Solvothermal Synthesis, Characterization and Mode of Formation of Aluminophosphate Chains, Layers and Frameworks

by

Scott R. J. Oliver

A thesis submitted in conformity with the requirements
for the degree of Doctor of Philosophy
Department of Chemistry
University of Toronto

Solvothermal Synthesis, Characterization and Mode of Formation

of Aluminophosphate Chains, Layers and Frameworks

Doctor of Philosophy

1997

Scott R. J. Oliver

Department of Chemistry

University of Toronto

ABSTRACT

The solvothermal synthesis of aluminophosphates is described, using organic amine additives ranging from primary to quaternary to cyclic. A tetraethylene glycol solvent led to a series of novel aluminophosphate crystal structures, denoted UT-n, where UT denotes University of Toronto and n denotes structure type. Of the eight structures that were discovered to date, two are one-dimensionally extended chains, five are two-dimensional layers and one is a three-dimensional framework. For all, the inorganic architecture is anionic and is charge-balanced by occluded alkylammonium template molecules. The chain and layered structures each contain an extensive hydrogen bonding network between the terminal oxygens of the phosphate groups and the ammonium hydrogens. A series of alkylammonium phosphate structures were also

discovered, which contain layers of phosphate molecules separated by interdigitated or bilayers of alkylammoniums.

The aluminophosphate and phosphate solids were characterized by a variety of techniques, including VT-PXRD, TGA, MS, SEM and solid state NMR. Many interesting results were found, such as a topotactic anionic framework to neutral framework transformation. The data also showed an unprecedented aluminophosphate chain to layer solid state transformation, where both end products were previously synthesized and fully solved UT-n crystal strucures.

This is followed by a new model for the mode of formation of aluminophosphates, which points out previously unrecognized structural aspects and is based on experimental evidence. The model involves a crystallizable chain precursor, which on hydrolysis, rearrangement and condensation, leads to a theoretically infinite number of possible chain types. These chains connect together and thereby account for the architectures, dimensionality and observed structural trends of potentially all known and theoretical aluminophosphate chains, layers and frameworks. Examples of each will be given.

Finally, changing the template molecule to an amphiphilic n-alkylamine ($C_nH_{2n+1}NH_2$) resulted in a series of novel mesolamellar aluminophosphates (MLA's). The phase(s), crystallinity and morphology of the resultant product were found to be highly dependent on carbon chain length. For n = 8 to 12, a series of remarkable surface morphologies were discovered. After the characterization of the MLA materials, a preliminary mode of formation will be described, involving an alkylammonium phosphate liquid crystal phase.

ACKNOWLEDGMENTS

I would like to thank my supervisor, Professor Geoffrey Ozin, for his guidance and seemingly perpetual effort and enthusiasm throughout my thesis. I also thank him for sparking my interest in the area while I was an undergraduate, which greatly influenced me to pursue research in his group. I also wish to thank Dr. Alex Kuperman for his help that allowed my research skills and independence to greatly develop. I also thank Dr. David Young for his help and discussion in all stages of my research.

I would like to acknowledge Dr. Alan Lough for crystallography, which my project depended greatly on. I also thank Dr. Neil Coombs for microscopy, especially on the work involving surfactants.

I would like to acknowledge the members of the Ozin group, past and present, for their friendship and help. The number of people I have known and the many discussions that I have had make clear the advantages of a being part of a large group. I thank Deepa Khushalani for thermogravimetry and Tong Jiang for DSC included in this work. I also thank the group members and the department for maintaining the equipment and services that I have used, as well as the computer network with the efforts of Dr. Scott Kirkby and Emmanuel Chomski.

Finally, I thank my family for their support. Most of all, I thank Dorothy for continuous support, motivation and patience throughout my graduate program.

TABLE OF CONTENTS

LIST OF TABLES

LIST OF FIGURES

LIST OF APPENDICES

CHAPTER 1: EXTENDED INORGANIC PHOSPHATE-BASED MATERIALS

1.0 INTRODUCTION

The synthesis and physicochemical study of extended inorganic materials has traditionally concentrated on the now well-established area of zeolite materials science. However, in the last twenty years, research into microporous aluminophosphates has been ongoing, both industrially and academically. To date, applications of these materials have been limited, but synthetic work has shown the structural diversity of aluminophosphates, and there now exists a large family of structure types. Some are isostructural to zeolites, while others are structurally unique. The frameworks and their preparation will be first considered in this chapter, as well as the mineral aluminophosphates.

The synthesis and characterization of lower dimensionality inorganic materials has also been an active area of research in recent years. Their method of preparation has, for the most part, followed the hydrothermal methods used for molecular sieves. The series of known one-dimensional chain and two-dimensional layered aluminophosphates will be discussed in some detail. There also exists data on molecular aluminophosphate clusters, and several crystal structures have been reported. Within other oxide-based compositional domains, there also exist numerous chain and layered structures to date. Due to their relevance to the present work, the metal phosphates will also be dealt with. However, the discussion will not be comprehensive, simply due to the large amount of literature that has amassed to date. Also pertinent is well-established polymeric and ringed condensed phosphates, and their hydrolysis chemistry.

The previously published models of aluminophosphate formation will be reviewed, as well as the solid state transformations that have been shown to occur for aluminophosphate frameworks. Since they are relevant to later chapters, the previously published alkylammonium phosphates will also be shown.

1.1 ALUMINOPHOSPHATE FRAMEWORKS: SYNTHESIS AND STRUCTURE TYPES

1.1.1 Occurrence

The natural aluminosilicate zeolites are well known,[1,2] and a wide variety of structure types occur in deposits all over the world.[3] Their relatively large abundance renders, in many

cases, the mining of zeolites more profitable than their large-scale synthesis. In the case of aluminophosphates, however, there are only limited types and amounts of mineral species. Augelite, berlinite, bolivarite, evansite, senegalite, trolleite, variscite, metavariscite and wavellite encompass all of the currently known aluminophosphate minerals.[4,5] This is partly due to the preference of Al^{3+} and P^{5+} cations to incorporate into other mineral phases. All were first reported in the nineteenth century, with the exception of metavariscite (1925), bolivarite (1921) and senegalite (1976).[5] The origin of the aluminophosphate minerals is also of interest and a source of debate for geologists.[6]

Berlinite is the aluminophosphate analog of quartz, comprised of tetrahedral aluminum, while most of the other aluminophosphate minerals may be considered as hydrated frameworks. Of the latter, the aluminum centres are octahedral, connected to four phosphate groups through bridging oxygens, with their coordination sphere completed by two terminal waters. These water molecules introduce a small degree of openness in the framework, such as for variscite[7] and metavariscite.[8] However, their channel sizes do not compare to those of the more open natural zeolites, such as faujasite. Further, zeolites may be reversibly dehydrated, whereas the aluminophosphate minerals are only partially reversible. Complete removal of the water causes collapse of the framework.[4]

Applications of natural aluminophosphates are limited. Berlinite is of interest for its piezoelectric properties.[9] However, this requires high quality single crystals and for this reason, synthetic berlinite is more appropriate. Aluminophosphates occur in large amounts as a minor component in many deposits of "phosphate rock", such as in Brazil and Senegal.[10] "Phosphate rock" is rock that contains a high concentration of phosphate minerals, primarily calcium phosphate, and is the world's main source of phosphorus.[11] In this way, aluminophosphate acts as a source of phosphorus, while aluminophosphate rock is also used directly for feedstuffs.[10] Aluminophosphate rock as a source of phosphorus ranks far above guano, the latter used only locally by villagers as fertilizer. Guano is found in caves where limestone has reacted over time with bat excrement, and less often, bird excrement.[5]

1.1.2 Dense Phase Aluminophosphates

An enormous amount of synthetic work has been performed for aluminophosphates. Part of the initial driving force for this was due to their natural occurrence, but more of a factor was the isostructurality of the high-temperature polymorphs of $AlPO_4$ to some of those of SiO_2,

namely berlinite, tridymite and cristobalite.[10,12-14] They not only display the same α and β (and γ for tridymite) forms of each, but also undergo the analogous transformations between the phases, although at slightly lower temperatures. This parallelism is attributed to the isoelectronic substitution of aluminum and phosphorus for two silicon atoms, and that the average ionic radii of aluminum and phosphorus is almost the same as that of silicon[13] [(Al^{3+} 0.39Å + P^{5+} 0.17Å)/2 = 0.28Å; Si^{4+} = 0.26Å].[14] Both $AlPO_4$ and SiO_2 form melts above approximately 1600°C and 1713°C, respectively, which may be quenched to produce glasses. High temperatures also lead to many crystalline forms of aluminum metaphosphates, including cubic[15] and monoclinic.[16] The latter is a framework comprised of octahedral aluminum connected to chains of condensed phosphate tetrahedra. All aluminophosphates, both natural and synthetic, contain tetrahedral phosphorus, while aluminum may exist as four-, five- and/or six-coordinate.

The pioneering work of d'Yvoire in 1961 was the first in-depth investigation into the synthesis and characterization of aluminophosphates.[17] Prior to this, only the dense phases such as berlinite or $AlPO_4$-cristobalite were synthesized. His experiments led to a series of new aluminophosphate hydrates, labeled $AlPO_4$-H1 to $AlPO_4$-H6 and $AlPO_4$-A to $AlPO_4$-E, some of which remain unsolved to date. $AlPO_4$-A to $AlPO_4$-E are obtained by the heating and accompanying dehydration of mineral or $AlPO_4$-Hn phases.

Kniep did a great deal of work in the 1970's to further the understanding of the ternary Al_2O_3-P_2O_5-H_2O system. He also elucidated much of the earlier work of d'Yvoire. In an excellent review of his work and that of others,[18] he takes a differing view of aluminophosphates by classifying them as acidic (Al:P <1), neutral (Al:P = 1) and basic (Al:P > 1), where there is a limiting range of 1:3 to 3:1. Therefore, the mineral aluminophosphate hydrates such as wavellite [$Al_3(OH)_3(PO_4)_2 \bullet 5H_2O$] are basic, while variscite and metavariscite ($AlPO_4 \bullet 2H_2O$) are neutral. Acid phases are synthesized by heating a concentrated phosphoric acid solution with Al_2O_3. Some were reported by d'Yvoire but were unsolved until the work of Kniep. One of the $Al(H_2PO_4)_3$ phases so reported is a framework structure, consisting of a network of octahedral aluminums connected by $O_2P(OH)_2$ groups.[19] The terminal hydroxyls of the tetrahedral phosphates are involved in hydrogen bonds. These methods using high concentrations also led to a number of lower-dimensionality layers, chains and clusters, as will be discussed in turn in section 1.2. Surprisingly, the work of Kniep has been ignored by those working in the area of

aluminophosphate synthesis. Notwithstanding, his work is an important contribution to the understanding of the aluminophosphate compositional domain.

1.1.3 Aluminophosphate Molecular Sieves

1.1.3.1 Hydrothermal Synthesis

A breakthrough came in 1982, when Wilson and coworkers at Union Carbide reported a new family of aluminophosphate molecular sieves.[20,21] These $AlPO_4$-n structures, where n denotes structure type, were synthesized under realtively mild hydrothermal conditions (i.e., autogenous pressure and low temperatures of 100-250°C, where water is the solvent). The resultant frameworks are highly open, much more so than the aluminophosphate hydrates discussed above, and their interior pores are filled by entrapped organic amines or quaternary ammonium salts and water. This work was based on the same methods used for zeolite synthesis, which itself was only 20 years old. In 1961, Barrer successfully prepared zeolites using organic amines and quaternary ammoniums rather than metal cations, as was already well-established and also known to occur naturally.[2] These organic agents exist in the final structure and are known as templates, the role of which is more fully explained in section 1.1.4.1.

The $AlPO_4$-n family displays a large degree of structural diversity. Most were novel, but others were isostructural to zeolite topologies, such as erionite ($AlPO_4$-17) and sodalite ($AlPO_4$-20). Some could only by synthesized with one template, such as tetramethylammonium hydroxide (TMAOH) for $AlPO_4$-20, while others were much less template specific, such as $AlPO_4$-5, which can be prepared with one of over 23 templates. The frameworks are comprised of tetrahedral aluminum and tetrahedral phosphorus, connected at their vertices by oxygens. The AlO_4 and PO_4 tetrahedra are strictly alternating, so that there are no Al-O-Al or P-O-P linkages.[4] Consequently, the $AlPO_4$ inorganic skeleton is neutral and the interior pores are filled by neutral organics.

The AlO_4 and PO_4 tetrahedra connect to define rings, necessarily with an even number of T-atoms (where T = Al, P). The smallest is a four-ring, which actually represents a ring of eight atoms, namely four T-atoms and four oxygens. The openness of the framework arises from the larger eight-, ten-, and twelve-rings. The various $AlPO_4$-n architectures have been compiled by Szostak.[22] An example that will be given here is $AlPO_4$-11, where edge-sharing four-rings and six-rings are arranged in the **ab** plane and define ten-rings (Figure 1-1a). Each T-atom in the **ab** plane is three-connected, and has its tetrahedron completed by adjoining to the next such layer

(a)

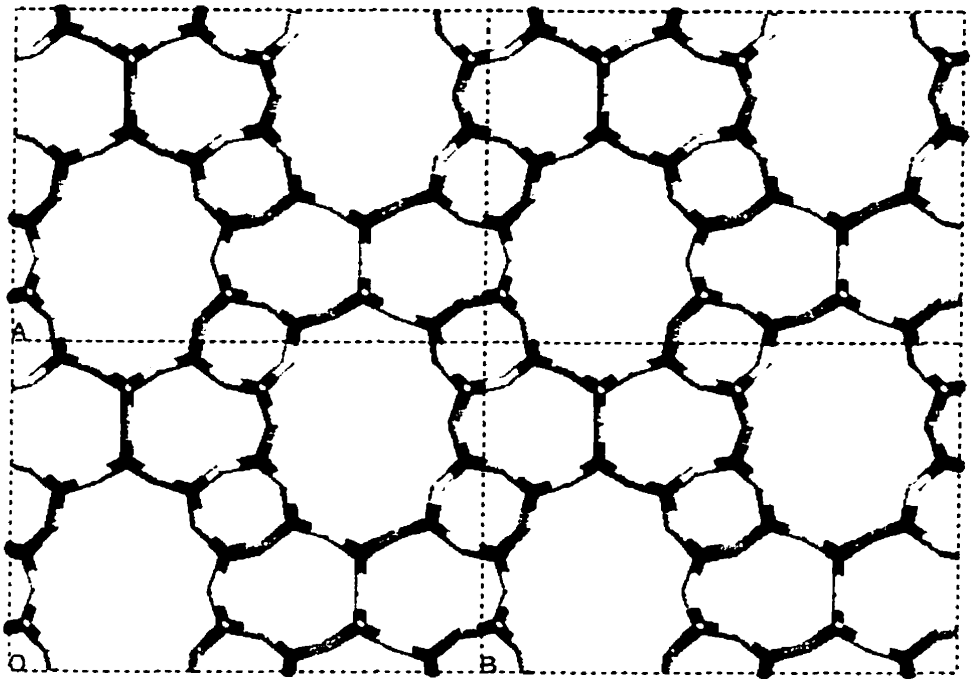

(b)

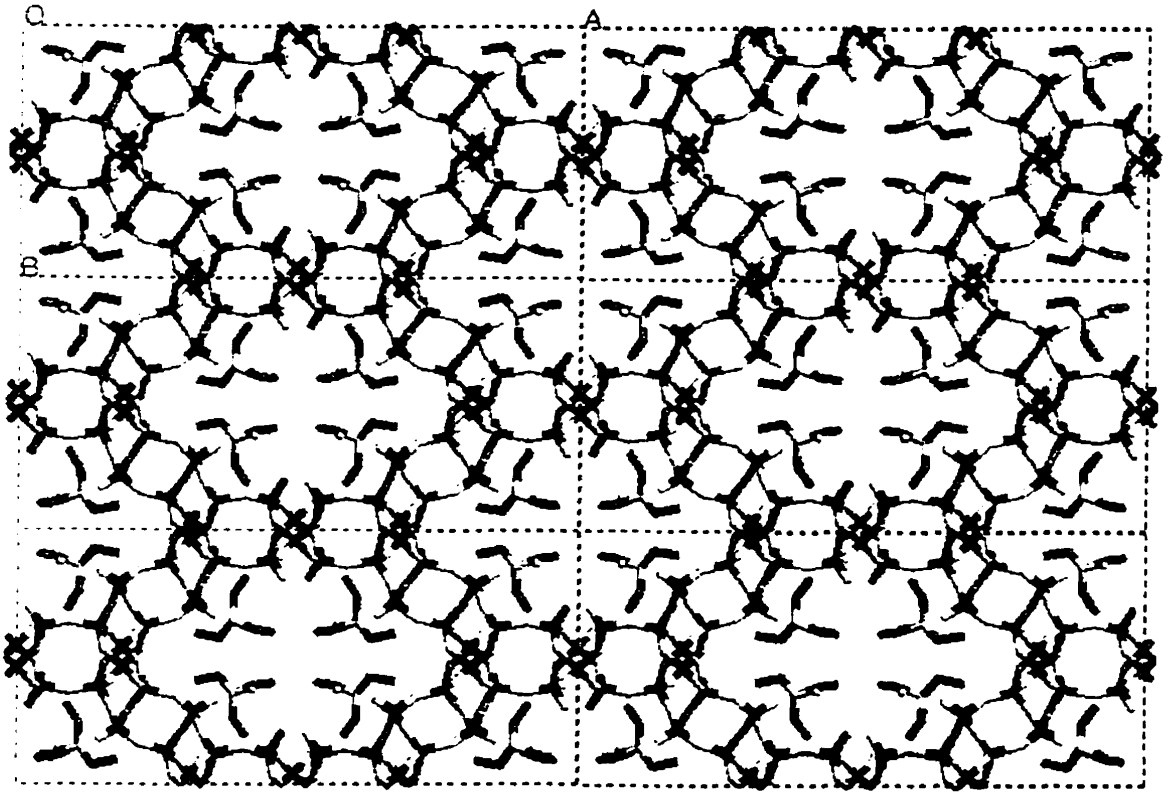

Figure 1-1. Two examples of three-dimensional aluminophosphate frameworks. (a) $AlPO_4$-11. (b) JDF-20. The shading scheme used in all figures is as follows: oxygen, nitrogen and hydrogen: white; phosphorus: black; aluminum and carbon: grey.

along the c-axis. In this way, ten-ring channels propagate down the c-axis. Layers of edge-sharing n-rings in the **ab** plane such as this are commonly found among the $AlPO_4$-n structures, therefore leading to a predominence of unidimensional channel systems. The fourth connectivity typically alternates up and down with respect to neighbouring T-atoms, thereby defining channel walls comprised of edge-sharing six-rings. Interestingly, this arrangement is analogous to the "double-pyroxene" chain building block of dense phases such as $AlPO_4$-tridymite.

The structures are termed molecular sieves since the organic species can be removed by heating the material, typically to 400-600°C. Many are stable to 1000°C. At the time of their discovery, it was hoped that the open materials would be of use for adsorptive and catalytic applications. However, to date, only the metal substituted (see section 1.1.3.3) SAPO-11 and SAPO-34 frameworks have found use as a support and catalyst, respectively.[23] This is due to their relatively low acidity and hydrolytic stability as compared to the extensively used zeolites.

This initial report of aluminophosphate molecular sieves of course led to much further work by others. Many of the initially unknown structures were then solved, including $AlPO_4$-H3,[24] $AlPO_4$-17,[25] $AlPO_4$-31[26] and others. This also resulted in the isolation of new phases, such as $AlPO_4$-12-TAMU (where TAMU represents Texas A&M University)[27] and $AlPO_4$-14A.[28] Many were solved by Rietveld refinement of powder X-ray diffraction due to the small crystal sizes. It was found that aluminum can exist as both tetrahedral and trigonal bipyramidal in the framework, such as in $AlPO_4$-21,[29] both tetrahedral and octahedral, such as in $AlPO_4$-H3,[24] or exclusively octahedral, as in the aluminophosphate analog of the mineral tinsleyite[30] (also referred to as $AlPO_4$-15[31]).

In 1989, VPI-5 (VPI for Virginia Polytechnical Institute) was reported,[32] producing much excitement at the time. This highly open framework material is related to $AlPO_4$-5, but contains an additional set of four-rings between the six-rings, which results in an 18-ring channel rather than a 12-ring channel. It can by synthesized with dipropylamine or tetrabutylammonium hydroxide (TBAOH), but the organics do not end up in the channel, and contain only water. Despite the expectation of future applications, none have been shown to date. Nonetheless, it sparked much interest and research into aluminophosphates. New hydrothermally synthesized aluminophosphates are being continually reported,[33-35] and there is every reason to believe that this will continue in future years through further synthetic work.

1.1.3.2 Non Aqueous Synthesis

The synthesis of molecular sieves from a predominantly non aqueous solvent was first reported as recently as 1985 by Bibby and Dale.[36] Other than the solvent, conditions were similar to hydrothermal methods, and this type of synthesis was subsequently dubbed "organothermal". They prepared sodalites with a wide range of Si:Al ratios from ethylene glycol and propanol solvents, where water was present in only minor amounts. Following this initial work, others broadened the number of solvents that could be used for zeolites,[37-39] including glycerol, pyridine, C_2-C_7 alcohols and DMSO. This inevitably led to the first report of the synthesis of aluminophosphate molecular sieves from predominantly non aqueous solvents by Xu and coworkers.[40] With a variety of templates, $AlPO_4$-5, $AlPO_4$-11 and $AlPO_4$-21 were isolated from alcohol and diol solvents, namely sec-butanol, hexanol, ethylene glycol and 1,3-propanediol. The same group more recently reported the synthesis of $AlPO_4$-17 from an ethylene glycol solvent.[41] Aluminum triisopropoxide was the Al_2O_3 source used in all experiments.

To date, two novel aluminophosphate frameworks have been synthesized by non aqueous methods. Both are anionic, containing extraframework organic cations in the channels. The first is JDF-20,[42] possessing a large unidimensional channel with triethylammoniums charge-balancing the framework (Figure 1-1b). The channel contains 20-membered rings that are "bifurcated",[43] that is to say, alternate paths may be traced around the ring, since there are branching sites at one or more points. The material holds little promise for use as a molecular sieve, since the channels are elliptical and contain P=O and P-OH groups that point into the channel and reduce its free aperture. Moreover, template removal leads to collapse of the framework, on account of its negative charge. The second novel framework has eight-membered ring channels containing methylammonium cations and was prepared from ethylene glycol.[44] Attempts to calcine the framework also led to its collapse.

The effect and role of the solvent in the organothermal systems has not been well understood nor even discussed in much detail in the literature. One report put forth by Xu *et al.* summarized their non aqueous work and discussed the main factors of the systems, such as template, temperature, time and solvent.[45] Of the latter, they attribute the polarity of the solvent as its key role in affecting the synthesis results. To do this, they compared the solvent's empirical solvent polarity parameter with the phase(s) obtained for a given template. They state that the polarity influences the precursor species that act as the nutrients for crystallization,

although this was not corroborated with any data or any specification of the nature of these precursor species.

In their initial report of the non aqueous synthesis of $AlPO_4$-n materials,[40] Xu and coworkers were correct in stating that much more work and discoveries remain to be made with non aqueous solvents. It has led to a large number of lower dimensionality aluminophosphates and metal phosphates, as will be discussed later. However, their statement that not all templating agents that are effective in aqueous solution, such as ethylenediamine, can be so in non aqueous solvents, will turn out to be incorrect.

1.1.3.3 Metal-Substituted Frameworks

A large amount of work has been devoted towards the isomorphic substitution of metal atoms into the aluminophosphate framework.[4,22] The metal is usually a divalent cation, and a wide range have been incorporated, including Be, Mg, Mn, Fe, Co, Ni and Zn. The materials are denoted MeAPO-n, sometimes written as MAPO-n. The interest in these materials is that the metal substitutes for an aluminum, and therefore introduces negative charge and a potentially catalytically active acid site to the framework. Silicon has also been shown to substitute for phosphorus, leading to anionic SAPO-n materials.

Some MAPO-n structures can be synthesized as the pure $AlPO_4$-n aluminophosphate, such as $AlPO_4$-5, while others cannot. For example, SAPO-37, has the faujasite (or zeolite Y) topology,[22] but synthesis of the $AlPO_4$-37 analog has not yet been realized. However, these missing aluminophosphate end-members are slowly being discovered through continued experimentation, such as $AlPO_4$-34 and $AlPO_4$-39,[46] $AlPO_4$-41[47] and, most recently, $AlPO_4$-36.[48] The latter was achieved by first aging a purely aluminophosphate gel for 5 days at 120°C, followed by the usual MAPO-36 synthesis conditions of 140°C for 3 days. Without the initial aging step, $AlPO_4$-5 was obtained.

In most MAPO-n materials, the metals are distributed randomly throughout the framework. An example is the recently discovered $Mg_{0.22}Al_{0.78}PO_4$ novel framework.[49] The level of substitution can in some cases be quite substantial, particularly for silicon. A few MAPO-n frameworks have the metal at crystallographically defined sites, such as MAPO-46 or CoAPO-50.[22] Recently, two nickel aluminophosphates were reported, where the nickel is octahedral.[50,51] An interesting structural aspect of these crystallographically defined materials is that the metal atoms covalently link together aluminophosphate layers.

1.1.3.4 Fluoroaluminophosphate Frameworks

Guth *et al.* developed a fluoride medium for the synthesis of $AlPO_4$-n structure types.[52] For example, they synthesized high quality crystals of $AlPO_4$-5, with tetrapropylammonium (TPA) cations located in the channels and F^- anions between two four-rings of the framework wall.[53] They also synthesized $AlPO_4$-11, $AlPO_4$-16, SAPO-34, SAPO-37, SAPO-40, SAPO-42 and other frameworks with fluorinated templates located in the channels.[54-56] This method also proved successful for many zeolites and a series of gallium phosphate frameworks (section 1.3.4). In an overview of their work, they noted the multi-functional role of fluoride anions as a template, structure-directing agent and mineralizer.[57]

Novel fluoroaluminophosphate frameworks were also prepared by these methods. In an original report by Yu *et al.*, a hydrothermal synthesis with a hexamethylenetetramine organic additive led to a novel small-pore framework.[58] However, the crystal report left several ambiguities. For example, charge-balancing cation was not shown, and no supporting evidence was given for the presence of fluorine in the framework. In a reexamination by Férey *et al.*,[59,60] it was found that the PO_4 tetrahedra were connected to AlX_5 trigonal bipyramids and AlX_6 octahedra, where $X = O^{2-}$ and a statistical average of OH^- and F^-. The extraframework cation was ammonium and was indicative of the decomposition of the organic additive. Indeed, the structure may also be synthesized with one of a variety of other organic amines, such as cyclohexylamine, piperidine and N,N,N',N'-tetramethylethylenediamine, but not stable quaternary ammonium salts such as TMAOH.

Two further examples of novel fluoroaluminophosphate frameworks were recently reported. One was grown hydrothermally and contains potassium cations in its channels.[61] It is built up of AlO_4F_2 octahedra, where the oxygens connect to four phosphates and the two cis fluorines connect to two other such AlO_4F_2 octahedra to form a chain of linked octahedra. The other framework was grown from a predominantly non aqueous triethylene glycol solvent and is closely related to the framework of the zeolite gismondine.[62] One half of the aluminums are tetrahedral while the other half are AlO_4F_2 octahedra interconnected to define doubly fluorine-bridged $[O_4Al\text{-}(\mu\text{-}F)_2\text{-}AlO_4]$ dimers. The $[Al_2P_2O_8F]^-$ framework pores contain dimethylammonium cations that were not added to the synthesis mixture, but evidently formed by the decomposition of the N,N-dimethylformamide that was added. Heating the phase above

340°C released HF, dimethylamine and collapsed the framework to $AlPO_4$-tridymite. Interestingly, the purposeful addition of dimethylamine did not allow this phase to form.

1.1.4 Mode of Formation of Aluminophosphate Molecular Sieves

1.1.4.1 Role of Template and Gel Chemistry

The traditional model for the formation of zeolites is template theory,[63] which was later extended to aluminophosphates. A template has been defined as any additive agent which induces the formation of a particular structure that does not form in its absence.[4] However, there are two contradictory trends, namely one template leading to many structure types versus many templates that lead to one structure. Further adding to the confusion is that a template is sometimes labeled so only if it exists in the resultant framework,[57] while this is commonly done even when it is not present in the framework. A more generic term of structure-directing, structure-promoting or organic additive is therefore quite often used, such as when applied to HCl for directing the structures of $AlPO_4$-H1 through $AlPO_4$-H4.[64]

There are certainly a multitude of chemical reactions and equilibria that occur during the crystallization of a molecular sieve. As discussed in a review by Davis and Lobo,[65] evidence has been presented for both solution-mediated transport and solid-phase transformation mechanisms. For example, zeolite Y can be synthesized from clear solution, when no gel is present. Alternatively, a dehydrated gel treated in triethylamine leads to ZSM-5, with no inorganic solution species present at any point during the crystallization. Generally, it is agreed that the template plays a role in conjunction with the gel chemistry that is taking place.[63,65,66]

This has been the opinion for aluminophosphate systems as well.[67] The correct gel chemistry is influenced by many factors, such as the aluminum and phosphorus sources, mixing procedure, gel composition and pretreatment (if any), and pH evolution of the reaction mixture. Therefore, the template structure-directs to a varying degree, while also influencing all of these gel chemistry parameters.

More recently, there has been much discussion on the role of the organic template by Lewis *et al.*[68,69] Their theoretical calculations were focused on the stability and concentration of metal-substitution into microporous aluminophosphates. However, they did find a correlation between the stability of certain frameworks and the presence of a template of specific shape. They also found that certain frameworks are more stable when the template is removed, which is

consistent with the observed conversion of the $AlPO_4$-CHA framework to $AlPO_4$-5 upon calcination.

One important role usually attributed to the template is the stabilization of the openness and consequent metastability of the framework. This prevents its collapse to a dense phase structure. However, Hu *et al.* have recently made thermochemical calculations of both microporous and dense phase aluminophosphates.[70] They found that in aqueous solution, open frameworks such as $AlPO_4$-5 are energetically comparable to dense phases such as berlinite. Therefore, the open inorganic architecture is not energetically unfavourable, since the inorganic species dense-pack around the template molecules to form a stable composite. Certainly, the mechanism of molecular sieve formation is of current interest and debate, and requires much further study. Nonetheless, it is leading to a better understanding of the template role and the complex chemistry that leads to molecular sieve frameworks.

1.1.4.2 Inorganic Building Blocks

Much evidence of the existence of silicate and aluminosilicate anions in solution has been uncovered, primarily by the use of NMR techniques.[4,71-73] Examples are four-rings, six-rings, double-four-rings and many others. Recent studies show that only certain aluminosilicate fragments are energetically reasonable to exist and that Lowenstein's rule is strictly obeyed.[74] Accordingly, many propose that these secondary building units (SBU's, where the primary building unit is a single metal oxide polyhedra) condense together to build up the final framework.[75-77] However, no direct evidence has been shown for this to occur, and the actual processes that take place are not known, as discussed in the previous section.

Much less is known or even discussed for aluminophosphate molecular sieves. Molecular aluminophosphate anions have been detected in solution,[78,79] but are mostly dimeric or trimeric and do not display any ring or double-ring structures as do the aluminosilicate anions. Férey has recently proposed the formation of fluorinated aluminophosphates and gallium phosphates to occur by the connection of various SBU units, the type and relative abundance of which depend on the fluorine source, pH and the amine that is present.[80] Others have indicated chain species that run through the final framework, parallel to the main channel system. Examples are narsarsukite, double-crankshaft[81,82] and triple-crankshaft chains[83] (Figure 1-2a-c). Narsarsukite chains account for the structure of $AlPO_4$-5 (Figure 1-2d). Triple-crankshaft chains

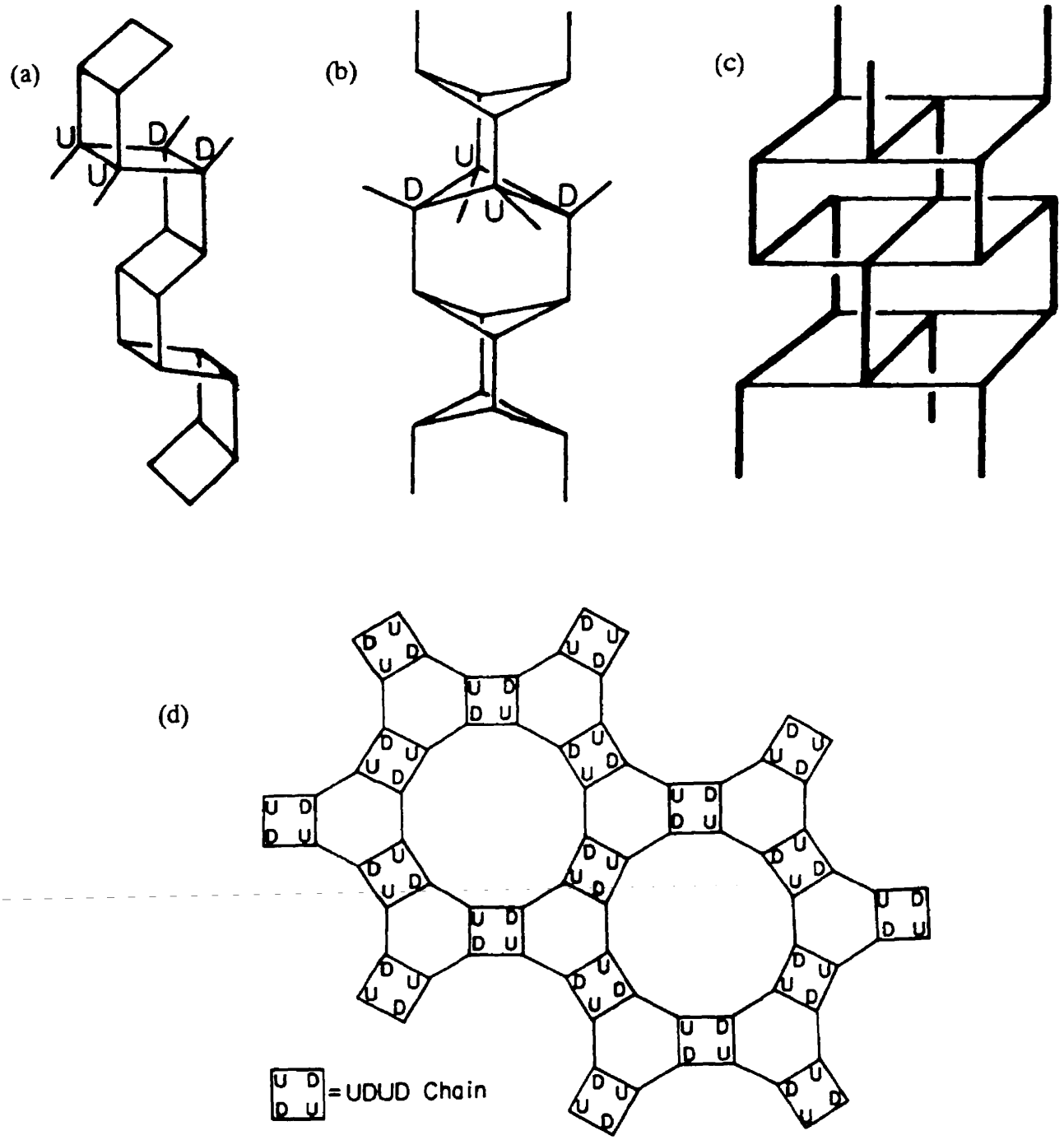

Figure 1-2. Proposed chain building blocks for aluminophosphate frameworks. (U denotes a T-atom pointing up, D denotes down.) (a) Double-crankshaft (UUDD) chain. (b) Narsarsukite (UDUD) chain. (c) Triple-crankshaft chain. (d) As an example, the $AlPO_4$-5 framework is comprised of UDUD chains.

are present in VPI-5 and $AlPO_4$-H2 and are proposed to assemble together to form the final structure.[83]

Smith and co-workers have classified aluminophosphate molecular sieve architectures, as well as those of other compositions such as zeolites, by pointing out theoretical two-dimensional nets that account for known and theoretical molecular sieve frameworks.[84-86] Similar evaluation of zeolites has more recently been made.[87,88] Again, no direct evidence has been provided for any of these SBU, chain or layered building blocks to exist in solution or undergo condensation to the final framework. It is noteworthy that no discussions yet exist concerning the mode of formation of the lower-dimensionality aluminophosphate layers, chains and clusters that have been discovered in recent years (section 1.2).

1.1.4.3 Layered Precursor

In the synthesis of VPI-5, some data have suggested that psuedoboehmite is intercalated by phosphate and organic amines, which then expands to form an amorphous aluminophosphate layered intermediate.[89] This disordered layered material is proposed to crystallize by undergoing cross-linking of the layers to give the final framework. Unrelated solid state NMR studies of reaction gels[90] suggest that the pseudoboehmite layers are linked together by phosphate, leading to an amorphous layered phase containing 6-coordinate aluminum. This phase reacts further with phosphate to give an amorphous solid containing 4-coordinate aluminum. This latter phase is said to act as a solid precursor to the VPI-5 product. Others state that aluminophosphate solution phase molecular species are initially formed, which then lead to a layered solid precursor to VPI-5.[91,92] All of these studies give the same overall suggestion, that a psuedoboehmite-phosphate reaction gives rise to a layered precursor to the final framework. Due to the interest in VPI-5, this is the most studied aluminophosphate synthesis system. It would be interesting to see how these results would compare to related studies of the reaction gels of other aluminophosphate frameworks.

Recently, a layered precursor to the zeolite ferrierite was reported.[93] Variable temperature powder X-ray diffraction showed the crystalline material to transform to a poorly ordered intermediate at 150°C, and then to ferrierite at 500°C. While the nature of the structure of the layered precursor was not fully elucidated, it was closely related to ferrierite, in fact proposed to be layers of ferrierite that are not yet connected, judging by the similarity of its diffraction pattern and ^{29}Si MAS NMR to that of ferrierite. A similar layer to zeolite transformation was

also reported for a layered borosilicate that transforms to the zeolite MCM-22.[94] Furthermore, the crystal structure of a layered silicate solved by Rietveld analysis was very recently reported.[95] The layer contains interlamellar TMA cations and was labeled as a zeolite precursor. However, no such transformation was shown and was only proposed to occur. Nonetheless, these reports represent a new way of rationalizing zeolite formation; it will be interesting to see if further progress is made and its implications into the mode of formation of aluminophosphates.

1.1.4.4 Framework to Framework Transformations

Any collapse of a framework, such as $AlPO_4$-5 to $AlPO_4$-tridymite, in itself represents a solid state framework to framework reconstructive transformation. However, there are a number of known thermal transformations where collapse does not take place but rather lead to another open framework. They have been shown to occur for some zeolites, such as zeolite E to sodalite[96] and chabazite to sodalite.[97] A large number of solid state transformations also occur for the aluminophosphate minerals and acid phases.[18]

An example is $AlPO_4$-H3, which reversibly transforms at 100°C to $AlPO_4$-C by loss of water.[81] The former contains $AlO_4(H_2O)_2$ octahedra, while the latter contains AlO_4 tetrahedra. The two closely related structures contain double-crankshafts, but are elongated in $AlPO_4$-H3. Further, the six-rings in the **ab** plane are much more distorted for $AlPO_4$-H3. Therefore, only a subtle, displacive rearrangement allows the interconversion between the two frameworks. In turn, $AlPO_4$-C irreversibly transforms at 250°C to $AlPO_4$-D, which contains nasarsukite chains. Therefore, the mechanism of this reconstructive transformation is said to involve the conversion of double-crankshaft chains of Figure 1-2a to narsarsukite chains of Figure 1-2b, by their hydrolysis and the moving of oxygens to the opposite side of the four-rings. $AlPO_4$-D reversibly hydrates to $AlPO_4$-H6 at 50°C, and collapses above 650°C to $AlPO_4$-tridymite.

A very similar transition occurs for the irreversible transformation of $AlPO_4$-21 to $AlPO_4$-25 at 500°C.[82] $AlPO_4$-21 contains double-crankshaft chains, while $AlPO_4$-25 contains narsarsukite chains. At 250°C, $AlPO_4$-25 also undergoes a displacive high-low transition analogous to that of $AlPO_4$-tridymite. A reversible transformation has also been shown to occur at 65°C for calcined $AlPO_4$-5.[98] While the exact nature of the transformation could not be elucidated, a similar process appears to be occurring[99] at 100°C for SSZ-24, the all-silica zeolitic analog of $AlPO_4$-5.[100]

A final example is the well-studied VPI-5 to $AlPO_4$-8 transformation, which occurs at 100°C.[101-103] $AlPO_4$-8 was discovered long before VPI-5, but the product was always dried at 100°C.[21] Therefore, this transformation must have been occurring and the VPI-5 framework was missed. The mechanism of this transformation has been proposed, involving the opening and rearrangement of the hydrated triple crankshafts.[104]

As of yet, $AlPO_4$-H1 is a material with an unknown structure, but is very closely related to VPI-5, as judged by its powder X-ray pattern. It has been contrasted to VPI-5 by its differing thermal behaviour, as it does not transform to $AlPO_4$-8 but instead collapses to $AlPO_4$-tridymite at 110°C.[105] Collectively, these framework transformations help us to understand the chemistry of the aluminophosphates and provide some insight into their mode of formation.

1.2 LOW-DIMENSIONAL ALUMINOPHOSPHATES

1.2.1 Aluminophosphate Layers

Since 1991, there has been a steady increase in the number of known layered aluminophosphate structures. In spite of this fact and that a large number of organic amine templates have been successfully employed, almost all of the layers display a stoichiometry of $[Al_3P_4O_{16}]^{3-}$. In addition, many possess the same inorganic architecture. For all, the P:Al ratios are greater than 1.0, since phosphate groups with terminal oxygens cap the layers, thereby terminating the Al-O-P connectivity in the third dimension. As seen for some frameworks, these phosphates usually introduce negative charge to the inorganic architecture, therefore requiring cationic molecules to exist between the layers.

The $[Al_3P_4O_{16}]^{3-}$ layers display two polymorphs. The first is an $AlPO_4$-5-like layer, containing the same arrangement of four-, six- and twelve-rings in the **ab** plane. However, the aluminums of the six-rings are capped by triply-bridging phosphate groups that alternate above and below the layers (Figure 1-3a). These phosphates contain one terminal phosphonyl oxygen that interacts with the interlamellar alkylammonium cations. Two structures have been shown to possess this layer structure, one containing 1,4-diammoniumbutane[106] and the other containing 1,4-diammoniumcyclohexane.[107]

The second type of $[Al_3P_4O_{16}]^{3-}$ layer contains four-, six- and eight-rings in an identical arrangement to the **ab** plane of $AlPO_4$-25.[4] Again, the six-rings are capped by triply bridging phosphate groups that alternate above and below the layer (Figure 1-3b). Two polytypes were synthesized organothermally, one from ethylene glycol with ethylenediammonium and ethylene

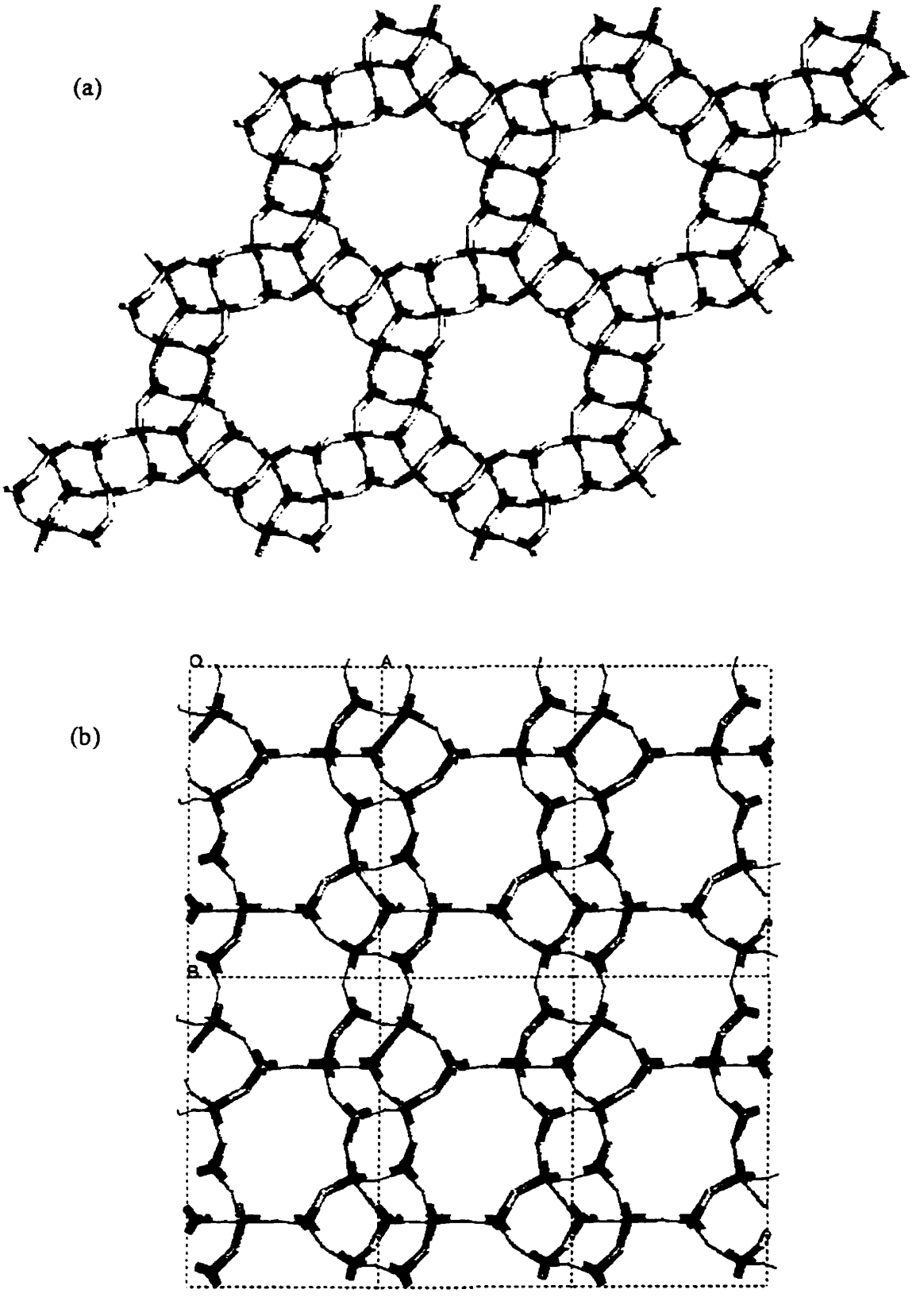

Figure 1-3. Two examples of $[Al_3P_4O_{16}]^{3-}$ layered aluminophosphates. (a) $AlPO_4$-5-like layer. (b) $AlPO_4$-25-like layer.

glycol between the layers.[108] The other was synthesized from a triethylene glycol solvent using two templating species, 1,5-diammoniumpentane and piperidinium.[109]

Several other organothermally grown layers have been reported that are structurally unique to the above layers, and that do not contain any two-dimensional connectivity that is present in an $AlPO_4$-n framework. One is an $[Al_2P_3O_{12}H_2]^-$ layer, separated by pyridinium cations and prepared from a sec-butanol solvent.[110] The second used the same solvent,[110] and contains two types of sec-$BuNH_3^+$ molecules between $[Al_2P_3O_{12}H]^{2-}$ layers (Figure 1-4a). A recently reported layer was prepared from an ethylene glycol solvent,[111] and contains a chiral $[NH_3CHMeCH_2NH_3]^{2+}$ template between lower symmetry $[(Al_3P_4O_{16})_2]^{6-}$ layers (see Figure 4-9b, Chapter 4).

An intriguing development occurred for aluminophosphates in general with the report of two layered structures templated by chiral transition metal complexes. The first displayed a novel $[Al_3P_4O_{16}]^{3-}$ layered architecture,[112] which may be thought of as a layer of edge-sharing six-rings with each aluminum connected to a triply-bridging phosphate capping group. Between the layers reside tris(ethylenediamine)cobalt(III) $[Co(en)_3]^{3+}$ octahedral complexes. The orange crystals were prepared hydrothermally and the chiral complexes lie in chiral pockets of the layer, which the authors state requires the presence of a chiral template. An equal number of each enantiomer and chiral pocket renders the structure non-chiral overall.

The second such layer (Figure 1-4b) contained chiral tris(propylenediamine)cobalt(III) complexes between the $[Al_3P_4O_{16}]^{3-}$ layer of Figure 1-3b.[113] Remarkably, a given crystal of the product contained only one enantiomer of the complex, and the layer is said to also be chiral due to the modification of its shape by the metal complexes. This may lead to aluminophosphate materials useful for chiral separation and catalysis. More importantly, the use of transition metal complexes as template represents a new and unexplored domain in the synthesis of aluminophosphates. Similarly, the very recent report of the first layered aluminum organophosphonate[114] shows that there is much promise for the synthesis of new low-dimensionality structures of this type.

Finally, Kniep *et al.* prepared two layered structures of high P:Al ratios by heating a concentrated aluminum oxide - phosphoric acid solution. The first contains layers of linked chains (Figure 1-5a).[115] The building chains are isostructural to the $Al(PO_4)_2$ chains (Figure 1-7a, below), but the aluminums are octahedral in this case. The layers are neutral due to the mono- and diprotonated phosphates, and are directly hydrogen bonded together. The second layer,

(a)

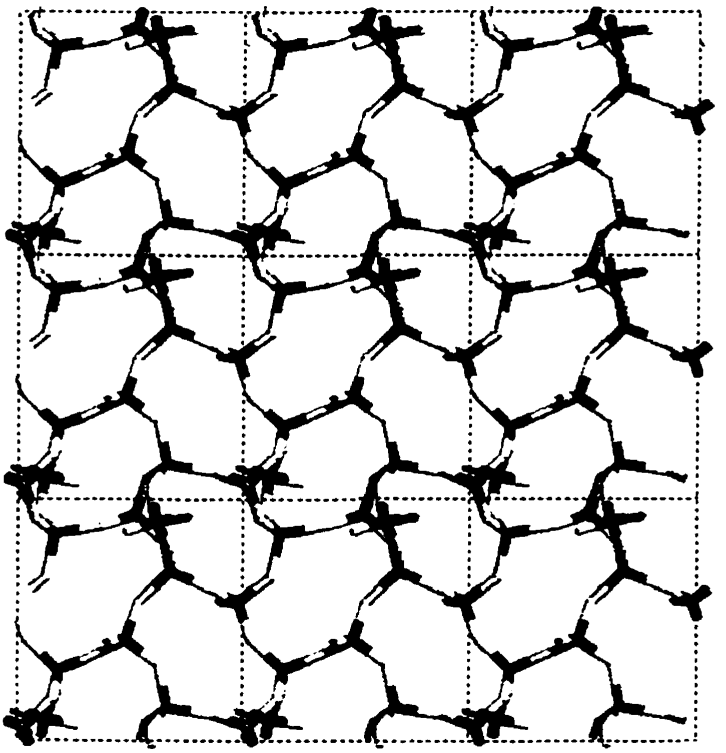

(b)

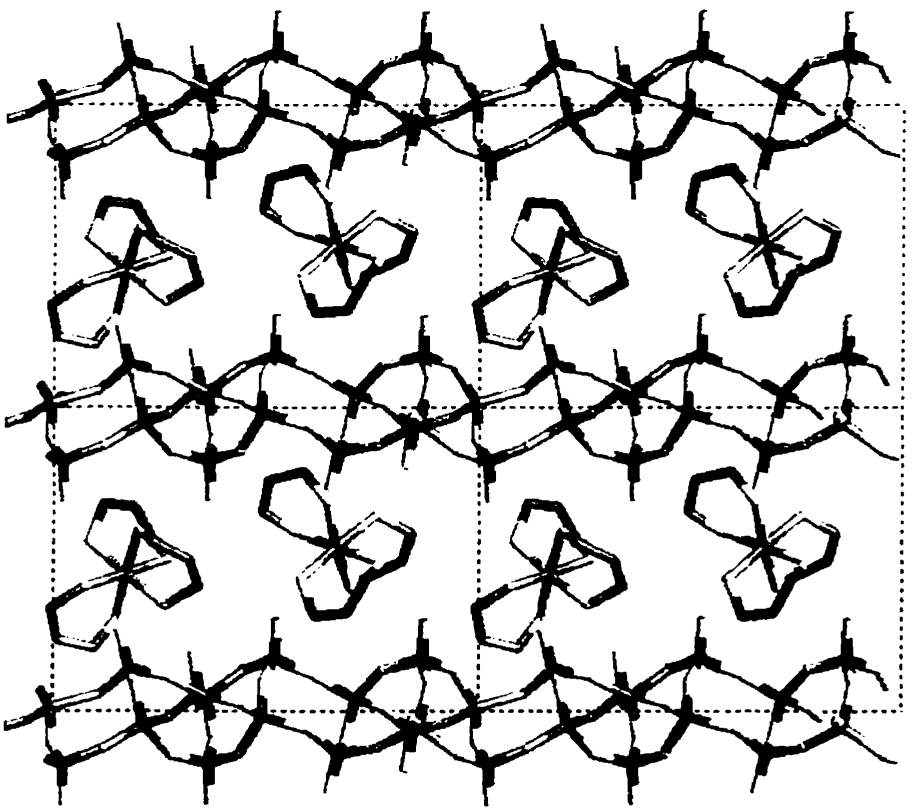

Figure 1-4. Further examples of two-dimensionally extended aluminophosphates. (a) $[Al_2P_3O_{12}H]^{2-}[sec\text{-}BuNH_3^+]_2$. (b) $[Al_3P_4O_{16}]^{3-}[Co(pn)_3]^{3+}$.

(a)

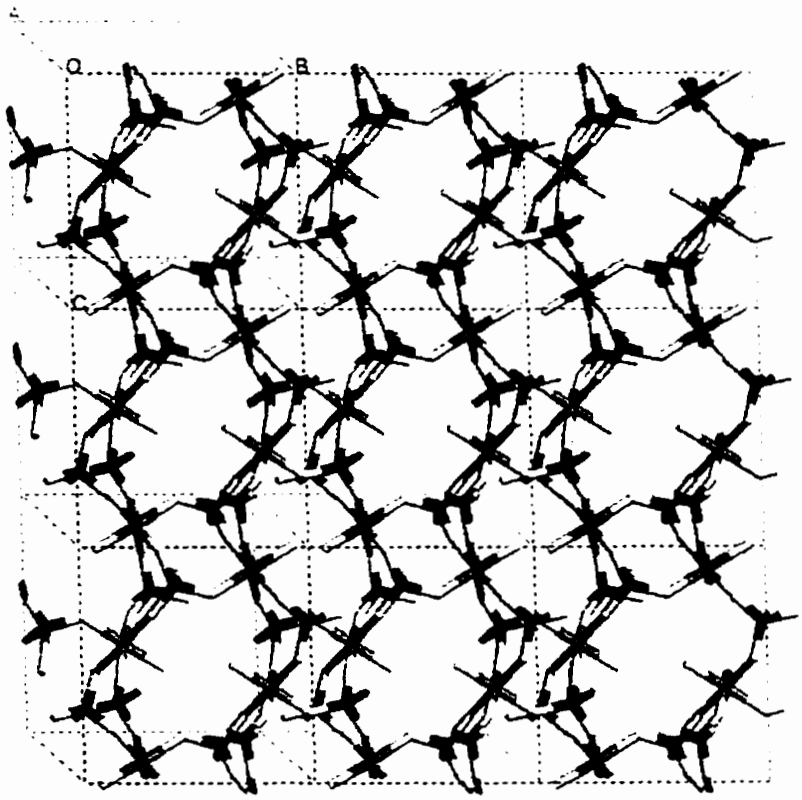

(b)

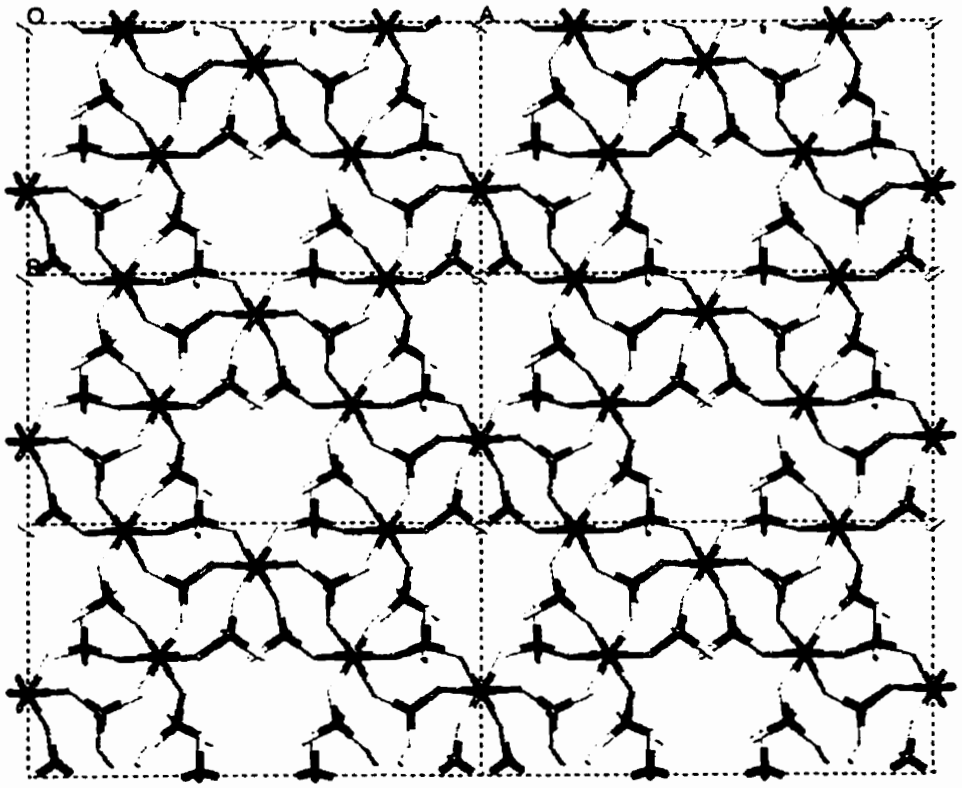

Figure 1-5. Layered aluminophosphates of Kniep *et al.* (a) $Al(H_2PO_4)(HPO_4)(H_2O)$. (b) $(H_3O)[Al_3(H_2PO_4)_6(HPO_4)_2]4(H_2O)$.

prepared by similar methods,[116] is slightly anionic and is charge-balanced by hydronium ions. The unique $[Al_3(H_2PO_4)_6(HPO_4)_2]^-$ layers contain octahedral aluminum and doubly- and triply-bridging phosphate groups (Figure 1-5b). Again, the layers are directly connected by hydrogen bonds.

1.2.2 Fluoroaluminophosphate Layers

A mixed aqueous - non aqueous system led to the only two known examples of layered fluoraluminophosphates. The first was formed with a solvent of molar ratio 20 ethylenediamine : 30 H_2O, and an NH_4F fluoride additive, to give a layered material comprised of PO_4 tetrahedra and distorted $Al(O_3F_2N)$ octahedra.[117] The nitrogen belongs to one end of an ethylenediamine which extend into the interlamellar region (Figure 1-6a). This is the first observation of a nitrogen ligand among the extended aluminophosphates, which the authors attribute to the high concentration of amine.

The second layered solid was synthesized from a mixed 40 EtOH : 60 H_2O solvent, templated by 1,6-hexanediammonium.[118] The layers contain PO_4 tetrahedra, three types of AlO_4F_2 octahedra and one type of AlO_3F tetrahedra, the latter with its fluorine atom in a terminal position. The layers are also separated by water molecules. An interesting hydrophobic effect is observed in the partial bending of the hexylene chains around and away from the water molecules (Figure 1-6b).

1.2.3 Aluminophosphate Chains

Metal phosphate "aggregation polymers" are known to exist in concentrated, viscous gels. This has been shown for a number of metals, but the most studied are the aluminophosphate polymers.[12,13,119-121] They form when the P:Al ratio is raised above 1.0,[12,13,121] and are stable in acidic medium, but precipitate on rendering the medium alkaline.[120] They may be dried to an amorphous solid and again brought back to the same state simply by adding water. Some have suggested that the solution-bound chains exist as a three-dimensional network of branched chains,[120] while others state that they are connected by a complex system of hydrogen bonds.[12]

In the early studies on these viscous gels, it was thought that the main solution species is aluminum tripolyphosphate (a condensed phosphate, section 1.4), due to the 3:1 P:Al ratio. However, chromatography later showed no P-O-P bonds to exist in the solid.[12] The crystal

(a)

(b)

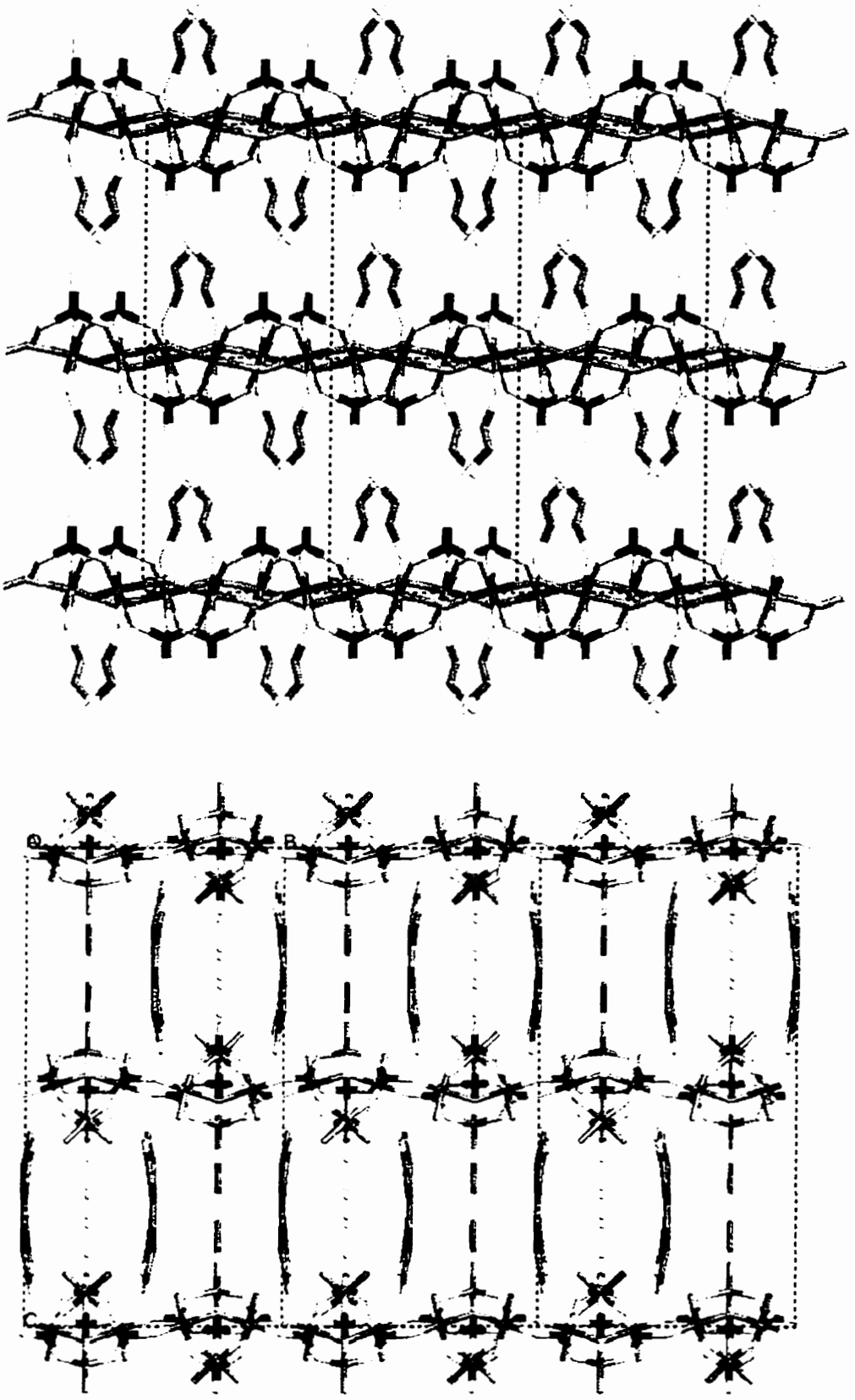

Figure 1-6. Layered fluoroaluminophosphates. (a) $AlF(HPO_4)en$, with en bonded to aluminum. (b) $Al_4(PO_4)_3(HPO_4)F_6$ (1,6-Hexanediammonium)$_{2.5}3H_2O$. Note the bending of the alkyl chains away from the water molecules.

structure of Kniep *et al.*[122] would seem to have conclusively dispelled this. Their $Al(H_2PO_4)_3$ chain structure was prepared by simply allowing the viscous solution of aggregation polymers to evaporate at 50°C. The crystals are made up of chains of AlO_6 octahedra connected to six phosphate groups. Three phosphate groups on either side of the octahedron are connected to the next aluminum of the chain. The neutral chains are connected by hydrogen bonds. This chain architecture seems to be common among the metal phosphates. Unfortunately, the atomic coordinates of the entirely inorganic $Al(H_2PO_4)_3$ were unavailable, but it is isostructural to the chain of Figure 1-8b, section 1.3.1.

Solvothermal methods have thus far led to only two chain crystal structures.[123,124] They are isostructural, and are very similar to the chain of Kniep *et al.* The chain contains isolated aluminum tetrahedra, and are therefore only connected by two doubly-bridging phosphates (Figure 1-7a). Again, this architecture has been shown for other inorganic chains, including a zinc phosphate chain (section 1.3.3) and the borosilicate chains of the mineral garrelsite.[4] The anionic $[Al(HPO_4)_2]^-$ chains may be synthesized hydrothermally with ethylenediammonium and water molecules hydrogen bonding the chains together into layers of chains (Figure 1-7b).[123] It was also isolated from a non aqueous sec-BuOH solvent, where the chains are arranged hexagonally and triethylammonium exist between the chains.[124] No other aluminophosphate chains nor any fluoroaluminophosphate chains have yet been reported.

1.2.4 Aluminophosphate Molecules and Clusters

The existence of solution bound aluminophosphate molecules has been shown and discussed at length in many reports.[78,79] In one, the existence of a diphosphatoaluminate anionic complex was determined by isolating its TMA salt.[125] The complex was interpreted as having a central octahedral aluminum connected at the axial oxygens to terminal phosphate groups.

As far as crystal structures are concerned, there are only a few examples. One was reported by Kniep *et al.*,[126] and may be considered as a piece of the $Al(H_2PO_4)_3$ aluminophosphate chain mentioned above. The hexameric $[Al_2(H_{1+x}PO_4)_3(H_2O)_6]^{+3x}$ clusters (where x is between 0 and 1) consist of two aluminum octahedra connected by three doubly-bridging phosphates, with isolated $(H_{3-3x}PO_4)$ orthophosphates residing between the clusters (Figure 1-7c).

Crystals of an octameric cubane-like $[Al(PO_4)(EtOH)_4]_4(HCl)_4$ cluster separate out from ethanol at room temperature by the reaction of anhydrous aluminum chloride and phosphoric

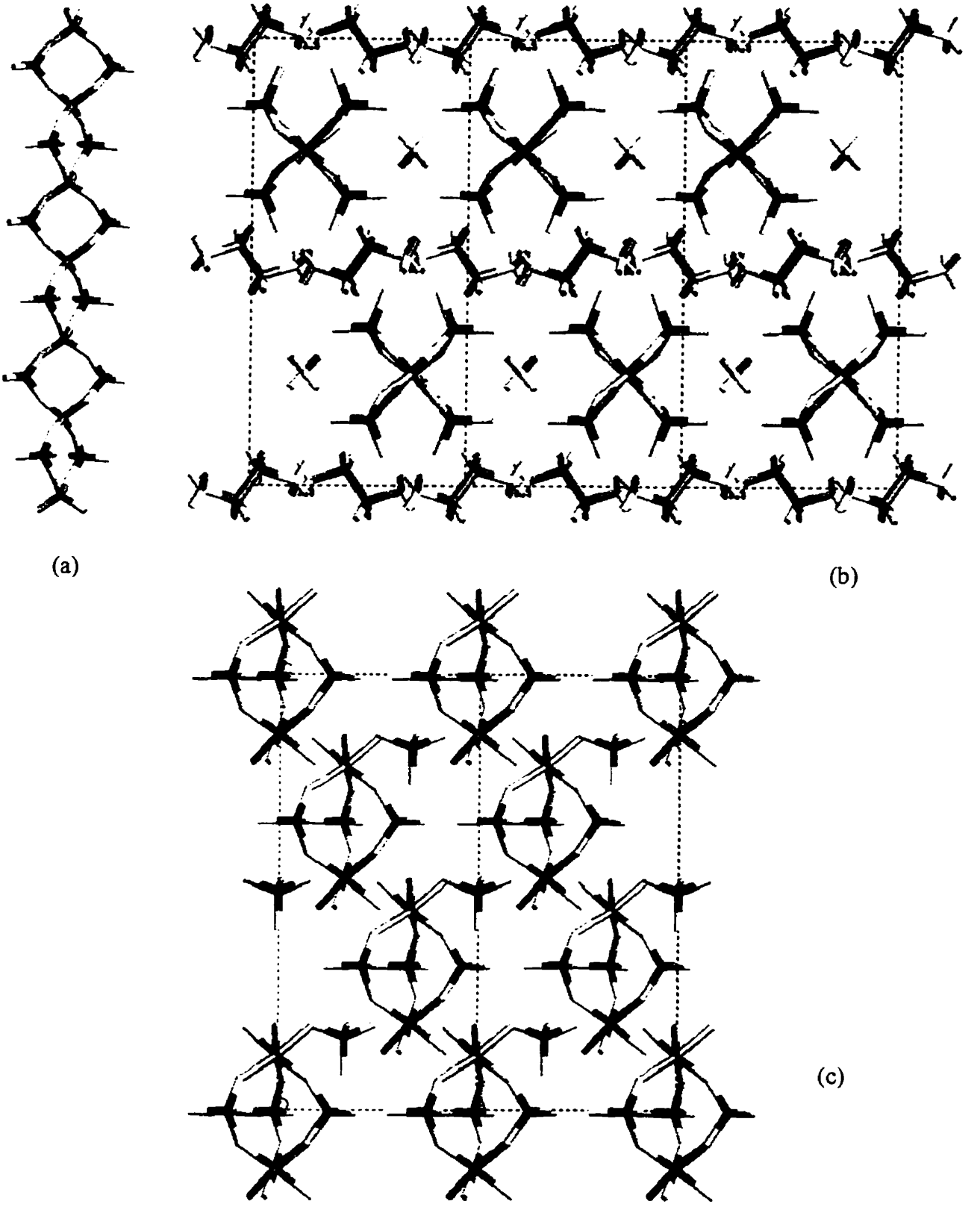

Figure 1-7. (a) $[AlP_2O_8H_2]^-$chain. (b) One of its structures, synthesized hydrothermally. (c) $Al(H_2PO_4)(HPO_4)(H_2O)$ cluster of Kniep *et al.*

acid.[127] Lower temperatures of 0°C or below allowed the formation of larger crystals. The cubes contain four octahedral aluminums and four triply-bridging phosphates, where the eight metal atoms occupy the corners of the cube. Therefore, each aluminum is connected to three phosphates. The aluminums have their coordination spheres completed by ethanol ligands. These terminal ethanols render the complex soluble in water and alcohol solvents. Heating the solid to above 50°C also allows their removal and concomitant cross-linking of the clusters to a glassy aluminophosphate.

Riou *et al.* isolated a pentameric $[AlP_4O_{16}]^{9-}$ cluster that is charge-balanced by four ethylenediammoniums and one ammonium molecule.[128] The clusters contain one tetrahedral aluminum, fully coordinated by four terminal phosphate groups. Interestingly, it was isolated from the same 20 ethylenediamine : 30 H_2O experiment that yielded a fluoroaluminophosphate layer (section 1.2.2).[117] The authors postulate that the cluster may be a precursor phase to the layered fluoroaluminophosphate.

1.3 EXTENDED METAL PHOSPHATES

The last number of years has seen a tremendous growth in the number of known metal phosphate cluster, chain, layered and open framework structures. A variety of transition and main group metals have been successfully employed in this respect. The majority have been prepared hydrothermally using an organic amine template. Following the trend of zeolites and aluminophosphates, non aqueous routes have only in the last several years been exploited and this still remains a largely unexplored area. As for the aluminophosphates, most known structures are frameworks, less are two-dimensional layers, and there are only a limited number of chain structures. The discussion below will be broken down by metal type, beginning with the frameworks for each. Due to the large number of known structure types, the examples that will be given are in many cases only representative.

1.3.1 Vanadium Phosphates and Arsenates

Haushalter and coworkers have summarized the over ten types of known vanadium phosphate frameworks, which contain extraframework s-block metals and/or organic amines.[129] They also prepared a framework where the tetrameric building unit is corner-sharing vanadium(IV) square pyramids that are doubly-bridged by phosphate groups.[129] As for the other frameworks, the restricted size of cavity windows prevent the removal of the organic cations and

the potential application of the material. Interestingly, the 1,3-propanediammonium molecules reside in the "less polar" cavities bordered by vanadyl groups, while the potassiums reside in the "hydrophilic" regions of phosphate groups.

The same group also prepared a layered vanadium(IV) phenylphosphonate, which they based on the as-yet unpublished preparation of vanadium organophosphonate clusters.[130] Intriguingly, the material has the phenyl groups pointing to one side of the layer to define a bilayer, while the vanadyl groups point to the diethylammonium and methylammonium molecules on the other side of the layer, to form alternating interlayer types (Figure 1-8a). This is an interesting observation of the effect of hydrophobic versus hydrophilic interactions. Furthermore, it opens the possibility of the synthesis of other metal phosphonates.

A layered vanadium phosphate hydrate, comprised of layers of connected "double-chains" of $(\mu_2\text{-}PO_4)_3$ vanadium(IV) octahedra, was prepared by directly refluxing V_2O_5 and phosphoric acid.[131] Octahedral vanadium is also observed in several chain structures. In one, V(III) octahedra are linked by three doubly-bridging phosphates (Figure 1-8b).[132] The chains are connected by hydrogen bonds and strontium cations. Two vanadium arsenate chains were also synthesized.[133] One contains V(IV) octahedra connected at the axial oxygens and doubly-bridged by arsenate groups, where the chains are hydrogen bonded into layers and 1,4-diammoniumbutane occupies the interlamellar region. The other contains vanadium(III) arsenate chains templated by ethylenediammonium, and are structurally similar to the vanadium phosphate chains of Figure 1-8b. Very recently, an octameric vanadium fluoroaluminophosphate cluster was reported, containing four V^VO_5F octahedra that are capped by four triply-bridging phosphate tetrahedra.[134] Quinuclidinium and hydronium cations occupy the space between the clusters, and the single fluorine is four-coordinated with respect to vanadium at the centre of the cluster, as observed by ^{19}F MAS NMR.

1.3.2 Iron Phosphates and Arsenates

Iron(III) displays structural similarities to aluminum in its oxide and oxyhydroxide phases. For example, hematite ($\alpha\text{-}Fe_2O_3$) is isostructural to corundum ($\alpha\text{-}Al_2O_3$) and lepidocrocite (γ-FeOOH) is isostructural to boehmite (γ-AlOOH).[135] In fact, for some phases, a solid solution between pure end members may be formed by the isomorphous substitution of Fe^{3+} for Al^{3+}, attributed to their similar ionic radii (0.64Å and 0.53Å, respectively).

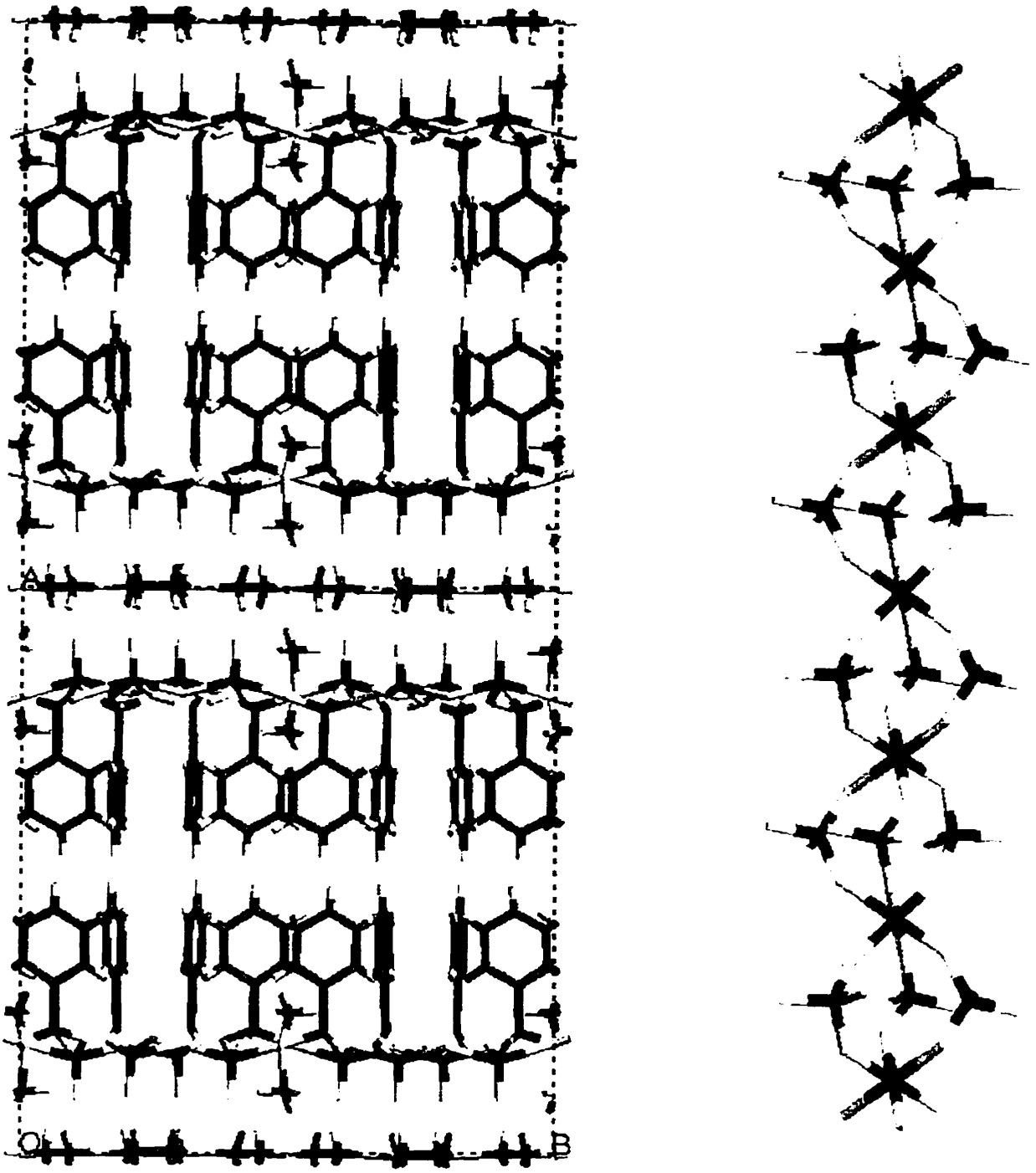

(a) (b)

Figure 1-8. Low-dimensional vanadium phosphates. (a) Layer, with alternating bilayer regions. (b) Chain structure, characteristic of metal phosphates.

The iron aluminophosphate framework cacoxenite occurs naturally. Its highly open $[Al(Al,Fe)_3Fe_{21}O_6(OH)_{12}(PO_4)_{17}(H_2O)_{24}]$ structure[22] contains a 14.2Å free diameter channel system containing mostly water and in fact represents the largest pore of any crystalline framework. To the author's knowledge, this mineral has not been synthesized to date, and is an indication of the limitations of molecular sieve science. It will be interesting to see if materials chemists can meet the challenge of synthesizing this interesting material in the future. However, one should note that it is not stable to dehydration, which limits its potential for future applications.

There are only a limited number of synthesized extended iron phosphates. Hydrothermal syntheses with TPAOH and TBAOH did not lead to open frameworks containing the organic ammoniums. Instead, small-pore frameworks were obtained that were the pure iron phosphate analogues of the minerals hureaulite and alluaudite.[136] Only one layered structure has been reported, a mixed-valence fluorinated iron phosphate containing monoprotonated ethylenediamine.[137] The iron phosphate chain structure isostructural to that of Figure 1-8b was obtained, also containing strontium cations.[132] Similarly, an iron arsenate chain was obtained that is isostructural to the chain of Figure 1-8b, but hydrogen bonded to water molecules that exist between the chains.[138]

1.3.3 Zinc Phosphates

The zinc phosphate structures are unique to the other metal phosphates discussed in this chapter since zinc exists as the divalent cation. Nonetheless, they display some isostructurality to other metal phosphates, where the lower positive charge of the metal atom imposes a negative charge on the inorganic skeleton, therefore requiring additional charge-balancing cations. For example, Gier *et al.* achieved the low-temperature (70°C) synthesis of several zincophosphate and arsenate frameworks that are zeolite analogues.[139] One of them was sodalite, which is also the structure of $AlPO_4$-20. However, the zinc phosphate framework is anionic and charge-balanced by sodium cations. Two novel zincophosphate framework topologies were very recently reported. One is chiral and contains sodium cations,[140] while the second possesses irregular 18-membered rings and guanidinium (CN_3H_6) template molecules.[43] A small-pore framework was also synthesized organothermally using an ethylene glycol solvent and ethylenediamine template.[141]

Harrison *et al.* synthesized a zinc phosphate chain structure also at mild temperatures of 70°C.[142] The chain is built of vertex-sharing zinc tetrahedra, each bridged by one doubly-bridging phosphate groups (Figure 1-9a). Similar methods led to another chain structure[143] that is isostructural to the aluminophosphate chain of Figure 1-7a, but the terminal oxygens of the phosphates are instead connected to ethyl groups (Figure 1-9b). The chains are therefore neutral and the ethyl groups of neighbouring chains interact by van der Waals forces to from a herringbone arrangement down the b-axis (Figure 1-9c). Only weak hydrophobic interactions exist between the chains, which render them soluble and recrystallizable from several polar and nonpolar solvents. NMR data suggests that it retains an oligomeric state in solution, with approximately 12 repeat units.

The same group reported two $[H(ZnPO_4)_2]^-$ layered materials prepared at 70°C, one containing sodium cations and the other cesium cations between the layers.[144] They also used a freezer held at temperatures of 4°C, to synthesize an anionic layered zinc phosphate, $[Zn(HPO_4)_2]^{2-}$, containing sodium cations.[145] They attribute the large crystal sizes (> 0.5mm) and the low experimental temperatures for all of the zinc phosphates to the greater solubility of the precursors as compared to aluminosilicates and aluminophosphates.

1.3.4 Gallium Phosphates

Gallium is directly below aluminum in group 13, and not surprisingly gallium phosphate also forms dense phases isostructural to quartz and cristobalite with similar thermal transitions.[146] Similarly, a gallium phosphate hydrate framework[146] was discovered in the 1960's that is isostructural to $AlPO_4$-tinsleyite.[30] Parise also synthesized the $GaPO_4$-12(en)[147] and $GaPO_4$-21[148] analogues of the corresponding $AlPO_4$-n structures.

However, it was not until the discovery of the large-pore framework cloverite, in 1991 by Kessler and coworkers,[149] that the synthesis of novel gallium phosphate frameworks was stimulated. They used the hydrothermal fluoride method also used for aluminophosphates (section 1.1.3.4).[52] Since then, several fluorinated gallium phosphate frameworks have been reported by Férey and coworkers.[150-153] Attfield *et al.* isolated a gallium phosphate framework hydrothermally, built of GaO_6 octahedra, GaO_5 trigonal bipyramids and PO_4 tetrahedra, with sodium cations and water molecules in the channels.[154] Chippindale *et al.* synthesized a novel cobalt-substituted gallium phosphate framework from a non aqueous butan-1-ol solvent,[155] as well as another, from an ethylene glycol solvent, that is isostructural with the zeolite

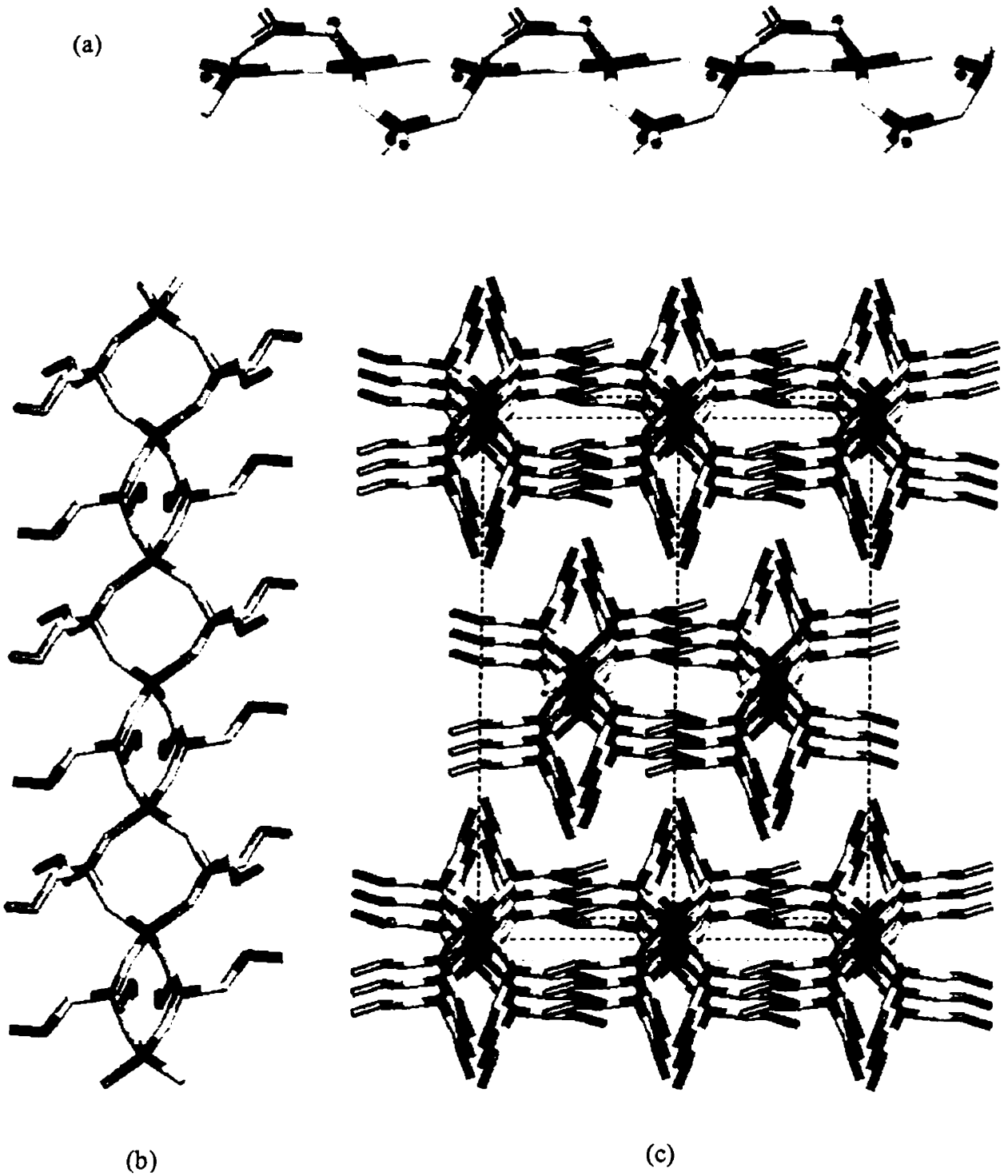

Figure 1-9. One-dimensional zinc phosphate chain structures. (a) $Na_2ZnPO_4OH \cdot 7H_2O$. (b) ZnPOEt. (c) b-projection of ZnPOEt, showing the interchain herringbone arrangement of terminal ethoxy groups.

gismondite.[156] Despite the structural diversity displayed by the gallium phosphate frameworks, there is a noticeable absence of any layered or chain structures amongst this class of compounds. Perhaps they await discovery.

1.3.5 Zirconium Phosphates and Phosphonates

As far as the direct synthesis of structural types is concerned, the zirconium phosphates are very limited. $Zr(HPO_4)\bullet nH_2O$ may be synthesized hydrothermally or by simply refluxing a zirconium phosphate gel in strong phosphoric acid.[157] In the crystals so obtained, n is variable and leads to several forms, such as α-ZrP, γ-ZrP, η-ZrP and many others. However, the interest in "ZrP" lies in the rich amount of intercalation chemistry which it displays. Even though this is a well-established area, interest in them does not appear to be fading.[158] Aside from the zirconium phosphates and arsenates and intercalated derivatives, there exists an entire family of related tetravalent acid salts [$M^{IV}(HXO_4)_2\bullet nH_2O$, where M^{IV} = tetravalent metal (e.g.: Groups 4, 5 and 14 except for carbon, Ce, U), X = P, As]. For these, intercalation also leads to a wide range of metal phosphates and phosphonates. All of the above collectively represent a huge area of study and are discussed at length in several books and reviews.[10,157,159]

1.3.6 Molybdenum Phosphates

Several layered and a large number of three-dimensional molybendum phosphates were reported, primarily in the 1980's, and are summarized in an excellent review by Haushalter and Mundi.[160] They can be synthesized by high temperature routes or hydrothermally. The former is carried out by simply heating a molybdenum oxide source with P_2O_5 or a metal phosphate and molybdenum metal to temperatures of 750°C or higher. These extreme conditions and absence of water, not surprisingly (section 1.4), lead in some cases to the coexistence of condensed, dimeric P_2O_7 groups in the final structure and Mo:P ratios of less than unity. The charge balancing cations are usually alkali metals or alkaline earth metals. Hydrothermal methods form structures with no such P_2O_7 groups and Mo:P ratios greater than unity. The cation in this case can be a metal cation or an organic amine template. Examples of the latter are TPA, diethylammonium and 4-phenylpyridinium for layers, and TMA, methylammonium and ammonium for frameworks.[160]

To date, only a few molybdenum phosphate chain structures have been published. The first was published in 1958,[161] and is a "double chain" of Mo(VI) octahedra and PO_4 tetrahedra defining an infinite connectivity of edge-sharing four-rings (Figure 1-10a). The neutral $Mo(OH)_3PO_4$ chains are connected by hydrogen bonds. The crystals were prepared by allowing a viscous solution of molybdenum oxide in concentrated phosphoric acid to evaporate, not unlike the method used for aluminophosphate aggregation polymers.

More recently, Haushalter and Lai hydrothermally synthesized orange crystals of two unidimensional structures comprised of Mo(V) octahedra, with one terminal molybdenyl oxygen on each octahedron, and doubly- and triply-bridging phosphate groups.[162,163] As for the layers and frameworks, hydrothermal methods preferentially formed Keggin type and larger heteropolymolybdate clusters if Mo was in an oxidation state of +6.[160] Synthesis of a higher dimensionality structure only occurred if the Na_2MoO_4 reagent was reduced by adding molybdenum metal to the synthesis mixture. The Mo(V) then allowed the formation of an extended structure.

Still, the tendency of molybdenum phosphates to form clusters is reflected in the final chain structures, which consist of one-dimensionally linked clusters. In one, there are $[Mo_6P_4O_{24}(OH)_7]^{5-}$ clusters with the six molybenums arranged approximately in a plane, and Mo-Mo bonds between alternating pairs of molybdenums.[162] The clusters are in turn sodium-bridged, which they term a sodium molybdenum phosphate polymer. A purely molybdenum phosphate chain was synthesized with charge-balancing tetraethylammonium cations.[163] The chain contains Mo_4O_4 cubane-like clusters that are both capped and connected by phosphate groups (Figure 1-10b). Interestingly, the doubly-bridging phosphate on the sides of the clusters hydrogen bond the chains into layers of chains (Figure 1-10c).

1.3.7 Indium Phosphates

The indium phosphates are much less developed. Despite the fact that indium is in group 13 and would be expected to show a structural diversity at least partially comparable to that of aluminum and gallium, only a handful of structures have been discovered to date. The first structure of any dimensionality was reported in 1993, and is a framework comprised of indium octahedra which are fully connected to six triply-bridging monohydrogen phosphates.[164] The anionic framework is charge-balanced by ethylenediammonium molecules. Only two other frameworks have been described.[165,166] It was not until very recently that a layered indium

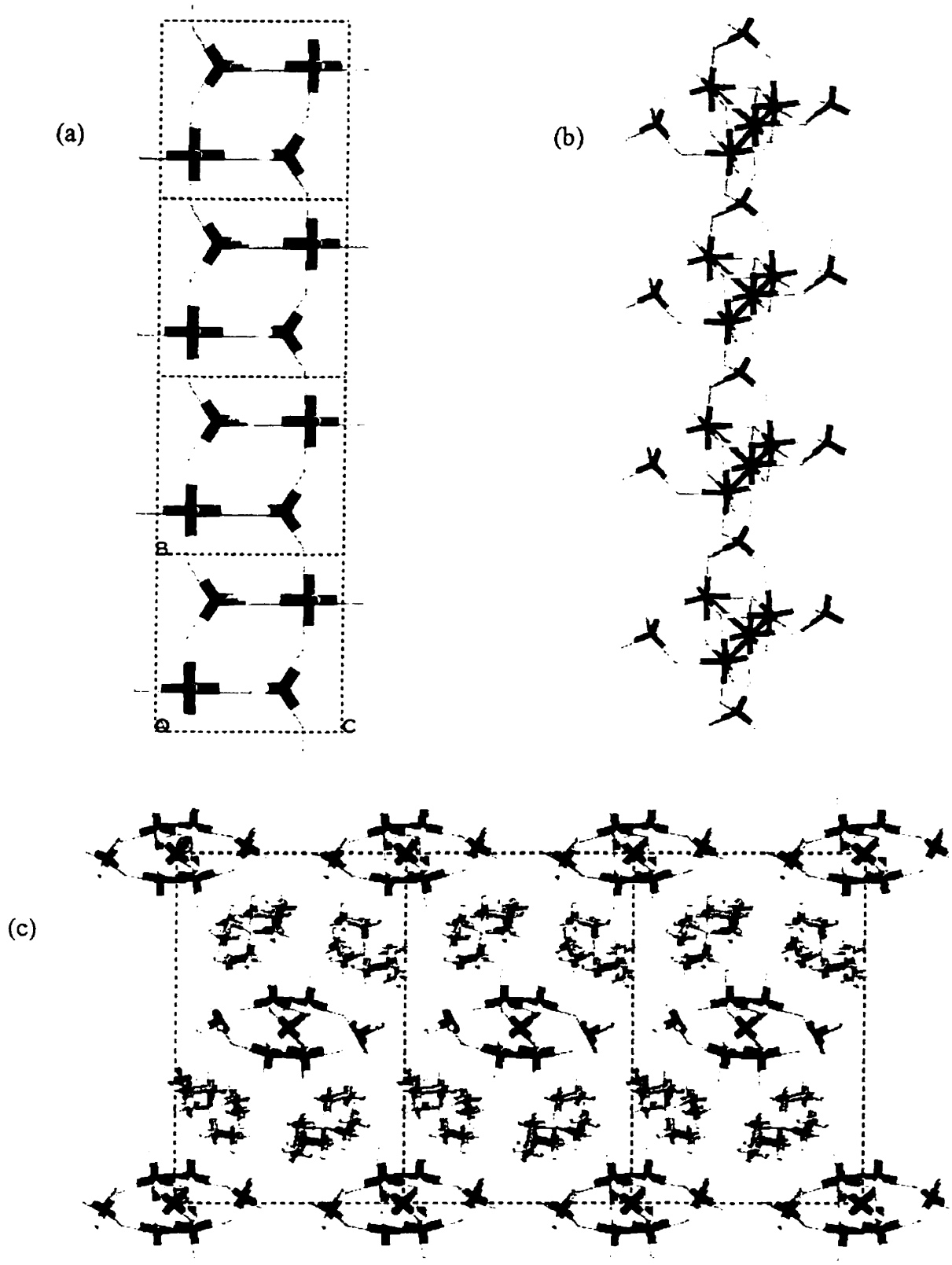

Figure 1-10. Molybdenum phosphate chain structures. (a) $Mo(OH)_3PO_4$. (b) $(Et_4N)_2[Mo_4O_8(PO_4)_2(H_{1.5}PO_4)_2]\cdot 2H_2O$. (c) c-projection of the latter. The chains are hydrogen bonded into layers.

phosphate was reported, synthesized from a butan-2-ol solvent using a pyridine organic amine template.[167] In this case, the indium octahedra are again connected to six phosphates, but there exists two doubly- and three triply-bridging phosphate groups. Notably, the sixth type of phosphate is singly-bridging and accepts as well as donates an interlayer hydrogen bond to another such phosphate group on the adjacent layer.

1.4 CONDENSED PHOSPHATES

Orthophosphoric acid is the name traditionally given to monomeric trihydrogen phosphate. Its most common form is as a concentrated acid solution in which varying degrees of hydrogen bonding occurs, depending on concentration. Two crystalline forms of orthophosphoric acid have been shown to exist.[168] Phosphates also exhibit heterocatenation,[169] where the tetrahedra undergo condensation polymerization to form various oligomeric species by sharing oxygen atoms. These are collectively termed the condensed phosphates and are classified into three groups, namely the chain polyphosphates, cyclic metaphosphates and branched ultraphosphates. They were initially discovered by Graham in the 1830's when he made a material still known as "Graham's salt". However, this material turned out to actually be a randomnly polymerized glass formed by quenching a sodium phosphate melt.[170]

The simplest example of a condensed phosphate is pyrophosphoric acid, the dimeric species. The linear trimer is also known and one example, sodium tripolyphosphate, was in fact extensively used as a detergent builder until its pollutant effects on rivers and lakes became well known.[10] It was not until the 1950's that chromatography allowed the characterization of the higher condensed phosphates. Since then, the chain polyphosphates have been isolated and characterized for n = 4 to 10.[171] Longer "macromolecular" polyphosphates exist for n > 10 to several thousand.[170] There are a large number of infinitely extended polyphosphate salts, to give overall stoichiometry $[M^{x+}(PO_3)_x]_n$. Various cations may be used, and for many, one or more polymorphs exist since the chain may take on different configurations.[10,170]

The metaphosphates are cyclic phosphates, and as expected, there are less examples of them. Since there are no end-groups, the formula is invariantly $(PO_3)^-$, as for the macromolecular polyphosphates. For this reason, the latter has been mistakenly labeled as a metaphosphate, particularly before chromatographic methods were in use. The smallest and yet most common ring is trimetaphosphate, most commonly known as its sodium or aluminum salt. Evidence has

been shown for an aluminum compound of tetrametaphosphate,[12] while the larger penta-, hexa-, octa-, deca- and dodecametaphosphate cyclic phosphates have all been isolated.[10,170]

Less studied due to their instability are the branched ultraphosphates, which generally have a $M_2O:P_2O_5$ ratio less than unity due to the branching phosphate groups. They are commonly referred to as having a branched chain structure,[172] but some structures have been suggested, such as an isobutyl-like arrangement.[10] The ultraphosphates are unstable in solution, since the branching points are attacked by hydrolysis, thereby forming smaller polyphosphates and orthophosphates. This is due to the reduced negative charge of the oxygens at a branching $PO_{2.5}$ site over that of the negative PO_3^- groups of the chain, rendering the former highly susceptible to removal by hydrolysis. This is known as the antibranching rule of condensed phosphates.[170] For the same reason, phosphorus pentoxide, which possesses the tetrameric P_4O_{10} cage structure, is vigorously attacked by water.

In contrast to the silicate anions in solution, which at room temperature polymerize to silica or hydrolyze to orthosilicate depending on whether the pH is low or high, respectively, the condensed phosphates are relatively stable in solution, and only slowly hydrolyze to the monomer.[120] The only significant degree of polymerization occurs under strongly acidic conditions, when the monomer forms a small mole percent of pyrophosphoric acid.[170]

1.5 ALKYLAMMONIUM PHOSPHATE SALTS

Despite the fact that large crystals of this type of compound may be easily recrystallized from a number of solvents and that the phosphate can exist in any of its three protonated forms, only seven crystal structures have been reported to date. The majority contain an alkylenediammonium cation. Some also exist as the polyhydrate, which gives additional structural diversity to this type of compound. There also exist alkylammonium phosphates with, for example, sodium coexisting in the structure[173] or containing instead an alkylamine derivative as cation, such as an amino acid.[174] However, the discussion here will be limited to alkylammonium phosphates.

Ethylenediammonium monohydrogen phosphate was reported independently by two groups.[175,176] The unit cell axes were defined differently for each report but the overall structure is the same. The structure consists of discrete monohydrogen phosphate molecules arranged approximately in layers, in which they are hydrogen bonded into chains (Figure 1-11a). These layers are separated by monolayers of ethylenediammonium (Figure 1-11b). As in all of the

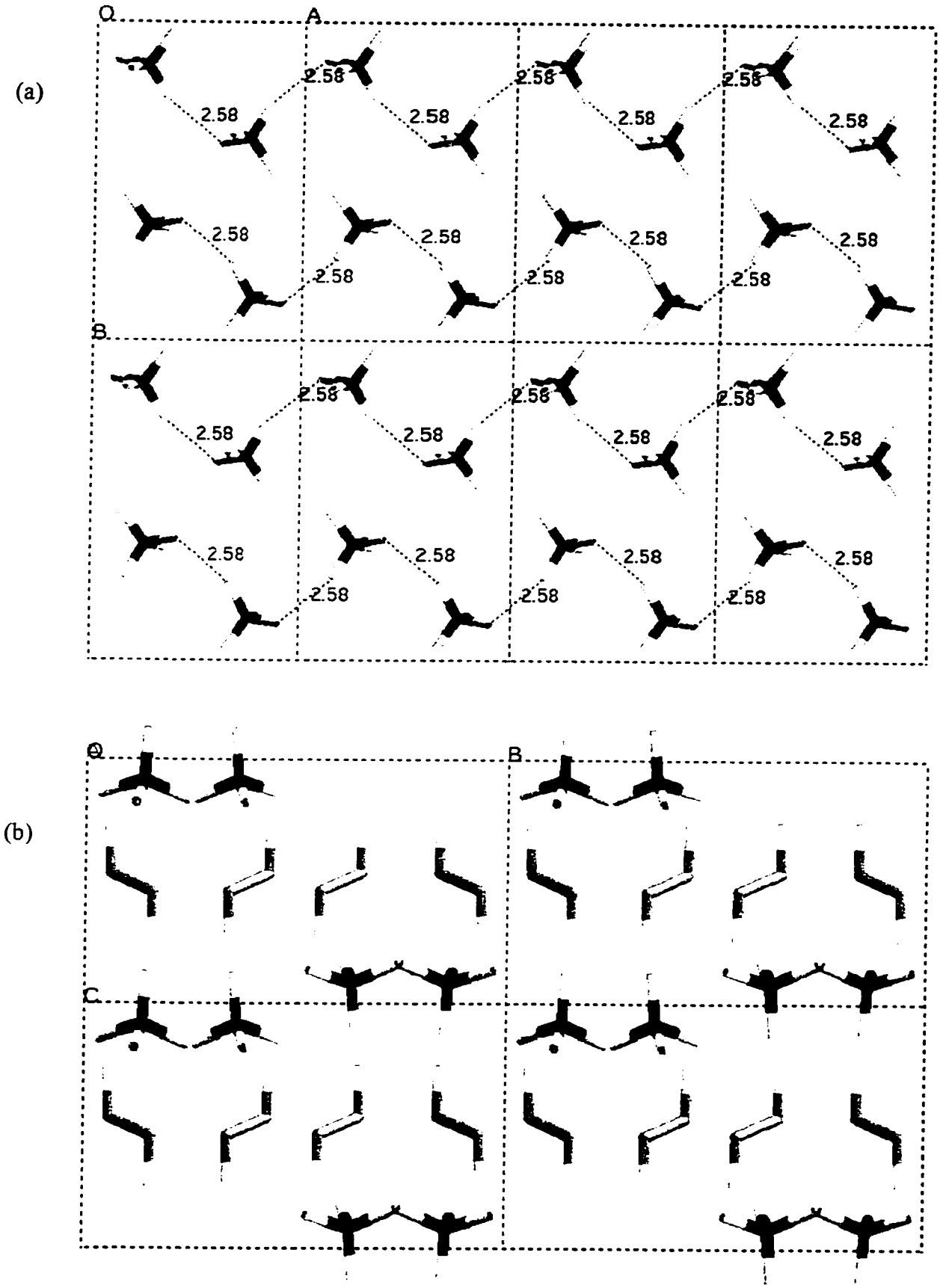

Figure 1-11. Ethylenediammonium monohydrogen phosphate. (a) c-projection of one phosphate layer, showing hydrogen bonding. (b) a-projection.

other alkylammonium phosphate structures, every N-H bond donates a hydrogen bond to an oxygen of a phosphate, creating a three-dimensional network of hydrogen bonding. The isostructural ethylenediammonium monohydrogen arsenate was also reported.[176]

The dihydrogen phosphate salt of ethylenediammonium has been reported,[177] also comprised of phosphate layers separated by monolayers of ethylenediammonium. However, in this case, the phosphates each donate and accept two hydrogen bonds (Figure 1-12a). The layout of the hydrogen bonds may be thought of as chains extending along the a-axis, connected to the next chain by doubly hydrogen bonded phosphates, to define a continuous layer in the **ab** plane. One such layer is seen in the b-projection (Figure 1-12b), although, in this case, the organic molecules are not perpendicular to the phosphate layer. For all dihydrogen phosphate salts, there is an expectedly larger amount of intralayer hydrogen bonding due to the additional proton on each phosphate group.

A hydrogen bonded layered configuration is not observed for the dihydrogen phosphate pentahydrogen bisphosphate structure,[178] which contains two types of dihydrogen phosphates and one trihydrogen phosphate. Instead, the phosphates define a hydrogen bonded three-dimensional framework, with the ethylenediammoniums occupying the voids. The coexistence of trihydrogen phosphate is likely due to the lower pH of the solution from which the crystals were grown, prepared by directly mixing 10 ml of ethylenediamine with 40 ml of 85 wt.% phosphoric acid.[178]

1,3-propanediammonium monohydrogen phosphate monohydrate[179] contains phosphate chains with only one hydrogen bond between two adjacent phosphates. Unlike the ethylenediammonium structures, the chains are isolated and not arranged in layers. Nonetheless, they do interact with the cations to build a three-dimensional network. The 1,3-propanediammonium dihydrogen phosphate salt[180] contains chains of phosphates that are doubly hydrogen bonded, due to the presence of two hydrogens on each. The chains are arranged in layers, similar to that shown in Figure 1-11a. The longest alkylenediamine used to date is 1,4-diaminobutane, also known as putrescine due to its rancid odour. The phosphate salt has been reported in its dihydrogen phosphate form.[181] The dihydrogen phosphates are arranged in a novel, uninterrupted two-dimensional layer of hydrogen bonds, with an average interlayer distance of *ca.* 8.1Å.[182]

Aakeröy *et al.* have synthesized a number of dihydrogen phosphate salts containing cyclic amines.[183] They obtained the crystal structures of only the piperidinium and benzylammonium salts by recrystallization from methanol and aqueous solution, respectively.

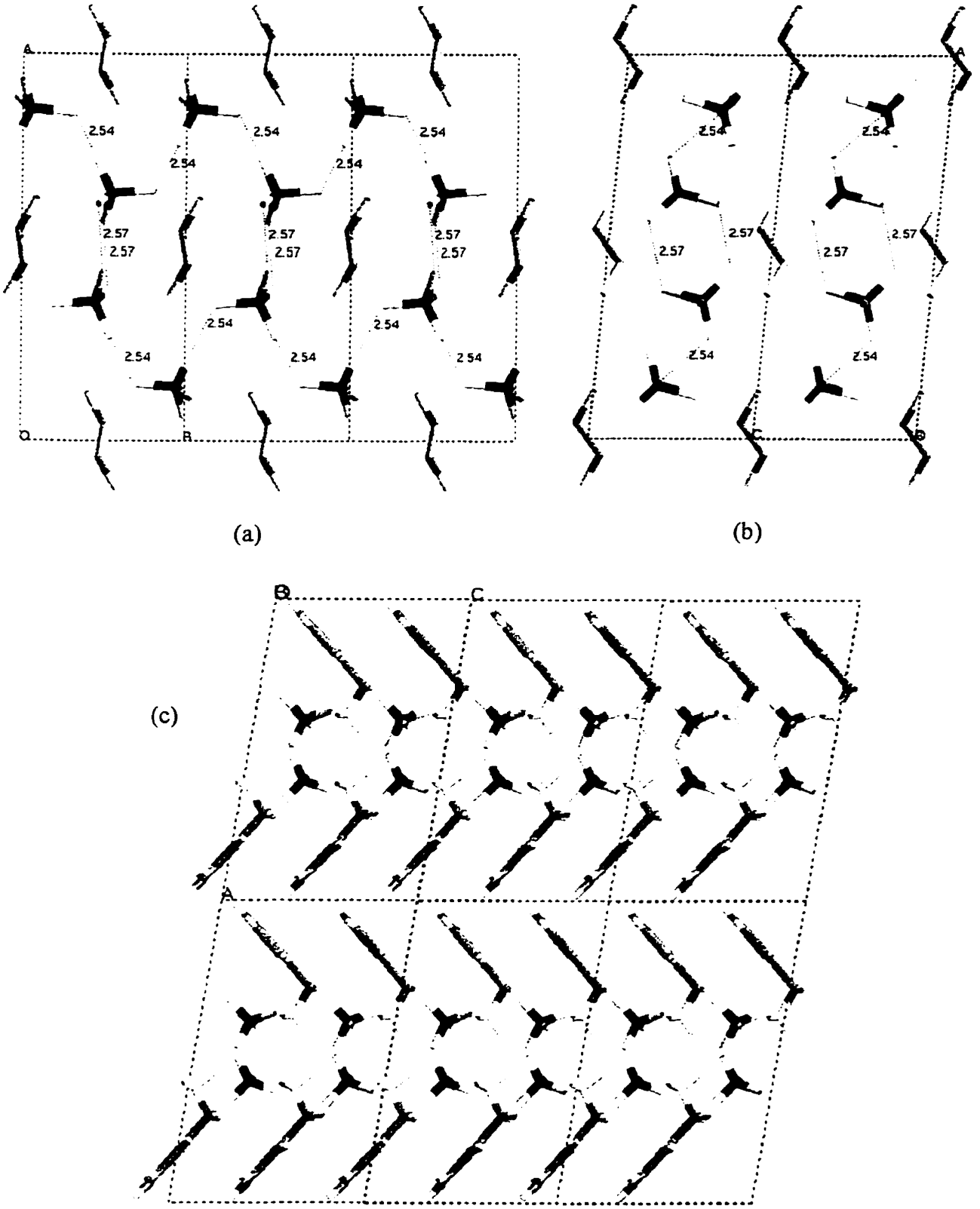

Figure 1-12. (a) c-projection of ethylenediammonium dihydrogen phosphate. (b) b-projection, showing an edge-on view of the phosphate layers. (c) The herringbone packing arrangement of the phenyl rings of benzylammonium dihydrogen phosphate.

The former contains doubly hydrogen bonded chains of phosphate arranged into layers, where the secondary piperidiniums interact with two adjacent phosphate layers, thereby cross linking them *via* two hydrogen bonds. The benzylammonium structure contains a complex two-dimensional array of hydrogen bonds between neighbouring phosphates and the methylammonium groups that extend off the phenyl rings and into the phosphate layers. The phenyl rings of the benzylammoniums define an interesting herring-bone packing arrangement (Figure 1-12c). This group also claims to have prepared 24 salts of various primary, secondary and tertiary amines. This indicates that many more alkylammonium phosphate crystal structures still await discovery.

Riou *et al.* reported the piperazinium monohydrogen phosphate monohydrate crystal structure.[184] Its consists of a three-dimensional network of hydrogen bonds between piperaziniums and, notably, isolated phosphates. No hydrogen bonding exists between phosphate groups. Even more interesting is that they synthesized the crystals in a hydrothermal fluoroaluminophosphate experiment containing piperazine.

The alkylammonium phosphate salts form readily in most solvents. Correspondingly, they would be expected to form in the reaction gels of aluminophosphate experiments, and even ascoprecipitates in the products. Only Bibby and coworkers discussed a dipropylamine-related phosphate salt that forms initially in the reaction mixture, as evidenced by powder X-ray diffraction.[185] They postulate that it is the dihydrogen phosphate salt, but did not determine the structure. No further mention of alkylammonium phosphate salts has been made in the aluminophosphate literature and by and large they have been ignored by those working in the area. Additionally, no characterization has been performed to date for any of the alkylammonium phosphate salts.

1.6 THESIS OUTLINE

A large volume of synthetic work was collected and organized using small molecule templates and a predominantly non aqueous solvent. After a description of the experimental methods, the results will be broken down into sections by template in Chapter 2. Chapter 2 will present only the experimental results; discussion of these results will be presented at the end of Chapter 4. The characterization of the related solid aluminophosphates and phosphates will be described in Chapter 3. In Chapter 4, the mode of formation of aluminophosphates will be described, and a new model will be presented involving an interconverting chain

aluminophosphate precursor. A series of examples of the construction of known chain, layer and framework structures will be illustrated. This will be followed by a discussion of some of the more important aspects of the numerous synthesis parameters that are responsible for the observed results. Chapter 5 will encompass the work involving amphiphilic primary n-alkylamines and alkylenediamines. The characterization of the aluminophosphate and phosphate materials so obtained will first be shown, followed by a proposed mode of formation for the mesolamellar phases and their macroscopic surface patterning. Finally, Chapter 6 will suggest just some of the possibilities for future work.

1.7 REFERENCES

1. R. M. Barrer, *Zeolites and Clay Minerals as Sorbents and Molecular Sieves*; Academic Press, Inc.: New York, 1978, ch. 1.
2. J. M. Newsam, *Science* **1986**, *231*, 1093.
3. L. B. Sand, F. A. Mumpton (eds.), *Natural Zeolites: Occurrence, Properties, Use*; Pargamon Press: New York, 1978.
4. R. Szostak, *Molecular Sieves: Principles of Synthesis and Identification*; Van Nostrand Reinhold: Toronto, 1989.
5. J. O. Nriagu, P. B. Moore (eds.), *Phosphate Minerals*; Springer-Verlag: New York, 1984.
6. W. S. Wise, S. E. Loh, *American Mineralogist* **1976**, *61*, 409, and references therein.
7. R. Kniep, D. Mootz, A. Vegas, *Acta Cryst.* **1977**, *B33*, 263.
8. R. Kniep, D. Mootz, *Acta Cryst.* **1973**, *B29*, 2292.
9. O. Cambon, A. Goiffon, E. Philippot, *J. Mat. Sci.* **1991**, *26*, 846.
10. T. Kanazawa (ed.), *Inorganic Phosphate Materials, Materials Science Monographs*, **52**, Elsevier Science: New York, 1989.
11. Mineral Facts and Problems No. 9, *Monograph on Rock Phosphate*; Indian Bureau of Mines: Nagpur, 1988.
12. J. H. Morris, P. G. Perkins, A. E. A. Rose, W. E. Smith, *Chem. Soc. Rev.* **1977**, *6*, 173.
13. J. R. Van Wazer, *Phosphorus and Its Compounds: Vol. I*; Interscience: New York, 1958; pp. 550-559.
14. S. T. Wilson, B. M. Lok, C. A. Messina, T. R. Cannan, E. M. Flanigen, in *Intrazeolite Chemistry*, G. D. Stucky, F. G. Dwyer (eds.); ACS Symp. Ser. 218, American Chemical Society: Washington, D. C., 1983, pp. 79.

15. L. Pauling, J. Sherman, *Z. Kristallogr.* **1937**, *96*, 481.

16. H. van der Meer, *Acta Cryst.* **1976**, *B32*, 2423.

17. F. D'Yvoire, *Bull. Soc. Chim. Fr.* **1961**, 1762.

18. R. Kniep, *Angew. Chem., Int. Ed. Engl.* **1986**, *25*, 525.

19. D. Brodalla, R. Kniep, D. Mootz, *Z. Naturforsch.* **1981**, *36B*, 907.

20. S. T. Wilson, B. M. Lok, C. A. Messina, T. R. Cannan, E. M. Flanigen, *J. Am. Chem. Soc.* **1982**, *104*, 1146.

21. S. T. Wilson, B. M. Lok, E. M. Flanigen, U. S. Patent 4 310 440.

22. R. Szostak, *Handbook of Molecular Sieves*; Van Nostrand Reinhold: New York, 1992.

23. S. I. Zones, M. E. Davis, *Current Opinion in Solid State & Mater. Sci.* **1996**, *1*, 107.

24. J. J. Pluth, J. V. Smith, *Nature* **1985**, *318*, 165.

25. J. J. Pluth, J. V. Smith, J. M. Bennett, *Acta Cryst.* **1986**, *C42*, 283.

26. J. M. Bennett, R. M. Kirchner, *Zeolites* **1992**, *12*, 338.

27. P. R. Rudolf, C. Saldarriaga-Molina, A. Clearfield, *J. Phys. Chem.* **1986**, *90*, 6122.

28. J. J. Pluth, J. V. Smith, *Acta Cryst.* **1987**, *C43*, 866.

29. J. M. Bennett, J. P. Cohen, G. Artioli, J. J. Pluth, J. V. Smith, *Inorg. Chem.* **1985**, *24*, 188.

30. J. B. Parise, *Acta Cryst.* **1984**, *C40*, 1641.

31. J. J. Pluth, J. V. Smith, J. M. Bennett, J. P. Cohen, *Acta Cryst.* **1984**, *C40*, 2008.

32. (a) M. E. Davis, C. Saldarriaga, C. Montes, J. Garces, C. Crowder, *Nature* **1988**, *331*, 698. (b) M. E. Davis, C. Saldarriaga, C. Montes, J. Garces, C. Crowder, *Zeolites* **1988**, *8*, 362. (c) M. E. Davis, C. Montes, J. M. Garces, *ACS Symp. Ser.* **1989**, *398*, 291.

33. D. E. Akporiaye, H. Fjellvag, E. N. Halvorsen, J. Hustveit, A. Karlsson, K. P. Lillerud, *J. Chem. Soc., Chem. Commun.* **1996**, 601.

34. S. Natarajan, J. P. Gabriel, A. K. Cheetham, *J. Chem. Soc., Chem. Commun.* **1996**, 1415.

35. P. A. Barrett, R. H. Jones, J. M. Thomas, G. Sankar, I. J. Shannon, C. R. A. Catlow, *J. Chem. Soc., Chem. Commun.* **1996**, 2001.

36. D. M. Bibby, M. P. Dale, *Nature* **1985**, *317*, 157.

37. W. A. van Erp, H. W. Kouwenhoven, J. M. Nanne, *Zeolites* **1987**, *7*, 286.

38. Q. Huo, S. Feng, R. Xu, *J. Chem. Soc., Chem. Commun.* **1988**, 1486.

39. C. Liu, S. Li, K. Tu, R. Xu, *J. Chem. Soc., Chem. Commun.* **1993**, 1645.

40. Q. Huo, R. Xu, *J. Chem. Soc., Chem. Commun.* **1990**, 783.

41. Q. Gao, S. Li, R. Xu, *J. Chem. Soc., Chem. Commun.* **1994**, 1465.

42. (a) Q. Huo, R. Xu, S. Li, Z. Ma, J. M. Thomas, R. H. Jones, A. M. Chippindale, *J. Chem. Soc., Chem. Commun.* **1992**, 875. (b) R. H. Jones, J. M. Thomas, J. Chen, R. Xu, Q. Huo, S. Li, Z. Ma, A. M. Chippindale, *J. Solid State Chem.* **1993**, *102*, 204.

43. W. W. T. A. Harrison, M. L. F. Phillips, *J. Chem. Soc., Chem. Commun.* **1996**, 2771.

44. A. M. Chippindale, A. V. Powell, R. H. Jones, J. M. Thomas, A. K. Cheetham, Q. Huo, R. Xu, *Acta Cryst.* **1994**, *C50*, 1537.

45. R. Xu, Q. Huo, W. Pang, in *Proceedings of the Ninth International Zeolite Conference*, Vol. I, eds. R. von Ballmoos *et al.*, Butterworth-Heinemann, London, 1993, p. 271.

46. E. M. Flanigen, R. L. Patton, S. T. Wilson, *Stud. Surf. Sci. Catal.* **1988**, *37*, 13.

47. R. M. Kirchener, J. M. Bennett, *Zeolites* **1994**, *14*, 523.

48. M. H. Zahedi-Niaki, P. N. Joshi, S. Kaliaguine, *J. Chem. Soc., Chem. Commun.* **1996**, 1373.

49. P. A. Wright, R. H. Jones, S. Natarajan, R. G. Bell, J. Chen, M. B. Hursthouse, J. M. Thomas, *J. Chem. Soc., Chem. Commun.* **1993**, 633.

50. M. Helliwell, B. Gallois, B. M. Kariuki, V. Kaucic, J. R. Helliwell, *Acta Cryst.* **1993**, *B49*, 420.

51. L. M. Meyer, R. C. Haushalter, *Chem. Mater.* **1994**, *6*, 349.

52. J. L. Guth, H. Kessler, R. Wey, *Stud. Surf. Sci. Catal.* **1986**, *28*, 121.

53. S. Qiu, W. Pang, H. Kessler, J. L. Guth, *Zeolites* **1989**, *9*, 440.

54. L. Delmotte, M. Soulard, F. Guth, A. Seive, A. Lopez, J. L. Guth, *Zeolites* **1990**, *10*, 778.

55. E. Klock, L. Delmotte, M. Soulard, J. L. Guth, in *Proceedings of the 9th International Zeolite Conference*, R. von Ballmoos *et al.* (eds.); Butterworth-Heinemann: London, 1993, pp. 611.

56. L. Sierra, J. Patarin, C. Deroche, H. Gies, J. L. Guth, *Stud. Surf. Sci. Catal.* **1994**, *84*, 2237.

57. J. L. Guth, H. Kessler, P. Caullet, J. Hazm, A. Merrouche, J. Patarin, in *Proceedings of the 9th International Zeolite Conference*, R. von Ballmoos *et al.* (eds.); Butterworth-Heinemann: London, 1993, pp. 215.

58. L. Yu, W. Pang, L. Li, *J. Solid State Chem.* **1990**, *87*, 241.

59. G. Férey, T. Loiseau, P. Lacorre, F. Taulelle, *J. Solid State Chem.* **1993**, *105*, 179.

60. G. Férey, T. Loiseau, P. Lacorre, F. Taulelle, *J. Solid State Chem.* **1993**, *105*, 191.

61. S. J. Kirkby, A. J. Lough, G. A. Ozin, *Z. Kristollogr.* **1995**, *210*, 956.

62. J. L. Paillaud, B. Marler, H. Kessler, *J. Chem. Soc., Chem. Commun.* **1996**, 1293.

63. B. M. Lok, T. R. Cannan, C. A. Messina, *Zeolites* **1983**, *3*, 283.

64. B. Duncan, M. Stöcker, D. Gwinup, R. Szostak, K. Vinje, *Bull. Soc. Chim. Fr.* **1992**, *129*, 98.

65. M. E. Davis, R. F. Lobo, *Chem. Mater.* **1992**, *4*, 756.

66. E. M. Flanigen, *Adv. Chem. Ser.* **1973**, *121*, 119.

67. X. Ren, S. Komarneni, D. M. Roy, *Zeolites* **1991**, *11*, 142.

68. D. W. Lewis, C. R. A. Catlow, J. M. Thomas, *Chem. Mater.* **1996**, *8*, 1112.

69. D. W. Lewis, D. J. Willock, C. R. A. Catlow, J. M. Thomas, G. J. Hutchings, *Nature* **1996**, *382*, 604.

70. Y. Hu, A. Navrotsky, C. Chen, M. E. Davis, *Chem. Mater.* **1995**, *7*, 1816.

71. R. F. Mortlock, A. T. Bell, C. J. Radke, *J. Phys. Chem.* **1991**, *95*, 372.

72. R. F. Mortlock, A. T. Bell, C. J. Radke, *J. Phys. Chem.* **1991**, *95*, 7847.

73. W. E. E. Stone, G. M. S. El Shafei, J. Sanz, S. A. Selim, *J. Phys. Chem.* **1993**, *97*, 10127.

74. C. R. A. Catlow, A. R. George, C. M. Freeman, *J. Chem. Soc., Chem. Commun.* **1996**, 1311.

75. J. Twu, P. K. Dutta, C. T. Kresge, *J. Phys. Chem.* **1991**, *95*, 5267.

76. G. J. Bratton, B. R. Currell, D. ap Kendrick, H. G. Midgley, J. R. Parsonage, *J. Mater. Chem.* **1993**, *3*, 465.

77. M. Wiebcke, J. Emmer, J. Felsche, *J. Chem. Soc., Chem. Commun.* **1993**, 1604.

78. R. F. Mortlock, A. T. Bell, C. J. Radke, *J. Phys. Chem.* **1993**, *97*, 767.

79. R. F. Mortlock, A. T. Bell, C. J. Radke, *J. Phys. Chem.* **1993**, *97*, 775

80. G. Férey, *J. Fluorine Chem.* **1995**, *72*, 187.

81. E. B. Keller, W. M. Meier, R. M. Kirchner, *Solid State Ionics* **1990**, *43*, 93.

82. J. W. Richardson, Jr., J. V. Smith, J. J. Pluth, *J. Phys. Chem.* **1990**, *94*, 3365.

83. H. Li, M. E. Davis, J. B. Higgins, R. M. Dessau, *J. Chem. Soc., Chem. Commun.* **1993**, 403.

84. J. V. Smith, W. J. Dytrych, *Nature* **1984**, *309*, 607.

85. J. W. Richardson, Jr., J. V. Smith, J. J. Pluth, *J. Phys. Chem.* **1989**, *93*, 8212.

86. J. V. Smith, *Stud. Surf. Sci. Catal.* **1989**, *49*, 29.

87. D. E. Akporiaye, *Stud. Surf. Sci. Catal.* **1994**, *84*, 575.

88. A. Fogden, M. Jacob, *Z. Kristallogr.* **1995**, *210*, 398.

89. E. Jahn, D. Mueller, J. Richter-Mendau, in *Synthesis of Microporous Materials, Vol. 1: Molecular Sieves*, M. L. Occelli, H. E. Robson, (eds.); Nelson Canada: Scarborough, 1992; pp. 248.

90. H. He, J. Klinowski, *J. Phys. Chem.* **1994**, *98*, 1192.

91. M. E. Davis, D. Young, *Stud. Surf. Sci. Catal.* **1991**, *60*, 53.

92. M. E. Davis, B. D. Murray, M. Narayana, in *Novel Materials in Heterogeneous Catalysis*, R. T. K. Baker, L. L. Murrell, (eds.); ACS Symp. Ser. **437**: Washington, 1990; pp. 48.

93. L. Schreyeck, P. Caullet, J. C. Mougenel, J. L. Guth, B. Marler, *J. Chem. Soc., Chem. Commun.* **1995**, 2187.

94. R. Millini, G. Perego, W. O. Parker, Jr., G. Bellussi, L. Carluccio, *Microporous Mater.* **1995**, *4*, 221.

95. U. Oberhagemann, P. Bayat, B. Marler, H. Gies, J. Rius, *Angew. Chem., Int. Ed. Engl.* **1996**, *35*, 2869.

96. W. M. Meier, M. Groner, *J. Solid State Chem.* **1981**, *37*, 204.

97. S. Cartlidge, W. M. Meier, *Zeolites* **1984**, *4*, 218.

98. D. Schultze, P. Kölsch, K. Jancke, G. Finger, J. Kornatowski, *J. Chem. Soc., Faraday Trans.* **1992**, *88*, 2971.

99. J. W. Richardson, Jr., J. V. Smith, S. Han, *J. Chem. Soc., Faraday Trans.* **1990**, *86*, 2341.

100. R. Bialek, W. M. Meier, M. Davis, M. J. Annen, *Zeolites* **1991**, *11*, 438.

101. S. Prasad, I. Balakrishnan, *Inorg. Chem.* **1990**, *29*, 4830.

102. M. Stocker, D. Akporiaye, K. Lillerud, *Appl. Catal.* **1991**, *69*, L7.

103. J. Rocha, W. Kolodziejski, I. Gameson, J. Klinowski, *Angew. Chem., Int. Ed. Engl.* **1992**, *31*, 610.

104. E. T. C. vogt, J. W. Richardson, Jr., *J. Solid State Chem.* **1990**, *87*, 469.

105. M. J. Annen, D. Young, M. E. Davis, O. B. Cavin, C. R. Hubbard, *J. Phys. Chem.* **1991**, *95*, 1380.

106. J. M. Thomas, R. H. Jones, R. Xu, J. Chen, A. M. Chippindale, S. Natarajan, A. K. Cheetham, *J. Chem. Soc., Chem. Commun.* **1992**, 929.

107. P. A. Barrett, R. H. Jones, *J. Chem. Soc., Chem. Commun.* **1995**, 1979.

108. R. H. Jones, J. M. Thomas, R. Xu, Q. Huo, A. K. Cheetham, A. V. Powell, *J. Chem. Soc., Chem. Commun.* **1991**, 1266.

109. (a) R. H. Jones, A. M. Chippindale, S. Natarajan, J. M. Thomas, *J. Chem. Soc., Chem. Commun.* **1994**, 565. (b) A. M. Chippindale, S. Natarajan, J. M. Thomas, R. H. Jones, *J. Solid State Chem.* **1994**, *111*, 18.

110. A. M. Chippindale, A. V. Powell, L. M. Bull, R. H. Jones, A. K. Cheetham, J. M. Thomas, R. Xu, *J. Solid State Chem.* **1992**, *96*, 199.

111. I. D. Williams, Q. Gao, J. Chen, L. Ngai, Z. Lin, R. Xu, *J. Chem. Soc., Chem. Commun.* **1996**, 1781.

112. K. Morgan, G. Gainsford, N. Milestone, *J. Chem. Soc., Chem. Commun.* **1995**, 425.

113. D. A. Bruce, A. P. Wilkinson, M. G. White, J. A. Bertrand, *J. Chem. Soc., Chem. Commun.* **1995**, 2059.

114. L. Sawers, V. J. Carter, A. R. Armstrong, P. G. Bruce, P. A. Wright, B. E. Gore, *J. Chem. Soc., Dalton Trans.* **1996**, 3159.

115. R. Kniep, D. Mootz, A. Wilms, *Z. Naturforsch.* **1978**, *33B*, 1047.

116. D. Brodalla, R. Kniep, , *Z. Naturforsch.* **1980**, *35B*, 403.

117. D. Riou, T. Loiseau, G. Férey, *J. Solid State Chem.* **1993**, *102*, 4.

118. J. Renaudin, G. Férey, *J. Solid State Chem.* **1995**, *120*, 197.

119. H. H. Greger, *Brick and Clay Record* **1950**, *117*, 63.

120. C. F. Callis, J. R. Van Wazer, P. G. Arvan, *Chem. Rev.* **1954**, *54*, 777.

121. D. E. C. Corbridge, *The Structural Chemistry of Phosphorus*; Elsevier: New York, 1974; pp. 124-126.

122. R. Kniep, M. Steffen, *Angew. Chem., Int. Ed. Engl.* **1978**, *17*, 272.

123. W. Tieli, Y. Long, P. Wengin, *J. Solid State Chem.* **1990**, *89*, 392.

124. R. H. Jones, J. M. Thomas, R. Xu, Q. Huo, Y. Xu, A. K. Cheetham, D. Bieber, *J. Chem. Soc., Chem. Commun.* **1990**, 1170.

125. G. Kühl, *J. Inorg. Nucl. Chem.* **1969**, *31*, 1043.

126. R. Kniep, A. Wilms, *Z. Naturforsch.* **1979**, *34B*, 750.

127. J. E. Cassidy, J. A. J. Jarvis, R. N. Rothon, *J. Chem. Soc., Dalton Trans.* **1975**, 1497.

128. D. Riou, T. Loiseau, G. Férey, *J. Solid State Chem.* **1992**, *99*, 414.

129. V. Soghomonian, Q. Chen, R. C. Haushalter, J. Zubieta, *Chem. Mater.* **1993**, *5*, 1595.

130. 25. M. I. Khan, Y. Lee, C. J. O'Connor, R. C. Haushalter, J. Zubieta, *J. Am. Chem. Soc.* **1994**, *116*, 4525.

131. M. E. Leonowicz, J. W. Johnson, J. F. Brody, H. F. Shannon, Jr., J. M. Newsam, *J. Solid State Chem.* **1985**, *56*, 370.

132. K. Lii, T. Lee, S. Liu, S. Wang, *J. Chem. Soc., Dalton Trans.* **1993**, 1051.

133. R. C. Haushalter, Z. Wang, L. M. Meyer, S. S. Dhingra, M. E. Thompson, J. Zubieta,. *Chem. Mater.* **1994**, *6*, 1463.

134. D. Riou, F. Taulelle, G. Férey, *Inorg. Chem.* **1996**, *35*, 6392.

135. U. Schwertmann, R. M. Cornell, *Iron Oxides in the Laboratory*; VCH Publishers, Inc.: New York, 1991, pp. 5-9.

136. D. R. Corbin, J. F. Whitney, W. C. Fultz, G. D. Stucky, M. M. Eddy, A. K. Cheetham, *Inorg. Chem.* **1986**, *25*, 2279.

137. M. Cavellec, D. Riou, G. Férey, *J. Solid State Chem.* **1994**, *112*, 441.

138. A. Boudjada, J. C. Guitel, *Acta Cryst.* **1981**, *B37*, 1402.

139. T. E. Gier, G. D. Stucky, *Nature* **1991**, *349*, 508.

140. W. T. A. Harrison, T. E. Gier, G. D. Stucky, R. W. Broach, R. A. Bedard, *Chem. Mater.* **1996**, *8*, 145.

141. T. Song, J. Xu, Y. Zhao, Y. Yue, Y. Xu, R. Xu, N. Hu, G. Wei, H. Jia, *J. Chem. Soc., Chem. Commun.* **1994**, 1171.

142. W. T. A. Harrison, T. M. Nenoff, T. E. Gier, G. D. Stucky, *Inorg. Chem.* **1992**, *32*, 2437.

143. W. T. A. Harrison, T. M. Nenoff, T. E. Gier, G. D. Stucky, *Inorg. Chem.* **1992**, *31*, 5395.

144. W. T. A. Harrison, T. M. Nenoff, T. E. Gier, G. D. Stucky, *J. Solid State Chem.* **1993**, *107*, 285.

145. W. T. A. Harrison, T. M. Nenoff, T. E. Gier, G. D. Stucky, *J. Solid State Chem.* **1994**, *113*, 168.

146. R. C. L. Mooney-Slater, *Acta Cryst.* **1966**, *20*, 526.

147. J. B. Parise, *Inorg. Chem.* **1985**, *24*, 4312.

148. J. B. Parise, *Acta Cryst.* **1986**, *C42*, 283.

149. M. Esterman, L. B. McCusker, C. Baerlocher, A. Merrouche, H. Kessler, *Nature* **1991**, *352*, 320.

150. T. Loiseau, G. Férey, *J. Chem. Soc., Chem. Commun.* **1992**, 1197.

151. T. Loiseau, G. Férey, *Eur. J. Soild State Inorg. Chem.* **1993**, *30*, 369.

152. G. Férey, T. Loiseau, P. Lacorre, F. Taulelle, *J. Solid State Chem.* **1993**, *105*, 179.

153. T. Loiseau, G. Férey, *J. Mater. Chem.* **1996**, *6*, 1073.

154. M. P. Attfield, R. E. Morris, E. Gutierrez-Puebla, A. Monge-Bravo, A. K. Cheetham, *J. Chem. Soc., Chem. Commun.* **1995**, 843.

155. A. M. Chippindale, R. I. Walton, *J. Chem. Soc., Chem. Commun.* **1994**, 2453.

156. A. R. Cowley, A. M. Chippindale, *J. Chem. Soc., Chem. Commun.* **1996**, 673.

157. A. Clearfield (ed.), *Inorganic Ion Exchange Materials*; CRC Press, Inc.: Boca Raton, Fla, 1982.

158. See, for example, (a) B. Shpeizer, D. M. Poojary, K. Ahn, C. E. Runyan, Jr., A. Clearfield, *Science* **1994**, *266*, 1357. (b) N. Kinomura, N. Kumada, *Inorg. Chem.* **1990**, *29*, 5217.

159. G. Alberti, U. Costantino, in: *Intercalation Chemistry*, M. S. Whittingham, A. J. Jacobson (eds.); Academic Press, Inc: New York, 1982, pp. 147-180.

160. R. C. Haushalter, L. A. Mundi, *Chem. Mater.* **1992**, *4*, 38.

161. P. Kierkegaard, *Acta Chem. Scand.* **1958**, *12*, 1701.

162. R. C. Haushalter, F. W. Lai, *Inorg. Chem.* **1989**, *28*, 2904.

163. L. A. Mundi, R. C. Haushalter, *J. Am. Chem. Soc.* **1991**, *113*, 6340.

164. S. S. Dhingra, R. C. Haushalter, *J. Chem. Soc., Chem. Commun.* **1993**, 1665.

165. S. S. Dhingra, R. C. Haushalter, *J. Solid State Chem.* **1994**, *112*, 96.

166. A. M. Chippindale, S. J. Brech, A. R. Cowley, W. M. Simpson, *Chem. Mater.* **1996**, *8*, 2259.

167. A. M. Chippindale, S. J. Brech, *J. Chem. Soc., Chem. Commun.* **1996**, 2781.

168. D. E. C. Corbridge, *Topics in Phosphorus Chemistry 3*, 57 (1966).

169. J. E. Huheey, *Inorganic Chemistry, 3rd. ed.*; Harper & Row, Publishers: New York, 1983, pp. 684.

170. A. E. R. Westman, *Topics in Phosphorus Chemistry 9*, 231 (1977).

171. E. J. Griffith, R. L. Buxton, *J. Am. Chem. Soc.* **1967**, *89*, 2884.

172. T. Glonek, T. C. Myers, P. Z. Han, J. R. Van Wazer, *J. Am. Chem. Soc.* **1970**, *92*, 7214.

173. M. T. Averbuch-Pouchot, A. Durif, J. C. Guitel, *Acta Cryst.* **1987**, *C43*, 1896.

174. D. Xu, M. Jiang, Z. Tan, *Acta Chim. Sinica* **1983**, *2*, 230.

175. S. M. Golubev, Y. D. Kondrashev, *Zh. Strukt. Khim.* **1984**, *25*, 471.

176. M. T. Averbuch-Pouchot, A. Durif, *Acta Cryst.* **1987**, *C43*, 1894.

177. S. Kamoun, A. Jouini, M. Kamoun, A. Daoud, *Acta Cryst.* **1989**, *C45*, 481.

178. M. Bagieu-Beucher, A. Durif, J. C. Guitel, *Acta Cryst.* **1989**, *C45*, 421.

179. S. Kamoun, A. Jouini, A. Daoud, *Acta Cryst.* **1991**, *C47*, 117.

180. S. Kamoun, A. Jouini, A. Daoud, A. Durif, J. C. Guitel, *Acta Cryst.* **1992**, *C48*, 133.

181. F. Takusagawa, T. F. Koetzle, *Acta Cryst.* **1979**, *B35*, 867.

182. F. Takusagawa, T. F. Koetzle, *Acta Cryst.* **1978**, *B34*, 1910.

183. C. B. Aakeröy, P. B. Hitchcock, B. D. Moyle, K. R. Seddon, *J. Chem. Soc., Chem. Commun.* **1989**, 1856.

184. D. Riou, T. Loiseau, G. Férey, *Acta Cryst.* **1993**, *C49*, 1237.

185. N. J. Tapp, N. B. Milestone, D. M. Bibby, *Zeolites* **1988**, *8*, 183.

CHAPTER 2: EXPERIMENTAL AND SUMMARY OF SYNTHETIC SYSTEMS

2.0 INTRODUCTION

Through on-going research, more is being learned about the synthesis, structures and properties of extended inorganic materials. In many cases, the method of exploratory synthetic research, particularly in the early stages, has been to a varying degree "trial and error". Those working in the area commonly refer to the "rational design" of new structures, where by controlling the structure one can control or tune its properties. For the most part, this has not yet been achieved. Before the chemist can be at such a stage, a much greater amount of data and knowledge is required of the complex series of chemical events that take place before, during and after the formation of a particular phase. This can only be realized with further synthetic, characterizational and theoretical research.

To date, there has not been publsihed a systematic nor even a large amount of study of non aqueous aluminophosphate systems. The volume of synthetic work that was performed in the present study will be summarized in this chapter. The typical source reagents and synthetic methods that were used will initially be described, followed by a brief description of the main characterization techniques. The synthesis results will be broken down according to organic amine templating agent, ranging from secondary to quaternary to cyclic amine species. Some sections will be further subdivided according to various parameters such as reagent molar ratios and solvent type. Primary n-alkylamines and alkylenediamines will be the subject of Chapter 5.

2.1 SYNTHESIS AND METHODS OF MATERIALS PREPARATION

2.1.1 Reagents

Unless otherwise specified, all laboratory reagents were used as received. Aluminum source material was almost exclusively added in the form of pseudoboehmite, $Al_2O_3 \bullet nH_2O$ (Dispal 23N4-80, Vista Chemical Co.), where n is *ca.* 2.5. The small particles of this white powder may be seen in the SEM of Figure 2-1(a). The low crystallinity of the material is reflected in its characteristic PXRD pattern, shown for future reference in Figure 2-1(b). Other sources of aluminum were pseudoboehmite in the form of Catapal A Alumina (Vista Chemical Co.) and Catapal B Alumina (Vista Chemical Co.). Dispal is much more dispersible and of

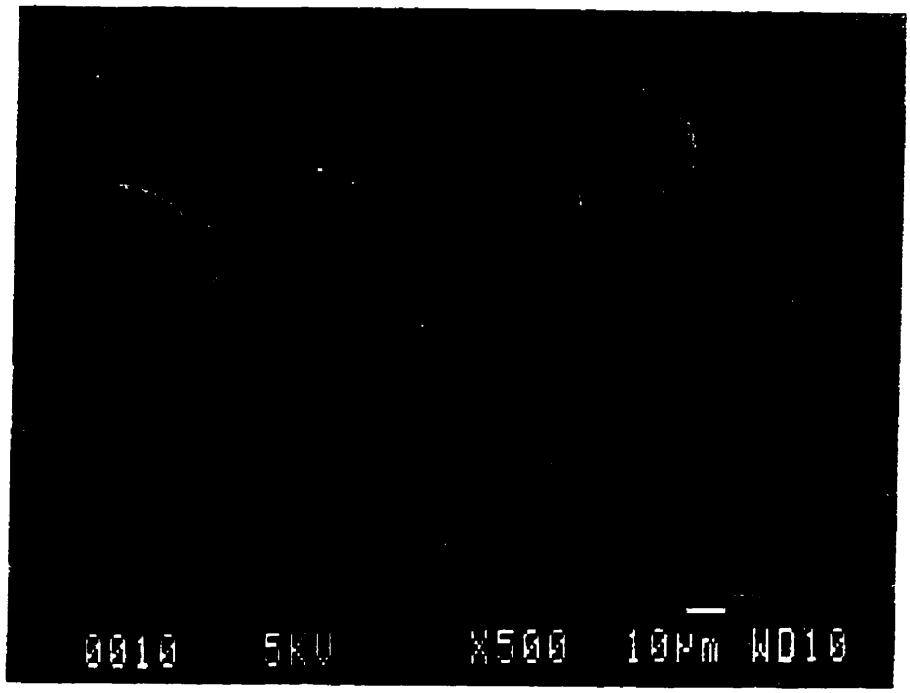

(a)

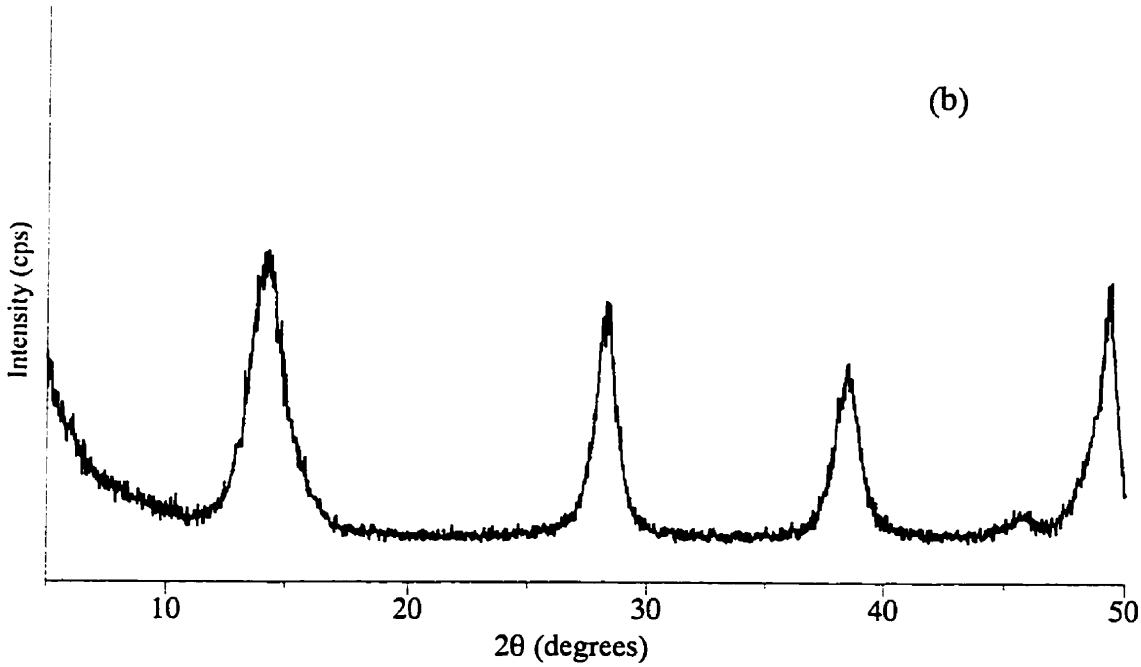

Figure 2-1. The Dispal form of psuedoboehmite. (a) SEM. (b) PXRD.

smaller average particle size (10 μm) as compared to Catapal A (55 μm) and Catapal B (60 μm).[1] Another source used at times was aluminum triisopropoxide (99.999% Gold Label, Aldrich).

Phosphorus was added in the form of an 85 wt.% solution of H_3PO_4 (Aldrich or Mallinckrodt AR). The molar composition of this phosphoric acid may be expressed as (P_2O_5•4.9H_2O). Other phosphorus sources included pyrophosphoric acid, $H_4P_2O_7$ (technical grade, Aldrich) and polyphosphoric acid (Aldrich). Both were very hygroscopic.

The solvents that were investigated were one or more of the following: ethylene glycol (EG, 98%, Aldrich), diethylene glycol (DEG, 99%, Aldrich), triethylene glycol (tEG, Aldrich), tetraethylene glycol (TEG, 99%, Aldrich or Sigma), polyethylene glycol, average MW 200 (PEG 200, Aldrich), PEG 300, PEG 400, PEG 600, PEG 1000, PEG 10,000 (Aldrich), tripropylene glycol (TPG, 97%, Aldrich), polypropylene glycol , average MW 425 (PPG 425, Aldrich), ±sec-2-butanol (99%, Aldrich), pyridine (ACS grade, BDH), glycerol (ACS Grade, BDH), mineral oil (Saybolt viscosity 335/350, Fisher) and deionized water.

Sources of fluorine were either hydrofluoric acid (48 wt.%, BDH) or an anhydrous organofluoride, namely hydrogen fluoride-pyridine (70 wt.% HF in pyridine, 98%, Aldrich), triethylamine-trihydrogen fluoride (37 wt.% HF in triethylamine, 98%, Aldrich) or poly[4-vinylpyridinium poly(hydrogen fluoride)] (Aldrich). The hydrogen fluoride-pyridine was added in a glove bag filled with nitrogen due to its sensitivity to air.

The brand and purity of the variety of organic template additives and other reagents that were used will be mentioned in the relevant sections.

2.1.2 Solvothermal Synthesis

The synthetic procedure was, for the most part, identical for all systems. Magnetic stirring was used throughout, and manual stirring was applied after the addition of each reagent. The solvent of choice was first weighed into a Nalgene beaker, followed by the second solvent, if used. At this point, if hydrogen fluoride was to be added, it was delivered dropwise by a polypropylene dispopipette (Samco). The alumina powder was then dropped in slowly, allowing the powder to disperse and slurry into the solvent. The pseudoboehmite powder particles were very light, and care had to be taken in this step to minimize the amount that became airborne by the pull of the fumehood exhaust. Some powder always adhered to the walls of the beaker, and was manually mixed into the solvent.

The phosphoric acid was then added dropwise. If water was used as all or part of the solvent, the mixture turned opaque and was observed to gel. If no water was used, this did not occur, but a small amount of hard material was observed to form on the bottom of the beaker by the action of the stirring bar, and this was scraped off with a spatula and mixed into the slurry.

Finally, the organic amine was added, and for most amines, the mixture turned thick and opaque and heat was evolved. As is the case for most molecular sieve syntheses, ensuring homogeneity of the reaction gel prior to its heating was an important step in the procedure. Extensive manual stirring was therefore applied in the final step. No aging of the mixture was necessary, but they were typically stirred magnetically for approximately ten minutes.

The synthesis mixtures were then loaded into Teflon-lined stainless steel autoclaves. The autoclaves used were 15 ml capacity (constructed in-house), 45 ml capacity (Parr No. 4744 Acid Digestion Bomb) and 125 ml capacity (Parr Bomb No. 4748 Acid Digestion Bomb). The reaction chambers were sealed as tightly as possible to prevent leakage and heated statically in a forced convection oven at the required synthesis temperature. The temperature of the oven was set using a thermocouple inserted into the centre of the oven. The 45 ml capacity autoclaves were sealed using a Parr-designed implement, while the 125 ml capacity autoclaves were closed using its tightening bolts.

For synthesis temperatures below 100°C, the slurry was placed into a wide-mouthed polypropylene bottle, initially covering its thread with Teflon tape, and treated statically in a forced convection oven.

Experiments involving agitation were placed in a forced convection oven containing a rotary device (constructed in-house) which continuously revolves the autoclaves. The oven was held at the desired synthesis temperature. Rotation speeds could be varied, but were approximately 7 rpm.

2.1.3 Sample Recovery

After thermal treatment for the desired amount of time, the autoclaves were removed from the oven and quickly brought to room temperature by quenching under a continuous flow of cold water. At least five minutes of this cooling were necessary to completely cool the mixture, longer for the larger capacity bombs. The solid product was then recovered by suction filtration and washed with acetone and/or water, depending on its solubilities. For mother liquor studies,

the filtrate was collected prior to washing the product and kept in a stoppered, sealed glass vial for subsequent measurements. All solid products were left to dry in ambient air overnight.

2.1.4 Teflon Liner Cleaning Treatment and Impregnation

Due to the highly porous nature of the Teflon liners,[2] it was necessary to treat them in an acid bath between synthetic runs, in an attempt to remove inorganic, organic and solvent impurities from the walls of the liner introduced by prior syntheses. This involved first washing the liner with soap and water, and then submerging it in a bath comprised of 1.0 M HF and 0.1 M HNO_3. The liners were kept in this bath until at least the next day, and then submerged in distilled water for at least 24 hours.

As will be seen, this usually annoying characteristic of Teflon was at times advantageous. In such cases, the liners were intentionally impregnated prior to their use in the synthesis with "impurities". This was achieved simply by charging the liner with a solution of the desired impurity in varying concentrations and heating at 200°C.

2.1.5 Recrystallization

The ionic salt materials relevant to this work, namely the series of alkylammonium-phosphate compounds, could be readily prepared as a powder in many solvents such as water or tetraethylene glycol. In order to solve their structures by single crystal X-ray diffraction, sufficiently large crystals needed to be grown. Since the salts were soluble in water, this was achieved by recrystallization using the evaporation method.

A saturated solution was first prepared by placing a small amount of the solid in a solution and mildly heating it until the solid dissolved. The solution was then allowed to cool to room temperature. If no solid had formed upon cooling, some solid was added to induce precipitation. This mixture was then allowed to stand for several days, after which the two phases were separated by gravity filtration. The filtrate was placed in a clean beaker and allowed to stand undisturbed, until the solvent had completely or partially evaporated and large crystals could be seen on the beaker walls or bottom. Depending on the starting reagents and volumes, this took anywhere from several days to several months. Most recrystallizations were performed in water, or an equal volume mixture of methanol and water. The temperature of recrystallization was usually room temperature, but ranged anywhere from 0 to 80°C.

2.2 CHARACTERIZATION METHODS

2.2.1 Powder X-ray Diffraction (PXRD)

Samples were finely ground and spread evenly on a Plexiglas sample holder. Powder X-ray diffraction patterns were collected on a Siemens D5000 diffractometer using Ni-filtered CuKα radiation (λ = 1.54178Å). The typical accelerating conditions were 50kV and 35mA. For strongly diffracting samples, the intensity of the 100% peak was first checked by quick manual scans of the angles in the region of the strongest peak under lower accelerating conditions, typically 40kV and 20 mA. The step size was 0.03° and the step time was 1.0 seconds, with a scan range of 1 to 50° (2θ). The detector in the instrument was a Kevex 2005-212 solid state detector. A slit size of 1 mm was used on the X-ray tube, and 1 mm and 0.2 mm for the detector slits. The latter was changed to 0.1 mm for more strongly diffracting samples. If diffraction was still intense (over 10,000 cps), folded aluminum foil was placed over the detector opening, or in more extreme cases, a copper film was placed between the two detector slits.

2.2.2 Single Crystal X-ray Diffraction (SC-XRD)

All SC-XRD data were collected and refined by Dr. Alan Lough in the X-ray facilities of the Department of Chemistry at the University of Toronto. The instrument used was either an Enraf-Nonius CAD4 diffractometer or a Siemens P4 diffractometer, both with graphite monochromated MoKα radiation (λ = 0.71073Å). The intensities of several standard reflections were measured throughout the data collection, and showed no decay. Reflections were considered observed for $I > 2\sigma(I)$. The data were corrected for Lorentz and polarization effects and for absorption.[3]

The structures were solved using the SHELXTL\PC V5.0 package[4] and refined by full-matrix least-squares on F^2 using all data (negative intensities included). The weighting scheme was $w = 1/[\sigma^2(F_o^2)+(aP)^2+bP]$, where $P = (F_o^2+2F_c^2)/3$, F_o is the observed structure factor and F_c is the calculated structure factor. Hydrogen atoms were included in calculated positions and treated as riding atoms. For many of the structures, the hydrogen atom of the P-OH group(s) and the ammonium hydrogens were refined with an isotropic thermal parameter. Attempts to model the organic template molecules as disordered rigid groups did not give as satisfactory a refinement as allowing all carbon atoms of the molecules to refine freely with anisotropic thermal parameters.

2.2.3 Scanning Electron Microscopy (SEM)

Scanning electron micrographs were collected on a JEOL 840 SEM, with accelerating conditions of 5kV or less. All mounted samples were pre-treated by sputter-coating an approximately 20Å layer of gold to create a conducting surface layer and reduce charging effects which were common for most samples. Most of the SEM work was obtained by Dr. Neil Coombs of Imagetek Analytical Imaging, Toronto, on a Hitachi S-570 SEM and the above instrument.

2.2.4 Thermal Analysis

Thermogravimetric Analysis (TGA) was performed on a Perkin Elmer 7 Series Analyzer, under nitrogen atmosphere and with a 5°C/min heating rate. Temperatures used were typically in the 25 to 600°C range. Samples were ground to a powder before placing in the platinum pan.

Differential Scanning Calorimetry (DSC) was also performed on the Perkin Elmer 7 Series Analyzer, with a heating rate of 5°C/min, and continuous temperature cycling between 25°C and 100°C to 200°C. Approximately 10 mg of ground sample was accurately weighed and sealed in an aluminum sample holder.

Variable-Temperature Powder X-ray Diffraction (VT-PXRD) patterns were obtained *in situ* on the Siemens D5000 diffractometer using a Siemens HTK 10 attachment. Samples were placed on a platinum strip from a slurry of the powder in isopropanol, allowing the latter to evaporate. The strip was placed on the goniometer in the chamber of the HT attachment, and data was collected in air or sealed under a nitrogen flow. The heating rate commonly used was 10°C/min between scans, and 1°C/min during data collection (the latter being reduced to minimize the increase in temperature during a particular scan). For higher resolution data, a heating rate of 1°C/min was used throughout the experiment, stopping at a particular temperature, if desired. For each VT-PXRD pattern, a quick scan was run from 1 to 37° (2θ), with 0.05° step size and 0.7 second step time. Due to the lower resolution of the scans and the decreased amount of sample, the second slit on the detector was changed to 0.6 mm.

Simple thermal heating for transformation and calcination experiments was performed in a heating chamber attached to a temperature programmer (Omega, model 2010). Samples were placed in a quartz tube and heated in the chamber in air. Heating rates were between 1 and 5°C per minute, and soaking times were 2 to 8 hours.

2.2.5 NMR

^{1}H and ^{13}C solution NMR spectra were collected on a Gemini 200 MHz NMR using 5mm borosilicate glass tubes and benzene-d6 inserts. ^{31}P NMR spectra were collected on a Gemini 300 MHz NMR using 10mm borosilicate glass tubes and a Wilmad special stem coaxial insert that was sealed containing benzene-d6. Solid state NMR was run by Varian and Bruker. The experimental conditions and the nuclei that were studied will be given in the discussion at the appropriate times.

2.2.6 Chemical Analysis

Qualitative Energy Dispersive X-ray (EDX) analyses of uncoated or carbon-coated samples were obtained by Dr. Neil Coombs of Imagetek Analytical Imaging, Toronto, on an AN 10,000 EDX device equipped with a solid state detector, on the Hitachi S-570 Field Emission SEM.

Chemical analysis was performed at Galbraith Laboratories, Knoxville, Tennessee. Elements that were analyzed included Al, P, O, F, N, C and H.

2.2.7 Computer Modeling

Inspection and evaluation of structures made use of the Cerius^2 software package (v. 2.0) of Molecular Simulations, Inc., on a Silicon Graphics workstation. All printed views of structures in this work, both from fractional coordinates of single crystal XRD data and theoretically constructed structures, were created using this program. Desired views or projections of a structure were first printed to a postscript file and transferred (by ftp) to a PC computer. The images were then converted to TIFF format using Corel 6 PhotoPaint, and further manipulated using Aldus Photostyler v. 2.0 and/or Adobe Photoshop. The shading scheme used in all figures is as follows: oxygen, nitrogen and hydrogen: white; phosphorus: black; aluminum and carbon: grey. PXRD patterns based on known and theoretical structures were also projected and indexed with Cerius^2.

2.3 SYNTHESIS RESULTS

This last section of the chapter will describe in turn the various synthesis systems that were explored, and the preliminary characterization of the products by PXRD and SEM. The sections will be arranged according to the degree and type of organic amine or ammonium

species. The different solvents studied for a given template will be included within each section. A large amount of data was obtained using cyclic amines (which themselves range from primary to tertiary), and will be discussed separately. In most cases, if a product is identified as a certain phase, it is due to the similarity of the experimental PXRD pattern to that published, or to that projected from the Cerius[2] program. Note also that for any of the "unknown" phases discussed in this chapter where a number is given in Angstroms to indicate its 100% peak, its presence was indicated by the close inspection of the overall diffraction pattern, comparing and indexing the patterns of different products and accounting for the peaks of known phases.

In order to organize the large amount of data, each product is assigned a code, numbered sequentially. These are shown in the text and next to the section titles. Correspondingly, the reaction conditions and results are tabulated in Appendix A. For selected products, as indicated in Appendix A, PXRD patterns are shown in Appendix B and SEM micrographs in Appendix C.

2.3.1 Secondary Amines

2.3.1.1 Diethylamine (Et_2NH) [II-1]

This organic does template zeolite frameworks such as ZSM-5,[5] but is not documented as giving any aluminophosphate structure. Its use (BDH) in TEG led to an amorphous product (II-1). It is possible that crystalline materials could be obtained with further modification of conditions.

2.3.1.2 Dipropylamine (Pr_2NH) [II-2 to II-5]

Dipropylamine (99+%, Aldrich) leads to many $AlPO_4$-n and MAPO-n framework structures, including $AlPO_4$-11 and VPI-5.[5] It was also said to form a dihydrogen phosphate salt in the initial aqueous synthesis mixture (section 1.5). In the TEG system, an amorphous, "open" material is present after one day of heating at 180°C (II-2). After 3 days, $AlPO_4$-11 is present as a minority phase, with an unknown phase whose first peak is at approximately 20Å (II-3). Use of 200°C for 3 days gave a similar product to II-3 (not shown).

The PXRD pattern after 10 days of heating (II-4) corresponds to that of $AlPO_4$-11. The SEM of the product shows a morphology of small platelets. It is interesting to consider that the unknown 20Å material could be a previously unobserved precursor phase to $AlPO_4$-11 or VPI-5, which were obtained under aqueous conditions (II-5), as expected. As for most systems, the

relative instability of the open materials is indicated by the observation that after 24 days at 200°C, only dense-phase berlinite was present.

2.3.2 Tertiary Amines

2.3.2.1 Trimethylamine (Me_3N) [II-6]

Since trimethylamine is a gas under ambient conditions, it was added as a 25 vol.% solution (Aldrich). It is commonly used for templating $AlPO_4$-21.[5] The PXRD pattern of the product from TEG after 10 days of heating at 180°C (II-6) appears to be $AlPO_4$-21. The peak at 9.5Å could be due to another phase in the product.

2.3.2.2 N,N-Diethylmethylamine ($MeEt_2N$) [II-7]

Due to the large number of materials that were observed in the triethylamine system, often of considerable crystal sizes, and the close relationship of the shape of triethylamine with the channels of JDF-20 (Figure 1-1b), it was decided to use an amine with one of the three ethyl groups shortened by one carbon (98%, Aldrich). The PXRD pattern of the product (II-7) displays an unknown material not observed to form in the triethylamine system. Use of a shorter time of 3 days formed the same material, but with lower crystallinity. Since the material is unknown in nature, it is not certain if it is phase pure or a mixture of phases.

2.3.2.3 Triethylamine (Et_3N) [II-8 to II-96]

An extensive number of experiments were conducted using triethylamine (99%, Aldrich) due to the variety of structure types, the large crystal sizes, and the observed water-dependence of the products. Therefore, this section will be broken down into a number of sub-sections, each representing one experimental parameter that was varied. All experiments used the Dispal form of pseudoboehmite, with the exception of those involving different sources of aluminum and phosphorus (section 2.3.2.3.6). Note that temperatures indicated as 195°C imply that the reaction chambers were placed at the bottom of a 180°C oven, which served to heat the bomb to approximately 195°C, as measured by a thermocouple placed under a bomb in the oven.

2.3.2.3.1 Non Aqueous TEG Solvent [II-8 to II-17]

This section deals with the variation of the time and temperature of the primarily non aqueous TEG-Al_2O_3-P_2O_5-Et_3N system. The initial reaction mixture is simply a slurry of the

alumina in the TEG solvent (II-8), and the PXRD of the dried solid obtained by filtering this slurry gives only the characteristic pattern of pseudoboehmite, as shown previously in Figure 2-1b. The pattern was identical after 1 to 4 months of aging statically at room temperature. It was also identical in the absence of phosphate and/or amine. Not present in the solid is any triethylammonium phosphate salt, as found for other templates, such as the cycloalkylamines (section 2.3.5) and alkylamines (Chapter 5).

A series of time-dependence studies were performed (II-9 to II-15). After one day of heating at 195°C, unreacted pseudoboehmite is present, as well as an amorphous material (broad hump centred at 25° (2θ)), and a small amount of another phase with peaks at *ca.* 12.9Å and 5.7Å (II-9). These peaks are at the same positions as the most intense peaks of JDF-20,[6] and evidently the phase is in its initial stages of formation at this point. Two days of heating at 195°C gave a highly crystalline JDF-20 product (II-10). Also present in the pattern is a smaller amount of the aluminophosphate chain structure $[AlP_2O_8H_2]^-[Et_3NH^+]$,[7] whose characteristic 100% peak resides at *ca.* 8.9Å. Longer heating times gave decreasing amounts of JDF-20 and increasing amounts of the chain phase (II-11, II-12), until the product was almost phase-pure after 9 days (II-13). Prior to discovering the chain structure in the literature, the SC-XRD data was collected and analyzed (section 3.1). Note the large crystal sizes that are usually obtained (II-13A, Appendix C). Also seen in the SEM are the spherical aggregates of needles of JDF-20, and its surface can be seen in a close up SEM of one of the spheres (II-13B).

It should be pointed out that the results shown above for the Et_3N system are for the materials obtained from the walls of the reaction chamber. At the bottom of the reaction chamber is a hard, densely packed material comprised of other phases. For example, the PXRD pattern and the large crystals of II-13 are in fact the crystals that grew on the walls of the Teflon liner, while the packed material from the bottom is comprised mostly of JDF-20 and a only trace amount of chains (II-14). This is typical of the triethylamine experiments that contain minority amounts of water. In fact, with extended periods of time, little or no crystals are observed on the liner walls, and all the product resides at the bottom of the liner. After 4.5 months at 180°C, the chain phase is observed at the liner bottom with trace amounts of JDF-20 (II-15).

An example of the sensitivity of the system to temperature is shown by the products using a lower temperature of 180°C. 2 or 3 days of heating yielded pseudoboehmite and an amorphous material (broad hump centred around 27° (2θ); no crystalline phase is observed at this point

(II-16). JDF-20 is observed after 6 days, which only required 2 days at 195°C. Higher temperatures of 200°C gave almost entirely the chain phase (II-17).

The results above are not dependent on the capacity of the reaction chambers. Nearly identical results were obtained with larger 45 ml and 125 ml capacity bombs, with similar crystal sizes and an expected increase in yield.

2.3.2.3.2 Reagent Amounts of Water [II-18 to II-40]

Before discussing the effects of addition of water, a few words should be mentioned concerning dilution. No matter what solvent was used, the concentration of all reagents in the solvent was important for all systems. An example is II-18, where the solvent volume was doubled by using 28 moles of TEG. The product was a majority phase of $AlPO_4$-5, with some JDF-20 present. Such a product is usually only obtained with the usual 14 moles of TEG solvent when significant amounts of water are added (see below). Similarly, if the starting mixture is too dilute, the product will ultimately be berlinite (as for aqueous conditions, II-39, below). Therefore, dilution should be taken into account, particularly when water is being added and increasing the volume of the solvent.

Small amounts of water have little effect on the resultant products. 1.8 moles of water (chosen for an H_2O:Al ratio of 1.0) gave essentially the same product as when no water was added (II-19). However, 3.6 moles of water gave the chains with a larger amount of JDF-20 at 180°C (II-20), and phase-pure JDF-20 at 200°C (II-21). 7.2 moles of water yielded only JDF-20, and the product was a homogenous, gelatinous mixture that filtered to yield a fine powder of small needles (II-22).

10.0 moles of water also gave JDF-20, and the PXRD patterns of the products show the temperature-dependence of the crystallinity of the JDF-20 phase with 3 days of heating (II-23 to II-25, Appendix B). Rather than forming a novel material, higher temperatures and/or longer heating times served only to produce $AlPO_4$-5 and dense-phase $AlPO_4$-tridymite and decrease the yield of JDF-20 (II-26, II-27). After 10 days at 220°C, $AlPO_4$-tridymite was the only phase present (II-28).

On a number of occasions, another phase was obtained using 10.0 moles of water and 195°C (II-25). They were large, hexagonal plates, several millimetres across (Optical micrograph, Figure 2-2) and grew on the lower walls or on top of the material at the bottom of the liner. One such crystal was studied by SC-XRD, and was found to be a layered

Figure 2-2. Optical micrograph of UT-1 crystal.

aluminophosphate, denoted UT-1. Its structure is the $AlPO_4$-5-like layer (sections 1.2.1 and 3.3). Interestingly, the material could not be formed reproducibly; many experiments were performed, varying different parameters, but were unsuccessful. It was subsequently discovered that the problem was undoubtedly due to impurities entrapped in the walls of the Teflon liner (see section 2.3.2.3.7). UT-1 gives rise to the peak observed at 10.1Å in the PXRD pattern of II-25, present as a minority phase. Although the inorganic architecture of UT-1 was solved, its irreproducibility was further complicated by the inability to resolve the interlamellar species from the data set (section 3.3). Without knowing the nature of the templating species, it becomes even more difficult to purposely synthesize this phase.

Slightly increasing the amounts of water and/or temperature failed to produce any UT-1, and gave only JDF-20 (II-29). Larger amounts of water yielded varying amounts of JDF-20, $AlPO_4$-5 and dense-phase $AlPO_4$-cristobalite, gradually increasing the yield of the latter two more hydrolyzed phases (II-30 to II-33). One general trend is the higher the amount of water, the greater is the dependence of the phases on both temperature and time.

Interestingly, at 89.4 moles of added water (half-aqueous by volume), large crystals of tinsleyite were obtained (II-34). The structure, solved by SC-XRD (section 3.4), is templated by ammonium rather than triethylamine, indicative of the large degree of template decomposition that takes place at these temperatures.

Further increase of water showed a very strong temperature-dependence (II-35, II-36). The effective increase of water concentration was also achieved by decreasing the amount of TEG, giving $AlPO_4$-5 and trace $AlPO_4$-cristobalite (II-37). Complete removal of TEG, i.e. aqueous conditions, yielded $AlPO_4$-5 (II-38A, 100 μm hexagonal rods) and a significant proportion of $AlPO_4$-cristobalite with an interesting morphology (II-38B, 300 μm octahedra). Dilution on the aqueous side of the system gave $AlPO_4$-5 (II-39) and ultimately berlinite (II-40, PXRD shown for future reference).

2.3.2.3.3 Agitation [II-41]

Since a hard, packed material was present on the bottom of the reaction chamber and crystals grow on the liner walls, an agitation experiment was performed. The product was JDF-20, all collected together into a solid ellipsoidal clump, whose width was slightly less than that of the liner (II-41). The solvent also contained a small amount of powder, which was analyzed

separately. It was comprised of poorly crystalline JDF-20. Due to these results, no further experiments with agitation were carried out.

2.3.2.3.4 Moles of Template [II-42 to II-46]

The important role of the template is indicated by the product using 2.9 moles of triethylamine (a molar reduction of 50%). At 180°C, the product is an approximately equal amount of $AlPO_4$-tridymite and chains, with a trace amount of $AlPO_4$-5 (II-42). 200°C gave $AlPO_4$-tridymite and a small amount of chains (II-43). This effect in combination with that of water is demonstrated by the experiment using 3.6 moles of water and 2.9 moles of Et_3N, which gave only $AlPO_4$-tridymite (II-44). Increase in the amount of Et_3N, namely 6.0 or 7.0 moles, only served to decrease crystal size and quality, producing fragmented crystals. In the absence of triethylamine, not surprisingly, berlinite was the product (II-45). The vital role of the amine functionality in general is also implied by the fact that 6.95 moles of cyclohexane (rather than cyclohexylamine) gave no open aluminophosphate phase, but rather berlinite (II-46).

2.3.2.3.5 Phosphorus to Aluminum Ratio [II-47 to II-53]

Most aluminophosphate syntheses use a 1:1 P:Al ratio.[5] Correspondingly, aluminophosphate frameworks tend to have a 1:1 P:Al ratio and are neutral. One of the reasons for the discovery of new structures in this work is the 2:1 P:Al ratio that was used, which helped to produce phases with a P:Al ratio greater than one (section 4.2.3). This ratio was therefore varied to study its effect on the products of the TEG-triethylamine system.

Addition of no phosphate (i.e., 0.0 P:Al) gave unreacted pseudoboehmite, as expected (II-47). An experiment equimolar in phosphorus and aluminum (1.0 P:Al) gave, notably, an approximately equal yield of JDF-20 and $AlPO_4$-5 after only 3 days (II-48), not achievable with a 2.0 P:Al ratio under such conditions. Unreacted Dispal pseudoboehmite could be seen in the product from the bottom of the liner. Semi-aqueous and aqueous solvents with P:Al equal to 1.0 gave $AlPO_4$-5 (II-49 and II-50).

Increasing the P:Al ratio to 3.0 and 4.0 under non aqueous conditions gave the chain structure as the preferred product (II-51 and II-52). The product at the bottom in this case was a much softer material. A 6.0 P:Al ratio gave berlinite as the only product (II-53). It should also

be noted that due to the aqueous component of the 85 wt.% phosphoric acid (P_2O_5•$4.9H_2O$), changing the P:Al ratio significantly alters the amount of water present in the TEG solvent.

2.3.2.3.6 Aluminum and Phosphorus Source Reagents [II-54 to II-62]

At all temperatures and conditions, aluminum isopropoxide gave similar product phases, but of much lower crystal quality and crystallinity (II-54). Similarly, Catapal A gave results comparable to Dispal, forming JDF-20 but of smaller crystal size (II-55). A fluoroaluminate source yielded only dense-phase aluminum phosphite in the product (II-56).

Condensed phosphates were used as phosphate sources, but were not stable to hydrolysis in the system. Pyrophosphoric acid and polyphosphoric acid both behaved as if monomeric orthophosphoric acid had been added (II-57, II-58). Clearly, the P-O-P linkages are hydrolyzed apart. Interestingly, the material from the bottom of the liners was mostly pseudoboehmite, with some poorly crystalline JDF-20 in the case of pyrophosphoric acid and chains in the case of polyphosphoric acid. This could be due to the anhydrous nature of these phosphate sources as compared to orthophosphoric acid, allowing for less hydrolysis of the pseudoboehmite reagent. The higher water content of pyrophosphoric acid ($H_4P_2O_7$) accounts for the presence of JDF-20 in the product rather than chains.

Triethyl phosphate was tried due to its templating of the zinc phosphate analog of the chain structure (section 1.3.3),[8] in which the hydrophobic ethyl groups separate the chain moieties. No other species was therefore used as templating agent. However, the ethyl groups were hydrolyzed off the phosphate, and the product was berlinite (II-59). In the presence of Et_3N, the product was poorly crystalline $AlPO_4$-5 with unreacted pseudoboehmite (II-60). The removal of the ethyl groups is attributable to the much higher temperatures used, as compared to those used for the zinc phosphates.

Aluminum metaphosphate, itself a dense phase aluminophosphate (section 1.1.2), remains unreacted at milder temperatures (II-61). It is indeed a higher temperature phase, and it is therefore reasonable that it should be stable under these conditions. However, at higher temperatures of 195°C, the product was $AlPO_4$-tridymite and $AlPO_4$-5, with some aluminum metaphosphate still present (II-62).

2.3.2.3.7 Other Additives: Effects of Fluorine [II-63 to II-74]

Other reagents were added to the triethylamine system and perturbed it to varying degrees. For example, acetic acid had only a slight effect, producing a small amount of $AlPO_4$-5 under non aqueous conditions (II-63). In another experiment, 0.5 moles of hydrochloric acid were added to reduce the pH, but had no effect on the product either in the presence or absence of triethylamine (II-64 and II-65, respectively). When 4.5 moles of HCl were added, the triethylamine formed a water-soluble chloride salt, $Et_3NH^+Cl^-$, as observed by SC-XRD of the large needles (II-66), while the aluminophosphate crystallized as berlinite.

On the contrary, fluorine had a drastic effect on the phases that form. Fluorine was added in two ways: by impregnating the liner with fluoride, or by directly adding an HF reagent source. In a typical non aqueous Et_3N synthesis, the former (achieved by pre-treating the Teflon liner in a 16 Py/4.0 HF-Py mixture at 200°C for 7 days, thereby "overloading" the liner with fluoride and allowing fluoride to be released during a typical synthesis) yielded, remarkably, a majority phase of $AlPO_4$-5, and only a small amount of JDF-20 and chains (II-67). A semi-aqueous experiment in such a pre-treated liner gave $AlPO_4$-cristobalite and a small amount of $AlPO_4$-5 and tinsleyite (II-68).

A liner pre-treated with a lower fluoride concentration (16 Py/2.0 HF-Py, 200°C, 10 days) gave a lower amount of $AlPO_4$-5, and a majority chain phase (II-69). The introduction of fluorine therefore appears to be somewhat controllable by this method, ideally allowing for a desired ratio of phases. For both II-68 and II-69, all of the product was soft and on the bottom of the liner.

Direct addition of HF in the form of $(HF)_3Et_3N$ had drastic effects. A micropipette should really have been used for the addition of such small amounts of HF: only one drop added to the normal synthesis mixture gave the chain phase, with $AlPO_4$-5, JDF-20 and, notably, UT-1 (II-70). This appears to have solved the way in which UT-1 forms; namely, when liners were used that had large amounts of fluorine impurity present in its walls. Indeed, 3 drops of fluoride yielded $AlPO_4$-5 and UT-1 again (II-71).

Similarly, only a trace amount of JDF-20 and chain phase were formed with only the two additional drops of the HF source, along with the beginnings of an unknown phase with 100% peak at 19.2Å. Larger amounts of HF, namely 1.0 or 2.0 moles, gave this unknown 19.2Å phase as what appears to be a pure phase (II-72). This is undoubtedly a fluoroaluminophosphate phase, as the addition of fluoride with cyclic amines tends to change the aluminophosphate product to

other fluorinated phases (see below). HF did not have as great an effect under semi-aqueous conditions (II-73).

Poly[4-vinylpyridinium poly(hydrogen fluoride)] (Aldrich) was used as a fluorine source in the hopes of slowly releasing fluorine and thus forming large crystals of known phases or the unknown 19.2Å phase. However, it formed only small needles of the latter, and a small amount of $AlPO_4$-5, but did serve to greatly increased the crystallinity of the unknown (II-74).

2.3.2.3.8 Other Non Aqueous Solvents [II-75 to II-96]

Many triethylamine-related experiments were performed with other solvents, mostly various oligo- and polyalkylene glycols. In all cases, the solvent molecules do not end up in the aluminophosphate crystals, possibly with the exception of UT-1 (section 3.3). An equal volume of solvent was used to keep concentrations constant. Ethylene glycol gave $AlPO_4$-5 as the only product phase (II-75). Published results of the formation of $AlPO_4$-5 in EG using aluminum triisopropoxide as the aluminum source[9] were reproduced (II-76). Diethylene glycol afforded small crystals of JDF-20 (II-77).

Triethylene glycol (tEG) was, in fact, investigated prior to any TEG experiments. tEG gave results similar to tetraethylene glycol, but with smaller, more fragmented crystals and lower crystallinity (II-78, II-79). As a result, tetraethylene glycol was used for all future experiments. Similarly, aluminum isopropoxide gave poorer crystals and crystallinity (II-80), and Dispal pseudoboehmite was thereafter used. The order of addition was also probed in the triethylene glycol system and was observed to have little or no effect. Consequently, the amine was added in the last step for almost all experiments.

Higher molecular weight polyethylene glycols gave the chain phase, with a small amount of JDF-20 (II-81 to II-83). For PEG 1000 and higher molecular weights, the glycol is a waxy solid at room temperature and the synthesis procedure had to be conducted at slightly elevated temperature, such as *ca.* 60°C for PEG 1000 (MP 39°C) Additionally, the products had to be filtered with the mother liquor still above 39°C, washing with warm water and acetone. Crystal sizes of the resultant chain phase were still large (II-84), but smaller and much thinner than those from TEG.

As observed for TEG, 200°C gave JDF-20 for PEG 1000 (II-85), while dilution by doubling the volume of solvent gave the chain phase and an unknown 9.8Å phase (II-86). PEG

4600 also gave the chain phase (II-87), while the highly viscous PEG 10,000 yielded an amorphous material with a small amount of berlinite (II-88).

Tripropylene glycol (TPG) and polypropylene glycol average MW 425 (PPG 425) also formed the chain phase (II-89 and II-90), and the results were essentially identical to the tEG and PEG 400 results, respectively. For this reason, the wide range of other commercially available polyalkylene glycols were not studied. There was no observable chelating effect that was unique to TEG by the various polyalkylene glycols.

Mineral oil yielded only $AlPO_4$-tridymite (II-91) and, in the absence of HF, pyridine solvents resulted in triethylamine-related products similar to TEG (II-92, II-93). With the addition of HF-Py, pyridine-related phases were formed (section 2.3.4.2). Sec-butanol also gave results related to TEG, and even showed a similar water-dependence (II-94 and II-95). It would be interesting to further probe the water-dependence of the other solvent systems to compare with the TEG-H_2O results.

While no triethylammonium-phosphate salt was observed in any of the experiments above, it can be formed from a concentrated mixture of TEG-H_3PO_4-Et_3N (II-96). That this phase is not relevant in the chemistry taking place during the aluminophosphate reactions is implied by the observation that these crystals will decompose in a short time when left exposed to air. It is therefore unlikely that the compound is present in the reaction mixtures.

2.3.2.4 Triethanolamine [$(HOCH_2CH_2)_3N$] [II-97]

$AlPO_4$-5 is templated by this amino alcohol.[5] Its use (98%, Aldrich) in TEG gave rise to an unknown PXRD pattern (II-97), mixed with $AlPO_4$-5, judging by the characteristic, more intense peaks of the latter at 11.8Å, 6.84Å, 5.93Å, 4.50Å, 4.24Å and 3.97Å.[5]

2.3.2.5 Tripropylamine (Pr_3N) [II-98]

All experiments with tripropylamine (98%, Aldrich) gave berlinite as the only product (II-98). This is likely due to the biphasic nature of the synthesis mixture: the tripropylamine would not disperse into the TEG solvent, and floated on top of the mixture. Therefore, it is not present in the phase in which the aluminophosphate reaction is occurring. Shorter heating times of 3 days also gave the same result.

2.3.2.6 Tributylamine (Bu_3N) [II-99]

As found for tripropylamine, berlinite was the only product using tributylamine (99%, Aldrich). For this system, phosphoric acid was added last, but it still did not mix with the TEG solvent. All of the berlinite solid was residing in the lower glycol phase of the reaction chamber (II-99). Milder conditions of 180°C and 4 days gave the same result.

2.3.3 Quaternary Tetraalkylammoniums

2.3.3.1 Ammonium Hydroxide (NH_4OH) [II-100 to II-101]

Ammonium hydroxide (30 wt.%, BDH) was used as the ammonium source reagent. Ammonium can be considered as the first in the series of quaternary tetraalkylammoniums. By itself, the only aluminophosphate structure it promotes is $AlPO_4$-tinsleyite.[10,11] In conjunction with other templates, it forms several low-dimensional aluminophosphate (section 1.2). However, in TEG it forms an ammonium phosphate salt (II-100). It appears that in the absence of water, the ammonium reacts with the phosphate and therefore cannot do so with the alumina. The addition of 5.9 moles of triethylamine to this system had no effect, and the PXRD pattern was identical to the above pattern (II-101), which is in agreement with the published results of the analogous H_2O-Al_2O_3-P_2O_5-NH_4OH-Et_3N system.[11]

2.3.3.2 Tetramethylammonium Hydroxide (TMAOH) [II-102]

TMAOH was added as its pentahydrate (97%, Aldrich). The spherical shape of the TMA molecule promotes the cuboctahedral beta-cage in zeolite synthesis,[12] as well as for aluminophosphates, forming the isostructural sodalite and $AlPO_4$-20,[5] respectively, and $AlPO_4$-12-TAMU.[13] However, the PXRD of the TEG-related product matched that of $AlPO_4$-18 (II-102). This represents the first synthesis of $AlPO_4$-18 in non aqueous conditions.

2.3.3.3 Tetraethylammonium Hydroxide (TEAOH) [II-103]

TEAOH was added as the 40% aqueous solution (Aldrich). It also led to an $AlPO_4$-18 product (II-103). No larger quaternary alkylammonium templates were utilized due to the similarity of the results of TMAOH and TEAOH to previously reported materials.

2.3.4 π-Conjugated Cyclic Amines

2.3.4.1 Pyrrole (C_4H_4NH) [II-104]

Pyrrole (98%, Aldrich) is the five-ring analog of pyridine, and was therefore used to compare results. The product gave an unknown PXRD pattern (II-104). The crystals were of poor quality and very small size, and consequently this system was not further explored.

2.3.4.2 Pyridine (C_5H_5N) [II-105 to II-110]

By far, this was the most successful π-conjugated amine and allowed for some interesting results. The first synthesis performed with TEG as solvent yielded a majority phase of berlinite and a trace amount of large, orthorhombic crystals which could visually be seen in the product (II-105). One such crystal was isolated from the product and its structure solved SC-XRD data (section 3.5). The structure, denoted UT-6, is a partially fluorinated aluminophosphate framework, $[Al_3P_3O_{12}F]^-[C_5H_5NH]^+ \bullet 0.15(H_2O)$. The remarkable aspect of this result was that no source of fluorine was added to the synthesis mixture. Evidently, fluorine was present in the Teflon liner and was released during the synthesis. It is likely that it had been adsorbed into its pores from the HF acid bath used between syntheses (section 2.1.4). The often annoying porous properties of Teflon[2,14] proved to be quite valuable in this case in isolating a new fluoroaluminophosphate framework structure.

Indeed, the purposeful addition of fluorine in the form of hydrogen fluoride-pyridine yielded UT-6 in pure phase, with a greatly reduced crystal size (II-106). The introduction of fluorine from the liner is further corroborated by the following: use of a new liner, not yet exposed to the HF acid bath, yielded only the previously reported layered aluminophosphate containing interlamellar pyridinium[15] (II-107), as was the initially expected product. Not even an impurity amount of UT-6 is present. The result of producing a trace amount of UT-6 in a majority phase of berlinite without adding any source of fluorine was reproduced under semi-aqueous conditions at 180°C (II-108), while 200°C yielded only berlinite.

With the UT-6 structure solved, its PXRD pattern was checked with previous experiments. It then became clear that in the pyridine solvent system, having been extensively studied in prior years, UT-6 was repeatedly being synthesized under various conditions (II-109, II-110). The UT-6 structure was forming if no template was added to the pyridine solvent (II-109), or in the presence of triethylamine (II-110), which was added for the purpose of acting as

template and evidently did not do so. UT-6 was also synthesized inadvertently several times by Susan Nadimi during experimentation in the pyridine solvent-aluminophosphate system.[14]

In the absence of HF-pyridine for the experiment of II-110, triethylamine-templated phases were obtained (II-92 and II-93, section 2.3.2.3.8), which again displays the important role of fluorine. The stronger templating power of cyclohexylamine is displayed by the result that replacing the triethylamine with cyclohexylamine forms cyclohexylamine-related phases (II-154, section 2.3.5.12).

2.3.4.3 (3,5)-Lutidine ($Me_2C_5H_3N$) [II-111]

Since pyridine proved to be a successful template, 3,5-lutidine (Lancaster) was chosen as template, as it is closely related to pyridine, with methyl groups on two carbons of the six-ring. However, the product was berlinite (II-111). As was seen for the pyridine system, conditions could have been too hydrolytic or dilute to form a templated phase. It would be interesting to see through further experiments if any of the several isomers of lutidine could form a novel structure, in light of the success of pyridine.

2.3.4.4 (4)-Aminopyridine ($NH_2C_5H_4N$) [II-112]

Also chosen for its likeness to pyridine, this organic (98%, Aldrich) may be considered as similar to an alkylenediamine, where the alkyl chain of the alkylenediamine is instead a phenyl ring. The product was a poorly crystalline unknown phase of very small crystal size (II-112).

2.3.4.5 Benzylamine ($C_6H_5CH_2NH_2$) [II-113 to II-115]

As observed below for the cycloalkylamines, 14 moles of TEG formed a too concentrated synthesis mixture. With 28 moles of TEG, the benzylamine (99%, Aldrich) system formed several unknown materials, depending on temperature. The similarity of the 150°C product (II-113) to the cycloalkylamine aluminophosphate chain structures below makes it likely that this is the isostructural compound containing interlamellar benzylammonium. Therefore, this is a candidate for Rietveld refinement of PXRD data.

At 180°C, another unknown material is formed, possibly a layered structure (II-114). At still higher temperatures, trace amounts of this second unknown phase are present, and the dominant phase becomes a third unknown (II-115). The products of this system formed crystals which at first appeared of large size and good quality. However, a crystal from II-114 mounted

on the diffractometer was not of sufficient quality to give rise to diffraction. Closer inspection shows that many of the crystals are multi-crystalline aggregates.

2.3.5 Saturated Cyclic Amines

2.3.5.1 N,N-Diethylcyclohexylamine ($Et_2NC_6H_{11}$) [II-116]

This template (97%, Aldrich) was chosen as a logical bridge between triethylamine and cyclohexylamine. The system with TEG as solvent formed $AlPO_4$-5 with an impurity amount of $AlPO_4$-cristobalite at 180°C (II-116) and $AlPO_4$-tridymite at 220°C. It is interesting to note the difference in results to the cyclohexylamine system and the triethylamine system, and the effect of the two N-ethyl groups. Cyclohexylamine formed layered structures under such conditions (section 2.3.5.12).

2.3.5.2 (2,3)-Dimethylcyclohexylamine ($Me_2C_6H_9NH_2$) [II-117]

Unlike cyclohexylamine, all temperatures probed for this template (99%, Aldrich) from 150°C to 220°C formed the same unknown material in TEG (II-117). A small number of large plates were observed in the powder, and should allow the solution of its structure. However, the only crystal that was isolated to date for SC-XRD was not of sufficient thickness to allow collection of a data set.

The same material was also prepared from a PEG 600 solvent. An EG solvent at 180°C gave a small amount of this material, with a majority $AlPO_4$-5 phase, while 220°C yielded pure-phase $AlPO_4$-5.

The resemblance of the unknown PXRD pattern to the cycloalkylamine chain structures, below (sections 2.3.5.11 and 2.3.5.13), could also be easily clarified by a Rietveld refinement procedure. Nonetheless, it is interesting to note the similarity of the results of 2,3-dimethylcyclohexylamine to cyclohexylamine, and the lack of similarity of N,N-diethylcyclohexylamine to both. Despite the common cyclohexylamine functionality, the nature of the amine head group plays a vital role in determining the aluminophosphate materials that form, as will become apparent in later chapters.

2.3.5.3 Morpholine ($O(C_2H_4)_2NH$) [II-118]

Morpholine (99+%, Aldrich) is analogous to the structure of piperidine (section 2.3.5.4), where the carbon of the six-ring "*para*-" to the nitrogen has been replaced by an oxygen atom. It

was reported as forming a chabazite-like aluminophosphate structure by Guth *et al.* under aqueous conditions.[16] The TEG product gave only unreacted pseudoboehmite and a single peak at 11.3Å (II-118), perhaps due to a morpholinium phosphate phase, judging by the narrowness of the peak.

2.3.5.4 Piperidine ($C_5H_{10}NH$) [II-119]

This organic imine (99%, Adlrich) is related to pyridine, where the carbons of the six ring are instead saturated. Piperidine templates both $AlPO_4$-5 and $AlPO_4$-17, as well as a layered aluminophosphate when used together with 1,5-diaminopentane[17] (section 1.2.1). Its use in TEG yielded an unknown material (II-119). The crystals were small, but the structure should be able to be solved with further work.

2.3.5.5 Hexamethyleneimine ($C_6H_{12}NH$) [II-120]

Hexamethyleneimine (DuPont, also known as homopiperidine) is related to piperidine, containing an additional methylene group to define a seven-ring. The unknown pattern of the product obtained in TEG could likely be a chain or layered structure (II-120). Large, octagonal plates were found in the product and could quite easily be solved by SC-XRD methods if they are of sufficient thickness.

2.3.5.6 Quinuclidine ($HC(CH_2CH_2)_3N$) [II-121]

The structure of quinuclidine may be considered as a piperidine ring with an ethyl group connected across the six-ring to both the nitrogen and the opposite carbon. It templates the large-pore gallium phosphate known as cloverite[18] To date, there is no known aluminophosphate analog or other compositional analog. It also promotes many $AlPO_4$-n frameworks, including $AlPO_4$-16, $AlPO_4$-17, MAPO-5, MAPO-17, MAPO-20 and MAPO-35.[5] The TEG-quinuclidine (97%, Aldrich) experiment produced another unknown pattern (II-121) and did not match any of the expected $AlPO_4$-n frameworks or cloverite. Cloverite has its first diffraction peak at 28.8Å, and in this case is *ca.* 15Å. Moreover, the rest of the pattern does not index to an aluminophosphate analog of cloverite. This is not surprising, however, as cloverite requires the addition of HF to promote its formation, where the fluoride anions reside in the double four-rings.[18]

2.3.5.7 (±)-exo-2-aminonorborane [II-122]

This cage-like amine (99%, Aldrich) is structurally similar to quinuclidine, making it an attractive candidate as a templating species. The unknown product shows excellent crystallinity (II-122). However, the crystals were very small and the structure remains unsolved. Until further experimentation is performed, it is unsure whether the product is phase-pure or is a mixture of phases.

2.3.5.8 Hexamethylenetetramine [II-123]

This template (99%, Aldrich) in TEG formed only ammonium phosphate (II-123), as the PXRD pattern was identical to the product obtained using ammonium hydroxide (II-100, section 2.3.3.1). Evidently, the template decomposed at the high synthesis temperatures of 180°C. This appears to have also occurred for a small-pore fluoroaluminophosphate framework previously reported, although the original authors made no mention of the nature of the occluded organic species.[19] Hexamethylenetetramine was initially used at a synthesis temperature of 150°C. Judging by the small size of the interior cages in the reported structure, the template must be ammonium. This was later confirmed in a reinvestigation by Férey *et al.* in an improved SC-XRD analysis[20] and solid state NMR of several nuclei (section 1.1.3.4).[21]

2.3.5.9 Cyclopropylamine ($C_3H_5NH_2$) [II-124]

Cyclopropylamine (98%, Aldrich), the smallest of the cycloalkylamines, was tried since the larger cycloalkylamines were successful. However, due to the ring-strain of the cyclopropyl ring, the molecule not surprisingly decomposed at 180°C, and the familiar ammonium phosphate material was obtained (II-124); the PXRD pattern was identical to that obtained from the NH_4OH system (II-100, section 2.3.3.1) and the hexamethylenetetramine system (II-123, section 2.3.5.8).

2.3.5.10 Cyclobutylamine ($C_4H_7NH_2$) [II-125 to II-127]

Cyclobutylamine (98%, Aldrich) was utilized subsequent to the success of the larger cycloalkylamines (see below). A crystalline product was obtained on the first attempt and appears to be multiphasic (II-125). Use of more dilute conditions, less moles of amine and lower temperature appeared to isolate one of the phases (II-126). Both dilution and higher temperatures of 180°C also showed a small peak at 28.3Å, perhaps due to another phase (II-127). At least one

crystal structure should be obtainable from this system due to the relatively large crystal sizes that were observed.

2.3.5.11 Cyclopentylamine ($C_5H_9NH_2$) [II-128 to II-146]

Several novel structures with very large crystal sizes were readily produced with this amine (99%, Aldrich). Consequently, it was the most explored of the cycloalkylamines. The chemistry taking place was observed to be similar to that of many of the other cyclic amines, particularly the larger cycloalkylamines, and information obtained from this system may be, at least partially, projected to others.

As previously mentioned, not only does the alumina exist as solid particles in the slurry of the synthesis mixture prior to its heating, but in many cases the phosphate and amine do so as well, as solid particles of an alkylammonium phosphate phase. More intriguing is the complete lack of mention of such phosphate salts in the aluminophosphate literature, the only exception being the report of Bibby and coworkers,[22] where they propose the existence of dipropylammonium dihydrogen phosphate (section 1.5). The alkylammonium phosphates have only been dealt with in a series of unrelated papers where the structures were purposely synthesized (section 1.5).

It will be seen that the phosphate and amine can self-assemble into a lamellar phosphate salt structure only if the conditions are correct, such as reagent concentrations or the proper size and shape of the template. In these structures, the hydrophobic alkyl tails define a hydrophobic interlayer region and the ammonium head groups hydrogen bond to the phosphate layers.

That not all templates can achieve this is reflected in the results of the triethylamine system, where no salt material is formed under normal synthesis conditions (II-96, section 2.3.2.3). Evidently, the shape of the triethylamine molecule is not suitable to readily form a phosphate salt. Moreover, triethylamine is tertiary and therefore cannot be involved extensive hydrogen bonding. However, the cycloalkylamines are primary and have an amphiphilic character which is not as strong as, but is comparable to, the primary alkylamines that will be discussed in Chapter 5 (Figure 2-3).

Consequently, the starting mixture is comprised of a cyclopentylammonium monohydrogen phosphate structure, and strongly diffracts in the PXRD pattern of the synthesis mixture prior to heating (II-128). The small crystals that form in the TEG slurry (see SEM) are soluble in water, and large crystals were grown by recrystallization from a methanol-water

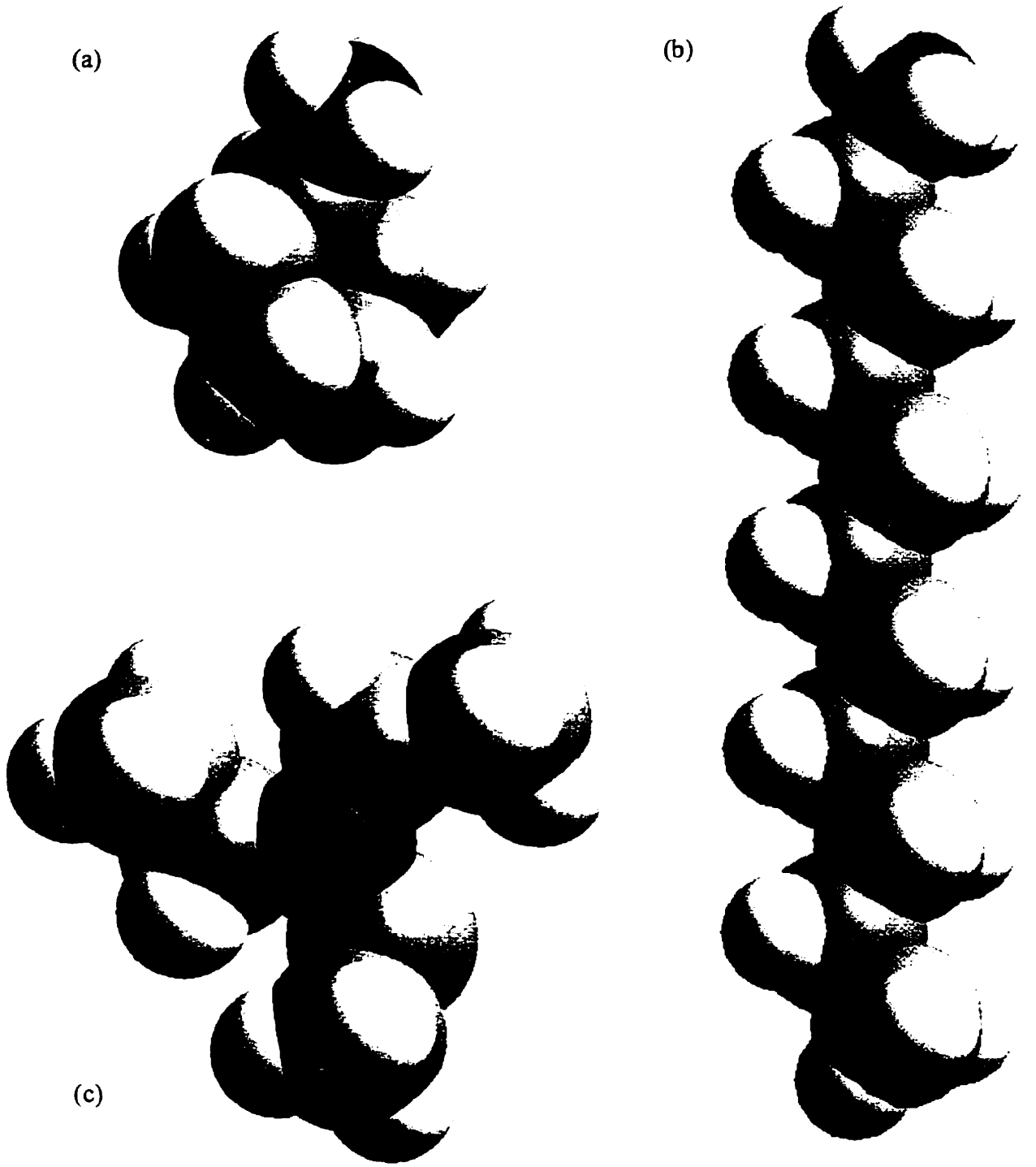

Figure 2-3. Space-filling view of three different templates. Nitrogens are shaded black. (a) Cyclopentylamine. (b) Decylamine. (c) Triethylamine.

solution (II-129), whose PXRD pattern was identical to that of II-128. Its structure was solved by SC-XRD (section 3.6), and a theoretical PXRD pattern also matched that of II-128.

Heating the TEG-alumina-phosphate-cyclopentylamine starting reaction mixture at relatively lower temperatures of 100°C to 130°C gives an open, amorphous aluminophosphate material that is likely layered in nature (II-130). This material is similar to that observed by others in related systems (section 1.1.4.3). Higher temperatures of 150°C gives a mixture of this phase and a crystalline aluminophosphate chain structure (II-131), denoted UT-2, obtained in pure-phase at 180°C (II-132). The large crystals of the chain structure allowed its structure to be solved by SC-XRD methods and the material was further characterized (section 3.7).

In this series of PXRD patterns, it is interesting to note that with respect to synthesis temperature, the UT-2 aluminophosphate chain structure (which itself is comprised of chains arranged in layers) appears to grow at the expense of the amorphous, open layered material. Often, using the conditions of II-132 (i.e., 180°C), a larger amount of the latter material would be observed in the PXRD pattern. It is entirely possible that the crystalline UT-2 chain structure is formed by a reconstructive solid state transformation of the amorphous material.

Slightly higher temperatures of 200°C gave a completely different material, namely UT-3 (II-133). UT-3 is a layered aluminophosphate structure (section 3.8), and can also be produced as a pure-phase at 220°C with very large crystal size.

Reagent amounts of water were added to this system, and the same 100°C to 220°C temperature range was probed (II-134 to II-144). Results using 3.6 moles of water (H_2O:H_3PO_4 ratio of 1.0) were very similar to those when no water was added (II-134), so 10.0 moles were added and the temperature range again probed (II-135 to II-138). Results were also similar to those above, but at 200°C, the product was comprised of long needles with a very high aspect ratio (II-137). The PXRD pattern had a first peak at lower d-spacing (*ca.* 13.7Å), and at first it appeared to be a different material. However, careful inspection of the diffraction pattern implies that it is in fact the UT-3 material with a contracted unit cell. The PXRD patterns differ with 0k0 peaks, attributable to a slight contraction of the b-axis of the unit cell. This is corroborated by the fact that non aqueous conditions where no water was added, and a temperature of only 180°C, gave an identical pattern to product II-137 after five months of heating (II-139). Such a contraction under these relatively milder conditions would be expected only after such a long period of heating. Preferred orientation effects could also be a factor in the differences in PXRD

patterns. Conditions of 220°C and 10.0 H_2O gave large, thick crystals of UT-3 from which the SC-XRD data set was actually collected (II-138).

Further increase of water suppresses the formation of the UT-2 and UT-3 phases and results in other, unknown phases. For example, 50.0 moles of water added to the mixture gives several unknown materials (II-140, II-141). Some large crystals exist in the powdery product and their structures should be able to be solved by SC-XRD. Further addition of water (to 134.4 moles, 50% aqueous by volume) gave similar results, containing mixtures of these three unknown phases in varying ratios (II-142 to II-144).

The morphology of the unknown 17.5Å material obtained at 150°C as an almost pure phase (II-142) displayed monodisperse, spherical spheres (see SEM), which could be easily rolled around on surfaces as if they were ball bearings. In fact, it was difficult to keep them stationary on a slide for observation in the optical microscope. The monodispersity of the particle size could have various applications, particularly if its unknown structure is a very open microporous framework: its PXRD pattern resembles that of VPI-5, with the exception that this unknown has its first diffraction peak at lower angle. Aqueous conditions also yielded the unknown 17.5Å material (II-145). Initial Raman spectra implies that this phase could be a framework structure, comparing with those published for framework aluminophosphates. Further work would be interesting in elucidating the nature of this highly open phase.

The strong effect of fluorine is again indicated by the addition of 1.0 moles of fluorine to the synthesis mixture, in the form of trihydrogen fluoride-triethylamine (II-146). A different unknown phase (majority peak at 14.9Å) is formed at the various temperatures probed, with a higher crystallinity at 200°C.

The large amount of data collected for the cyclopentylamine system, and the results obtained will be continued in the next chapter, in the discussion of the UT-2 chain and UT-3 layered crystal structures and their characterization. The results will have direct implications with respect to the mode of formation of aluminophosphates in Chapter 4.

2.3.5.12 Cyclohexylamine ($C_6H_{11}NH_2$) [II-147 to II-155]

Cyclohexylamine (99+%, Aldrich) is a commonly used organic in molecular sieve synthesis. In aluminophosphate synthesis, it templates the $AlPO_4$-5 and $AlPO_4$-17 frameworks, and the MAPO-5, MAPO-17 and MAPO-44 frameworks with a variety of metals.[5] Its use in the

TEG system in the present work, however, led to several novel materials, of which two were solved by SC-XRD analysis.

The 130°C to 200°C temperature range was probed (II-147 to II-150). Up to 180°C, the PXRD patterns show the presence of what appears to be an open, amorphous material in the product, similar to that seen in the cyclopentylamine system, above. Co-precipitating with the products are a varying ratio of two other phases, whose 100% peaks are located at *ca.* 17.5Å and 14.2Å. At 180°C, the latter phase forms large plates (II-149) and its structure was solved by SC-XRD. The material is a layered aluminophosphate, denoted UT-4 (section 3.9). The structure of the 17.5Å phase to this point remains unknown, but could likely be a chain structure.

Higher temperatures yielded UT-4 and another phase with 100% peak at 15.3Å (II-150). A gel aging experiment gave similar results (II-151). The second phase was isolated with only a trace amount of UT-4 when the experiment mixture contained lower amounts of organic and a small amount of nickel sulfate (II-186, section 2.3.7.4). Large enough crystals of this second phase were so obtained and its structure solved (section 3.10). Interestingly, its structure, denoted UT-5, is also layered, and is isostructural to UT-3, the cylcopentylamine-templated layered material. The same experiment as II-149, but using a Teflon liner which had been pre-treated with a 16 Pyridine: 4.0 HF-Py mixture at 200°C for 6 days, also gave UT-4 and UT-5, but with a higher yield of the latter.

Addition of water to semi-aqueous conditions by volume gave, at 150°C, what appeared to be UT-4 with preferred orientation, and a smaller amount of an unknown phase with its first peak at 18.1Å (II-152). It is unclear if the latter phase is just a more crystalline version of the unknown 17.5Å phase above (II-147 to II-149). Judging by the stark differences in results between the non aqueous and semi-aqueous conditions for other related systems (such as cyclopentylamine), it is unlikely that the phases are the same, particularly in light of the fact that the yield of the 18.1Å phase increases with respect to temperature (II-152 vs. II-153), whereas the 17.5Å phase was no longer present in the higher-temperature products, even under primarily non aqueous conditions (II-150). Indeed, the 18.1Å phase was obtained as almost a pure phase at 200°C, with an even smaller amount of UT-4 after 17 days at 200°C.

The stronger templating action of cyclohexylamine as compared to other templates is revealed by the results obtained from a pyridine solvent. As seen in the pyridine system (section 2.3.4.2), the formation of pyridinium-containing phases was insensitive to the addition of 4 moles of triethylamine to the synthesis mixture; the pyridinium-containing UT-6 framework was

obtained with or without the addition of triethylamine (II-109 and II-110, respectively). However, the same experiment with 4 moles of cyclohexylamine in place of triethylamine yielded cyclohexylamine-related phases. The pyridine solvent tended to form a majority 16.5Å unknown phase (II-154). Other phases are present in the PXRD pattern, namely a 15.3Å phase and a trace amount of a phase with peaks at 18.23Å and 9.08Å. The 15.3Å phase appears to not be UT-5, but a poorly formed fluoroaluminophosphate phase, as indicated by similarity of the product to that of a TEG experiment containing cyclohexylamine and 1.0 moles of HF-Py (II-155). This again demonstrates the drastic influence of HF (e.g., comparing II-155 and II-149). It also implies that the relative templating strengths would therefore be cyclohexylamine > pyridine > triethylamine.

2.3.5.13 Cycloheptylamine ($C_7H_{13}NH_2$) [II-156 to II-164]

Cycloheptylamine (99%, Aldrich) and larger cycloalkylamines formed synthesis mixtures that thickened to a greater degree when using 14 moles of TEG. In fact, the mixture could not even be stirred and the product was of low crystallinity, comprised of very small needles (II-156). Consequently, 28 moles of TEG were used in all subsequent experiments.

The initial reaction mixture contains crystalline cycloheptylammonium-phosphate and pseudoboehmite (II-157). The product from 150°C was large plates (II-158), and its structure, denoted UT-7, was solved by SC-XRD (section 3.11). It proved to be an aluminophosphate chain isostructural to UT-2. The structures differ only in their interlayer spacing due to the difference in size of carbon rings.

A small amount of another unknown material with 100% peak at *ca.* 18.1Å was also present at 150°C (II-158). At 180°C and 200°C, the two phases are obtained in approximately equal amounts (II-159), while at 220°C, some UT-7 is present and another unknown is the majority phase whose 100% peak resides at 16.0Å (II-160). Both of these unknowns remain unsolved, although the 16.0Å phase of product II-160 were large plates, and further work should elucidate its structure. The similarity of these results to the cyclopentylamine system make it likely that the smaller d-spacing 16.0Å unknown (also formed at higher temperatures) is a layered material. In fact, it will be shown in the following chapter that the UT-7 material thermally transforms in the solid state to what appears to be this unknown material.

Addition of water to the synthesis mixture had a drastic effect on the products for this template. With 20.0 moles of water, the two unknown 18.1Å and 16.0Å phases occurred in

equal amounts only at 150°C (II-161). At 180°C, the 16.0Å unknown phase was isolated (II-162). Semi-aqueous conditions gave yet a third unknown 18.9Å phase, with a small amount of UT-7 present in the product from 150°C (II-163). Temperatures of 180, 200 and 220°C all gave a pure phase of this 18.9Å unknown material (II-164), and large crystal sizes. It would be interesting to observe what these unknown structures are, in light of the similarity of the results and the isostructuralities among the cyclopentylamine, cyclohexylamine and cycloheptylamine systems.

2.3.5.14 Cyclooctylamine ($C_8H_{15}NH_2$) **[II-165 to II-173]**

Very similar results were obtained with this organic template (97%, Aldrich). As was observed for cycloheptylamine, only 14 moles of TEG creates conditions that are too concentrated for a fluid mixture, and the starting gel became more like a solid (II-165). 28 moles of TEG and 150°C gave the same PXRD pattern as II-165, but with some larger crystals (II-166). Temperatures of 180°C to 220°C produced similar products. A number of larger plates, obtained in small yield at 180°C after 3 days, were larger in size with 14 days of heating at 180°C. Perhaps with even longer times, large enough crystals could be isolated to solve the unknown structure.

In order to try and induce larger crystals to form, the amount of template was reduced in an attempt to lower the levels of supersaturation, or to make the reaction mixture less viscous, and perhaps more able to transport solution species to the growing crystals. Only 180°C and 220°C were probed, since larger crystals were formed at 220°C in the above experiments. However, 2.9 moles of cyclooctylamine (a molar reduction of 50%) produced the same 17.2Å material with similar crystal sizes (II-167). The template was then further decreased to 0.9 moles, and yielded only berlinite (II-168). Evidently, the template was too dilute to act as template to the aluminophosphate species.

Another attempt at forming larger crystals was made by adding a buffer which would increase the pH of the reaction mixture and hopefully solubilize the source nutrients. However, the sodium bicarbonate which was added only served to prevent the alumina and phosphate from reacting, by forming a sodium phosphate solid product. Therefore, the alumina remained in the form of pseudoboehmite (II-169).

The semi-aqueous cyclooctylamine system was also examined, and the second, more open 18.5Å phase was isolated as a pure phase at 135°C and 150°C (II-170), with a small amount

of the 17.2Å unknown in the 180°C product (II-171). A temperature of 200°C produced mostly the latter material with only a trace of the 18.5Å phase and a small amount of a third unknown 19.5Å phase (II-172). The crystals of the 200°C product were quite large, and a crystal was mounted for SC-XRD, but diffracted poorly and must have been multi-crystalline. At 220°C, the 17.2Å phase dominates, with no 18.5Å present and a more prevalent 19.5Å phase (II-173). It is likely that this third unknown, which is beginning to appear in these semi-aqueous products from higher temperatures, could be formed as a pure phase if more aqueous or fully aqueous conditions were used.

2.3.5.15 Cyclododecylamine ($C_{12}H_{23}NH_2$) [II-174 to II-178]

The largest cycloalkylamine commercially available is cyclododecylamine; the nine-, ten- and eleven-ring cyclic amines (and larger) are not available. Cyclododecylamine (98%, Aldrich) also forms a phosphate salt in the initial synthesis mixture. Recrystallization attempts were unsuccessful in forming large crystals (II-174). It is interesting to note the large d-spacing of this material as well as the cyclododecylamine-related aluminophosphate phases that will be shown below. They are comparable to those obtained using surfactants (Chapter 5), and it is should be noted that crystalline aluminophosphate phases are still obtained in the present case, a point that will be discussed further in Chapter 5.

The use of 14 moles of TEG again forms a too concentrated, solid-like mixture and a powdery, finely crystalline product (II-175). With 28 moles of TEG at 100°C, the phosphate salt was produced (implying its higher stability over that of the other cycloalkylamine phosphate salts under these conditions) and an unknown phase with 100% peak at 21.3Å (II-176); the peak at 17.0Å is due to the same phase. The phosphate salt phase is a kinetic phase in this system, and disappeared after 1 month at 80°C, giving only the unknown aluminophosphate material. Temperatures from 130°C to 220°C all gave this same unknown phase, with only slight shifts in the PXRD peaks and changes in crystallinity with respect to temperature (II-177). All gave powders comprised of small needles (see SEM). It is interesting to note the difference in chemistry compared to the smaller cycloalkylamines. In fact, semi-aqueous conditions also gave the same, single phase, under all temperatures and times used from 80°C to 220°C (II-178), indicating its relative thermodynamic and hydrolytic stability.

The product yield was measured and the percent yield calculated for the cyclododecylamine-phosphate recrystallization experiment (II-174). This was also done for a

number of other aluminophosphate and phosphate salt syntheses (Table 2-1). The experimental yield is based on a 100% product of the expected phase, such as $[Al_2P_3O_{12}H]^{2-}[C_5H_9NH_3^+]_2$ for the UT-3 product of II-137 or $[AlP_2O_8H_2]^-[Et_3NH^+]$ for the TEG-Et_3N synthesis of II-67 (Table 2-1). The values are in an acceptable range, since a reduction of product weight is expected due to several factors. Examples are product solubility in the mother liquor, loss of material during product recovery, incomplete reaction and the formation of other phase(s) with differing stoichiometries. The percent yields for the phosphate salts are higher, attributable to the fact that the reaction occurs quickly under ambient conditions and that the product is always phase-pure.

2.3.6 Mixed Amine Systems [II-179 to II-181]

A large number of syntheses were performed using mixtures of two or more amines, in an attempt to produce a new material. Several aluminophosphates are promoted only when mixtures of amines are used,[5,17] but represent only a small fraction of the number of known structure types. The procedure typically involved the mixture of leftover synthesis gels in a desired ratio, each containing one of the respective amines. In some cases, the mixtures were prepared by adding the amines sequentially to the TEG-alumina-phosphate slurry.

Most attempts were unsuccessful, in the sense that products were multiphasic, where each phase is templated by only one amine; the amines did not combine into one material. Just a few examples of the unsuccessful mixed amine systems that were explored were: hexamethyleneimine-cyclopentylamine; benzylamine-pyridine; cyclopentylamine - 2,3-dimethylcycloyhexylamine; pyrrole-cyclopropylamine; cyclopentylamine-triethylamine; cyclopentylamine-decylamine and cyclopentylamine-dodecylamine.

However, one synthesis was successful, namely the cyclobutylamine-piperidine system, in which a layered structure formed, denoted UT-8 (II-179). A 100% yield of large crystals was obtained, and the structure was solved by SC-XRD (section 3.12).

Some of the mixed cyclic amine combinations gave products that appeared to be monophasic unknown materials of a new, crystalline structure. Examples are cyclopentylamine-cycloheptylamine (II-180) and cyclopentylamine-cyclohexylamine (II-181). Conditions other than those of II-180 and II-181 gave multiphasic products of the corresponding cycloalkylamine phases comprised of one template. These mixed cycloalkylamine systems were chosen due to the isostructurality of UT-2 to UT-7, and UT-3 to UT-5. It is possible that the same inorganic architecture was formed, but contain mixed bilayers of the cyclic amines. It would be interesting

Table 2-1. Measurements of weight and percent yields for various aluminophosphate and phosphate salt products.

Ref. #	Experiment	Expected Product[a]	Actual Yield[b]	Percent Yield[c]
II-12	14 TEG : 0.9 Al_2O_3•nH_2O : 3.6 H_3PO_4 : 5.9 Et_3N, 180°C, 7 days	JDF-20, $[Al_5P_6O_{24}H]^{2-}[Et_3NH^+]_2$	0.92g	74.6%
II-67	14 TEG : 0.9 Al_2O_3•nH_2O : 3.6 H_3PO_4 : 5.9 Et_3N, 195°C, 9 days, liner pre-treated with 2 HF-Py	Aluminophosphate Chain Structure, $[AlP_2O_8H_2]^-[Et_3NH^+]$	2.72g*	73.5%
II-129	1.11 H_2O : 9.18 mmol H_3PO_4 : 11.0 mmol $C_5H_9NH_2$, RT	Cyclopentylammonium Monohydrogen Phosphate (CMP), $[C_5H_9NH_3^+]_2[HPO_4^{2-}]$	1.15g	86.3%
II-137	14 TEG : 10.0 H_2O : 0.9 Al_2O_3•nH_2O : 3.6 H_3PO_4 : 5.9 $C_5H_9NH_2$, 200°C, 1 day	UT-3, $[Al_2P_3O_{12}H]^{2-}[C_5H_9NH_3^+]_2$	2.15g*	74.5%
II-141	14 TEG : 50.0 H_2O : 0.9 Al_2O_3•nH_2O : 3.6 H_3PO_4 : 5.9 $C_5H_9NH_2$, 200°C, 25 days	Unknown 11.7Å phase, 11.4Å phase	2.06g*	Unable to calculate, unknown
N/A	14 TEG : 0.9 Al_2O_3•nH_2O : 3.6 H_3PO_4 : 4.6 $C_6H_{11}NH_2$, 180°C, 4 days, liner pre-treated with 4 HF-Py	UT-4, $[Al_2P_3O_{12}H]^{2-}[C_6H_{11}NH_3^+]_2$, UT-5, $[Al_2P_3O_{12}H]^{2-}[C_6H_{11}NH_3^+]_2$	1.53g	82.4%
II-164	14 TEG : 134.3 H_2O : 0.9 Al_2O_3•nH_2O : 3.6 H_3PO_4 : 5.9 $C_7H_{13}NH_2$, 220°C, 4 days	Unknown layered material, $[Al_2P_3O_{12}H]^{2-}[C_7H_{13}NH_3^+]_2$, isostructural to UT-4 or UT-5	0.93g	79.4%
II-174	1.1 H_2O : 11.0 mmol H_3PO_4 : 11.0 mmol $C_{12}H_{23}NH_2$, RT	Cyclododecylammonium Monohydrogen Phosphate, $[C_{12}H_{23}NH_3^+]_2[HPO_4^{2-}]$	2.15g	88.8%

[a]As established by PXRD of the product.

[b]Yield of product is dependent on the capacity of the reaction vessel, which was 15 ml, except for those denoted by an asterisk, indicating 45 ml. Also based on degree of filling, which was typically 65%. Yield of phosphate salts are based simply on the amounts of reagents used.

[c]Calculation based on the formula of the expected product.

to obtain the crystal structure of these materials, and observe in what manner the cyclics reside in the structure: randomly distributed; separated to define interlamellar regions alternating with each cyclic amine; or possibly arranged into mixed bilayers with one cyclic comprising one half of the bilayer, and the other cyclic comprising the other half. However, the crystal sizes were typically very small, with the exception of II-181.

2.3.7 Metal Aluminophosphate and Metal Phosphates [II-182 to II-188]

There is an extensive amount of literature involving framework substitution of metal sites in aluminophosphates (section 1.1.3.3).[5] Most research has been directed towards replacing aluminum sites with various elements to introduce charge to the framework, and consequently acid sites, for a variety of applications. Attempts to construct new materials from the TEG system were unsuccessful, and each metal will be discussed briefly in turn below. This is not discouraging, however, as it provides supporting data for the mode of formation studies that will be discussed in Chapter 4.

2.3.7.1 Silicoaluminophosphates [II-182]

The most studied metal substitution into $AlPO_4$-n structures is silicon, to give materials denoted SAPO-n. However, addition of silica in the form of Ludox AS-40 (DuPont) had no effect on the products. Only JDF-20 and the chain structures were obtained from the triethylamine system (II-182). It is unlikely that any silicon has substituted into the structures. A white powder, not usually present in the aluminophosphate products, could be seen mixed with the JDF-20 and chain crystals, and is likely amorphous silica.

2.3.7.2 Iron Phosphates, Iron Aluminophosphates [II-183 to II-184]

Attempts at forming open iron phosphates from the TEG system were not successful (II-183). Part of the problem could be due to the low solubility of the iron oxide source, which was Fe_2O_3. Better results may have been obtained using a more soluble source of iron, such as iron acetate.

The large-pore framework cacoxenite was a target material,[23] which contains a high Fe:Al ratio (section 1.3.2). A similar ratio was used to try and induce formation of this material (II-184). However, a poorly crystalline dense-phase iron phosphate was the majority phase, with a

small amount of an unknown material whose 100% peak was at 10.8Å. Further experiments with a more suitable iron source are necessary to deduce the nature of this unknown material.

2.3.7.3 Cobalt Aluminophosphates [II-185]

Cobalt is also a well-studied metal for substitution into aluminophosphate frameworks, substituting randomly into several frameworks such as $AlPO_4$-5 and $AlPO_4$-34.[5] Cobalt is also present in the MeAPO-46 and MeAPO-50 frameworks in a crystallographically defined position throughout the framework, capping the opposite side of the six ring of the $AlPO_4$-5-like layer (section 4.2.6). An experiment analogous to those that produce the CoAPO-n materials was performed in TEG (II-185). The blue powdery products were JDF-20 and CoAPO-34. No new materials were formed, nor was a metal-substituted chain structure.

2.3.7.4 Nickel Aluminophosphates [II-186]

Nickel has been observed to form novel crystalline structures with aluminophosphates, incorporating into the inorganic architecture (section 1.1.3.3). Nickel (II) sulfate hexahydrate (99%, Aldrich) was added to a TEG-cyclohexylamine experiment, but was not included into the aluminophosphate phase (II-186). Only the cyclohexylamine-templated layered structure UT-5 was observed. However, the UT-5 crystals were larger than those obtained in the absence of the nickel reagent, and allowed the structure to be solved by SC-XRD (section 3.10). Presumably, the nickel precipitated as nickel oxide, which gave the product its green hue. The lack of incorporation of other metal atoms into the aluminophosphate phase is a commonly observed phenomenon.[24]

2.3.7.5 Other Metal Phosphates [II-187 to II-188]

Due to the vast number of metal phosphate chain, layered and framework materials that are now known (section 1.3), some of the corresponding metal oxides were added in place of Al_2O_3 to the TEG-phosphate-Et_3N system. Attempts at synthesizing a vanadium phosphate material were unsuccessful, giving rise to only a dense phase structure (II-187). However, a small amount of a poorly crystalline, open material was also formed. The vanadium was added as a green vanadium (III) oxide powder and was perhaps not a suitably soluble vanadium source. Similar results were obtained in trying to form an indium phosphate material (II-188). The indium (III) oxide source (Alfa) may also be insoluble in the TEG solvent. In context of the

work that will be shown in Chapter 5, it is interesting to note that the hard, dense product obtained at the bottom of the reaction chamber for II-188 contained large holes and surface impressions through the material, several millimetres in diameter.

These and other metal phosphate systems, such as molybdenum phosphate, are attractive candidates for future research due to the ever-increasing amount of low-dimensionality materials being reported. Most of these materials were synthesized under aqueous conditions. The few recent examples of successful non aqueous systems[25-27] show the potential of further exploration in this area. As was observed for aluminophosphates, there could likely be some interesting results using organothermal synthesis conditions.

2.4 REFERENCES

1. *Introduction to Catapal and Dispal Aluminas*, Vista Chemical Company: Houston, Texas.
2. Acid Digestion Bombs Bulletin 4745, Parr Instrument Company, 1986.
3. G. M. Sheldrick, *SHELXA-90*, Program for Absorption Correction, University of Göttingen, Germany, 1990.
4. G. M. Sheldrick, *SHELXTL/PC Version 5.0* (Siemens Analytical X-Ray Instruments Inc., Madison, Wisconsin, U.S.A., 1995).
5. R. Szostak, *Handbook of Molecular Sieves*; Van Nostrand Reinhold: New York, 1992.
6. (a) Q. Huo, R. Xu, S. Li, Z. Ma, J. M. Thomas, R. H. Jones, A. M. Chippindale, *J. Chem. Soc., Chem. Commun.* **1992**, 875. (b) R. H. Jones, J. M. Thomas, J. Chen, R. Xu, Q. Huo, S. Li, Z. Ma, A. M. Chippindale, *J. Solid State Chem.* **1993**, *102*, 204.
7. R. H. Jones, J. M. Thomas, R. Xu, Q. Huo, Y. Xu, A. K. Cheetham, D. Bieber, *J. Chem. Soc., Chem. Commun.* **1990**, 1170.
8. W. T. A. Harrison, T. M. Nenoff, T. E. Gier and G. D. Stucky, *Inorg. Chem.* **1992**, *31*, 5395.
9. Q. Huo and R. Xu, *J. Chem. Soc., Chem. Commun.* **1990**, 783.
10. J. B. Parise, *Acta Cryst.* **1984**, *C40*, 1641.
11. N. Bilba, A. Azzouz, N. Naum and D. Nibou, *Stud. Surf. Sci. Catal.* **1994**, *84A*, 605.
12. D. W. Breck, *Zeolite Molecular Sieves*; John Wiley & Sons: New York, 1974.
13. P. R. Rudolf, C. Saldarriaga-Molina and A. Clearfield, *J. Phys. Chem.* **1986**, *90*, 6122.
14. Souzan Nadimi, Ph.D. Thesis, University of Toronto, 1993.
15. R. H. Jones, J. M. Thomas, J. Chen, R. Xu, Q. Huo, S. Li, Z. Ma, A. M. Chippindale, *J. Solid State Chem.* **1992**, *96*, 199.

16. J. L. Guth, H. Kessler, P. Caullet, J. Hazm, A. Merrouche and J. Patarin, in *Proceedings of the 9th International Zeolite Conference,* Vol. I, eds. R. von Ballmoos *et al.*, Butterworth-Heinemann, London, 1993, pp. 215.

17. A. M. Chippindale, S. Natarajan, J. M. Thomas and R. H. Jones, *J. Solid State Chem.* **1994**, *111*, 18.

18. M. Esterman, L. B. McCusker, C. Baerlocher, A. Merrouche, H. Kessler, *Nature* **1991**, *352*, 320.

19. L. Yu, W. Pang and L. Li, *J. Solid State Chem.* **1990**, *87*, 241.

20. G. Férey, T. Loiseau, P. Lacorre and F. Taulelle, *J. Solid State Chem.* **1993**, *105*, 179.

21. G. Férey, T. Loiseau, P. Lacorre and F. Taulelle, *J. Solid State Chem.* **1993**, *105*, 191.

22. N. J. Tapp, N. B. Milestone, D. M. Bibby, *Zeolites* **1988**, *8*, 183.

23. R. Szostak, *Molecular Sieves: Principles of Synthesis and Identification*; Van Nostrand Reinhold: Toronto, 1989.

24. See, for example, J. M. Thomas, R. H. Jones, R. Xu, J. Chen, A. M. Chippindale, S. Natarajan and A. K. Cheetham, *J. Chem. Soc., Chem. Commun.* **1992**, 929.

25. T. Song, J. Xu, Y. Xhao, Y. Yue, Y. Xu, R. Xu, N Hu, G. Wei and H. Jia, *J. Chem. Soc., Chem. Commun.* **1994**, 1171.

26. A. M. Chippindale and R. I. Walton, *J. Chem. Soc., Chem. Commun.* **1994**, 2453.

27. A. R. Cowley and A. M. Chippindale, *J. Chem. Soc., Chem. Commun.* **1996**, 673.

CHAPTER 3: SINGLE CRYSTAL XRD STRUCTURES AND MATERIALS CHARACTERIZATION

3.0 INTRODUCTION

A series of new crystal structures were discovered in the course of non aqueous synthesis using cyclic amines. The structures and properties of these and other relevant materials will be the topic of this chapter. In addition to single crystal X-ray diffraction (SC-XRD), the main characterization methods employed were thermal analyses through several techniques, namely TGA, VT-PXRD, DSC and mass spectrometry (MS). The presentation will follow that of Chapter 2, using the same names and reference number system. Crystal data and refinement parameters will be summarized in tables, while fractional atomic coordinates are included in Appendix D. The aluminophosphate and phosphate-based structures containing primary alkylamines and diaminoalkanes will be discussed separately in Chapter 5.

3.1 The "Aluminophosphate Chain Structure", $[AlP_2O_8H_2]^-[Et_3NH^+]$

As was seen in the previous chapter, the TEG-triethylamine system afforded large crystals of a chain structure (II-13). The SC-XRD data was collected for this material prior to discovering that the structure existed in the literature.[1] The data proved to be almost the same as those published, slightly outside experimental error.[2] The unit cell and refinement data, for comparison, are given in Table 3-1. In the present case, the a and c axes were defined in an opposite manner to that published (due to the arbitrary choices of the respective crystallographers), while the unique b-axis of the monoclinic unit cell is the same for both studies. The chain structure was described previously in section 1.2.3.

Due to the relevance of this structure to the mode of formation studies that will be described in Chapter 4, its thermal properties were investigated. It was considered that the chain structure may behave as a solid state precursor to JDF-20 (or vice-versa, next section), as well as other aluminophosphate materials. However, heating the chain structure under vacuum led mostly to $AlPO_4$-tridymite (III-1 to III-3). Intriguingly, treatment at 300°C yielded a mixture of $AlPO_4$-tridymite and a poorly crystalline material which diffracts in the 15Å region (III-2). The transformation is hardly quantitative, but it is interesting to consider that this unknown material may in some way be related to JDF-20. Heating the chain sample in air led to $AlPO_4$-tridymite

Compound	$[AlP_2O_8H_2]^-$ $[Et_3NH^+]$	UT-1	Tinsleyite	UT-6
Empirical Formula	$C_6H_{18}AlNO_8P_2$	$Al_3O_{16}P_4R_3$	$H_9Al_2NO_{11}P_2$	$C_5H_6Al_3FNO_{12}P_3{\cdot}0.15(H_2O)$
M_r	321.14	-	314.98	467.66
Crystal size, mm	0.30×0.03×0.02	0.25×0.25×0.28	0.24×0.13×0.12	0.40×0.10×0.10
Crystal Class	Monoclinic	Trigonal	Monoclinic	Triclinic
Space Group	$P2_1/n$	P-3	$P2_1/c$	$P\bar{1}$
Temperature, K	293	173	293	293
a, Å	8.534(2)	13.072(10)	9.548(2)	9.118(1)
b, Å	13.237(2)	13.072(10)	9.567(2)	9.161(1)
c, Å	12.058(2)	10.048(10)	9.611(2)	9.335(1)
α, °	90	90	90	85.98(1)
β, °	97.29	90	103.57(3)	77.45(1)
γ, °	90	120	90	89.01(1)
V, A^3	1351.2(4)	1486.9(2)	853.4(3)	759.25(14)
Z	4	6	4	2
D_{calc}, g cm^{-3}	1.564	-	2.452	2.046
μ(MoKα), cm^{-1}	4.06	-	7.78	6.44
F(000)	660	-	640	467
ω scan width, °	1.40 + 0.30tanθ			0.59 + 0.50tanθ
range θ collected, °	3.00 to 25.00	3.12 to 29.99	2.71 to 26.30	2.23 to 26.30
absorption correction	Lorentz			Psi scans
min. and max. transmission				0.596, 0.616
no. reflections collected	2684	3111	1821	3292
independent reflections	2508	2806	1719	3087
R_{int}	0.021	0.0388	0.0487	0.0159
no. observed data [I>2σ(I)]	1775			2725
R_1 [I>2σ(I)]	0.055	0.0562	0.0409	0.0280
wR_2 (all data)	0.058	0.2144	0.1207	0.0830
weighting a,b				0.0372, 0.92
goodness of fit	3.42	0.935	1.045	1.072
parameters refined	163	168	181	232
max density in ΔF map, e $Å^{-3}$	0.940	0.661	0.627	0.454

Definition of R indices: $R_1 = \Sigma(F_o-F_c)/\Sigma(F_o)$, $wR_2 = [\Sigma[w(F_o^2-F_c^2)^2]/\Sigma[w(F_o^2)^2]]^{1/2}$

Table 3-1. Summary of crystal data, details of intensity collection and least-squares refinement parameters for the solved structures.

Compound	$[C_5H_9NH_3^+]_2[HPO_4^{2-}]$	UT-2	UT-3	UT-4
Empirical Formula	$C_{10}H_{25}N_2O_4P$	$C_{25}H_{61}Al_3N_5O_{20}P_5$	$C_{10}H_{25}Al_2N_2O_{12}P_3$	$C_{12}H_{29}Al_2N_2O_{12}P_3$
M_r	268.29	987.6	512.19	540.24
Crystal size, mm	0.12×0.26×0.32	0.40×0.35×0.08	0.32×0.30×0.11	0.52×0.50×0.21
Crystal Class	Monoclinic	Triclinic	Monoclinic	Monoclinic
Space Group	$P2_1/n$	$P\bar{1}$	$P2_1/c$	$P2_1/c$
Temperature, K	173	293	293	293
a, Å	14.197(3)	10.063(2)	9.120(3)	14.739(3)
b, Å	5.992(1)	15.447(2)	28.289(6)	18.837(4)
c, Å	16.580(3)	15.736(2)	9.010(3)	8.601(2)
α, °	90	71.72(1)	90	90
β, °	98.57(2)	80.07(1)	111.82(1)	105.89(3)
γ, °	90	79.57(1)	90	90
V, A^3	1394.7(5)	2266.6(6)	2158.0(11)	2296.7(9)
Z	4	2	4	4
D_{calc}, g cm^{-3}	1.278	1.447	1.576	1.562
μ(MoKα), cm^{-1}	2.04	3.36	4.17	3.96
F(000)	584	1040	1064	1128
ω scan width, °		0.43	0.54	1.15 + 0.85tanθ
range θ collected, °	2.90 to 25.99	2.07 to 30.02	3.07 to 30.00	2.60 to 26.30
absorption correction		ΔF method	ΔF method	ΔF method
min. and max. transmission		0.3970, 0.9775	0.1682, 0.9655	0.3372, 0.9812
no. reflections collected	2850	13680	6642	4958
independent reflections	2737	12992	6288	4637
R_{int}	0.0478	0.0309	0.0622	0.0481
no. observed data [I>2σ(I)]		8573	0.3628	3147
R_1 [I>2σ(I)]	0.0610	0.0646	0.0622	0.0604
wR_2 (all data)	0.1559	0.1871	0.2016	0.1947
weighting a,b		0.0851, 2.41	0.1161, 0.00	0.0988, 2.77
goodness of fit	0.868	1.026	1.001	1.055
parameters refined	177	532	270	284
max density in ΔF map, e $Å^{-3}$	0.337	1.021	0.689	0.705

Definition of R indices: $R_1 = \Sigma(F_o-F_c)/\Sigma(F_o)$, $wR_2 = [\Sigma[w(F_o^2-F_c^2)^2]/\Sigma[w(F_o^2)^2]]^{1/2}$

Table 3-1 (Cont'd). Summary of crystal data, details of intensity collection and least-squares refinement parameters for the solved structures.

Compound	UT-5	UT-7	UT-8
Empirical Formula	$C_{12}H_{29}Al_2N_2O_{12}P_3$	$C_{35}H_{81}Al_3N_5O_{20}P_5$	$C_{13}H_{32}Al_3N_3O_{16}P_4$
M_r	540.24	1127.84	691.24
Crystal size, mm	0.48×0.42×0.08	0.32×0.22×0.05	0.31×0.24×0.08
Crystal Class	Monoclinic	Triclinic	Monoclinic
Space Group	$P2_1/c$	$P\bar{1}$	$P2_1$
Temperature, K	173	293	173
a, Å	9.104(3)	10.118(3)	8.993(4)
b, Å	30.848(11)	15.691(4)	14.884(8)
c, Å	9.004(3)	18.117(3)	9.799(9)
α, °	90	72.91(2)	90
β, °	111.17(3)	85.18(2)	103.52(3)
γ, °	90	79.49(2)	90
V, A^3	2357.9(14)	2701.7(11)	1275(2)
Z	4	2	2
D_{calc}, g cm^{-3}	1.522	1.386	1.800
μ(MoKα), cm^{-1}	3.86	2.92	4.82
F(000)	1128	1200	716
ω scan width, °	0.45	0.82	0.51
range θ collected, °	2.50 to 25.00	2.10 to 25.00	3.10 to 60.00
absorption correction	ΔF method	ΔF method	ΔF method
min. and max. transmission	0.2530, 0.9579	0.9799, 0.4250	0.4017, 0.9667
no. reflections collected	4412	9970	3188
independent reflections	4137	9386	3033
R_{int}	0.1385	0.050	0.083
no. observed data [I>2σ(I)]	2319	5721	2259
R_1 [I>2σ(I)]	0.0976	0.0774	0.0557
wR_2 (all data)	0.2974	0.2206	0.1989
weighting a,b	0.1734, 0.00	0.0960, 5.92	0.1072, 0.00
goodness of fit	1.015	1.038	0.953
parameters refined	279	620	339
max density in ΔF map, e $Å^{-3}$	1.081	1.255	0.631

Definition of R indices: $R_1 = \Sigma(F_o-F_c)/\Sigma(F_o)$, $wR_2 = [\Sigma[w(F_o^2-F_c^2)^2]/\Sigma[w(F_o^2)^2]]^{1/2}$

Table 3-1 (Cont'd). Summary of crystal data, details of intensity collection and least-squares refinement parameters for the solved structures.

with a small amount of what appears to be the hydrated aluminophosphate mineral variscite (III-4).

It was also attempted to use the chain structure as the source reagents for aluminum and phosphorus in a typical TEG-triethylamine synthesis, subtracting out the moles of triethylamine that is present in the chain solid. However, milder conditions of 80°C simply gave unreacted chains (III-5), while higher temperatures yielded a mixture of unreacted chains and $AlPO_4$-tridymite (III-6).

Hydrochloric acid is known to promote the formation of several neutral aluminophosphate hydrates, including VPI-5, $AlPO_4$-H1 to $AlPO_4$-H4 and the variscite and metavariscite minerals.[3-5] The chain material used as a reagent in an analogous synthesis wth HCl gave a mixture of variscite and metavariscite at 100°C (III-7). At higher temperatures, $AlPO_4$-H4 was obtained (III-8). These three phases have been synthesized in the absence of any organic additive, where $AlPO_4$-H4 is favoured at higher P:Al ratios and higher temperatures.[5] This is in agreement with the results of III-7 and III-8.

Some of the $AlPO_4$-H4 crystals for III-8 were found on the walls of the liner despite the fact that all of the reagent chain crystals resided on the bottom of the liner at the beginning of the synthesis. This indicates that the material had grown by the dissolution of the chain solid and not by a solid state transformation. The orthorhombic $AlPO_4$-H4 crystals were up to 10μm in size, making it possible that this structure, which still remains unknown to date, could be solved by SC-XRD methods. The relatively large crystal size can be attributed to the slow release of nutrients into the solvent from the gradual dissolution of the chain solid.

VT-PXRD of the chain phase showed it to simply collapse to $AlPO_4$-tridymite somewhere between 100°C and 200°C. It should be noted that the heating rate of this preliminary VT-PXRD was quite rapid; a slower heating rate should be used between these temperatures to observe if any other transformations are taking place.

3.2 JDF-20, $[Al_5P_6O_{24}H]^{2-}[Et_3NH^+]_2$

The SC-XRD analysis was not performed for JDF-20, since the PXRD pattern and crystal morphology were the same as those published[6] and the PXRD matched the projected pattern from Cerius. The thermal properties of JDF-20 in the original report of the structure were only briefly mentioned, where it was stated that it transformed upon "calcination" to a mixture of

$AlPO_4$-5 and $AlPO_4$-tridymite at 500°C.[6] All attempts in the present work gave no evidence for this to occur, nor did JDF-20 calcine with its structure intact, but simply collapsed to $AlPO_4$-tridymite (III-9). VT-PXRD confirmed this result, showing JDF-20 to collapse in the 175°C region. No $AlPO_4$-5 or any other open phase even began to form in any of the thermal studies.

Use of JDF-20 as a reagent in the aqueous HCl synthesis analogous to III-7 and III-8 led to an amorphous product at 100°C (III-10), and a mixture of $AlPO_4$-tridymite and $AlPO_4$-H4 at 140°C (III-11). The observation of an amorphous phase at lower temperatures implies that JDF-20 decomposes prior to formation of $AlPO_4$-H4. The thermal data also indicates that JDF-20 is not transforming to the chain phase.

3.3 UT-1, $[Al_3P_4O_{16}]^{3-}[R^+]_3$

The large UT-1 crystals, observed to grow only a number of times from the identical experiment (II-25), was studied by SC-XRD. Data are summarized in Table 3-1, and its structure was the $AlPO_4$-5-like layer, previously shown in Figure 1-3a (section 1.2.1). In the two other reported polytypes, the interlayer regions are occupied by 1,4-diammoniumbutane[7] and 1,4-diammoniumcyclohexane.[8] However, for UT-1, the interlamellar species were disordered and could not be resolved from the data set; thus, the use of a generic "R" in the formula above.

Several attempts were made to fully solve this structure, whenever the large crystals were observed in the product. However, in all cases, the templating species could not be determined. The partial or complete disorder of interlamellar species is a commonly observed phenomenon in layered aluminophosphates.[9] It did appear as if there was some oligomeric species containing carbons and oxygens between the layers, but they would not converge during structure refinement. It is possible that protonated and/or neutral polyethylene glycol is the templating species, in a similar manner to the layered aluminophosphate containing ethylenediammonium and both singly-protonated ethylene glycol ($HOCH_2CH_2OH_2^+$) and space-filling neutral ethylene glycol ($HOCH_2CH_2OH$) between its layers.[10]

The reproducible synthesis of UT-1, albeit in trace amounts, using small amounts of hydrogen fluoride in the TEG-Et_3N system (II-70, II-71, section 2.3.2.3.7) makes it possible that UT-1 contains fluorine, present on either the aluminums of the inorganic layer or the interlamellar organic species. This would imply that the occasions on which it was obtained without the addition of hydrogen fluoride was due to the presence of fluorine impurities in the liner, as was the case for UT-6 (sections 2.3.4.2 and 3.5). This is corroborated by the fact that

UT-1 was never observed to grow when a new liner was used. Certainly, the characterization of UT-1 would aid in this respect, such as solid state NMR or chemical analysis. Unfortunately, due to the limited amount of this material that is available, UT-1 was not further characterized.

3.4 Tinsleyite, $[Al_2P_2O_8(OH)^-][NH_4^+]\bullet 2H_2O$

Crystals of tinsleyite were observed to form in the TEG-H_2O-Et_3N system under certain conditions (II-34, section 2.3.2.3.7). The SC-XRD data so obtained, summarized in Table 3-1, gave a structure identical to that previously published.[11] The framework material contains ammonium molecules in its channels which charge-balance the negative charge of the hydroxides that reside on the aluminum centres. The presence of ammonium indicates the decomposition of triethylamine, and also implies the relatively stronger templating action of ammonium over that of triethylamine, which is in agreement with the work of others in the closely related aqueous H_2O-Al_2O_3-P_2O_5-Et_3N-NH_4OH system.[12]

$AlPO_4$-tinsleyite is exclusively built of octahedral AlO_6 and tetrahedral PO_4 units (for a view of the structure, see Chapter 4, Figure 4-12c). All phosphorus centres are connected to four aluminums through the bridging oxygens. Four vertices of the aluminum octahedra are occupied by oxygens connected to phosphates. One third of the aluminum sites have their coordination sphere completed by two terminal oxygens (OH^-, H_2O) while the remaining two thirds achieve this as doubly oxygen-bridged pairs (Al-(μ-O)$_2$-Al).

The observed octahedral coordination of aluminum is not surprising, as five- and six-coordinated aluminum are commonly observed in other aluminophosphate structures (sections 1.1 and 1.2). Aluminum is octahedral in more acidic conditions, and in solution can partially exist as condensed oxide polyhedra, including Al_2O_{10} dimers.[13,14] It is therefore possible that such species exist in the mother liquor during the synthesis of tinsleyite, a point that will be discussed further in Chapter 4. Again, the low yield of this material prevented its further characterization.

3.5 UT-6, $[Al_3P_3O_{12}F]^-[C_5H_5NH^+]\bullet 0.15(H_2O)$

The UT-6 fluoroaluminophosphate framework can be obtained from a TEG (II-106) or pyridine (II-109, II-110) solvent (section 2.3.4.2). A more crystalline and phase-pure product is obtained from the latter. The structure of the material was solved from the large crystals that

grow when no fluorine was added to the synthesis, but was present in minority amounts as an impurity. The large crystals allowed for a full structure refinement (Table 3-1), including the pyridinium hydrogen and recognition of the unexpected bridging fluorine atoms, as opposed to similarly diffracting oxygen. The empirical formula $[Al_3P_3O_{12}F]^-$ reflects the negative charge of the framework, which is charge-balanced by the pyridinium cations. The structure refinement strongly implied the presence of doubly-bridging fluorines between the octahedral aluminums. Chemical analysis of the as-synthesized material confirms the presence of fluorine on the framework (3.66 wt.% F). This is further supported by the ^{19}F MAS NMR spectrum of UT-6, containing one strong peak at *ca.* -120 ppm, referenced to C_6F_6 (Figure 3-1a), comparing well to the data of Klock *et al.* (see below). Chemical analysis showed the UT-6 product to contain 13.64 wt.% C, 2.31 wt.% H, 2.19 wt.% N, 3.66 wt.% F, 18.64 wt.% Al and 17.18 wt.% P, giving a molar ratio of $Al_{3.00}P_{2.41}C_{4.93}N_{0.68}H_{9.95}F_{0.84}$.

The crystallographic view down the a-axis shows one of the three independent eight-membered ring channel systems of UT-6 (Figure 3-1b). The channels intersect to define interior cages, each containing two pyridinium cations. The overall structure of the framework is related to the aluminophosphate and metal aluminophosphate analogues ($AlPO_4$-34, MAPO-34, MAPO4-44, MAPO-47)[3] of the microporous zeolite chabazite (CHA), whose aluminum centres are exclusively tetrahedral. These aluminophosphate frameworks, collectively termed "$AlPO_4$-CHA", may be considered as a primitive array of hexagonal prisms connected by four-rings (Figure 3-2a). In UT-6, however, one aluminum of each six-ring of the hexagonal prisms is octahedral and connects to that of another hexagonal prism through not only a four-ring, as for $AlPO_4$-CHA, but also two bridging fluorines [Al-F 1.854(2), 1.894(2) Å] (Figure 3-2b). The octahedra are thereby dimerized into double-octahedra, while the remaining aluminum atoms are tetrahedral, as in $AlPO_4$-CHA. The pyridiniums are hydrogen bonded to one of the bridging oxygens of the octahedral aluminums [N-H•••O 1.849 Å].

The solid state NMR of the UT-6 material obtained from TEG showed one peak for each crystallographically unique metal atom, as expected. The ^{31}P CP-MAS NMR contained three strong and sharp resonances of equal intensity at *ca.* -8.5 ppm, -25.2 ppm and -31.1 ppm (referenced to $[NH_4][H_2PO_4]$, 400.13 MHz, 10 kHz spinning rate, 3.0 μs pulse duration and 4.0 s recycle time), and were typical for aluminophosphate materials.[15] The flourine-decoupled ^{27}Al MAS NMR showed two peaks at *ca.* 29.5 ppm and -17.9 ppm (referenced to Al_2O_3, 17 kHz

(a)

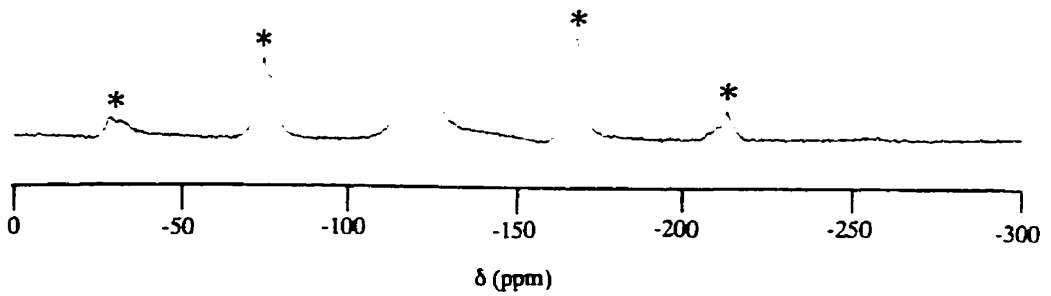

(b)

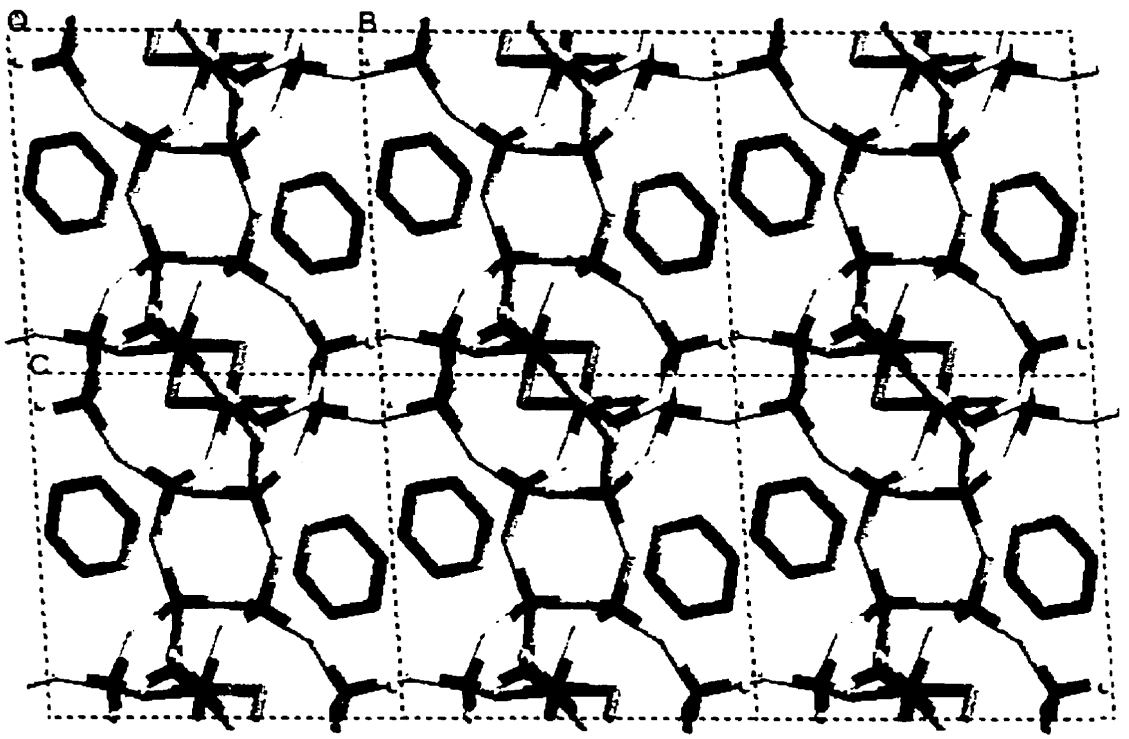

Figure 3-1. (a) ^{19}F MAS NMR of as-synthesized UT-6. Referenced to C_6F_6; asterisks denote spinning sidebands. (b) a-projection of UT-6.

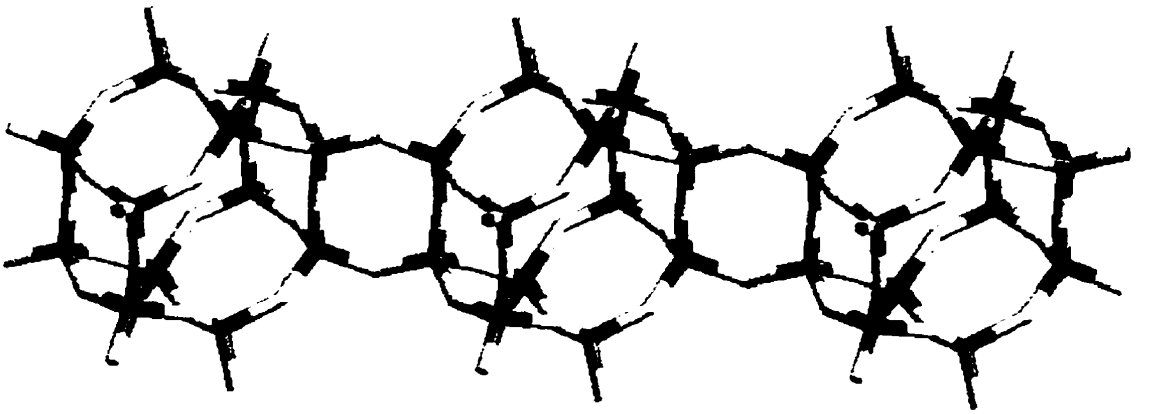

(a)

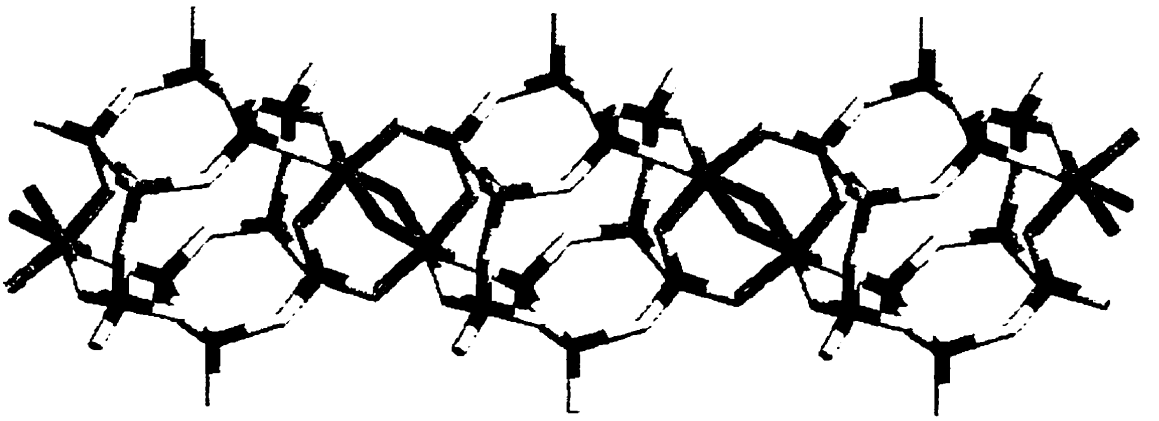

(b)

Figure 3-2. (a) The nature of the connection of hexagonal prisms through four-rings in $AlPO_4$-CHA. (b) A similar view of UT-6, and their connection through Al-(μ-F)$_2$-Al links.

spinning rate), in an approximately 2:1 intensity ratio. The former, downfield peak was resolved into two peaks by a ^{27}Al MQ-MAS experiment. The values also agree with published values,[15] where the two peaks resolved by MQ-MAS are due to the two crystallographically unique tetrahedral aluminums, and the upfield peak is due to the one type of octahedral aluminum.

Since UT-6 is a microporous framework containing large chabazite-like cages and a relatively large free aperture between the cages (eight-ring windows, *ca.* 6.5 to 6.9 Å), it should be possible to remove the extraframework organic molecules from the material. Indeed, the van der Waal size of the planar pyridinium cations is *ca.* 6.3 Å in the largest dimension. However, this would render the framework unstable, since it is anionic and is stabilized by the charge-balancing pyridinium molecules. Therefore, the negative charge of the framework would also have to be removed, or compensated for, in the process of calcination.

The TGA of the material (Figure 3-3a) shows a thermal event just above 400°C, which may be attributed to loss of the extra-framework pyridiniums and framework fluorines (observed weight loss: 20.3 wt.%; expected: 20.5 wt.%). Correspondingly, this event in the VT-PXRD shows a phase transformation from UT-6 to a fully indexable, neutral, non-fluorinated $AlPO_4$-CHA (Figure 3-3b). Mass spectrometry confirms the release of pyridine and hydrogen fluoride at these temperatures. The resulting $AlPO_4$-CHA structure is observed to still be intact at 1200°C, which is the upper operating limit of the VT-PXRD instrument. The loss of *ca.* 5 wt.% at 200°C may be attributed to the release of the water molecules that are present in the framework channels.

This was not the case for samples heated in air. The above TGA and VT-PXRD experiments use a nitrogen atmosphere (section 2.2.4). Simply heating UT-6 in air to temperatures of 250 to 500°C transforms it to a mixture of unreacted UT-6, $AlPO_4$-5 and $AlPO_4$-tridymite, the relative ratios of each depending on the heating conditions. The $AlPO_4$-CHA to $AlPO_4$-5 transformation is not surprising, as it is a well known occurrence.[16]

Since the framework is anionic, it is also possible that the cations may be ion-exchanged, as is commonly performed with zeolites. Although anionic aluminophosphate frameworks are known to exist,[11,17-19] ion exchange has not yet been demonstrated due to the restricted dimensions of their channels, which reduces the free aperture for the diffusion of molecules through the structure. The relative openness of UT-6, however, may render the material as the first example of a non metal-substituted aluminophosphate ion-exchanger.

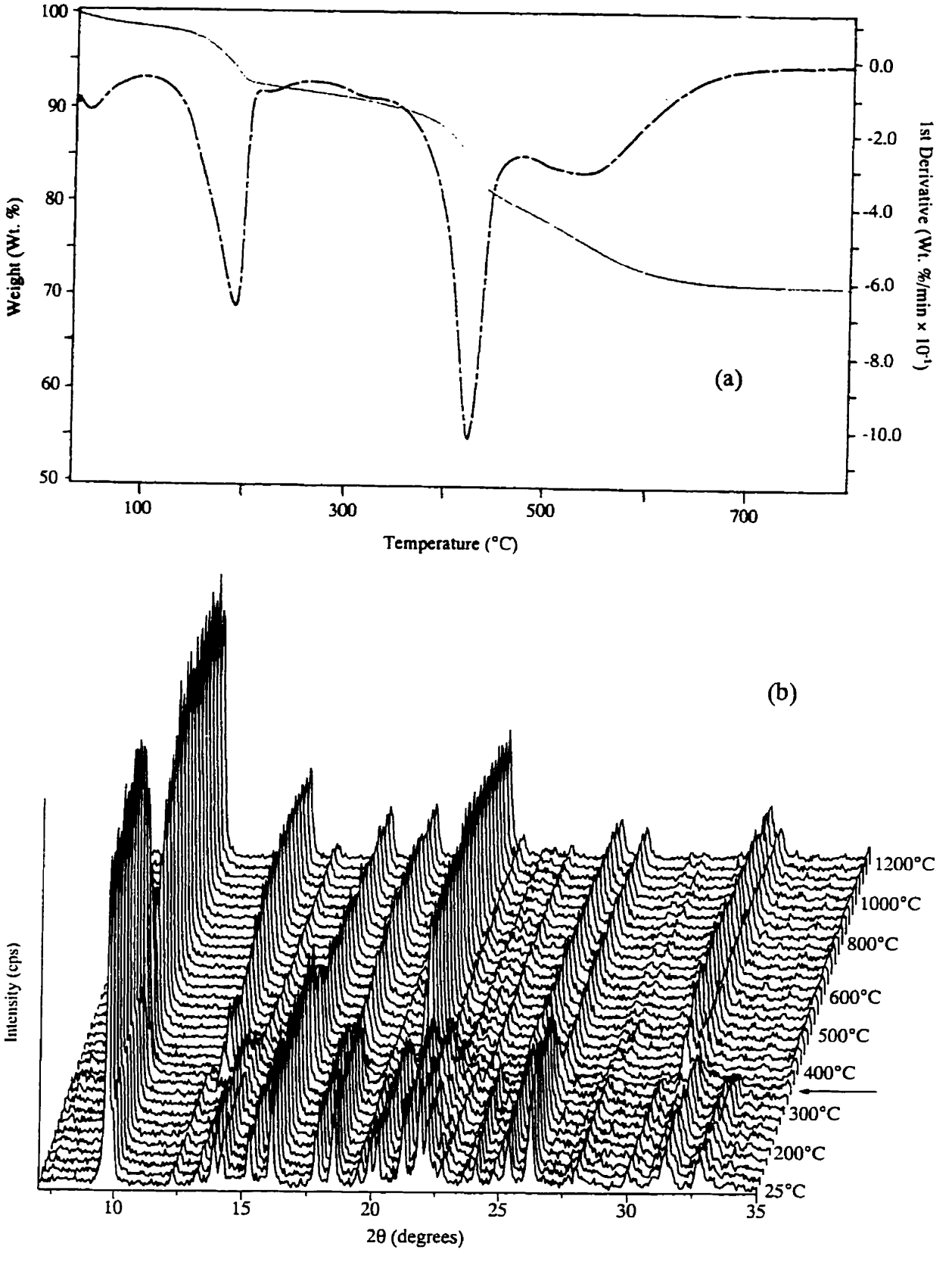

Figure 3-3. (a) TGA of UT-6. (b) VT-PXRD of UT-6.

Finally, the discovery of UT-6 provides insight into a "triclinic aluminophosphate with the chabazite-like topology" that was reported by Kessler.[20] Their material was synthesized aqueously in the presence of HF and with morpholine as a template. Based on the Rietveld refinement data, it was proposed that in this novel structure, two fluorine atoms bridge two aluminums of a four T-atom ring (T = Al, P) that connect two double six-rings of the chabazite structure, which is the case for UT-6 (Figure 3-2b). This was confirmed later by ^{27}Al MAS NMR.[21-23] The crystal structure of the material was not reported in detail in the literature and, presumably, has yet to be precisely solved. Further, the ^{19}F MAS NMR data reported by Klock *et al.*[24] agrees very well to that shown above for UT-6. It is therefore likely that their "chabazite-like" material is isostructural to the UT-6 framework, containing extraframework morpholinium rather than pyridinium.

3.6 Cyclopentylammonium Monohydrogen Phosphate (CMP), $[C_5H_9NH_3^+]_2[HPO_4^{2-}]$

This phase was observed to form in the starting TEG-cyclopentylamine synthesis mixture (II-128) and was subsequently recrystallized from water (II-129). Its structure is akin to the published alkylammonium phosphate structures[25] (section 1.5), where the phosphate molecules are arranged approximately into layers (Figure 3-4a). The cyclic amines define a bilayer-like interlayer region, similar to their arrangement in the cycloalkylamine-related aluminophosphates, below. Interestingly, for CMP, only the alpha carbon of the five-ring is stationary, and the other four carbons are distributed equally between two sites (Figure 3-4a). This is an observation of the weak nature of the hydrophobic interactions of the bilayer region, and the difference in the way in which the carbon ring defines the interlayer region versus the carbon chain of n-alkylamines (section 5.3.3).

The phosphate layers themselves contain monohydrogen phosphate hydrogen bonded into pairs (Figure 3-4b). While an extensive hydrogen bonding network exists between the phosphates and the R-NH_3^+ groups of the cyclopentylammoniums, no intralayer hydrogen bonding exists between adjacent phosphate pairs. They are only indirectly connected through hydrogen bonds to common cyclopentylammonium molecules. The CMP material decomposes in the 175°C region, as observed in its TGA trace (Figure 3-4c).

The observation of the singly-protonated monohydrogen phosphate in CMP is likely due to the relatively more basic conditions, arising from the larger mole ratios of amine used in this case (5.9 molar equivalents). The alkylamines, added in much lower ratios (typically 3.0 molar

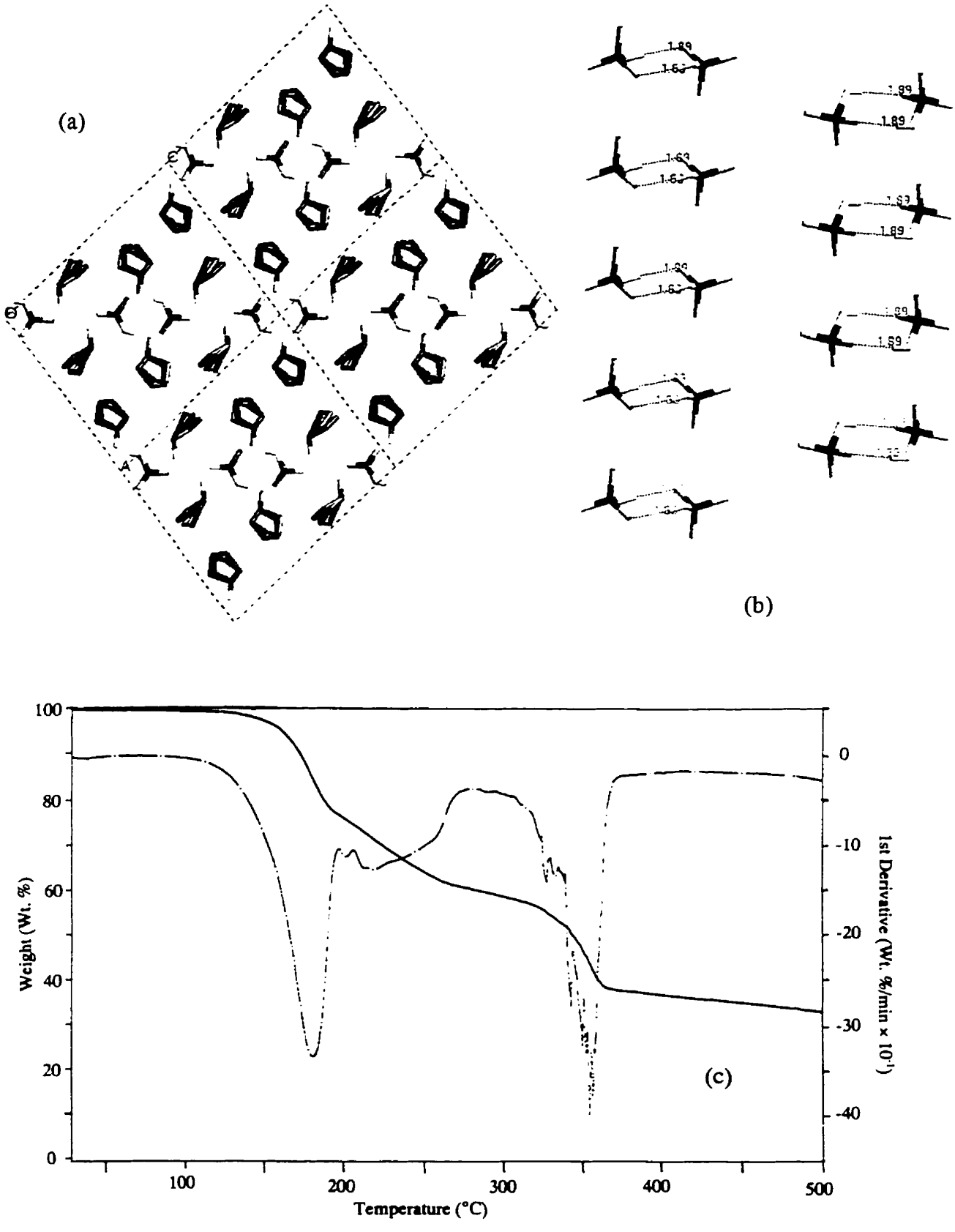

Figure 3-4. (a) b-projection of CMP. Note the bilayer arrangement and partial disorder of the cyclopentylammoniums between two sites. (b) View of CMP phosphate layer, containing hydrogen bonded dimers. (c) TGA of CMP.

equivalents), tend to form the dihydrogen phosphate salt (section 5.1.2). The basicity of the amine is also a factor in this respect, as it would necessarily affect the pH of the synthesis mixture. The size and shape of the alkyl group should also be important, since it will determine the packing of the molecules in the structure, which would in turn effect the nature of the phosphate layers. The relative basicity of the cyclopentylamine and its preference to exist in the protonated form could prevent its functioning as a neutral space-filler, as observed for 1,8-diammoniumoctane, 1,8-diaminooctane dihydrogen phosphate (DODP, section 5.1.1.5).

3.7 UT-2, $[Al_3P_5O_{20}H]^{5-}[C_5H_9NH_3^+]_5$

Large crystals of UT-2 were obtained from the TEG-cyclopentylamine system under primarily non aqueous conditions and relatively lower temperatures of 180°C (II-132). Its structure is a one-dimensional aluminophosphate chain, arranged into layers of chains (Figure 3-5a). Each chain hydrogen bonds to its two neighbouring chains through terminal P-OH and P=O groups (P-OH•••O-P distance, 1.855 Å). The crystallographic asymmetric unit contains five distinct cyclopentylammoniums, three aluminum atoms and five phosphorus atoms. UT-2 is the first aluminophosphate structure to contain a 5:3 P:Al ratio, and represents only the third reported case of an aluminophosphate chain structure. The two previously reported chain types[1,26,27] were discussed in section 1.2.3. Chemical analysis showed the UT-2 product to contain 29.84 wt.% C, 7.27 wt.% H, 6.70 wt.% N, 9.87 wt.% Al and 17.16 wt.% P, giving a molar ratio of $Al_{3.00}P_{4.54}C_{20.38}N_{3.92}H_{59.15}$.

The UT-2 chain contains three types of $P(O\text{-}Al)_nO_{4-n}$ units, where n = 1, 2 and 3. It should be noted that n = 1 represents a phosphate group with only one bridging oxygen to an aluminum and three terminal oxygens (P-OH 1.572(3) Å, $P\text{-}O_{bridging}$ 1.543(2) Å, $P{=}O_{terminal}$ 1.499(3) and 1.509(3) Å). This is the first observation of a singly-bridged, triply-terminal phosphate group among all of the reported chain, layered and framework aluminophosphate crystal structures to date. The only other metal phosphate it has been observed for is the recently reported layered indium phosphate (section 1.3.7).[28]

Extensive hydrogen bonding exists between the anionic layers of chains and the interlamellar cyclopentylammonium cations ($P\text{-}O\bullet\bullet\bullet H\text{-}N_{av}$ 2.08Å). The bilayer-like arrangement of the cyclic amines may be observed in the a-projection of UT-2 (Figure 3-5b). This view also shows the chains end-on. Unlike the CMP structure, the template molecules in UT-2 are not

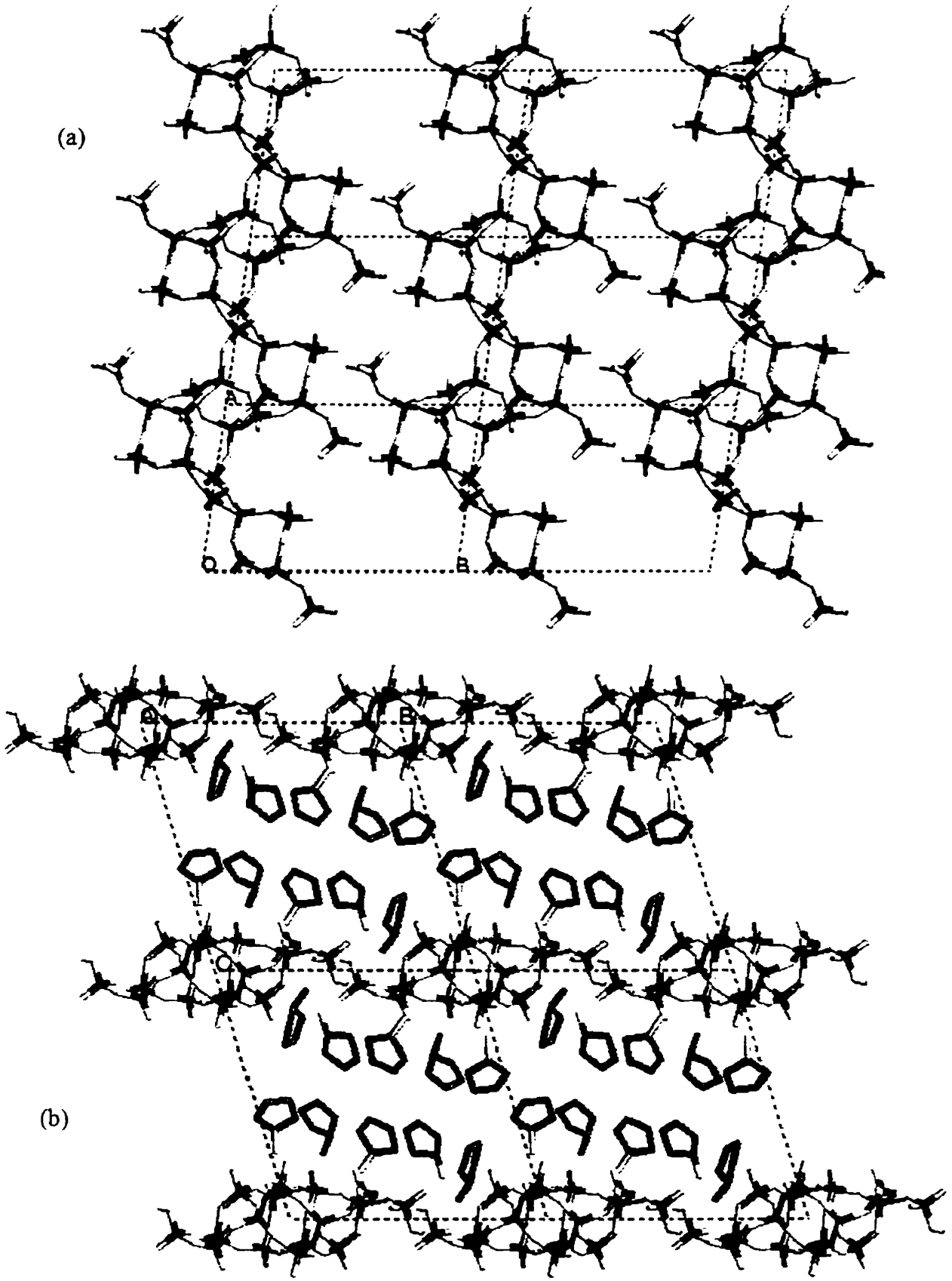

Figure 3-5. (a) c-projection of UT-2, showing one layer of hydrogen bonded chains. (b) a-projection of UT-2. In this view, the chains may be seen end-on.

disordered. The anisotropic thermal parameters were expectedly larger for the non-alpha carbons of the rings.

The repeat unit of the UT-2 chain structure may be visualized as sections of three corner-sharing four-rings, where the apices are occupied by aluminum atoms, as in the aluminophosphate chain structure of Figure 1-7a. These sections are connected to three edge-sharing four-rings in a double-crankshaft conformation to define sections of five edge-sharing four-rings. This seemingly complex architecture should become clearer when it is considered further in the mode of formation discussion of Chapter 4. In fact, prior to its discovery, this chain structure had been theoretically predicted to exist during the development of the model, and will turn out to be a highly significant structure.

UT-2 was heated in air under various conditions to study its thermal properties (III-12 to III-15). No reaction occurred after heating at 100°C, and the PXRD pattern was identical to the starting UT-2 material (III-12). At 150°C, however, a remarkable solid-state transformation occurred: the product was a perfectly clean, indexable and phase-pure UT-3. A minor amount of the contracted UT-3 material (section 2.3.5.11) was present, which became the majority phase at 175°C (III-14). These samples were ground up to a powder prior to heating them. When unground crystals of UT-2 were heated at 175°C, the uncontracted, 14.2Å UT-3 material was the majority phase (III-15). Clearly, the lower surface area of the crystals had an effect in discouraging the further reaction of the UT-3 layered structure.

This UT-2 to UT-3 chain to layer transformation is the first aluminophosphate transformation of its kind, and has several ramifications. It certainly has implications into the mode of formation of extended aluminophosphate structures (Chapter 4). It also suggests that in the various syntheses of UT-3 shown in the previous chapter (section 2.3.5.11), the UT-2 to UT-3 chain to layer transformation was being induced by one or all of the following: the addition of reagent amounts of water, higher temperatures and longer reaction time. It is also becomes clear that the UT-3 layer is the more thermodynamically stable structure, while the UT-2 chain is the metastable precursor phase.

All of the above transformation findings are confirmed by VT-PXRD studies, run in air (Figure 3-6a). The UT-2 pattern is unchanged up to 150°C, and the peaks belonging to UT-3 begin to appear at 155°C. By 165°C, the transformation is almost complete, and UT-3 then begins to collapse to $AlPO_4$-tridymite and an open, amorphous material (broad peak centred at

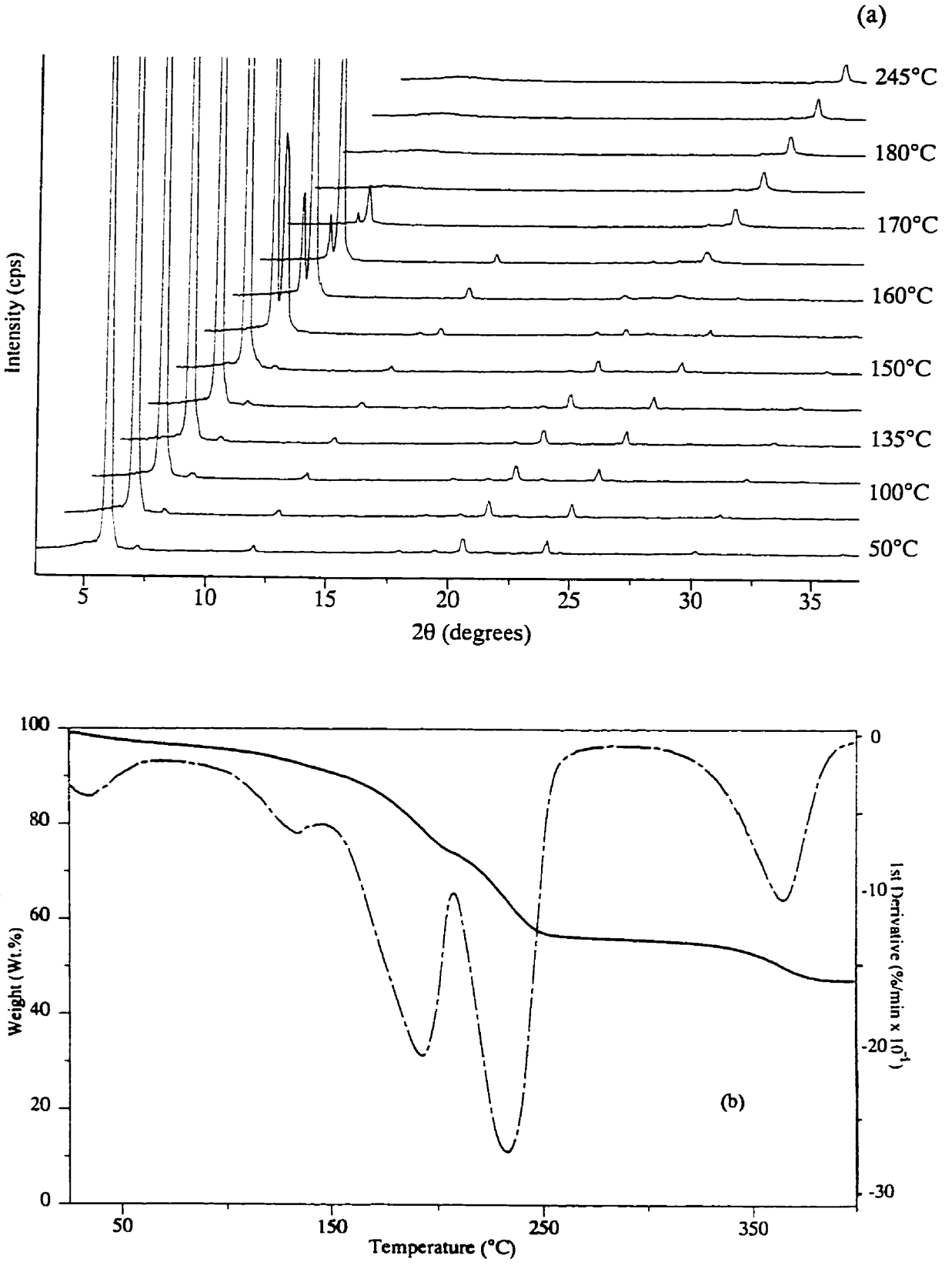

Figure 3-6. (a) VT-PXRD of UT-2. (b) TGA of UT-2.

ca. 5° (2θ)). The latter collapses by 365°C. Certainly, the UT-2 to UT-3 transformation could have gone to completion, with no accompanied collapse to $AlPO_4$-tridymite, if the temperature had been held at 150°C, as was done for III-13.

These observations may also be followed in the TGA of UT-2 (Figure 3-6b), where the first peak at approximately 180°C is attributed to the UT-2 to UT-3 transformation, and the second in the 230°C region to the collapse of UT-3. The latter peak agrees well with the TGA of UT-3 (section 3.8) The collapse of the open, amorphous material gives rise to the peak just above 350°C. The slightly higher transformation temperatures as compared to those above are due to the nitrogen flow used in the TGA apparatus. VT-PXRD studies under a nitrogen atmosphere gave similar results. Mass spectrometry at these temperatures showed the characteristic pattern of cyclopentylamine.

An experiment aimed at ion-exchanging the interlamellar species with ammonium were unsuccessful (III-16). The conditions used were obviously too basic, as all aluminophosphates are unstable in strongly alkaline medium.[29,30] Accordingly, UT-2 was observed to immediately dissolve in 40% methylamine solution. Nonetheless, ion-exchange should be possible with the correct choice of conditions and concentrations. Interestingly, the UT-2 to UT-3 transformation was not induced when heated in water. Rather, the UT-2 material decomposed after 3 days at 80°C (III-17), an indication of the hydrothermal instability of both structures.

3.8 UT-3, $[Al_2P_3O_{12}H]^{2-}[C_5H_9NH_3^+]_2$

UT-3, obtained from synthesis conditions slightly higher in temperatures and/or water content than UT-2 (e.g.: II-133, II-138), is a novel layered aluminophosphate. Chemical analysis showed the UT-3 product to contain 22.88 wt.% C, 5.50 wt.% H, 4.99 wt.% N, 12.54 wt.% Al and 19.72 wt.% P, giving a molar ratio of $Al_{2.00}P_{2.74}C_{8.20}N_{1.53}H_{23.48}$.

. The layers consist of alternating tetrahedral phosphorus and aluminum centres connected by bridging oxygens, arranged into a three-connected two-dimensional net of edge-sharing six-rings (Figure 3-7a). The four-coordination of phosphorus is completed by one terminal phosphonyl group ($P=O_{av}$ 1.477(3) Å), while aluminum completes its tetrahedron with the oxygen of an out-of-plane doubly-bridging phosphate group that connects two aluminums of the six-rings (Figure 3-7a). Only one-half of the six-rings contain this phosphate group, since this is sufficient to fully coordinate all of the aluminum centres. These phosphate groups alternate above and below the

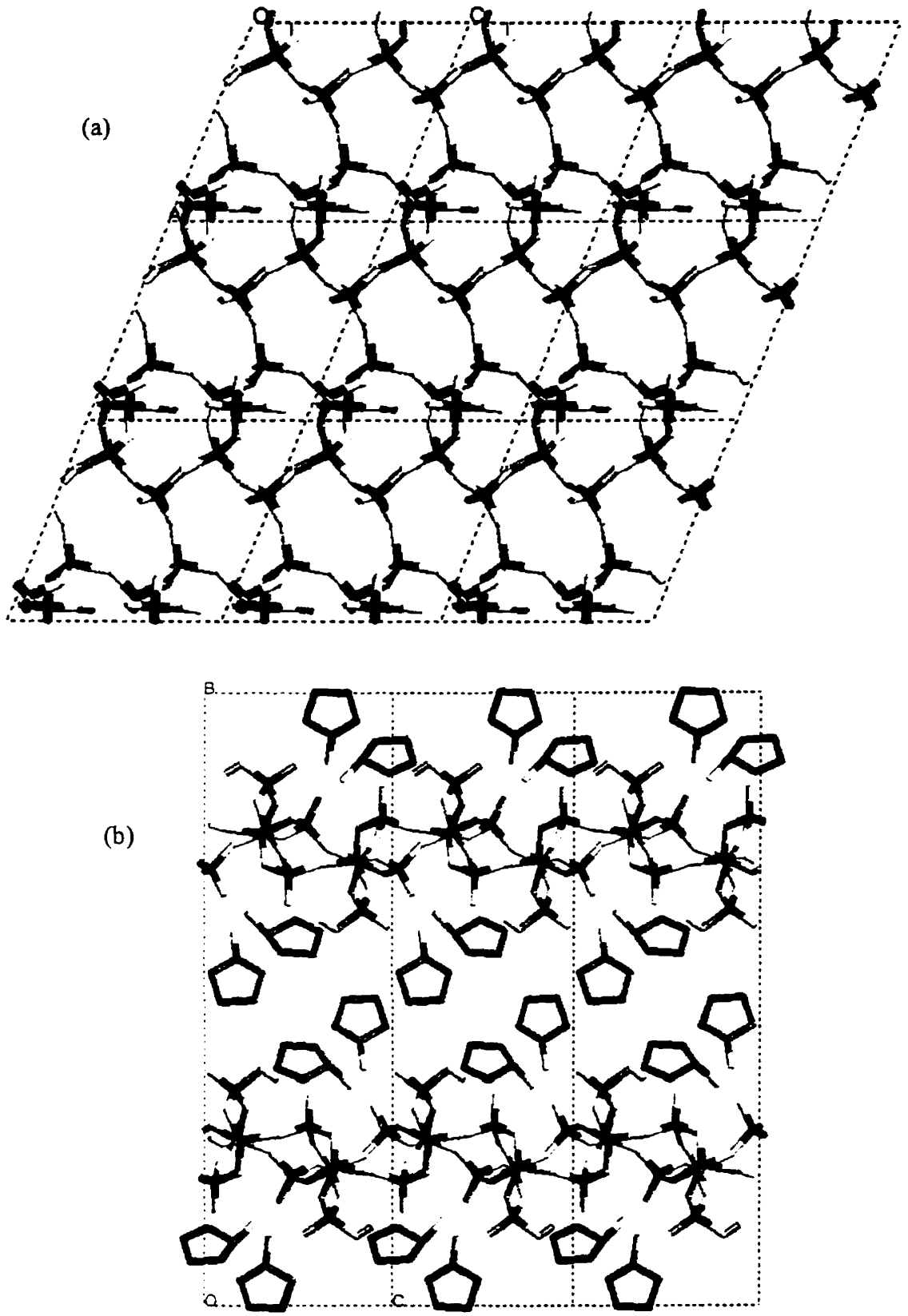

Figure 3-7. (a) b-projection of UT-3. (b) a-projection of UT-3. In this view, the doubly-bridging phosphate groups that reside above and below the plane of the layer may be seen.

plane of the layer along each row of six-rings and may be seen in the a-projection of Figure 3-7b. They each possess two terminal oxygens, one of which is protonated (P=O 1.476(3) Å, P-OH 1.551(3) Å). The P-OH group participates in an intralayer hydrogen bond to a phosphonyl group belonging to the two-dimensional net (P-OH•••O=P, 1.821 Å). UT-3 also contains cyclopentylammonium bilayers interdisposed between the anionic aluminophosphate layers, in an arrangement different from that of UT-2 (Figure 3-7b). Again, they are involved in an extensive network of hydrogen bonds with the phosphate groups (P-O•••H-N_{av} 1.994(3) Å).

Although the layer architecture is novel, it is structurally similar and stoichiometrically equivalent to a previously reported layered structure of Chippindale *et al.*[31] Inspection of the respective $[Al_2P_3O_{12}H]^{2-}[R^+]_2$ structures show the arrangement of six-rings and doubly-bridging phosphate groups to be different in each case (cf. Figure 3-7a, Figure 1-4a). It is also similar to the layer of Morgan *et al.* containing interlamellar $[Co(en)_3]^{3+}$ octahedral complexes (section 1.2.1),[32] but the aluminums of the two-dimensional net of six-rings of their layer are instead capped by triply-bridging phosphates to give a layer stoichiometry of $[Al_3P_4O_{16}]^{3-}$. UT-3 is also identical in stoichiometry but has an architecture different to that of UT-4, a layered aluminophosphate templated by cyclohexylammonium (section 3.9) and is, in fact, isostructural with UT-5, a second layer templated by cyclohexylammonium (section 3.10).

The thermal analysis of UT-3 was actually well-characterized in the previous section, since UT-3 was formed during each analysis of UT-2. The specific analysis of UT-3, however, helps to "deconvolute" the data of UT-2 and UT-3. Thermal treatment of UT-3, either as-synthesized or obtained by thermal treatment of UT-2, partially transformed it to a material with first peak at 13.3Å, and partially collapsed it to $AlPO_4$-tridymite (III-18). Comparison of the full PXRD patterns shows that this new phase is a contracted UT-3 (section 2.3.5.11). Proper heating rate and temperature should allow its isolation, as it can be synthesized in pure-phase (II-137, II-139). Heating the 13.3Å phase in air led only to its collapse (III-19).

The VT-PXRD of UT-3 shows collapse to $AlPO_4$-tridymite and an open, amorphous phase (broad PXRD reflection, *ca.* 14Å) in the region of 175°C (Figure 3-8a). This is identical to the behaviour of UT-2 subsequent to its transformation to UT-3. The VT-PXRD of the contracted UT-3 is very similar (Figure 3-8b), aside from the initial differences in the PXRD pattern (using product II-137). Heating rates were likely too rapid to resolve the subtle differences in behaviour of the two phases, although the technique has limited resolution for such

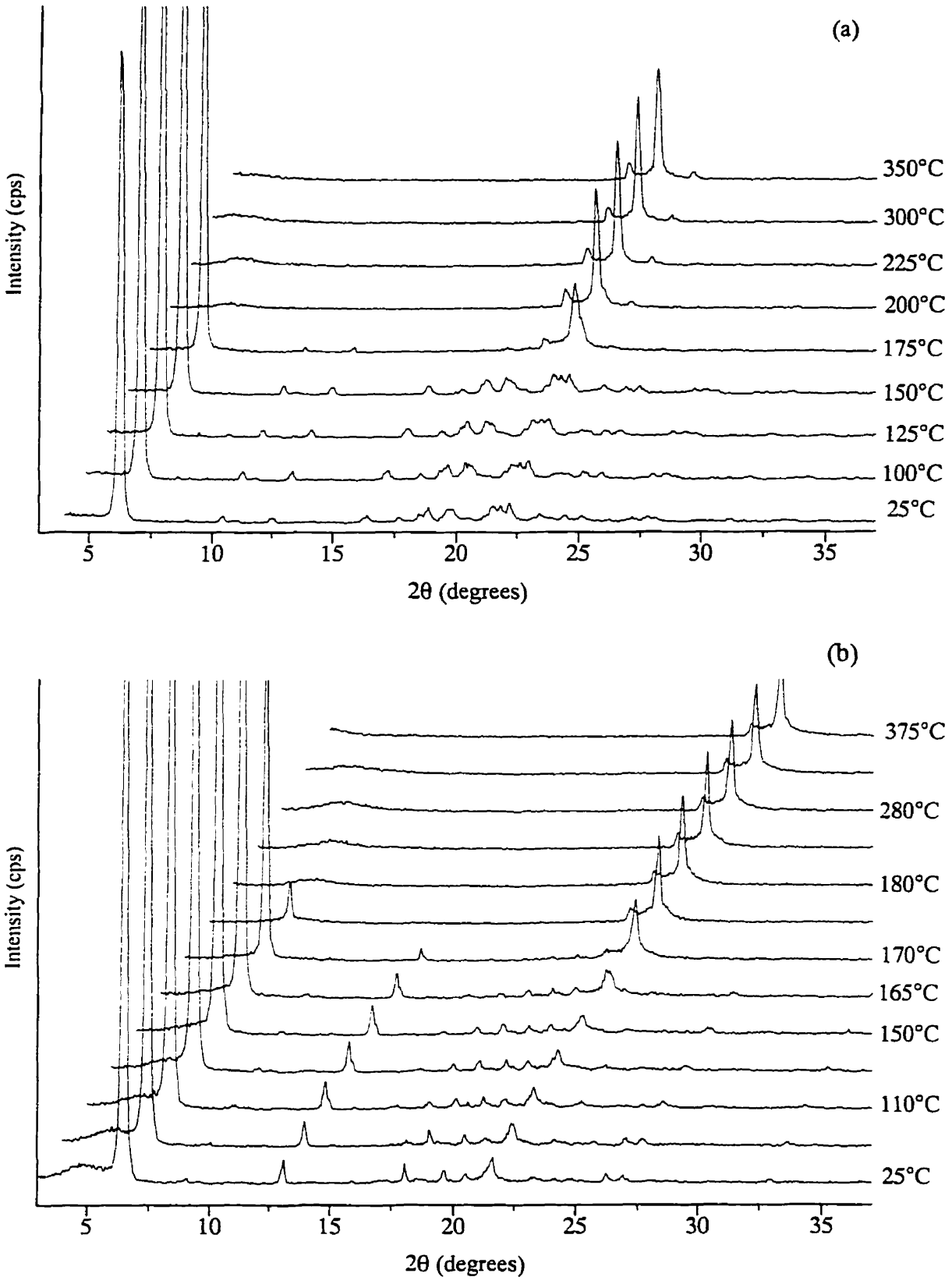

Figure 3-8. (a) VT-PXRD of UT-3. (b) VT-PXRD of "contracted" UT-3.

observation. The contracted UT-3 phase was observed to slightly expand prior to its collapse, which could imply that the contraction is reversible. Such a slight expansion would, of course, not be seen in the heating experiment of III-19 since it is not *in situ*.

The TGA traces of the two phases, however, more accurately depicts their differences (Figure 3-9a,b). The TGA analyses are nearly identical, except for the small peak at approximately 175°C in the uncontracted UT-3, which may be attributed to its contraction. Presumably, this involves some reconstruction process in which water and/or organic is removed, accounting for the observed weight loss. It should not be ruled out, however, that the "contraction" is actually forming a new layered structure (see data and discussion for UT-5, below).

For comparison, the TGA of the unknown 17.5Å phase that formed spherical aggregates of needles under semi-aqueous and aqueous conditions (e.g.: II-142, II-145, respectively) is shown in Figure 3-9c. The thermal behaviour material shows a large weight loss at 300°C, implying that the material is of higher thermal stability as compared to the various layered aluminophosphates.

3.9 UT-4, $[Al_2P_3O_{12}H]^{2-}[C_6H_{11}NH_3^+]_2$

UT-4 is another novel layered aluminophosphate, templated by cyclohexylammonium. Its layers also contain tetrahedral Al and P centres connected through bridging oxygens and are separated by double-layers of cyclohexylammonium cations. Chemical analysis showed the UT-4 product to contain 27.24 wt.% C, 5.75 wt.% H, 4.76 wt.% N, 12.04 wt.% Al and 19.15 wt.% P, giving a molar ratio of $Al_{2.00}P_{2.77}C_{10.16}N_{1.52}H_{25.57}$. The layer architecture of UT-4 may again be thought of as a two-dimensional net of three-connected Al and P centres, but where rows of edge-sharing six-rings are connected instead by four- and eight-rings (Figure 3-10a). The phosphorus atoms each possess one terminal oxygen as a phosphonyl group (P=O distances 1.487(4), 1.494(3) Å), while the fourth oxygen of the aluminum tetrahedra are defined by doubly-bridging phosphate groups that essentially "cap" the layers. These phosphate groups reside exclusively on the six rings, and alternate above and below the plane of the layers with respect to the c-axis (Figure 3-10a). Since they are doubly-bridging, they possess two terminal oxygens, of which one is protonated (P=O 1.494(3) Å, P-OH 1.552(3) Å). This P-OH group donates an intralayer hydrogen bond to an adjacent phosphate group. All of the terminal phosphate oxygens are involved in an intricate hydrogen bonding network with the bilayer of

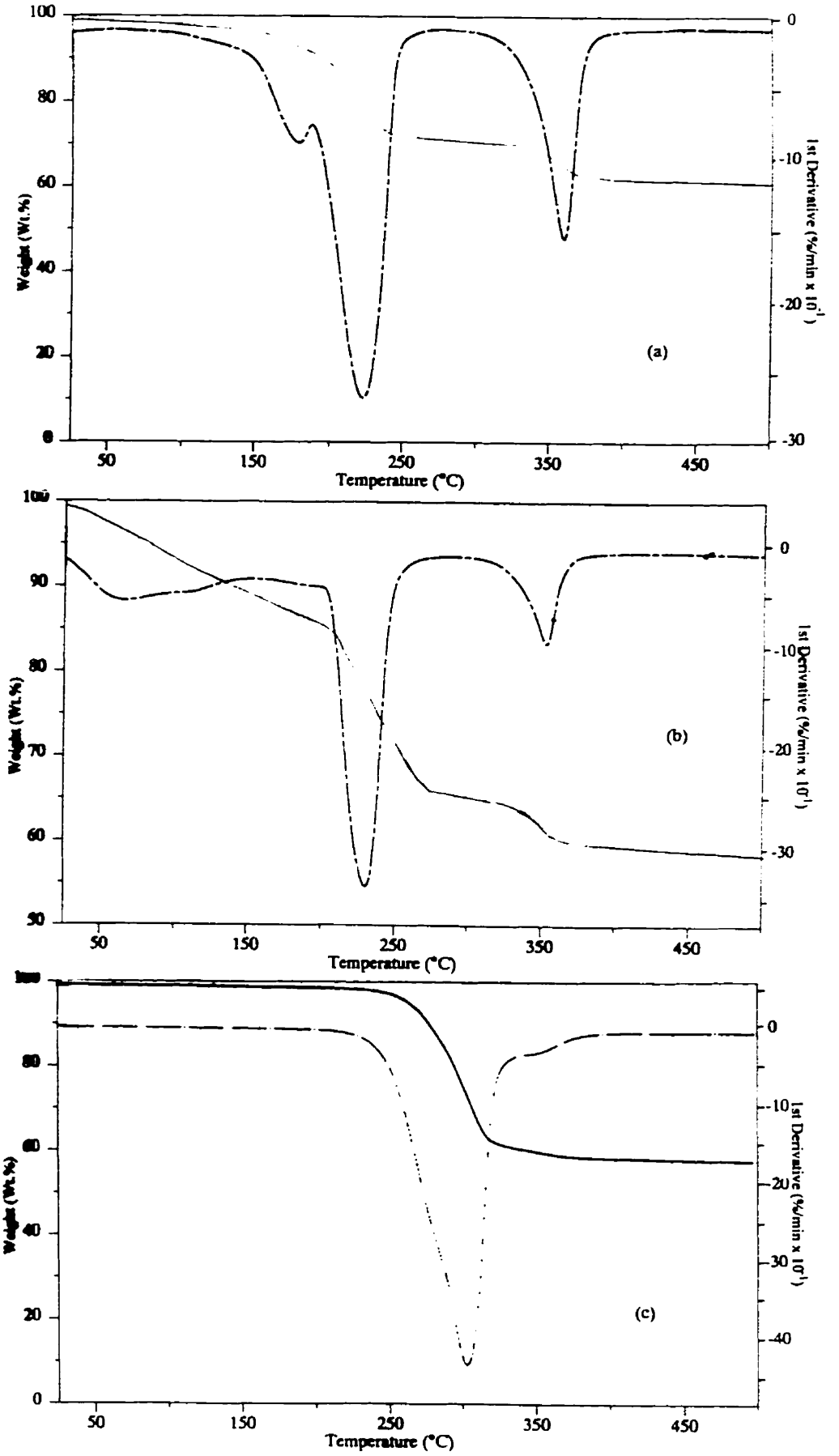

Figure 3-9. (a) TGA of UT-3. (b) TGA of contracted UT-3. (c) TGA of unknown 17.5Å phase.

(a)

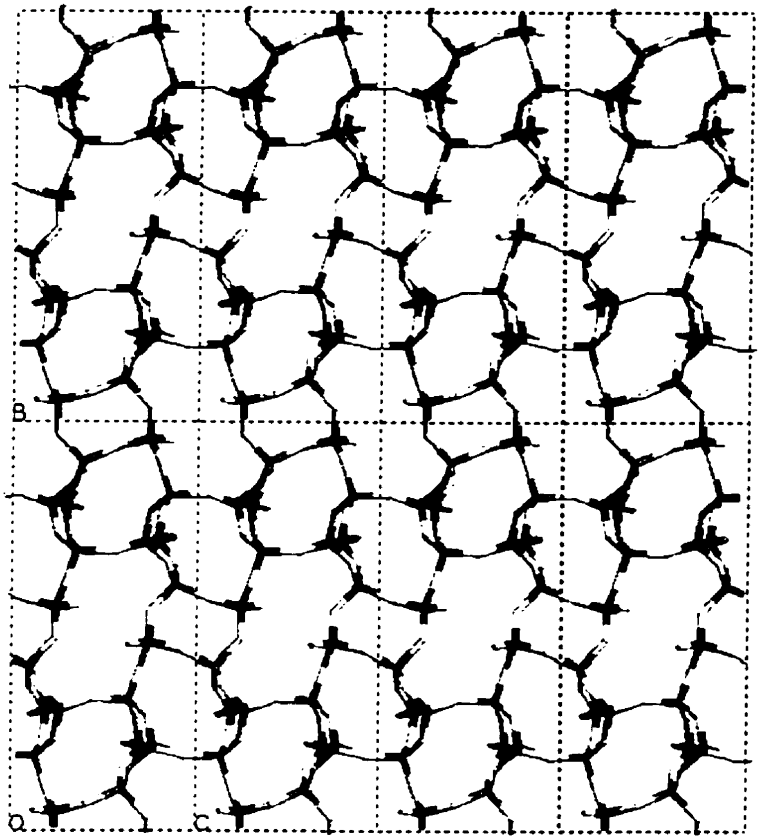

(b)

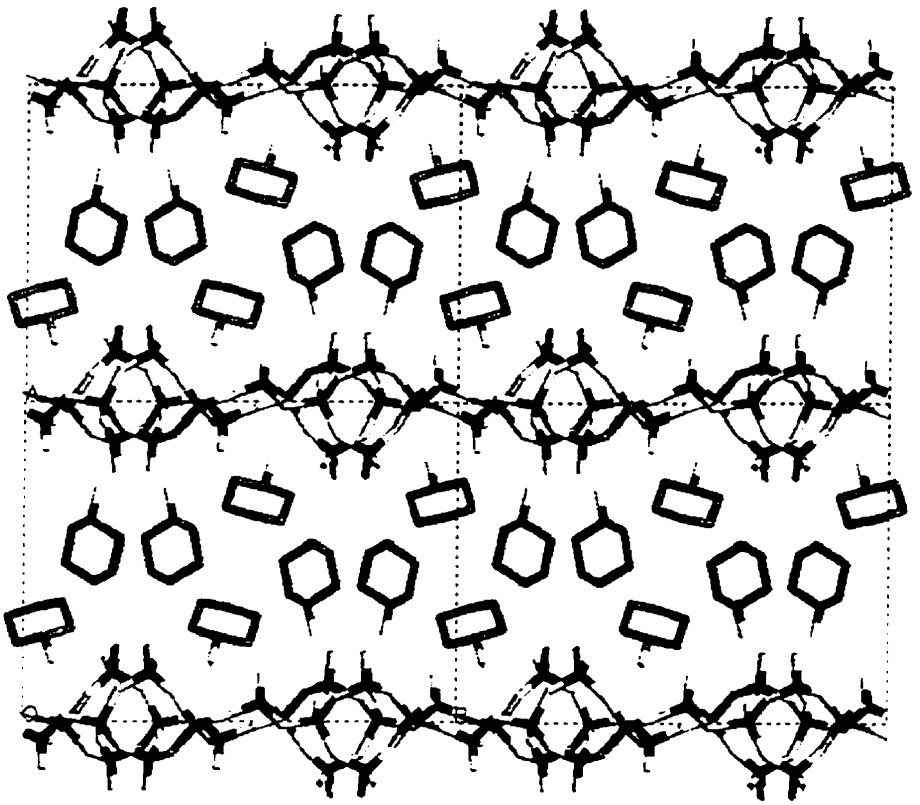

Figure 3-10. (a) a-projection of UT-4. (b) c-projection of UT-4, showing bilayer-like arrangement of cyclohexylammoniums.

chair-conformation interlamellar cyclohexylammoniums (Figure 3-10b). Each oxygen accepts two hydrogen bonds from the hydrogens of the template ammonium head groups.

UT-4 demonstrates moderate thermal stability typical of an aluminophosphate layer. While a VT-PXRD of UT-4 was not collected, its TGA shows a transformation at approximately 250°C (Figure 3-11a), which is certainly the collapse of the layer. Partial formation of an open, amorphous material must have also occurred, which collapses at approximately 350°C. No further characterization of UT-4 was performed. Based on comparison of PXRD patterns, it is possible that an unknown aluminophosphate obtained from an aqueous aluminophosphate-cyclohexylamine system[33] is in fact UT-4.

3.10 UT-5, $[Al_2P_3O_{12}H]^{2-}[C_6H_{11}NH_3^+]_2$

As previously mentioned, a second layered structure using cyclohexylammonium was obtained. UT-5 is isostructural to UT-3 (section 3.8). Chemical analysis showed the UT-5 product to contain 25.96 wt.% C, 5.64 wt.% H, 4.72 wt.% N, 11.76 wt.% Al and 21.19 wt.% P, giving a molar ratio of $Al_{2.00}P_{3.14}C_{9.92}N_{1.55}H_{25.68}$. The bilayer-like cyclic amines reside in the same positions for both structures, and are accordingly involved in an isostructural hydrogen bonding network. The hydrogen bonds are slightly longer than those of UT-3 (N-H•••O=P_{ave} 2.018(3) Å for UT-5, 1.994(3) Å for UT-3). The d_{0k0} peaks in the PXRD of UT-5 shift to lower angles with respect to UT-3 due to the expansion of the unit cell in the b-dimension to accomodate the larger carbon six-rings of the cyclohexylammoniums, as can be seen in the a-projection of UT-5 (Figure 3-12a, cf. Figure 3-7b). The values of a and c remain almost the same for the two structures, and the layers can be virtually superimposed. For a view of a layer of UT-5, one may look at that of UT-3 (Figure 3-7a).

Similarly, a discussion of the inorganic architecture would read the same as that given in section 3.8, above. For comparison, the distances of the terminal oxygens of the doubly-bridging phosphate groups are P=O 1.494(3) Å and P-OH 1.575(3) Å, which are longer than those of UT-3 (P=O 1.476(3) Å, P-OH 1.551(3) Å). While the UT-5 crystals are quite thin, diffraction was of sufficient intensity to allow anisotropic refinement of the data and location of the non-aliphatic protons.

The TGA of UT-5 (Figure 3-11b) looks almost the same as UT-4 (Figure 3-11a). VT-PXRD studies show a collapse of UT-5 to an open, poorly crystalline material which diffracts at

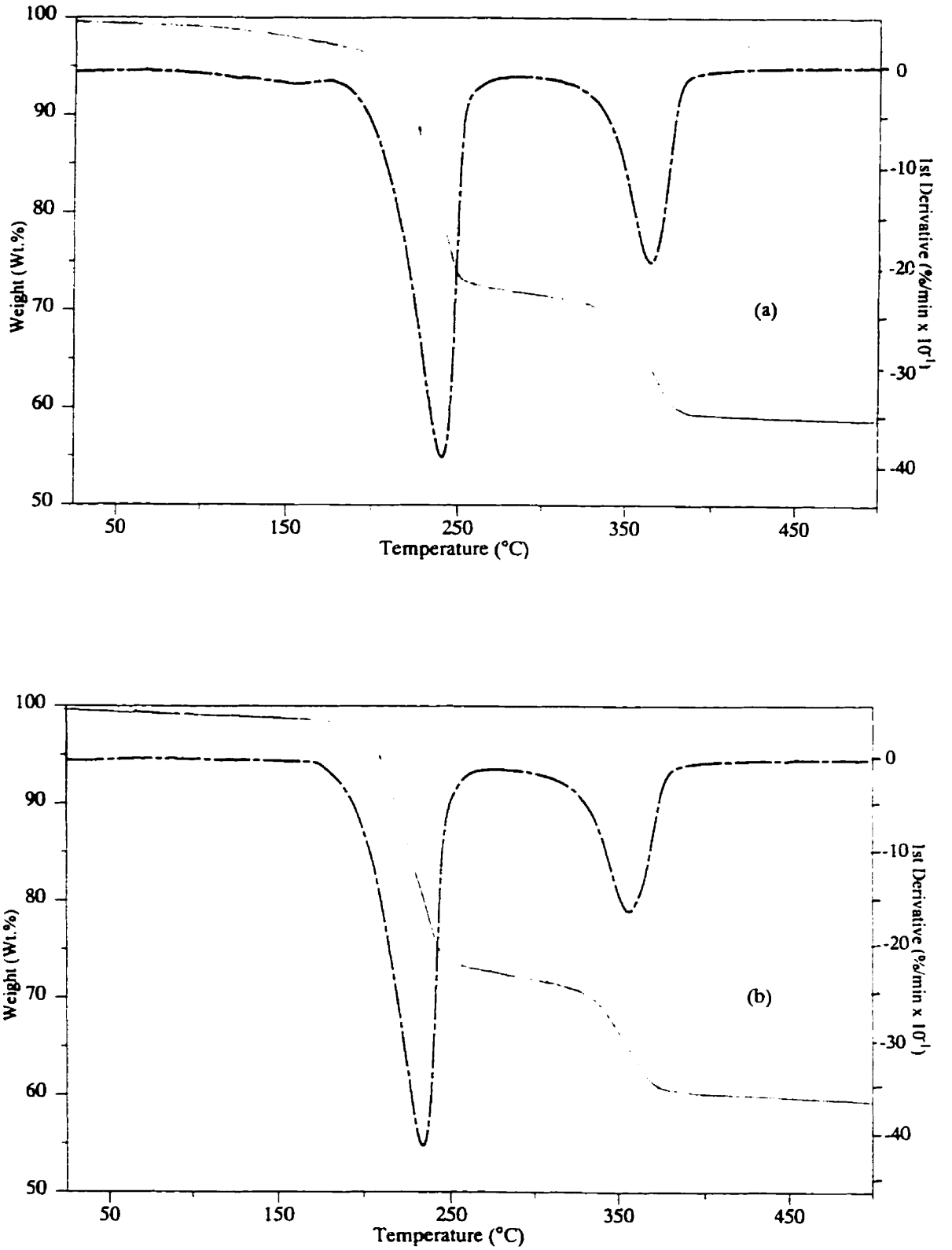

Figure 3-11. (a) TGA of UT-4. (b) TGA of UT-5.

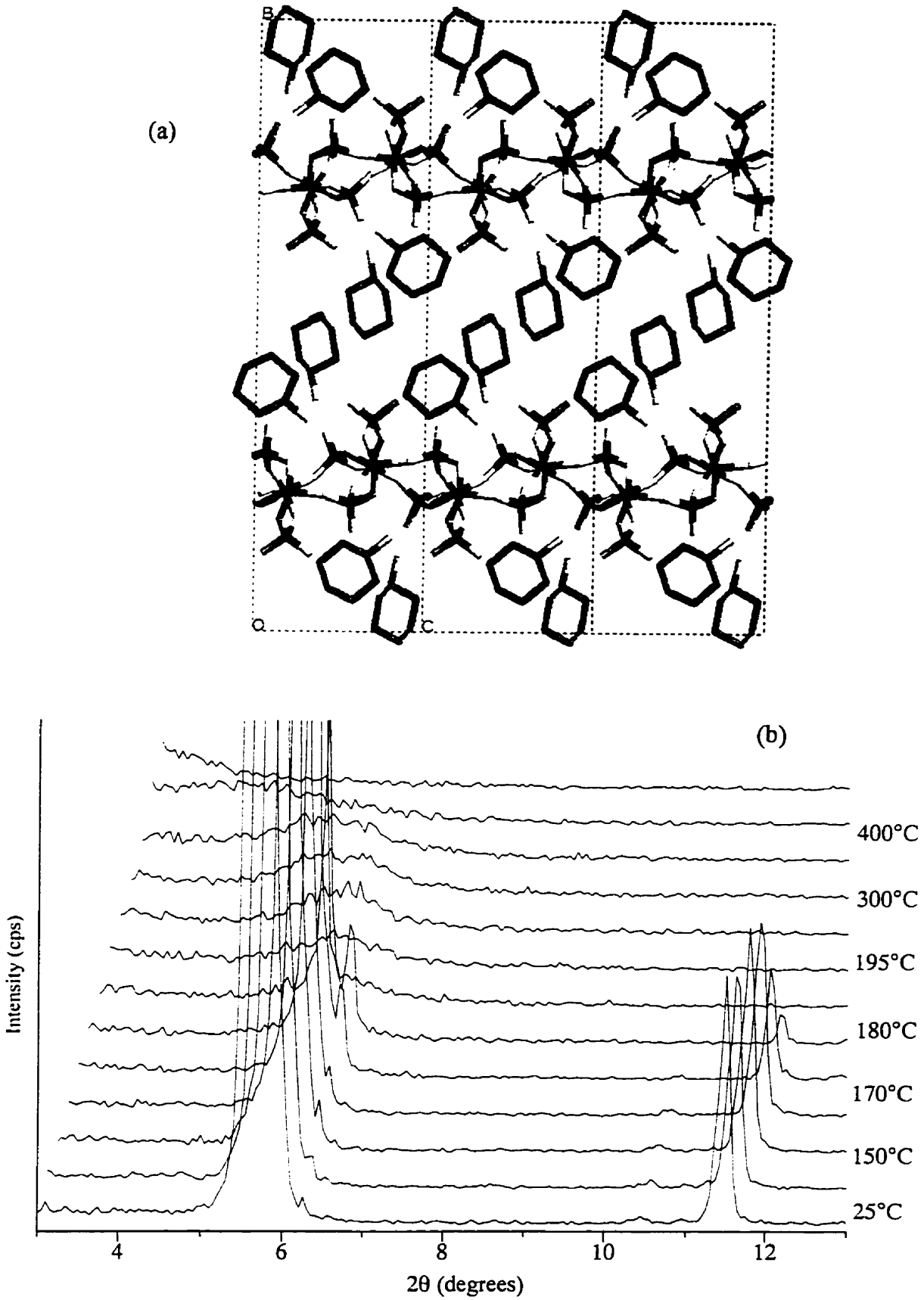

Figure 3-12. (a) a-projection of UT-5, which is isostructural to UT-3 (cf. Figure 3-7b). (b) VT-PXRD of UT-5.

a similar value of d-spacing (Figure 3-12b). This material collapses to $AlPO_4$-tridymite at about 350°C. The VT-PXRD pattern also reveals that an intriguing transformation occurs for UT-5. As the material begins to transform and its PXRD peaks start to decrease in intensity, new peaks appear at the positions belonging to the major peaks in the diffraction pattern of UT-4. However, this transformation remains incomplete, and both materials collapse to the open amorphous phase and $AlPO_4$-tridymite.

A repeat of this experiment, holding the temperature constant at 155°C or 160°C, allowed this transformation to continue, but the peaks of the new 14.2Å phase began to slowly disappear after about 20 minutes. Nevertheless, based on these observations, it is possible that UT-4 forms in the reaction mixture *via* a solid state transformation of UT-5. Indeed, UT-5 would not even have to change its composition, as the two phases are stoichiometrically equivalent. It would only need to undergo a small contraction in the unit cell from 15.424Å to 14.739Å, comparing the interlayer distance of the two structures, and a series of hydrolysis and condensation steps. Furthermore, since UT-3 and UT-5 are isostructural, this transformation does have implications into the UT-3 to "contracted UT-3" transformation discussed in the previous section.

It should also be noted that, as the isostructural UT-3 layer grows from the UT-2 chain precursor phase, it is quite likely that UT-5 is formed from a cyclohexylamine-related chain precursor phase that is isostructural to UT-2. Indeed, the chain phase was solved in the cycloheptylamine system (next section). This may in fact be the structure of the as-yet unsolved 17.5Å phase that was observed at lower temperatures in the TEG-cyclohexylamine system (II-147 to II-149).

3.11 UT-7, $[Al_3P_5O_{20}H]^{5-}[C_7H_{13}NH_3^+]_5$

Several materials were observed to form in the TEG-cycloheptylamine system (section 2.3.5.13). At lower temperatures, large crystals of UT-7 were obtained (II-158). The structure of UT-7 turned out to be a one-dimensional chain aluminophosphate isostructural to UT-2 (section 3.7). The structure of the chain was discussed in section 3.7 and will be considered further in Chapter 4. Chemical analysis showed the UT-7 product to contain 37.92 wt.% C, 8.96 wt.% H, 3.37 wt.% N, 5.00 wt.% Al and 8.38 wt.% P, giving a molar ratio of $Al_{3.00}P_{4.38}C_{51.11}N_{3.90}H_{143.91}$. A view of the layer of chains is identical to that previously shown for UT-2 (Figure 3-5a). The increase of the unit cell in the b-dimension by 2.381(3) Å may be observed in the a-projection of

UT-7 in Figure 3-13a. Note the remarkable similarity of the conformation and position of the cyclic amines in the two structures, comparing Figure 3-5b and Figure 3-13a.

For comparison, the bond lengths of UT-7 are as follows: Al-O_{av} 1.734(1) Å; three of the five crystallographically distinct phosphorus are triply-bridging (P-O_{av} 1.537(1) Å) with one terminal phosphonyl oxygen (P=O_{av} 1.486(1) Å); the fourth phosphate group is doubly-bridging (P-$O_{bridging}$ distances 1.553(4) and 1.563(4) Å), with two non-protonated terminal oxygens (P=O distances 1.482(4), 1.500(5) Å); the remaining fifth phosphorus is connected to only one aluminum (P-$O_{bridging}$ 1.539(4) Å) and contains three terminal oxygens, of which one is protonated (P=O distances 1.495(5) and 1.495(5) Å, P-OH 1.576(5) Å). The interchain hydrogen bond between the protonated phosphate group and the terminal oxygen of a triply-bridged phosphate group on an adjacent chain is 1.72Å in length.

UT-7 was thermally treated in air at 150° (III-20) and, remarkably, transformed it to a low-crystallinity material that compares well to the unknown phase obtained from the TEG-cycloheptylamine system at higher temperatures (II-160). As postulated in section 2.3.5.13, this is strong evidence that this unknown material is indeed a layered aluminophosphate isostructural to UT-3, obtained by an analogous chain to layer transformation.

This UT-7 transformation may also be followed in the TGA (Figure 3-13b) and VT-PXRD studies (Figure 3-14a), which display very similar behaviour to UT-2 when it transformed to UT-3. The unknown 16.5Å pattern appears at 175°C in the VT-PXRD, collapsing by 200°C to $AlPO_4$-tridymite and an open, amorphous phase. Note that the sample originally contained a fraction of the second unknown whose d-spacing is 18.4Å (product II-158 was used). This second unknown does not overlap with the UT-7 transformation; it appears to simply collapse in the 200°C region. Since the unknown 16.5Å phase formed quite large crystals in its synthesis (II-160), it should be possible to obtain the SC-XRD data of the unknown and verify this transformation. The isostructurality and phase behaviour among the chain and layered aluminophosphates containing cyclic amines is, in itself, an interesting observation and will be discussed further in the next chapter.

3.12 UT-8, $[Al_3P_4O_{16}]^{3-}[C_4H_9NH_3^+]_2[C_5H_{10}NH_2^+]$

UT-8 was obtained using a TEG mixture equimolar in cyclobutylamine and piperidine (II-179, section 2.3.6). The large crystals allowed the solution of the structure by SC-XRD (Table 3-1). Chemical analysis showed the UT-8 product to contain 19.06 wt.% C, 4.28 wt.% H,

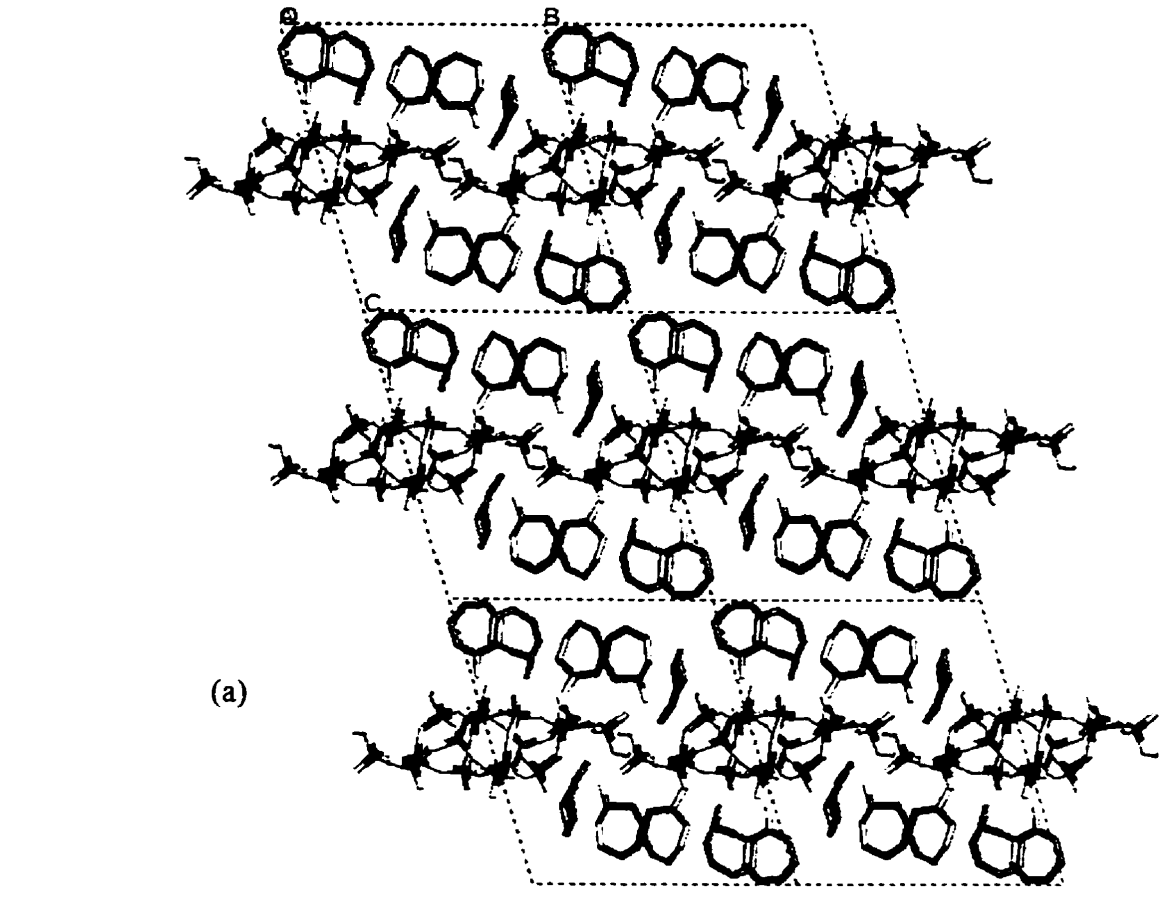

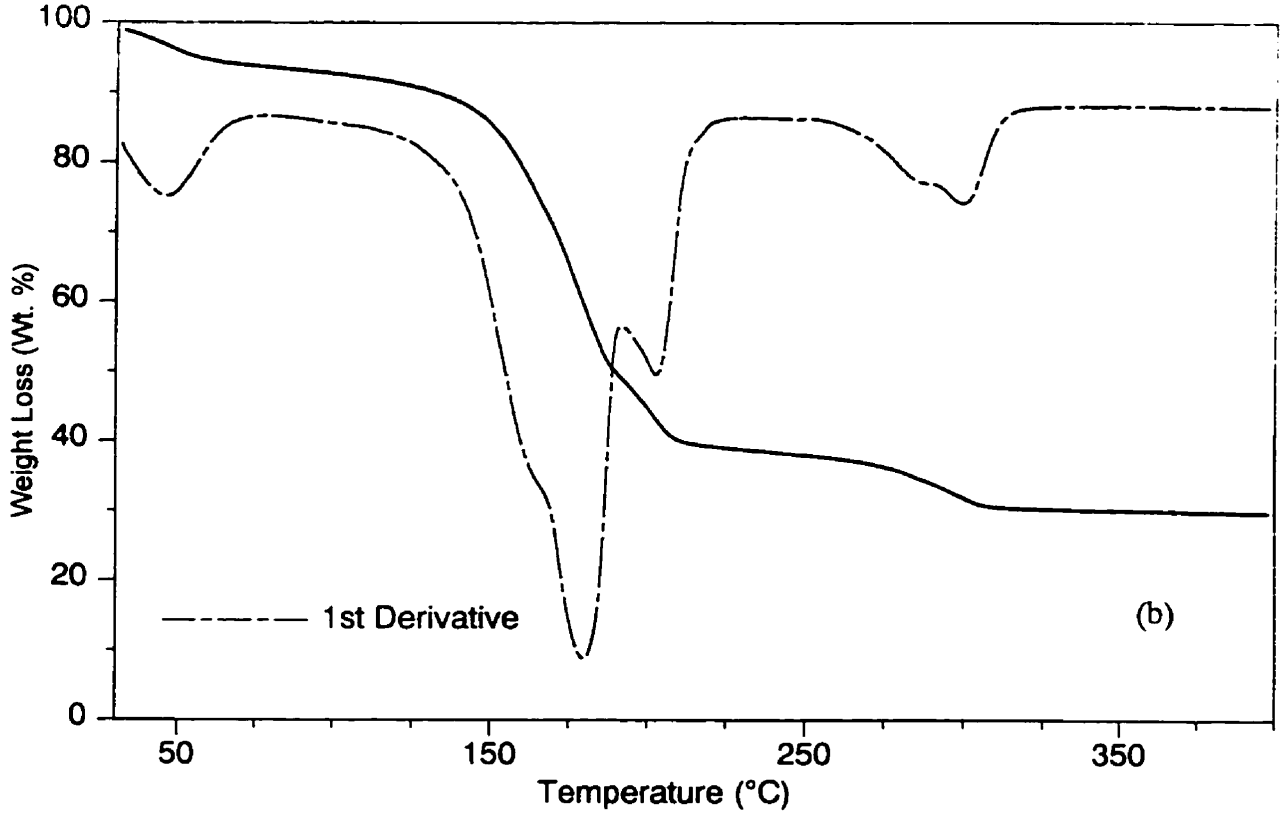

Figure 3-13. (a) a-projection of UT-7, which is isostructural to UT-2 (cf. Figure 3-5b). (b) TGA of UT-7.

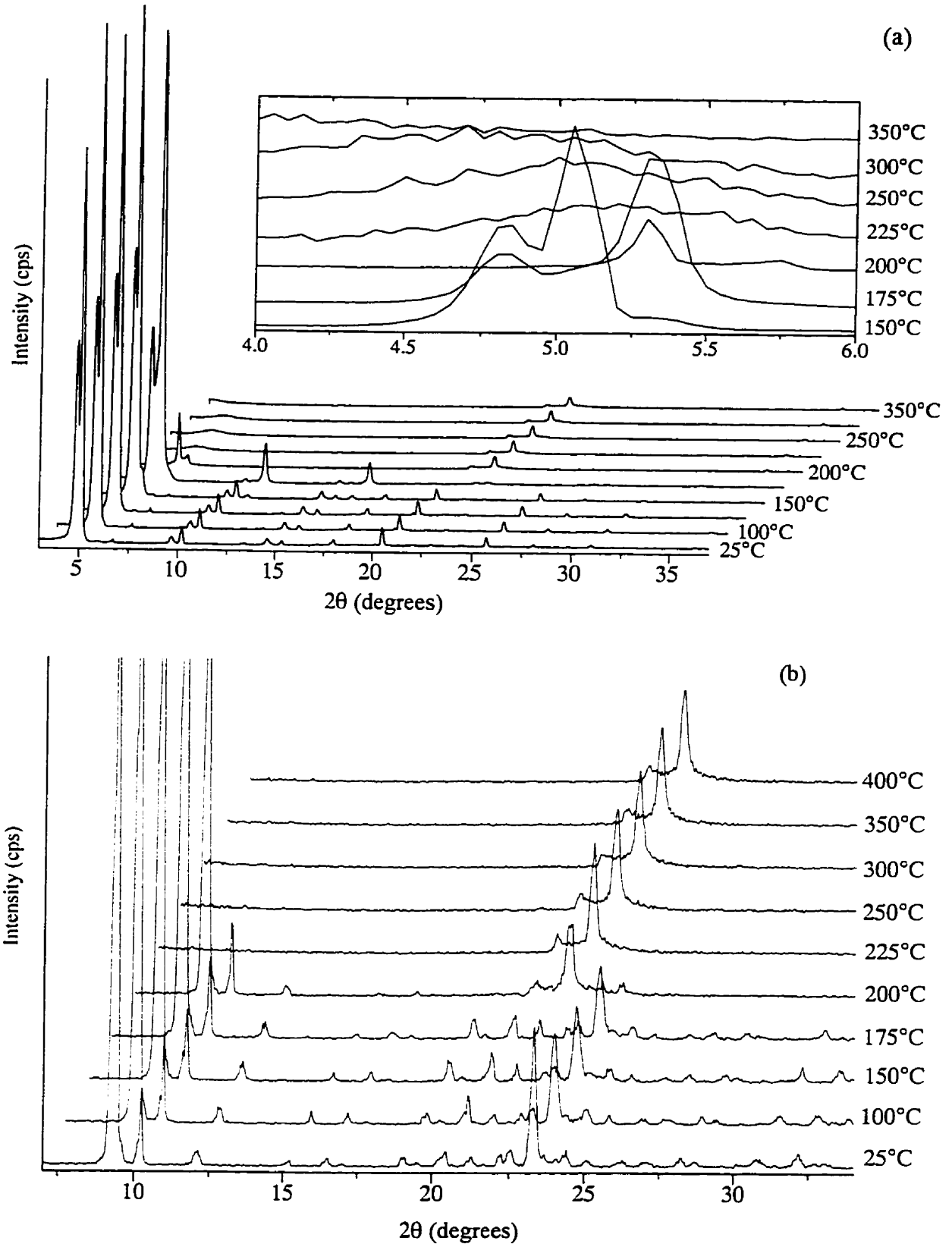

Figure 3-14. (a) VT-PXRD of UT-7. Inset: expansion of the low-angle region, and the solid state transformation to an unknown phase; (b) VT-PXRD of UT-8.

5.83 wt.% N, 13.91 wt.% Al and 19.10 wt.% P, giving a molar ratio of $Al_{3.00}P_{3.59}C_{9.24}N_{2.42}H_{24.71}$. The $[Al_3P_4O_{16}]^{3-}$ layered structure of UT-8 is a three-connected two-dimensional net of alternating tetrahedral aluminum and phosphorus centres connected by bridging oxygens (P-O_{av} 1.535(1) Å, Al-O_{av} 1.732(1) Å), defining an array of edge-sharing four-, six- and eight-rings that is identical to the **ab** plane of the $AlPO_4$-12 or $AlPO_4$-25 frameworks.[3] However, in UT-8, the fourth oxygen of the phosphorus atoms are not linked to another layer, but are terminal phosphonyl groups (P=O_{av} 1.501(1) Å). The six-rings are capped alternatively above and below the plane of the layer by a triply-bridging phosphate group, as observed for the capped six-rings of the $AlPO_4$-5-like layered structure of UT-1 (section 3.3) and others.[7,8]

UT-8 is isostructural to the layered material reported by Jones *et al.*,[34] which contains one interlamellar diprotonated 1,5-diaminopentane and one piperidinium (section 1.2.1). See Chapter 1, Figure 1-3b for a view of the layer. UT-8, however, contains two crystallographically independent cyclobutylammoniums and one piperidinium in the interlayer region (Figure 3-15a). These two structures are also isostructural to the $[Al_3P_4O_{16}]^{3-}$ layer reported by Jones *et al.* containing protonated interlamellar ethylenediamine and ethylene glycol,[10] as well as the recently reported $[Al_3P_4O_{16}]^{3-}$ layer containing interlamellar octahedral $[Co(pn)_3]^{3+}$ complexes.[35]

Each terminal oxygen of the phosphate groups accepts two hydrogen bonds from the template ammoniums (NH•••OP *ca.* 1.92 to 2.35 Å). The piperidiniums reside in the same position and conformation with respect to the inorganic layers as in the material reported by Jones *et al.*,[34] with the secondary ammonium groups interacting with only one layer. Interestingly, the two cyclobutylammoniums in UT-8 fill the same role as the one pentane-1,5-diammonium. Consequently, each cyclobutylammonium donates one hydrogen-bond to one layer and two to the adjacent layer, as for each end of the diamine. This, however, does not increase the thermal stability of the material, as revealed in the TGA (Figure 3-15b). The layer simply collapses to $AlPO_4$-tridymite at approximately 225°C, confirmed by VT-PXRD (Figure 3-14b).

It is interesting to note the somewhat accidental way in which the $[Al_3P_4O_{16}]^3$ mixed-amine layers of UT-8 and Jones *et al.*[34] were discovered. UT-8 was initially discovered when approximately equal volumes of leftover gels of the respective TEG-cyclobutylamine (II-125) and TEG-piperidine (II-119) experiments were combined and treated at the synthesis temperature

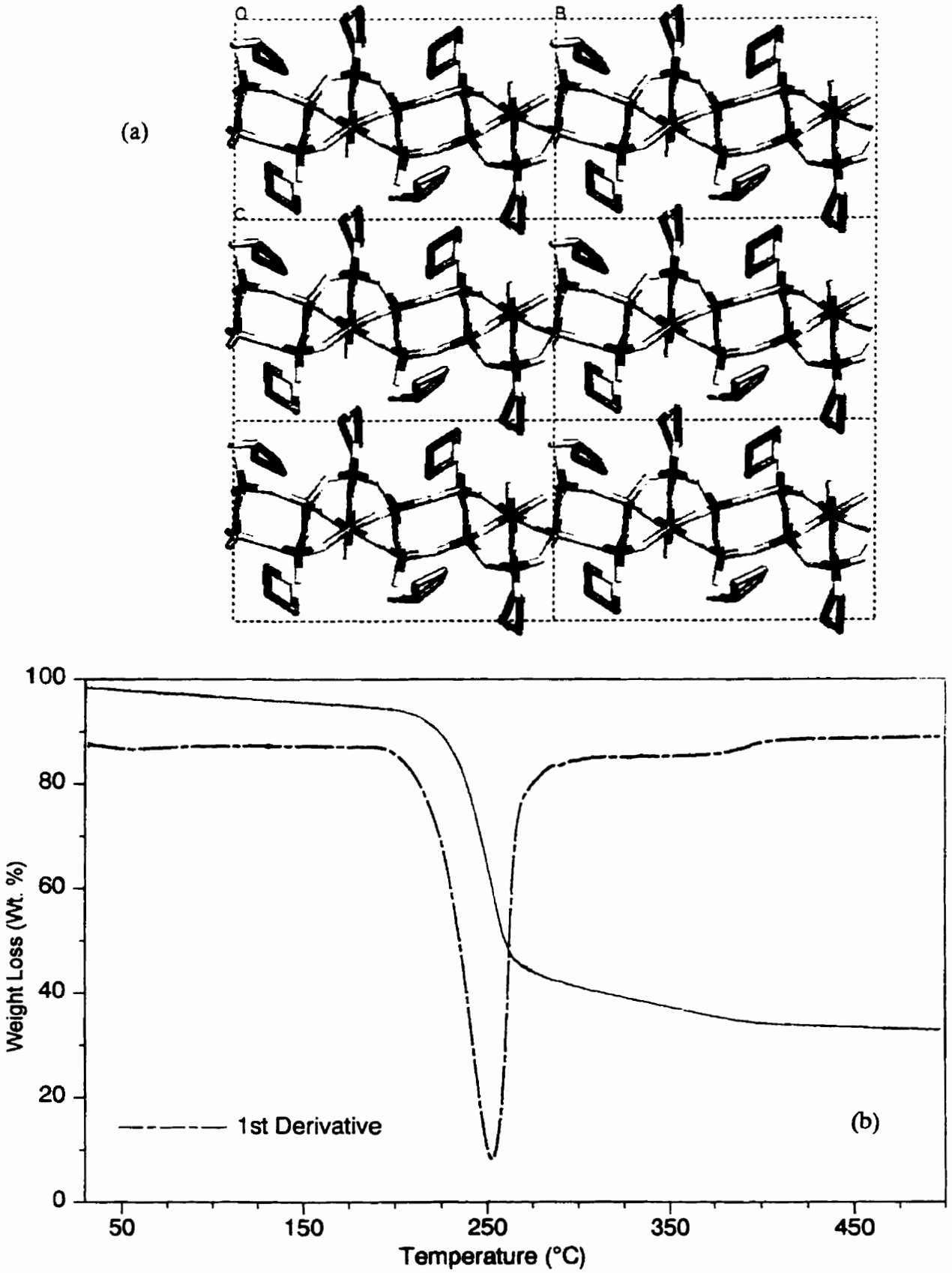

Figure 3-15. (a) a-projection of UT-8, which has the capped $AlPO_4$-25-like layer (cf. Figure 1-4b). (b) TGA of UT-8.

of 180°C. Jones *et al.* crystallized their material using only 1,5-diaminopentane as the organic additive, which partially decomposed and ring-closed to form piperidine.

3.13 CONCLUSIONS

The large crystal sizes that were obtained using a TEG solvent allowed the determination of a series of novel aluminophosphate structures by SC-XRD. With the various structures solved and the unequivocal identification of a particular phase or phases by its projected PXRD pattern, the characterization of both known and unknown phases could be carried out. Certainly, there exists much potential for future research into not only new structure types and their characterization, but possible solid state applications of these materials, as well as heretofore undiscovered structural relationships between the phases (Chapter 6).

Perhaps one of the most significant discoveries of this study was the thermal behaviour of UT-2 and UT-3 and an aluminophosphate chain to layer transformation that was both surprising and unprecedented. The data shown in this chapter was not the initial basis for the mode of formation studies of the next chapter, but nonetheless provides some important substantiating evidence for the model. It will also be interesting to compare and contrast the results to those using long-chain primary alkylamines and alkylenediamines in Chapter 5.

3.14 REFERENCES

1. R. H. Jones, J. M. Thomas, R. Xu, Q. Huo, Y. Xu, A. K. Cheetham, D. Bieber, *J. Chem. Soc., Chem. Commun.* **1990**, 1170.
2. SC-XRD data collection and refinement by P. Rudolf, Dow Chemical Co.
3. R. Szostak, *Handbook of Molecular Sieves*; Van Nostrand Reinhold: New York, 1992.
4. F. D'Yvoire, *Bull. Soc. Chim. Fr.* **1961**, 1762.
5. B. Duncan, M. Stocker, D. Gwinup, R. Szostak, K. Vinje, *Bull. Soc. Chim. Fr.* **1992**, *129*, 98.
6. (a) Q. Huo, R. Xu, S. Li, Z. Ma, J. M. Thomas, R. H. Jones, A. M. Chippindale, *J. Chem. Soc., Chem. Commun.* **1992**, 875. (b) R. H. Jones, J. M. Thomas, J. Chen, R. Xu, Q. Huo, S. Li, Z. Ma, A. M. Chippindale, *J. Solid State Chem.* **1993**, *102*, 204.
7. J. M. Thomas, R. H. Jones, R. Xu, J. Chen, A. M. Chippindale, S. Natarajan, A. K. Cheetham, *J. Chem. Soc., Chem. Commun.* **1992**, 929.
8. P. A. Barrett, R. H. Jones, *J. Chem. Soc., Chem. Commun.* **1995**, 1979.

9. See, for example: I. D. Williams, Q. Gao, J. Chen, L. Ngai, Z. Lin, R. Xu, *J. Chem. Soc., Chem. Commun.* **1996**, 1781.

10. R. H. Jones, J. M. Thomas, R. Xu, Q. Huo, A. K. Cheetham, A. V. Powell, *J. Chem. Soc., Chem. Commun.* **1991**, 1266.

11. J. B. Parise, *Acta Cryst.* **1984**, *C40*, 1641.

12. N. Bilba, A. Azzouz, N. Naum, D. Nibou, *Stud. Surf. Sci. Catal.* **1994**, *84A*, 605.

13. R. J. Moolenaar, J. C. Evans, L. D. McKeever, *J. Phys. Chem.* **1970**, *74*, 3629.

14. J. W. Akitt, N. N. Greenwood, B. L. Khandelwal, G. D. Lester, *J. Chem. Soc., Dalton Trans.* **1972**, 604.

15. C. S. Blackwell and R. L. Patton, *J. Phys. Chem.* 1988, **92**, 3965, and references therein.

16 D. W. Lewis, C. R. A. Catlow, J. M. Thomas, *Chem. Mater.* **1996**, *8*, 1112, and references therein.

17. J. Paillaud, B. Marler and H. Kessler, *J. Chem. Soc., Chem. Commun.* **1996**, 1293.

18. S. J. Kirkby, A. J. Lough, G. A. Ozin, *Z. Kristallogr.* **1995**, *210*, 956.

19. S. Natarajan, J. P. Gabriel, A. K. Cheetham, *J. Chem. Soc., Chem. Commun.* **1996**, 1415.

20. H. Kessler, in *Synthesis/Characterization and Novel Applications of Molecular Sieves*; R.L. Bedard, T. Bein, M. E. Davis, J. Garces, V. A. Maroni, G. D. Stucky (eds.), MRS **233**, Pittsburg, Penn, 1991, pp. 47.

21. J. L. Guth, H. Kessler, P. Caullet, J. Hazm, A. Merrouche, J. Patarin, in *Proceedings of the 9th International Zeolite Conference;* Vol. I, R. von Ballmoos *et al.* (eds.), Butterworth-Heinemann: London, 1993, pp. 215.

22. L. Delmotte, M. Soulard, F. Guth, A. Seive, A. Lopez, J. L. Guth, *Zeolites* **1990**, *10*, 778.

23. C Fernandez, J.P. Amourex, L. Delmotte, H. Kessler, *Microporous Materials*, **1996**, *6*, 125.

24. E. Klock, L. Delmotte, M. Soulard, J. L. Guth, in *Proceedings from the Ninth International Zeolite Conference*; Vol. I, R. von Ballmoos *et al.* (eds.), Butterworth-Heinemann: London, 1993, pp. 611.

25. See, for example: (a) M. T. Averbuch-Pouchot, A. Durif, *Acta Cryst.* **1987**, *C43*, 1894. (b) S. Kamoun, A. Jouini, A. Daoud, A. Durif, J. C. Guitel, *Acta Cryst.* **1992**, *C48*, 133. (c) F. Takusagawa, T. F. Koetzle, *Acta Cryst.* **1979**, *B35*, 867. (d) C. B. Aakeroy, P. B. Hitchcock, B. D. Moyle, K. R. Seddon, *J. Chem. Soc., Chem. Commun.* **1989**, 1856.

26. W. Tieli, Y. Long, P. Wengin, *J. Solid State Chem.* **1990**, *89*, 392.

27. R. Kniep, M. Steffen, *Angew. Chem., Int. Ed. Engl.* **1978**, *17*, 272.

28. A. M. Chippindale, S. J. Brech, *J. Chem. Soc., Chem. Commun.* **1996**, 2781.

29. V. R. Choudhary, D. B. Akolekar, A. P. Singh, S. D. Sansare, *J. Catal.* **1988**, *111*, 254.

30. B. Hampson, H. Frank Leach, B. M. Lowe, C. D. Williams, *Zeolites* **1989**, *9*, 521.

31. A. M. Chippindale, A. V. Powell, L. M. Bull, R. H. Jones, A. K. Cheetham, J. M. Thomas, R. Xu, *J. Solid State Chem.* **1992**, *96*, 199.

32. K. Morgan, G. Gainsford, N. Milestone, *J. Chem. Soc., Chem. Commun.* **1995**, 425.

33. H. Li, M. E. Davis, *J. Chem. Soc., Faraday Trans.* 1993, **89**, 957.

34. (a) R. H. Jones, A. M. Chippindale, S. Natarajan, J. M. Thomas, *J. Chem. Soc., Chem. Commun.* **1994**, 565. (b) A. M. Chippindale, S. Natarajan, J. M. Thomas, R. H. Jones, *J. Solid State Chem.* **1994**, *111*, 18.

35. D. A. Bruce, A. P. Wilkinson, M. G. White, J. A. Bertrand, *J. Chem. Soc., Chem. Commun.* **1995**, 2059.

CHAPTER 4: A CHAIN MODEL FOR THE FORMATION OF ONE-, TWO- AND THREE-DIMENSIONAL ALUMINOPHOSPHATES

4.0 INTRODUCTION

The mode of formation of extended aluminophosphates remains a topic of ongoing discussion and debate. Only formation of the frameworks has been discussed in the literature (section 1.1.4). In this chapter, a new chain-related model will be discussed, that accounts for aluminophosphate structures extended in any of one, two or three dimensions. It is based in part on direct experimental evidence presented in previous chapters. It should be pointed out that the ideas discussed hereinafter are novel, and point out structural and experimental aspects that have not been previously realized.

After consideration of the the source reagents that exist at the beginning stages of synthesis, the "parent chain" species will be presented, where a simple hydrolysis-condensation pathway allows its conversion to a theoretically infinite number of possible chain types. The new chain type can crystallize to give a one-dimensional aluminophosphate material, or condense further to more complex layered or framework structures. A nomenclature scheme will be given to aid in identifying particular chain types. The model applies not only to the structures discovered in the course of the present work, but also to other known and theoretical extended aluminophosphate structures. It is potentially a universal model for aluminophosphate formation. Representative examples of the build-up of their seemingly complex, extended architectures will be shown. This will be followed by a brief discussion of the results of Chapter 2 and 3, and conclusions.

4.1 SOURCE REAGENTS AND GENERATION OF ALUMINOPHOSPHATE SPECIES

The source materials generally employed in the synthesis of aluminophosphates are phosphoric acid and an aluminum oxide or alkoxide. The mineralization of alumina by phosphoric acid is a well-documented process due to its relevance to soil and environmental science.[1-4] Generally, phosphate links through bridging oxygens to aluminum centres by ligand exchange of OH^- or H_2O and breaking any Al-O-Al linkages that may exist, such as in an alumina mineral. Molecular phosphatoaluminum complexes are thereby leached into the supernatant and have been detected experimentally by ion-exchange, pH measurements and

NMR.[5-11] They include monomeric, dimeric and oligomeric species. Mortlock *et al.* also performed theoretical calculations to model these complexes.[10]

At the same time, aluminum ions and phosphate ions are known to strongly interact.[1-4] Accordingly, phosphate shows a tendency to surround aluminum centres in the phosphatoaluminum complexes, such as the two terminal phosphates that surround an octahedral aluminum in the diphosphatoaluminate complex,[8] or evidence of the existence of $[Al(HPO_4)_3(H_2O)_3]^{3-}$ and $[Al(H_2PO_4)_3(H_2O)_3]$ complexes.[7,10,11] For a tetrahedral aluminum, this is further demonstrated by the pentameric $[AlP_4O_{16}]^{9-}$ cluster of Riou *et al.*[12] All of the vertices of the aluminum centre are occupied by a bridging oxygen connected to a phosphate. A tetrahedral geometry is often found for the central metal atom when surrounded by many other metal oxide polyhedra, as in the $[AlP_4O_{16}]^{9-}$ cluster or the Keggin ion.[13]

As was seen in Chapter 1, phosphate groups are also found to commonly doubly- and triply-bridge the metal centres in inorganic molecular and chain structures, such as the aluminum phosphates,[14,15] (and in UT-2 and UT-7, Chapter 3), zinc phosphates,[15-17] molybdenum phosphates,[18-20] vanadium phosphates[21] and arsenates,[22] as well as in the chain building units of higher dimensionality metal phosphate structures.[23] Similarly, the layered aluminophosphates contain exclusively doubly- and triply-bridging phosphates (section 1.2.1 and the UT-n layers of Chapter 3). This is also the case for other layered metal phosphates, such as indium phosphates,[24] vanadium phosphates[25] and iron phosphates[26] (section 1.3).

There is evidence that "aggregation polymers" exist for metal phosphates in viscous gels, the most studied being the aluminophosphate polymers.[27-31] The materials were found to be amorphous upon precipitation. The aggregation polymers have also been suggested as a "transition between the heteropoly acids and soluble complexes."[29] It should also be noted that they tend to form as the Al:P ratios of the solution is raised above 1:1.[29-31]

Therefore, by what pathway do the aluminophosphate clusters combine to form an extended aluminophosphate, if this is indeed the case? They can simply connect together directly to build up the final structure. However, in view of the above discussion, a reasonable and likely candidate is an oligomeric precursor species, containing tetrahedral or octahedral aluminums that are fully coordinated by doubly-bridging phosphates. This is the arrangement found for what will be considered as the parent chain, as well as the chain of Kniep *et al.*, prepared by simply allowing an aggregation polymer solution to evaporate (section 1.2.3).

4.2 THE CHAIN MODEL

4.2.1 The Parent Chain Precursor

Of all the aluminophosphate experiments that were conducted, the first were in the TEG-triethylamine system. The large crystals so obtained (II-13) were studied by SC-XRD (section 3.1), and turned out to be the previously reported one-dimensional chain structure.[14] The product also contained varying amounts of JDF-20 (II-8 to II-15), and structural aspects of the two phases led to the initial stages of the chain-related model.[32] The relationship between the chain structure and JDF-20 will be discussed later in section 4.2.7. Importantly, this "parent chain" structure can also be obtained under aqueous conditions, using ethylenediamine as template.[15] This shows that the structure can form under aqueous conditions, which is an important and supporting observation for the present model. However, this should not be surprising in light of the method in which Kniep *et al.* discovered the $Al(H_2PO_4)_3$ chain (section 1.2.3).

The rather simple structure of the parent chain consists of an infinite one-dimensional connection of skewed, corner-sharing four-rings bridged at the aluminum centres, with two doubly-bridging phosphates per four-ring, (section 1.2.3, Figure 1-7a). It will only crystallize if the shape of the template, reagent concentration and synthesis conditions are correct, which would explain the lack of its observation in other synthetic systems. The identical arrangement of mutually orthogonal four-rings exists for other mixed metal oxide chains, as discussed in section 1.3. Interestingly, the isostructural zinc phosphate chain structure can be recrystallized from various solvents, and the authors indicate that NMR data suggests that the chain exists as an oligomer in solution, maintaining its polymeric structure.[16]

The structure is quite reasonably a highly stable polymeric aluminophosphate species, as it is structurally very simple, containing only one type of aluminum and phosphorus site. It also readily sets up the oxygen-bridged, strictly alternating aluminum and phosphorus centres and thereby obeys Lowenstein's rule, which is operative for all known aluminophosphates. Moreover, it follows the trends observed for metal phosphates, as discussed above.

A non-bridged, oligomeric species is supported by the polymeric nature of the condensed phosphates. Termed the non-branching rule of condensed phosphates (section 1.4),[33] the polyphosphates and ring metaphosphates avoid branching due to the reduced negative charge of branching sites, rendering them highly susceptible to removal by hydrolysis. Similar tendency to

avoid chain branching at the doubly-bridging phosphates may occur for the aluminophosphates in solution, resulting in non-branched, one-dimensional chains.

That the importance of this intermediate aluminophosphate chain has not been previously proposed or realized could, among other reasons, be due to the fact that most of the synthetic research for aluminophosphates to date have used aqueous conditions. It is known that the rigorous, hydrothermal conditions cause a higher degree of polymerization and cross-linking to occur upon the precipitation of aluminophosphate solids.[28,31] Consequently, the materials obtained should tend to be the higher-dimensionality layers and frameworks, primarily the latter. Not surprisingly, the recent non aqueous synthetic work described in chapters 2, 3 and 5 and by others has yielded a new series of lower dimensionality chain and layered aluminophosphates.

4.2.2 Chain Nomenclature

Since the chain structures are rather complicated on first sight, and because it is necessary to discuss different chain types, it is helpful at this point to introduce a nomenclature scheme. Only the repeat unit of a chain need be described, and each section is given a specific label for chain type, with a subscript for its length in number of aluminums (or, equivalently, number of four-rings). In this way, any chain type or theoretical chain type may be labelled. The nomenclature scheme is summarized in Table 4-1, and will be used throughout the remainder of this chapter. Examples using this scheme are also given in the figure captions.

4.2.3 Chain Hydrolysis and Condensation

The parent chain would be expected to undergo hydrolysis of the Al-O-P bonds in solution.[28-31] Even under predominantly non aqueous conditions this will be the case, as water is always present in reagent amounts from various sources. Depending on the pH, acid or base hydrolysis breaks the Al-O-P linkage, and two terminal Al-OH and P-OH bonds are thereby formed (Figure 4-1a-b).

Such a polymeric species in solution would also be expected to be highly flexible, particularly at synthesis conditions. Rapid rotation and bending would therefore be expected to occur about the remaining and only Al-O-P linkage (Figure 4-1b), as occurs for polymers in solution or in a melt. Rotation would at times bring the Al-OH and P-OH groups within vicinity of each other (Figure 4-1c), allowing intra-chain condensation to occur and regeneration of a water molecule (Figure 4-1d). In this way, the two corner-sharing four-rings are quickly and

Table 4-1. Nomenclature scheme for the description of the aluminophosphate chain repeat units.

$\Diamond_n$	Section of n corner-sharing four-rings of the unhydrolyzed parent chain
T_n	Section of n edge-sharing four-rings in a Trans conformation
$(T_P)_n$	Section of n edge-sharing four-rings in a Trans conformation, with terminal phosphates remaining on the aluminum centres
C_n	Section of n edge-sharing four-rings in a Cis-Trans conformation
$(C_P)_n$	Section of n edge-sharing four-rings in a Cis-Trans conformation, with terminal phosphates remaining on the aluminum centres
O_n	Section of n corner-sharing four-rings that have been ring-Opened (and have lost their terminal phosphate groups)
$(O_P)_n$	Section of n corner-sharing four-rings that have been ring-Opened, with terminal phosphates remaining on the aluminum centres
$[Z(a,b)]_n$	Section of n edge-sharing four-rings in a Zig-Zag conformation, of lengths a four-rings and b four-rings per leg
$[Z(a,b)_P]_n$	Section of n edge-sharing four-rings in a Zig-Zag conformation, of lengths a four-rings and b four-rings per leg, with terminal phosphates remaining on the aluminum centres

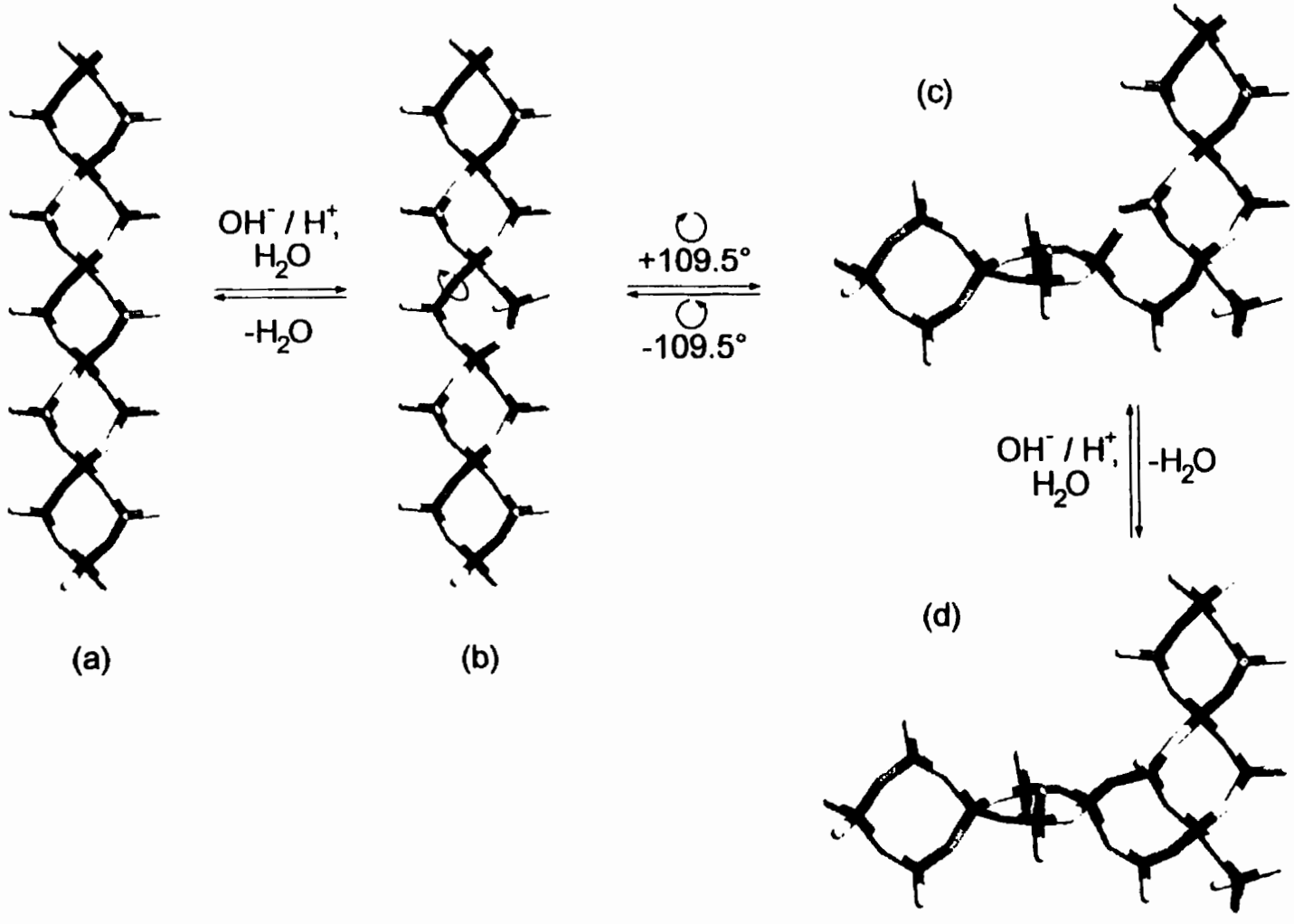

Figure 4-1. Scheme for the transformation of the parent chain, forming edge-sharing four-rings and a singly-bridging, triply-terminal phosphate group. (a) $\Diamond_n$, the parent chain. (b) Ring-opening hydrolysis. (c) Rotation about the remaining bridging oxygen brings the Al-OH group to the P-OH group of the next four-ring of the chain. (d) Condensation to define two edge-sharing four-rings.

easily transformed into two edge-sharing four-rings. Note that the reverse process is equally likely, indicated by the equilibrium arrows for each step. A dynamic equilibrium is therefore expected, and the chain to rapidly interconvert on very short timescales between these two states in the synthesis mixture. Also note the terminal phosphate group that necessarily resides at the aluminum atom common to the two four-rings (Figure 4-1d). This phosphate can remain on the chain or be cleaved off by hydrolysis, allowing another degree of freedom for possible transformation pathways.

If the process shown in Figure 4-1 is not undone by the reverse process, hydrolysis will occur further down the chain backbone at, for example, the next four-ring of the parent chain. There are now several choices as to the manner in which the third four-ring connects with respect to the first two, Figures 4-2 to 4-4. Each Al-O-P bond in the next four-ring is equally likely to be hydrolyzed apart. Hydrolysis at sites 3 or 4 (Figure 4-2a) leads to an open chain type (see below). Ring-opening at site 1 and rotation about the remaining bridging oxygen in the direction shown (Figure 4-2b) will bring the Al-OH group only within the P-OH group also labelled 1 (note that in this perspective, P-OH group 1 is hidden behind P-OH group 2_1). The third four-ring thereby connects to form a new section in which the three edge-sharing four-rings are "cis" with respect to the linking four-ring (Figure 4-2d).

Alternatively, for hydrolysis at site 2, rotation can bring the Al-OH group within vicinity of one of two P-OH groups, labelled 2_1 and 2_2. Rotation in one direction ("+109.5°") connects the chain onto phosphate group 2_1, to define a section in which the edge-sharing four-rings are "trans" to each other, Figure 4-3. Rotation in the other direction ("-109.5°") results in condensation to phosphate group 2_2, and a "zig-zag" chain that is bent back upon itself (Figure 4-4).

Subsequent four-ring "foldings" would continue down the chain, giving an infinite chain type with a new connectivity. For the trans chain, the process can continue down the chain without steric hindrance (Figure 4-5a). Similarly, the zig-zag chain can readily be formed (Figure 4-5b). Note the necessity of an odd number of four-rings per leg (in this case, three). The reason for this is that the chain transformation must propagate through the aluminum atoms in opposite corners of the four-rings down the axis of the parent chain. Therefore, the two four-rings cannot connect in the manner shown in Figure 4-5d.

In the case of the cis chain, the chain must bend back in the opposite direction in order to avoid folding back onto itself (Figure 4-5c). In this way, an alternating, "cis-trans" chain is

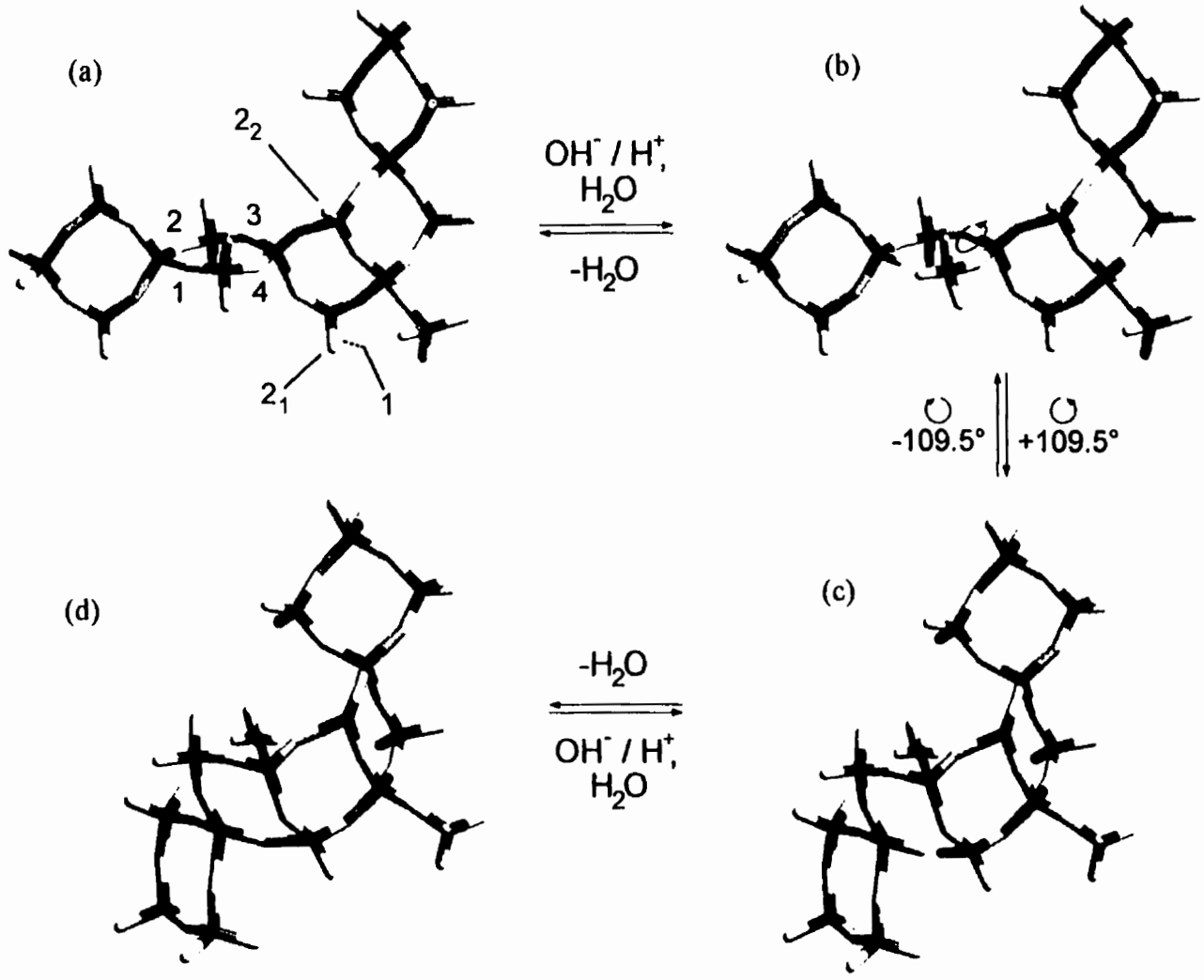

Figure 4-2. One possible pathway for the next step in the formation of three edge-sharing four-rings: a "cis" $\Diamond_n(C_p)_3\Diamond_n$ section: (a) Hydrolysis occurs at one of the four bridging oxygens of the next four-ring. (b) Ring-opening hydrolysis at position 1. (c) Rotation around the bridging oxygen brings the Al-OH group in vicinity of P-OH group 1. (d) Condensation and regeneration of a water molecule.

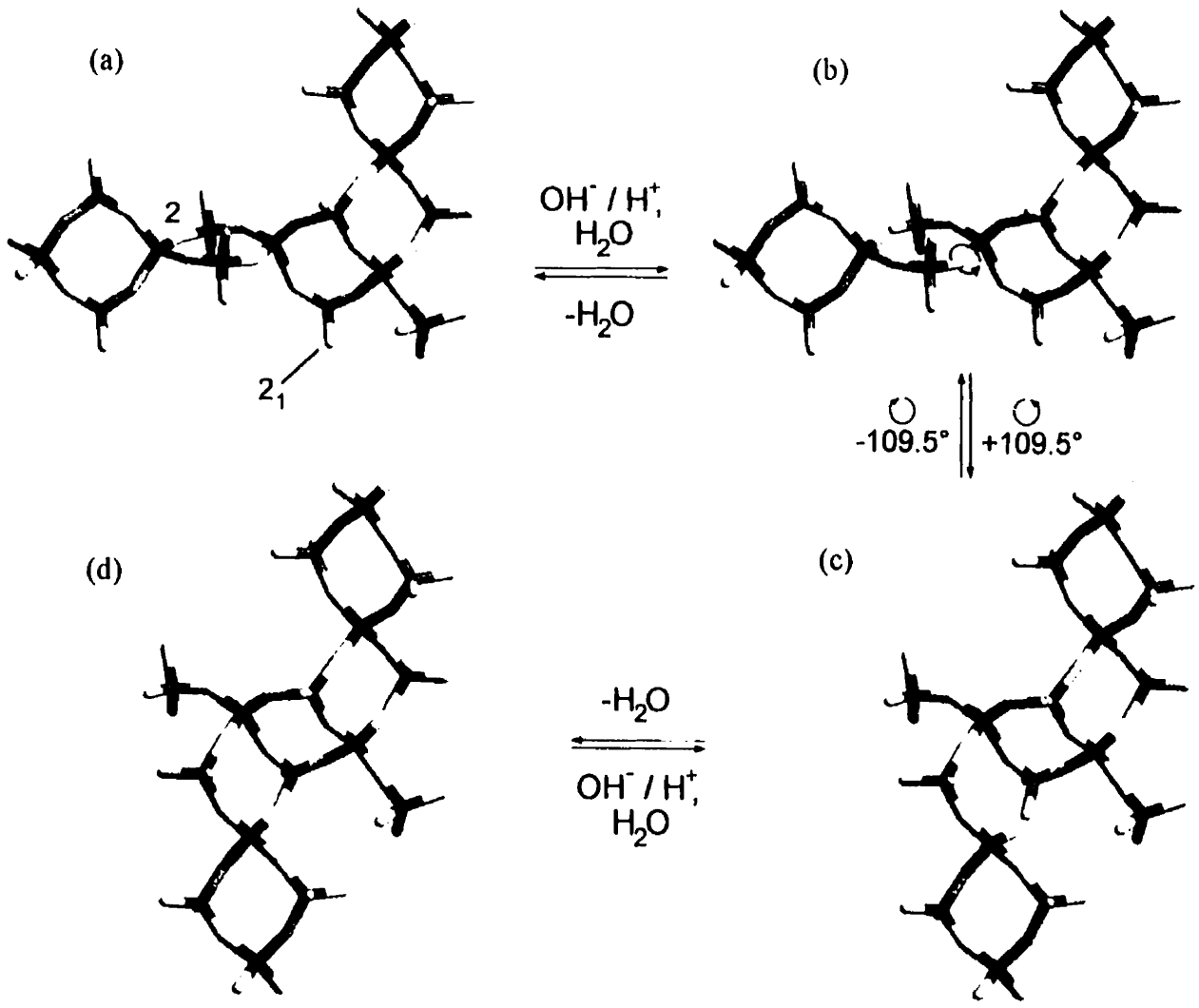

Figure 4-3. A second possible pathway for the next step in the formation of three edge-sharing four-rings: a "trans" $\Diamond_n(T_p)_3\Diamond_n$ section: (a) The chain prior to hydrolysis. (b) Ring-opening at position 2. (c) Rotation around the bridging oxygen in one direction, "+109.5°", brings the Al-OH group close to P-OH group 2_1. (d) Condensation.

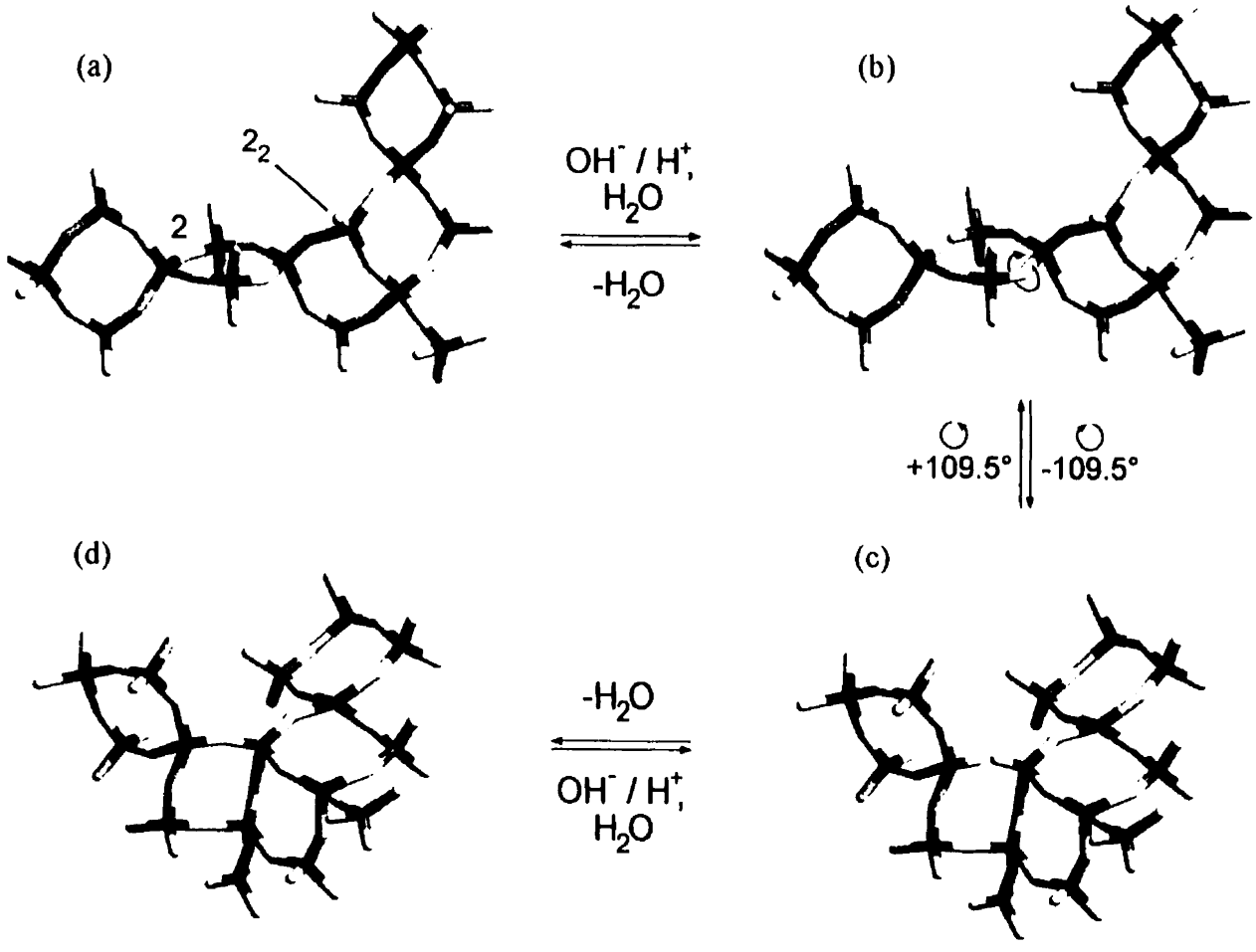

Figure 4-4. A third possible pathway for the next step in the formation of three edge-sharing four-rings: a "zig-zag" $\Diamond_n[Z(2,2)_p]_3\Diamond_n$ section. (a) The chain prior to hydrolysis. (b) Ring-opening at position 2. (c) Rotation in the opposite direction, "-109.5°", brings the Al-OH group to P-OH group 2_2. (d) Condensation.

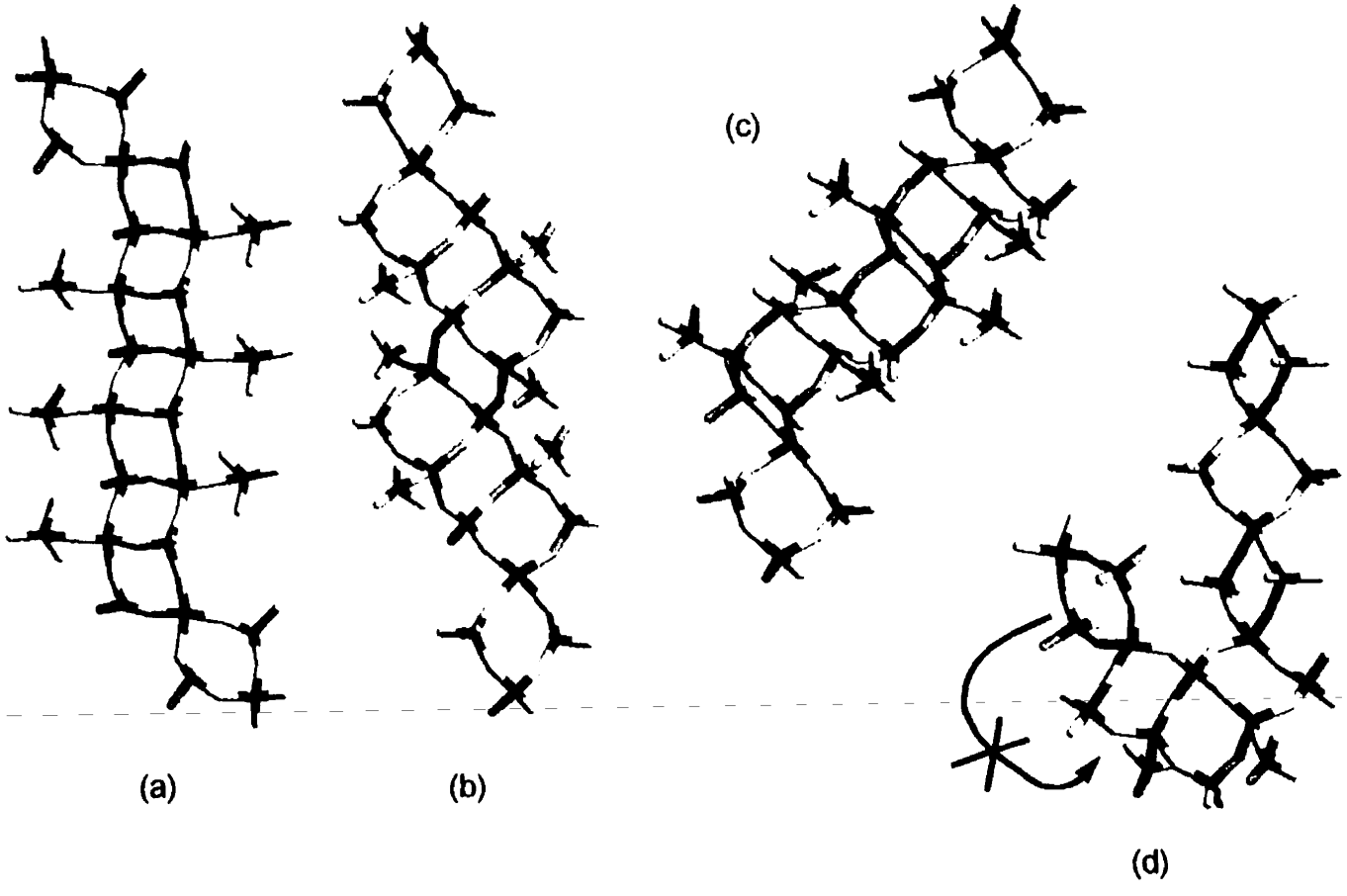

Figure 4-5. Examples of fully transformed chains. The terminal phosphate groups have been retained on each aluminum in these examples. (a) A trans chain secion, $(T_p)_7$. (b) A zig-zag chain section, $[Z(3,3)_p]_7$. (c) An alternating cis-trans chain section, $(C_p)_7$. (d) The zig-zag chain of Figure 4-4d. The point of hydrolysis of the next four-ring makes it impossible to create a zig-zag chain with only two four-rings per leg.

formed. An infinite connection of this type would be equivalent to the double-crankshaft chain that has been previously proposed as an aluminophosphate building block[34,35] (section 1.1.4.2), except that in the present case, there are terminal phosphate groups on each aluminum centre. However, only small sections of the cis-trans chain type are necessary to rationalize aluminophosphate formation.

There are yet many other degrees of freedom for chain transformations. For example, any number of corner-sharing four-rings can remain intact and be skipped in the hydrolysis process (Figure 4-6a-e). Another example is that no condensation and only ring-opening of the four-rings may take place, resulting in an "open" chain (Figure 4-6a,d). Each resulting chain type represents an infinite family: the different chain sections can be of any length, such as for the two chains shown in Figures 4-6b and c. Combinations of these processes can also occur on a single chain, allowing an unlimited number of mixed chain types, such as the chain of Figure 4-6e. These are but a few examples of the infinite number of possibilities.

Additional intra-chain condensation of a transformed chain is equally probable to occur, resulting in, for example, capped six-rings (Figure 4-6f-g), or sections of five edge-sharing four-rings connected to sections of three corner-sharing four-rings (Figure 4-6h-i). It will be shown that this additional intra-chain condensation and the formation of a chain with phosphate-capped six-rings is an important pathway for many extended aluminophosphates. It should be pointed out that modeling studies show all chain types to be of high conformational stability. All tetrahedra remain slightly distorted, as found in aluminophosphate solids, and bond lengths and angles do not need to be changed beyond their energetically accessible limits.[36]

While the chain transformations can be thought of as a chain "zipping", it is more probable that the various chain operations occur simultaneously or in short succession to each other, on parts of the chain or along its entire length. Indeed, the very short timescales expected for these processes make it not unreasonable that they are occurring during the extremely short synthesis times observed for many aluminophosphate materials, such as mere seconds for the high-temperature or microwave synthesis of $AlPO_4$-5.[37,38] A typical chain transformation, such as the seemingly complicated transformation of Figure 4-1a to Figure 4-6c, involves only a small number of hydrolysis, rotation and condensation processes per asymmetric unit.

The chain model quite readily accounts for the phosphorus to aluminum ratios that are observed in aluminophosphates. The extended aluminophosphate structures prepared hydrothermally contain a P:Al ratio between 2.0 and 1.0. This has been generally attributed to

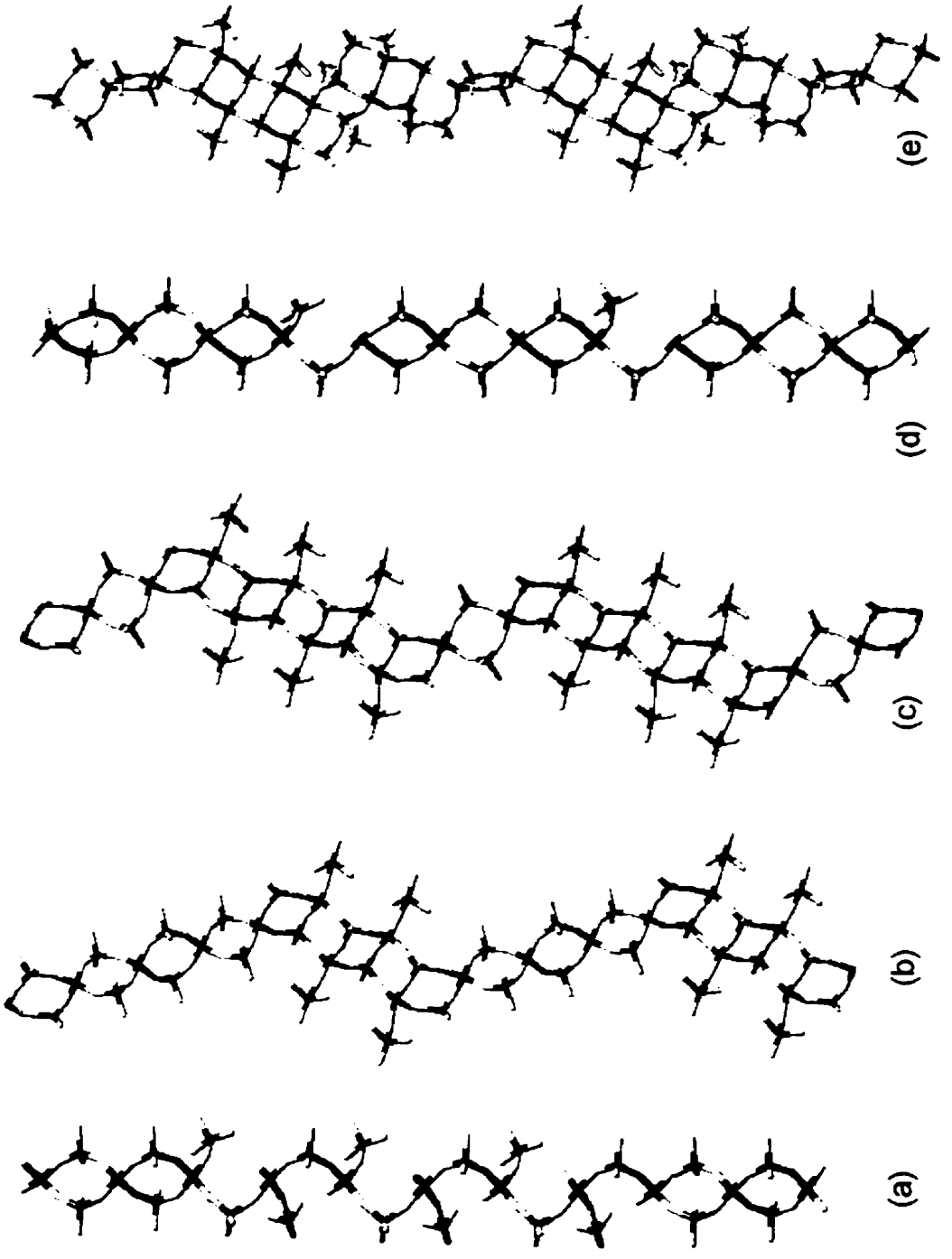

Figure 4-6. Further examples of some of the possible chain types. (a) $\diamond_2(O_p)_7$. (b) $\diamond_5(T_p)_5$. (c) $\diamond_3(T_p)_7$. (d) $\diamond_3(O_p)_1$. (e) $\diamond_3(T_p)_3[Z(3,3)_p]_5$.

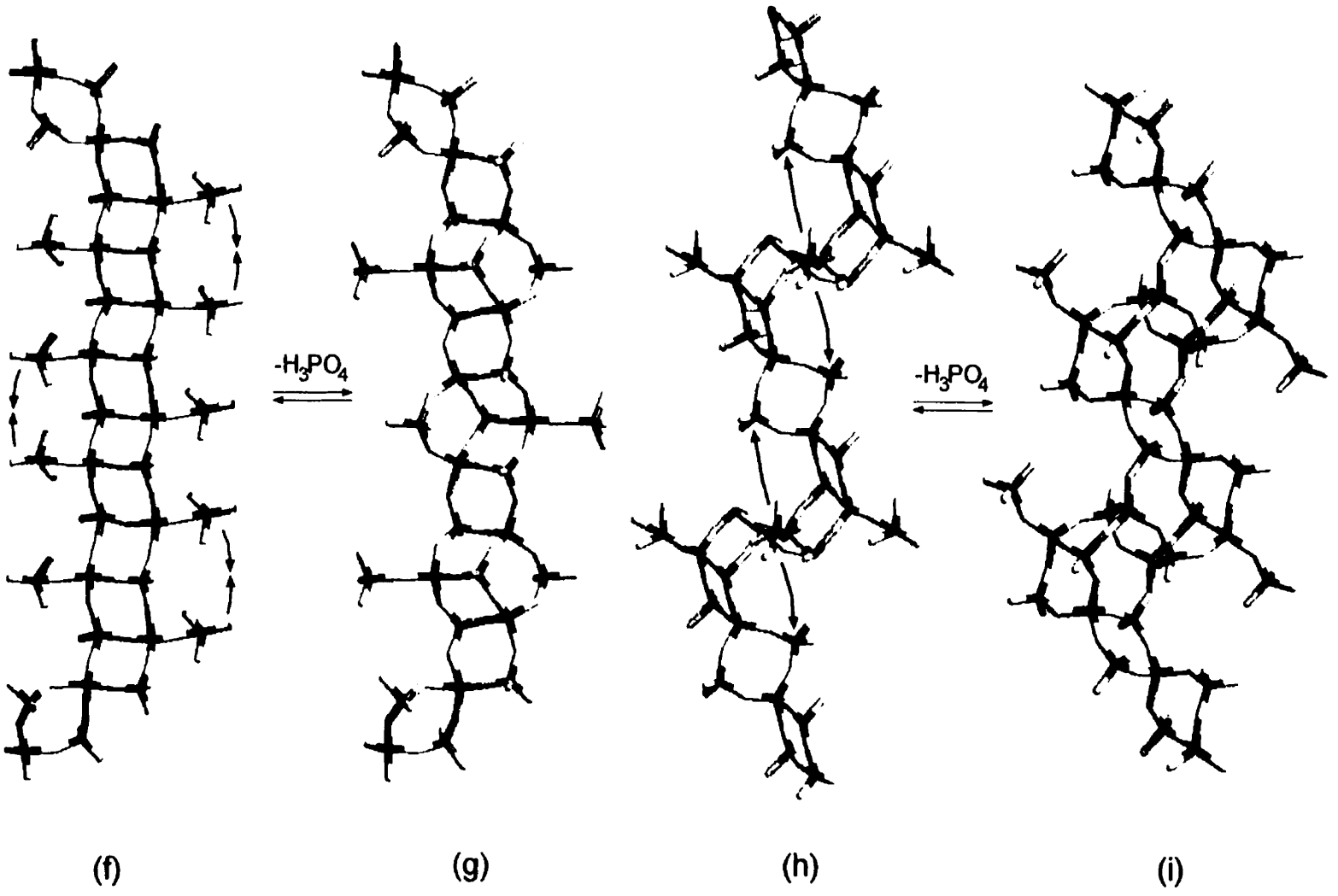

Figure 4-6 (Cont'd). (f) The trans chain, $\Diamond_n(T_P)_{10}\Diamond_n$. (g) Intra-chain condensation to give a chain with edge-sharing four-rings and capped six-rings. (h) $\Diamond_3(C_P)_5$. (i) Intra-chain condensation of the C_P section to the parent chain section.

the starting P:Al molar ratios of the synthesis mixture. However, the largest value of 2.0 is present on what is proposed as the parent chain. By hydrolyzing terminal phosphates off transformed chains, the P:Al ratio is gradually reduced. This allows virtually any chain stoichiometry to be formed, and will necessarily be the same as the materials which they build up. The greater the degree of hydrolysis, the more phosphates that are removed, particularly in condensing to layers and frameworks. This accounts for the generally lower P:Al ratios of the higher dimensionality aluminophosphates.

As for zeolites, all aluminophosphates avoid direct Al-O-Al linkages between AlO_4 tetrahedra according to Lowenstein's rule.[39] Recent energy of formation calculations show this rule to be strictly obeyed for aluminophosphates.[40] There are also no P-O-P linkages in the non - metal-substituted, tetrahedral aluminophosphate frameworks, and the P:Al ratio is therefore always 1.0. These rules are also obeyed by the parent chain, which initiates the alternating Al and P centres. It is interesting to note that the aggregation polymers of aluminophosphates prefer to form in solutions with P:Al ratio from 1 to 2,[29-31,41] which are also the ratios used for the synthesis of chain, layer and framework aluminophosphates.

4.2.4 Chain to Chain Transformations

Having introduced the various chain types and the way in which they form, examples will be given that illustrate how they comprise the architectures of aluminophosphate materials, beginning with the lower dimensionality structures. The above hydrolysis, rotation and condensation processes in themselves represent chain to chain transformations. However, there is only one actual example of such a transformation, owing to the simple fact that there are only two known chain aluminophosphate crystal structures to date, namely the parent chain and the chain of UT-2 and UT-7. This transformation was shown in Figure 4-6h-i (cf. Figure 3-5a). The chain of Figure 4-6h may be formed by transformation of the parent chain to a partial cis-trans chain, $\Diamond_3(C_P)_5$, in a like manner to Figure 4-2.

Notably, the chain of UT-2 and UT-7 was predicted to exist by this model prior to obtaining its crystal structure. UT-2 may be considered as a trapped kinetic intermediate, where the typically unstable singly-bridging, triply-terminal $P(O_{Al})_1O_3$ phosphates interact with those of the neighbouring chains *via* hydrogen bonds, not allowing the chains to covalently cross-link to a layer or framework. This is the case when the conditions are not too rigorous; at higher

temperatures or hydrolytic conditions, a layer or framework is the product (see below). Note the location of the terminal phosphate groups on the edge-sharing four-rings, as expected (Figure 4-6i). UT-2 is the first example of an extended aluminophosphate structure to contain such a group. The only other aluminophosphates that contain a singly-bridging phosphate group are monomeric clusters.[1-3,6,7,10-12] The amphiphilic property of the cycloalkylamine molecules may have also been important in obtaining this structure (section 4.3.4).

4.2.5 Chain to Layer Transformations

Numerous aluminophosphate layers are now known, where many possess the same layered architecture and differ only in the species present between the layers (section 1.2.1). Consequently, the four examples that will be shown in this section encompass almost all of the layered aluminophosphates known to date.

The first example is the $AlPO_4$-5-like layer, $[Al_3P_4O_{16}]^{3-}[R^+]_3$, which is found in UT-1[42] and other polytypes.[43,44] Intra-chain condensation of the $\Diamond_3(T_P)_5$ chains (Figure 4-7a) creates $[Al_3P_4O_{16}]^{3-}$ chains containing capped six-rings (Figure 4-7b). These further condense to create four-rings and twelve-rings, defining the two-dimensional net[45] (Figure 4-7c). The resemblance of the layered structure to $AlPO_4$-5 itself is likely not a coincidence (section 4.2.6).

Another chain to layer transformation is given in Figure 4-8. The $[Al_3P_4O_{16}]^{3-}$ layer structure[46-48] has been isolated from several non aqueous systems, such as UT-8 from TEG. As was shown in Figure 4-6f-g, the $[Al_3P_4O_{16}]^{3-}$ chain of Figure 4-8a is formed from an all-trans $(T_p)_n$ chain by loss of terminal phosphate groups and additional intra-chain condensation. Connection of these chains forms the layered architecture (Figure 4-8b).

The third example is the recently reported layered aluminophosphate of Williams *et al.*[49] Its novel layered structure may be accounted for by the $\Diamond_2(T)_3$ chain of Figure 4-9a. The $\Diamond_2(T)_3$ chains connect together to form six-rings and create the layer (Figure 4-9b). Interestingly, in light of the present discussion, the authors proposed a new "double-diamond" secondary building unit (SBU), which is two corner-sharing four-rings connected at the aluminum centre. However, they must be arranged correctly in an array to fully define the layer structure. Their proposed SBU may be considered as just a small section of the $\Diamond_2(T)_3$ chain.

The final chain to layer example is the previously discussed UT-2 to UT-3 transformation (section 3.7). Prior to discovering the structural relationship between the two phases, the

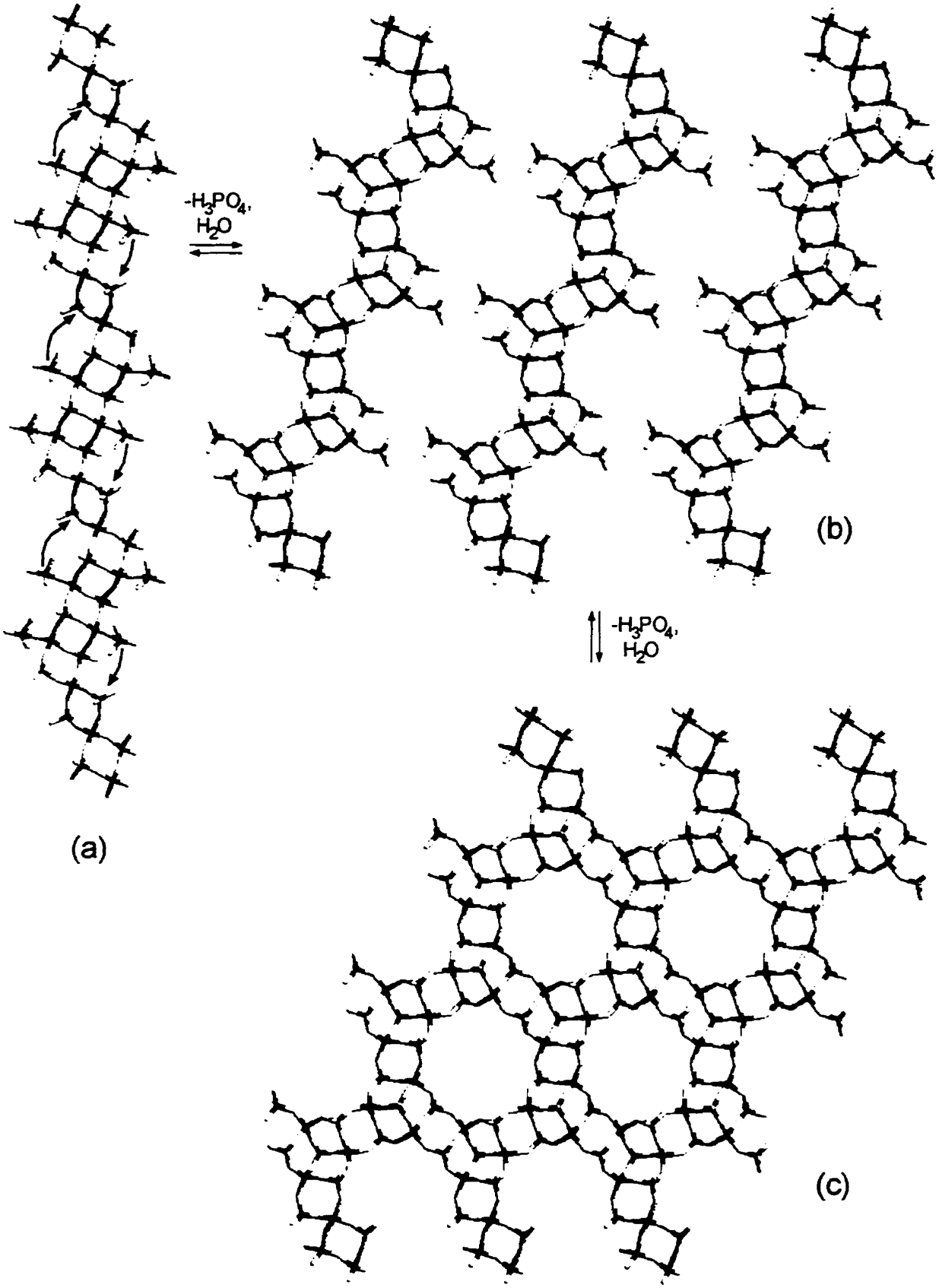

Figure 4-7. Formation of the capped $AlPO_4$-5-like layer. (a) The $\Diamond_3(T_P)_7$ chain. (b) Intra-chain condensation. (c) Inter-chain condensation.

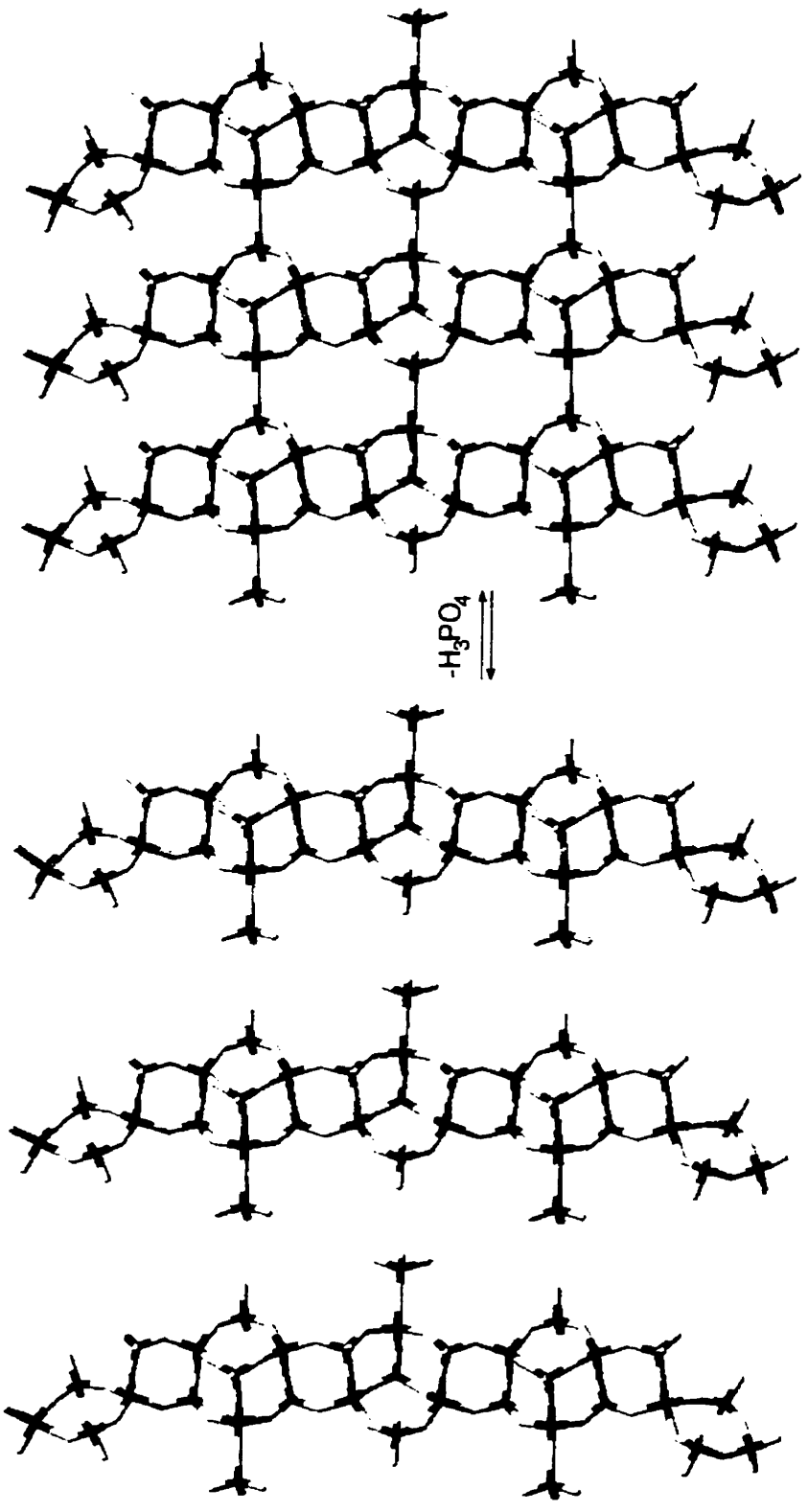

Figure 4-8. Construction of the capped $[Al_3P_4O_{16}]^{3-}$ layer. (a) The chain of Figure 4-6g, formed by intra-chain condensation of the $(T_P)_{10}$ chain of Figure 4-6f. (b) Condensation with loss of terminal phosphate groups and water.

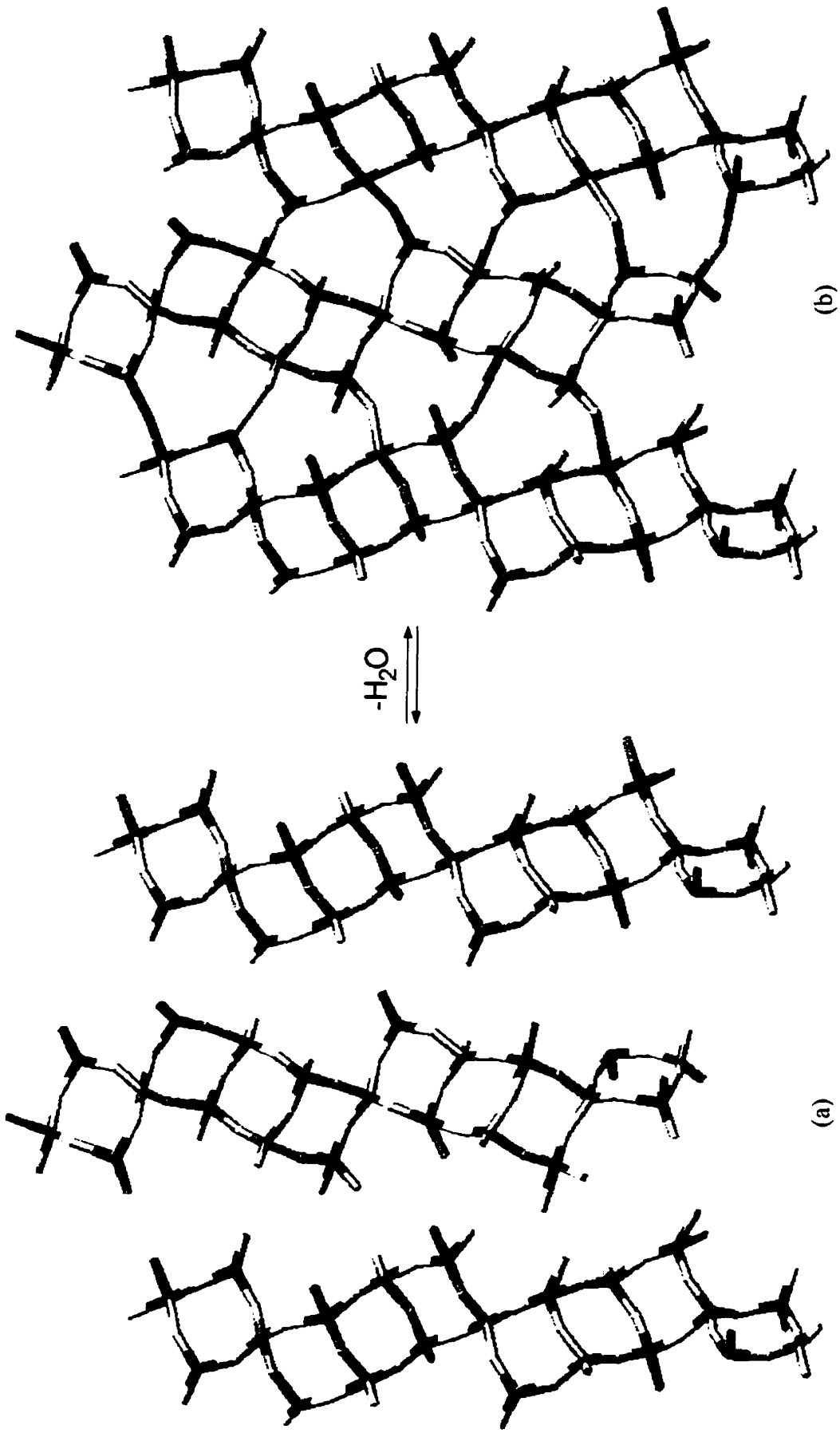

Figure 4-9. Formation of the recently reported layer of Xu *et al.*[49] (a) A partial trans chain, $\diamond_2(T)_3$. (b) Connection through six-rings creates the layer.

building chain of the UT-3 layer (Figure 3-7a), as well as those of UT-4, UT-5 and the sec-$BuNH_3^+$-templated layer,[50] was thought to be an open $\Diamond_1(O)_1$ chain. However, this turned out not to be the case, since the layer is directly formed by the solid state transformation of the UT-2 chain, and this almost certainly occurs in the synthesis of UT-3. The actual rearrangement that must occur, comparing the two structures, is rather complex and will not be shown here. One possible pathway was worked out, and is not unlike the chain transformations that are shown above. It involves a series of hydrolysis, translation, rotation and condensation processes, where the chains also link together to form layers.

The source of UT-2 appeared to be an open, amorphous phase (II-130 to II-132). Judging by the observed UT-2 to UT-3 transformation, it strongly implies that such a process is occurring for the other aluminophosphate layers. Therefore, chain species initially exist in solution, which aggregate together to form a solid-state precursor of a layer of chains, which subsequently transforms to a layered structure. This would be in agreement with the *in situ* studies of others, where an unknown, open "layered" aluminophosphate material is formed prior to the appearance of a crystalline layer or framework.[51-54] The crystalline product will be a one-dimensional chain only if the conditions and the template properties are correct. Otherwise, the chains cross-link to form a layer or framework and the initial chain structure is often obscured in the process.

Consideration of the isostructurality among the UT-n chain and layered crystal structures also implies that the analogous chain to layer process is occurring for the other cycloalkylamine-related phases, as discussed in chapter 3. Just as UT-2 transforms to UT-3, and UT-5 is isostructural to UT-3, there is likely a cyclohexylammonium-related aluminophosphate chain structure that is isostructural to UT-2. Similarly, since UT-7 is isostructural to UT-2, there should exist a cycloheptylammonium-related layer that is isostructural UT-3, as implied by the VT-PXRD of UT-7 (Figure 3-14a, section 3.11).

4.2.6 Chain to Layer to Framework Transformations

As previously mentioned, the similarity of the structures of the $AlPO_4$-5-like layer and $AlPO_4$-5 framework already implies that the phases are related. An obvious way to account for the formation of the framework is by removal of the capping phosphate groups present on the six-rings of the layer, followed by interlayer condensation to define the $AlPO_4$-5 framework. However, there is little reason for the capping phosphate groups to be the most susceptible to

removal. Moreover, no evidence has shown that any of the $AlPO_4$-5-like layers transform even in part to the $AlPO_4$-5 framework.

Therefore, the pathway in Figure 4-7b-c need not be followed in the formation of the $AlPO_4$-5 framework. The $\Diamond_3(T_P)_5$ chains of Figure 4-7a responsible for the $AlPO_4$-5-like layer could bypass the layer "intermediate" and undergo simultaneous chain to framework connection to create the framework (as will be shown below for the VPI-5 framework, section 4.2.8). The choice of $AlPO_4$-5 layer or $AlPO_4$-5 framework is determined by the template that is used or the degree of hydrolysis that occurs on the chain-building species. Under more hydrolytic conditions, be it in terms of temperature, P:Al ratio, reagent concentrations or water concentrations, extensive cross-linking occurs and a framework material is formed. This would account for the relative ease of synthesizing $AlPO_4$-5, which can be accomplished with a large number of different templates in both aqueous[55] and non aqueous systems.[32,56] In contrast, the $AlPO_4$-5 like layer has been synthesized in a limited number of systems and with only a few possible templating agents.

Worthy of mention in light of a layered versus framework $AlPO_4$-5, are two metal-substituted MAPO-n frameworks.[55] MAPO-46 is comprised of two capped $AlPO_4$-5-like layers arranged back to back, with the caps pointing in opposite directions. One layer is the phosphate-capped $AlPO_4$-5-like layer, while the other contains six-rings in which, instead, the phosphorus centres of the six-rings are capped by a metal atom. This "double-layer" connects to the next through the respective phosphate and metal caps to define the overall framework. The second MAPO-n framework, CoAPO-50, is comprised exclusively of the $AlPO_4$-5-like layer structure, where the tetrahedral cobalt atoms triply cap the opposite side of the six-rings, and connect to the phosphate caps of the next layer. While the predominance of the $AlPO_4$-5 framework architecture is commonly noted,[55] it appears that the capped $AlPO_4$-5-like layer structure is also a predominant architecture among the $AlPO_4$-n frameworks. This in turn underlines the important role of the $\Diamond_3(T_P)_5$ chain of Figure 4-7a in the formation of aluminophosphate chains, layers and frameworks.

In this context, it is also noteworthy that the arrangement of four-, six- and eight-rings in the $[Al_3P_4O_{16}]^{3-}$ layer (Figure 4-8b) is identical to that of $AlPO_4$-12 and $AlPO_4$-25, where the six-rings of the $[Al_3P_4O_{16}]^{3-}$ layer are again capped by a triply-bridging phosphate.[8] As for the $AlPO_4$-5-like layer, the $[Al_3P_4O_{16}]^{3-}$ layers can cross-link to form the $AlPO_4$-12 or $AlPO_4$-25

framework by removing the capping phosphate groups, or the starting chains of Figure 4-8a could by-pass the layer to directly form $AlPO_4$-12 or $AlPO_4$-25.

4.2.7 Chain to Framework Transformations

An example of the connection of chains directly to a framework is displayed by the example of JDF-20.[58] This framework structure was obtained in the TEG-triethylamine system, in a mixed phase product also containing the parent chain (section 2.3.2.3). The structural similarities of these two phases led to the initial development[32] of the present model. The JDF-20 structure can be accounted for by two chain types, namely the $\Diamond_n$ parent chain itself and the $[Z(3,3)]_n$ zig-zag chain of Figure 4-5b. The $\Diamond_n$ parent chain connects to two $[Z(3,3)]_n$ zig-zag chains *via* six-rings, Figure 4-10a-b. Each of these two $[Z(3,3)]_n$ chains is in turn connected to two $[Z(3,3)]_n$ chains, thereby forming two sets of eight-ring channels, Figure 4-10c-d. The presence of parent and zig-zag chains in the final product requires hydrolysis conditions that are less severe, making it not surprising that this material was discovered in the predominantly non aqueous tEG system.

The one-dimensional building chains are arranged around the unidimensional elliptical channels containing the triethylammonium template molecules (see Figure 1-1b). The empirical formulae of the building chains are $[AlP_2O_8H_2]^-$ for the $\Diamond_n$ parent chain and $[Al_4P_4O_{17}]^{2-}$ for the $[Z(3,3)]_n$ zig-zag chain. However the latter are exactly double the length per formula unit than the former. Therefore, the chain formulae may be written as $[AlP_2O_8H_2]^-$ and $[Al_2P_2O_{8.5}]^{2-}$. The ratio of the chains in the JDF-20 framework are 1 to 2, respectively, and the overall formula of the JDF-20 framework (after loss of water by condensation of the chains) is accordingly $[Al_5P_6O_{24}H]^{2-}$.

4.2.8 Chain Encapsulation

Just as two or more chain types can co-crystallize to build up a structure, it is also expected that the chains will connect to any other inorganic species that co-exist in the system to which it can condense, such as monomeric or oligomeric aluminum oxide, aluminophosphate or metal oxide species. This would be the case for the "metal-substituted" MAPO-46 and CoAPO-50 frameworks, above.

As discussed in Chapter 1, the coordination and aggregation state of aluminum oxide,[59,60] aluminophosphate small molecules[10,11] and aluminophosphate aggregation polymers[28-31] are all

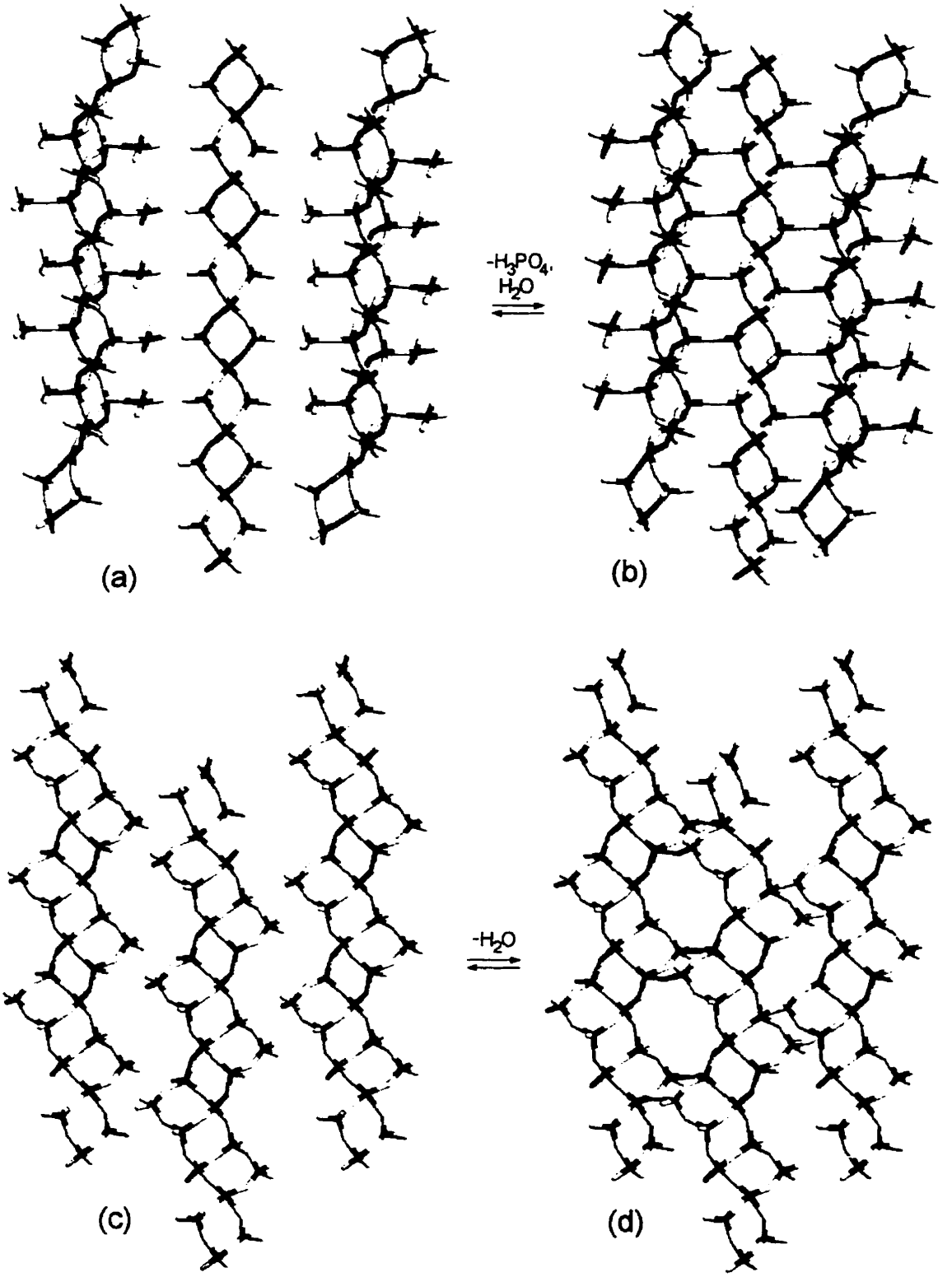

Figure 4-10. Chain condensation to define the JDF-20 framework. (a) Two zig-zag chains, $[Z(3,3)_p]_n$, connect to a parent chain, $\Diamond_n$. (b) Formation of six-rings on either side of the parent chain. (c) End-on view of three units from part b. (d) Connection of zig-zag chains forms to eight-ring channels.

known to be highly dependent on pH. Therefore, under the correct synthesis conditions, other aluminum oxide and aluminophosphate species are anticipated to be present in solution. These species should end up in the structures that are isolated from such systems, surrounded (or "encapsulated") by and connected to the chains. This represents yet another degree of freedom for the present model and accounts for a number of structure types.

One example of chain encapsulation is the UT-6 chabazite-like fluoroaluminophosphate framework (section 3.5). Its structure becomes easy to rationalize with the $\Diamond_3(T)_3$ chain (Figure 4-11a). These chains surround one aluminum of partially fluorinated Al-$(\mu$-F$)_2$-Al double octahedra, to form the bottom six-ring of the hexagonal prisms (emphasized by the hexagon, Figure 4-11b). The other aluminums of these double octahedra connect to the next layer of chains, below the plane of the page. Likewise, a plane of double octahedra above the plane of the page would complete the upper six-ring of the hexagonal prisms (second hexagon, Figure 4-11c). In this way, the UT-6 framework is constructed, containing a primitive array of hexagonal prisms.

Another example is $AlPO_4$-tinsleyite,[61] Figure 4-12. The build-up of the tinsleyite framework (section 3.4) can be rationalized by the $(O_p)_n$ chain of Figure 4-12a, which connects to Al_2O_{10} aluminum double octahedra on either side of the chain, Figure 4-12b-c. The aluminum centres of the $(O_p)_n$ chain are rendered octahedral by the terminal water ligands. This is commonly seen in other aluminophosphate frameworks, such as VPI-5,[62,63] $AlPO_4$-H2,[63,64] or the aluminophosphate hydrates.[65]

Similarly, chain encapsulation accounts for some layered aluminophosphates. For example, the layered structure of ULM-13[66] can be thought of as the $[Al_3P_4O_{16}]^{3-}$ capped $AlPO_4$-25-like layer of Figure 4-8b, where an extra aluminum is connected to the layer. The presence of an extra aluminum results in a molecular formula of $[Al_4P_4O_{16}]^{3-}$, excluding the phosphate hydrogens and fluorines of the aluminums.

The final example, also involving chain encapsulation of AlO_6 octahedra, is VPI-5 (Figure 4-13). The synthesis of this material has been the subject of many studies.[51-54,62-64,67-71] Thus far, the reasons for the formation of such a large-pore material have not been fully elucidated. Here, an $(O_P)_2(T)_2$ chain is proposed to be the building chain of VPI-5. By loss of one quarter of the terminal phosphates, a less symmetric $(O)_2(T)_2(O)_1(O_P)_1(T)_2$ chain type is formed (Figure 4-13a). Connection of these chains to AlO_6 octahedra gives rise to the 18-

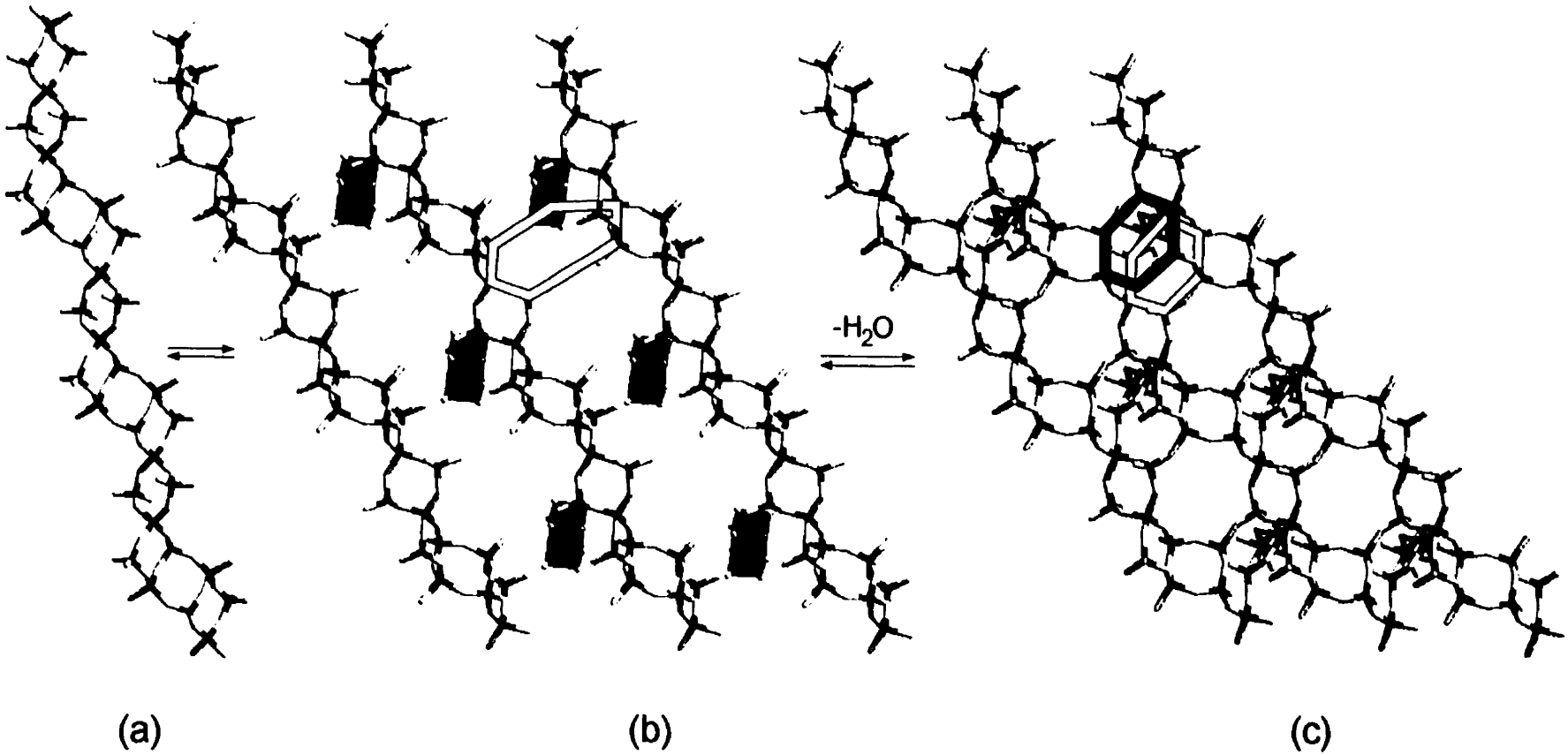

Figure 4-11. Formation of UT-6. (a) $\Diamond_3(T)_3$ chain. (b) The chains surround one octahedron of the $Al_2F_2O_8$ dimers to create the bottom six-ring (hexagon). (c) Connection to another plane of dimers above the plane of the page results in the top six-ring (second hexagon).

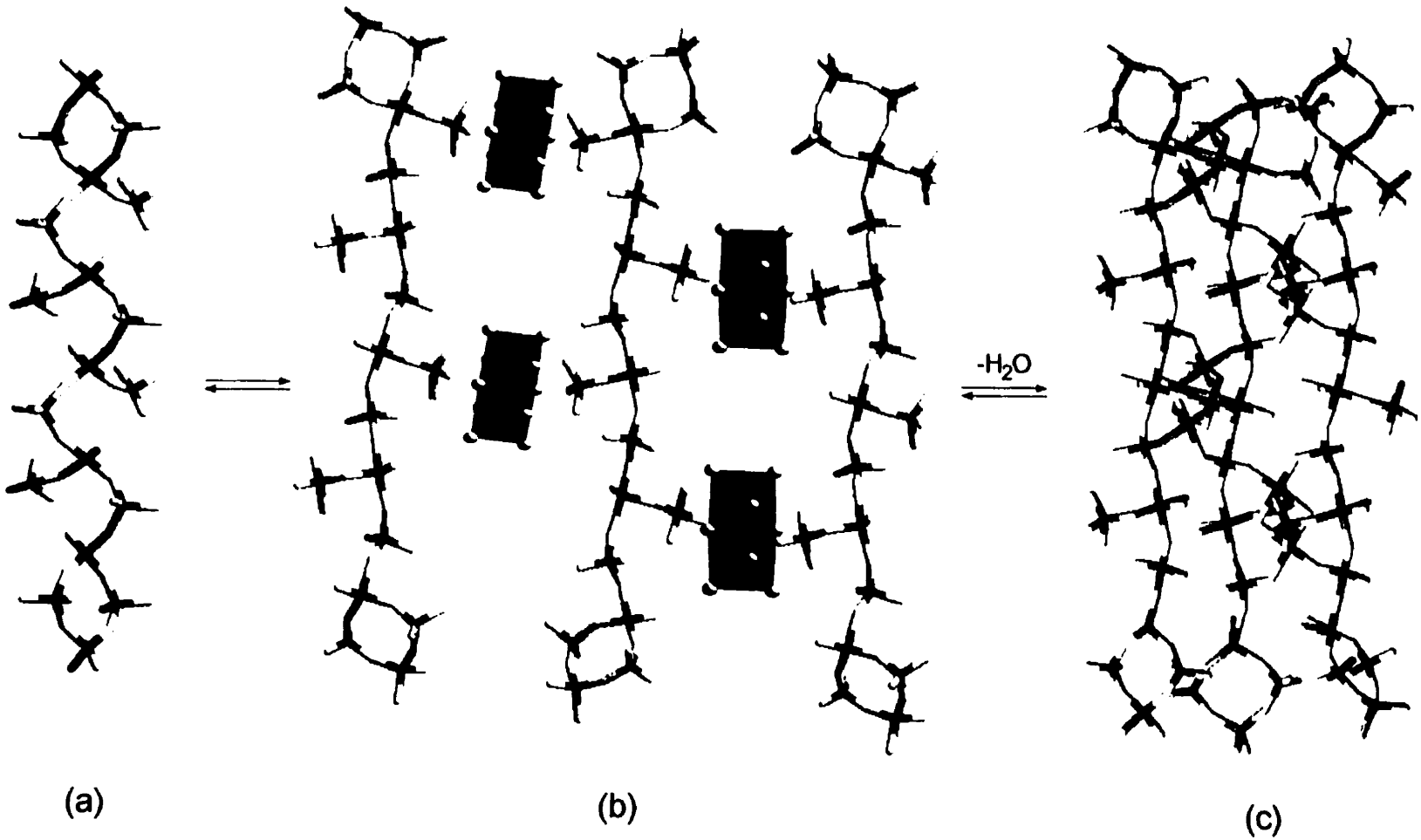

Figure 4-12. Construction of $AlPO_4$-tinsleyite. (a) The open chain type, $(O_p)_n$. (b) The terminal phosphate groups extend above (left in this view) and below (right in this view) the Al_2O_{10} double octahedra. (c) Condensation to form the distorted eight-rings of the framework.

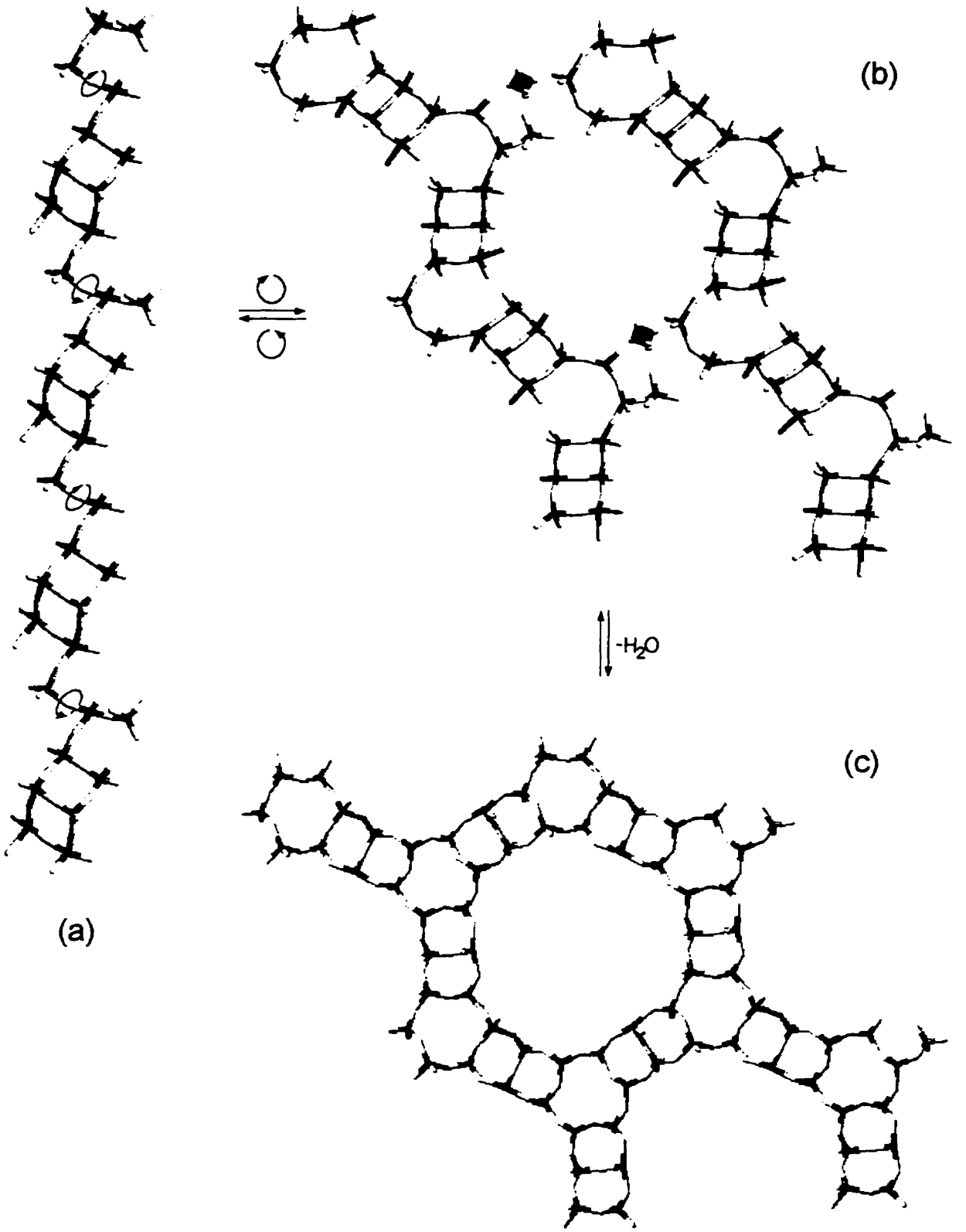

Figure 4-13. Construction of VPI-5, by-passing any capped VPI-5-like layered "intermediate". (a) A low-symmetry $(O)_2(T)_2(O)_1(O_P)_1(T)_2$ chain. (b) Rotation around the linkages, as shown in part a, surround aluminum octahedra with terminal phosphate groups. (c) Condensation to give the framework.

membered rings (Figure 4-13b-c). The aluminums are octahedral due to the terminal waters that reside in the main channel.[62,63,72] This pathway would be consistent with the difficulty of synthesizing VPI-5,[53,54] as one must first age the gel, and then carefully control the pH. In order for the process of Figure 4-13 to occur, one must first leach aluminum oxide species into the gel, as well as build up the more complex chain type of Figure 4-13a.

4.2.9 Framework to Framework Transformations

There also exist a series of known aluminophosphate framework to framework transformations (section 1.1.4.4). Examples are $AlPO_4$-21 to $AlPO_4$-25,[34] $AlPO_4$-C to $AlPO_4$-D,[35] VPI-5 to $AlPO_4$-8[73-77] and UT-6 to $AlPO_4$-CHA (section 3.5). These topotactic rearrangements occur by heating the starting material. They are said to involve a series of hydrolysis, reconstructional and condensation processes. The chemistry that is occurring is identical to the various chain-related processes that have been proposed, as well as the UT-2 to UT-3 chain to layer transformation, or even the collapse of an open aluminophosphate to a dense phase. The only difference is the dimensionality of the material or species that is being considered. The framework to framework transformations therefore provide supporting evidence for the chain model.

The UT-6 structure thermally transforms in the solid state to $AlPO_4$-CHA, with removal of the bridging fluorines and extra-framework template cations (section 3.5). This suggests that this is the mode by which $AlPO_4$-CHA is formed. Without the UT-6 "missing link" or precursor phase, it would be extremely difficult to rationalize the formation of the chabazite structure. Similarly, only with the knowledge of the structures of the two end-products can the VPI-5 to $AlPO_4$-8[78,79] transformation be proposed.[76,77,80]

4.3 DISCUSSION OF SYNTHESIS RESULTS

Now that the chain model for the formation of extended aluminophosphates has been demonstrated, a discussion of the synthesis results of Chapter 2 can proceed. Several of the more important parameters will be discussed, and arranged into sections according to one particular parameter. As with most synthetic systems, this represents only a fraction of the large number of variables that are responsible for the formation of the final product. However, it is hoped that the discussion will serve to sort out the large amount of results that were shown in Chapter 2.

4.3.1 Reaction of Phosphate and Pseudoboehmite

One important aspect of the chemistry that is occurring in the system is the phosphate-psuedoboehmite reaction. As mentioned previously, this reaction has been well studied.[1-4] Spectroscopic investigations of aged reaction gels showed that the reaction proceeds with time at ambient conditions.[4,81] With longer time, aluminophosphate complexes are produced by the reaction of phosphate with the pseudoboehmite. This would account for the necessity of gel aging in the synthesis of some aluminophosphate materials such as VPI-5.[53,54,81]

Similarly, both the rate[4,81] and mechanism[2] of the phosphate-pseudoboehmite reaction have been shown to be dependent on the phosphate concentration. Holding other variables constant, this equates to the P:Al ratio. Higher ratios produced more hydrolyzed phases in the TEG-Et_3N system (II-47 to II-53). This ratio also has a profound effect on the phases of the aluminophosphate minerals and hydrates that form.[41] Aluminum isopropoxide, on the other hand, hydrolyzes rapidly in solution and reacts immediately with phosphate to form aluminophosphate complexes.[81] Consequently, no gel aging is needed for experiments with this source of aluminum. The fast reaction accounts for the generally lower crystal sizes and reduced crystallinity when using aluminum isopropoxide (e.g., II-54, II-93).

Another factor affecting the phosphate reaction with pseudoboehmite would be any compound that complexes the alumina. For example, waste-water treatment studies for the removal of phosphate have shown that organic anions such as citrate compete with phosphate for the adsorption sites of aluminum oxides.[82] Alumina has been shown to react with ethylene glycol to form covalently linked aluminoglycolate anions.[83] More importantly, "glycothermal" treatment of gibbsite with ethylene glycol forms boehmite with ethylene glycol intercalated between the layers and covalently linked to the aluminum centres.[84,85] The TEG solvent may therefore be competing with phosphate for the pseudoboehmite surface, resulting in a slow release of aluminophosphate species. This may be important in the formation of large crystals that were often obtained from TEG systems (e.g. UT-2, II-132). In this respect, it is reasonable that the lower solubility of the reaction gel in non aqueous solvents compared to aqueous solution is at least partially a factor.[57]

4.3.2 Concentration Effects

The changing of concentration by altering the volume of solvent has a marked effect on the resulting product. On the dilution side, dense phases prevail (e.g., II-39, II-40), which can be

attributed to the reduction in effective concentration of template. In the absence of a template, an open structure cannot form and the aluminophosphate species simply connect to form a condensed structure which is most stable under the given conditions. Holding the volume of solvent the same and decreasing the moles of template has the same effect (e.g., II-42 to II-45, II-168 and references 39, 78, 81).

As for zeolite synthesis,[39] more concentrated conditions result in a thick, highly cross-linked reaction gel when water is the solvent. The products are often the expected phase for that template but are of low crystallinity and crystal size. In the TEG system, this was also the case. Certain amines caused the synthesis mixture to thicken to a greater degree even using the same reagent ratios, such as cyclooctylamine (II-165) or cyclododecylamine (II-175). In these cases, the thickening of the mixture is due to the formation of an alkylammonium-phosphate solid. A gradual increase in viscosity of the mixture was observed for cyclopropylamine through cyclododecylamine, as well as the n-alkylamines (Chapter 5).

The use of aluminophosphates as source reagent or crystal seeds were unsuccessful. Large UT-1 crystals were placed into a TEG-10.0 H_2O-Et_3N experiment of II-25. However, the product was only the usual JDF-20 material. Evidently, the crystals simply dissolved and behaved as an additional source of aluminophosphate. Use of a larger amount of a particular phase may give more interesting results, either by a controllable, slower release of aluminophosphate species, as in the formation of 10 μm crystals of $AlPO_4$-H4 from $[AlP_2O_8H_2]^-$ $[Et_3NH^+]$ (III-8), or by inducing a transformation to a new or unsolved phase.

Finally, the slow-release of other compounds from the Teflon liners may also occur due its porosity, such as the formation of UT-6, a fluoroaluminophosphate, without the addition of a fluorine source (II-105). In this way, not only does the liner behave as the source of fluorine, but it could be releasing the fluorine at a controlled rate to yield a small number of large UT-6 crystals. A similar process could be occurring with the reproducible synthesis of UT-1 (II-70, II-71). The slow-release phenomenon certainly warrants further study, and could be a procedure for the formation of large crystal sizes of both known and novel phases.

4.3.3 Role of Solvent and Concentration of Water

As was observed, the type of solvent greatly influenced the phases and/or morphology that were obtained. For example, higher molecular weight polyethylene glycols resulted in

smaller crystals for the triethylamine system (II-81 to II-90, section 2.3.2.3.8). This may be attributed to the high viscosity of these solvents, which in turn decreases the rate of convection of the overall reaction mixture. As a result, there is a higher yield of smaller crystals since the nutrient species quickly condense to the nearest growing crystal rather than being transported or diffusing to a large, growing crystal. A similar argument can be made for the difference in crystallinity of the UT-6 product from a pyridine solvent versus a TEG solvent (II-109 and II-106, respectively, section 2.3.4.2). However, the solubility of the source reagents could also be a factor in this respect, as well as a chelating-effect of the polyethylene glycol solvent. This can only be elucidated with further experimentation.

The higher polarity of the EG solvent accounts for the formation of $AlPO_4$-5 (II-76, section 2.3.2.3.8) rather than the typical product of the chain structure or JDF-20 using TEG. However, DEG (II-77) and tEG (II-78 to II-80) each contain an ether linkage and therefore give results similar to TEG. The polarity of the solvent likely contributes towards the hydrolysis of the aluminophosphate species and/or solid intermediates, resulting in a more hydrolyzed phase.

The concentration of water had a major influence in all of the non aqueous systems. Examples are the sec-BuOH-H_2O-Et_3N system (II-94 and II-95, section 2.3.2.3.8), the TEG-H_2O-Et_3N system (section 2.3.2.3.2) and the TEG-H_2O-cycloalkylamine systems (section 2.3.5). To demonstrate this point, a qualitative plot of the resultant aluminophosphate phase versus water content is shown for the TEG-H_2O-Et_3N system, Figure 4-14. The explanation of this effect follows directly from the chain model introduced above. The higher the water content of the non aqueous solvent, the more hydrolysis that occurs on the aluminophosphate chain precursor species, and therefore the more hydrolyzed the phase that is obtained. This is certainly reflected in the results obtained when only water is used as the solvent, for example with triethylamine (II-39, II-40) or cyclopentylamine (II-145).

Similar plots may be made for any of the other organothermal systems, and indeed it would be interesting to explore further the effect of water concentration on the non aqueous synthesis of extended inorganic materials in general.

4.3.4 Role of Template

The vital role of the template agent is clearly evident, since in its absence, only dense phase aluminophosphates or hydrates are formed in both organothermal (II-45, section 2.3.2.3.4) and hydrothermal systems.[78,79,81] Similarly, the resultant structure(s) is (are) dependent on the

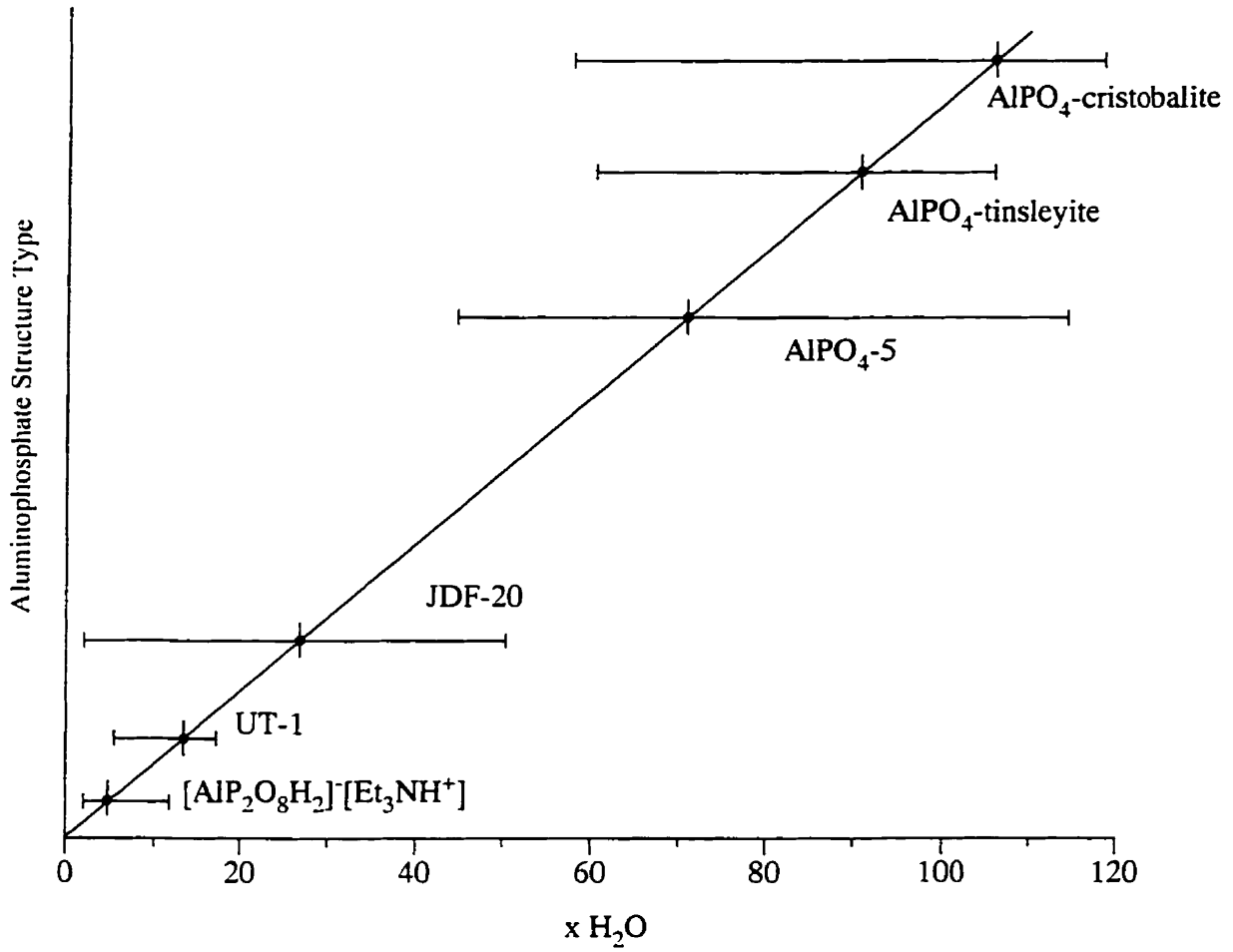

14 TEG : 0.9 $Al_2O_3 \cdot nH_2O$: 3.6 H_3PO_4 : 5.9 Et_3N : x H_2O

Figure 4-14. Dependence of the resultant aluminophosphate phases on the water content of the TEG-H_2O-Et_3N system.

template, where the organic amine occupies the interior pores, channels or interlayer space and stabilizes the openness of the material. It also charge-balances the anionic aluminophosphate architecture. In these ways, the organic assumes the role described by template theory.[39,87-89] However, the complete role of template is certainly not fully understood. Generally, the template is believed to play a structure-directing role in parallel with the gel chemistry that is occurring (section 1.1.4.1).[88,90] As for zeolites and other extended inorganic materials, there exist both template-dependent and template-independent structures, such as tinsleyite and $AlPO_4$-5, respectively.

Under the chain model, the final structure is controlled by both chain type and the template properties. For example, JDF-20 is built of two chain types that can account for its structure. However, their arrangement into unidimensional elliptical channels follows the shape of the occluded triethylammonium molecules (Figure 1-1b). The latter must cooperatively arrange the chain building-blocks during the formation of the framework. Since triethylamine is the only organic amine known to allow the synthesis of JDF-20, this is an example of a template-dependent structure.

The phenomenon of template-independence may be rationalized by the prevalence of a certain chain type. For example, the $\Diamond_3(T_p)_7$ chain forms the $AlPO_4$-5-like layer or $AlPO_4$-5 framework. In fact, the $\Diamond_n(T)_n$ chain types are present in many of the examples that were shown, such as $\Diamond_3(T)_3$ for UT-6, or $\Diamond_2(T)_3$ for the layer of Williams *et al.*[49] This simplifies the model by minimizing the number of reconstructional processes necessary to incur on the parent chain. Another reason for template-independence of the as-synthesized $AlPO_4$-n frameworks is their electroneutrality. In these cases, the template exists in its neutral form in the interior channels, such as TPAOH for $AlPO_4$-5,[55] and there are only weak interactions between framework and template. Therefore, there is a greatly reduced dependence on a particular template.

The template amphiphilicity will be important in directing the formation of the aluminophosphate product. For example, the cycloalkylamines always formed a bilayer in the interlayer region for the chain or layered UT-n aluminophosphates. This may separate the layers and prevent them from cross-linking to a framework structure.

The chain or layered phases always contain doubly- or triply-bridging phosphate groups that essentially cap the layers and terminate the connectivity along the interlayer axis. These phosphate groups necessarily contain terminal oxygens and are involved in hydrogen bonds with

the ammonium hydrogens of the template. Therefore, an amine with less alkyl groups, particularly primary amines such as ethylenediamine, are more effective in forming lower dimensionality aluminophosphates. Indeed, none of the layers to date are templated by tertiary or quaternary ammoniums, which are so commonly used for the synthesis of framework aluminophosphates.[55]

Finally, it is interesting to compare the results of different templates that contain similar functionalities. Cyclohexylamine formed two layers, UT-4 and UT-5, and other unknowns (section 2.3.5.12). However, N,N-diethylcyclohexylamine formed only $AlPO_4$-5 and dense phases (section 2.3.5.1). One explanation is that the tertiary nitrogen is sterically crowded and can only possess one hydrogen in its protonated form. Therefore, it cannot interact with the aluminophosphate layers as cyclohexylammonium does in UT-4 and UT-5, which has its primary $R\text{-}NH_3^+$ ammonium group pointing at the layers and involved in three strong hydrogen bonds (Figure 3-10b, Figure 3-12a). Similarly, N,N-diethylcyclohexylamine differs with triethylamine in only one of its alkyl groups (ethyl versus cyclohexyl). However, the former is too sterically crowded to form any of the various phases that triethylamine can lead to (section 2.3.2.3). Therefore, subtle differences in template structure have a profound effect on the aluminophosphate structures that result.

4.3.5 Solution Phase Studies

The presence of at least some type of aluminophosphate solution-bound species was confirmed by boiling off the TEG solvent of the mother liquor of a typical TEG-triethylamine synthesis product (e.g., II-13). Thermal treatment of the resulting black gum-like material in air at *ca.* 500°C resulted in a grey powder, whose PXRD pattern was that of aluminum phosphite. However, all attempts at crystallizing out a solution species by heating, cooling, solvent extraction or adding a chelating agent, were unsuccessful.

Preliminary ^{31}P NMR experiments (300 MHz Gemini instrument, referenced to 85% H_3PO_4) were performed to see if a solution-bound chain or any other aluminophosphate species could be identified. The spectrum of the starting mixture of the TEG-triethylamine system contained only a singlet at approximately 0.0 ppm. Judging by the chemical shift and the mid-range pH values of the synthesis mixtures, this peak may be assigned to dihydrogen phosphate.[91,92] The spectrum remained the same for synthesis mixtures aged for 1 to 4 months.

The mother liquors of the TEG-triethylamine experiments were run, after filtering out the solid phase. After 2 to 4 days of heating, the strong peak at 0.0 ppm was still present, along with a weak peak at *ca.* -2.5 ppm. This more upfield peak is assigned to monohydrogen phosphate.[91] Agreeably, the mother liquors from cyclopentylamine experiments (which form a monohydrogen phosphate salt) showed only a singlet at -2.7 ppm.

A third, weak, broad peak centred at -4 to -6 ppm was also present in the triethylamine mother liquor after 2 or more days. This more upfield peak is of similar chemical shift to the small molecule and oligomeric aluminophosphate species shown to exist in aqueous solution by ^{31}P NMR.[9-11,81] However, these published spectra contained a series of narrow peaks in these ranges and could be assigned to particular aluminophosphate complexes. The broadness of the peak in the present case could be due to an oligomeric aluminophosphate species, since it should be rapidly converting and possess a distribution of chemical shifts, as observed in short chain polymers as well as the lower condensed polyphosphates.[93] Further NMR studies, including solution, solid state and variable-temperature NMR, could be highly beneficial in elucidating the solution aluminophosphate species that are present in the system.

4.4 CONCLUDING REMARKS

It is interesting to note that in a paper by Vaughan, the build-up of zeolite frameworks is discussed not only from sheet and columnar building units, but also a chain unit comprised of edge-sharing four-rings.[94] The latter accounts the zeolite frameworks of offretite, mazzite, Linde type L, gismondine, merlinoite and phillipsite. Even more interesting is that the framework of analcime (which is isostructural to $AlPO_4$-24) may be thought of as built of chains of corner-sharing four-rings. Indeed, it was discovered in the present work that the sodalite framework (isostructural to $AlPO_4$-20) may be thought of as comprised of the parent chain, but this was not included in the examples given in this chapter. It is possible that the model developed in the current work is also applicable to extended structures of other compositions, including zeolites.

In the proposed model of aluminophosphates presented in this work, the chain to layer, chain to layer to framework, chain to framework and framework to framework transformations often obscure the original shape of the building chain in the process. In the absence of the chain intermediates, one could not have proposed such a model by simply studying the final structures. It has been developed only through a series of crystal structures obtained by non aqueous methods. Particularly attractive to the model is that the proposed building units may be

crystallized from the synthetic system, unlike any other model previously put forth. Furthermore, it accounts for the existence of lower dimensionality aluminophosphates and their structures. It is likely that new aluminophosphate chain structures will be discovered in the future and will fall into the categories of the examples that have been given. The desired end-result of this (and any) model is that it will allow for a more complete understanding of aluminophosphate formation and the structures themselves. With such knowledge, one is closer to the rational design of new structure types with desired materials properties.

4.5 REFERENCES

1. D. Muljadi, A. M. Posner, J. P. Quirk, *J. Soil Sci.* **1966**, *17*, 212, and references therein.
2. S. S. S. Rajan, K. W. Perrott, W. M. H. Saunders, *J. Soil Sci.* **1974**, *25*, 438.
3. S. S. S. Rajan, *Nature* **1976**, *262*, 45.
4. E. Laiti, P. Persson, L. Öhman, *Langmuir* **1996**, *12*, 2969, and references therein.
5. R. F. Jameson, J. E. Salmon, *J. Chem. Soc.* **1954**, 4013.
6. A. Holroyd, J. E. Salmon, *J. Chem. Soc.* **1956**, 269.
7. J. E. Salmon, J. G. Wall, L. *J. Chem. Soc.* **1958**, 1128.
8. G. Kühl, *J. Inorg. Nucl. Chem.* **1969**, *31*, 1043.
9. J. W. Akitt, N. N. Greenwood, G. D. Lester, *J. Chem. Soc. (A)* **1971**, 2450.
10. R. F. Mortlock, A. T. Bell, C. J. Radke, *J. Phys. Chem.* **1993**, *97*, 767.
11. R. F. Mortlock, A. T. Bell, C. J. Radke, *J. Phys. Chem.* **1993**, *97*, 775
12. D. Riou, T. Loiseau, G. Férey, *J. Solid State Chem.* **1992**, *99*, 414.
13 D. F. Shriver, P. Atkins, C. H. Langford, *Inorganic Chemistry, 2nd ed.*; W. H. Freeman and Company: New York, 1994; pp. 199.
14. R. H. Jones, J. M. Thomas, R. Xu, Q. Huo, Y. Xu, A. K. Cheetham, D. Bieber, *J. Chem. Soc., Chem. Commun.* **1990**, 1170.
15. W. Tieli, Y. Long, P. Wengin, *J. Solid State Chem.* **1990**, *89*, 392.
16. W. T. A. Harrison, T. M. Nenoff, T. E. Gier, G. D. Stucky, *Inorg. Chem.* **1992**, *31*, 5395.
17. W. T. A. Harrison, T. M. Nenoff, T. E. Gier, G. D. Stucky, *Inorg. Chem.* **1992**, *32*, 2437.
18. P. Kierkegaard, *Acta Chem. Scand.* **1958**, *12*, 1701.
19. R. C. Haushalter, F. W. Lai, *Inorg. Chem.* **1989**, *28*, 2904.
20. L. A. Mundi, R. C. Haushalter, *J. Am. Chem. Soc.* **1991**, *113*, 6340.

21. M. E. Leonowicz, J. W. Johnson, J. F. Brody, H. F. Shannon, Jr., J. M. Newsam, *J. Solid State Chem.* **1985**, *56*, 370.

22. R. C. Haushalter, Z. Wang, L. M. Meyer, S. S. Dhingra, M. E. Thompson, J. Zubieta,. *Chem. Mater.* **1994**, *6*, 1463.

23. K. Lii, T. Lee, S. Liu, S. Wang, *Chem. Soc., Dalton Trans.* **1993**, 1051.

24. A. M. Chippindale, S. J. Breech, *J. Chem. Soc., Chem. Commun.* **1996**, 2781.

25. M. I. Khan, Y. Lee, C. J. O'Connor, R. C. Haushalter, J. Zubieta, *J. Am. Chem. Soc.* **1994**, *116*, 4525.

26. M. Cavellec, D. Riou, G. Férey, *J. Solid State Chem.* **1994**, *112*, 441.

27. H. H. Greger, *Brick and Clay Record* **1950**, *117*, 63.

28. C. F. Callis, J. R. Van Wazer, P. G. Arvan, *Chem. Rev.* **1954**, *54*, 777.

29. J. R. Van Wazer, *Phosphorus and Its Compounds: Vol. I*; Interscience: New York, 1958; pp. 550-559.

30. D. E. C. Corbridge, *The Structural Chemistry of Phosphorus*; Elsevier: New York, 1974; pp. 124-126.

31. J. H. Morris, P. G. Perkins, A. E. A. Rose, W. E. Smith, *Chem. Soc. Rev.* **1977**, *6*, 173.

32. S. Oliver, A. Kuperman, A. Lough, G. A. Ozin, J. M. Garcés, M. M. Olken, P. Rudolf, *Stud. Surf. Sci. Catal.* **1994**, *84A*, 219.

33. A. E. R. Westman, in *Topics in Phosphorus Chemistry 9*, E. J. Griffith, M. Grayson, eds.; John Wiley and Sons: New York, 1977, pp. 247-256.

34. J. W. Richardson, Jr., J. V. Smith, J. J. Pluth, *J. Phys. Chem.* **1990**, *94*, 3365.

35. E. B. Keller, W. M. Meier, R. M. Kirchner, *Solid State Ionics* **1990**, *43*, 93.

36. R. Carson, E. M. Cooke, J. Dwyer, A. Hinchcliffe, P. J. O. Malley, in *Zeolites as Catalysts, Sorbents and Detergent Builders*, H. G. Karge, J. Weitkamp, eds.; *Stud. Surf. Sci. Catal. 46*, Elsevier Science Publishers: Amsterdam, 1989; pp. 39.

37. Q. Huo, R. Xu, *J. Chem. Soc., Chem. Commun.* **1992**, 168.

38. S. L. Cresswell, J. R. Parsonage, P. G. Riby, M. J. K. Thomas, *J. Chem. Soc., Dalton Trans.* **1995**, 2315.

39. R. Szostak, *Molecular Sieves: Principles of Synthesis and Identification*; Van Nostrand Reinhold: Toronto, 1989.

40. C. R. A. Catlow, A. R. George, C. M. Freeman, *J. Chem. Soc., Chem. Commun.* **1996**, 1311.

41. R. Kniep, *Angew. Chem., Int. Ed. Engl.* **1986**, *25*, 525.

42. A. Kuperman, S. Nadimi, S. Oliver, G. A. Ozin, J. M. Garcés, M. M. Olken, *Nature* **1993**, *365*, 239.

43. J. M. Thomas, R. H. Jones, R. Xu, J. Chen, A. M. Chippindale, S. Natarajan, A. K. Cheetham, *J. Chem. Soc., Chem. Commun.* **1992**, 929.

44. P. A. Barrett, R. H. Jones, *J. Chem. Soc., Chem. Commun.* **1995**, 1979.

45. J. V. Smith, *Stud. Surf. Sci. Catal.* **1989**, *49*, 29.

46. R. H. Jones, J. M. Thomas, R. Xu, Q. Huo, A. K. Cheetham, A. V. Powell, *J. Chem. Soc., Chem. Commun.* **1991**, 1266.

47. (a) R. H. Jones, A. M. Chippindale, S. Natarajan, J. M. Thomas, *J. Chem. Soc., Chem. Commun.* **1994**, 565. (b) A. M. Chippindale, S. Natarajan, J. M. Thomas, R. H. Jones, *J. Solid State Chem.* **1994**, *111*, 18.

48. D. A. Bruce, A. P. Wilkinson, M. G. White, J. A. Bertrand, *J. Chem. Soc., Chem. Commun.* **1995**, 2059.

49. I. D. Williams, Q. Gao, J. Chen, L. Ngai, Z. Lin, R. Xu, *J. Chem. Soc., Chem. Commun.* **1996**, 1781.

50. A. M. Chippindale, A. V. Powell, L. M. Bull, R. H. Jones, A. K. Cheetham, J. M. Thomas, R. Xu, *J. Solid State Chem.* **1992**, *96*, 199.

51. E. Jahn, D. Mueller, J. Richter-Mendau, in *Synthesis of Microporous Materials, Vol. 1: Molecular Sieves*, M. L. Occelli, H. E. Robson, eds.; Nelson Canada: Scarborough, 1992; pp. 248.

52. H. He, J. Klinowski, *J. Phys. Chem.* **1994**, *98*, 1192.

53. M. E. Davis, D. Young, *Stud. Surf. Sci. Catal.* **1991**, *60*, 53.

54. M. E. Davis, B. D. Murray, M. Narayana, in *Novel Materials in Heterogeneous Catalysis*, R. T. K. Baker, L. L. Murrell, eds.; ACS Symp. Ser. **437**: Washington, 1990; pp. 48.

55. R. Szostak, *Handbook of Molecular Sieves*; Van Nostrand Reinhold: New York, 1992.

56. Q. Huo, R. Xu, *J. Chem. Soc., Chem. Commun.* **1990**, 783.

57. R. Xu, Q. Huo, W. Pang, in *Proceedings of the Ninth International Zeolite Conference*, Vol. I, eds. R. von Ballmoos *et al.*, Butterworth-Heinemann, London, 1993, p. 271.

58. (a) Q. Huo, R. Xu, S. Li, Z. Ma, J. M. Thomas, R. H. Jones, A. M. Chippindale, *J. Chem. Soc., Chem. Commun.* **1992**, 875. (b) R. H. Jones, J. M. Thomas, J. Chen, R. Xu, Q. Huo, S. Li, Z. Ma, A. M. Chippindale, *J. Solid State Chem.* **1993**, *102*, 204.

59. R. J. Moolenaar, J. C. Evans, L. D. McKeever, *J. Phys. Chem.* **1970**, *74*, 3629.

60. J. W. Akitt, N. N. Greenwood, B. L. Khandelwal, G. D. Lester, *J. Chem. Soc., Dalton Trans.* **1972**, 604.

61. J. B. Parise, *Acta Cryst.* **1984**, *C40*, 1641.

62. P. J. Grobet, J. A. Martens, I. Balakrishnan, M. Mertens, P. A. Jacobs, *Appl. Catal.* **1989**, *56*, L21.

63. H. Li, M. E. Davis, J. B. Higgins, R. M. Dessau, *J. Chem. Soc., Chem. Commun.* **1993**, 403.

64. H. Li, M. E. Davis, *J. Chem. Soc., Faraday Trans.* **1993**, *89*, 951.

65. F. D'Yvoire, *Bull. Soc. Chim. Fr.* **1961**, 1762.

66. J. Renaudin, G. Férey, *J. Solid State Chem.* **1995**, *120*, 197.

67. M. E. Davis, C. Montes, P. E. Hathaway, J. M. Garcés, *Stud. Surf. Sci. Catal.* **1989**, *49*, 199.

68. M. E. Davis, C. Montes, J. M. Garcés, *ACS Symp. Ser.* **1989**, *398*, 291.

69. D. Young, M. E. Davis, *Zeolites* **1991**, *11*, 277.

70. W. Schmidt, F. Schüth, H. Reichert, K. Unger, *Zeolites* **1992**, *12*, 2.

71. M. J. Franco, A. Mifsud, J. Perez-Pariente, *Zeolites* **1995**, *15*, 117.

72. M. J. Duer, H. He, W. Kolodziejski, J. Klinowski, *J. Phys. Chem.* **1994**, *98*, 1198.

73. S. Prasad, I. Balakrishnan, *Inorg. Chem.* **1990**, *29*, 4830.

74. M. Stocker, D. Akporiaye, K. Lillerud, *Appl. Catal.* **1991**, *69*, L7.

75. M. J. Annen, D. Young, M. E. Davis, O. B. Cavin, C. R. Hubbard, *J. Phys. Chem.* **1991**, *95*, 1380.

76. L. Maistriau, Z. Gabelica, E. G. Derouane, E. T. C. Vogt, J. van Oene, *Zeolites* **1991**, *11*, 583.

77. H. He, P. Barnes, J. Munn, X. Turrillas, J. Klinowski, *Chem. Phys. Lett.* **1992**, *196*, 267.

78. S. T. Wilson, B. M. Lok, C. A. Messina, T. R. Cannan, E. M. Flanigen, *J. Am. Chem. Soc.* **1982**, *104*, 1146.

79. S. T. Wilson, B. M. Lok, E. M. Flanigen, U. S. Patent 4 310 440.

80. H. Li, M. E. Davis, *J. Chem. Soc., Faraday Trans.* **1993**, *89*, 957.

81. S. Prasad, S. Liu, *Chem. Mater.* **1994**, *6*, 633.

82. K. F. Ng Kee Kwong, P. M. Huang, *Nature* **1978**, *271*, 336, and references therein.

83. G. J. Gainsford, T. Kemmitt, N. B. Milestone, *Inorg. Chem.* **1995**, *34*, 5244.

84. M. Inoue, Y. Kondo, T. Inui, *Inorg. Chem.* **1988**, *27*, 215.

85. M. Inoue, H. Kominami, T. Inui, *J. Mater. Sci.* **1994**, *29*, 2459.

86. X. Ren, S. Komarneni, D. M. Roy, *Zeolites* **1991**, *11*, 142.

87. D. W. Breck, *Zeolite Molecular Sieves*; John Wiley & Sons: New York, 1974.

88. B. M. Lok, T. R. Cannan, C. A. Messina, *Zeolites* **1983**, *3*, 283.

89. M. E. Davis, R. F. Lobo, *Chem. Mater.* **1992**, *4*, 756.

90. E. M. Flanigen, *Adv. Chem. Ser.* **1973**, *121*, 119.

91. M. M. Crutchfield, C. F. Callis, R. R. Irani, G. C. Roth, *Inorg. Chem.* **1962**, *1*, 813.

92. P. Hartmann, J. Vogel, B. Schnabel, *J. Mag. Res.* **1994**, *111A*, 110.

93. M. M. Crutchfield, R. R. Irani, *J. Am. Chem. Soc.* **1965**, *87*, 2815.

94. D. E. W. Vaughan, *Stud. Surf. Sci. Catal.* **1991**, *65*, 275.

CHAPTER 5: PRIMARY ALKYLAMINES AND ALKYLENEDIAMINES

5.0 INTRODUCTION

Only a limited amount of reports have been made to date for the synthesis of aluminophosphates using primary alkylamines and alkylenediamines. This last chapter will deal with the synthetic work that was performed with this type of organic additive, in order of increasing alkyl chain length, followed by the characterization of some of the more relevant materials. The results showed a marked dependence on alkyl chain length, ranging from a typical small molecule that promotes the formation of crystalline aluminophosphates to amphiphilic behaviour and the formation of a series of mesolamellar phosphates and aluminophosphates.

5.1 SYNTHESIS RESULTS

5.1.1 ALKYLENEDIAMINES

5.1.1.1 Ethylenediamine (en, $H_2NCH_2CH_2NH_2$) [V-1 to V-6]

This organic is an important reagent in inorganic chemistry in general as a strong bidentate ligand.[1] However, in materials chemistry, it is a common templating agent. For aluminophosphates alone, it forms one pentameric cluster,[2] one chain structure,[3] one layered material[4] and two framework materials.[5] A layered fluoroaluminophosphate is formed only by ethylenediamine, where the nitrogen is coordinated to the octahedral aluminums.[6] As was seen in Chapter 1, a variety of other extended metal-oxide, metal-phosphate and metal-arsenate chains,[7] layers[8] and frameworks[9] are formed with ethylenediamine, as well as the salts of monohydrogen phosphate,[10] dihydrogen phosphate,[11] and a mixed trihydrogen phosphate dihydrogen phosphate.[12]

The choice of ethylenediamine (99%, Aldrich) was made due to its templating of the parent chain structure.[3] The chain was synthesized aqueously, while the $[Al_3P_4O_{16}]^{3-}$, $AlPO_4$-25-like layered material was isolated from EG.[4] Therefore, H_2O, EG and TEG solvents were used (V-1 to V-6). The multiphasic products appeared to contain several unknowns, and could not be indexed to any of the known aluminophosphates. Examples are shown in the PXRD patterns of

V-1 and V-3, Appendix B. The monohydrogen phosphate salt was the product from a TEG solvent (V-6).

5.1.1.2 (1,3)-Diaminopropane ($H_2N(CH_2)_3NH_2$) [V-7]

This reagent (99+%, Aldrich) has recently been shown to template a framework aluminophosphate,[13] and forms a monohydrogen phosphate monohydrate salt[14] and dihydrogen phosphate salt.[15] A TEG experiment in fact led to a 1,3-diammoniumpropane monohydrogen phosphate monohydrate as the only product (V-7); unreacted pseudoboehmite can also be seen in the PXRD pattern. Use of higher temperatures (195°C) gave the same phase, with slightly higher crystallinity.

5.1.1.3 (1,4)-Diaminobutane (putrescine, $H_2N(CH_2)_4NH_2$) [V-8]

One of the several polytypes of the $AlPO_4$-5-like layered material forms with this alkylenediamine,[16] as well as a dihydrogen phosphate salt.[17] An experiment similar to that for 1,3-diaminopropane was performed with 1,4-diaminobutane (99%, Aldrich), and gave a crystalline product (V-8). Higher temperatures of 195°C gave a slightly more crystalline product of the same phase. While the PXRD pattern did not match that of the dihydrogen phosphate salt, it is possibly that of the monohydrogen phosphate salt, judging by the results for 1,3-diaminopropane, above. Further work would easily clarify this point, as the salt could be grown by recrystallization.

5.1.1.4 (1,6)-Diaminohexane ($H_2N(CH_2)_6NH_2$) [V-9]

1,6-Diaminohexane (Sigma) is the template of a layered fluoroaluminophosphate.[18] The initial TEG-aluminophosphate synthesis mixture displayed the presence of pseudoboehmite and a crystalline phase (V-9), which is undoubtedly a phosphate salt. However, after heating for 11 days at 180°C, the product was pseudoboehmite and an amorphous material.

5.1.1.5 (1,8)-Diaminooctane ($H_2N(CH_2)_8NH_2$) [V-10 to V-11]

The tendency to form phosphate salts with alkylenediamines continues with this longer alkyl chain (98%, Aldrich). The product after heating for 5 days gave a multiphasic product containing plates, some large enough for SC-XRD analysis (V-10, see SEM). The analysis and a subsequently projected PXRD pattern showed that the low-angle peaks at 13.5Å and 12.2Å and

the higher-angle peaks are due to a phosphate salt, 1,8-diammoniumoctane dihydrogen phosphate (DODP). The DODP structure is present in the intial reaction mixture, and can be recrystallized as a pure phase from water (V-11).

The structure of DODP is shown in Figure 5-1. The phosphates are arranged into layers, with a monolayer of 1,8-diammoniumoctanes arranged at an angle to the layers (Figure 5-1a). A view of the phosphate layer reveals that the phosphates are hydrogen bonded into chains (Figure 5-1b). Note the intriguing arrangement of the alkylenediamines with respect to the z-axis, where the chains are inclined at opposite angles to its neighbour (Figure 5-1c). The space between the chains is occupied by a disordered 1,8-diaminooctane, which gave rise to residual peaks in the refinement. These are shown for visualization purposes in the view of one monolayer of alkylenediamines (Figure 5-1c).

The peaks at 16.5Å and 15.7Å in the aluminophosphate-based synthesis (V-10) are therefore likely due to one or more unknown aluminophosphate structures. The 16.5Å phase agrees with an aluminophosphate material that was synthesized by others in an aqueous system with 1,8-diaminooctane.[19] This was the longest alkylenediamine used in the present work. However, the cited authors grew aluminophosphate phases using longer alkylenediamines, namely 1,10-decylenediamine and 1,12-dodecylenediamine, suggesting that further discoveries await to be made with these templates.

5.1.2 PRIMARY ALKYLAMINES

5.1.2.1 Ethylamine ($CH_3CH_2NH_2$) [V-12]

The synthesis of $AlPO_4$-21 from an EG solvent or a sec-butanol solvent was reported using ethylamine as template.[20] The same experimental conditions were used for an EG solvent (ethylamine: 70 wt.% solution, Aldrich), but gave a pattern which could not be identified (V-12).

5.1.2.2 Propylamine ($CH_3(CH_2)_2NH_2$) [V-13]

A similar experiment with propylamine (98%, Aldrich) and an EG solvent gave an amorphous product (V-13). Aluminum isopropoxide was used as the aluminum source, and perhaps a crystalline material could have been formed using pseudoboehmite, which had this effect in other systems (Chapter 2). Propylamine is used only in the synthesis of $AlPO_4$-21.[5]

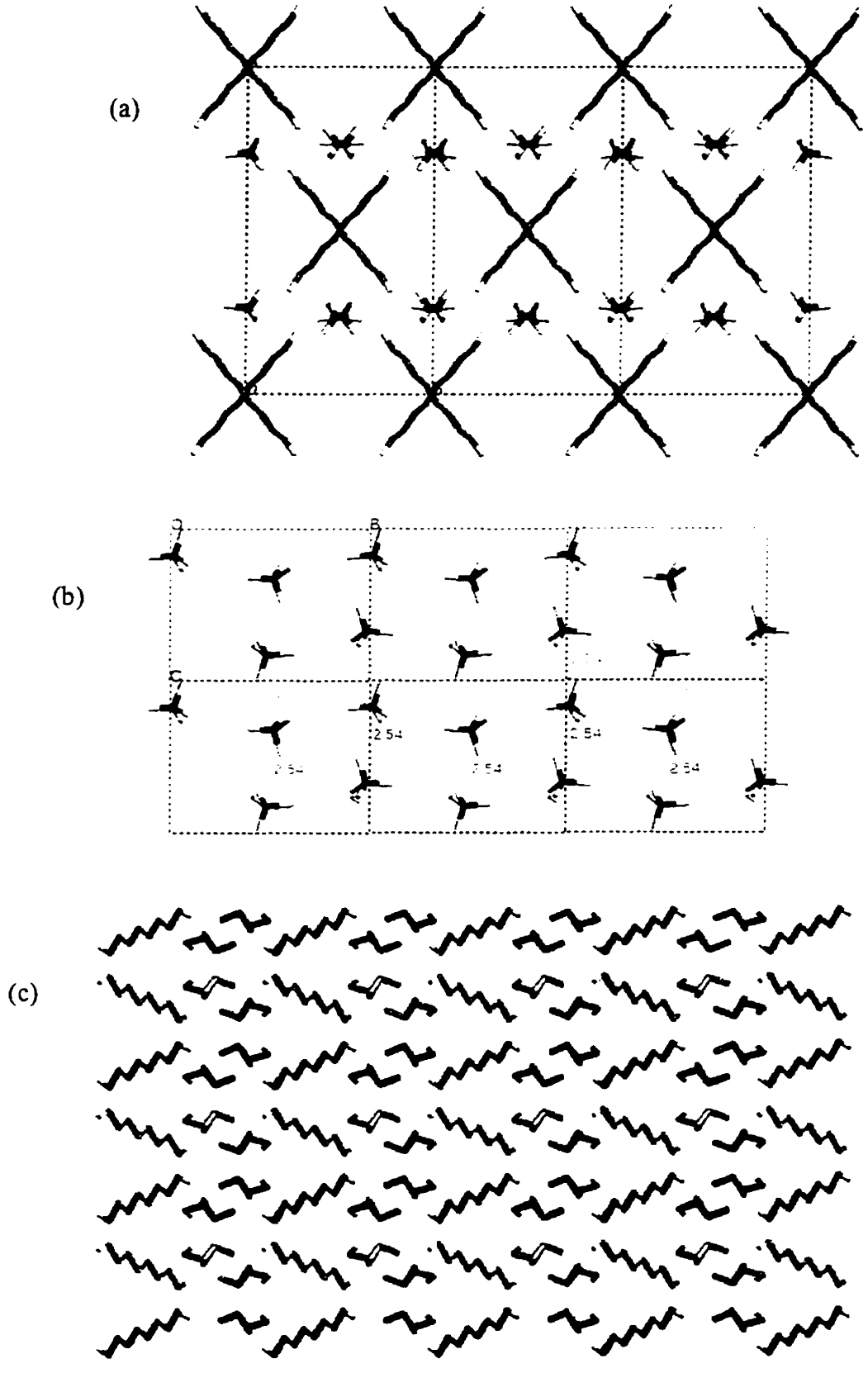

Figure 5-1. (a) c-projection of DODP. (b) a-projection of a phosphate layer of DODP, where phosphates are hydrogen bonded into chains. (c) A view of one monolayer of organics. The residual atoms have been included.

Isopropylamine would be an interesting choice, as it is a commonly used template among $AlPO_4$-n, MAPO-n and gallium phosphate frameworks.[5,21]

5.1.2.3 ±Sec-Butylamine ($CH_3CH_2CH(CH_3)NH_2$) [V-14]

Sec-butylamine is chiral at the alpha carbon, and templates a layered structure from a sec-butanol solvent system.[22] The reagent used was a racemic mixture of the two isomers (99%, Aldrich). In TEG, the product was a poorly ordered material which diffracts at low-angle, with a small amount of an unknown crystalline material (V-14). It is interesting to compare this PXRD pattern with that of the cyclopentylamine system at lower temperatures (II-131).

5.1.2.4 Hexylamine ($CH_3(CH_2)_5NH_2$) [V-15 to V-18]

The phosphate salt of this amine (99%, Aldrich) forms in the TEG synthesis mixture (V-15), which was also the case for all of the longer chain alkylamines. Large crystals may be recrystallized, but were stacked, multicrystalline plates and did not allow for SC-XRD data collection. The material is most likely isostructural to the octylammonium and decylammonium dihydrogen phosphate structures, below. The phosphate salt was the product after heating if no Al_2O_3 was added to the synthesis mixture (e.g. 180°C, 12 days).

In the presence of Al_2O_3, the product (V-16) was the first in a series of mesolamellar aluminophosphates (MLA). The material, "hexylamine-MLA", is of low crystallinity, but does show some degree of short-range order, as indicated by the presence of higher-angle peaks. It also forms at lower temperatures, but of much lower crystallinity (e.g. 80°C, 1 month). At 180°C, the product is similar to V-16, but a peak at 4.08Å begins to appear (V-17), and becomes highly prevalent in the 200°C product (V-18). This peak will be seen in most of the MLA products, and is attributed to the presence of $AlPO_4$-tridymite, as evidenced by the accompanying peaks of this phase. The morphology of the hexylamine-based products was small granules and platelets (e.g. SEM of V-17).

Recently, Gao *et al.* used hexylamine and a mixed solvent comprised primarily of EG to form the same material.[23] The authors make no mention of the beginning synthesis mixture or a hexylammonium phosphate salt. Only the second-order and third order reflections of the MLA peak were shown in their PXRD pattern, as it ends at 15° (2θ). Nonetheless, their report is

complementary to the present work, and shows that the MLA material may also be grown in other solvents.

5.1.2.5 Octylamine ($CH_3(CH_2)_7NH_2$) [V-19 to V-23]

The slurry of the synthesis mixture in TEG (octylamine: 99%, Aldrich) contained a highly crystalline phosphate salt (V-19), which forms very large crystals by recrystallization from water at room temperature. The morphology and crystal size of the phosphate salt are nearly identical to that of the hexylamine system, above (see SEM of V-15). The SC-XRD analysis (Table 5-1) showed the material to be octylammonium dihydrogen phosphate (ODP), comprised of dihydrogen phosphate arranged in layers (Figure 5-2a). One oxygen of the phosphate is static and the other three are shared equally between two sites. Each hydrogen of the ammonium headgroup donates a hydrogen bond to the terminal oxygens of the phosphates. The octylammonium molecules are interdigitated between the phosphate layers to define a hydrophobic interlayer region (Figure 5-2b). Again, if no Al_2O_3 is added to the synthesis, ODP is the only product after heating.

Temperatures of 150°C gave an MLA product with two d-spacings, and a trace amount of ODP (V-20). The 180°C product displayed a similar pattern, but with no ODP in the product (V-21). At 200°C, the larger d-spacing MLA was the major product, with a small amount of $AlPO_4$-tridymite (V-22). The morphology was often plate-like (V-21), while surface impressions and holes could often be seen on some of the particles (V-22). For the synthesis at 180°C, material was also observed at the top and on the cap of the liner (V-23). PXRD of specifically this material showed what appears to be an MLA material of 22.1Å d-spacing and smaller peaks at 28.2Å and 19.6Å. The SEM showed an extraordinary rhomobohedral mesh morphology continuing over the surface of the particles (V-23).

5.1.2.6 Nonylamine ($CH_3(CH_2)_8NH_2$) [V-24 to V-28]

A nonylammonium phosphate phase (nonylamine: 99%, Aldrich) was also formed initially in TEG (V-24). Results were very similar to the octylamine system, forming an MLA product of expectedly larger d-spacing, between 24Å and 27Å (V-25 to V-28). The higher-angle peaks are due to $AlPO_4$-tridymite. No ordered surface patterning was observed in the products despite the results of octylamine, decylamine and larger alkylamines. This may simply be due to lack of experimentation in this system; a limited amount of SEM work was performed on the

Compound	$[^{+}H_3N(CH_2)_8NH_3^{+}]$ $[H_2N(CH_2)_8NH_2]$ $[H_2PO_4^{-}]_2$ (DODP)	$[CH_3(CH_2)_7NH_3^{+}]$ $[H_2PO_4^{-}]$ (ODP)	$[CH_3(CH_2)_9NH_3^{+}]$ $[H_2PO_4^{-}]$ (DDP)
Empirical Formula		$C_8H_{21}NO_4P$	$C_{10}H_{26}NO_4P$
M_r		226.23	255.29
Crystal size, mm		0.35×0.16×0.21	0.35×0.32×0.20
Crystal Class	Monoclinic	Monoclinic	Monoclinic
Space Group	C2/c	$P2_1/c$	$P2_1/n$
Temperature, K		173	173
a, Å	21.118(4)	4.554(1)	7.358(2)
b, Å	11.049(2)	34.652(3)	39.749(12)
c, Å	9.273(2)	7.328(1)	9.131(4)
α, °	90	90	90
β, °	109.05(3)	90.66(1)	90.45(2)
γ, °	90	90	90
V, A^3		1156.3(2)	2671(2)
Z		4	4
D_{calc}, g cm^{-3}		1.300	1.270
μ(MoKα), cm^{-1}		2.30	2.07
F(000)		492	1120
range θ collected, °		2.84 to 25.00	2.71 to 24.01
no. reflections collected		2291	4416
independent reflections		2031	4067
R_{int}		0.0211	0.0342
no. observed data [I>2σ(I)]			2962
R_1 [I>2σ(I)]		0.0476	0.0679
wR_2 (all data)		0.1584	0.1861
weighting a,b			0.0272, 10.92
goodness of fit		1.165	1.135
parameters refined		160	329
max density in ΔF map, e $Å^{-3}$		0.393	0.689

Definition of R indices: $R_1 = \Sigma(F_O-F_C)/\Sigma(F_O)$, $wR_2 = [\Sigma[w(F_O^2-F_C^2)^2]/\Sigma[w(F_O^2)^2]]^{1/2}$

Table 5-1. Summary of crystal data, details of intensity collection and least-squares refinement parameters for the solved phosphate salt structures.

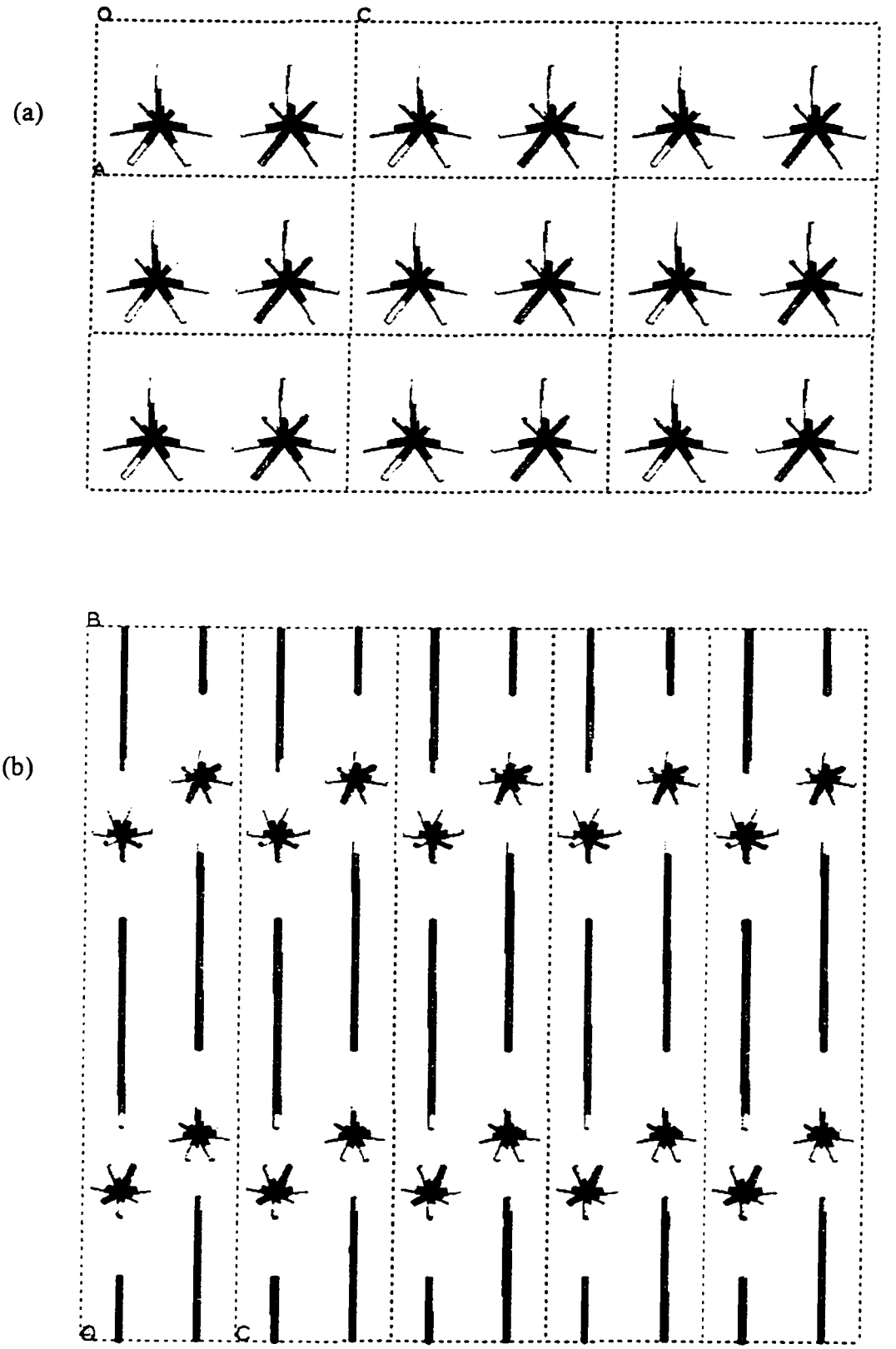

Figure 5-2. (a) b-projection of ODP. Three of the phosphate oxygens are disordered between two sites. (b) a-projection of ODP, showing interdigitated structure.

nonylamine-MLA products. Judging by the decylamine and undecylamine results below, interesting morphologies should be obtainable from this system with further investigation.

5.1.2.7 Decylamine ($CH_3(CH_2)_9NH_2$) [V-29 to V-48]

Decylamine (95%, Aldrich) gave the most intriguing results, and was therefore the most explored system of the alkylamines. The synthesis mixture contained pseudoboehmite and decylammonium dihydrogen phosphate (DDP, V-29). DDP was recrystallized from water at 50°C and its structure was solved by SC-XRD (Table 5-1). It is isostructural to ODP, above, but the phosphates in DDP are not disordered (Figure 5-3a). There are two crystallographically distinct phosphates and decylammoniums, as opposed to one phosphate and one octylammonium for ODP. Each dihydrogen phosphate donates two hydrogen bonds and accepts two hydrogen bonds to define a continuous, uninterrupted phosphate layer (P-O•••H-OP distances 1.54 Å to 1.80Å, Figure 5-3a). The primary ammonium head groups each donate three hydrogen bonds (N-H•••O-P distances 1.89 Å to 2.09 Å). The decylammonium chains are again interdigitated (Figure 5-3b, cf. Figure 5-2b).

The DDP structure was still present in the TEG synthesis mixture at room temperature after aging for two months. It was the only observed product if no Al_2O_3 was added to the synthesis mixture, for example after heating at 180°C for 5 days. The PXRD pattern of the synthesis mixture (V-29) is identical to both the recrystallized DDP material and the projected powder pattern from Cerius[2] based on the SC-XRD structure.

As for the products of other alkylamine systems, lower temperatures yielded a mixture of the MLA and DDP materials (V-30, V-31), while higher temperatures contained a trace amount or an absence of DDP and increasing amounts of $AlPO_4$-tridymite (V-32, V-33). The interlayer distances for the MLA material varied between 26Å and 30Å, with more than one often appearing in a given product (e.g. V-31, V-33).

Many unexpected morphologies were observed for the decylamine-MLA products. A series of ten SEM micrographs for the 180°C product (V-32) is shown in Appendix C. A significant portion of the product was a powder consisting of small MLA plates (V-32A). The product also afforded a number of spherical growths. They were 1 to 2 mm in size and could therefore be isolated from the rest of the product (V-32B) for separate characterization. PXRD showed them to be comprised exclusively of the MLA material, containing none of the DDP or

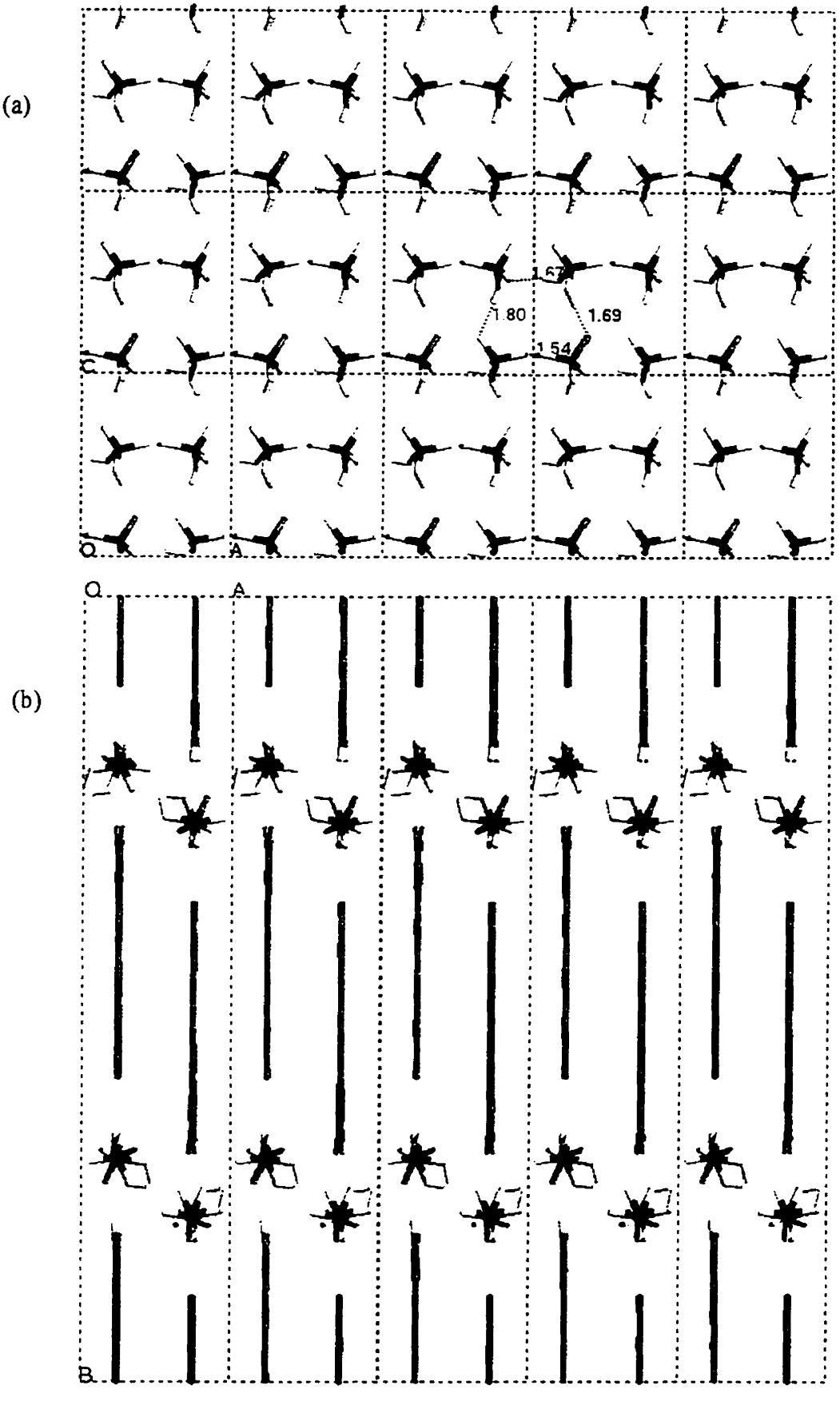

Figure 5-3. (a) b-projection of DDP. The phosphates in this case are not disordered. (b) c-projection of DDP and its interdigitated structure.

$AlPO_4$-tridymite impurities that are always present in the bulk product. Much of the surface of these spheres contain bowl-like impressions (V-32C), sometimes with a circular arrangement of smaller platelets extruding from the surface (V-32D). Other areas contained smaller impressions of monodisperse size that were connected to define a honeycomb-like pattern (V-32E) or other patterns with hexagonal symmetry (V-32F).

The surface of some spheres possessed hollow spheres (V-32G). These hollow spheres in turn contain a fine-structure of surface bowls (V-32H), often with a concentric arrangement of platelets (V-32I). Hollow spheres were also observed as an aggregated plate-like collection on the lower portion of the walls or bottom of the liner (V-32J), which showed similar patterning on their surfaces.

Further experiments were conducted to probe this system and the conditions under which these patterned particles occur. Temperatures above or below 180°C gave the MLA material, as previously shown (V-30, V-31, V-33), but only in the form of the small plate-like morphology, as shown in V-32A. Increase in the molar ratio of decylamine resulted in a more phase-pure and strongly diffracting MLA material (V-34, V-35). However, the products were devoid of any patterned or hollow spheres. Decrease in the molar ratio of decylamine only served to yield a majority phase of berlinite (V-36 to V-38), with any trace of MLA or DDP absent at higher temperatures.

Agitation by vigorously shaking the reaction chamber in the middle of the synthesis, after 1 day of heating, was performed (V-39). The product after 3 days was the MLA phase, with hollow spheres as the dominant morphology (see SEM). Inspection of the hollow spheres showed their surface to be granular in appearance and not at all like those obtained from static conditions, above. Continuous tumbling of the autoclaves also gave small MLA platelets (V-40), with a solid cylinder of material, as observed for the triethylamine-related tumbling experiments (Chapter 2).

The solvent was changed from TEG to observe the role of the solvent. EG gave the MLA material (V-41), but with a stacked-plate morphology (see SEM). Similar results were obtained using a mixed EG-TEG solvent (V-42), as well as with DEG and tEG solvents. Increase of molecular weight to PEG 400 (V-43) gave surface features similar to those obtained from TEG (V-43A, V-43B). Further increase in molecular weight to PEG 1000 (waxy at room temperature) formed a highly viscous synthesis mixture, and yielded only MLA platelets (V-44).

Water was added to the TEG solvent, to give a solvent reversed in terms of volumes of H_2O and TEG (V-45). The product was still the MLA material, but devoid of any surface patterning similar to V-32. What was initially thought to be patterning turned out to be large voids with a granular surface (see SEM of V-45). Fully aqueous conditions gave DDP as the majority phase under all temperatues (V-46). The MLA material may be prepared aqueously in pure phase by using more concentrated conditions and/or a lower P:Al ratio, also shown by others for the alkylamines spanning octylamine to hexadecylamine.[24]

Finally, the order of addition of phosphate and amine was reversed, adding the phosphoric acid last. The starting synthesis mixture in this case showed the presence of an entirely different phase (V-47), with a small amount of DDP. This new material is likely decylammonium monohydrogen phosphate (DMP), since only 1.8 moles of H_3PO_4 were added, as the slurry was becoming extremely viscous with the addition of phosphate. The DMP structure remains unsolved to date, but an initial recrystallization from ethanol formed crystals which appeared to be large enough for SC-XRD. The aluminophosphate product of this reverse-order experiment was the MLA material, consisiting only of small granules (V-48).

5.1.2.8 Undecylamine ($CH_3(CH_2)_{10}NH_2$) [V-49 to V-53]

The starting mixture with this alkylamine (98%, Aldrich) also contained the phosphate salt (V-49). Recrystallization attempts to date gave only smaller crystals. Synthesis temperatures of 150°C to 220°C led to an MLA material of 29 to 31Å d-spacing (V-50 to V-53). Again, lower temperatures yielded a small amount of phosphate salt (V-50) and higher temperatures yielded no phosphate salt, but increasing amounts of $AlPO_4$-tridymite (V-51 to V-53).

The interesting patterns arose from the 180°C and 200°C products; no such patterns were observed for the 150°C or 220°C products. For 180°C (V-51), the particles of interest were plate-like aggregates of hollow spheres that grew on the lower wall of the liner (V-51A), very similar to their decylamine counterpart in size, shape and morphology. A close-up of these hollow spheres also shows a fine-structure of surface impressions (V-51B). The 200°C product (V-52) afforded a number of *ca.* 1 to 2 mm diameter spheres (V-52A), also very similar to the decylamine-related spheres. Again, the PXRD of only the spheres gave a phase-pure MLA pattern. A mesh-like feature was present on most of the surface, whether on flat regions (V-52B)

or on the interior of surface bowls (V-52C). The surface bowls appear to space-fill the surface (V-52D) and many of them contain an interesting growth feature at their centres (V-52E).

5.1.2.9 Dodecylamine ($CH_3(CH_2)_{11}NH_2$) [V-54 to V-55]

Chenite *et al.* recently prepared hydrothermally an interesting coaxial cylindrical mesophase, comprised of an aluminophosphate-dodecylamine composite.[25] The use of dodecylamine (99+%, Aldrich) in TEG led to a 34Å MLA material (V-54, V-55). Some dodecylammonium-phosphate salt is present in the product (peaks at 22.5Å, 11.2Å) as well as $AlPO_4$-tridymite. The only noteworthy surface feature was large indentations (see SEM, V-54); the rest of the product consisted of small granules.

5.1.2.10 Tetradecylamine ($CH_3(CH_2)_{13}NH_2$) [V-56 to V-58]

The increase in d-spacing of both the phosphate salt (V-56) and MLA product (V-57) continued with tetradecylamine (96%, Aldrich). The high viscosity of the synthesis slurry required a smaller amount of amine to be added. The morphology of the product was exclusively small granules. Since the alkylamine source is a solid when the alkyl chain is larger than twelve carbons, it becomes rather easy to mistake the product as a mesolamellar material when it is actually just unreacted amine. Tetradecylamine itself gives rise to PXRD peaks at 39.8Å or 34.5Å and a series of higher-angle peaks (V-58). However, the product of V-57 does not contain the peaks of the tetradecylamine reagent and is therefore considered as tetradecylamine-MLA.

5.1.2.11 Hexadecylamine ($CH_3(CH_2)_{15}NH_2$) [V-59 to V-60]

This was the longest n-alkylamine used (90% tech., Aldrich or 99+%, Fluka), and gave an MLA product for all temperatures used (V-59). The "unpatterned platelets" are shown for the 180°C product (see SEM). Unreacted hexadecylamine reagent (V-60) is not present in the aluminophosphate product, and was affirmed by washing the product with 1M HCl in methanol during filtration of the product. Extensive washing in this way also served to partially decompose the MLA and $AlPO_4$-tridymite to an amorphous material.

5.1.3 CETYL TRIALKYLAMMONIUMS [V-61 to V-65]

An aqueous synthesis using cetyltrimethylammonium bromide (CTAB, $C_{16}H_{33}NMe_3^+Br^-$, 29 wt.% solution, Pfaltz & Bauer) gave poorly crystalline metavariscite and variscite at lower

temperatures (V-61) and $AlPO_4$-H4 at higher temperatures (V-62) The bromide anion must have promoted the formation of $AlPO_4$-H4, as reported by others.[26] Both non aqueous TEG or semi-aqueous TEG-H_2O solvents led only to berlinite at 180°C (V-63). Similarly, cetylpyridinium chloride monohydrate (CPC, $C_{16}H_{33}NC_5H_5^+Cl^-\bullet H_2O$, 98%, Aldrich) in a TEG system led to $AlPO_4$-H4 at 80°C (V-64) and berlinite at 180°C (V-65).

5.1.4 SILICA-DECYLAMINE SYSTEM [V-66]

The crucial role of aluminum oxide is indicated by the experiments in which it was replaced by an equimolar amount of silica (EH-5 Cab-O-Sil, Cabot). Both the starting mixture and the product (V-66) showed only the DDP material and amorphous silica in its PXRD, at all synthesis temperatures probed. Interestingly, the product from 180°C contained large depressions in its particles (V-66A). A closer view of the walls showed them to be made up of fine crystals (V-66B). The EDX of these crystals indicated only the presence of phosphorus (and no silicon). Evidently, the walls are comprised of the DDP material. This was not the case for the MLA products of the aluminophosphate syntheses, above.

5.2 MATERIALS CHARACTERIZATION

5.2.1 TEM of the Mesolamellae

The mesolamellar nature of the MLA material already indicated by PXRD was confirmed by the TEM of sample V-32 (Figure 5-4). The mesolamellae displayed an approximate interlayer distance of slightly less than 30Å, as illustrated by the scale bar. It was also a direct observation of the excellent ordering of the layers over the long-range.

5.2.2 MLA Thermal Properties

The TGA of decylamine-MLA is shown in Figure 5-5a; the TGA of undecylamine-MLA was almost identical (Figure 5-5b). The large weight loss between 150°C and 225°C appears to contain two overlapped events, with a final event around 350°C. These transformations may be followed in the VT-PXRD, Figure 5-6a. A gradual contraction of the interlayer spacing is observed from 29.0 Å at 25°C to 27.6 Å at 150°C. At 175°C, the MLA suddenly transforms to a mixture of $AlPO_4$-tridymite and a new MLA material, with 100% peak at 24.5 Å. The peak area is greatly reduced for this new phase, which agrees with the partial collapse to $AlPO_4$-tridymite.

Figure 5-4. TEM of the mesolamellae of the decylamine-related MLA. Scale bar = 30nm.

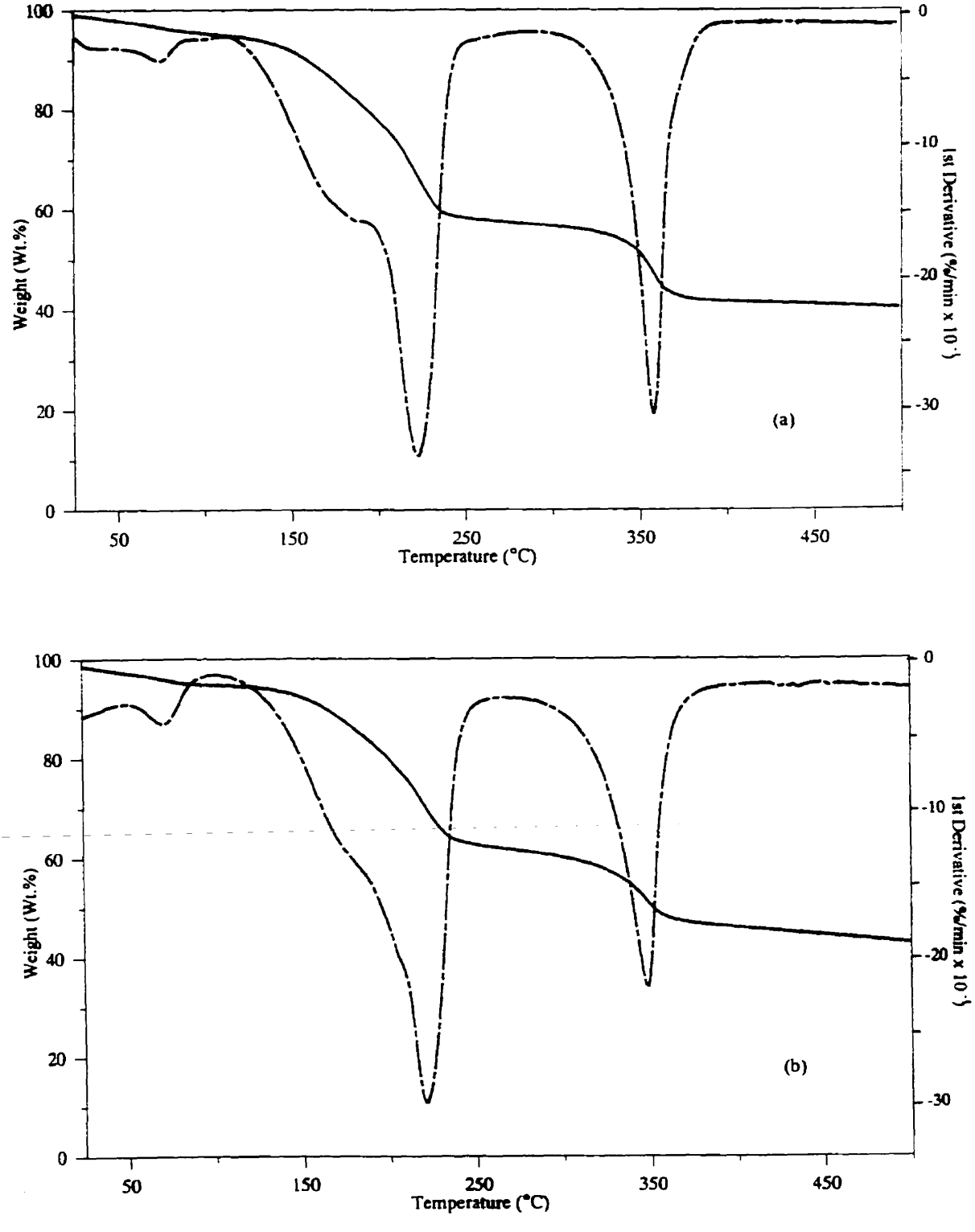

Figure 5-5. (a) TGA of decylamine-MLA. (b) TGA of undecylamine-MLA.

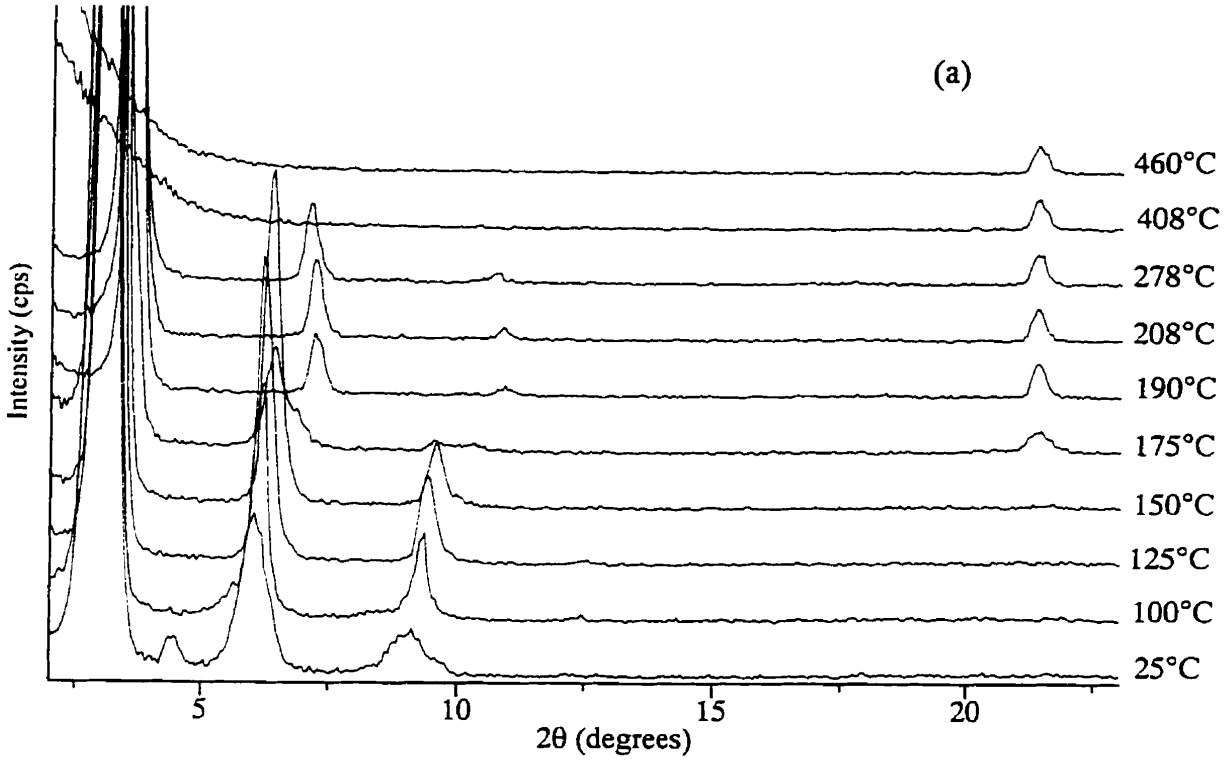

(b)

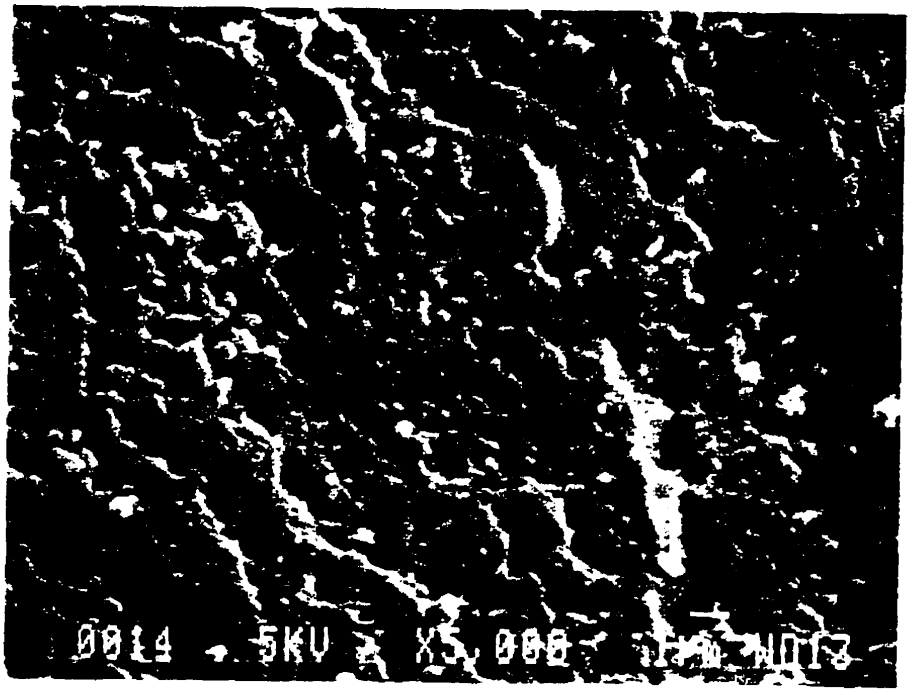

Figure 5-6. (a) VT-PXRD of decylamine-related MLA. (b) SEM of the honeycomb-like morphology of V-32E after heating to 200°C.

This 24.5 Å layer collapses somewhere between 280°C and 400°C, accounting for the last TGA peak. MS confirms the release of decylamine at these temperatures. Chemical analysis of as-synthesized decylamine-MLA showed it to contain 41.70 wt.% C, 4.62 wt.% N, 4.55 wt.% Al and 10.49 wt.% P, giving a molar ratio of $Al_{1.00}P_{2.02}C_{20.61}N_{1.96}$.

Heating the MLA samples in air gave similar results. Treatment of the solid (V-32) at 200°C (7 hour ramp, 2 hour soak) resulted in an approximately equal amount of a 25.7Å and 23.2Å MLA, with a small amount of $AlPO_4$-tridymite in the product. The surface morphologies appeared to partially or completely decompose; the original sample used possessed the honeycomb pattern (V-32E), and after heating was barely recognizable (Figure 5-6b). After heating the MLA at 300°C (7 hour ramp, 2 hour soak), only $AlPO_4$-tridymite and berlinite were present in the PXRD. The DSC of the MLA material showed an exothermic event at approximately 65°C (Figure 5-7), which may be attributed to a contraction of the layers, arising due to a loss of physisorbed water (small peak in TGA at *ca.* 60°C, Figure 5-5a). Presumably, the alkyl chains tilt with respect to the layers, as evidenced by the change in the PXRD patterns between 25°C and 100°C (Figure 5-6a).

5.2.3 DDP and DMP Thermal Properties

The DDP phase showed several unexpected thermal transitions. It was present and unaltered (100% peak, 19.9Å) up to 80°C in the VT-PXRD (Figure 5-8a). By 100°C, a new crystalline phase appears, with d_{010} peak expanded to *ca.* 24.0 Å and a series of new, distinct higher-angle peaks. This new phase in turn transforms by 125°C to a phase with interlayer distance increasing further to *ca.* 25.7 Å, where the only other peaks present are the second- and third-order reflections. It remains in the VT-PXRD until it decomposes in the 350°C region. The TGA of DDP remains unaltered with little or no weight loss up to 300°C, and then undergoes rapid weight loss.

Each of the transitions were found to be completely reversible. Cooling the sample after each shows the sample to revert back to its original state, with an hysteresis of approximately 10 to 20°C. For example, the crystal to crystal transformation occurs at 90°C in the forward direction and somewhere between 80°C and 50°C in the reverse direction (Figure 5-8b). The second transformation is also reversible (Figure 5-8c). The three transformations may in fact be continuously performed, with increase in ordering of the DDP phase after each cycle (Figure 5-8d).

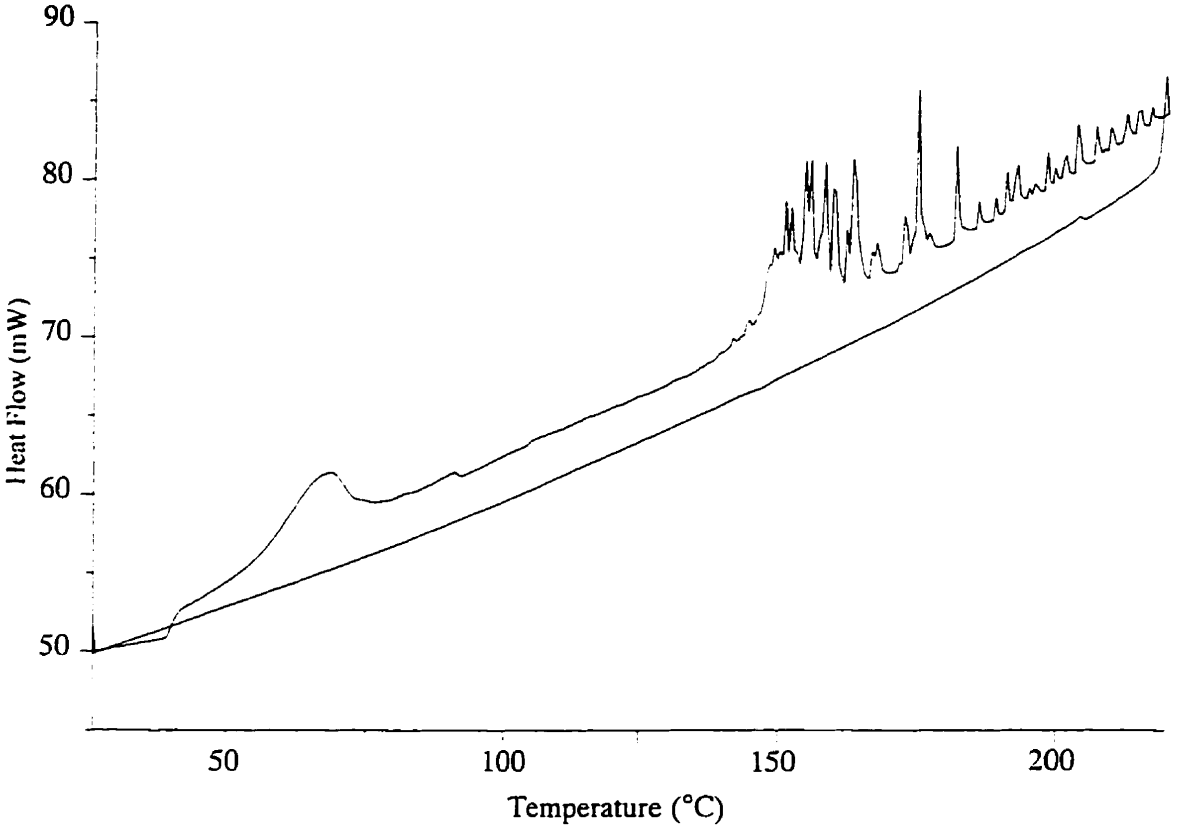

Figure 5-7. DSC of decylamine-MLA.

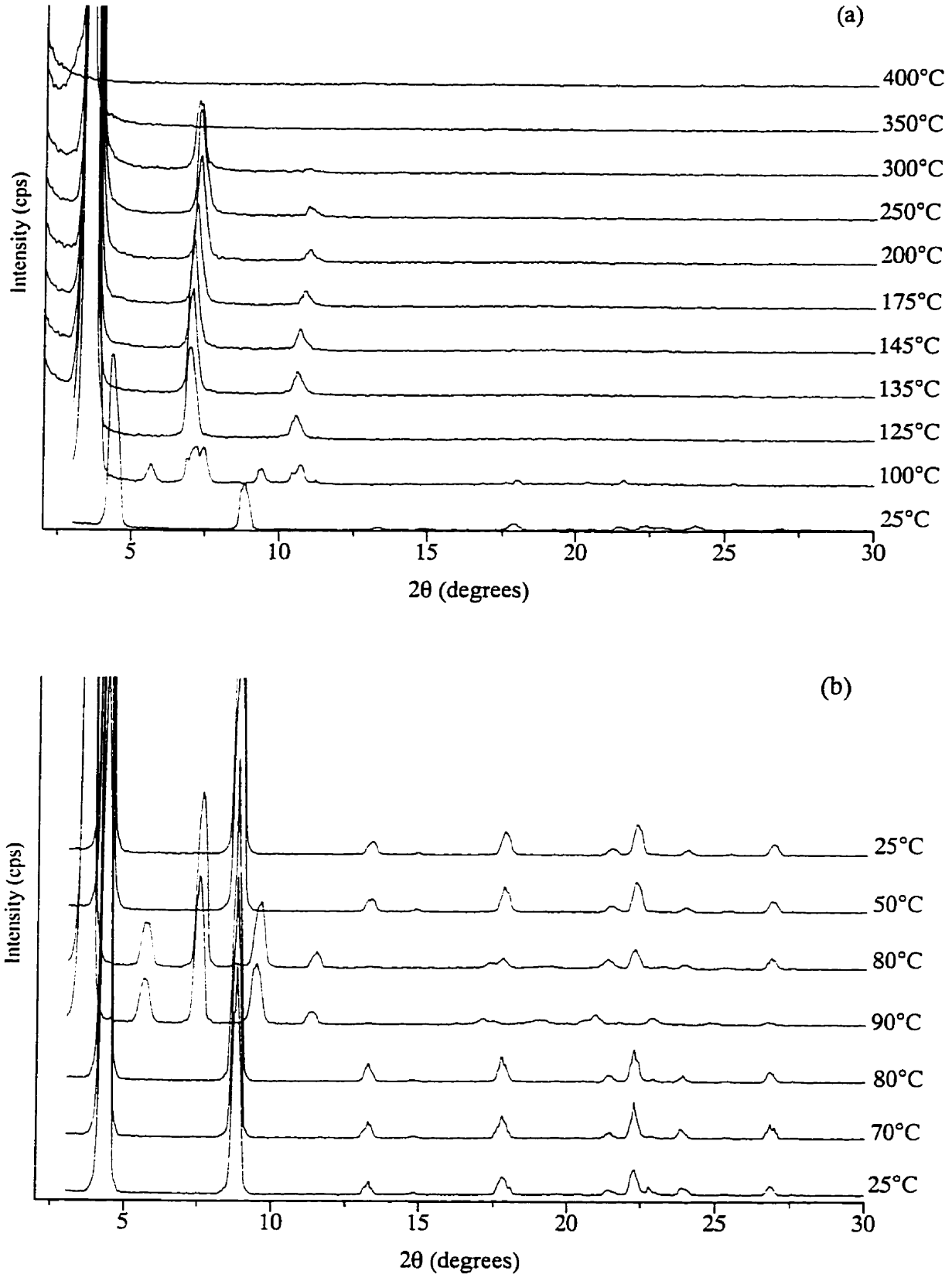

Figure 5-8. (a) VT-PXRD of DDP. (b) DDP crystal to crystal transition.

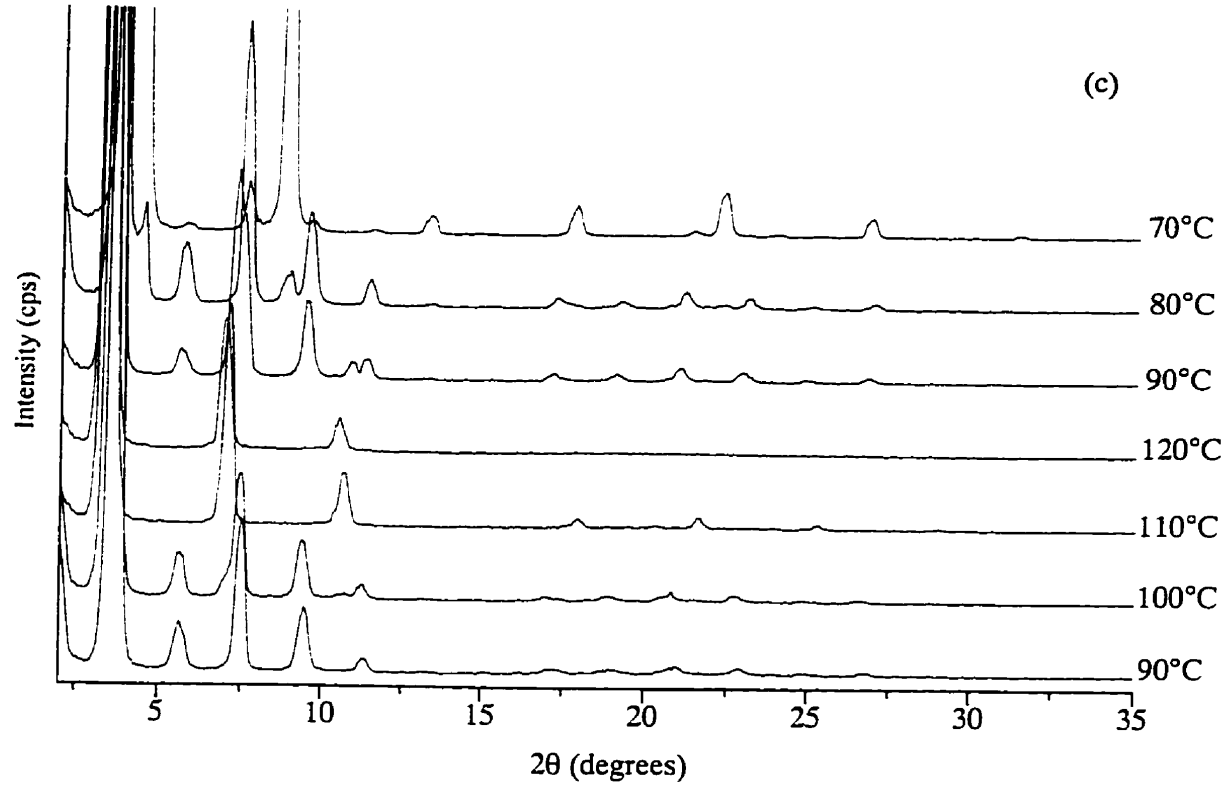

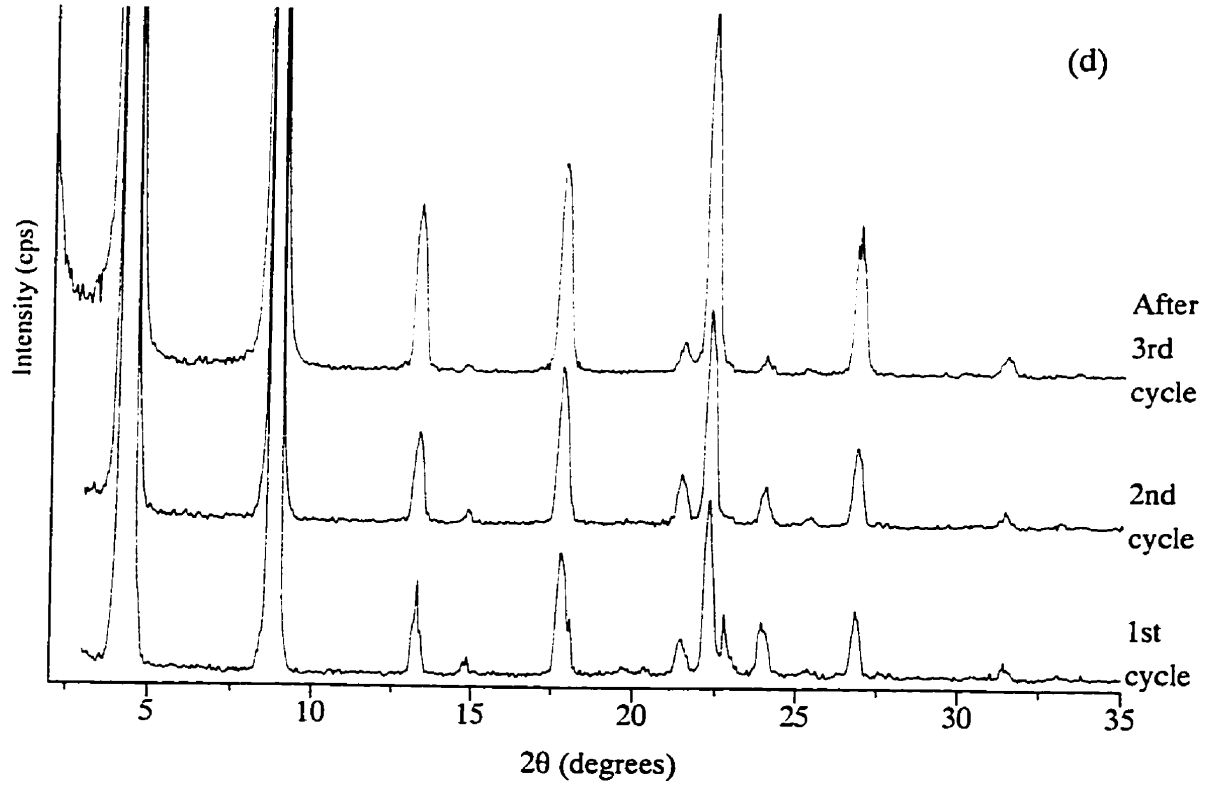

Figure 5-8 (Cont'd). (c) High-temperature crystal to liquid crystal transition. (d) Increase in order of DDP with cycling.

These transformations may be followed in the DSC (Figure 5-9a). The reversibility and hysteresis can be seen in the three cycles shown. The first, sharp transition corresponds to the first transition in the VT-PXRD. The VT-PXRD showed only a second transition. However, there appears to be both a second and a third transition in the DSC, the second being the broad peak which begins before 90°C, and the third being the sharp peak at *ca.* 95°C (Figure 5-9a). These two peaks are overlapped during increase of temperature, but appear to occur at different temperatures during cooling. The DSC of what is considered as decylammonium monohydrogen phosphate (DMP, V-47) was collected for comparison (Figure 5-9b). There are two weakly exothermic, reversible events at *ca.* 50°C and 60°C.

5.2.4 Solid State NMR

The ^{31}P MAS NMR of DDP showed two sharp resonances of equal intensity at 1.13 and -0.65 ppm (spinning rate 6 kHz, referenced to $NH_4H_2PO_4$), one for each of the two crystallographically unique dihydrogen phosphates. The ^{31}P MAS NMR of decylamine-MLA (spinning rate 10 kHz, referenced to $NH_4H_2PO_4$) displayed at least four distinct peaks in the 0 to -20 ppm range (Figure 5-10a). The MLA and DDP spectra agree with the recently reported dodecylamine-MLA and what was termed as a "template-phosphate complex".[24] While the authors did not know the nature of the alkylammonium dihydrogen phosphate (ADP) phase, a synthesis with P:Al ratios of 1 : 0 gave a product with only one peak in the 0.0 ppm range, which they assigned to the "complex". This peak gave way to a series of more upfield peaks at intermediate P:Al ratios of 1 : 0.6, which was shown to be the MLA material.

The ^{27}Al MAS of decylamine-MLA shows two peaks at 48.7 and 0.0 ppm (spinning rate 13.0 kHz), corresponding to tetrahedral and octahedral aluminum, respectively.[24,27-30] A third peak was also observed between these two, at 23.9 ppm, and was of much smaller peak area. A similar third peak was also observed for the published dodecylamine-based MLA, and was attributed to excess amorphous alumina.[24] This was based on the fact that it was the only peak observed when no phosphorus was used in the synthesis (i.e., P:Al = 0 : 1). Therefore, this middle peak in the present case is best attributed to unreacted pseudoboehmite.

The ^{13}C CP-MAS NMR of the DDP and MLA solids showed peaks in the regions expected for decylammonium,[31] downfield of TMS. For DDP (Figure 5-10b), the broadness of the peaks increases from the methyl end of the alkyl chain (13.66 ppm) to the alpha carbon (40.46 ppm). Decylamine-MLA displays a similar effect, but all of the peaks were broader than

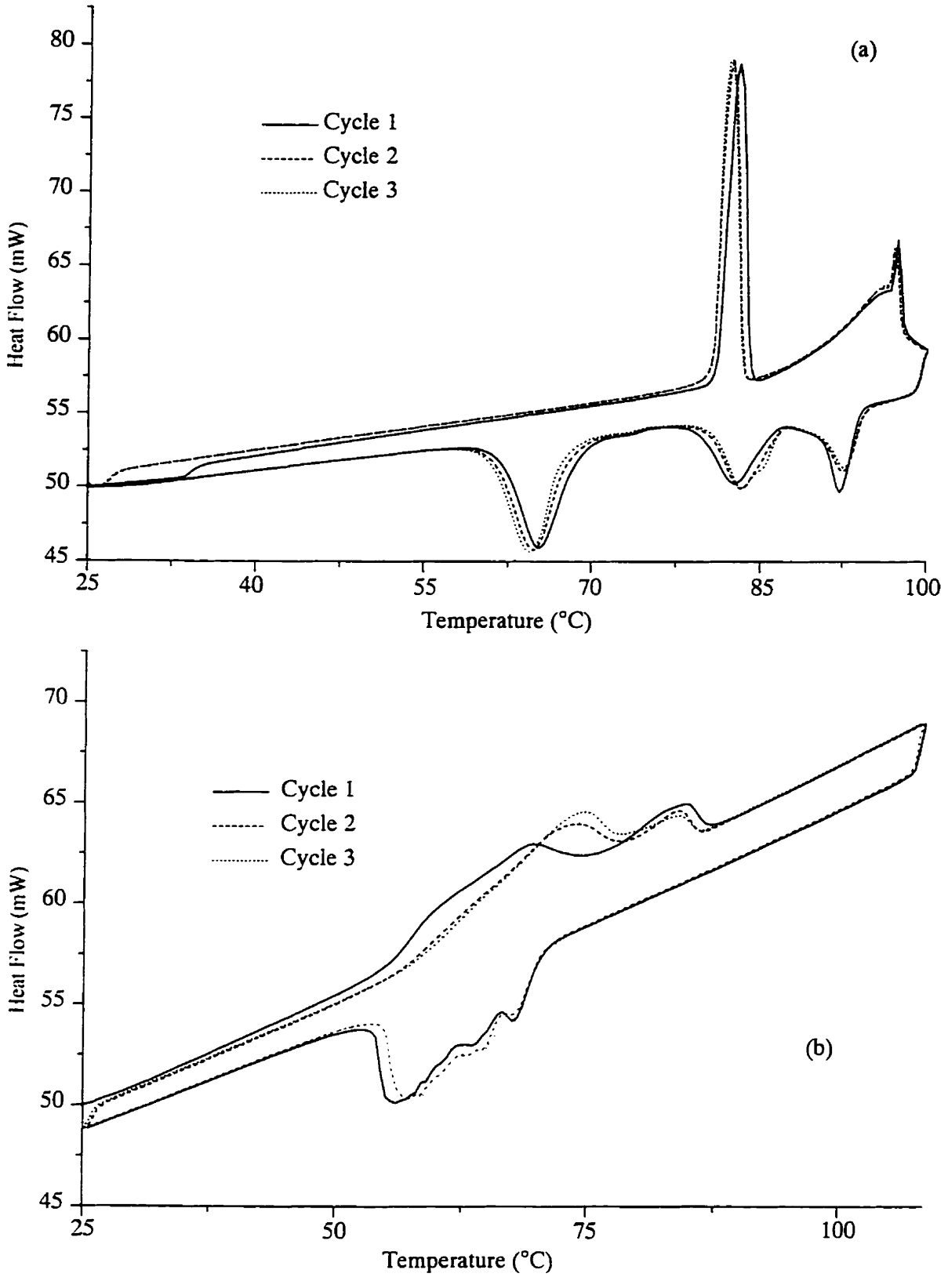

Figure 5-9. (a) DSC of DDP. (b) DSC of DMP.

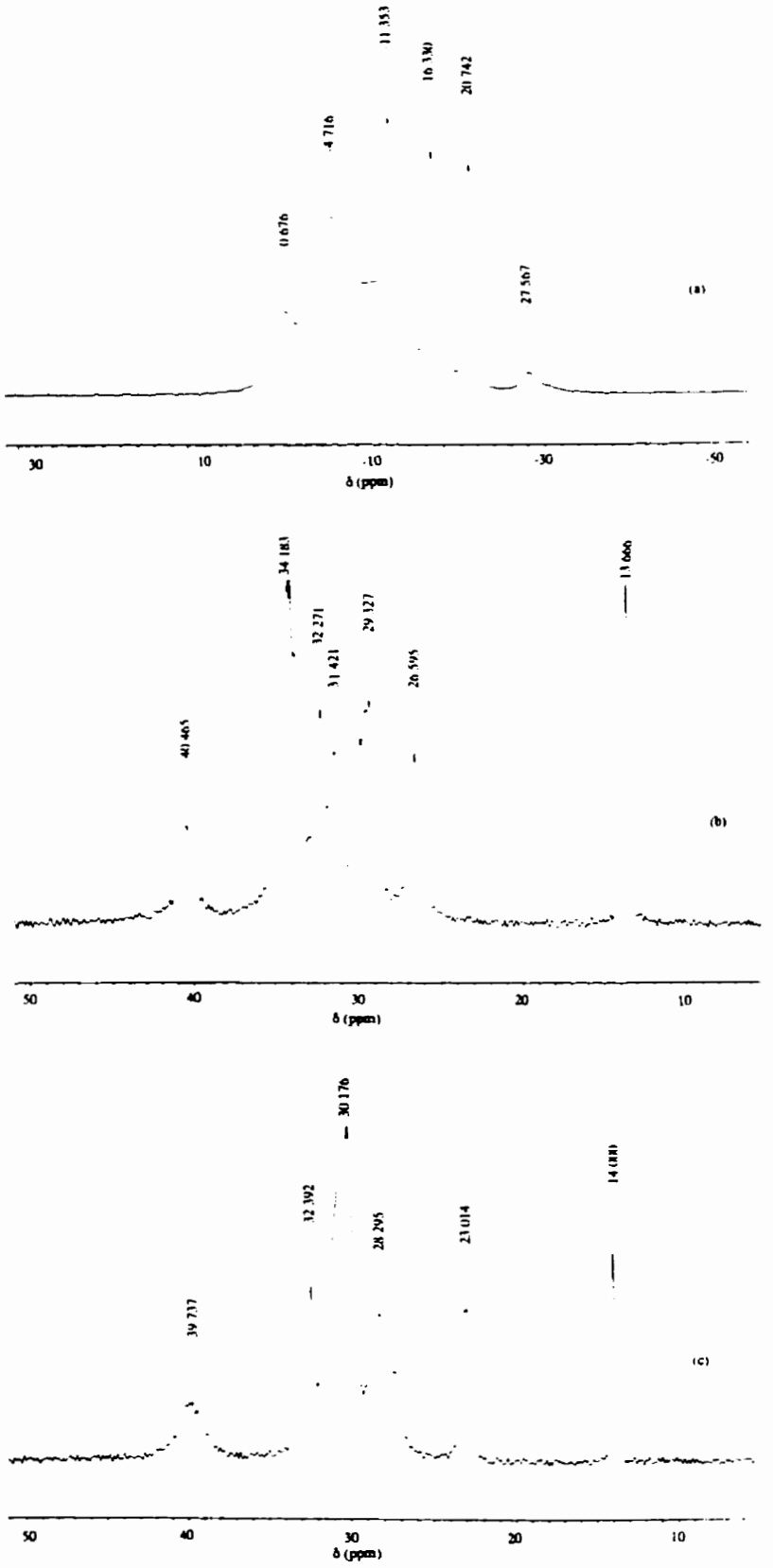

Figure 5-10. (a) ^{31}P MAS NMR of decylamine-MLA. (b) ^{13}C CP-MAS NMR of DDP. (c) ^{13}C CP-MAS NMR of decylamine-MLA.

for DDP, particularly for the alpha and neighbouring carbons (Figure 5-10c). The relationship of the ^{13}C NMR spectra of decylamine-MLA to decylamine itself is, for the most part, identical to the relationship of the recently published hexylamine-MLA[23] to hexylamine.

5.3 DISCUSSION

5.3.1 DDP: Liquid Crystal Formation

As discovered in the SC-XRD analysis, the initial DDP phase has its alkyl chains interdigitated (Figure 5-3b). Such an arrangement is favourable when a relatively larger space needs to be filled by the alkyl chain, such as the ionic salt containing interdigitated CPC molecules and large chlorometalate(II) anions.[32] In the case of DDP, this occurs in order to maintain electroneutrality with the anionic dihydrogen phosphate layers.

The thermal processes that were observed in section 5.2.3 for DDP as a solid are illustrated schematically in Figure 5-11. The first strongly exothermic thermal transition of DDP involved the formation of a second crystalline phase of a larger interlayer spacing. This is attributed to the de-interdigitation of the DDP phase, Figure 5-11b. This step is not gradual but rapid, as indicated by the sudden change of VT-PXRD patterns and the narrowness of the DSC peak. The transition to a second crystalline phase was observed (Figure 5-11c), followed by a transition to a disordered lamellar phase, which is attributed to a thermotropic liquid-crystal (l.c.) phase (Figure 5-11d). Interdigitated to bilayer liquid crystal phase (and reverse) transitions commonly occur for phospholipid membranes and vesicles.[33-36] Often, these observations are also made by DSC and VT-PXRD.

The unique structural aspects of DDP are the reasons for its thermal properties. Firstly, it is the first alkylammonium phosphate to contain an amphiphile, which is necessary for liquid crystal formation. This would not occur for the phosphate salts of other amines, such as triethylamine (Figure 2-3). Secondly, other phosphate salts, such as cyclopentylammonium monohydrogen phosphate (Figure 3-4a,b) or ethylenediammonium monohydrogen phosphate (Figure 1-11a), contain disjointed phosphate layers, hydrogen bonded into dimers or chains (section 1.5). In DDP, however, a continuous hydrogen bonded sheet exists, where each phosphate donates and accepts two hydrogen bonds to define a layer of "four-rings" (Figure 5-3a).

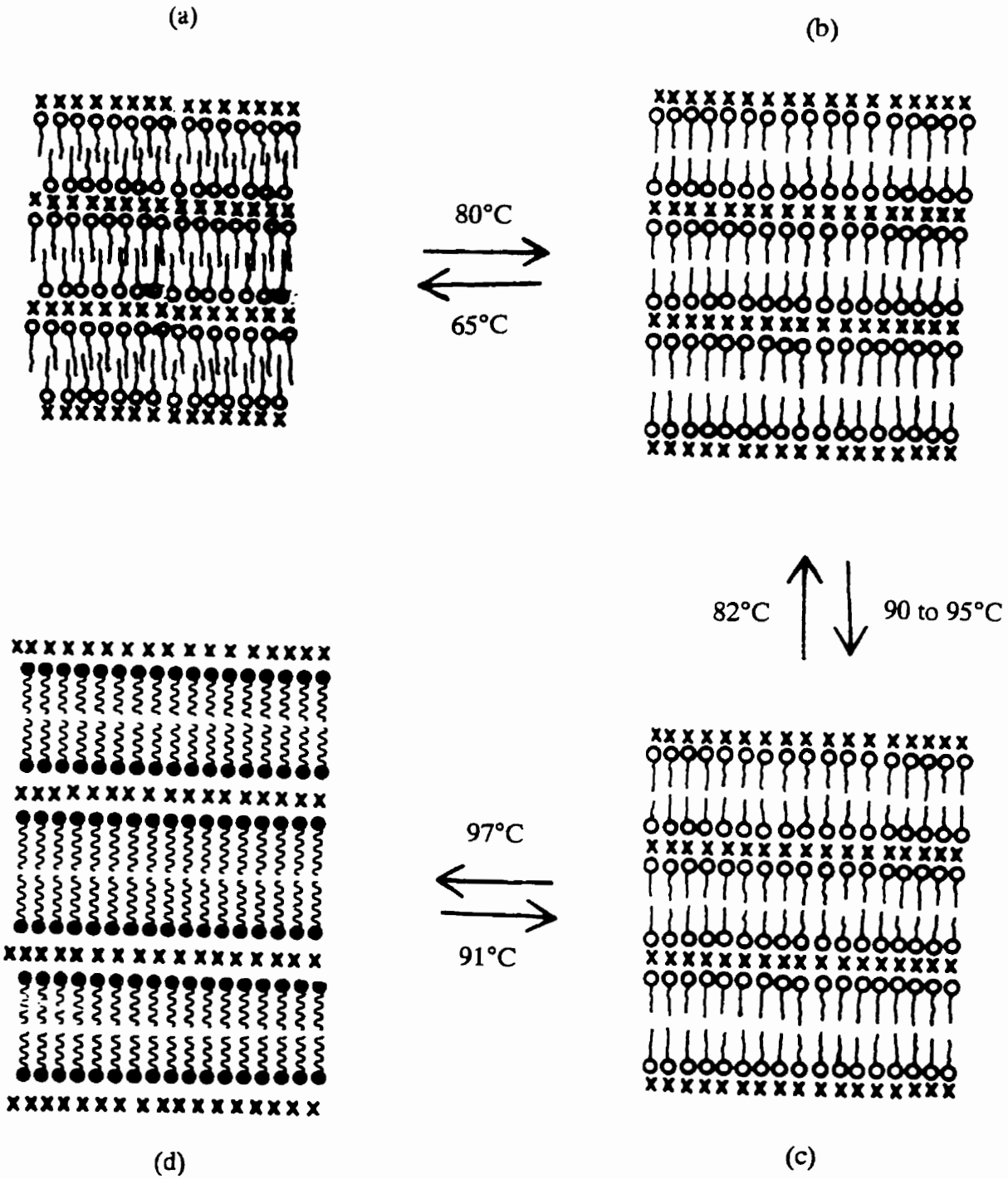

Figure 5-11. Diagram of the thermal transitions observed for DDP; temperatures are approximate and taken from the DSC. (a) The interdigitated phase at room temperature. (b) First high temperature crystal state. (c) Second high temperature crystal state. (d) Transition to a thermotropic liquid crystal.

The DDP solid becomes a soft, semi-translucent paste when heated above its transition temperature. It was also observed that by simply heating the synthesis mixture (i.e., the opaque, white, viscous TEG-pseudoboehmite-DDP slurry) in a beaker to *ca.* 55°C, the mixture separated into an orange-brown liquid with a clump of soft material present in the solvent. The soft DDP present in the heated TEG slurry is therefore attributed to the liquid crystal phase, where it undergoes the same processes shown in Figure 5-11. Accordingly, the soft DDP hardens upon cooling to room temperature in both cases. This also occurred for solid DDP itself.

It should be noted that since the DDP transitions are completely reversible, the thermal investigations had to be *in situ* to observe these effects. These transitions must have occurred, but were not observed, for the aqueous experiments of V-46, the TEG-silica-DDP experiment of V-66, and the experiments identical to V-31, V-32 or V-33, but without the addition of pseudoboehmite which gave only DDP products.

5.3.2 Alkylamine Concentration and Alkyl Chain Length

The MLA material may be synthesized with primary alkylamines of carbon chain length six or greater, from aqueous, non aqueous or mixed solvents. As was observed in the previous chapters, the type of solvent and conentration of reagents will influence the amount of hydrolysis that occurs and therefore the relative yield of MLA, DDP and dense-phase products. The MLA material forms under higher concentrations of alkylamine and/or inorganic reagents, be it under non aqueous (e.g. V-31 to V-35) or aqueous conditions.[24,37] Lower concentrations of alkylamine gave the DDP material and unreacted pseudoboehmite under aqueous conditions (V-46), and berlinite from TEG (V-37, V-38).

The resultant phases were highly dependent on the alkylamine chain length. While a phosphate salt may be formed for any chain length under the correct conditions (Figure 5-12a), the aluminophosphate products range from crystalline molecular sieves for ethylamine[20] and propylamine,[5] to lamellar phases with decreasing short-range order and increasing interlayer distance (Figure 5-12b). The different symbols in Figure 5-12b represent the second and/or third MLA d-spacing that was observed in the PXRD of the aluminophosphate product, as was the case for many of the alkylamines (section 5.1.2).

The important role of the terminal methyl of the alkyl chain is directly observed by considering the results obtained using an alkylamine versus an alkylenediamine template. 1,8-diaminooctane, for example, formed a phosphate salt containing a monolayer of template

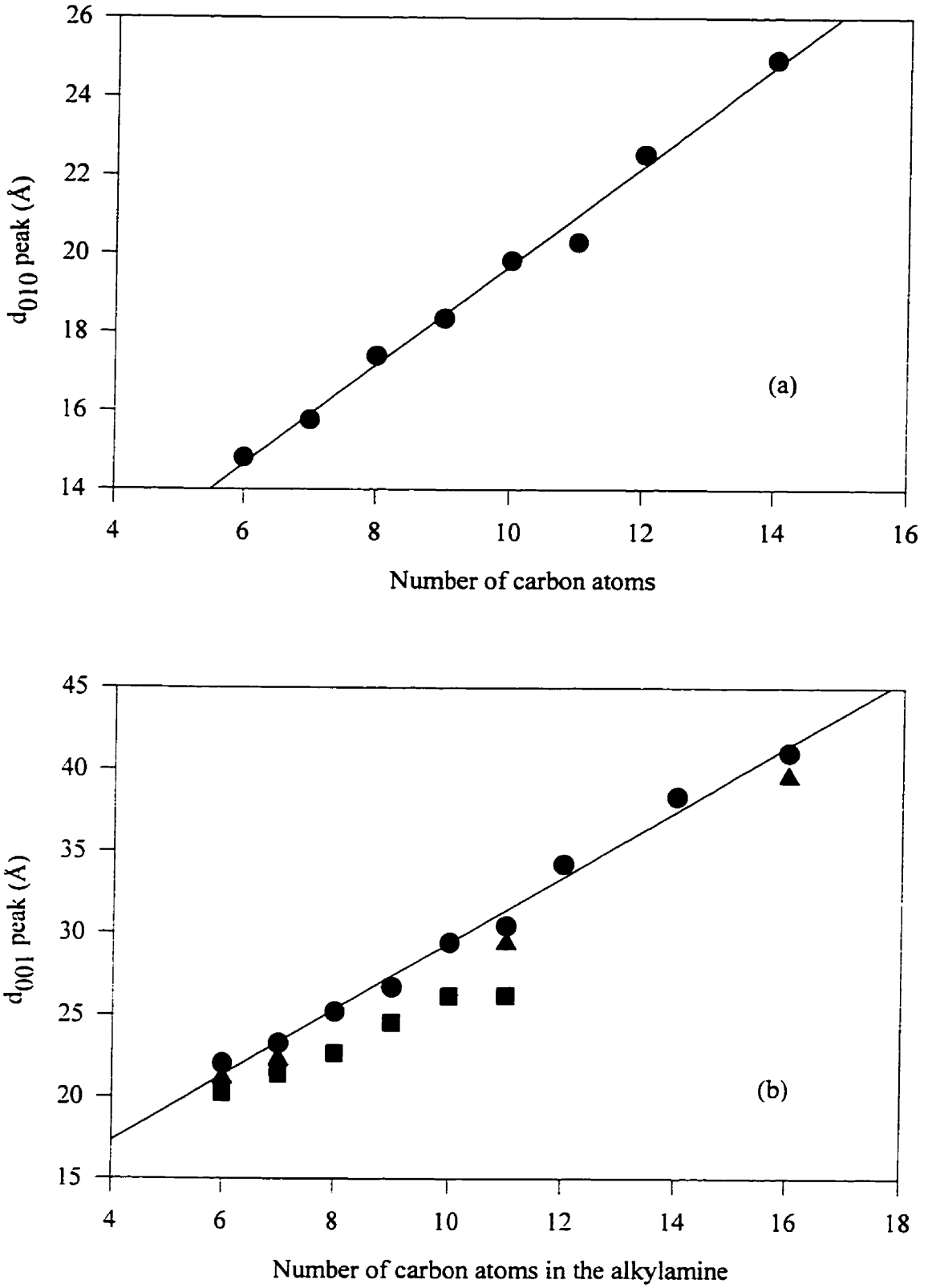

Figure 5-12. Interlayer spacing versus carbon chain length.
(a) ADP. (b) MLA.

molecules. In contrast, octylamine formed the MLA material containing a bilayer of ocytalmmonium molecules. The presence of a terminal methyl is necessary for formation of a bilayer or even an interdigitated configuration, as in ODP.

5.3.3 MLA Morphologies

Much data has been collected for the alkylamine systems, and the MLA and ADP materials. However, by what means do the macroscopic MLA surface patterns form? Unfortunately, this represents the first exploration of the TEG-aluminophosphate-alkylamine system, and there is no precedence for the synthesis of these aluminophosphate morphologies. However, much is known concerning emulsions, which are mixtures of two immiscible liquids, stabilized by an emulsifier. This will be the basis for a preliminary mode of formation that will be offered here.

Two types of emulsions exist, a microemulsion, which is thermodynamically stable, and a macroemulsion, which is thermodynamically unstable.[38,39] As their prefix implies, the latter involves larger length scales. A microemulsion is stabilized only by a surfactant, while a macroemulsion can be stabilized by a surfactant, polymer or small particles. These species prevent the discrete drops of the emulsion from reaching molecular contact and undergoing coalescence. The most common example of an emulsifier is a monolayer film of surfactants that reside at the polar-apolar interface.[38] However, Friberg *et al.* have prepared macroemulsions where the emulsifier is a lamellar liquid crystal.[40,41]

Therefore, the following is proposed for the formation of the MLA morphologies: Polyethylene glycols (PEG) of a wide range of molecular weights are known to be water soluble at moderate temperatures, but undergo phase separation at higher temperatures.[42-45] At the same time, the DDP was shown to form a liquid crystal phase at these temperatures. Therefore, a macroemulsion can exist, where the polar component is water, the apolar component is TEG and the DDP liquid crystal exists at the interface and stabilizes the macroemulsion. Subsequent aluminophosphate growth at the interface would result in an MLA material with a patterned surface, such as the surface bowls (e.g. V-32C, V-52A). This would necessarily occur at the particle surface, since it is where aluminophosphate growth is occurring and water is produced by condensation polymerization. The growth of the surface pattern ends by the exhaustion of the source reagents or by the quenching of the reaction.

Since the above model involves a water-in-oil (W/O) type of macroemulsion,[38,39] it would explain the lack of pattern formation under aqueous conditions. Likewise, a reverse microemulsion experiment, TEG in H_2O (V-45, 134.4 H_2O : 0.58 TEG), gave the MLA material but with no such surface patterning. If an emulsion indeed exists, the results would be expected to be sensitive to agitation. This would account for the lack of observation of such surface patterns under dynamic conditions (V-39, V-40).

It would appear that another process is occurring for formation of the hollow spheres. One explanation is the existence of bubbles in the solvent, which is well understood for one-component or many-component systems.[46,47] Bubbles are known to coagulate and adhere on a surface, which would account for their occurrence only on the bottom or sides of the Teflon liner (V-32J, V-51A), or on the surface of a solid sphere (V-32G). The deposition of MLA material around these bubbles would lead to the growth of a hollow sphere. Once it has begun to develop, it should undergo the same type of macroemulsion patterning process as occurs for the solid spheres. Their respective surface patterning are certainly quite similar (cf. V-32H, V-32D).

Finally, some of the undecylamine-MLA patterned spheres were cross-sectioned to observe the nature of the underlying material and if any patterns or voids were present under the surface. The SEM micrographs of the cross-sections are shown in Figure 5-13. The lamellar morphology follows the outer contour of the sphere in some areas, but is tortuous in others (Figure 5-13a,b). Similar results were observed for the decylamine-related spheres. The "burial" of a surface feature may be observed in Figure 5-13c; what likely was once a surface bowl, in the bottom right of the micrograph, has been deposited over (the outer surface of the sphere is on the lower half of this view).

5.4 CONCLUSIONS

The preliminary work involving alkylamines has led to a series of new mesolamellar phosphates and aluminophosphates. The mode of formation of the aluminophosphate morphologies warrants further investigation. The morphologies are unprecedented within the aluminophosphate domain and bear resemblance to biomineral forms.[48] The synthesis of inorganics with natural form is certainly not a new notion.[49,50] However, in recent years, it has become an area of developing interest, known today as biomimetic materials chemistry.[51,52] This is one area with which the work of this chapter overlaps. Another is the area of hierarchical

(a)

(b)

(c)

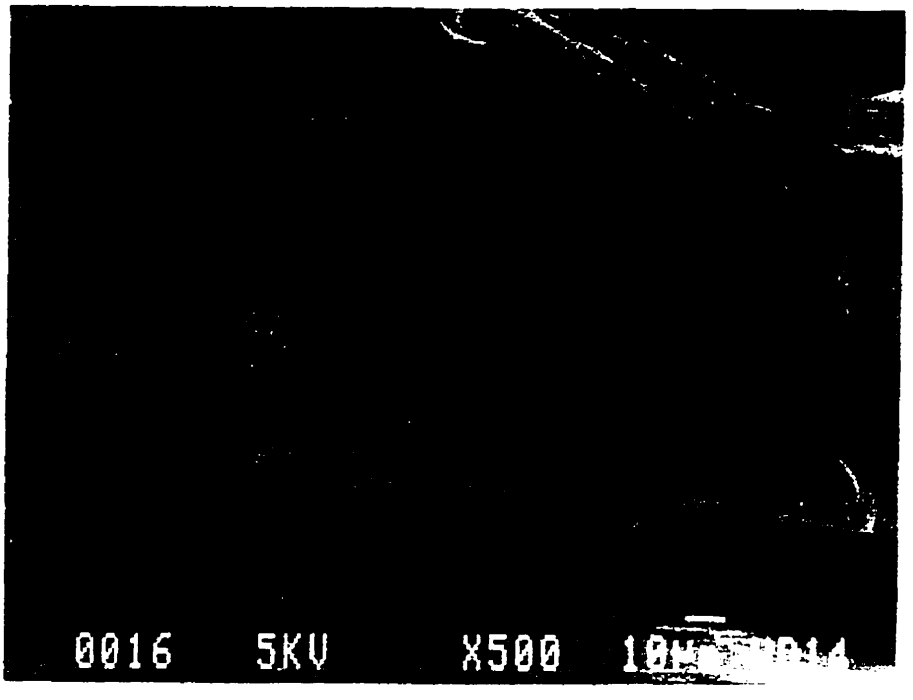

Figure 5-13. Cross-sectional SEM's. (a) Undecylamine patterned sphere. (b) Close-up of the surface of a cut sphere. (c) Another close-up of a cut sphere, showing the nature of the underlying material.

inorganic materials chemistry.[53,54] The MLA composite is mesolamellar, while the MLA fabric is sculpted into macroscopic shapes and patterns.

5.5 REFERENCES

1. D. F. Shriver, P. Atkins, C. H. Langford, *Inorganic Chemistry, 2nd ed.*; W. H. Freeman and Company: New York, 1994, pp. 239.
2. D. Riou, T. Loiseau, G. Férey, *J. Solid State Chem.* **1992**, *99*, 414.
3. W. Tieli, Y. Long, P. Wengin, *J. Solid State Chem.* **1990**, *89*, 392.
4. R. H. Jones, J. M. Thomas, R. Xu, Q. Huo, A. K. Cheetham, A. V. Powell, *J. Chem. Soc., Chem. Commun.* **1991**, 1266.
5. R. Szostak, *Handbook of Molecular Sieves*; Van Nostrand Reinhold: New York, 1992.
6. D. Riou, T. Loiseau, G. Férey, *J. Solid State Chem.* **1993**, *102*, 4.
7. See, for example, R. C. Haushalter, Z. Wang, L. M. Meyer, S. S. Dhingra, M. E. Thompson, J. Zubieta, *Chem. Mater.* **1994**, *6*, 1463.
8. See, for example, M. Cavellec, D. Riou, G. Férey, *J. Solid State Chem.* **1994**, *112*, 441.
9. See, for example, (a) S. S. Dhingra, R. C. Haushalter, *J. Chem. Soc., Chem. Commun.* **1993**, 1665. (b) T. Song, J. Xu, Y. Zhao, Y. Yue, Y. Xu, R. Xu, N. Hu, G. Wei, H. Jia, *J. Chem. Soc., Chem. Commun.* **1994**, 1171.
10. (a) M. T. Averbuch-Pouchot, A. Durif, *Acta Cryst.* **1987**, *C43*, 1894. (b) S. M. Golubev, Y. D. Kondrashev, *Zh. Strukt. Khim.* **1984**, *25*, 471.
11. S. Kamoun, A. Jouini, M. Kamoun, A. Daoud, *Acta Cryst.* **1989**, *C45*, 481.
12. M. Bagieu-Beucher, A. Durif, J. C. Guitel, *Acta Cryst.* **1989**, *C45*, 421.
13. S. Natarajan, J. P. Gabriel, A. K. Cheetham, *J. Chem. Soc., Chem. Commun*, **1996**, 1415.
14. S. Kamoun, A. Jouini, A. Daoud, *Acta Cryst.* **1991**, *C47*, 117.
15. S. Kamoun, A. Jouini, A. Daoud, A. Durif, J. C. Guitel, *Acta Cryst.* **1992**, *C48*, 133.
16. J. M. Thomas, R. H. Jones, R. Xu, J. Chen, A. M. Chippindale, S. Natarajan, A. K. Cheetham, *J. Chem. Soc., Chem. Commun.* **1992**, 929.
17. F. Takusagawa, T. F. Koetzle, *Acta Cryst.* **1979**, *B35*, 867.
18. J. Renaudin, G. Férey, *J. Solid State Chem.* **1995**, *120*, 197.
19. B. Kraushaar-Czarnetzki, W. H. J. Stork, R. J. Dogterom, *Inorg. Chem.* **1993**, *32*, 5029.
20. Q. Huo, R. Xu, *J. Chem. Soc., Chem. Commun.* **1990**, 783.

21. J. J. Pluth, J. V. Smith, *Acta Cryst.* **1987**, *C43*, 866.

22. A. M. Chippindale, A. V. Powell, L. M. Bull, R. H. Jones, A. K. Cheetham, J. M. Thomas, R. Xu, *J. Solid State Chem.* **1992**, *96*, 199.

23. Q. Gao, R. Xu, J. Chen, R. Li, S. Li, S. Qiu, Y. Yue, *J. Chem. Soc., Dalton Trans.* **1996**, 3303.

24. A. Sayari, V. R. Karra, J. S. Rddy, I. L. Moudrakovski, *J. Chem. Soc., Chem. Commun.* **1996**, 411.

25. A. Chenite, Y. Le Page, V. R. Karra, A. Sayari, *J. Chem. Soc., Chem. Commun.* **1996**, 413.

26. B. Duncan, M. Stocker, D. Gwinup, R. Szostak, K. Vinje, *Bull. Soc. Chim. Fr.* **1992**, *129*, 98.

27. C. S. Blackwell, R. L. Patton, *J. Phys. Chem.* **1984**, *88*, 6135.

28. C. S. Blackwell, R. L. Patton, *J. Phys. Chem.* **1988**, *92*, 3965.

29. H. He, J. Klinowski, *J. Phys. Chem.* **1993**, *97*, 10385.

30. M. P. J. Peeters, L. J. M. van de Ven, J. W. de Haan, J. H. C. van Hooff, *J. Phys. Chem.* **1993**, *97*, 8254.

31. C. J. Pouchert, J. Behnke (eds.), *The Aldrich Library of ^{13}C and ^{1}H FT NMR Spectra*; Aldrich Chemical Co.: Milwauke, 1993.

32. C. J. Bowlas, D. W. Bruce, K. R. Seddon, *J. Chem. Soc., Chem. Commun.* **1996**, 1625.

33. V. Skita, D. W. Chester, C. J. Oliver, J. G. Turcotte, R. H. Notter, *J. Lipid Res.* **1995**, *36*, 1116.

34. S. Maruyama, H. Matsuki, H. Ichimori, S. Kaneshina, *Chem. Phys. Lipids* **1996**, *82*, 125.

35. I. Hatta, S. Kato, H. Takahashi, *Phase Transitions* **1993**, *45*, 157.

36. F. S. Hing, G. G. Shipley, *Biochem.* **1995**, *34*, 11904.

37. G. Shen, S. Oliver, G. A. Ozin, unpublished results.

38. D. F. Evans, H. Wennerström, *The Colloidal Domain: Where Physics, Chemistry and Biology Meet*; VCH Publishers, Inc.: New York, 1994, ch. 11.

39. J. Sjöblom, R. Lindberg, S. E. Friberg, *Adv. Colloid Int. Sci.* **1996**, *95*, 125.

40. S. Friberg, L. Rydhag, G. Jederström, *J. Pharm. Sci.* **1971**, *60*, 1883.

41. S. Friberg, J. *Am. Oil. Chem. Soc.* **1971**, *48*, 578.

42. T. Kuhl, Y. Guo, J. L. Alderfer, A. D. Berman, D. Leckband, J. Israelachvili, S. W. Hui, *Langmuir* **1996**, *12*, 3003.

43. M. L. Sierra, E. Rodenas, *Langmuir* **1994**, *10*, 4440.

44. M. L. Sierra, E. Rodenas, *Langmuir* **1996**, *12*, 573.

45. E. Rodenas, M. L. Sierra, *Langmuir* **1996**, *12*, 1600.

46. S. D. Lubetkin, *Chem. Soc. Rev.* **1995**, *24*, 243.

47. W. L. Ryan, E. A. Hemmingsen, *J. Colloid Interface. Sci.* **1993**, *157*, 312.

48. H. A. Lowenstam, *Science* **1981**, *211*, 1126.

49. P. Harting, *Natuurkd. Verh. Koninkl. Acad.* **1873**, *13*, 1.

50. D. W. Thompson, *On Growth and Form*; Cambridge University Press: Cambridge, 1917.

51. S. Mann, *J. Mater. Chem.* **1995**, *5*, 1.

52. R. Kniep, S. Busch, *Angew. Chem., Int. Ed. Engl.* **1996**, *35*, 2624.

53. National Materials Advisory Board, *Hierarchical Structures in Biology as a Guide for New Materials Technology*; National Academy Press: Washington D.C., 1994.

54. Q. Huo, J. Feng, F. Schüth, G. D. Stucky, *Chem. Mater.* **1997**, *9*, 14.

CHAPTER 6: FUTURE WORK

The volume of data that was compiled in this course of this work led to many new discoveries that contribute to the area of aluminophosphate materials. At the same time, there is much future research that could be pursued, on the long or short term. Some suggestions will be offered here, which of course represent only a fraction of the possiblities.

Firstly, new aluminophosphate crystal structures await discovery. Many of the products from tetraethylene glycol were comprised of one or more unknown phases, with crystals often sufficiently large for single crystal XRD. Other systems could be optimized to increase crystal size, as was accomplished in the isolation of large crystals of UT-3. The discovery of additional aluminophosphate structures was not essential to the present work and effort was instead concentrated elsewhere. Nonetheless, such work could quickly and easily lead to a series of new structures. Furthermore, the amines that were chosen represent only some of the possible organic templating species. It would also be interesting to see if transition metal coordination complexes could be successful as templating agents, as was only shown very recently for aqueous systems.[1,2]

It should be straightforward to discover a large number of new phosphate salt structures. They formed spontaneously in most solvents by simply adding phosphoric acid and the alkylamine in the proper amounts. Large crystals may be grown by recrystallization, or solvothermally, as for DODP. In many cases, there exists more than one structure type for a given alkylamine due to the polyprotic nature of the phosphate anion.[3,4] Of the limited number of phosphate salt structures reported to date, some are of interest as a model for understanding the interactions of amines with nucleic acids.[5] Others have shown that alkylammonium dihydrogen phosphate salts display second harmonic generation (SHG) activity.[6] The main advantages of an ADP phase over related materials, such as $LiNbO_3$ or KH_2PO_4,[7] are, firstly, the organic amine may be chosen from a wide range of possible species, which in turn determines the optical properties and photostability of the compound, and, secondly, they are in many instances much more soluble. Therefore, they are easier to process and can be incorporated into, for example, an organic polymer to form an SHG-active composite.[6] They are also transparent in the visible region. Investigation of the SHG properties of the ADP and AMP compounds are therefore a candidate for future work.

The more detailed materials characterization of the aluminophosphate and phosphate solids represents a large area of possible research. Although there exists much spectroscopic data

on the aluminophosphate frameworks,[8,9] the data for the lower dimensionality materials is rather scarce. For example, IR spectra were not collected for any of the UT-n or phosphate materials. Solid state NMR was performed on only a limited number of the discovered materials. This could also be done for the unknown compounds, which would reveal the coordination state and number of crystallographic sites of aluminum and phosphorus, and could be compared to those of known structures.

The Raman spectra of only a few aluminophosphate frameworks have been published and displayed many non-template bands, attributed to aluminophosphate four-rings and the larger rings of the main channel.[10,11] It would be interesting to compare these to the lower-dimensionality chain and layered aluminophosphates, such as the $AlPO_4$-5 framework versus the $AlPO_4$-5-like layer. Preliminary Raman data collected for UT-2, UT-3 and others showed promising results and warrants further study.

More in-depth thermal studies of the aluminophosphate solids could elucidate some unanswered questions. For example, is the chain to layer transformation that was observed for the cyclopentylammonium-related phases indeed occurring for the other cycloalkylamine-related materials? This would confirm the proposed isostructurality amongst the unknowns of these systems, without the need for SC-XRD analysis. Thermal studies of the n-alkylamine ADP phases could also be studied by, for example, DSC, VT-PXRD, hot-stage polarizing optical microscopy (POM) and variable temperature ^{13}C and ^{31}P MAS NMR. This could reveal the range of carbon chain length that leads to a thermotropic liquid crystal and therefore possibly account for the narrow range of alkylamines that lead to macroscopic surface patterning.

Further synthetic work with alkylamines could also be performed to better define the conditions necessary for pattern formation, by the systematic variation of synthesis parameters such as TEG/H_2O concentration, P:Al ratio, temperature, time and others. There should also exist further interesting morphologies, such as geometric variations of the honeycomb or rhombohedral mesh. More importantly, emphasis could be placed on the isolation of one particular morphology, which would be necessary for any potential applications. However, a more developed model for their mode of formation would likely be more helpful in this regard.

Further development of the mode of formation studies of Chapter 4 could be beneficial, since a better understanding brings one closer to the rational design of structure types for specific applications. Further examples of the build-up of other chain, layered and framework structures were derived but not included in this write-up. Perhaps there are other chain transformations that

could better account for certain structures. More experimental work is certainly necessary, and some possibilities include:

- Solubilization and recrystallization of the parent chain or any other chain species. The isostructural zinc phosphate chain was believed to exist in solution.[12] This chain undergoes different solution chemistry since there were no template molecules in the structure, as the phosphate groups contain terminal ethoxy groups which solubilize the chain. Nonetheless, the reversible dehydration-hydration of the solution-bound aluminophosphate aggregation polymers, from a viscous liquid to a solid and back, suggests that this is quite possible. Indeed, this was how the crystal structure of the $Al(H_2PO_4)_3$ chain was obtained.[13] In the present work, all attempts were unsuccessful, although only a limited number of such experminets were conducted.

- "Capping" of a solution-bound chain, thereby precipitating it out of solution. An example of a capping agent would be trimethylchlorosilane, which is commonly used to precipitate out silicate solution species by "trimethylsilylation".[14,15] Another possibility is to connect an alkyl group to the phosphate groups by condensing terminal P-OH groups with an alcohol. This would render the chain reversibly soluble and crystallizable due to the terminal alkoxy groups, as for the zinc phosphate chain. The ideal case would be to crystallize out the various known and theoretical aluminophophate chain types.

- Gel phase chromatography, a common technique for determining molecular weight and molecular weight distribution of polymers and in fact for the trimethylsilylated silicate oligomers and clusters[14,15] and higher length oligomers of condensed polyphosphates.[16,17] This could be performed for various mother liquors, which may lead to evidence of a chain species and its MW and distribution.

- Real-time *in situ* PXRD of reaction gels heated under synthesis conditions. Recently, O'Hare and coworkers have shown this to be an excellent and powerful technique for monitoring intercalation chemistry and the hydrothermal syntheses of molecular sieves.[18,19] Advantages include the observation of the formation of a particular phase under actual synthesis conditions, as well as that of any solid intermediates and their transformations, and direct observation of the effect of varying synthesis parameters. This would corroborate many of the observed solid state transformations and allow observation of any precursor phases, such

as the poorly crystalline phases that diffract at low-angle, often observed prior to the crystalline aluminophosphate product.

Since the Teflon liners contain impurities that appear to be responsible for the isolation of large crystals such as UT-6, this warrants further study. Such research could lead to other new phases and large crystal sizes of either known or unknown phases. Some degree of control of this process could be obtained by adding to the synthesis mixture a piece of Teflon impregnated with a chosen "impurity".

The use of fluorine in any of the synthesis systems should lead to new fluoroaluminophosphate phases. Very small amounts made a marked difference in the results, such as one drop or more, and demonstrates the power of its effect. For any such future work, a micropipette should be used to quantitatively measure the volumes of fluorine that are added.

The structural modification of any of the aluminosphosphate solids is another area which could be of interest. Ion exchange of the extraframework pyridinium cations of UT-6 is a definite possibility. There is an entire sub-discipline of intercalation chemistry for layered inorganic compounds,[20] which could be relevant to the layered aluminophosphates. It would also be interesting to exfoliate the layers of, for example, UT-3, as shown for many layered inorganic compounds by Mallouk and coworkers.[21,22] The layers may then be deposited epitaxially onto a film from solution to form various superstructurred multilayered films. Similarly, thin film growth has been demonstrated for oriented films of $AlPO_4$-5 and zincophosphate molecular sieves.[23] However, the film consisted of discrete, pregrown crystals. Performing this type of chemistry with the various layered aluminophosphates, most of which already possess a plate-like morphology, would be much more sensible in trying to grow a smooth, continuous film, as is essential for any thin film device applications.

There is a previously unexplored world of aluminum organophosphates and aluminum organophosphonates, where one of the phosphate oxygens is connected to or replaced by the carbon of an organic group, respectively. As for the zinc organophosphates, the organic group would serve as the void space filler and separate the inorganic species, eliminating the need of an organic amine. Indeed, two aluminum methylphosphonate frameworks[24,25] and one layer[26] were recently prepared hydrothermally using methylphosphonic acid as the P_2O_5 source and no template. Haushalter and coworkers hydrothermally synthesized a layered vanadium organophosphonate,[27] where the inorganic layers are joined alternately by bilayers of phenyl

phosphonates and monolayers of dialkylammonium template molecules. The well-established area of layered zirconium and metal phosphates and phosphonates[28,29] is also a good area upon which to build.

Finally, the non aqueous synthesis and characterization of other metal phosphates or metal arsenates is a candidate for future research. The number of reported chain, layers and frameworks of this class of material continually increases. To date, most are synthesized hydrothermally. However, a layered indium phosphate prepared from an ethylene glycol solvent was recently reported.[30] As was found for aluminophosphates, the organothermal synthesis of other metal phosphates could be very rewarding.

REFERENCES

1. K. Morgan, G. Gainsford, N. Milestone, *J. Chem. Soc., Chem. Commun.* **1995**, 425.
2. D. A. Bruce, A. P. Wilkinson, M. G. White, J. A. Bertrand, *J. Chem. Soc., Chem. Commun.* **1995**, 2059.
3. S. Kamoun, A. Jouini, A. Daoud, *Acta Cryst.* **1991**, *C47*, 117.
4. D. Riou, T. Loiseau, G. Férey, *Acta Cryst.* **1993**, *C49*, 1237.
5. F. Takusagawa, T. F. Koetzle, *Acta Cryst.* **1979**, *B35*, 867.
6. C. B. Aakeröy, P. B. Hitchcock, B. D. Moyle, K. R. Seddon, *J. Chem. Soc., Chem. Commun.* **1989**, 1856.
7. C. N. R. Rao, J. Gopalakrishnan, *New Directions in Solid State Chemistry*; Cambridge University Press: New York, 1986, pp. 367.
8. C. S. Blackwell, R. L. Patton, *J. Phys. Chem.* **1988**, *92*, 3965.
9. R. Szostak, *Handbook of Molecular Sieves*; Van Nostrand Reinhold: New York, 1992.
10. R. J. Davis, *Chem. Mater.* **1992**, *4*, 1410.
11. A. J. Holmes, S. J. Kirkby, G. A. Ozin, D. Young, *J. Phys. Chem.* **1994**, *98*, 4677.
12. W. T. A. Harrison, T. M. Nenoff, T. E. Gier, G. D. Stucky, *Inorg. Chem.* **1992**, *31*, 5395.
13. R. Kniep, M. Steffen, *Angew. Chem., Int. Ed. Engl.* **1978**, *17*, 272.
14. R. Szostak, *Molecular Sieves: Principles of Synthesis and Identification*; Van Nostrand Reinhold: Toronto, 1989, pp. 162.
15. G. J. Bratton, B. R. Currell, D. Kendrick, H. G. Midgley, J. R. Parsonage, *J. Mater. Chem.* **1993**, *3*, 465.

16. D. E. C. Corbridge, *Topics Phosphorus Chem.* **1966**, *3*, 57.

17. E. J. Griffith, R. L. Buxton, *J. Am. Chem. Soc.* **1967**, *89*, 2884.

18. S. M. Clark, J. S. O. Evans, D. O'Hare, C. J. Nuttall, H. Wong, *J. Chem. Soc., Chem. Commun.* **1994**, 809.

19. R. J. Francis, S. J. Price, J. S. O. Evans, S. O'Brien, D. O'Hare, S. M. Clark, *Chem. Mater.* **1996**, *8*, 2102, and references therein.

20. See, for example, (a) M. S. Whittingham, A. J. Jacobson (eds.), *Intercalation Chemistry*; Academic Press, Inc.: New York, 1982. (b) M. S. Dresselhaus (ed.), *Intercalation in Layered Materials*; Plenum Press: New York, 1986.

21. Hong, H.; Sackett, D. D.; Mallouk, T. E. *Chem. Mater.* **1991**, *3*, 521.

22. Kepley, L. J.; Sackett, D. D.; Bell, C. M.; Mallouk, T. E. *Thin Solid Films.* **1992**, *208*, 132.

23. S. Feng, T. Bein, *Nature* **1994**, *368*, 834, and references therein.

24. K. Maeda, J. Akimoto, Y. Kiyozumi, F. Mizukami, *J. Chem. Soc., Chem. Commun.* **1995**, 1033.

25. K. Maeda, J. Akimoto, Y. Kiyozumi, F. Mizukami, *Angew. Chem., Int. Ed. Engl.* **1995**, *34*, 1199.

26. L. Sawers, V. J. Carter, A. R. Armstrong, P. G. Bruce, P. A. Wright, B. E. Gore, *J. Chem. Soc., Dalton Trans.* **1996**, 3159.

27. M. I. Khan, Y. Lee, C. J. O'Connor, R. C. Haushalter, J. Zubieta, *J. Am. Chem. Soc.* **1994**, *116*, 4525.

28. A. Clearfield, *Inorganic Ion Exchange Materials*; CRC Press, Inc.: Boca Raton, Florida, 1982.

29. T. Kanazawa, *Inorganic Phosphate Materials*; *Mater. Sci. Monographs*, **52**. Elsevier Science Publishers: New York, 1989, ch. 6.

30. A. M. Chippindale, S. J. Brech, *J. Chem. Soc., Chem. Commun.* **1996**, 2781.

Appendix A. Tabular summary of synthetic systems and results. PXRD and SEM data are shown for selected products in Appendices B and C, respectively, as indicated in the last two columns.

Ref #	Solvent	Al_2O_3 Source	P_2O_5 Source	Organic Additive	Temp (°C)	Time	Major Product(s)	Observed Morphology	PXRD	SEM
Chapter 2: Secondary, Tertiary, Quaternary and Cyclic Amines										
2.3.1 Secondary Amines										
II-1	9.3 TEG	0.9 Al_2O_3•nH_2O	3.6 H_3PO_4	5.9 Et_2NH	180	10 days	Amorphous			
II-2	9.3 TEG	0.9 Al_2O_3•nH_2O	3.6 H_3PO_4	5.9 Pr_2NH	180	1 day	Disordered layer	Some needles present	√	
II-3	9.3 TEG	0.9 Al_2O_3•nH_2O	3.6 H_3PO_4	5.9 Pr_2NH	180	3 days	Unknown 20Å phase, $AlPO_4$-11	Needles, up to 200 μm in length	√	
II-4	9.3 TEG	0.9 Al_2O_3•nH_2O	3.6 H_3PO_4	5.9 Pr_2NH	180	10 days	$AlPO_4$-11	1 μm small platelets	√	√
II-5	40 H_2O	1.0 Catapal B	2.0 H_3PO_4	1.0 Pr_2NH	150	1 day	VPI-5, trace $AlPO_4$-11	Small needles		
2.3.2 Tertiary Amines										
II-6	9.3 TEG	0.9 Al_2O_3•nH_2O	3.6 H_3PO_4	5.9 Me_3N	180	10 days	$AlPO_4$-21	5 μm platelets	√	
II-7	14 TEG	0.9 Al_2O_3•nH_2O	3.6 H_3PO_4	5.9 Et_2MeN	180	14 days	Unknown	150μm cuboctahedral	√	
II-8	14 TEG	0.9 Al_2O_3•nH_2O	3.6 H_3PO_4	5.9 Et_3N	RT	0 days, 1 or 4 months	Pseudoboehmite	Pseudoboehmite spheres		
II-9	14 TEG	0.9 Al_2O_3•nH_2O	3.6 H_3PO_4	5.9 Et_3N	195	1 day	Pseudoboehmite, trace JDF-20	Pseudoboehmite spheres, small crystals on wall	√	
II-10	14 TEG	0.9 Al_2O_3•nH_2O	3.6 H_3PO_4	5.9 Et_3N	195	2 days	JDF-20, chains	JDF-20 spheres and needles	√	
II-11	14 TEG	0.9 Al_2O_3•nH_2O	3.6 H_3PO_4	5.9 Et_3N	195	4 days	Chains, JDF-20	Needles and JDF-20 spheres	√	
II-12	14 TEG	0.9 Al_2O_3•nH_2O	3.6 H_3PO_4	5.9 Et_3N	195	7 days	Chains, JDF-20	Needles on walls, JDF-20 spheres	√	
II-13	9.3 TEG	0.9 Al_2O_3•nH_2O	3.6 H_3PO_4	5.9 Et_3N	195	9 days, wall	Chains, trace JDF-20	Needles on walls, some JDF-20 spheres	√	√ √
II-14	9.3 TEG	0.9 Al_2O_3•nH_2O	3.6 H_3PO_4	5.9 Et_3N	195	9 days, bottom	JDF-20, trace chains	Hard disk of material, comprised of small needles	√	
II-15	14 TEG	0.9 Al_2O_3•nH_2O	3.6 H_3PO_4	5.9 Et_3N	180	4.5 months	Chains, trace JDF-20	All needles on bottom of liner		
II-16	14 TEG	0.9 Al_2O_3•nH_2O	3.6 H_3PO_4	5.9 Et_3N	180	2 or 3 days	Pseudoboehmite, amorphous	Plate-like growths, pseudoboehmite spheres	√	
II-17	14 TEG	0.9 Al_2O_3•nH_2O	3.6 H_3PO_4	5.9 Et_3N	200	12 days	Chain phase	Large needles		
II-18	28 TEG	1.0 Al_2O_3•nH_2O	3.6 H_3PO_4	5.9 Et_3N	195	10 days	$AlPO_4$-5, JDF-20	Aggregates of needles	√	

Ref #	Solvent	Al_2O_3 Source	P_2O_5 Source	Organic Additive	Temp (°C)	Time	Major Product(s)	Observed Morphology	PXRD	SEM
II-19	9.3 TEG + 1.8 H_2O	0.9 Al_2O_3•nH_2O	3.6 H_3PO_4	5.9 Et_3N	195	9 days	Chains, JDF-20	Needles, JDF-20 spheres on wall		
II-20	9.3 TEG + 3.6 H_2O	1.0 Al_2O_3•nH_2O	3.6 H_3PO_4	5.9 Et_3N	180	9 days	Chains, more JDF-20	Needles, JDF-20 spheres		
II-21	9.3 TEG + 3.6 H_2O	1.0 Al_2O_3•nH_2O	3.6 H_3PO_4	5.9 Et_3N	200	9 days	JDF-20	JDF-20 spheres		
II-22	9.3 TEG + 7.2 H_2O	1.0 Al_2O_3•nH_2O	3.6 H_3PO_4	5.9 Et_3N	195	9 days	JDF-20	Powder of small needles		√
II-23	9.3 TEG + 10.0 H_2O	0.9 Al_2O_3•nH_2O	3.6 H_3PO_4	5.9 Et_3N	150	3 days	Poorly crystalline JDF-20	Very small needles	√	
II-24	9.3 TEG + 10.0 H_2O	0.9 Al_2O_3•nH_2O	3.6 H_3PO_4	5.9 Et_3N	180	3 days	Poorly crystalline JDF-20	Very small needles	√	
II-25	9.3 TEG + 10.0 H_2O	0.9 Al_2O_3•nH_2O	3.6 H_3PO_4	5.9 Et_3N	195	3 days	JDF-20, sometimes UT-1	Small needles, large hexagonal plates	√	
II-26	9.3 TEG + 10.0 H_2O	0.9 Al_2O_3•nH_2O	3.6 H_3PO_4	5.9 Et_3N	200	2 days	JDF-20, $AlPO_4$-5	Aggregates of small needles		
II-27	9.3 TEG + 10.0 H_2O	0.9 Al_2O_3•nH_2O	3.6 H_3PO_4	5.9 Et_3N	200	10 days	$AlPO_4$-tridymite, JDF-20, $AlPO_4$-5	Faceted crystals	√	
II-28	9.3 TEG + 10.0 H_2O	0.9 Al_2O_3•nH_2O	3.6 H_3PO_4	5.9 Et_3N	220	10 days	$AlPO_4$-tridymite	200 μm faceted crystals	√	
II-29	9.3 TEG + 15.0, 20.0 or 25.0 H_2O	0.9 Al_2O_3•nH_2O	3.6 H_3PO_4	5.9 Et_3N	180 or 200	2 or 3 days	JDF-20	Powder of small needles		
II-30	9.3 TEG + 40.0 H_2O	0.9 Al_2O_3•nH_2O	3.6 H_3PO_4	5.9 Et_3N	195	10 days	$AlPO_4$-cristobalite, $AlPO_4$-5, JDF-20	Octahedral crystals, small needles		
II-31	9.3 TEG + 60.0 H_2O	0.9 Al_2O_3•nH_2O	3.6 H_3PO_4	5.9 Et_3N	180	6 days	JDF-20, $AlPO_4$-5	Small needles		
II-32	9.3 TEG + 89.4 H_2O	0.9 Al_2O_3•nH_2O	3.6 H_3PO_4	5.9 Et_3N	150	3 days	Poorly crystalline JDF-20, trace $AlPO_4$-5	Small needles		
II-33	9.3 TEG + 89.4 H_2O	0.9 Al_2O_3•nH_2O	3.6 H_3PO_4	5.9 Et_3N	180	3 to 10 days	$AlPO_4$-5, trace $AlPO_4$-cristobalite	20 μm hexagonal rods		
II-34	9.3 TEG + 89.4 H_2O	0.9 Al_2O_3•nH_2O	3.6 H_3PO_4	5.9 Et_3N	195	10 days	Tinsleyite, $AlPO_4$-cristobalite, trace $AlPO_4$-5	200 μm hexagonal plates	√	√
II-35	9.3 TEG + 120.0 H_2O	0.9 Al_2O_3•nH_2O	3.6 H_3PO_4	5.9 Et_3N	150	6 days	Poorly formed JDF-20			
II-36	9.3 TEG + 120.0 H_2O	0.9 Al_2O_3•nH_2O	3.6 H_3PO_4	5.9 Et_3N	180	6 days	$AlPO_4$-5, trace $AlPO_4$-cristobalite			
II-37	89.5 H_2O + 4.67 TEG	0.9 Al_2O_3•nH_2O	3.6 H_3PO_4	5.9 Et_3N	180	5 days	$AlPO_4$-5, trace $AlPO_4$-cristobalite	3 μm $AlPO_4$-5 hexagonal rods		
II-38	89.5 H_2O	1.0 Al_2O_3•nH_2O	3.6 H_3PO_4	5.9 Et_3N	195	12 days	$AlPO_4$-5, $AlPO_4$-cristobalite	100 μm hexagonal rods, 300 μm octahedra		√ √
II-39	300 H_2O	0.9 Al_2O_3•nH_2O	3.6 H_3PO_4	5.9 Et_3N	195	11 days	$AlPO_4$-5, unknown 8.7Å phase	Needles, 5 μm square plates	√	
II-40	1000 H_2O	0.9 Al_2O_3•nH_2O	3.6 H_3PO_4	5.9 Et_3N	195	11 days	Berlinite	Large, frayed needles	√	

Ref #	Solvent	Al_2O_3 Source	P_2O_5 Source	Organic Additive	Temp (°C)	Time	Major Product(s)	Observed Morphology	PXRD	SEM
II-41	14 TEG	0.9 Al_2O_3•nH_2O	3.6 H_3PO_4	5.9 Et_3N	180, tumble	7 days	JDF-20	Solid clump of JDF-20, some small needles		
II-42	9.3 TEG	1.0 Al_2O_3•nH_2O	3.6 H_3PO_4	2.9 Et_3N	180	11 days	Chains, $AlPO_4$-tridymite, trace $AlPO_4$-5	Faceted spherical crystals, small needles		
II-43	9.3 TEG	1.0 Al_2O_3•nH_2O	3.6 H_3PO_4	2.9 Et_3N	200	11 days	$AlPO_4$-tridymite, trace chains	Faceted spherical crystals, small needles		
II-44	9.3 TEG + 3.6 H_2O	1.0 Al_2O_3•nH_2O	3.6 H_3PO_4	2.9 Et_3N	195 or 200	11 to 13 days	$AlPO_4$-tridymite	Faceted spherical crystals		
II-45	9.3 TEG	1.0 Al_2O_3•nH_2O	3.6 H_3PO_4	-	195 or 200	11 to 13 days	Berlinite	Brown powder of 20μm spherical, faceted crystals		
II-46	9.3 TEG	1.0 Al_2O_3•nH_2O	3.6 H_3PO_4	6.95 C_6H_{12}	180	4 days	Berlinite	Brown powder of 50μm spherical, faceted crystals		
II-47	14 TEG	0.9 Al_2O_3•nH_2O	-	5.9 Et_3N	180	3 days	Pseudoboehmite	Pseudoboehmite spheres		
II-48	14 TEG	0.9 Al_2O_3•nH_2O	1.8 H_3PO_4	5.9 Et_3N	180	3 days	JDF-20, $AlPO_4$-5, pseudoboehmite	JDF-20 spheres, pseudoboehmite spheres, needles		
II-49	9.3 TEG + 89.4 H_2O	1.0 Al_2O_3•nH_2O	2.0 H_3PO_4	5.9 Et_3N	195	11 days	$AlPO_4$-5	40μm hexagonal rods		
II-50	89.4 H_2O	1.0 Al_2O_3•nH_2O	2.0 H_3PO_4	5.9 Et_3N	195	11 days	$AlPO_4$-5	Large hexagonal rods		
II-51	9.3 TEG	0.9 Al_2O_3•nH_2O	5.4 H_3PO_4	5.9 Et_3N	195	3 days	Chains, trace $AlPO_4$-5	Frayed needles		
II-52	14 TEG	0.9 Al_2O_3•nH_2O	7.2 H_3PO_4	5.9 Et_3N	195	4 days	Chains	Large needles		
II-53	14 TEG	0.9 Al_2O_3•nH_2O	10.8 H_3PO_4	5.9 Et_3N	180 or 195	5 days	Berlinite	80μm cubic crystals		
II-54	14 TEG	2.0 $Al(isopr)_3$	3.6 H_3PO_4	5.9 Et_3N	150, 165, 180	10 days	Poorly crystalline JDF-20	Small needles		√
II-55	9.3 TEG	0.9 Catapal A	3.6 H_3PO_4	5.9 Et_3N	195	4 days	JDF-20	Fan-shaped aggregates of small needles		
II-56	14 TEG	0.9 $Na_3[AlF_6]$	3.6 H_3PO_4	5.9 Et_3N	150, 180, 195	6 days	$Al(PO_3)_3$		√	
II-57	9.3 TEG	0.9 Al_2O_3•nH_2O	1.8 $H_4P_2O_7$	5.9 Et_3N	180	3 days	Chains, some JDF-20	Large needles		
II-58	9.3 TEG	0.9 Al_2O_3•nH_2O	0.9 $H_6P_4O_{13}$	5.9 Et_3N	180	3 days	Chains	Small needles		
II-59	9.3 TEG	0.9 Al_2O_3•nH_2O	4.0 $(EtO)_3PO$	-	200	5 days	Berlinite	Large, faceted spherical crystals		
II-60	9.3 TEG	0.9 Al_2O_3•nH_2O	3.6 $(EtO)_3PO$	5.9 Et_3N	180	3 days	Poorly crystalline $AlPO_4$-5, pseudoboehmite	Pseudoboehmite spheres		
II-61	14 TEG	0.9 $Al(PO_3)_3$		5.9 Et_3N	150, 180	7 days	$Al(PO_3)_3$		√	
II-62	14 TEG	0.9 $Al(PO_3)_3$		5.9 Et_3N	195	7 days	$AlPO_4$-tridymite, $AlPO_4$-5, trace $Al(PO_3)_3$		√	

Ref #	Solvent	Al_2O_3 Source	P_2O_5 Source	Organic Additive	Temp (°C)	Time	Major Product(s)	Observed Morphology	PXRD	SEM
II-63	9.3 TEG	0.9 Al_2O_3•nH_2O	3.6 H_3PO_4	5.9 Et_3N + 4.2 CH_3COOH	195	3 days	Chains, JDF-20, $AlPO_4$-5	Large needles, JDF-20 spheres		
II-64	9.3 TEG	0.9 Al_2O_3•nH_2O	3.6 H_3PO_4	5.9 Et_3N + 0.5 HCl	180	3 days	Chains, JDF-20	Large needles, small needles		
II-65	9.3 TEG	0.9 Al_2O_3•nH_2O	3.6 H_3PO_4	0.5 HCl	180	3 days	Berlinite	30 μm faceted crystals		
II-66	9.3 TEG	0.9 Al_2O_3•nH_2O	3.6 H_3PO_4	5.9 Et_3N + 4.5 HCl	195	3 days	$Et_3NH^+Cl^-$, berlinite	Fibrous powder of long needles	√	√
II-67	14 TEG	0.9 Al_2O_3•nH_2O	3.6 H_3PO_4	5.9 Et_3N	195, liner: 4 HF-Py	9 days	$AlPO_4$-5, some JDF-20 and chains	Small needles		
II-68	14 TEG + 89.5 H_2O	0.9 Al_2O_3•nH_2O	3.6 H_3PO_4	5.9 Et_3N	195, liner: 4 HF-Py	9 days	$AlPO_4$-cristobalite, $AlPO_4$-5, trace tinsleyite	300 μm hexagonal plates		
II-69	14 TEG	0.9 Al_2O_3•nH_2O	3.6 H_3PO_4	5.9 Et_3N	195, liner: 2 HF-Py	11 days	Chains, JDF-20, $AlPO_4$-5	Large needles, small needles		
II-70	14 TEG	0.9 Al_2O_3•nH_2O	3.6 H_3PO_4	5.9 Et_3N + 1 drop of $(HF)_3Et_3N$	180	6 days	Chains, $AlPO_4$-5, JDF-20, UT-1	Large needles	√	
II-71	14 TEG	0.9 Al_2O_3•nH_2O	3.6 H_3PO_4	5.9 Et_3N + 3 drops of $(HF)_3Et_3N$	180	6 days	$AlPO_4$-5, UT-1, trace JDF-20, unknown 19.2Å phase	Small needles	√	
II-72	14 TEG	0.9 Al_2O_3•nH_2O	3.6 H_3PO_4	5.9 Et_3N + 0.33 to 0.67 $(HF)_3Et_3N$	180	6 to 10 days	Unknown 19.2Å phase	Very small needles	√	
II-73	14 TEG + 89.5 H_2O	0.9 Al_2O_3•nH_2O	3.6 H_3PO_4	5.9 Et_3N + 0.33 $(HF)_3Et_3N$	180 or 200	6 days	$AlPO_4$-5, trace tinsleyite	100 × 20 μm hexagonal rods		
II-74	14 TEG	0.9 Al_2O_3•nH_2O	3.6 H_3PO_4	5.9 Et_3N + ~0.5g of polyvinyl-pyridinium	195	6 days	Unknown 19.2Å phase, some $AlPO_4$-5	Small needles	√	
II-75	28.9 EG	0.9 Al_2O_3•nH_2O	3.6 H_3PO_4	5.9 Et_3N	195	13 days	$AlPO_4$-5	Small hexagonal rods		
II-76	60 EG	2.0 $Al(iospr)_3$	5.0 H_3PO_4	9.8 Et_3N	180	1 month	$AlPO_4$-5			
II-77	16.97 DEG	0.9 Al_2O_3•nH_2O	3.6 H_3PO_4	5.9 Et_3N	195	13 days	JDF-20	Poweder of small crystals		
II-78	12.07 tEG	0.9 Al_2O_3•nH_2O	3.6 H_3PO_4	5.9 Et_3N	195	9 days	JDF-20	Small, fragmented crystals		
II-79	18.0 tEG	1.0 Al_2O_3•nH_2O	3.6 H_3PO_4	4.7 Et_3N	150 or 180	5 days	JDF-20	Small, fragmented crystals		
II-80	18.0 tEG	2.0 $Al(iospr)_3$	3.6 H_3PO_4	6.0 Et_3N	180 or 200	2 days	JDF-20	Fan-like aggregates of needles		
II-81	6.04 PEG 300	0.9 Al_2O_3•nH_2O	3.6 H_3PO_4	5.9 Et_3N	180	10 days	Chains, some JDF-20	Small, fragmented crystals		
II-82	4.54 PEG 400	0.9 Al_2O_3•nH_2O	3.6 H_3PO_4	5.9 Et_3N	180	10 days	Chains, some JDF-20	Stacked needles on bottom of liner		
II-83	3.03 PEG 600	0.9 Al_2O_3•nH_2O	3.6 H_3PO_4	5.9 Et_3N	180	10 days	Chains, some JDF-20	Stacked needles on bottom of liner		

Ref #	Solvent	Al_2O_3 Source	P_2O_5 Source	Organic Additive	Temp (°C)	Time	Major Product(s)	Observed Morphology	PXRD	SEM
II-84	1.77 PEG 1000	0.9 Al_2O_3•nH_2O	3.6 H_3PO_4	5.9 Et_3N	150, 180	6 days	Chains, trace JDF-20, unknown 9.8Å phase	Thin, stacked needles		
II-85	1.77 PEG 1000	0.9 Al_2O_3•nH_2O	3.6 H_3PO_4	5.9 Et_3N	200	6 days	JDF-20	Small needles		
II-86	3.54 PEG 1000	0.9 Al_2O_3•nH_2O	3.6 H_3PO_4	5.9 Et_3N	200	6 days	Chains, unknown 9.8Å phase	Small needles	√	
II-87	0.39 PEG 4600	0.9 Al_2O_3•nH_2O	3.6 H_3PO_4	5.9 Et_3N	180	6 days	Chains, trace unknown 9.8Å phase	Small needles		
II-88	0.17 PEG 10,000	0.9 Al_2O_3•nH_2O	3.6 H_3PO_4	5.9 Et_3N	195	13 days	Amorphous, berlinite		√	
II-89	8.6 TPG	0.9 Al_2O_3•nH_2O	3.6 H_3PO_4	5.9 Et_3N	195	9 days	Chains	Small needles on bottom of liner		
II-90	3.8 PPG 425	0.9 Al_2O_3•nH_2O	3.6 H_3PO_4	5.9 Et_3N	195	9 days	Chains, trace JDF-20	Small needles on bottom of liner		
II-91	13.4 ml Mineral Oil	0.9 Al_2O_3•nH_2O	3.6 H_3PO_4	5.9 Et_3N	195	8 days	$AlPO_4$-tridymite			
II-92	16 Py	0.5 Al_2O_3•nH_2O	1.2 H_3PO_4	4.0 Et_3N	150, 180	4 days	Chains, $AlPO_4$-5, JDF-20	Small needles, fan-shaped aggregates of needles		
II-93	16 Py	1.0 Al(isopr)$_3$	1.2 H_3PO_4	4.0 Et_3N	150, 180	4 days	Amorphous, trace chains			
II-94	26.3 sec-BuOH	0.9 Al_2O_3•nH_2O	3.6 H_3PO_4	5.9 Et_3N	180	4 days	Chains	Needles		
II-95	26.3 sec-BuOH + 5 H_2O	0.9 Al_2O_3•nH_2O	3.6 H_3PO_4	5.9 Et_3N	180	4 days	Chains, some JDF-20	Needles		
II-96	14 TEG	-	3.6 H_3PO_4	6.0 Et_3N	RT	-	[Et_3NH^+]-phosphate salt	Large, air-sensitive needles		
II-97	9.3 TEG	0.9 Al_2O_3•nH_2O	3.6 H_3PO_4	5.9 (HOEt)$_3$N	180	10 days	Unknowns, $AlPO_4$-5	20μm needles	√	
II-98	9.3 TEG	0.9 Al_2O_3•nH_2O	3.6 H_3PO_4	5.9 Pr_3N	180, 195	3 to 10 days	Berlinite	200 μm cuboctahedral		√
II-99	9.3 TEG	0.9 Al_2O_3•nH_2O	3.6 H_3PO_4	3.6 Bu_3N	195, 200	4 to 13 days	Berlinite	10 μm cubes		
				2.3.3 Quaternary Tetraalkylammoniums						
II-100	9.3 TEG	0.9 Al_2O_3•nH_2O	3.6 H_3PO_4	5.9 NH_4OH	180	3 days	Phosphate salt		√	
II-101	9.3 TEG	0.9 Al_2O_3•nH_2O	3.6 H_3PO_4	5.9 NH_4OH, 5.9 ET_3N	180	3 days	Phosphate salt			
II-102	9.3 TEG	0.9 Al_2O_3•nH_2O	3.6 H_3PO_4	5.9 TMAOH• $5H_2O$	180	9 days	$AlPO_4$-18		√	
II-103	9.3 TEG	0.9 Al_2O_3•nH_2O	3.6 H_3PO_4	5.9 TEAOH	180	9 days	$AlPO_4$-18			

Ref #	Solvent	Al_2O_3 Source	P_2O_5 Source	Organic Additive	Temp (°C)	Time	Major Product(s)	Observed Morphology	PXRD	SEM
2.3.4 π-Conjugated Cyclic Amines										
II-104	14 TEG	0.9 Al_2O_3•nH_2O	3.6 H_3PO_4	5.9 Pyrrole	180	4 days	Unknown	Brown powder of small particles	√	
II-105	14 TEG	0.9 Al_2O_3•nH_2O	3.6 H_3PO_4	5.9 Pyridine	180	10 days	Berlinite, trace UT-6	Faceted crystals, 200 × 50 μm plates		√
II-106	14 TEG	0.9 Al_2O_3•nH_2O	3.6 H_3PO_4	8.0 Pyridine, 1.0 HF-Pyridine	180	2 days	UT-6	~ 30 μm orthorhombic plates	√	
II-107	14 TEG	0.9 Al_2O_3•nH_2O	3.6 H_3PO_4	10.0 Pyridine	180, new liner	4 days	$[Al_2P_3O_{12}H]^{2-}$ 2[PyH^+]	100 × 20 μm needles	√	
II-108	14 TEG + 134.4 H_2O	0.9 Al_2O_3•nH_2O	3.6 H_3PO_4	9.83 Pyridine	180	5 days	Berlinite, trace UT-6	Large faceted crystals, small number of plates		
II-109	16 Py + 8 H_2O	0.5 Al_2O_3•nH_2O	1.2 H_3PO_4	1.0 HF-Pyridine	120, 150, 180	1 to 5 days	UT-6	Small needles		
II-110	16 Py + 8 H_2O	1.0 Al(isopr)$_3$ or 0.5 Al_2O_3•nH_2O	1.2 H_3PO_4	4 Et_3N + 2.0 HF-Pyridine	150, 180	5 to 8 days	UT-6	Small needles		
II-111	14 TEG	0.9 Al_2O_3•nH_2O	3.6 H_3PO_4	5.9 (3,5)-Lutidine	180	3 days	Berlinite	50 μm cuboctahedral		
II-112	14 TEG	0.9 Al_2O_3•nH_2O	3.6 H_3PO_4	5.9 (4)-Amino-pyridine	180	3 days	Unknown	Small needles	√	
II-113	28 TEG	0.9 Al_2O_3•nH_2O	3.6 H_3PO_4	3.92 $BenzylNH_2$	150	5 days	Unknown 19Å phase	Small needles	√	
II-114	28 TEG	0.9 Al_2O_3•nH_2O	3.6 H_3PO_4	3.92 $BenzylNH_2$	180, 200	5 days	Unknown 19Å phase	Large plates, needles	√	√
II-115	28 TEG	0.9 Al_2O_3•nH_2O	3.6 H_3PO_4	3.92 $BenzylNH_2$	220	5 days	Unknown 10Å phase, trace 19Å	20 μm needles	√	
2.3.5 Saturated Cyclic Amines										
II-116	14 TEG	0.9 Al_2O_3•nH_2O	3.6 H_3PO_4	4.0 $C_6H_{11}NEt_2$	180	4 days	$AlPO_4$-5			
II-117	28 TEG or 9.09 PEG 600	0.9 Al_2O_3•nH_2O	3.6 H_3PO_4	5.34 (2,3)-dimethyl-$C_6H_{11}NH_2$	150 to 220	3 days	Unknown	Powder with small number of larger plates	√	
II-118	14 TEG	0.9 Al_2O_3•nH_2O	3.6 H_3PO_4	5.9 Morpholine	180	3 days	Pseudoboehmite, unknown	Powder with number of large needles	√	
II-119	14 TEG	0.9 Al_2O_3•nH_2O	3.6 H_3PO_4	5.9 Piperidine	180	6 days	Unknown	~3 μm needles	√	
II-120	14 TEG	0.9 Al_2O_3•nH_2O	3.6 H_3PO_4	4.4 $C_6H_{12}NH$	180	5 days	Unknown	Small needles and 300 × 300 μm octagonal plates	√	
II-121	14 TEG	1.0 Al_2O_3•nH_2O	3.6 H_3PO_4	5.16 Quinucl.	180	10 days	Unknown		√	
II-122	14 TEG	0.9 Al_2O_3•nH_2O	3.6 H_3PO_4	5.9 (±)-exo-2-amino-norborane	180	3 days	Unknown	Very small needles	√	√

Ref #	Solvent	Al_2O_3 Source	P_2O_5 Source	Organic Additive	Temp (°C)	Time	Major Product(s)	Observed Morphology	PXRD	SEM
II-123	9.3 TEG	0.9 Al_2O_3•nH_2O	3.6 H_3PO_4	2.9 $(CH_2)_6N_4$	180	11 days	Phosphate salt	Very small plates		
II-124	14 TEG	0.9 Al_2O_3•nH_2O	3.6 H_3PO_4	5.9 $C_5H_5NH_2$	180	4 days	Phosphate salt	Very small needles		
II-125	14 TEG	0.9 Al_2O_3•nH_2O	3.6 H_3PO_4	5.9 $C_5H_5NH_2$	180	6 days	Unknown	Needles, large plates (~200 μm width)	√	
II-126	28 TEG	0.9 Al_2O_3•nH_2O	3.6 H_3PO_4	3.0 $C_5H_5NH_2$	150	3 days	Unknown	Orthorhombic plates up to 150 μm in size	√	
II-127	28 TEG	0.9 Al_2O_3•nH_2O	3.6 H_3PO_4	3.0 $C_5H_5NH_2$	180	3 days	Unknown, unknown 28.3Å phase	Orthorhombic plates larger than II-126		
II-128	14 TEG	0.9 Al_2O_3•nH_2O	3.6 H_3PO_4	5.9 $C_5H_5NH_2$		0 days	$[C_5H_5NH_3^+]_2$ $[HPO_4]^{2-}$, Pseduo-boehmite	Powder of very small needles	√	√
II-129	0.28 MeOH + 0.83 H_2O		4.33 mmol H_3PO_4	5.53 mmol $C_5H_5NH_2$	RT	7 days	Large crystals of $[C_5H_5NH_3^+]_2$ $[HPO_4]^{2-}$	Large needles, hundreds of μm in length		
II-130	14 TEG	0.9 Al_2O_3•nH_2O	3.6 H_3PO_4	5.9 $C_5H_5NH_2$	100 to 130	13 days	Amorphous layered material		√	
II-131	14 TEG	0.9 Al_2O_3•nH_2O	3.6 H_3PO_4	5.9 $C_5H_5NH_2$	150	3 days	Amorphous layer, UT-2 chain structure	Small number of large plates in amorphous powder	√	
II-132	14 TEG	0.9 Al_2O_3•nH_2O	3.6 H_3PO_4	5.9 $C_5H_5NH_2$	180	3 days	UT-2, some amophous layer	Large plates	√	√
II-133	14 TEG	0.9 Al_2O_3•nH_2O	3.6 H_3PO_4	5.9 $C_5H_5NH_2$	200 to 220	3 days	UT-3	Very large plates, over 1 mm in size	√	
II-134	14 TEG + 3.6 H_2O	0.9 Al_2O_3•nH_2O	3.6 H_3PO_4	5.9 $C_5H_5NH_2$	130 to 220	3 days	Results similar to II-130 to II-133	Results similar to II-130 to II-133		
II-135	14 TEG + 10.0 H_2O	0.9 Al_2O_3•nH_2O	3.6 H_3PO_4	5.9 $C_5H_5NH_2$	130 to 150	4 days	Amorphous layer			
II-136	14 TEG + 10.0 H_2O	0.9 Al_2O_3•nH_2O	3.6 H_3PO_4	5.9 $C_5H_5NH_2$	180	4 days	UT-2, amorphous layer	Large needles		
II-137	14 TEG + 10.0 H_2O	0.9 Al_2O_3•nH_2O	3.6 H_3PO_4	5.9 $C_5H_5NH_2$	200	1 to 7 days	Fibrous contracted UT-3, UT-3	Long, thin needles	√	√
II-138	14 TEG + 10.0 H_2O	0.9 Al_2O_3•nH_2O	3.6 H_3PO_4	5.9 $C_5H_5NH_2$	220	6 days	UT-3	Large, thick plates		√
II-139	14 TEG	0.9 Al_2O_3•nH_2O	3.6 H_3PO_4	5.9 $C_5H_5NH_2$	180	5 mths	Contracted UT-3	Large plates		
II-140	14 TEG + 50 H_2O	0.9 Al_2O_3•nH_2O	3.6 H_3PO_4	5.9 $C_5H_5NH_2$	180	25 days	Unknown 17.5Å phase, 11.4Å phase	200 μm hexagonal plates	√	
II-141	14 TEG + 50 H_2O	0.9 Al_2O_3•nH_2O	3.6 H_3PO_4	5.9 $C_5H_5NH_2$	200	25 days	Unknown 11.7Å phase, 11.4Å phase	Very small needles, 200 × 50 μm plates, 200 μm square plates	√	
II-142	14 TEG + 134.4 H_2O	0.9 Al_2O_3•nH_2O	3.6 H_3PO_4	5.9 $C_5H_5NH_2$	150	6 days	Unknown 17.5Å phase, trace 11.7Å phase	200 μm spherical aggregates of small needles	√	√

Ref #	Solvent	Al_2O_3 Source	P_2O_5 Source	Organic Additive	Temp (°C)	Time	Major Product(s)	Observed Morphology	PXRD	SEM
II-143	14 TEG + 134.4 H_2O	0.9 Al_2O_3•nH_2O	3.6 H_3PO_4	5.9 $C_5H_9NH_2$	180	6 days	Unknown 11.4Å phase, small amount of 17.5Å phase	Very small needles, some spherical aggregates		
II-144	14 TEG + 134.4 H_2O	0.9 Al_2O_3•nH_2O	3.6 H_3PO_4	5.9 $C_5H_9NH_2$	200 to 220	6 days	Unknown 11.4Å phase	100 μm hexagonal plates		
II-145	134.4 H_2O	0.9 Al_2O_3•nH_2O	3.6 H_3PO_4	5.9 $C_5H_9NH_2$	150 to 180	1 day	Unknown 17.5Å phase	Monodisperse 500 μm shperical aggregates of needles		
II-146	14 TEG	0.9 Al_2O_3•nH_2O	3.6 H_3PO_4	5.9 $C_5H_9NH_2$ + 1.0 $(HF)_3$-Et_3N	150 to 200	25 days	Unknown 14.9Å phase	Very small needles	√	
II-147	14 TEG	0.9 Al_2O_3•nH_2O	3.6 H_3PO_4	5.9 $C_6H_{11}NH_2$	130	3 days	Open amorphous material, unknown 17.5Å phase	Small 25 × 10 μm needles	√	
II-148	14 TEG	0.9 Al_2O_3•nH_2O	3.6 H_3PO_4	5.9 $C_6H_{11}NH_2$	150	3 days	Unknown 17.5Å phase, UT-4, open amorphous material	Small 25 × 10 μm needles, some larger 100 × 20 μm needles	√	
II-149	14 TEG	0.9 Al_2O_3•nH_2O	3.6 H_3PO_4	5.9 $C_6H_{11}NH_2$	180	4 days	UT-4, unknown 17.5Å phase, open amorphous material	100 × 20 μm needles, very large plates	√	√
II-150	14 TEG	0.9 Al_2O_3•nH_2O	3.6 H_3PO_4	5.9 $C_6H_{11}NH_2$	200	3 days	UT-4, UT-5	Large plates, 100 × 50 μm plates	√	
II-151	14 TEG	0.9 Al_2O_3•nH_2O	3.6 H_3PO_4	5.9 $C_6H_{11}NH_2$	1 day at RT, 180	2 days	UT-5, UT-4	Similar to II-149		
II-152	14 TEG + 134.4 H_2O	0.9 Al_2O_3•nH_2O	3.6 H_3PO_4	5.9 $C_6H_{11}NH_2$	150	4 days	UT-4, unknown 18.0Å phase	Large plates	√	
II-153	14 TEG + 134.4 H_2O	0.9 Al_2O_3•nH_2O	3.6 H_3PO_4	5.9 $C_6H_{11}NH_2$	180 to 220	4 days	Unknown 18.0Å phase, UT-4	Small needles, some large plates	√	
II-154	16 Py + 8 H_2O	0.5 Al_2O_3•nH_2O or 1.0 Al(isopr)	1.2 H_3PO_4	4.0 $C_6H_{11}NH_2$ + 2.0 HF-Py	150	6 days	Unknowns: 16.5Å phase, 15.3Å phase, trace 18.2Å phase	Large plates, needles up to 200 μm in length	√	
II-155	14 TEG	0.9 Al_2O_3•nH_2O	3.6 H_3PO_4	4.0 $C_6H_{11}NH_2$ + 1.0 HF-Py	180	2 days	Unknown 15.3Å phase		√	
II-156	14 TEG	0.9 Al_2O_3•nH_2O	3.6 H_3PO_4	5.9 $C_7H_{13}NH_2$	180	3 days	Poorly crystalline UT-7	Fine powder		
II-157	28 TEG + 20 H_2O	0.9 Al_2O_3•nH_2O	3.6 H_3PO_4	5.44 $C_7H_{13}NH_2$	-	0 days	$[C_7H_{13}NH_3]^+$ phosphate salt, pseudoboehmite	Very small needles	√	
II-158	28 TEG	0.9 Al_2O_3•nH_2O	3.6 H_3PO_4	5.9 $C_7H_{13}NH_2$	150	3 days	UT-7, trace 18.1Å unknown	Small and large needles	√	√
II-159	28 TEG	0.9 Al_2O_3•nH_2O	3.6 H_3PO_4	5.9 $C_7H_{13}NH_2$	180, 200	3 days	Equal amount of UT-7 and unknown 16.0Å phase	Small needles, a few larger needles	√	
II-160	28 TEG	0.9 Al_2O_3•nH_2O	3.6 H_3PO_4	5.9 $C_7H_{13}NH_2$	220	3 days	16.0Å unknown phase, UT-7	Small needles, some large 200 × 100 μm plates	√	
II-161	28 TEG + 20 H_2O	0.9 Al_2O_3•nH_2O	3.6 H_3PO_4	5.44 $C_7H_{13}NH_2$	150	3 days	Equal amount of 18.1Å and 16.0Å unknowns	Very small needles		

Ref #	Solvent	Al_2O_3 Source	P_2O_5 Source	Organic Additive	Temp (°C)	Time	Major Product(s)	Observed Morphology	PXRD	SEM
II-162	28 TEG + 20 H_2O	0.9 Al_2O_3•nH_2O	3.6 H_3PO_4	5.44 $C_7H_{13}NH_2$	180	3 days	Unknown 16.0Å phase	Small needles, some 500 × 100 plates	√	
II-163	14 TEG + 134.4 H_2O	0.9 Al_2O_3•nH_2O	3.6 H_3PO_4	5.9 $C_7H_{13}NH_2$	150	4 days	Unknown 18.9Å phase, trace UT-7	Large plates	√	
II-164	14 TEG + 134.4 H_2O	0.9 Al_2O_3•nH_2O	3.6 H_3PO_4	5.9 $C_7H_{13}NH_2$	180, 200, 220	4 days	Unknown 18.9Å phase	Large plates		
II-165	14 TEG	0.9 Al_2O_3•nH_2O	3.6 H_3PO_4	5.9 $C_8H_{15}NH_2$	180	3 days	Unknown 17.2Å phase, trace 18.2Å phase	Fine powder of small needles		
II-166	28 TEG	0.9 Al_2O_3•nH_2O	3.6 H_3PO_4	5.9 $C_8H_{15}NH_2$	150 to 220	3 days	Same as above	Small needles, plates up to 200 × 200 µm	√	
II-167	28 TEG	0.9 Al_2O_3•nH_2O	3.6 H_3PO_4	2.9 $C_8H_{15}NH_2$	180, 220	3 days	Unknown 17.2Å phase	Same as II-166		
II-168	28 TEG	0.9 Al_2O_3•nH_2O	3.6 H_3PO_4	0.9 $C_8H_{15}NH_2$	180, 220	5 days	Berlinite	15 µm round particles		
II-169	28 TEG	0.9 Al_2O_3•nH_2O	3.6 H_3PO_4	3.65 $C_8H_{15}NH_2$ 3.78 NaHCO	150 to 220	3 to 6 days	Pseudoboehmite, sodium phosphate	Dispal spheres	√	
II-170	14 TEG + 134.4 H_2O	0.9 Al_2O_3•nH_2O	3.6 H_3PO_4	5.0 $C_8H_{15}NH_2$	135, 150	4 days	Unknown 18.5Å phase	Needles up to 200 × 100 µm	√	
II-171	14 TEG + 134.4 H_2O	0.9 Al_2O_3•nH_2O	3.6 H_3PO_4	5.0 $C_8H_{15}NH_2$	180	4 days	Unknown 18.5Å phase, 17.2Å phase	Large needles, up to 1 mm in length		
II-172	14 TEG + 134.4 H_2O	0.9 Al_2O_3•nH_2O	3.6 H_3PO_4	5.0 $C_8H_{15}NH_2$	200	4 days	Unknown 17.2Å, 18.5Å phases, trace 19.5Å phase	Plates up to 300 × 200 µm	√	√
II-173	14 TEG + 134.4 H_2O	0.9 Al_2O_3•nH_2O	3.6 H_3PO_4	5.0 $C_8H_{15}NH_2$	220	4 days	Unknown 17.2Å, trace 19.5Å phases	100 × 20 µm needles		
II-174	1.1 H_2O	-	11.0 mmol H_3PO_4	11.0 mmol $C_{12}H_{23}NH_2$	RT	-	$[C_{12}H_{23}NH_3]^+$ phosphate salt	Small needles, up to 100 × 20 µm	√	
II-175	14 TEG	0.9 Al_2O_3•nH_2O	3.6 H_3PO_4	4.5 $C_{12}H_{23}NH_2$	180	3 days	Unknown 21.2Å phase	Small needles		
II-176	28 TEG	0.9 Al_2O_3•nH_2O	3.6 H_3PO_4	4.5 $C_{12}H_{23}NH_2$	100	13 days	$[C_{12}H_{23}NH_3]^+$ phosphate salt, unknown 21.2Å phase	Small needles	√	
II-177	28 TEG	0.9 Al_2O_3•nH_2O	3.6 H_3PO_4	4.5 $C_{12}H_{23}NH_2$	130, 150, 180, 200, 220	3 to 13 days	Unknown 21.2Å phase	Small needles	√	√
II-178	14 TEG + 134.4 H_2O	0.9 Al_2O_3•nH_2O	3.6 H_3PO_4	4.0 $C_{12}H_{23}NH_2$	80, 150, 180, 200, 220	4 days to 1 month	Unknown 21.2Å phase	Small needles		
2.3.6 Mixed Amine Systems										
II-179	14 TEG	0.9 Al_2O_3•nH_2O	3.6 H_3PO_4	2.95 $C_4H_9NH_2$ + 2.95 $C_5H_{10}NH$	180	6 days	UT-8	Cubic plates, several hundred µm width	√	√
II-180	20 TEG	0.9 Al_2O_3•nH_2O	3.6 H_3PO_4	2.95 $C_5H_9NH_2$ + 2.95 $C_7H_{13}NH_2$	180 to 200	6 days	Unknown	Small needles and plates	√	
II-181	14 TEG	0.9 Al_2O_3•nH_2O	3.6 H_3PO_4	2.5 $C_5H_9NH_2$ + 2.5 $C_6H_{11}NH_2$	200	6 days	Unknown	Large plates, similar to UT-2 and UT-4	√	

Ref #	Solvent	Al_2O_3 Source	P_2O_5 Source	Organic Additive	Temp (°C)	Time	Major Product(s)	Observed Morphology	PXRD	SEM
2.3.7 Metal Aluminophosphate and Metal Phosphate Systems										
II-182	14 TEG	1.0 Al_2O_3•nH_2O + 0.56 SiO_2	3.6 H_3PO_4	5.9 Et_3N	180, 200	9 days	JDF-20, chains	Large needles		
II-183	9.3 TEG	0.9 Fe_2O_3•H_2O	3.6 H_3PO_4	5.9 Et_3N	180	5 days	Iron phosphate	Black powder	√	
II-184	14 TEG	1.62 Fe_2O_3•H_2O + 0.09 Al_2O_3•nH_2O	3.6 H_3PO_4	5.9 Et_3N	180	5 days	Iron phosphate, 10.8Å phase	Black powder	√	
II-185	14 TEG + 5.0 H_2O	0.9 Al_2O_3•nH_2O + 0.2 Co(II) acetate tetrahydrate	3.6 H_3PO_4	5.9 Et_3N	180	3 days	JDF-20, CoAPO-34	Blue powder of small particles	√	
II-186	14 TEG	0.9 Al_2O_3•nH_2O + 0.2 $NiSO_4$•6H_2O	3.6 H_3PO_4	3.67 $C_6H_{11}NH_2$	180	3 days	UT-5	Large plates, green hue to bulk product	√	√
II-187	14 TEG	0.9 V_2O_3	3.6 H_3PO_4	3.67 $C_6H_{11}NH_2$	180	3 days	Dense-phase, amorphous open material	Green product of large plates	√	
II-188	14 TEG	0.9 In_2O_3	3.6 H_3PO_4	5.9 Et_3N	180	6 days	Dense-phase, amorphous open material	Hard, grey material with holes and surface impressions	√	

Chapter 3: Single Crystal XRD Structures and Materials Characterization

Ref #	Aluminophosphate Source Material	Conditions of Heating or Synthesis	Temp (°C)	Time	Product(s)	PXRD
III-1	$[AlP_2O_8H_2]^-[Et_3NH]^+$	Vacuum	200	4 hours	$AlPO_4$-tridymite, unreacted chains	
III-2	$[AlP_2O_8H_2]^-[Et_3NH]^+$	Vacuum	300	4 hours	$AlPO_4$-tridymite, open, amorphous material	√
III-3	$[AlP_2O_8H_2]^-[Et_3NH]^+$	Vacuum	400	4 hours	$AlPO_4$-tridymite, trace variscite	
III-4	$[AlP_2O_8H_2]^-[Et_3NH]^+$	Air	500	16 hours	$AlPO_4$-tridymite, variscite	√
III-5	5.0 $[AlP_2O_8H_2]^-[Et_3NH]^+$	26.0 TEG : 15.0 H_2O : 1.0 Et_3N	80	4 to 23 days	Unreacted chains, amorphous	
III-6	1.0 $[AlP_2O_8H_2]^-[Et_3NH]^+$	9.3 TEG : 3.6 H_2O : 4.6 Et_3N	200	9 days	$AlPO_4$-tridymite, unreacted chains	
III-7	1.0 $[AlP_2O_8H_2]^-[Et_3NH]^+$	50.0 H_2O : 1.0 HCl	100	1 day	Variscite, metavariscite	√
III-8	1.0 $[AlP_2O_8H_2]^-[Et_3NH]^+$	50.0 H_2O : 1.0 HCl	140, 150	3 hours to 1 day	$AlPO_4$-H4	√
III-9	JDF-20	Vacuum	150, 200	4 hours	$AlPO_4$-tridymite	
III-10	0.27 JDF-20, $[Al_5P_6O_{24}H]^{2-}[Et_3NH^+]_2$	50.0 H_2O : 1.0 HCl	100	3 hours	Amorphous	
III-11	0.27 JDF-20, $[Al_5P_6O_{24}H]^{2-}[Et_3NH^+]_2$	50.0 H_2O : 1.0 HCl	140	3 hours to 1 day	$AlPO_4$-tridymite, $AlPO_4$-H4	
III-12	UT-2	Air	100	4 hours	UT-2	
III-13	UT-2	Air	150	4 hours	UT-3, trace contracted UT-3	
III-14	UT-2	Air	175	4 hours	Contracted UT-3, some UT-3	
III-15	Unground UT-2 Crystals	Air	175	5 hours	UT-3, some contracted UT-3	
III-16	0.27 mmol UT-2	3.22 mol H_2O, 3.41 mmol NH_4OH	RT	2 hours	Amorphous	

Ref #	Aluminophosphate Source Material	Conditions of Heating or Synthesis	Temp (°C)	Time	Product(s)	PXRD
III-17	0.12 mmol UT-2	0.67 mol H_2O	80	3 days	Amorphous	
III-18	UT-3	Air	175	4 hours	UT-3, contracted UT-3, $AlPO_4$-tridymite	√
III-19	Contracted UT-3	Air	175	4 hours	Contracted UT-3, $AlPO_4$-tridymite	
III-20	UT-7	Air	150	4 hours	16.3Å Unknown phase	√

Chapter 5: Primary Alkylamines and Alkylenediamines

5.11 Alkylenediamines

Ref #	Solvent	Al_2O_3 Source	P_2O_5 Source	Organic Additive	Temp (°C)	Time	Major Product(s)	Observed Morphology	PXRD	SEM
V-1	60 H_2O	1.0 Al_2O_3•nH_2O	3.2 H_3PO_4	1.8 en	150	10 days	Several unknowns	25 μm thin needles	√	
V-2	60 H_2O	1.0 Al_2O_3•nH_2O	4.0 H_3PO_4	1.8 en	120	10 days	Other unknowns	Long needles		
V-3	60 EG	1.0 Al_2O_3•nH_2O	3.6 H_3PO_4	12 en	180	7 days	Unknowns of smaller d-spacing	30 μm plates	√	
V-4	60 EG	2.0 Al(isopr)$_3$	3.6 H_3PO_4	12 en	180	7 days	Mixture of unknowns seen above	30 μm plates, 200×400 μm plates		
V-5	60 EG	2.0 Al(isopr)$_3$	3.6 H_3PO_4	12 en	180	8 days	Unknown	Small amount of large plates		
V-6	14 TEG	0.9 Al_2O_3•nH_2O	3.6 H_3PO_4	12 en	180	7 days	$[enH_2]^{2+}[HPO_4]^{2-}$	Small needles	√	
V-7	14 TEG	0.9 Al_2O_3•nH_2O	3.6 H_3PO_4	5.0 H_2NPrNH_2	180, 195	13 days	$[^+H_3NPrNH_3^+]$ $[HPO_4^{2-}]$•H_2O, pseudoboehmite	Small platelets	√	
V-8	14 TEG	0.9 Al_2O_3•nH_2O	3.6 H_3PO_4	2.8 H_2NBuNH_2	180	13 days	Unknown	25 μm plates	√	
V-9	14 TEG	0.9 Al_2O_3•nH_2O	3.6 H_3PO_4	2.71 $H_2NHexNH_2$	RT	0 days	Phosphate salt, psuedoboehmite	Small platelets	√	
V-10	14 TEG	0.9 Al_2O_3•nH_2O	3.6 H_3PO_4	2.71 $H_2NOctNH_2$	180	13 days	$[^+H_3NOctNH_3^+]$ $2[H_2PO_4^-]$, unknown(s)	Plates up to 300 × 100 μm	√	√
V-11	1.2 mol H_2O		5.0 mmol H_3PO_4	5.5 mmol $H_2NOctNH_2$	RT	1.5 mths	$[^+H_3NOctNH_3^+]$ $2[H_2PO_4^-]$	Small needles	√	

5.12 Alkylamines

V-12	45 EG	2.0 Al(isopr)$_3$	3.6 H_3PO_4	5.2 $EtNH_2$	180	14 days	Unknown		√	
V-13	60 EG	2.0 Al(isopr)$_3$	3.6 H_3PO_4	5.0 $PrNH_2$	180	15 days	Amorphous			
V-14	14 TEG	0.9 Al_2O_3•nH_2O	3.6 H_3PO_4	5.9 sec-$BuNH_2$	180	3 days	Open, amorhpous phase, unknown	Some large needles	√	
V-15	14 TEG	0.9 Al_2O_3•nH_2O	3.6 H_3PO_4	3.0 $HexNH_2$	RT	0 days	Phosphate salt, psuedoboehmite	30 × 10 μm plates	√	√
V-16	14 TEG	0.9 Al_2O_3•nH_2O	3.6 H_3PO_4	3.0 $HexNH_2$	150	3 days	Low-crystallinity MLA	Thin platelets	√	
V-17	14 TEG	0.9 Al_2O_3•nH_2O	3.6 H_3PO_4	3.0 $HexNH_2$	180	3 days	MLA, some $AlPO_4$-tridymite	Thin platelets, 150 μm hexagonal plates	√	√
V-18	14 TEG	0.9 Al_2O_3•nH_2O	3.6 H_3PO_4	3.0 $HexNH_2$	200	3 days	MLA, $AlPO_4$-tridymite		√	
V-19	14 TEG	0.9 Al_2O_3•nH_2O	3.6 H_3PO_4	3.0 $OctNH_2$	RT	0 days	ODP, psuedoboehmite	10 μm plates	√	

Ref #	Solvent	Al_2O_3 Source	P_2O_5 Source	Organic Additive	Temp (°C)	Time	Major Product(s)	Observed Morphology	PXRD	SEM
V-20	14 TEG	0.9 Al_2O_3•nH_2O	3.6 H_3PO_4	3.0 OctNH_2	150	3 days	MLA, trace ODP	10 μm plates	√	
V-21	14 TEG	0.9 Al_2O_3•nH_2O	3.6 H_3PO_4	3.0 OctNH_2	180	3 days	MLA	Plates	√	√
V-22	14 TEG	0.9 Al_2O_3•nH_2O	3.6 H_3PO_4	3.0 OctNH_2	200	3 days	MLA	Plates, some surface patterning	√	√
V-23	14 TEG	0.9 Al_2O_3•nH_2O	3.6 H_3PO_4	3.0 OctNH_2	180	3 days	MLA from top and cap of liner	Rhombohedral mesh pattern	√	√
V-24	14 TEG	0.9 Al_2O_3•nH_2O	3.6 H_3PO_4	3.0 NonylNH_2	RT	0 days	Phosphate salt, psuedoboehmite	Small plates	√	
V-25	14 TEG	0.9 Al_2O_3•nH_2O	3.6 H_3PO_4	3.0 NonylNH_2	150	4 days	MLA, trace phosphate salt		√	
V-26	14 TEG	0.9 Al_2O_3•nH_2O	3.6 H_3PO_4	3.0 NonylNH_2	180	4 days	MLA		√	
V-27	14 TEG	0.9 Al_2O_3•nH_2O	3.6 H_3PO_4	3.0 NonylNH_2	200	4 days	MLA, $AlPO_4$-tridymite		√	
V-28	14 TEG	0.9 Al_2O_3•nH_2O	3.6 H_3PO_4	3.0 NonylNH_2	220	4 days	MLA, $AlPO_4$-tridymite		√	
V-29	14 TEG	0.9 Al_2O_3•nH_2O	3.6 H_3PO_4	3.0 DecylNH_2	RT	0 days	DDP, pseudoboehmite	Small plates	√	
V-30	14 TEG	0.9 Al_2O_3•nH_2O	3.6 H_3PO_4	3.0 DecylNH_2	80	4 days	MLA, DDP	Small platelets		
V-31	14 TEG	0.9 Al_2O_3•nH_2O	3.6 H_3PO_4	3.0 DecylNH_2	150	3 days	MLA, trace DDP	Small platelets	√	
V-32	14 TEG	0.9 Al_2O_3•nH_2O	3.6 H_3PO_4	3.0 DecylNH_2	180	3 days	MLA, trace DDP	Small platelets, patterned spheres, hollow spheres		√ √ √
V-33	14 TEG	0.9 Al_2O_3•nH_2O	3.6 H_3PO_4	3.0 DecylNH_2	200, 220	3 days	MLA, $AlPO_4$-tridymite	Small platelets		
V-34	14 TEG	0.9 Al_2O_3•nH_2O	3.6 H_3PO_4	3.92 DecylNH_2	150	3 days	MLA, DDP	Small platelets		√
V-35	14 TEG	0.9 Al_2O_3•nH_2O	3.6 H_3PO_4	3.92 DecylNH_2	180, 200	3 days	MLA	Small platelets	√	
V-36	14 TEG	0.9 Al_2O_3•nH_2O	3.6 H_3PO_4	1.0 DecylNH_2	150	3 days	Berlinite, trace MLA	Small granules		
V-37	14 TEG	0.9 Al_2O_3•nH_2O	3.6 H_3PO_4	1.0 DecylNH_2	180	3 days	Berlinite, DDP	Small granules		
V-38	14 TEG	0.9 Al_2O_3•nH_2O	3.6 H_3PO_4	1.0 DecylNH_2	200	3 days	Berlinite	20 μm faceted crystals		
V-39	14 TEG	0.9 Al_2O_3•nH_2O	3.6 H_3PO_4	3.0 DecylNH_2	180, shaking	3 days	MLA, $AlPO_4$-tridymite	300 μm hollow spheres		√
V-40	14 TEG	0.9 Al_2O_3•nH_2O	3.6 H_3PO_4	3.0 DecylNH_2	180, tumbler	3 to 11 days	MLA, $AlPO_4$-tridymite	Small platelets, solid cylinder		
V-41	43.4 EG	0.9 Al_2O_3•nH_2O	3.6 H_3PO_4	3.0 DecylNH_2	80 to 180	3 days	MLA, $AlPO_4$-tridymite	Worm-like growths		√
V-42	43.4 EG + 1.0 TEG	0.9 Al_2O_3•nH_2O	3.6 H_3PO_4	3.0 DecylNH_2	180	3 days	MLA, $AlPO_4$-tridymite	Worm-like growths		
V-43	6.82 PEG 400	0.9 Al_2O_3•nH_2O	3.6 H_3PO_4	3.0 DecylNH_2	180, 200	4 days	MLA, $AlPO_4$-tridymite, trace DDP	Small platelets, patterned plates, hollow spheres		√ √
V-44	2.73 PEG 1000	0.9 Al_2O_3•nH_2O	3.6 H_3PO_4	3.0 DecylNH_2	180, 200	4 days	MLA, $AlPO_4$-tridymite, trace DDP	Small platelets		
V-45	134.3 H_2O + 0.58 TEG	0.9 Al_2O_3•nH_2O	3.6 H_3PO_4	3.0 DecylNH_2	180	3 days	MLA, trace DDP	Small platelets, large voids on top, granular walls		√

Ref #	Solvent	Al_2O_3 Source	P_2O_5 Source	Organic Additive	Temp (°C)	Time	Major Product(s)	Observed Morphology	PXRD	SEM
V-46	134.3 H_2O	0.9 Al_2O_3•nH_2O	3.6 H_3PO_4	1.0 DecylNH_2	80 to 200	6 days	DDP	Long, thin, intergrown needles		
V-47	14 TEG	0.9 Al_2O_3•nH_2O	3.0 DecylNH_2 + 1.8 H_3PO_4 (reverse order)		RT	0 days	DMP, DDP, pseudoboehmite	Small needles	√	
V-48	14 TEG	0.9 Al_2O_3•nH_2O	3.0 DecylNH_2 + 1.8 H_3PO_4 (reverse order)		180	3 days	MLA	Small granules		
V-49	14 TEG	0.9 Al_2O_3•nH_2O	3.6 H_3PO_4	3.0 UndecylNH_2	RT	0 days	Phosphate salt, pseudoboehmite	Small needles	√	
V-50	14 TEG	0.9 Al_2O_3•nH_2O	3.6 H_3PO_4	3.0 UndecylNH_2	150	4 days	MLA, trace phosphate salt	Granules	√	
V-51	14 TEG	0.9 Al_2O_3•nH_2O	3.6 H_3PO_4	3.0 UndecylNH_2	180	4 days	MLA, trace phosphate salt, $AlPO_4$-tridymite	Granules, patterned spheres and plates	√	√ √
V-52	14 TEG	0.9 Al_2O_3•nH_2O	3.6 H_3PO_4	3.0 UndecylNH_2	200	5 days	MLA, $AlPO_4$-tridymite	Granules, patterned spheres and plates	√	√ √ √
V-53	14 TEG	0.9 Al_2O_3•nH_2O	3.6 H_3PO_4	3.0 UndecylNH_2	220	5 days	MLA, $AlPO_4$-tridymite	Granules, some patterns		
V-54	14 TEG	0.9 Al_2O_3•nH_2O	3.6 H_3PO_4	3.0 DodecylNH_2	180	6 days	MLA, phosphate salt, $AlPO_4$-tridymite		√	√
V-55	14 TEG	0.9 Al_2O_3•nH_2O	3.6 H_3PO_4	3.0 DodecylNH_2	200	6 days	MLA, phosphate salt, $AlPO_4$-tridymite			
V-56	14 TEG	0.9 Al_2O_3•nH_2O	3.6 H_3PO_4	1.86 Tetradecyl NH_2	RT	0 days	Phosphate salt, psuedoboehmite	Orthorhombic plates up to 50 × 20 μm	√	
V-57	14 TEG	0.9 Al_2O_3•nH_2O	3.6 H_3PO_4	1.86 Tetradecyl NH_2	180	3 days	Phosphate salt, psuedoboehmite	Orthorhombic plates up to 50 × 20 μm	√	
V-58	Tetradecylamine Reagent								√	
V-59	14 TEG	0.9 Al_2O_3•nH_2O	3.6 H_3PO_4	2.60 HexadecylNH_2	150 to 220	4 days	MLA, $AlPO_4$-tridymite	Small platelets	√	√
V-60	Hexadecylamine Reagent								√	
	5.13 Cetyl Trialkylammoniums									
V-61	151 H_2O	0.9 Al_2O_3•nH_2O	3.6 H_3PO_4	0.50 CTAB	80	3 days	Metavariscite, variscite			
V-62	151 H_2O	0.9 Al_2O_3•nH_2O	3.6 H_3PO_4	0.50 CTAB	150	3 days	$AlPO_4$-H4			
V-63	14 TEG (+ 134 H_2O)	0.9 Al_2O_3•nH_2O	3.6 H_3PO_4	0.50 CTAB	180	3 days	Berlinite	Small, faceted crystals		
V-64	14 TEG	0.9 Al_2O_3•nH_2O	3.6 H_3PO_4	0.5 CPC	80	4 days	$AlPO_4$-H4	25 μm particles		
V-65	14 TEG	0.9 Al_2O_3•nH_2O	3.6 H_3PO_4	0.5 CPC	180	4 days	Berlinite	Small, faceted crystals		
	5.14 Silica-Decylamine System									
V-66	14 TEG	1.8 SiO_2	3.6 H_3PO_4	3.0 DecylNH_2	180	3 days	DDP	Fibrous needles enclosing surface depressions		√

Appendix B. PXRD Patterns of Selected Products.
Reference numbers are the same as those given in Appendix A and in the main text.

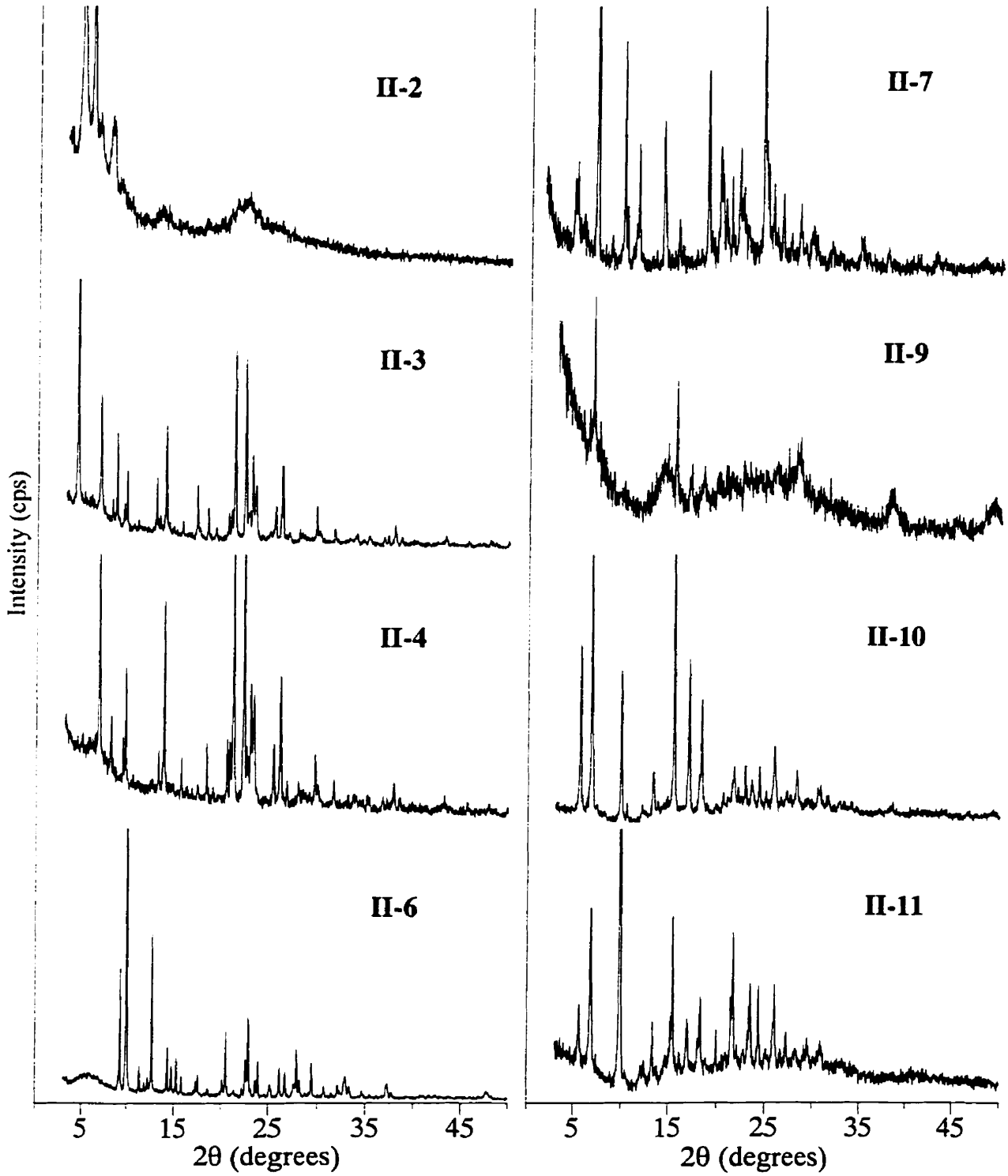

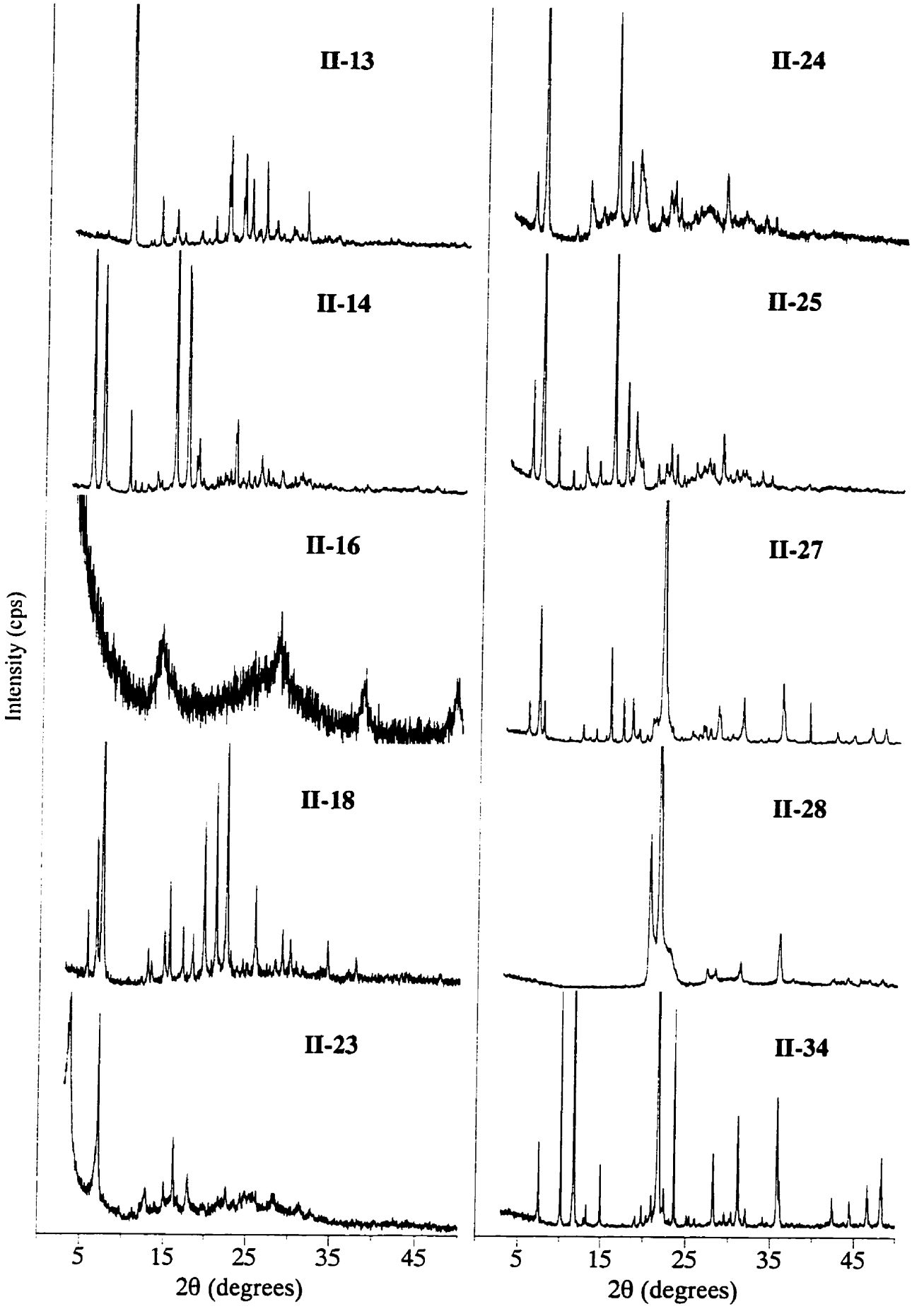
II-13
II-14
II-16
II-18
II-23
II-24
II-25
II-27
II-28
II-34
Intensity (cps)
5
15
25
35
45
2θ (degrees)
5
15
25
35
45
2θ (degrees)

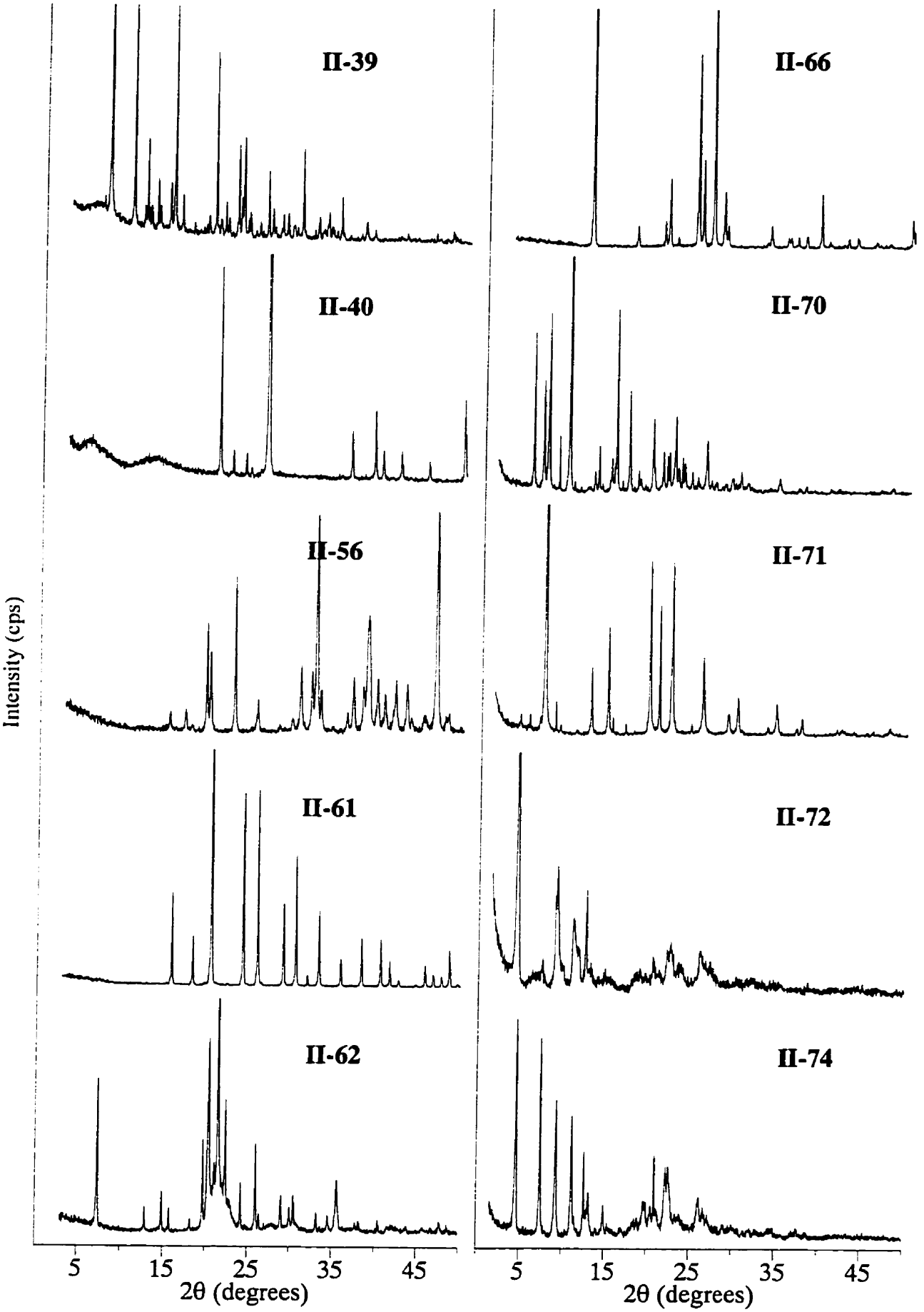
II-39
II-66
II-40
II-70
II-56
II-71
II-61
II-72
II-62
II-74
Intensity (cps)
5
15
25
35
45
2θ (degrees)
5
15
25
35
45
2θ (degrees)

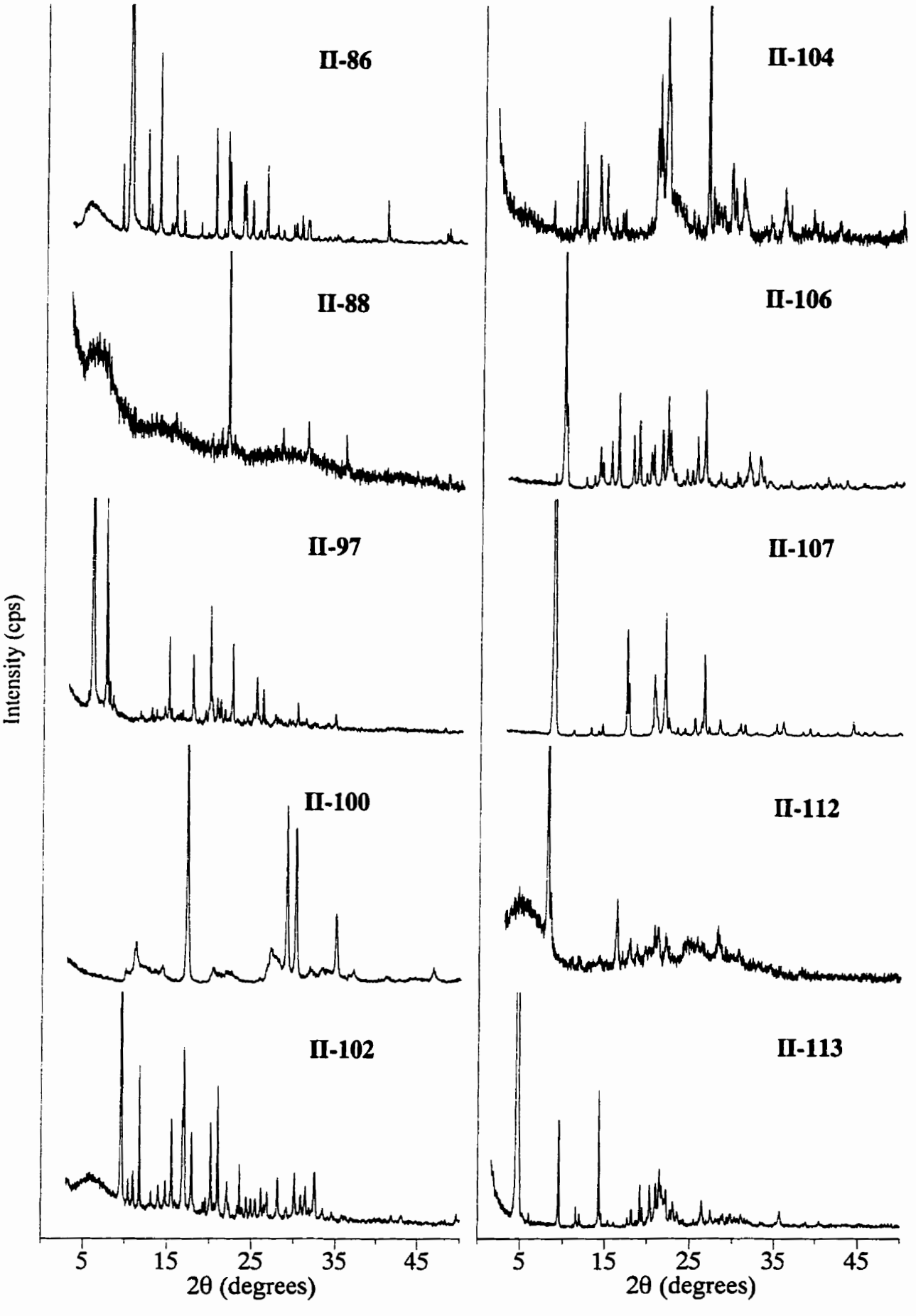
II-86
II-104
II-88
II-106
II-97
II-107
II-100
II-112
II-102
II-113
Intensity (cps)
5
15
25
35
45
2θ (degrees)
5
15
25
35
45
2θ (degrees)

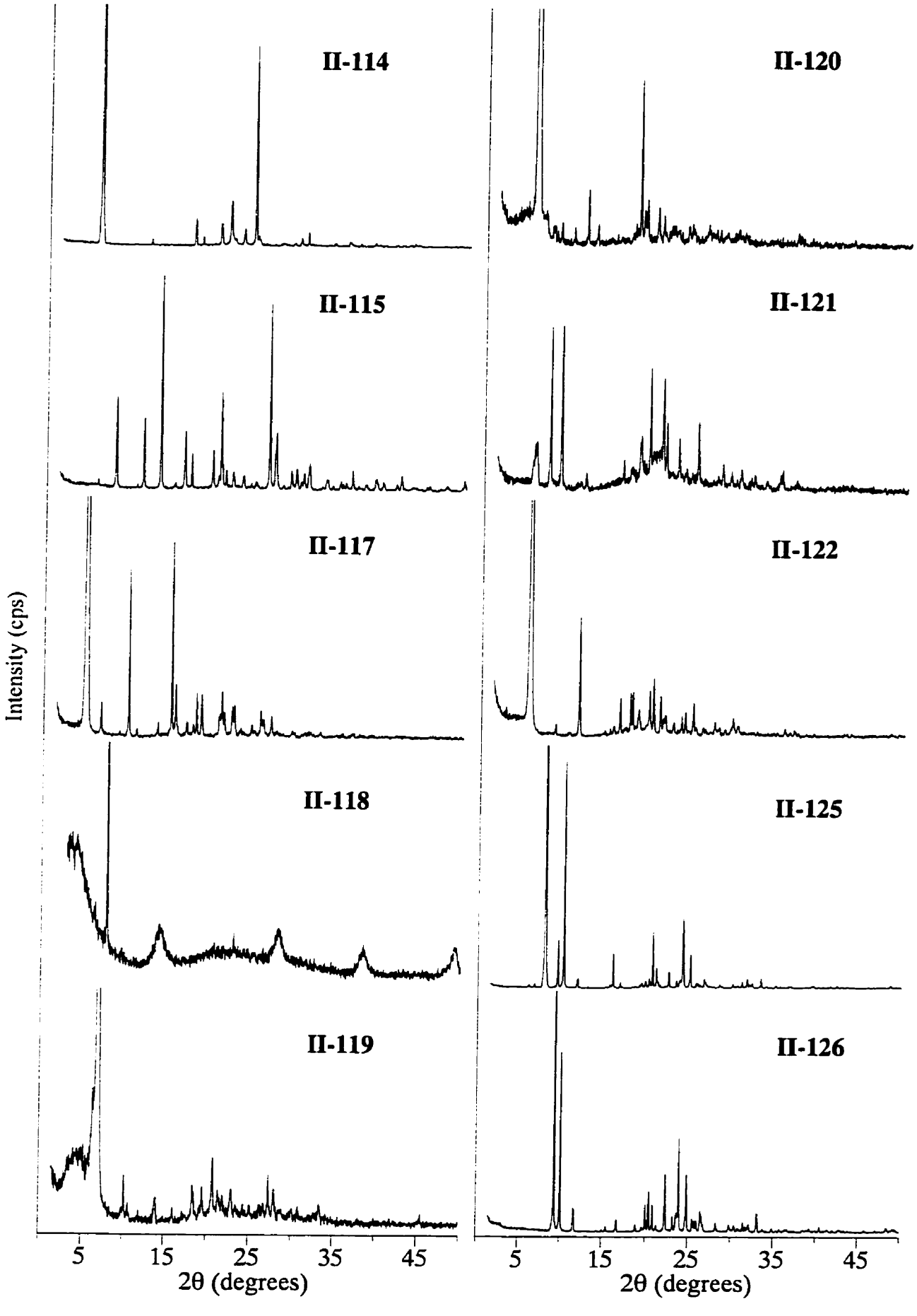
II-114
II-115
II-117
II-118
II-119
II-120
II-121
II-122
II-125
II-126
Intensity (cps)
5
15
25
35
45
2θ (degrees)
5
15
25
35
45
2θ (degrees)

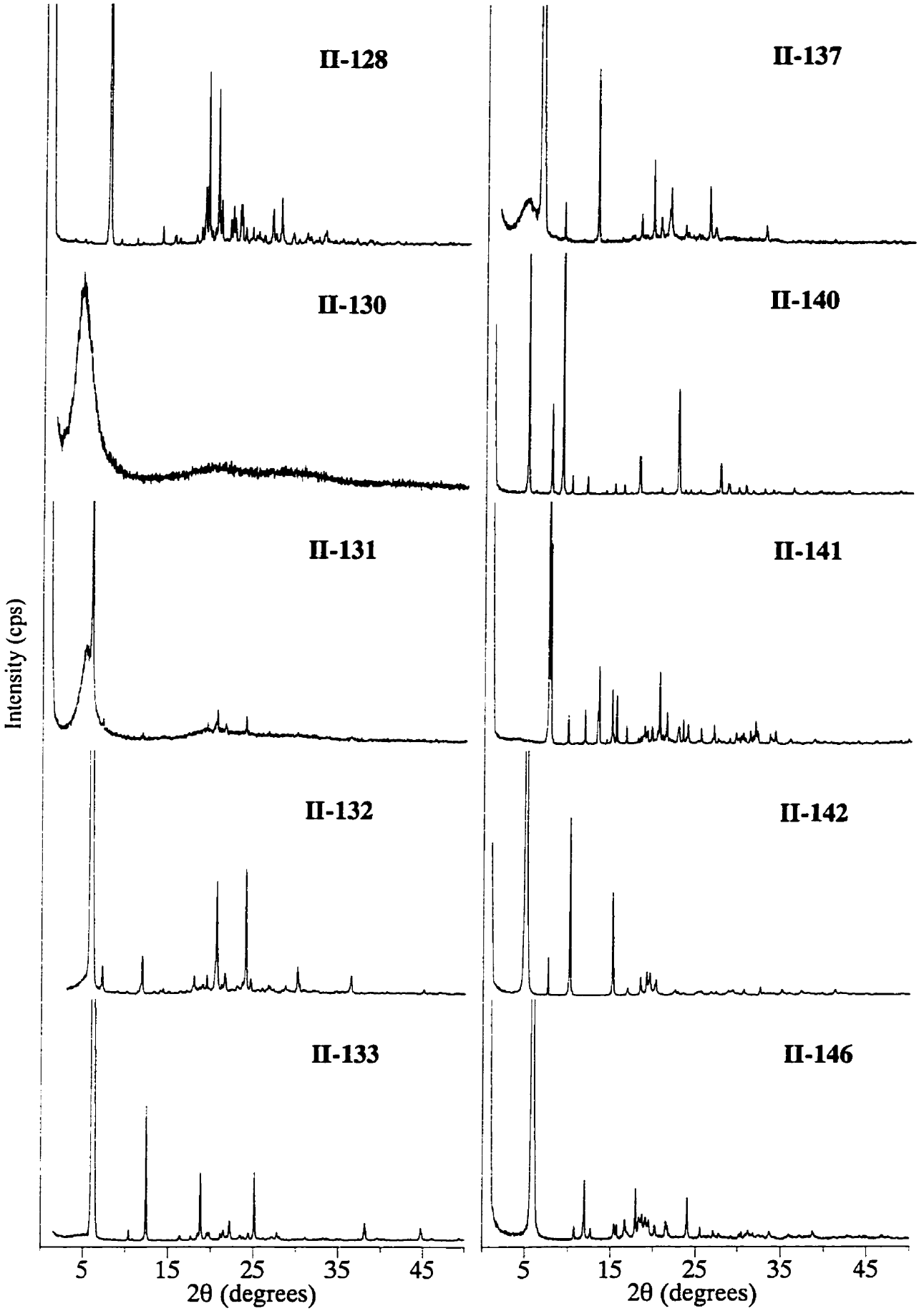
II-128
II-137
II-130
II-140
II-131
II-141
II-132
II-142
II-133
II-146
Intensity (cps)
5
15
25
35
45
2θ (degrees)
5
15
25
35
45
2θ (degrees)

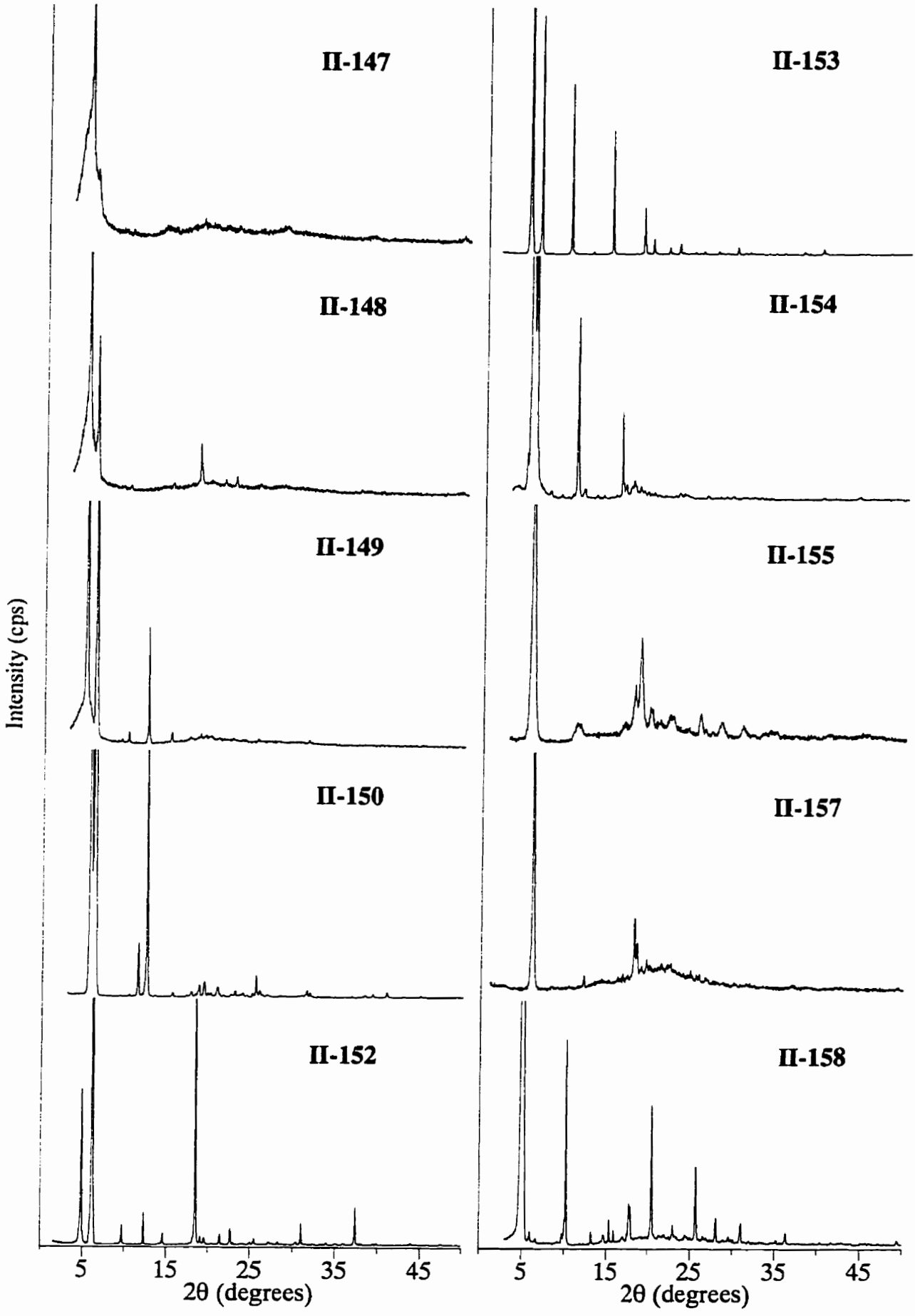
II-147
II-153
II-148
II-154
II-149
II-155
II-150
II-157
II-152
II-158
Intensity (cps)
5
15
25
35
45
2θ (degrees)
5
15
25
35
45
2θ (degrees)

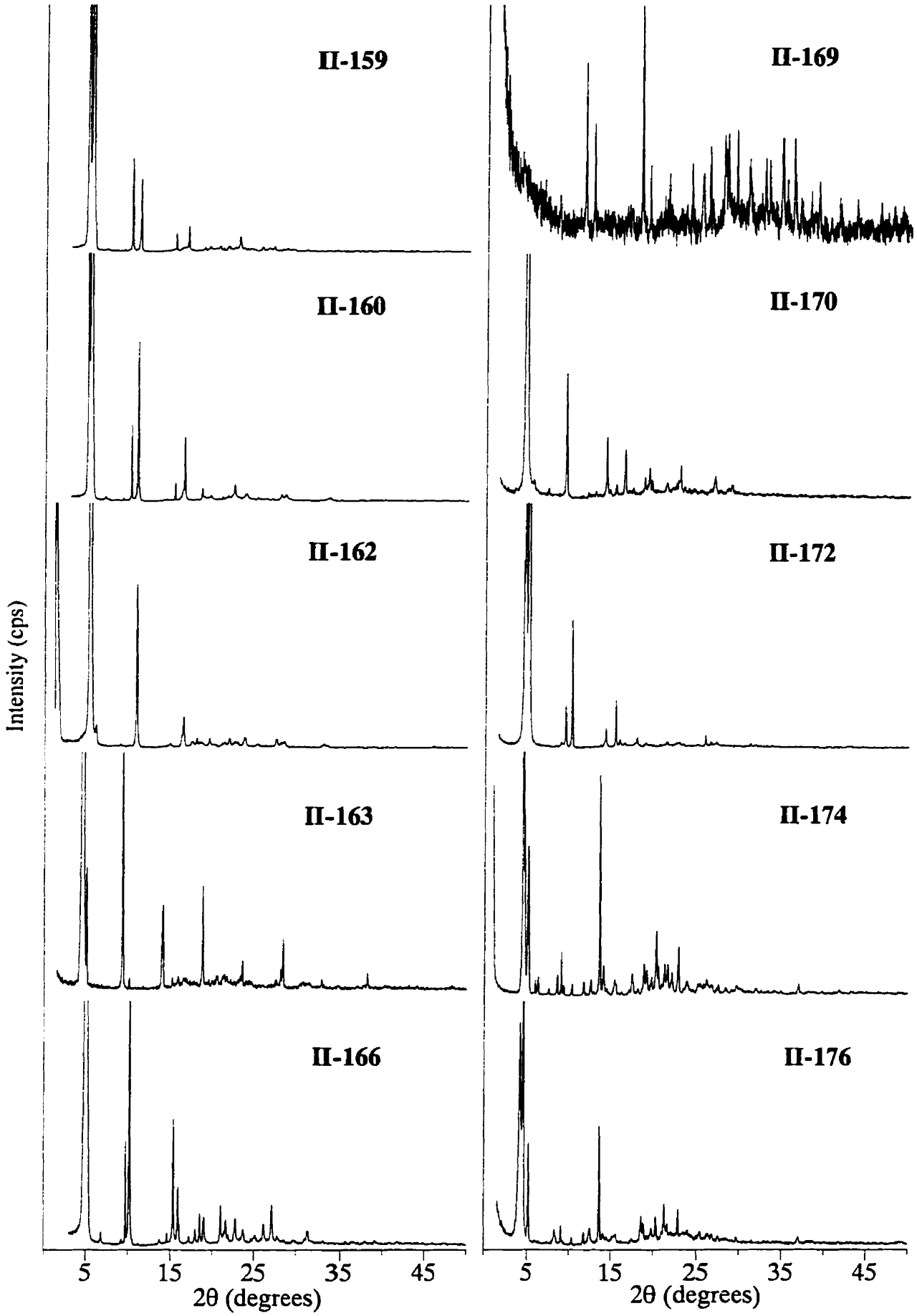
II-159
II-169
II-160
II-170
II-162
II-172
II-163
II-174
II-166
II-176
Intensity (cps)
5
15
25
35
45
2θ (degrees)
5
15
25
35
45
2θ (degrees)

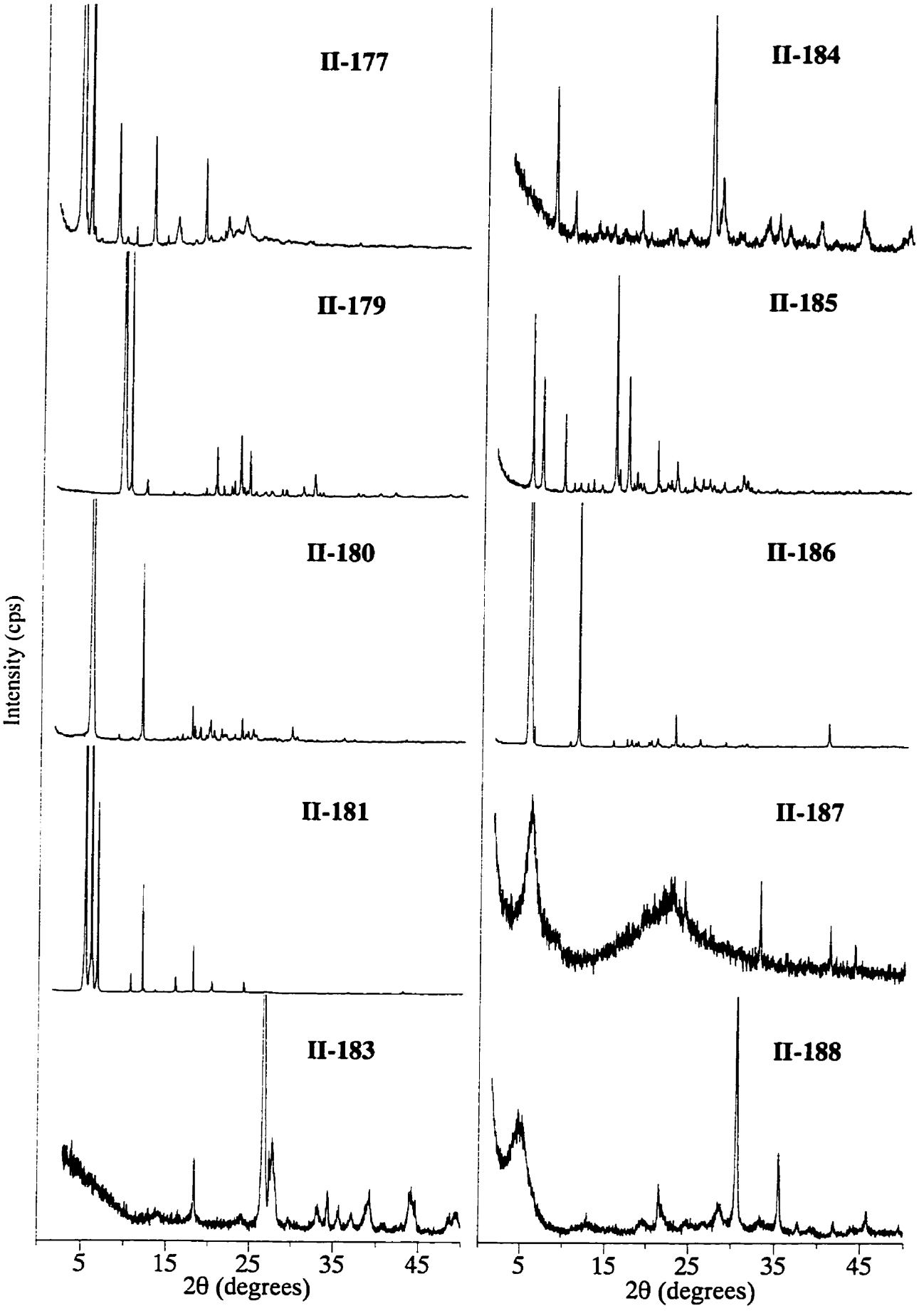
II-177
II-184
II-179
II-185
II-180
II-186
II-181
II-187
II-183
II-188
Intensity (cps)
5
15
25
35
45
2θ (degrees)
5
15
25
35
45
2θ (degrees)

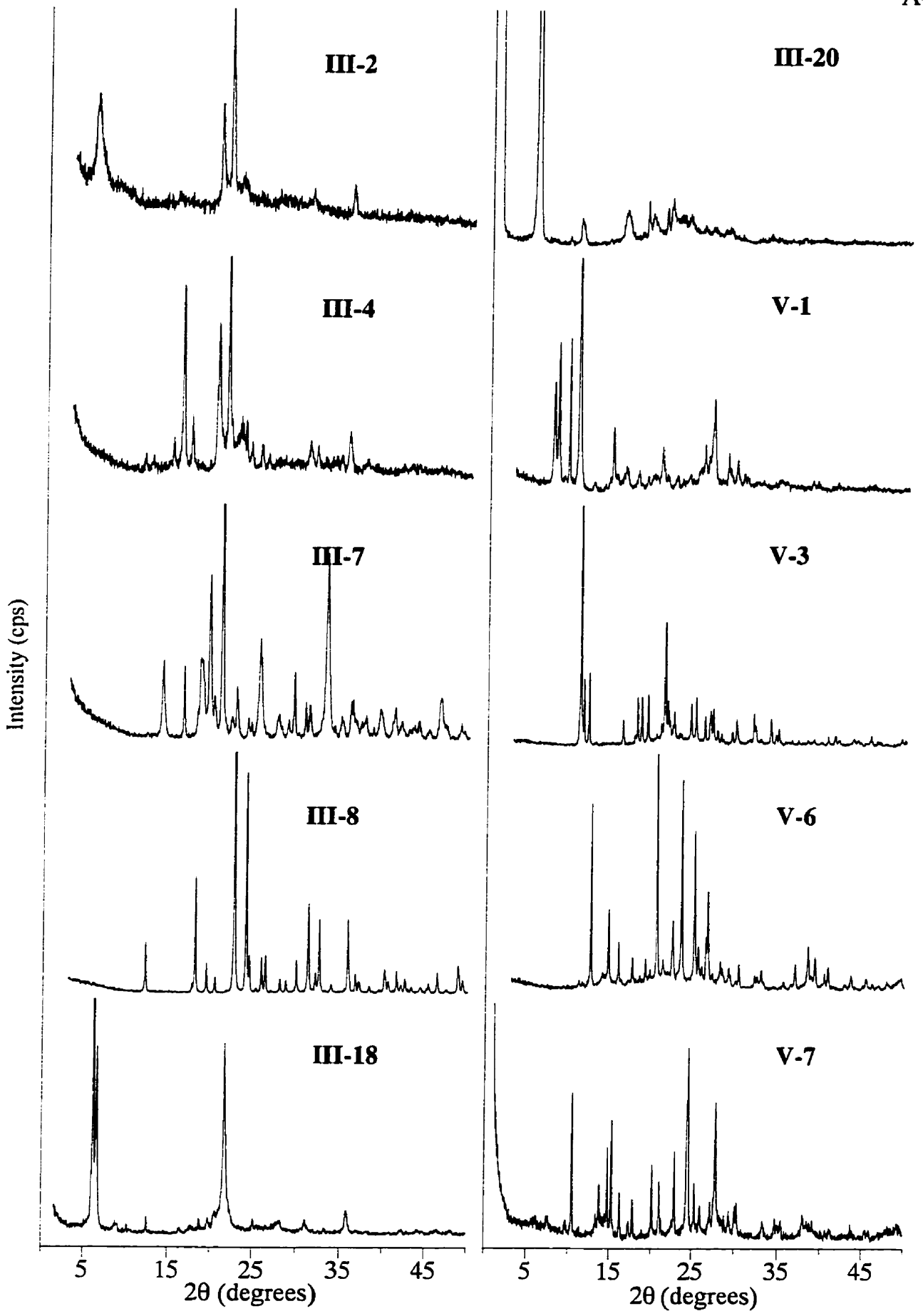
III-2
III-20
III-4
V-1
III-7
V-3
III-8
V-6
III-18
V-7
Intensity (cps)
5
15
25
35
45
2θ (degrees)
5
15
25
35
45
2θ (degrees)

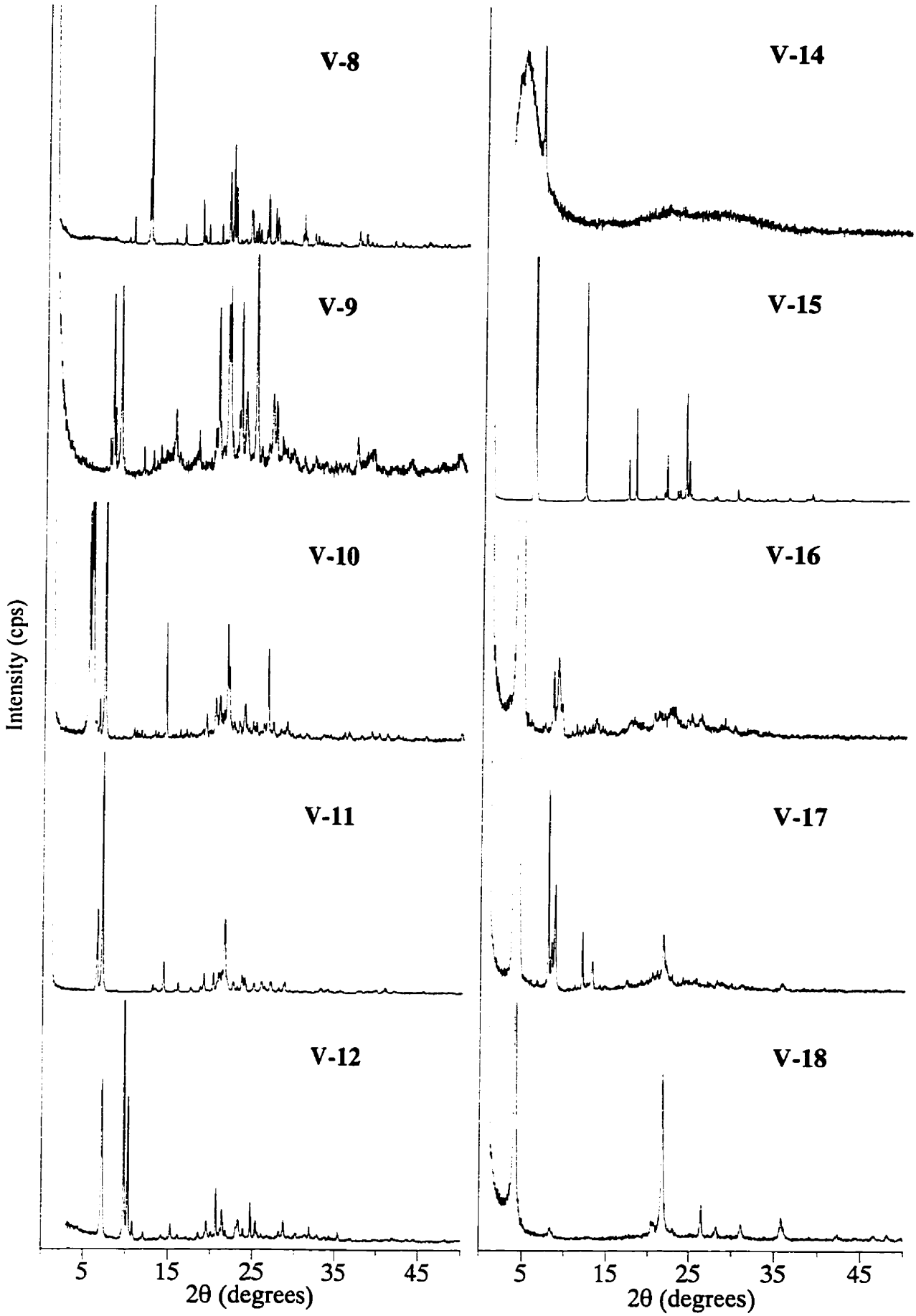
V-8
V-14
V-9
V-15
V-10
V-16
V-11
V-17
V-12
V-18
Intensity (cps)
5
15
25
35
45
2θ (degrees)
5
15
25
35
45
2θ (degrees)

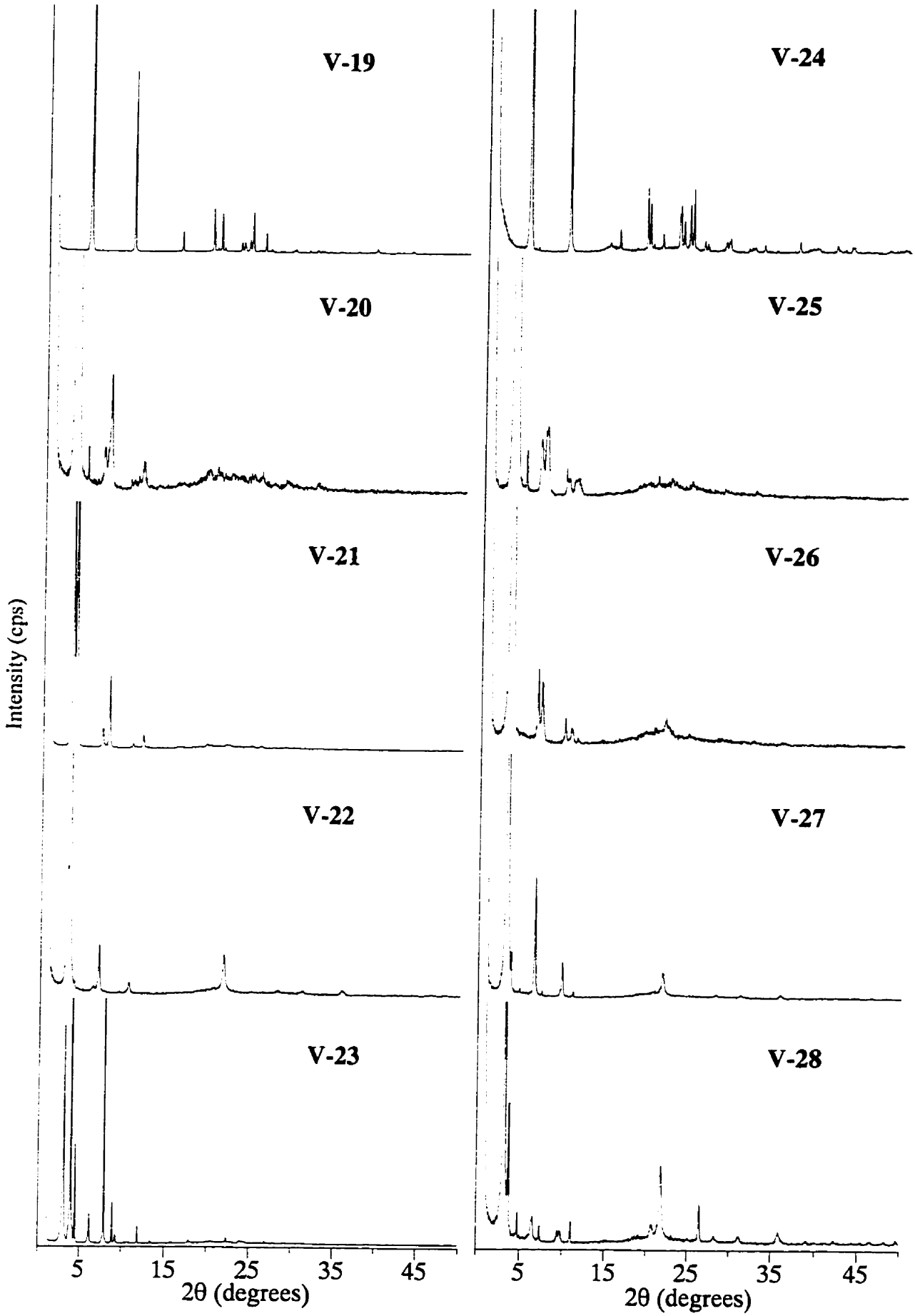
V-19
V-20
V-21
V-22
V-23
V-24
V-25
V-26
V-27
V-28
Intensity (cps)
5
15
25
35
45
2θ (degrees)
5
15
25
35
45
2θ (degrees)

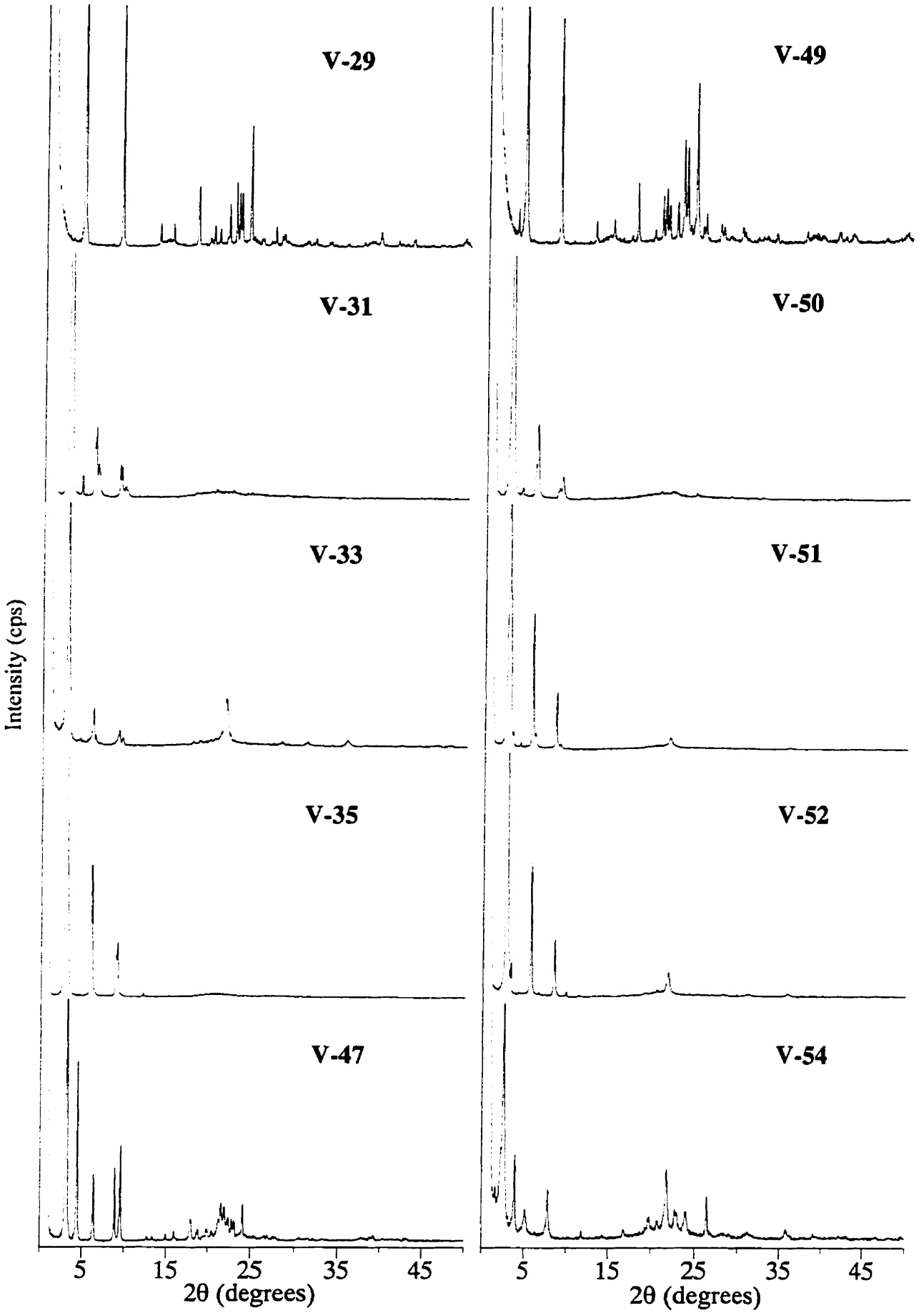
V-29
V-49
V-31
V-50
V-33
V-51
V-35
V-52
V-47
V-54
Intensity (cps)
5
15
25
35
45
2θ (degrees)
5
15
25
35
45
2θ (degrees)

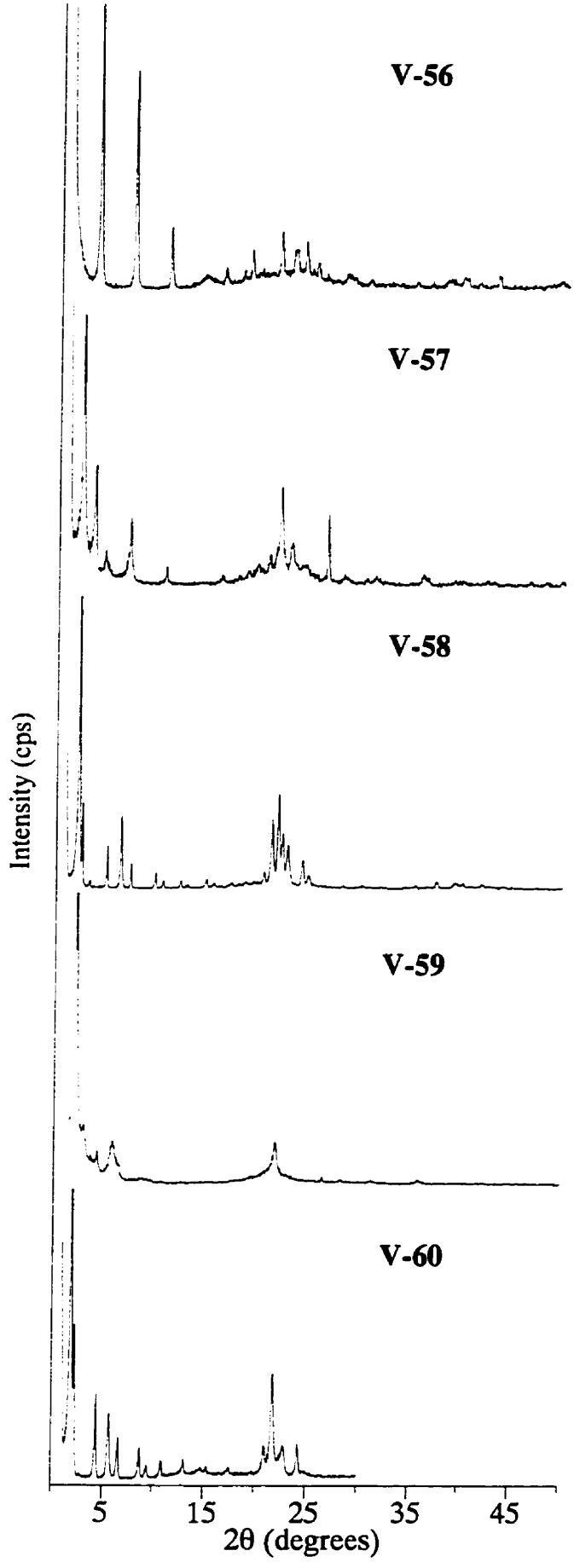
V-56
V-57
V-58
V-59
V-60
Intensity (cps)
5
15
25
35
45
2θ (degrees)

Appendix C: Scanning Electron Micrographs

II-4

II-13A

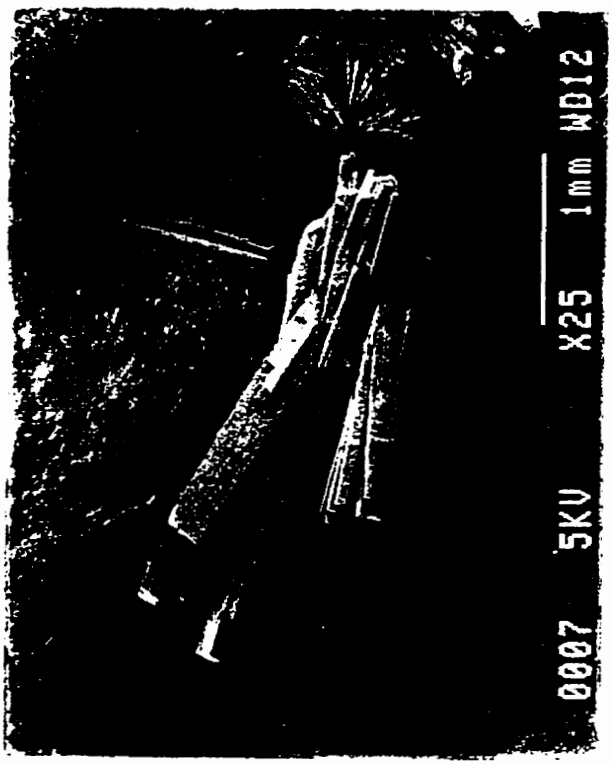

II-13B

II-22

II-34

II-38A

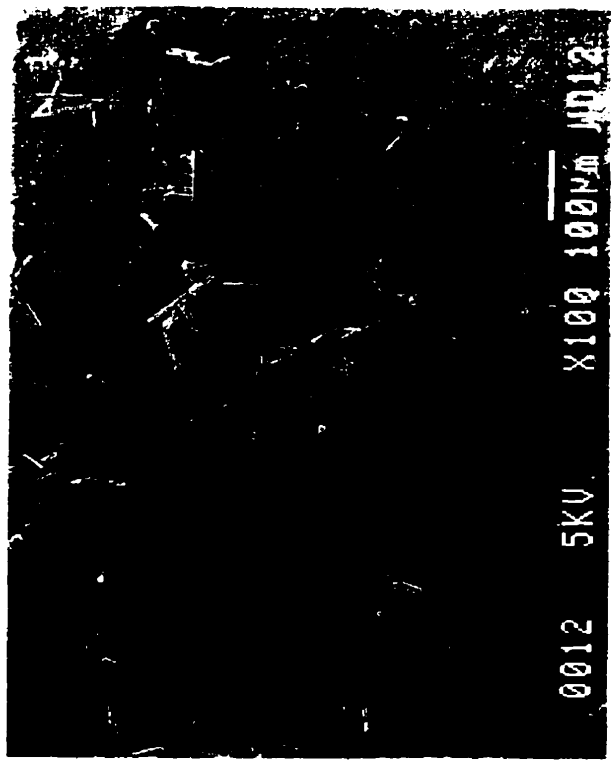

II-38B

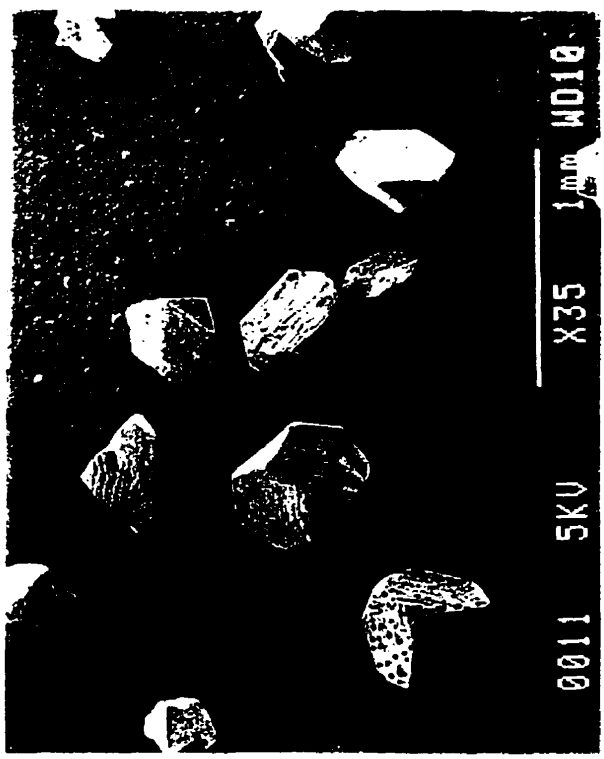

II-54

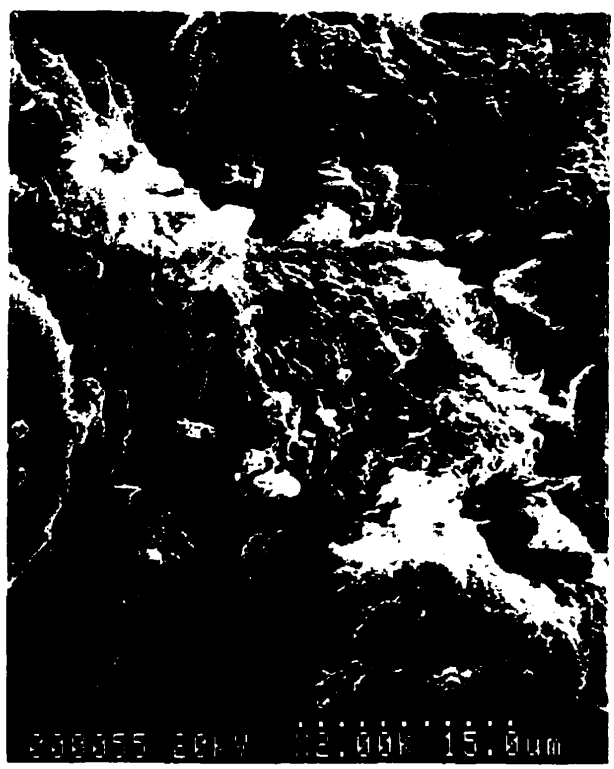

II-66

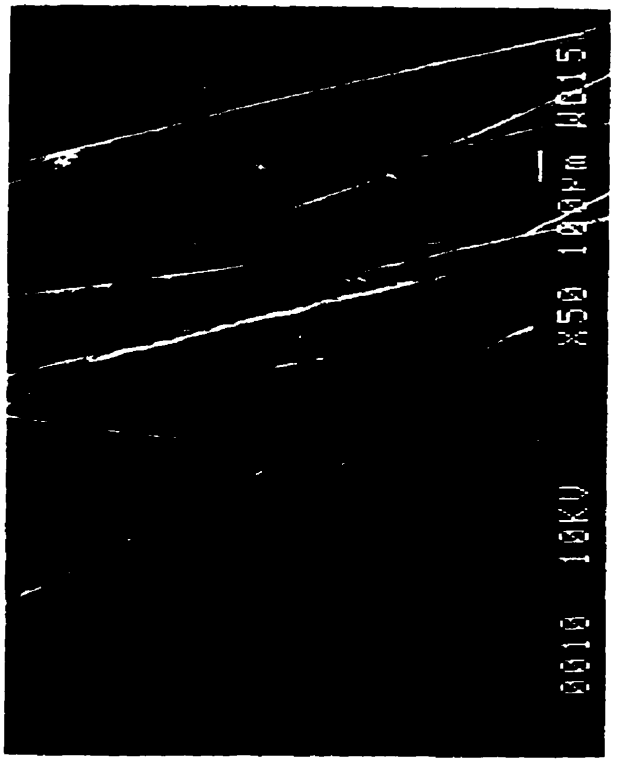

II-98

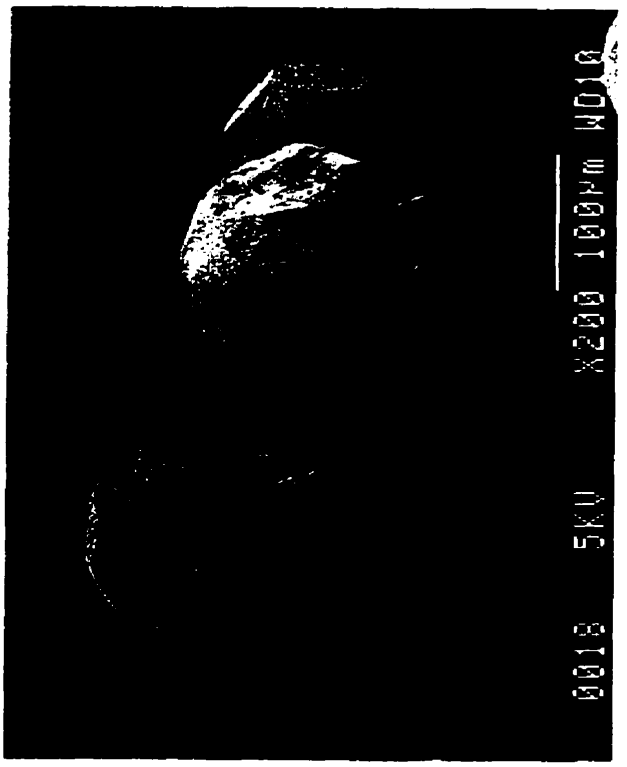

II-105

II-114

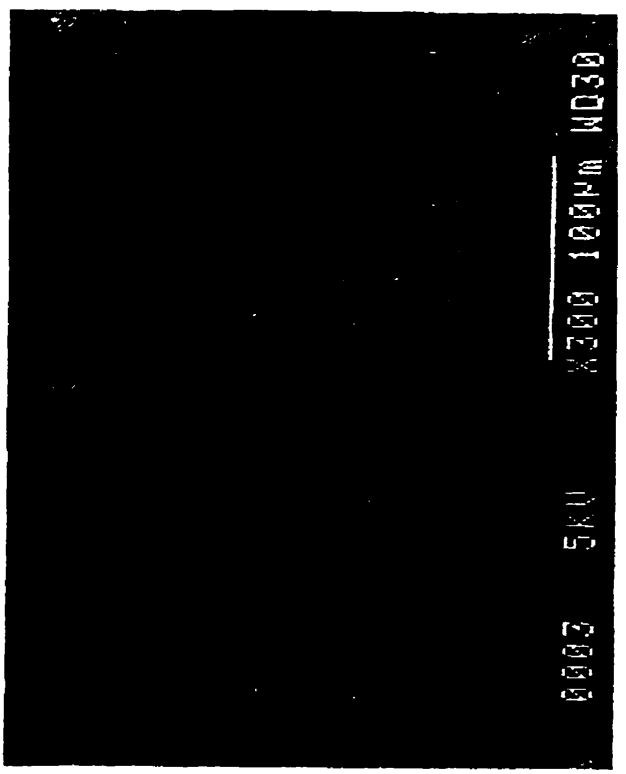

II-122

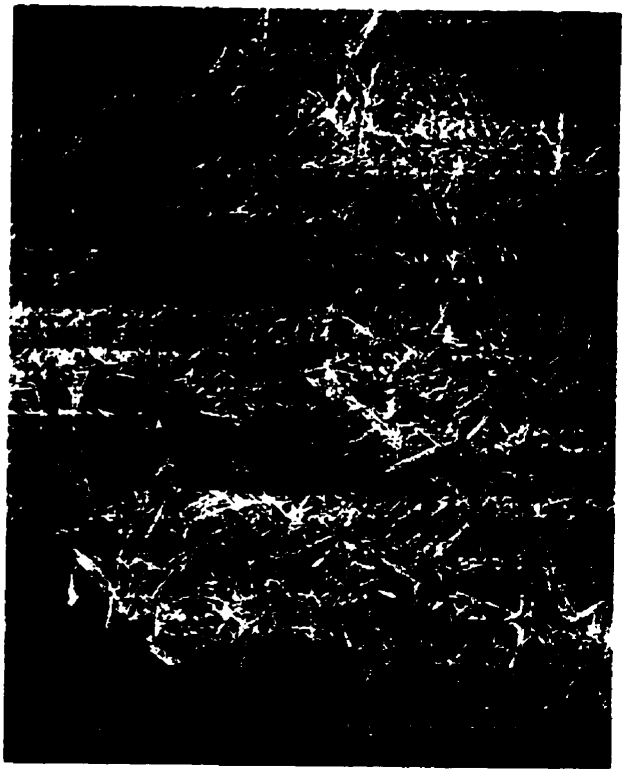

II-128

II-132

II-137

II-138

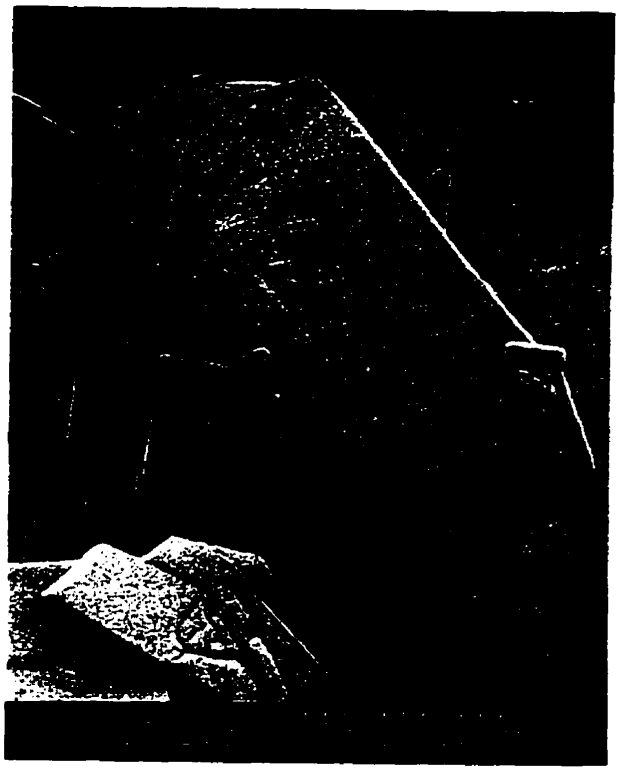

II-142

II-149

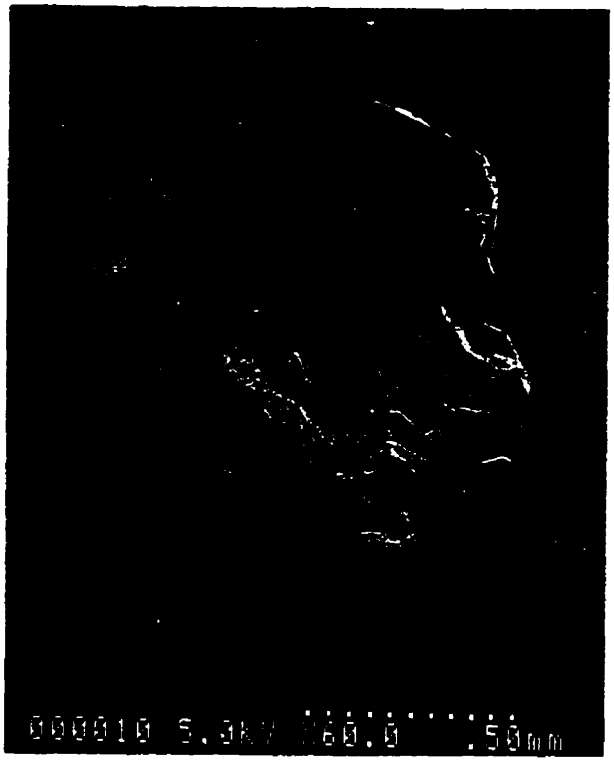

II-158

II-172

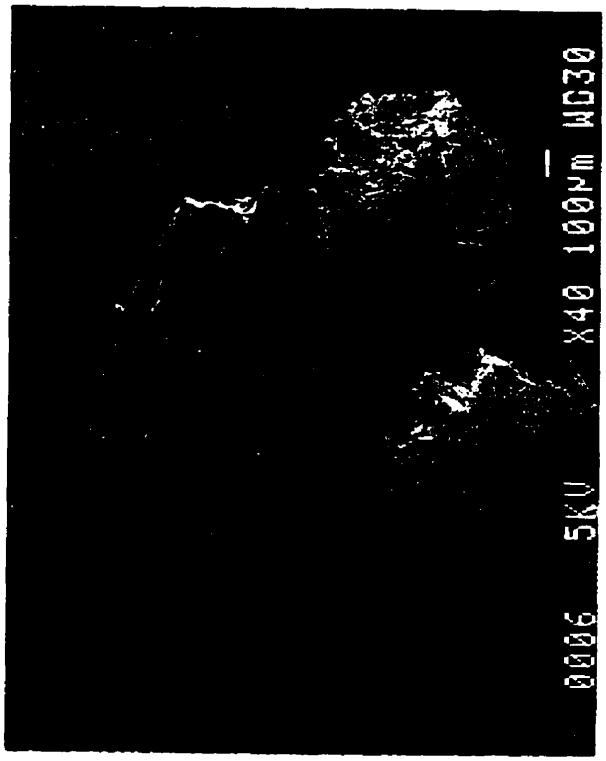

II-177

II-179

II-186

V-10

V-15

V-17

V-21

V-22

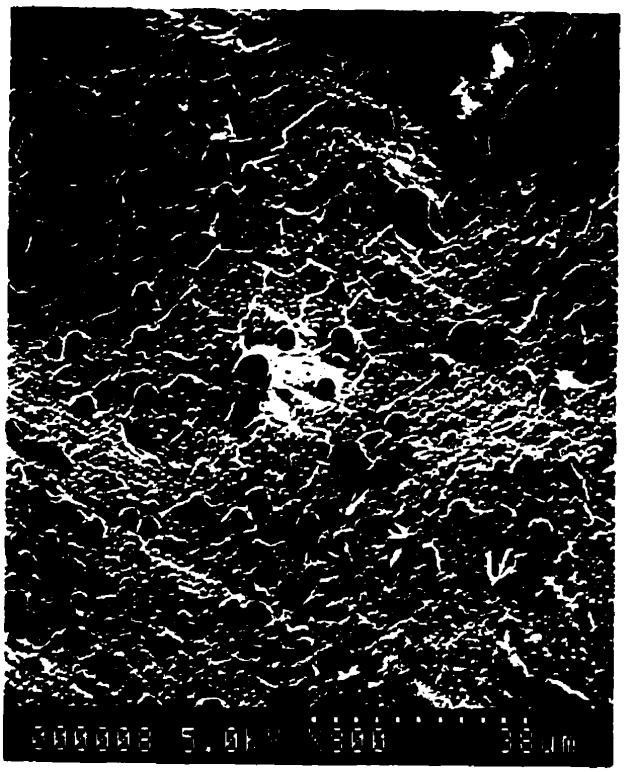

V-23

V-32A

V-32B

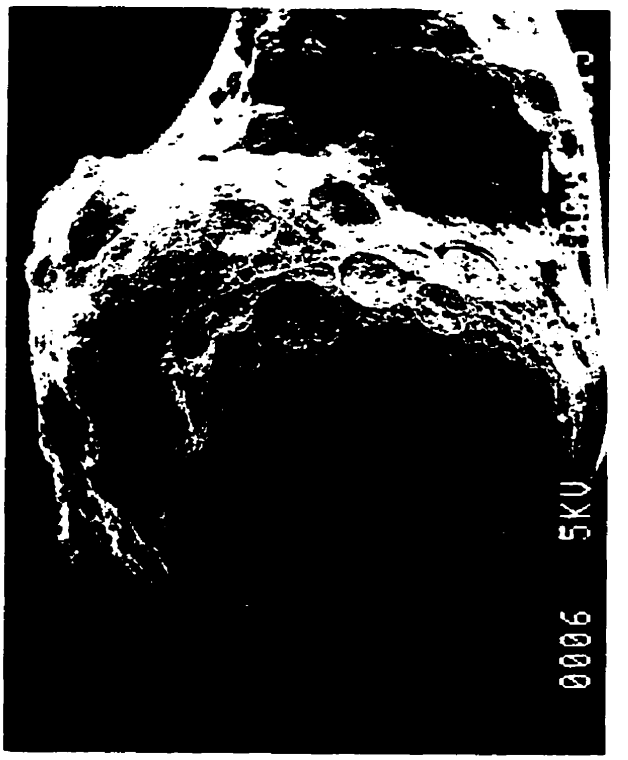

V-32C

V-32D

V-32E

V-32F

V-32G

V-32H

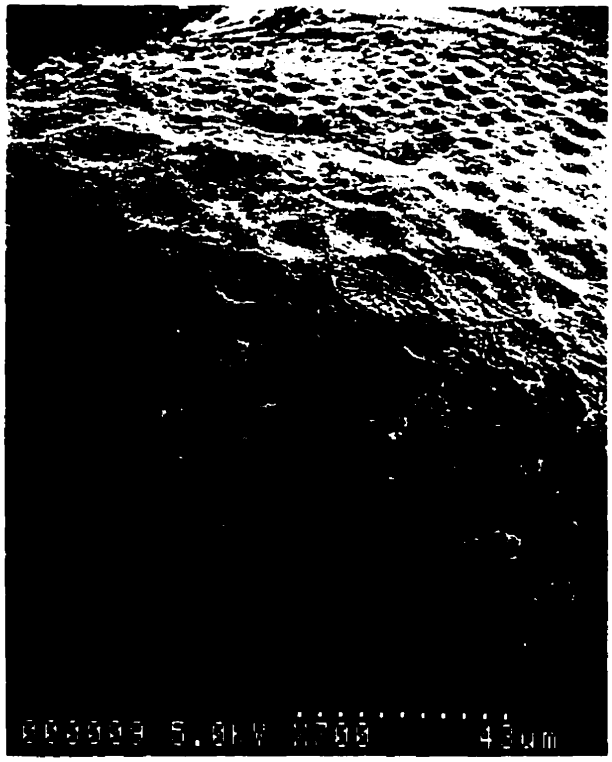

V-32I

V-32J

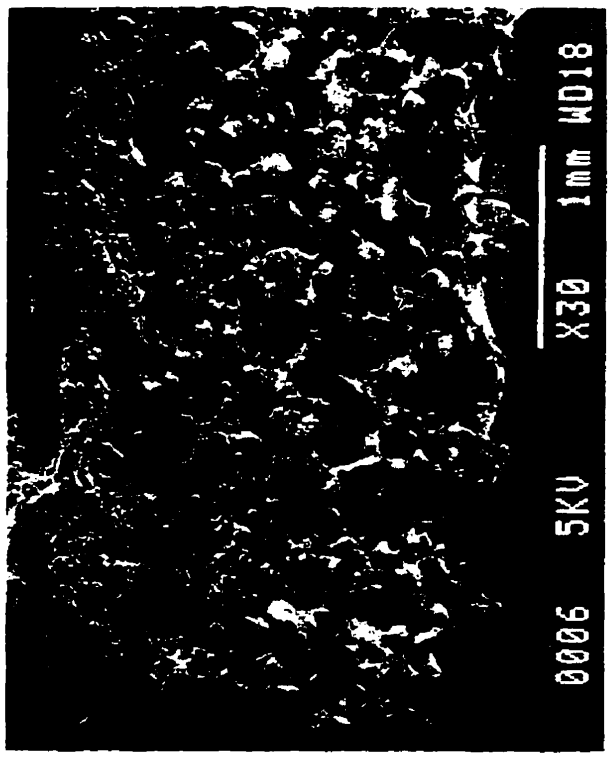

V-39

V-41

V-43A

V-43B

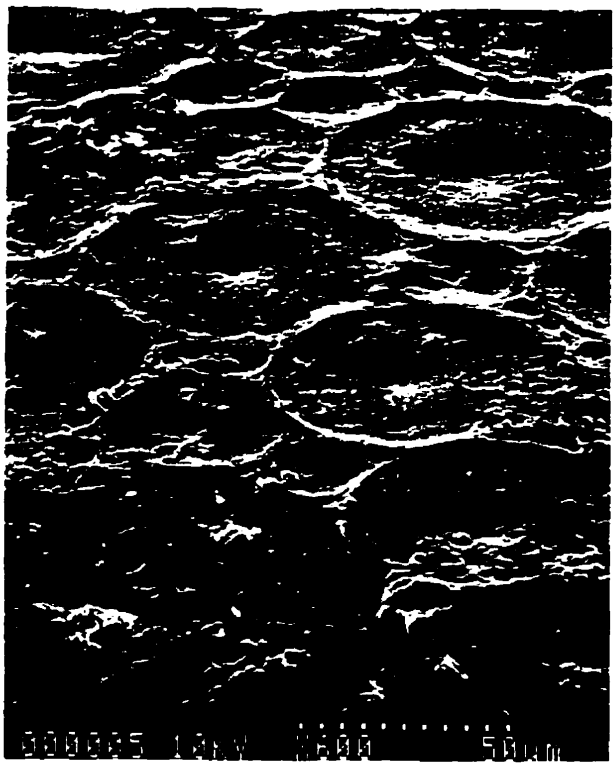

V-45

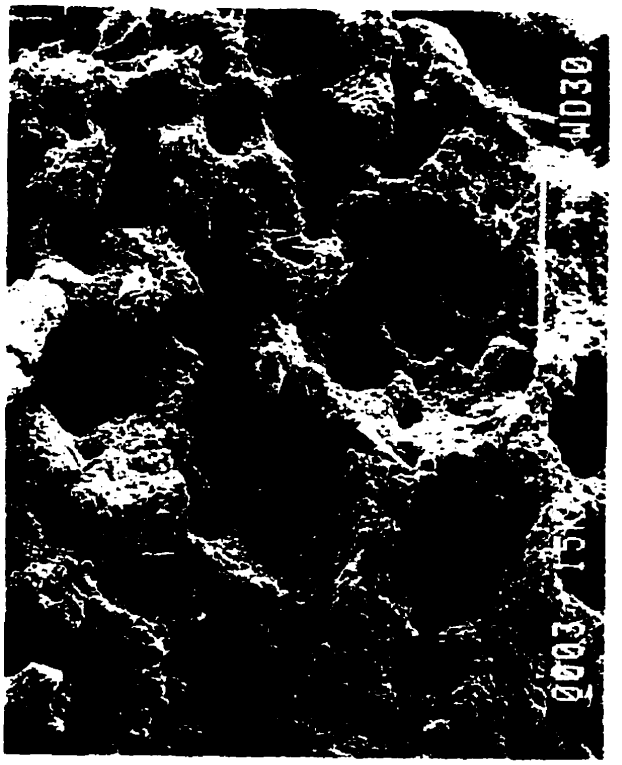

V-51A

V-51B

V-52A

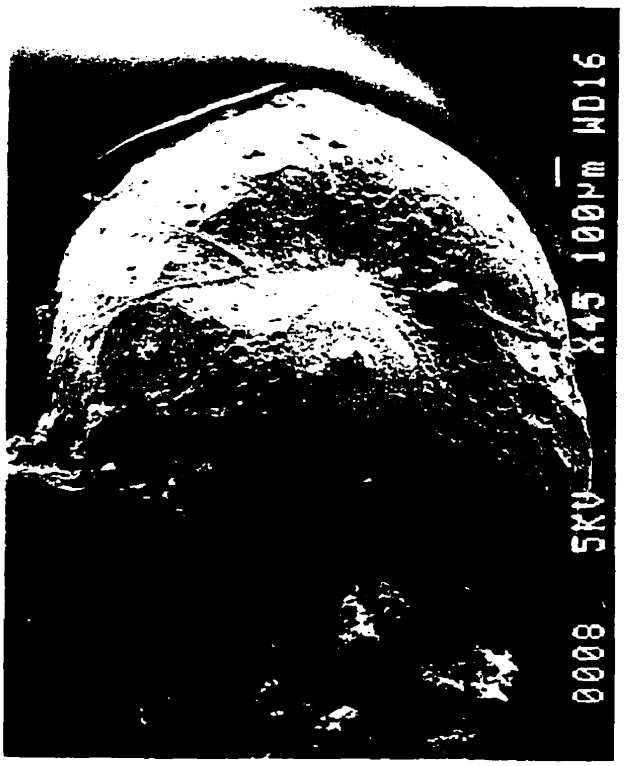

V-52B

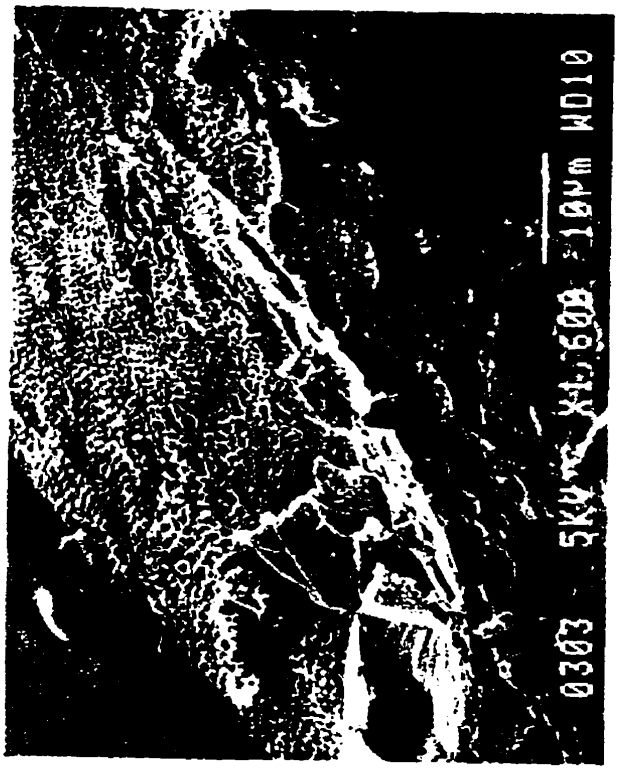

V-52C

V-52D

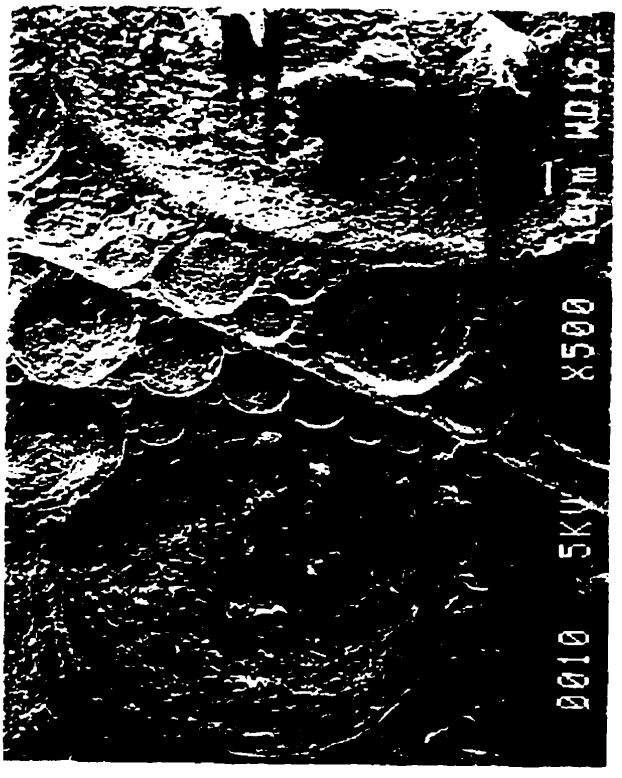

V-52E

V-54

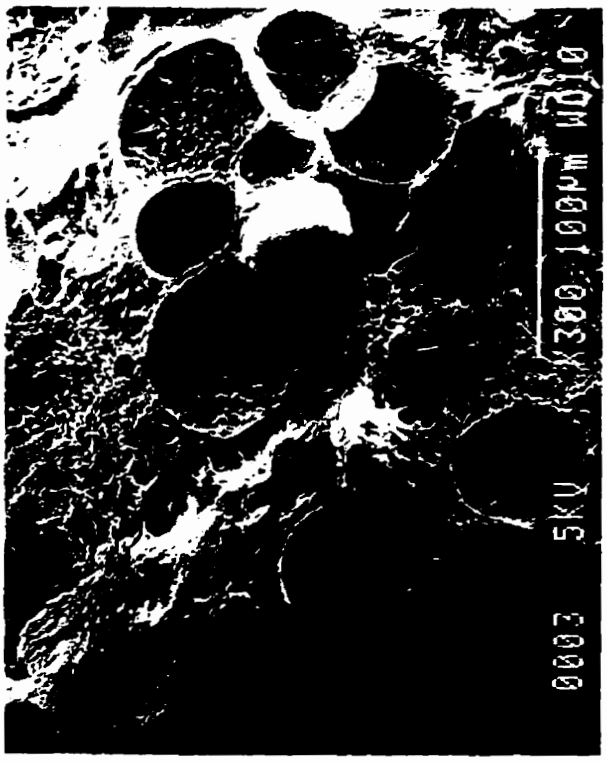

V-59

V-66A

V-66B

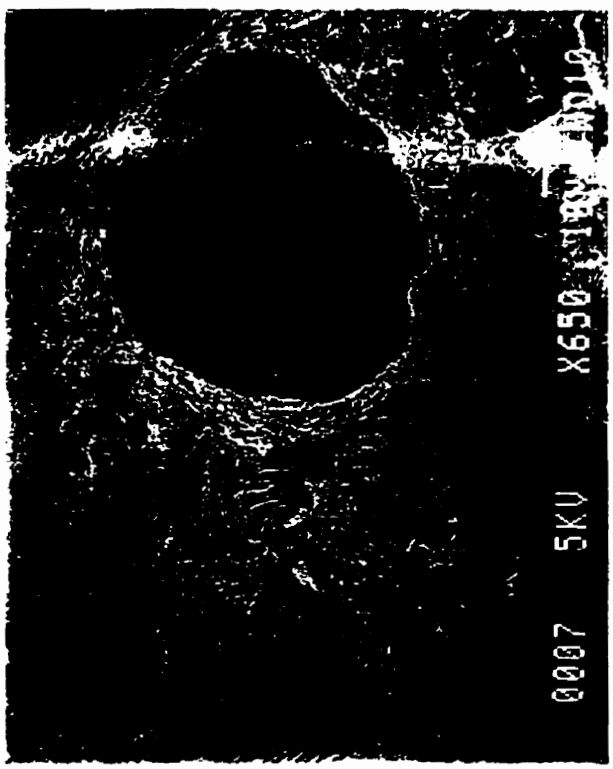

Appendix D. Fractional Atomic Coordinates, Theoretical PXRD Patterns and Tables of Relative Intensities versus d-spacing for the Novel UT-n and ADP Single Crystal XRD Structures

Order of Presentation:

(i) **UT-1,** $[Al_3P_4O_{16}]^{3-}[R^+]_3$

(ii) **UT-2,** $[Al_3P_5O_{20}H]^{5-}[C_5H_9NH_3^+]_5$

(iii) **UT-3,** $[Al_2P_3O_{12}H]^{2-}[C_5H_9NH_3^+]_2$

(iv) **UT-4,** $[Al_2P_3O_{12}H]^{2-}[C_6H_{11}NH_3^+]_2$

(v) **UT-5,** $[Al_2P_3O_{12}H]^{2-}[C_6H_{11}NH_3^+]_2$

(vi) **UT-6,** $[Al_3P_3O_{12}F]^-[C_5H_5NH^+]\bullet 0.15(H_2O)$

(vii) **UT-7,** $[Al_3P_5O_{20}H]^{5-}[C_7H_{13}NH_3^+]_5$

(viii) **UT-8,** $[Al_3P_4O_{16}]^{3-}[C_4H_9NH_3^+]_2[C_5H_{10}NH_2^+]$

(ix) **Cyclopentylammonium Monohydrogen Phosphate (CMP),** $[C_5H_9NH_3^+]_2[HPO_4^{2-}]$

(x) **1,8-Diammoniumoctane Dihydrogen Phosphate (DODP),** $[^+H_3N(CH_2)_8NH_3^+][H_2N(CH_2)_8NH_2][H_2PO_4^-]_2$

(xi) **Octylammonium Dihydrogen Phosphate (ODP),** $[CH_3(CH_2)_7NH_3^+][H_2PO_4^-]$

(xii) **Decylammonium Dihydrogen Phosphate (DDP),** $[CH_3(CH_2)_9NH_3^+][H_2PO_4^-]$

- For all structures, U(eq) is defined as one third of the trace of the orthogonalized U_{ij} tensor.
- For (i) and (x), residual electron density has been included as leftover atoms.
- For (x), standard deviations and thermal parameters are not included, as the data set was of poor quality.
- All PXRD data were produced by the Cerius^2 software program.
- Calculated peaks with relative intensity below 0.5% were omitted from the tables.

(i) UT-1, $[Al_3P_4O_{16}]^{3-}[R^+]_3$

Fractional Atomic Coordinates ($\times 10^4$) and Equivalent Isotropic Displacement Parameters ($Å^2 \times 10^3$) for UT-1

	x	y	z	U(eq)		x	y	z	U(eq)
Al(1)	3324(1)	-1480(1)	418(1)	12(1)	C(5)	3813(11)	896(9)	5779(10)	50(3)
P(1)	3333	-3333	2362(1)	11(1)	C(6)	3494(14)	340(13)	7197(11)	72(5)
P(2)	4458(1)	1175(1)	1174(1)	12(1)	N(3)	6667	3333	3467(5)	17(1)
O(1)	3333	-3333	3839(4)	19(1)	N(2)	0	0	0	82(44)
O(2)	3441(2)	-2183(2)	1815(3)	22(1)	C(4**)	2088(24)	-12(24)	3344(28)	56(6)
O(3)	3539(2)	-119(2)	896(3)	18(1)	C(4*)	1246(88)	-897(83)	5087(99)	112(28)
O(4)	4446(2)	1491(2)	2593(3)	21(1)	C(4)	1751(28)	-670(28)	4128(33)	66(7)
O(5)	4152(2)	1907(2)	235(3)	19(1)	C(27)	1558(47)	118(46)	-1240(52)	40(11)
O(6)	5686(2)	1378(2)	790(3)	22(1)	C(26)	0	0	392(87)	57(16)
N(1)	3875(11)	89(9)	4808(10)	40(2)	C(25)	1958(35)	-1035(36)	3942(40)	21(7)
C(1)	4664(19)	-397(10)	4859(15)	71(5)	C(24)	615(55)	1226(52)	-74(62)	46(12)
C(2)	5877(26)	247(31)	4423(38)	71(10)	C(23)	4372(74)	273(78)	5031(93)	54(20)
C(3)	2755(19)	-1046(10)	4616(14)	96(8)	C(21)	1015(74)	178(73)	857(82)	71(20)

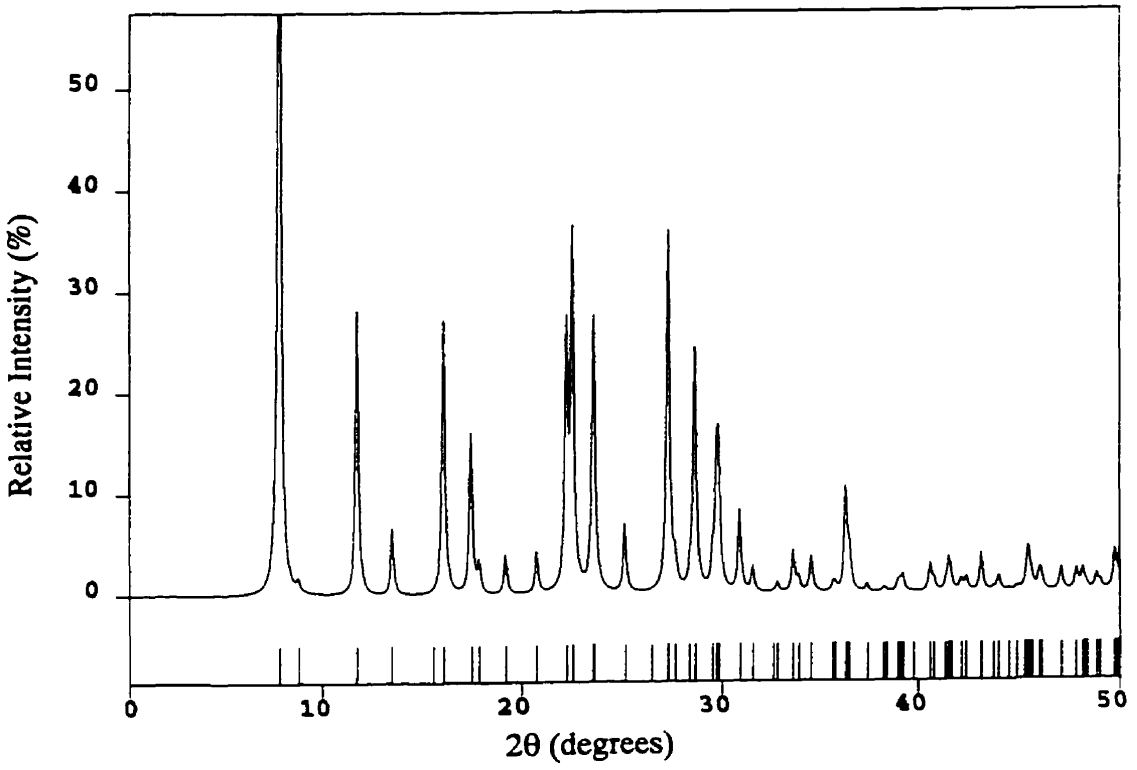

h	k	l	d-spacing	2θ	Relative Intensity	h	k	l	d-spacing	2θ	Relative Intensity
1	0	0	11.338	7.797	100.00%	4	0	2	2.4714	36.351	1.33%
0	0	1	10.093	8.761	0.95%	1	0	4	2.463	36.479	3.82%
1	0	1	7.5387	11.738	28.26%	4	1	1	2.403	37.423	0.82%
1	1	0	6.546	13.526	6.72%	1	1	4	2.3544	38.225	0.50%
1	1	1	5.492	16.138	27.39%	3	2	2	2.3121	38.953	0.84%
0	0	2	5.0465	17.574	15.98%	2	0	4	2.3052	39.073	0.68%
2	0	1	4.9427	17.946	2.70%	3	1	3	2.2973	39.213	1.62%
1	0	2	4.6104	19.251	3.82%	4	1	2	2.2215	40.609	2.76%
2	1	0	4.2854	20.727	4.12%	5	0	1	2.2124	40.783	1.13%
1	1	2	3.9967	22.242	25.17%	3	3	0	2.182	41.378	0.79%
2	1	1	3.9445	22.54	34.84%	2	1	4	2.1743	41.531	2.96%
3	0	0	3.7793	23.539	7.34%	4	0	3	2.1677	41.664	0.92%

2	0	2	3.7694	23.602	22.19%	4	2	0	2.1427	42.173	1.15%
3	0	1	3.5393	25.16	6.86%	3	3	1	2.1327	42.379	1.37%
2	2	0	3.273	27.246	1.61%	4	2	1	2.096	43.16	3.68%
2	1	2	3.2665	27.301	35.36%	3	2	3	2.0578	44.001	1.63%
1	0	3	3.2253	27.656	2.70%	2	2	4	1.9983	45.382	1.61%
3	1	0	3.1446	28.381	1.40%	5	1	1	1.9961	45.435	1.28%
2	2	1	3.1134	28.672	24.59%	4	1	3	1.9932	45.506	2.60%
3	0	2	3.0251	29.528	2.79%	1	0	5	1.9873	45.648	0.53%
3	1	1	3.0023	29.757	9.32%	4	2	2	1.9723	46.017	1.81%
1	1	3	2.9923	29.859	12.33%	3	1	4	1.968	46.122	1.20%
2	0	3	2.8932	30.906	8.27%	1	1	5	1.929	47.111	2.44%
4	0	0	2.8345	31.563	2.49%	2	0	5	1.9016	47.83	2.21%
4	0	1	2.7289	32.818	1.02%	6	0	0	1.8897	48.152	1.92%
3	1	2	2.6689	33.578	4.02%	4	3	0	1.864	48.86	1.61%
2	1	3	2.6463	33.873	1.33%	6	0	1	1.8574	49.043	0.80%
3	2	0	2.6011	34.479	3.59%	4	3	1	1.833	49.741	3.14%
3	2	1	2.5188	35.643	0.64%	3	3	3	1.8307	49.807	1.26%
4	1	0	2.4742	36.309	9.31%	2	1	5	1.8261	49.94	1.60%

(ii) UT-2, $[Al_3P_5O_{20}H]^{5-}[C_5H_9NH_3^+]_5$

Fractional Atomic Coordinates ($\times 10^4$) and Equivalent Isotropic Displacement Parameters ($Å^2 \times 10^3$) for UT-2

	x	y	z	U(eq)		x	y	z	U(eq)
Al(1)	-127(1)	-2974(1)	676(1)	25(1)	C(11)	-7221(5)	-3983(3)	2662(3)	55(1)
Al(2)	-1426(1)	342(1)	929(1)	25(1)	C(12)	-6187(7)	-4856(3)	2785(4)	79(2)
Al(3)	-3472(1)	-1203(1)	-89(1)	23(1)	C(13)	-5633(11)	-4949(9)	3635(6)	175(5)
P(1)	-4337(1)	-42(1)	1351(1)	23(1)	C(14)	-6368(13)	-4259(13)	4023(8)	212(8)
P(2)	-596(1)	-1550(1)	-1117(1)	24(1)	C(15)	-7351(12)	-3728(5)	3531(5)	129(4)
P(3)	703(1)	-1326(1)	1155(1)	24(1)	C(21)	5272(5)	-7381(4)	1479(3)	60(1)
P(4)	-3204(1)	-3190(1)	1120(1)	27(1)	N(2)	4679(3)	-6644(2)	754(2)	38(1)
P(5)	2136(1)	-4552(1)	563(1)	30(1)	C(22)	6259(7)	-7136(6)	1890(4)	126(4)
O(1)	-1798(2)	-1087(2)	-592(2)	33(1)	C(23)	6154(13)	-7741(10)	2841(6)	243(9)
O(2)	-3685(2)	-2358(2)	313(2)	32(1)	C(24)	4958(12)	-8180(9)	3033(5)	186(6)
O(3)	-4083(2)	-3112(2)	1980(2)	37(1)	C(25)	4195(6)	-7777(5)	2255(4)	84(2)
O(4)	-3237(3)	-4052(2)	896(2)	46(1)	N(3)	92(4)	-6369(2)	1701(2)	47(1)
O(5)	-3799(3)	-703(2)	777(2)	35(1)	C(31)	-674(7)	-6387(5)	2608(4)	78(2)
O(6)	-4890(3)	-542(2)	2284(2)	35(1)	C(32)	-1383(11)	-5512(7)	2665(5)	155(5)
O(7)	-5426(2)	698(2)	891(2)	36(1)	C(33)	-1345(22)	-5491(13)	3560(10)	331(15)
O(8)	-979(3)	-1661(2)	-1948(2)	38(1)	C(34)	-310(17)	-6100(13)	3905(10)	240(8)
O(9)	-87(3)	-2494(2)	-485(2)	35(1)	C(35)	298(9)	-6669(8)	3311(5)	146(4)
O(10)	758(3)	-4064(2)	893(2)	37(1)	N(4)	-2859(4)	-2051(2)	2591(2)	43(1)
O(11)	3234(3)	-3982(2)	482(2)	47(1)	C(41)	-2140(8)	-2550(5)	3389(4)	86(2)
O(12)	1930(3)	-4585(2)	-393(2)	45(1)	C(42)	-3067(13)	-2973(8)	4131(6)	167(6)
O(13)	2357(3)	-5517(2)	1190(2)	40(1)	C(43)	-3179(20)	-2454(17)	4711(12)	313(14)
O(14)	-544(2)	945(2)	1357(2)	35(1)	C(44)	-2396(26)	-1729(12)	4387(11)	304(14)
O(15)	-1757(2)	-3039(2)	1210(2)	40(1)	C(45)	-1482(11)	-1936(9)	3708(5)	169(6)
O(16)	1535(3)	-1422(2)	1882(2)	37(1)	N(5)	-7709(3)	-218(2)	2629(2)	37(1)
O(17)	-760(2)	-826(2)	1313(2)	33(1)	C(51)	-8297(6)	-446(4)	3593(3)	62(1)
O(18)	-3131(2)	432(2)	1377(2)	31(1)	C(52)	-7850(11)	-1415(5)	4085(4)	121(3)
O(19)	564(3)	-2290(2)	1129(2)	36(1)	C(53)	-7263(21)	-1401(9)	4809(12)	293(12)
O(20)	1332(2)	-781(2)	229(2)	35(1)	C(54)	-7028(17)	-465(9)	4711(10)	245(9)
N(1)	-6706(3)	-3242(2)	1880(2)	42(1)	C(55)	-7813(10)	132(6)	4080(4)	111(3)

Hydrogen Fractional Coordinates ($\times 10^4$) and Isotropic Displacement Parameters ($Å^2 \times 10^3$) for UT-2

	x	y	z	U(eq)		x	y	z	U(eq)
H(1O)	2264(53)	-4983(36)	-490(35)	56(16)	H(33A)	-2070(22)	-5532(13)	3862(10)	255(11)
H(1A)	-7248(3)	-2786(2)	1819(2)	66(4)	H(33B)	-1131(22)	-5003(13)	3516(10)	255(11)
H(1B)	-5998(3)	-3139(2)	1967(2)	66(4)	H(34A)	-669(17)	-6439(13)	4347(10)	255(11)
H(1C)	-6593(3)	-3401(2)	1432(2)	66(4)	H(34B)	251(17)	-5889(13)	4054(10)	255(11)
H(11B)	-7935(5)	-4080(3)	2580(3)	255(11)	H(35A)	1026(9)	-6517(8)	3084(5)	255(11)
H(12B)	-5608(7)	-4811(3)	2362(4)	255(11)	H(35B)	389(9)	-7212(8)	3553(5)	255(11)
H(12C)	-6554(7)	-5294(3)	2849(4)	255(11)	H(4A)	-3198(4)	-2406(2)	2447(2)	66(4)

H(13B)	-4856(11)	-4856(9)	3513(6)	255(11)
H(13C)	-5659(11)	-5453(9)	3980(6)	255(11)
H(14A)	-5873(13)	-3940(13)	4089(8)	255(11)
H(14B)	-6720(13)	-4516(13)	4512(8)	255(11)
H(15A)	-8090(12)	-3806(5)	3802(5)	255(11)
H(15B)	-7266(12)	-3198(5)	3419(5)	255(11)
H(21A)	5634(5)	-7793(4)	1278(3)	255(11)
H(2A)	5273(3)	-6463(2)	362(2)	66(4)
H(2B)	4151(3)	-6836(2)	556(2)	66(4)
H(2C)	4293(3)	-6229(2)	943(2)	66(4)
H(22A)	6099(7)	-6602(6)	1860(4)	255(11)
H(22B)	7009(7)	-7235(6)	1642(4)	255(11)
H(23A)	6082(13)	-7428(10)	3170(6)	255(11)
H(23B)	6819(13)	-8113(10)	2930(6)	255(11)
H(24A)	4504(12)	-8122(9)	3487(5)	255(11)
H(24B)	5180(12)	-8717(9)	3091(5)	255(11)
H(25A)	3839(6)	-8151(5)	2153(4)	255(11)
H(25B)	3624(6)	-7371(5)	2343(4)	255(11)
H(3A)	-429(4)	-6230(2)	1334(2)	66(4)
H(3B)	616(4)	-002(2)	564(2)	66(4)
H(3C)	501(4)	-6869(2)	721(2)	66(4)
H(31A)	-1203(7)	-6751(5)	2744(4)	255(11)
H(32A)	-2163(11)	-5463(7)	2592(5)	255(11)
H(32B)	-1036(11)	-5111(7)	2283(5)	255(11)

H(4B)	-440(4)	-1666(2)	2714(2)	66(4)
H(4C)	-330(4)	-1811(2)	2181(2)	66(4)
H(41A)	-1576(8)	-2939(5)	3258(4)	255(11)
H(42A)	-3784(13)	-2962(8)	3972(6)	255(11)
H(42B)	-2769(13)	-3496(8)	4363(6)	255(11)
H(43A)	-2975(20)	-2762(17)	5195(12)	255(11)
H(43B)	-3968(20)	-2252(17)	4774(12)	255(11)
H(44A)	-2064(26)	-1657(12)	4783(11)	255(11)
H(44B)	-2859(26)	-1261(12)	4160(11)	255(11)
H(45A)	-1290(11)	-1495(9)	3304(5)	255(11)
H(45B)	-810(11)	-2207(9)	3928(5)	255(11)
H(5A)	-7969(3)	-528(2)	2386(2)	66(4)
H(5B)	-942(3)	314(2)	2386(2)	66(4)
H(5C)	-897(3)	-313(2)	2597(2)	66(4)
H(51A)	-9110(6)	-355(4)	3622(3)	255(11)
H(52A)	-7343(11)	-1662(5)	3754(4)	255(11)
H(52B)	-8493(11)	-1688(5)	4281(4)	255(11)
H(53A)	-6536(21)	-1712(9)	4802(12)	255(11)
H(53B)	-7702(21)	-1606(9)	5283(12)	255(11)
H(54A)	-6246(17)	-397(9)	4545(10)	255(11)
H(54B)	-7232(17)	-363(9)	5188(10)	255(11)
H(55A)	-8448(10)	391(6)	4329(4)	255(11)
H(55B)	-7383(10)	509(6)	3726(4)	255(11)

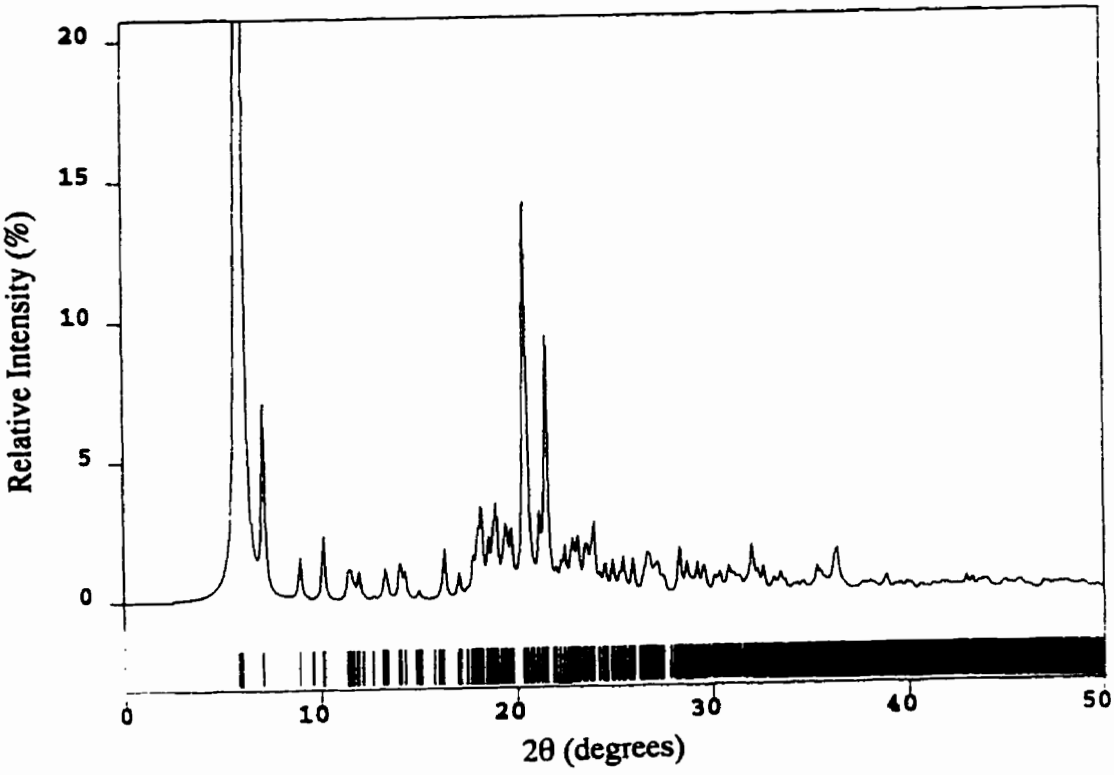

h	k	l	d-spacing	2θ	Relative Intensity	h	k	l	d-spacing	2θ	Relative Intensity
0	0	1	14.8268	5.961	100.00%	1	3	3	4.1253	21.54	4.80%
0	1	0	14.5318	6.082	5.52%	0	3	3	4.1099	21.622	0.73%
0	1	1	12.3297	7.169	6.65%	1	3	-1	4.0275	22.07	0.55%
1	0	0	9.8205	9.004	1.49%	1	-2	-3	3.9866	22.299	0.78%
1	1	0	8.7032	10.163	0.77%	1	-3	-2	3.9512	22.502	1.41%
1	0	1	8.6985	10.169	1.41%	2	3	1	3.9011	22.794	0.66%
1	0	-1	7.7571	11.407	0.89%	2	2	-1	3.8874	22.876	1.07%
1	-1	0	7.6682	11.539	0.77%	2	3	2	3.8395	23.165	1.11%

0	0	2	7.4134	11.937	0.93%	2	-2	0	3.8341	23.198	0.52%
1	0	2	6.3042	14.048	0.97%	0	2	4	3.7777	23.549	0.76%
1	2	0	6.2614	14.144	0.63%	2	-2	-1	3.7645	23.633	0.93%
0	2	2	6.1649	14.367	0.84%	2	0	3	3.7214	23.911	0.77%
1	-2	-1	5.4271	16.332	1.84%	2	3	0	3.7093	23.99	0.65%
1	-1	2	5.1839	17.104	0.57%	0	0	4	3.7067	24.007	1.43%
1	1	-2	4.9868	17.786	1.07%	2	-2	1	3.6616	24.307	0.50%
1	-2	1	4.9162	18.043	1.48%	0	2	-3	3.6245	24.56	0.52%
1	3	1	4.8789	18.182	1.58%	1	0	4	3.6192	24.597	0.57%
2	1	0	4.8561	18.269	1.37%	1	4	0	3.5685	24.951	1.05%
1	-2	-2	4.7734	18.588	1.46%	1	3	4	3.5184	25.313	0.55%
1	2	3	4.7086	18.846	1.66%	1	4	3	3.4945	25.488	1.14%
1	3	2	4.6708	19	2.68%	1	3	-2	3.4276	25.995	0.76%
1	3	0	4.5989	19.3	0.53%	1	-3	2	3.3384	26.702	0.62%
0	2	-2	4.5661	19.439	1.66%	1	-2	-4	3.314	26.902	0.54%
2	1	2	4.5462	19.525	0.85%	3	2	0	3.1489	28.341	1.02%
2	0	-1	4.498	19.737	1.87%	1	4	4	3.1434	28.392	0.66%
2	0	2	4.3492	20.419	3.36%	1	2	5	3.106	28.742	0.51%
2	1	-1	4.3411	20.458	10.62%	1	-4	-3	3.0526	29.255	0.62%
0	1	-3	4.3115	20.599	3.31%	1	-3	3	2.9002	30.829	0.63%
2	-1	1	4.3086	20.614	0.58%	3	-2	-1	2.796	32.009	1.08%
1	-3	-1	4.195	21.178	2.30%	3	4	2	2.7462	32.606	0.78%
1	-3	0	4.1276	21.528	3.26%	3	4	3	2.6782	33.457	0.58%
1	-2	2	4.1263	21.535	0.68%	4	1	2	2.483	36.175	0.50%

(iii) UT-3, $[Al_2P_3O_{12}H]^{2-}[C_5H_9NH_3^+]_2$

Fractional Atomic Coordinates ($\times 10^4$) and Equivalent Isotropic Displacement Parameters ($Å^2 \times 10^3$) for UT-3

	x	y	z	U(eq)		x	y	z	U(eq)
Al(1)	2872(1)	7725(1)	3044(1)	39(1)	O(11)	6932(3)	7458(1)	6569(3)	61(1)
Al(2)	8369(1)	7750(1)	3271(1)	41(1)	O(12)	7563(3)	7943(1)	4617(3)	55(1)
P(1)	1264(1)	7051(1)	4454(1)	40(1)	N(1)	3819(4)	8568(1)	7222(4)	57(1)
P(2)	744(1)	8535(1)	3373(1)	44(1)	C(11)	4732(6)	8933(2)	8373(6)	74(1)
P(3)	6339(1)	7856(1)	5363(1)	43(1)	C(12)	3767(7)	9226(2)	9054(7)	94(2)
O(1)	-230(3)	7328(1)	4178(3)	58(1)	C(13)	4724(12)	9258(4)	10788(9)	167(4)
O(2)	952(3)	6535(1)	4400(3)	53(1)	C(14)	5830(14)	8878(5)	11141(10)	222(7)
O(3)	2500(3)	7200(1)	6040(3)	51(1)	C(15)	5985(8)	8697(3)	9778(7)	114(3)
O(4)	893(4)	8830(1)	4772(3)	58(1)	N(2)	-1077(4)	6155(1)	1546(4)	58(1)
O(5)	694(4)	8856(1)	1960(4)	57(1)	C(21)	-1394(12)	5672(3)	1755(9)	144(4)
O(6)	-744(3)	8237(1)	2776(3)	55(1)	C(22)	-2558(13)	5431(3)	358(11)	185(5)
O(7)	2158(3)	8202(1)	3767(3)	51(1)	C(23)	-2674(22)	4971(4)	877(21)	301(11)
O(8)	1939(3)	7198(1)	3183(3)	48(1)	C(24)	-1859(26)	4999(5)	2626(21)	314(10)
O(9)	4854(3)	7662(1)	4060(3)	51(1)	C(25)	-1011(18)	5432(3)	3059(13)	239(8)
O(10)	6077(3)	8298(1)	6084(4)	61(1)					

Hydrogen Fractional Coordinates ($\times 10^4$) and Isotropic Displacement Parameters ($Å^2 \times 10^3$) for UT-3

	x	y	z	U(eq)		x	y	z	U(eq)
H(5O)	606(57)	8689(19)	1136(58)	70(15)	H(2A)	-423(29)	6273(3)	2471(10)	82(7)
H(1A)	2956(20)	8698(3)	6508(23)	82(7)	H(2B)	-1977(6)	6318(2)	1217(36)	82(7)
H(1B)	3540(33)	8339(6)	7743(6)	82(7)	H(2C)	-634(34)	6177(2)	820(28)	82(7)
H(1C)	4411(14)	8447(8)	6722(28)	82(7)	H(21A)	-490(12)	5558(3)	1519(9)	173
H(11A)	5244(6)	9141(2)	7843(6)	89	H(22A)	-3572(13)	5590(3)	20(11)	222
H(12A)	3578(7)	9538(2)	8572(7)	113	H(22B)	-2199(13)	5427(3)	-530(11)	222
H(12B)	2758(7)	9076(2)	8873(7)	113	H(23A)	-2158(22)	4746(4)	419(21)	361
H(13A)	5270(12)	9559(4)	11040(9)	201	H(23B)	-3770(22)	4879(4)	591(21)	361
H(13B)	4055(12)	9228(4)	11405(9)	201	H(24A)	-2627(26)	4979(5)	3134(21)	377
H(14A)	6851(14)	8988(5)	11868(10)	267	H(24B)	-1134(26)	4736(5)	2997(21)	377
H(14B)	5487(14)	8627(5)	11674(10)	267	H(25B)	-1306(18)	5600(3)	3845(13)	287
H(15A)	5836(8)	8357(3)	9727(7)	137	H(25A)	118(18)	5374(3)	3504(13)	287
H(15B)	7027(8)	8766(3)	9779(7)	137					

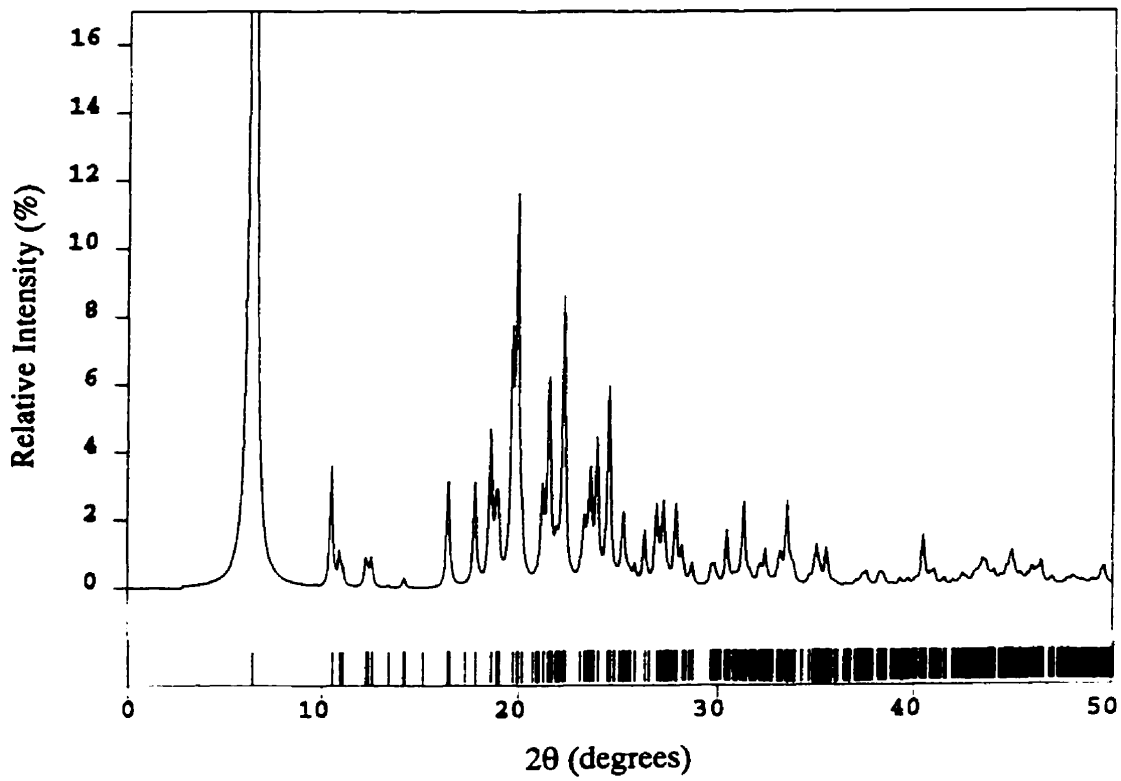

h	k	l	d-spacing	2θ	Relative Intensity	h	k	l	d-spacing	2θ	Relative Intensity
0	2	0	14.1445	6.248	100.00%	2	2	-2	3.6278	24.537	0.70%
1	0	0	8.4666	10.448	3.59%	0	8	0	3.5361	25.184	0.52%
1	1	0	8.1111	10.907	0.85%	2	5	-1	3.5281	25.242	1.68%
0	4	0	7.0722	12.516	0.78%	1	6	1	3.456	25.778	0.52%
0	4	1	5.4006	16.413	2.87%	2	5	0	3.3895	26.292	1.62%
1	1	1	5.0006	17.736	3.04%	2	4	-2	3.3154	26.891	2.24%
1	2	1	4.7815	18.556	4.39%	1	1	2	3.2727	27.248	2.19%
1	5	0	4.7041	18.864	1.32%	1	8	-1	3.199	27.889	2.30%
0	5	1	4.6864	18.936	1.72%	1	7	1	3.1628	28.215	0.97%
1	5	-1	4.5182	19.648	6.41%	1	3	2	3.1104	28.7	0.62%
1	3	1	4.4727	19.849	0.62%	2	7	-1	3.0106	29.673	0.52%
1	0	-2	4.4664	19.878	5.40%	2	6	-2	2.9365	30.439	1.42%
2	1	-1	4.4566	19.922	4.96%	2	5	1	2.8592	31.283	1.81%
1	1	-2	4.4118	20.126	1.14%	1	3	-3	2.859	31.285	0.61%
2	1	0	4.1867	21.221	2.48%	1	4	-3	2.762	32.414	0.52%
0	1	2	4.1373	21.477	2.72%	3	3	0	2.7037	33.132	0.55%
1	4	1	4.1263	21.535	2.83%	3	5	-1	2.6765	33.479	0.82%
1	6	0	4.1192	21.573	1.00%	3	4	-2	2.6751	33.497	1.00%
2	2	0	4.0556	21.915	0.62%	0	3	3	2.6737	33.515	0.53%
1	6	-1	3.9926	22.265	8.42%	2	7	1	2.5623	35.019	0.98%
0	3	2	3.8231	23.266	1.52%	2	1	2	2.5301	35.478	0.73%
2	4	-1	3.8044	23.382	0.53%	2	8	-3	2.2281	40.483	0.82%
1	5	1	3.7802	23.534	2.97%	2	5	-4	2.0773	43.568	0.54%
2	1	-2	3.7207	23.915	4.11%	3	1	2	2.0123	45.05	0.51%
2	4	0	3.6323	24.506	5.32%						

(iv) UT-4, $[Al_2P_3O_{12}H]^{2-}[C_6H_{11}NH_3^+]_2$

Fractional Atomic Coordinates ($\times 10^4$) and Equivalent Isotropic Displacement Parameters ($Å^2 \times 10^3$) for UT-4

	x	y	z	U(eq)		x	y	z	U(eq)
Al(1)	-134(1)	3995(1)	1081(1)	17(1)	O(12)	168(2)	4686(1)	2479(3)	21(1)
Al(2)	59(1)	6825(1)	3575(2)	16(1)	N(1)	2678(3)	6702(2)	4612(5)	29(1)
P(1)	1171(1)	7942(1)	2251(1)	17(1)	C(1)	3694(4)	6537(3)	5091(7)	40(1)
P(2)	-1552(1)	7926(1)	2962(1)	19(1)	C(2)	3983(5)	6111(5)	3921(12)	89(3)
P(3)	578(1)	5438(1)	2493(1)	16(1)	C(3)	5038(6)	5948(5)	4475(16)	124(5)
O(1)	600(3)	8200(2)	601(4)	40(1)	C(4)	5599(5)	6631(6)	4792(13)	96(3)
O(2)	2191(2)	7873(2)	2360(4)	29(1)	C(5)	5309(5)	7053(5)	5954(12)	89(3)
O(3)	988(2)	8462(2)	3488(4)	26(1)	C(6)	4266(5)	7214(4)	5505(9)	59(2)
O(4)	-858(2)	8498(2)	3864(4)	29(1)	N(2)	-1812(3)	5665(2)	4311(5)	27(1)
O(5)	-1982(2)	8109(2)	1228(4)	29(1)	C(7)	-2658(4)	5495(2)	2943(6)	29(1)
O(6)	-2337(2)	7849(2)	3841(4)	26(1)	C(8)	-2918(5)	6105(3)	1791(7)	47(2)
O(7)	1530(2)	5486(2)	3681(4)	25(1)	C(9)	-3752(6)	5900(4)	379(9)	74(2)
O(8)	621(2)	5630(2)	790(3)	22(1)	C(10)	-3564(6)	5244(4)	-462(8)	84(3)
O(9)	776(2)	7217(2)	2551(4)	30(1)	C(11)	-3287(6)	4637(4)	688(9)	82(3)
O(10)	-1036(2)	7209(2	3165(4)	28(1)	C(12)	-2446(5)	4829(3)	2118(7)	51(2)
O(11)	-140(2)	5942(2)	2939(3)	20(1)					

Hydrogen Fractional Coordinates ($\times 10^4$) and Isotropic Displacement Parameters ($Å^2 \times 10^3$) for UT-4

	x	y	z	U(eq)		x	y	z	U(eq)
H(1O)	-2173(25)	7555(33)	4569(65)	95(29)	H(2A)	-1917(10)	6062(10)	4796(26)	41
H(1A)	2351(3)	6307(4)	4273(38)	43	H(2D)	-1313(6)	5725(18)	3932(7)	41
H(1B)	2556(5)	7020(13)	3816(27)	43	H(2E)	-1702(15)	5310(8)	5020(21)	41
H(1C)	2514(5)	6878(16)	5456(12)	43	H(7B)	-3190(4)	5397(2)	3389(6)	35
H(1D)	3818(4)	6256(3)	6086(7)	48	H(8B)	-2384(5)	6233(3)	1394(7)	56
H(2B)	3840(5)	6362(5)	2898(12)	107	H(8C)	-3083(5)	6514(3)	2345(7)	56
H(2C)	3631(5)	5670(5)	3755(12)	107	H(9A)	-4301(6)	5823(4)	773(9)	89
H(3B)	5177(6)	5665(5)	5455(16)	148	H(9B)	-3894(6)	6289(4)	-389(9)	89
H(3C)	5217(6)	5676(5)	3649(16)	148	H(10A)	-4126(6)	5118(4)	-1306(8)	101
H(4B)	6266(5)	6522(6)	5193(13)	115	H(10B)	-3062(6)	5337(4)	-966(8)	101
H(4C)	5502(5)	6895(6)	3791(13)	115	H(11A)	-3123(6)	4232(4)	124(9)	98
H(5B)	5654(5)	7497(5)	6096(12)	107	H(11B)	-3818(6)	4503(4)	1087(9)	98
H(5C)	5479(5)	6806(5)	6984(12)	107	H(12A)	-2314(5)	4440(3)	2886(7)	61
H(6B)	4108(5)	7532(4)	4583(9)	71	H(12B)	-1892(5)	4906(3)	1738(7)	61
H(6C)	4111(5)	7450(4)	6401(9)	71					

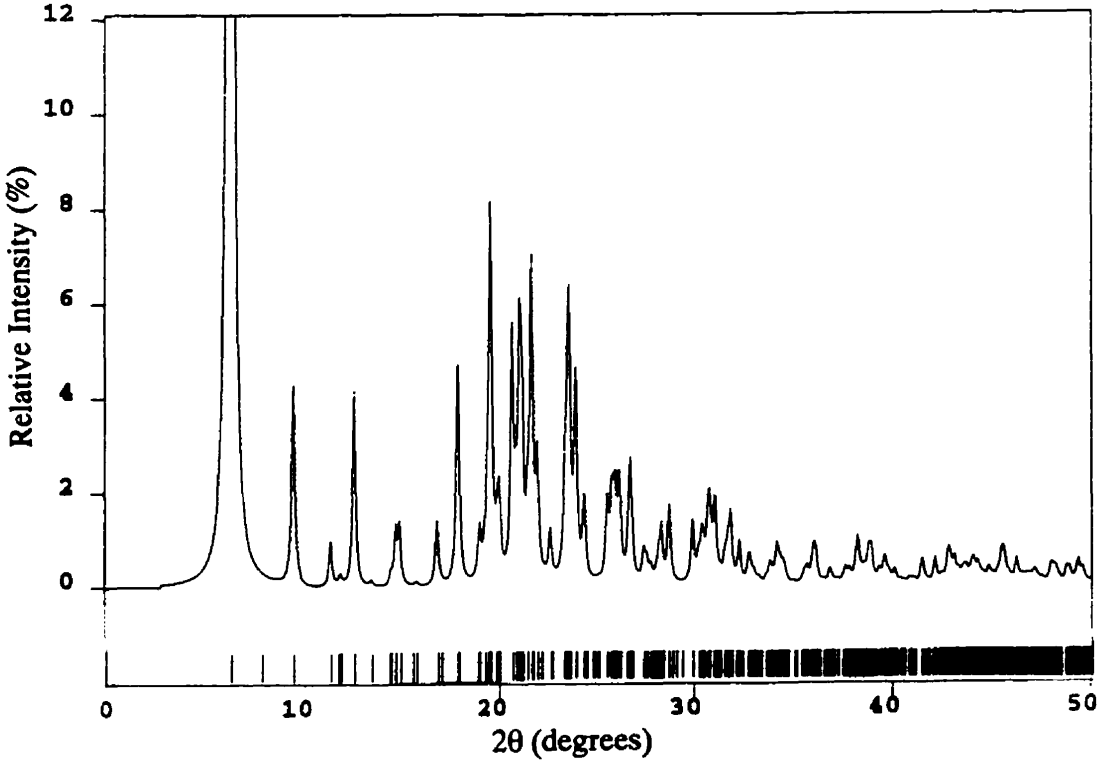

h	k	l	d-spacing	2θ	Relative Intensity	h	k	l	d-spacing	2θ	Relative Intensity
1	0	0	14.1758	6.235	100.00%	3	4	1	2.905	30.778	1.31%
3	1	-1	4.5544	19.49	7.52%	2	1	-1	5.9764	14.822	1.23%
0	4	1	4.0926	21.715	6.02%	1	3	-1	4.9823	17.802	1.20%
1	0	-2	4.2997	20.656	5.02%	2	6	-1	2.8101	31.844	1.09%
3	2	0	4.2235	21.033	4.32%	2	2	-2	3.7542	23.699	1.08%
0	2	0	9.4185	9.39	4.20%	1	1	1	6.0771	14.575	1.07%
2	0	0	7.0879	12.488	4.15%	2	2	1	4.259	20.856	1.06%
1	0	2	3.7071	24.005	4.15%	0	0	2	4.1362	21.483	1.02%
0	3	1	5.0014	17.733	3.79%	1	4	2	2.9128	30.693	1.02%
3	3	-1	3.7594	23.665	3.66%	4	3	-1	3.1478	28.351	1.00%
0	1	2	4.0399	22.001	2.39%	2	4	0	3.9224	22.669	0.97%
1	1	-2	4.1919	21.194	2.06%	1	2	0	7.8448	11.279	0.94%
3	1	0	4.5833	19.366	1.92%	1	2	2	3.4495	25.827	0.85%
1	4	1	3.7973	23.426	1.89%	2	5	-2	2.7721	32.293	0.84%
3	4	-1	3.3244	26.816	1.89%	2	3	0	4.7	18.88	0.80%
2	4	-1	3.7724	23.583	1.66%	0	5	1	3.4286	25.987	0.80%
2	3	-1	4.448	19.961	1.62%	0	3	2	3.4541	25.792	0.79%
0	4	2	3.1077	28.725	1.61%	0	8	0	2.3546	38.221	0.75%
4	1	0	3.4828	25.575	1.59%	3	4	0	3.3356	26.725	0.74%
3	2	-1	4.2009	21.148	1.56%	4	2	2	2.3143	38.913	0.68%
4	4	-1	2.879	31.062	1.53%	4	2	-1	3.3937	26.259	0.67%
3	2	-2	3.4002	26.208	1.48%	1	8	0	2.3228	38.766	0.65%
1	1	2	3.6373	24.472	1.40%	1	5	1	3.2493	27.448	0.62%
1	2	1	5.3051	16.711	1.37%	5	4	-1	2.4941	36.009	0.55%
4	2	-2	2.9882	29.9	1.31%	3	2	1	3.4364	25.927	0.52%

(v) UT-5, $[Al_2P_3O_{12}H]^{2-}[C_6H_{11}NH_3^+]_2$

Fractional Atomic Coordinates ($\times 10^4$) and Equivalent Isotropic Displacement Parameters ($Å^2 \times 10^3$) for UT-5

	x	y	z	U(eq)		x	y	z	U(eq)
Al(1)	12019(3)	2277(1)	1826(3)	10(1)	O(12)	11219(7)	1838(2)	2478(7)	15(1)
Al(2)	7476(3)	2265(1)	2107(3)	10(1)	N(1)	6803(9)	1552(3)	8053(9)	15(2)
P(1)	14025(3)	2141(1)	-317(3)	10(1)	C(1)	6239(11)	1247(3)	6685(10)	15(2)
P(2)	9059(3)	2908(1)	689(3)	9(1)	C(2)	4993(13)	1446(3)	5263(12)	24(2)
P(3)	9771(3)	1540(1)	1894(3)	12(1)	C(3)	4438(14)	1120(4)	3893(13)	33(3)
O(1)	12746(7)	2079(2)	427(7)	16(2)	C(4)	3872(14)	703(4)	4388(14)	37(3)
O(2)	13481(7)	2495(2)	-1568(7)	19(2)	C(5)	5093(14)	508(4)	5858(14)	36(3)
O(3)	14273(8)	1718(2)	-997(7)	19(2)	C(6)	5705(13)	833(3)	7254(12)	25(2)
O(4)	15504(7)	2313(2)	994(7)	16(2)	N(2)	11489(9)	1231(3)	-1484(9)	15(2)
O(5)	10545(7)	2651(2)	870(7)	16(2)	C(7)	11666(11)	768(3)	-1837(11)	15(2)
O(6)	7759(8)	2781(2)	-897(7)	16(2)	C(8)	10077(13)	549(4)	-2495(14)	31(3)
O(7)	9373(8)	3381(2)	790(7)	19(2)	C(9)	10282(16)	63(4)	-2792(17)	47(3)
O(8)	8436(7)	2756(2)	1999(7)	10(1)	C(10)	11394(17)	-159(4)	-1294(18)	49(4)
O(9)	8280(7)	1826(2)	1477(7)	14(1)	C(11)	12919(16)	62(4)	-669(16)	46(3)
O(10)	9696(8)	1266(2)	499(7)	18(2)	C(12)	12767(14)	542(4)	-352(13)	32(3)
O(11)	9841(8)	1237(2)	3323(8)	21(2)					

Hydrogen Fractional Coordinates ($\times 10^4$) and Isotropic Displacement Parameters ($Å^2 \times 10^3$) for UT-5

	x	y	z	U(eq)		x	y	z	U(eq)
H(11C)	9765(158)	1388(5)	4068(61)	57(43)	H(2C)	10869(58)	1367(5)	-2389(18)	23
H(1B)	7311(62)	1778(10)	7802(27)	22	H(2D)	12454(11)	1359(5)	-1110(68)	23
H(1C)	7476(54)	1411(6)	8920(21)	22	H(2E)	11036(66)	1249(3)	-735(54)	23
H(1D)	5966(11)	1653(15)	8276(46)	22	H(7A)	12154(11)	756(3)	-2668(11)	18
H(1A)	7157(11)	1173(3)	6372(10)	18	H(8A)	9424(13)	689(4)	-3507(14)	38
H(2A)	5423(13)	1707(3)	4921(12)	29	H(8B)	9528(13)	579(4)	-1731(14)	38
H(2B)	4089(13)	1538(3)	5553(12)	29	H(9A)	9242(16)	-82(4)	-3141(17)	56
H(3A)	3571(14)	1249(4)	2990(13)	39	H(9B)	10706(16)	34(4)	-3656(17)	56
H(3B)	5317(14)	1055(4)	3527(13)	39	H(10A)	10910(17)	-161(4)	-470(18)	59
H(4A)	3614(14)	492(4)	3502(14)	44	H(10B)	11556(17)	-464(4)	-1544(18)	59

H(4B)	2897(14)	761(4)	4602(14)	44	H(11A)	13457(16)	31(4)	-1442(16)	56
H(5A)	5993(14)	403(4)	5586(14)	43	H(11B)	13583(16)	-80(4)	336(16)	56
H(5B)	4628(14)	255(4)	6203(14)	43	H(12A)	12356(14)	575(4)	520(13)	38
H(6A)	4858(13)	900(3)	7664(12)	30	H(12B)	13819(14)	680(4)	-10(13)	38
H(6B)	6598(13)	704(3)	8132(12)	30					

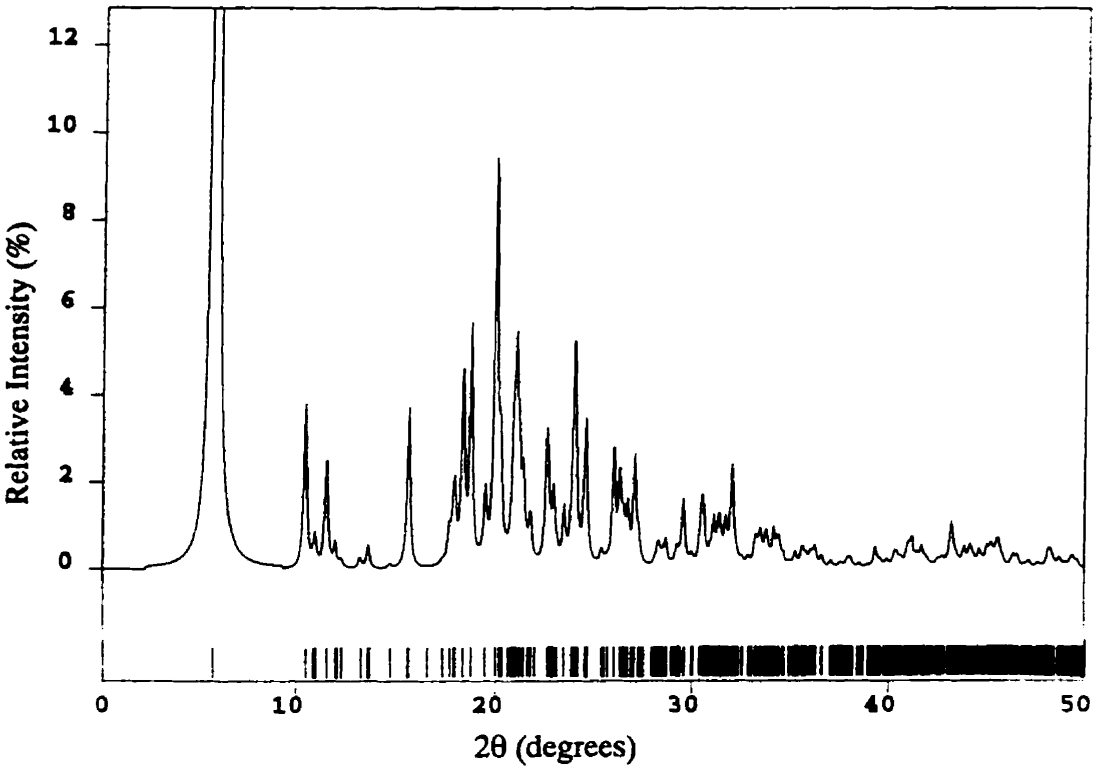

h	k	l	d-spacing	2θ	Relative Intensity	h	k	l	d-spacing	2θ	Relative Intensity
0	2	0	15.424	5.73	100.00%	2	3	0	3.9236	22.662	0.87%
1	0	0	8.4895	10.42	3.78%	0	3	2	3.8867	22.88	1.53%
0	1	1	8.1016	10.92	0.64%	1	7	-1	3.7954	23.438	1.20%
0	4	0	7.712	11.474	2.46%	2	4	0	3.7187	23.929	2.87%
1	2	0	7.4373	11.899	0.53%	2	1	-2	3.7072	24.004	2.87%
0	4	1	5.6797	15.601	3.67%	2	5	-1	3.6347	24.49	0.82%
1	1	1	5.048	17.568	0.71%	2	2	-2	3.6294	24.527	2.50%
1	5	0	4.9908	17.771	0.91%	1	8	-1	3.4263	26.005	2.61%
0	5	1	4.9717	17.84	1.40%	2	6	-1	3.3854	26.325	1.87%
1	2	1	4.8567	18.266	4.26%	2	4	-2	3.3609	26.52	0.60%
1	5	-1	4.7565	18.654	5.41%	1	7	1	3.3392	26.695	1.21%
1	3	1	4.5811	19.375	1.54%	1	1	2	3.2982	27.034	2.48%
1	0	-2	4.4565	19.922	6.23%	2	6	0	3.2733	27.243	0.52%
2	1	-1	4.4511	19.947	3.85%	1	9	-1	3.1151	28.655	0.58%
1	1	-2	4.4107	20.131	1.00%	2	6	-2	3.0214	29.564	1.49%
1	6	0	4.3977	20.191	1.62%	2	5	1	2.9333	30.473	1.09%
1	4	1	4.2638	20.833	2.24%	2	8	-1	2.9276	30.535	1.03%
2	0	0	4.2447	20.927	0.54%	3	0	-2	2.8769	31.086	0.87%
1	6	-1	4.2349	20.977	3.81%	1	10	-1	2.8512	31.374	0.67%
2	1	0	4.2051	21.127	1.80%	3	4	-1	2.823	31.695	0.74%
0	1	2	4.1598	21.359	1.77%	2	6	1	2.7975	31.991	1.52%
1	3	-2	4.089	21.734	0.65%	1	4	-3	2.7956	32.014	0.78%
1	5	1	3.9386	22.574	2.70%	0	4	3	2.6309	34.077	0.77%

(vi) UT-6, $[Al_3P_3O_{12}F]^-[C_5H_5NH^+]\bullet 0.15(H_2O)$

Fractional Atomic Coordinates ($\times 10^4$) and Equivalent Isotropic Displacement Parameters ($Å^2 \times 10^3$) for UT-6

	x	y	z	U(eq)		x	y	z	U(eq)
Al(1)	6296(1)	1572(1)	10791(1)	10(1)	O(7)	2251(2)	6216(2)	12879(2)	16(1)
Al(2)	1345(1)	4377(1)	9148(1)	10(1)	O(8)	-11(2)	6446(2)	11881(2)	13(1)
Al(3)	3938(1)	6214(1)	13440(1)	11(1)	O(9)	2540(2)	5081(2)	7417(2)	15(1)
P(1)	3812(1)	1856(1)	9004(1)	9(1)	O(10)	3524(2)	6754(2)	5231(2)	16(1)
P(2)	1700(1)	6455(1)	11433(1)	10(1)	O(11)	3627(2)	7551(2)	7652(2)	16(1)
P(3)	3724(1)	6207(1)	6762(1)	9(1)	O(12)	5293(2)	5531(2)	6613(2)	17(1)
F(1)	-129(1)	3924(1)	10822(1)	13(1)	N(1)	1140(4)	2363(4)	5518(4)	63(1)
O(1)	7744(2)	2022(2)	9276(2)	16(1)	C(2)	828(6)	2707(5)	4208(6)	74(1)
O(2)	4575(2)	1884(2)	10306(2)	20(1)	C(3)	1299(7)	1814(6)	3111(5)	80(2)
O(3)	3529(2)	269(2)	8735(2)	18(1)	C(4)	2115(6)	617(5)	3332(5)	73(1)
O(4)	4868(2)	2494(2)	7611(2)	19(1)	C(5)	2469(6)	338(5)	4666(6)	84(2)
O(5)	2339(2)	2648(2)	9306(2)	14(1)	C(6)	1927(6)	1227(6)	5767(5)	80(2)
O(6)	2353(2)	5308(2)	10378(2)	14(1)	O(1W)	-140(33)	241(31)	916(30)	104(8)

Hydrogen Fractional Coordinates ($\times 10^4$) and Isotropic Displacement Parameters ($Å^2 \times 10^3$) for UT-6

	x	y	z	U(eq)		x	y	z	U(eq)
H(1B)	783(4)	2942(4)	6257(4)	139(10)	H(4B)	2442(6)	-35(5)	2564(5)	139(10)
H(2B)	274(6)	3583(5)	4054(6)	139(10)	H(5B)	3096(6)	-483(5)	4824(6)	139(10)
H(3B)	1043(7)	2029(6)	2174(5)	139(10)	H(6B)	2145(6)	1023(6)	6722(5)	139(10)

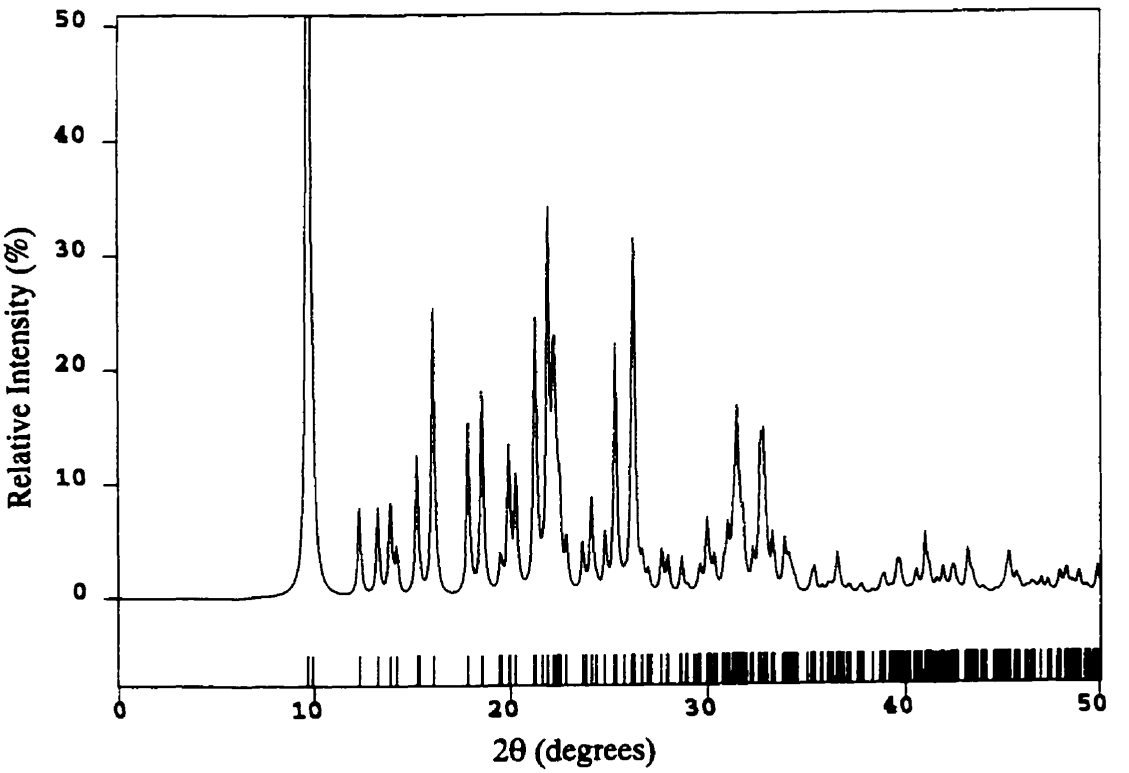

h	k	l	d-spacing	2θ	Relative Intensity	h	k	l	d-spacing	2θ	Relative Intensity
0	1	0	9.1384	9.678	67.52%	1	3	-1	2.6481	33.849	6.59%
0	0	1	9.0909	9.729	100.00%	2	-1	3	2.6329	34.05	3.24%
1	0	0	8.9001	9.938	13.78%	1	-1	-3	2.6288	34.105	0.55%

1	0	1	7.1853	12.318	11.97%	3	-1	2	2.6235	34.176	1.84%
0	1	1	6.6759	13.262	11.91%	0	3	2	2.614	34.304	1.01%
1	1	0	6.3826	13.874	2.06%	0	2	3	2.6084	34.38	0.98%
1	-1	0	6.3692	13.903	10.64%	3	2	1	2.5485	35.214	1.29%
0	1	-1	6.2365	14.201	5.57%	3	1	-1	2.538	35.364	3.25%
1	1	1	5.807	15.257	18.79%	2	-3	0	2.5112	35.755	0.91%
1	-1	1	5.5022	16.108	39.01%	3	-2	1	2.4912	36.052	0.89%
1	-1	-1	4.9709	17.843	23.17%	2	-3	1	2.4627	36.483	2.52%
1	1	-1	4.787	18.534	27.48%	2	2	3	2.4608	36.513	2.51%
0	2	0	4.5692	19.426	4.05%	0	3	-2	2.4545	36.61	1.32%
0	0	2	4.5454	19.529	1.26%	1	-3	-2	2.4265	37.047	0.71%
1	0	2	4.4581	19.915	17.44%	3	2	2	2.4188	37.17	0.87%
2	0	0	4.4501	19.951	2.47%	1	-2	-3	2.3852	37.713	1.16%
2	0	1	4.3901	20.227	14.96%	3	1	3	2.349	38.317	0.56%
0	2	1	4.1987	21.159	4.81%	3	-2	2	2.3272	38.69	0.60%
0	1	2	4.1848	21.23	34.35%	2	3	-1	2.3207	38.802	1.08%
1	1	2	4.1182	21.578	0.89%	3	-2	-1	2.3142	38.915	2.01%
1	2	0	4.0683	21.846	8.07%	1	3	-2	2.2992	39.18	0.67%
1	-2	0	4.0614	21.883	42.62%	4	0	1	2.2782	39.556	3.42%
2	1	1	4.0122	22.155	16.05%	0	0	4	2.2727	39.655	1.66%
2	1	0	4.0042	22.2	9.01%	3	0	-2	2.2695	39.714	1.92%
2	-1	0	3.9976	22.237	10.01%	2	0	4	2.2291	40.465	0.63%
0	2	-1	3.9755	22.362	3.02%	0	3	3	2.2253	40.537	1.92%
1	2	1	3.9562	22.472	10.34%	4	0	0	2.225	40.542	0.71%
2	-1	1	3.9043	22.775	4.19%	4	-1	1	2.2007	41.011	4.44%
1	-1	2	3.9039	22.777	2.00%	2	1	4	2.2002	41.021	3.70%
1	-2	1	3.7624	23.647	6.48%	2	1	-3	2.191	41.2	2.72%
2	0	-1	3.6934	24.095	12.71%	3	3	1	2.1716	41.585	1.13%
1	-2	-1	3.6562	24.344	1.13%	1	-4	-1	2.155	41.921	3.14%
2	0	2	3.5926	24.781	7.57%	4	1	2	2.1514	41.993	0.63%
1	2	-1	3.5104	25.371	33.76%	1	2	4	2.1344	42.345	0.94%
2	-1	-1	3.4555	25.781	0.68%	2	-1	4	2.1326	42.382	1.47%
2	1	2	3.4085	26.143	7.38%	3	3	0	2.1275	42.488	2.50%
2	1	-1	3.3939	26.257	32.40%	3	3	2	2.0972	43.134	1.56%
1	1	-2	3.3917	26.275	17.09%	1	4	-1	2.0942	43.197	1.96%
0	2	2	3.3379	26.706	3.82%	1	-3	3	2.0937	43.208	1.00%
1	2	2	3.3048	26.979	2.60%	0	2	4	2.0924	43.237	0.63%
2	2	1	3.2224	27.682	5.87%	1	4	2	2.0915	43.257	1.34%
2	-2	0	3.1846	28.017	4.35%	2	-2	-3	2.086	43.376	0.95%
0	2	-2	3.1182	28.626	0.88%	1	-3	-3	2.0816	43.473	1.27%
2	-2	1	3.1119	28.686	4.34%	3	1	4	2.0071	45.173	1.17%
1	0	3	3.0793	28.996	0.94%	4	1	-1	2.0044	45.239	0.70%
0	0	3	3.0303	29.475	0.98%	4	2	0	2.0021	45.292	3.16%
3	0	1	3.0199	29.579	3.03%	2	-3	3	1.9997	45.35	1.06%
1	1	3	2.9818	29.966	9.09%	2	-4	1	1.9982	45.385	1.45%
1	-2	-2	2.9723	30.064	2.24%	3	3	-1	1.9842	45.724	1.84%
0	3	1	2.9494	30.303	4.31%	1	-4	2	1.9795	45.839	0.85%
2	2	2	2.9035	30.794	3.11%	2	-4	-1	1.9658	46.176	0.64%
1	3	0	2.8839	31.009	5.89%	3	-1	4	1.955	46.446	0.54%
2	0	-2	2.8829	31.019	1.34%	2	-2	4	1.952	46.523	0.71%
1	3	1	2.8621	31.25	3.82%	4	-1	3	1.9473	46.642	0.69%
1	-1	3	2.8584	31.292	5.20%	3	3	3	1.9357	46.939	1.93%
3	-1	1	2.8465	31.426	20.99%	3	0	-3	1.922	47.294	1.38%
2	2	-1	2.8367	31.538	3.01%	3	2	4	1.8985	47.915	1.49%
0	3	-1	2.8309	31.604	2.96%	3	-1	-3	1.8968	47.959	1.33%
3	-1	0	2.82	31.729	1.59%	4	-2	-1	1.888	48.198	0.71%
0	1	-3	2.8196	31.734	5.25%	0	4	3	1.887	48.226	1.78%
1	2	-2	2.8163	31.772	1.72%	0	3	4	1.884	48.306	1.32%
3	0	2	2.7747	32.261	4.32%	4	2	3	1.8755	48.539	0.63%
2	-2	2	2.7511	32.546	1.24%	2	-3	-3	1.8736	48.593	0.57%
1	-3	-1	2.7411	32.668	16.59%	1	0	5	1.8623	48.907	1.43%
2	1	3	2.7295	32.811	17.26%	2	3	4	1.8599	48.973	1.68%
2	1	-2	2.717	32.966	3.50%	2	-1	-4	1.8491	49.278	0.55%
1	0	-3	2.6959	33.231	6.42%	0	5	0	1.8277	49.895	3.35%
3	1	2	2.6877	33.336	1.24%						

(vii) UT-7, $[Al_3P_5O_{20}H]^{5-}[C_7H_{13}NH_3^+]_5$

Fractional Atomic Coordinates (× 10^4) and Equivalent Isotropic Displacement Parameters (Å^2 × 10^3) for UT-7

	x	y	z	U(eq)		x	y	z	U(eq)
Al(1)	-30(2)	-2926(1)	5548(1)	29(1)	C(16)	2687(9)	-1995(7)	2772(4)	74(3)
Al(2)	1289(2)	-327(1)	4206(1)	27(1)	C(17)	3291(7)	-2609(7)	3464(5)	80(3)
Al(3)	6513(2)	-1187(1)	4904(1)	25(1)	N(2)	7311(5)	226(4)	2760(3)	39(1)
P(1)	2201(2)	-4531(1)	5487(1)	34(1)	C(21)	7670(11)	458(6)	1927(5)	75(3)
P(2)	854(2)	-1313(1)	5980(1)	27(1)	C(22)	7454(29)	-208(9)	1591(7)	308(19)
P(3)	-750(1)	-1515(1)	4024(1)	27(1)	C(23)	8071(35)	-223(13)	854(8)	406(29)
P(4)	4141(1)	54(1)	3845(1)	25(1)	C(24)	7621(34)	499(12)	199(9)	304(19)
P(5)	6964(2)	-3147(1)	5898(1)	30(1)	C(25)	7455(29)	1424(13)	147(8)	233(12)
O(1)	3309(5)	-3998(4)	5429(3)	57(1)	C(26)	7642(31)	1769(13)	760(6)	273(16)
O(2)	2448(5)	-5461(3)	6035(3)	45(1)	C(27)	7240(19)	1389(7)	1547(6)	149(7)
O(3)	1908(6)	-4584(3)	4663(3)	52(1)	N(3)	3548(6)	-3213(4)	6609(3)	51(2)
O(4)	875(4)	-4003(3)	5720(3)	45(1)	C(31)	3167(10)	-3891(6)	7313(5)	84(3)
O(5)	-124(4)	-2440(3)	4552(2)	37(1)	C(32)	4077(14)	-4744(7)	7421(7)	122(5)
O(6)	714(4)	-2263(3)	5955(3)	40(1)	C(33)	4391(31)	-5325(14)	8183(8)	327(21)
O(7)	-1243(4)	-1621(3)	3310(3)	43(1)	C(34)	4309(19)	-5129(15)	8913(8)	240(14)
O(8)	-1886(4)	-1081(3)	4489(2)	33(1)	C(35)	3172(25)	-4619(16)	9210(11)	265(16)
O(9)	-584(4)	-823(3)	6105(2)	35(1)	C(36)	2279(23)	-4013(14)	8636(9)	265(15)
O(10)	1769(4)	-1406(3)	6606(2)	40(1)	C(37)	2862(21)	-3485(8)	7929(6)	218(12)
O(11)	336(4)	-905(3)	3832(2)	34(1)	N(4)	307(6)	-6348(4)	6431(3)	49(2)
O(12)	1358(4)	-777(3)	5194(2)	37(1)	C(41)	-297(8)	-6320(4)	7212(4)	55(2)
O(13)	2931(4)	-408(3)	3830(2)	34(1)	C(42)	-845(11)	-5393(5)	7195(5)	83(3)
O(14)	4542(4)	553(3)	3048(2)	37(1)	C(43)	-1533(20)	-5169(10)	7853(6)	187(9)
O(15)	3705(4)	695(3)	4347(2)	35(1)	C(44)	-1270(22)	-5622(14)	8643(7)	242(13)
O(16)	5303(4)	-679(3)	4220(2)	37(1)	C(45)	-276(19)	-6380(10)	8984(7)	182(9)
O(17)	6347(4)	-2320(3)	5231(2)	35(1)	C(46)	170(16)	-7079(8)	8612(5)	135(6)
O(18)	8405(4)	-2988(3)	5986(3)	41(1)	C(47)	617(10)	-6877(7)	7809(4)	93(3)
O(19)	6218(4)	-3114(3)	6642(3)	41(1)	N(5)	-2530(5)	-2057(4)	7204(3)	42(1)
O(20)	6941(5)	-3977(3)	5669(3)	53(1)	C(51)	-1867(8)	-2498(5)	7953(4)	59(2)
N(1)	5179(6)	-3401(4)	4314(3)	43(1)	C(52)	-2862(12)	-2939(8)	8515(5)	108(4)
C(11)	4656(7)	-2724(10)	3648(6)	135(6)	C(53)	-2711(26)	-3084(15)	9346(7)	265(14)
C(12)	5679(10)	-2347(9)	3117(5)	110(5)	C(54)	-3041(19)	-2277(14)	9634(8)	177(9)
C(13)	5647(13)	-2289(15)	2320(7)	210(10)	C(55)	-2379(24)	-1469(13)	9341(10)	209(11)
C(14)	4611(11)	-1794(13)	1804(7)	160(7)	C(56)	-2117(16)	-1157(9)	8493(9)	170(9)
C(15)	3253(11)	-1948(12)	2013(6)	149(6)	C(57)	-1212(12)	-1834(7)	8175(6)	103(4)

Hydrogen Fractional Coordinates (× 10^4) and Isotropic Displacement Parameters (Å^2 × 10^3) for UT-7

	x	y	z	U(eq)		x	y	z	U(eq)
H(1O)	2349(82)	-5046(37)	4588(25)	113(40)	H(34A)	5141(19)	-4901(15)	8860(8)	288
H(1A)	4504(6)	-3622(22)	4612(13)	65	H(34B)	4433(19)	-5696(15)	9310(8)	288
H(1B)	5641(39)	-3162(8)	4577(14)	65	H(35A)	3641(25)	-4213(16)	9352(11)	318
H(1C)	5719(37)	-3844(15)	4172(3)	65	H(35B)	2786(25)	-4971(16)	9677(11)	318
H(11A)	4494(7)	-2249(10)	3895(6)	162	H(36A)	1718(23)	-3617(14)	8892(9)	318
H(12A)	6529(10)	-2679(9)	3318(5)	132	H(36B)	1739(23)	-4393(14)	8512(9)	318
H(12B)	5678(10)	-1725(9)	3083(5)	132	H(37A)	2329(21)	-2896(8)	7745(6)	261
H(13A)	5507(13)	-2893(15)	2370(7)	251	H(37B)	3731(21)	-3408(8)	8049(6)	261
H(13B)	6532(13)	-2243(15)	2093(7)	251	H(4A)	576(46)	-6920(4)	6430(9)	74
H(14A)	4872(11)	-1881(13)	1306(7)	192	H(4B)	1008(31)	-6057(29)	6326(13)	74
H(14B)	4643(11)	-1176(13)	1773(7)	192	H(4C)	-306(16)	-6082(30)	6073(5)	74
H(15A)	3218(11)	-2536(12)	1964(6)	178	H(41A)	-1047(8)	-6638(4)	7295(4)	66
H(15B)	2671(11)	-1519(12)	1635(6)	178	H(42A)	-1448(11)	-5153(5)	6773(5)	99
H(16A)	1758(9)	-2057(7)	2787(4)	89	H(42B)	-103(11)	-5067(5)	7062(5)	99
H(16B)	2710(9)	-1404(7)	2818(4)	89	H(43A)	-2469(20)	-5155(10)	7785(5)	225
H(17A)	2707(7)	-2547(7)	3898(5)	96	H(43B)	-1433(20)	-4555(10)	7791(6)	225
H(17B)	3261(7)	-3196(7)	3410(5)	96	H(44A)	-2120(22)	-5795(14)	8846(7)	290
H(2A)	7680(37)	561(21)	2979(6)	58	H(44B)	-1154(22)	-5158(14)	8866(7)	290
H(2B)	7616(38)	-356(8)	2979(6)	58	H(45A)	-616(19)	-6643(10)	9496(7)	218
H(2C)	6421(6)	333(28)	2826(3)	58	H(45B)	520(19)	-6155(10)	9039(7)	218
H(21A)	8631(11)	368(6)	1854(5)	91	H(46A)	-601(16)	-7358(8)	8617(5)	162
H(22A)	6558(29)	38(9)	1413(7)	370	H(46B)	826(16)	-7526(8)	8930(5)	162
H(22B)	7465(29)	-790(9)	1961(7)	370	H(47A)	1320(10)	-6531(7)	7782(4)	112

H(23A)	8287(35)	-808(13)	767(8)	487	H(47B)	1012(10)	-7423(7)	7683(4)	112
H(23B)	8878(35)	-16(13)	920(8)	487	H(5A)	-2910(39)	-2456(9)	7070(13)	64
H(24A)	6710(34)	390(12)	290(9)	365	H(5B)	-1921(10)	-1854(27)	6842(6)	64
H(24B)	7923(34)	420(12)	-297(9)	365	H(5C)	-3159(32)	-1597(19)	7250(8)	64
H(25A)	6636(29)	1757(13)	-96(8)	279	H(51A)	-1168(8)	-2964(5)	7864(4)	71
H(25B)	8159(29)	1594(13)	-228(8)	279	H(52A)	-2904(12)	-3500(8)	8412(5)	129
H(26A)	7159(31)	2376(13)	595(6)	327	H(52B)	-3728(12)	-2568(8)	8408(5)	129
H(26B)	8576(31)	1811(13)	764(6)	327	H(53A)	-1780(26)	-3317(15)	9452(7)	317
H(27A)	7448(19)	1742(7)	1862(6)	179	H(53B)	-3230(26)	-3539(15)	9628(7)	317
H(27B)	6280(19)	1433(7)	1563(6)	179	H(54A)	-2950(19)	-2465(14)	184(8)	213
H(3A)	2980(31)	-2696(11)	6554(16)	76	H(54B)	-3986(19)	-2095(14)	9546(8)	213
H(3B)	3515(49)	-3412(15)	6200(5)	76	H(55A)	-1574(24)	-1561(13)	9619(10)	250
H(3C)	4380(20)	-3123(25)	6648(13)	76	H(55B)	-2990(24)	-989(13)	9476(10)	250
H(31A)	2301(10)	-4006(6)	7227(5)	101	H(56A)	-1732(16)	-618(9)	8403(9)	204
H(32A)	4947(14)	-4585(7)	7250(7)	147	H(56B)	-2928(16)	-997(9)	8208(9)	204
H(32B)	3843(14)	-5063(7)	7085(7)	147	H(57A)	-749(12)	-1511(7)	7725(6)	123
H(33A)	5148(31)	-5784(14)	8154(8)	392	H(57B)	-554(12)	-2153(7)	8555(6)	123
H(33B)	3613(31)	-5617(14)	8267(8)	392					

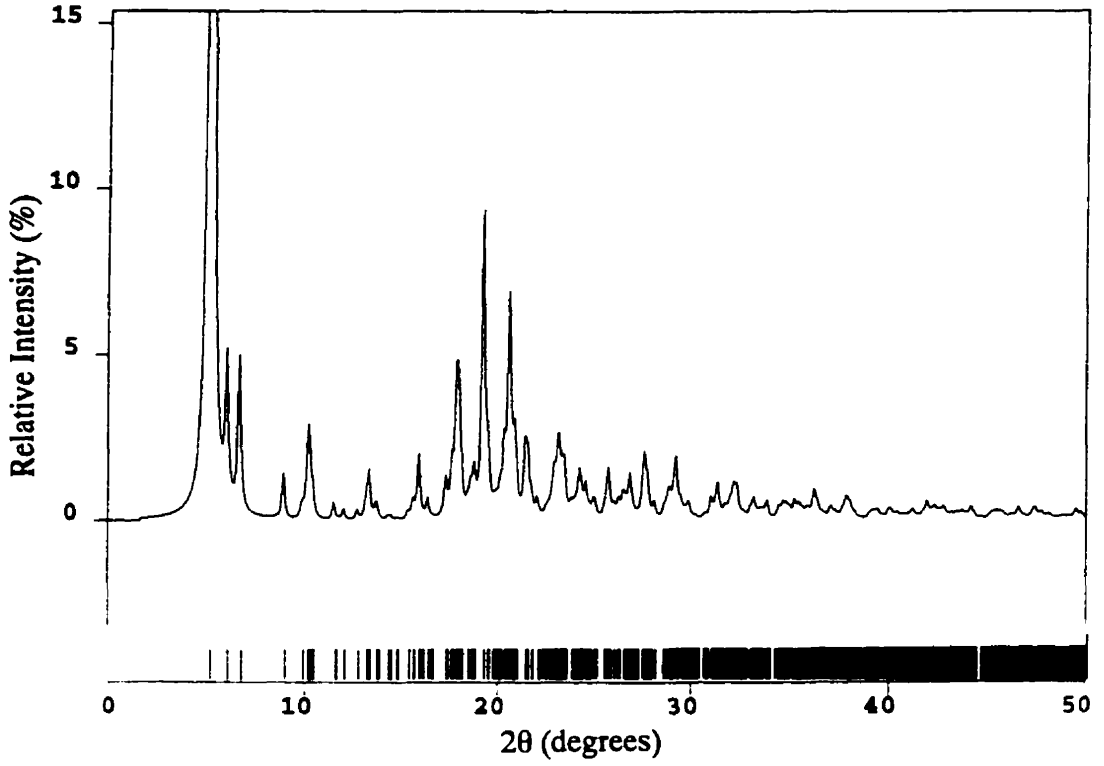

h	k	l	d-spacing	2θ	Relative Intensity	h	k	l	d-spacing	2θ	Relative Intensity
0	0	1	17.308	5.106	100.00%	1	3	3	4.3265	20.527	4.98%
0	1	0	14.7912	5.975	4.21%	0	2	4	4.3063	20.625	0.59%
0	1	1	13.2594	6.666	4.62%	2	-1	1	4.2898	20.705	0.58%
1	0	0	9.943	8.893	1.37%	1	-3	-1	4.2617	20.843	1.47%
1	0	1	8.7448	10.115	0.78%	2	0	-2	4.2518	20.892	0.54%
0	0	2	8.654	10.221	1.98%	1	-3	0	4.152	21.4	1.34%
1	0	-1	8.5036	10.403	0.75%	2	2	-1	4.1427	21.449	0.57%
1	-1	0	7.6838	11.516	0.50%	1	-3	-2	4.1244	21.545	1.60%
1	0	2	6.635	13.344	0.85%	2	1	-2	4.0884	21.737	0.52%
1	1	-2	5.6813	15.597	0.51%	2	3	2	3.8747	22.952	1.02%
1	-2	-1	5.575	15.896	1.86%	2	-2	-1	3.8519	23.089	0.56%
1	-1	2	5.4249	16.339	0.56%	2	3	0	3.8324	23.209	0.59%
1	-2	-2	5.1216	17.314	0.72%	2	0	3	3.8279	23.236	1.13%
1	2	3	5.0326	17.622	1.36%	1	4	2	3.8049	23.378	0.62%

1	-2	1	4.981	17.807	1.04%	1	3	4	3.7864	23.494	1.13%
2	0	0	4.9715	17.841	0.59%	1	4	0	3.6701	24.25	1.12%
0	2	-2	4.9678	17.854	1.36%	1	2	5	3.4657	25.704	0.54%
1	3	1	4.951	17.915	1.51%	0	0	5	3.4616	25.735	0.60%
0	1	-3	4.922	18.022	2.07%	1	-3	2	3.4517	25.81	0.63%
1	3	2	4.7798	18.563	0.67%	1	4	4	3.3221	26.835	0.88%
2	0	-1	4.7378	18.729	0.85%	3	2	0	3.2307	27.609	0.83%
2	1	-1	4.6206	19.208	8.98%	1	-4	-3	3.2145	27.751	0.54%
2	2	1	4.5701	19.422	0.51%	1	-3	3	3.0583	29.199	0.88%
2	1	2	4.5676	19.433	1.39%	3	-2	-1	2.853	31.352	0.66%
0	3	3	4.4198	20.09	0.54%	3	4	2	2.7685	32.336	0.79%
2	0	2	4.3724	20.31	1.69%	4	1	2	2.4746	36.302	0.50%
0	0	4	4.327	20.525	0.85%						

(viii) UT-8, $[Al_3P_4O_{16}]^{3-}[C_4H_9NH_3^+]_2[C_5H_{10}NH_2^+]$

Fractional Atomic Coordinates ($\times 10^4$) and Equivalent Isotropic Displacement Parameters ($Å^2 \times 10^3$) for UT-8

	x	y	z	U(eq)		x	y	z	U(eq)
Al(1)	-1466(3)	5123(2)	4361(3)	16(1)	O(14)	2709(7)	4710(5)	6159(7)	24(2)
Al(2)	-1503(3)	2348(2)	4111(2)	13(1)	O(15)	-3082(7)	2856(5)	4540(7)	25(2)
Al(3)	2922(2)	3741(3)	5271(2)	14(1)	O(16)	1630(5)	3711(7)	3645(5)	25(1)
P(1)	1542(2)	2100(2)	6557(2)	15(1)	N(1)	2393(9)	3591(8)	-312(8)	38(2)
P(2)	1613(2)	5318(2)	6748(2)	14(1)	C(1)	3696(29)	3416(17)	22(31)	147(12)
P(3)	-3509(2)	3669(2)	5330(2)	14(1)	C(2)	4881(33)	3953(34)	-601(26)	199(17)
P(4)	52(2)	3797(2)	2645(2)	13(1)	C(3)	5891(17)	3994(17)	1124(29)	133(12)
O(1)	2080(6)	6293(5)	6519(6)	22(1)	C(4)	4788(37)	3820(25)	1560(19)	161(12)
O(2)	1688(7)	5127(5)	8259(6)	23(2)	N(2)	1298(7)	-117(5)	1204(7)	21(2)
O(3)	2111(6)	1194(5)	6120(6)	24(1)	C(5)	2181(10)	729(9)	1103(10)	37(3)
O(4)	-741(8)	4626(5)	3056(7)	26(2)	C(6)	2015(19)	1472(11)	2081(18)	73(5)
O(5)	-910(8)	2960(5)	2826(6)	23(2)	C(7)	3588(26)	1629(31)	2547(30)	212(22)
O(6)	-5259(4)	3712(6)	4970(5)	20(1)	C(8)	3935(16)	687(15)	1839(27)	116(10)
O(7)	1444(7)	2094(5)	8062(6)	22(2)	N(3)	1671(8)	6954(7)	1929(8)	37(2)
O(8)	-2811(6)	3611(6)	6884(5)	30(2)	C(9)	4364(12)	6151(14)	1385(14)	81(6)
O(9)	169(5)	3862(6)	1140(5)	21(2)	C(10)	3575(15)	6999(16)	568(13)	87(6)
O(10)	-2983(7)	4525(5)	4691(7)	24(2)	C(11)	1897(13)	7010(12)	497(11)	51(3)
O(11)	2651(7)	2814(5)	6285(6)	20(1)	C(12)	2407(11)	6121(8)	2696(11)	36(3)
O(12)	-37(6)	2292(5)	5612(6)	25(2)	C(13)	4088(14)	6112(12)	2766(14)	58(4)
O(13)	-35(7)	5176(5)	5895(6)	25(2)					

Hydrogen Fractional Coordinates ($\times 10^4$) and Isotropic Displacement Parameters ($Å^2 \times 10^3$) for UT-8

	x	y	z	U(eq)		x	y	z	U(eq)
H(3B)	663(8)	6955(7)	1896(8)	44	H(2B)	4530(33)	4534(34)	-962(26)	239
H(3E)	2088(8)	7447(7)	2399(8)	44	H(2C)	5353(33)	3625(34)	-1231(26)	239
H(9B)	5444(12)	6139(14)	1438(14)	97	H(3C)	6336(17)	4564(17)	1448(29)	159
H(9C)	3908(12)	5625(14)	893(14)	97	H(3D)	6651(17)	3529(17)	1326(29)	159
H(10A)	3769(15)	7028(16)	-354(13)	104	H(4A)	4986(37)	3376(25)	2290(19)	193
H(10B)	4017(15)	7520(16)	1083(13)	104	H(4B)	4356(37)	4347(25)	1881(19)	193
H(11A)	1423(13)	7532(12)	5(11)	61	H(2D)	338(17)	23(6)	1213(57)	25
H(11B)	1452(13)	6486(12)	-8(11)	61	H(2E)	1730(36)	-408(19)	1990(29)	25
H(12A)	1973(11)	5593(8)	2195(11)	43	H(2F)	1302(52)	-466(17)	468(30)	25
H(12B)	2236(11)	6096(8)	3626(11)	43	H(5A)	1984(10)	942(9)	153(10)	45
H(13A)	4497(14)	6659(12)	3223(14)	70	H(6B)	1614(19)	1260(11)	2848(18)	88
H(13B)	4597(14)	5618(12)	3311(14)	70	H(6C)	1410(19)	1965(11)	1622(18)	88
H(1B)	1922(20)	3202(38)	-961(70)	57	H(7B)	3991(26)	1653(31)	3544(30)	255
H(1C)	2278(10)	4145(24)	-664(86)	57	H(7C)	3883(26)	2146(31)	2088(30)	255
H(1D)	1988(24)	3559(59)	433(21)	57	H(8B)	4576(16)	722(15)	1182(27)	139
H(1A)	3852(29)	2768(17)	-52(31)	177	H(8C)	4233(16)	202(15)	2491(27)	139

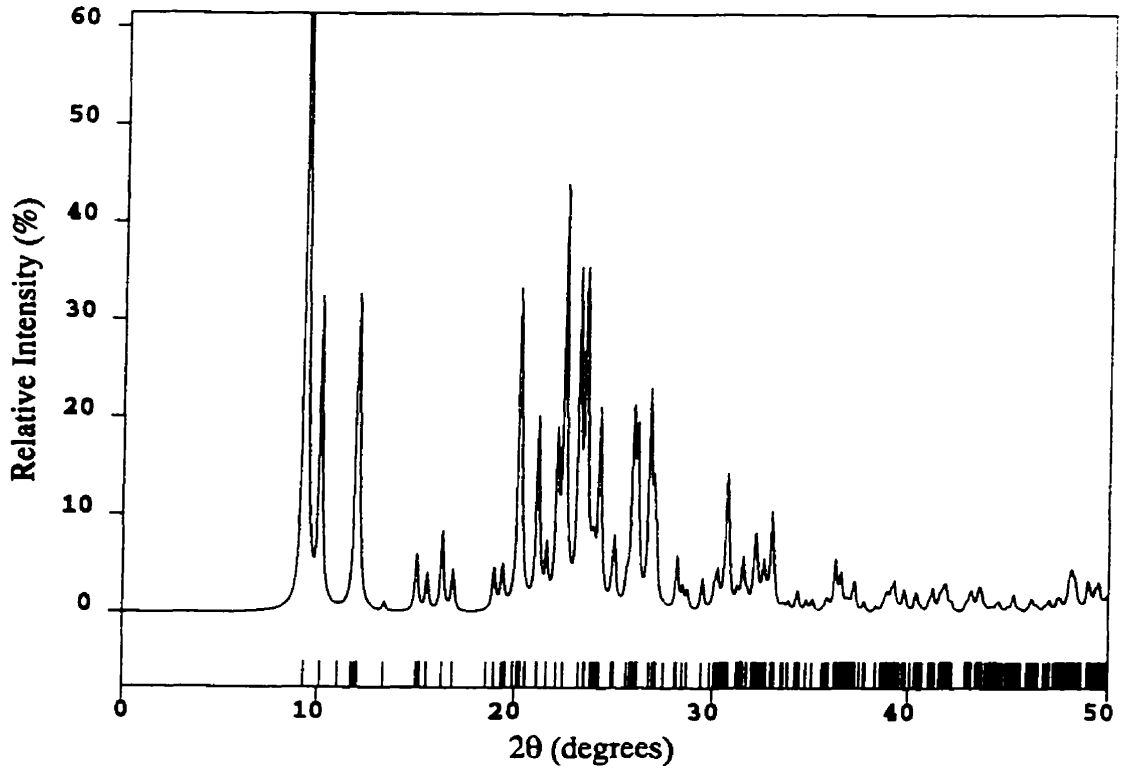

h	k	l	d-spacing	2θ	Relative Intensity	h	k	l	d-spacing	2θ	Relative Intensity
0	0	1	9.5275	9.282	100.00%	2	2	2	2.7028	33.144	1.06%
1	0	0	8.7438	10.116	31.30%	1	4	2	2.6669	33.603	0.56%
0	2	0	7.442	11.891	14.46%	1	5	1	2.6485	33.843	0.99%
1	0	-1	7.3554	12.032	29.10%	2	4	-2	2.6157	34.281	1.94%
1	1	-1	6.5941	13.427	0.95%	3	1	1	2.5812	34.753	1.25%
0	2	1	5.8649	15.106	6.01%	3	3	-1	2.5605	35.043	1.26%
1	2	0	5.6672	15.636	3.73%	2	3	-3	2.5125	35.736	0.93%
1	1	1	5.4056	16.398	8.37%	0	6	0	2.4807	36.21	5.33%
1	2	-1	5.2314	16.948	4.11%	3	2	1	2.4721	36.339	0.52%
1	0	-2	4.6665	19.017	4.27%	2	5	-1	2.4621	36.492	1.46%
1	2	1	4.5756	19.399	4.37%	2	5	0	2.4606	36.516	2.00%
0	3	1	4.4004	20.179	28.28%	1	4	-3	2.4426	36.795	0.84%
2	0	-1	4.3806	20.271	1.67%	1	3	3	2.4276	37.031	0.56%
2	0	0	4.3719	20.312	8.64%	3	1	-3	2.4192	37.163	1.37%
2	1	-1	4.2024	21.14	19.13%	1	1	-4	2.4154	37.224	1.72%
2	1	0	4.1947	21.18	0.66%	1	6	0	2.3865	37.692	1.04%
1	3	-1	4.1131	21.605	5.61%	1	5	2	2.3491	38.315	0.54%
0	2	2	4.0121	22.155	16.10%	3	3	1	2.3175	38.859	0.86%
1	2	-2	3.9536	22.488	42.96%	2	5	-2	2.3138	38.922	0.91%
1	0	2	3.8244	23.258	32.59%	2	1	-4	2.3051	39.075	1.62%
2	2	-1	3.7752	23.565	14.01%	3	4	0	2.2945	39.263	2.27%
1	3	1	3.7706	23.594	17.15%	0	2	4	2.2685	39.732	2.04%
2	2	0	3.7696	23.601	5.22%	3	0	2	2.2619	39.853	0.73%
0	4	0	3.721	23.913	2.70%	3	1	2	2.2362	40.331	1.22%
1	1	2	3.7041	24.024	3.40%	3	4	-2	2.2342	40.368	0.70%
2	0	-2	3.6777	24.199	2.08%	0	6	2	2.2002	41.02	0.65%
2	0	1	3.6622	24.303	19.15%	1	6	-2	2.1904	41.212	1.99%
2	1	-2	3.5703	24.939	1.78%	1	0	4	2.1729	41.559	1.09%
2	1	1	3.5562	25.04	6.42%	4	1	-2	2.167	41.678	0.68%
0	4	1	3.466	25.702	2.29%	4	1	0	2.1627	41.763	0.88%
0	3	2	3.4362	25.929	2.57%	2	6	-1	2.1586	41.848	1.15%
1	4	0	3.4239	26.024	16.45%	2	6	0	2.1575	41.869	0.98%
1	3	-2	3.3992	26.216	15.93%	0	3	4	2.1472	42.079	0.64%
1	4	-1	3.3203	26.85	21.32%	4	2	-2	2.1012	43.047	0.85%

2	2	-2	3.2971	27.043	7.92%	3	0	-4	2.1006	43.06	0.56%
2	3	-1	3.2838	27.155	5.20%	4	2	0	2.0973	43.13	1.37%
1	1	-3	3.1638	28.205	5.65%	3	5	0	2.0826	43.451	0.72%
1	4	1	3.1322	28.496	2.11%	3	1	-4	2.08	43.508	1.37%
0	1	3	3.1059	28.742	1.89%	0	7	1	2.0752	43.613	0.96%
1	3	2	3.0289	29.489	3.26%	3	5	-2	2.0372	44.471	0.86%
1	2	-3	2.969	30.099	2.04%	0	4	4	2.0061	45.198	1.74%
2	3	-2	2.9545	30.25	3.47%	2	4	3	1.9712	46.044	0.50%
0	2	3	2.921	30.605	1.13%	1	6	-3	1.9692	46.094	0.84%
3	0	0	2.9146	30.674	0.92%	3	0	3	1.9339	46.984	1.06%
1	4	-2	2.9093	30.731	10.35%	3	1	3	1.9178	47.403	1.06%
2	0	2	2.9009	30.823	4.23%	2	7	0	1.9121	47.551	0.55%
3	1	0	2.8603	31.271	1.52%	1	2	-5	1.895	48.01	1.91%
0	5	1	2.8413	31.485	0.56%	3	5	-3	1.8925	48.075	1.61%
2	4	-1	2.836	31.546	4.23%	1	5	-4	1.8907	48.125	0.74%
1	5	0	2.818	31.753	1.21%	2	6	-3	1.8888	48.175	0.65%
3	0	-2	2.7939	32.034	0.63%	4	4	0	1.8848	48.285	2.06%
1	0	3	2.7835	32.156	6.51%	0	8	0	1.8605	48.956	2.58%
3	2	-1	2.774	32.27	2.65%	2	2	-5	1.858	49.025	0.58%
1	5	-1	2.7594	32.445	0.80%	3	6	-2	1.855	49.111	0.57%
3	1	-2	2.7459	32.608	4.05%	0	2	5	1.8459	49.368	1.61%
1	1	3	2.7361	32.729	0.87%	2	7	-2	1.8408	49.516	2.03%
3	2	0	2.7139	33.005	8.17%	2	7	1	1.8388	49.572	0.62%
2	2	-3	2.7131	33.014	1.56%	0	8	1	1.826	49.944	1.48%

(ix) Cyclopentylammonium Monohydrogen Phosphate (CMP), $[C_5H_9NH_3^+]_2[HPO_4^{2-}]$

Fractional Atomic Coordinates ($\times 10^4$) and Equivalent Isotropic Displacement Parameters ($Å^2 \times 10^3$) for CMP

	x	y	z	U(eq)		x	y	z	U(eq)
P(1)	1076(1)	621(2)	945(1)	21(1)	C(4*)	-2917(10)	3186(25)	1608(9)	78(4)
O(1)	879(2)	3134(4)	966(2)	27(1)	C(5)	-1792(4)	3240(8)	1638(3)	47(1)
O(2)	1822(2)	-123(4)	1641(2)	30(1)	N(2)	1552(3)	-4230(6)	2275(2)	27(1)
O(3)	1293(2)	-51(4)	104(1)	26(1)	C(6)	746(3)	-4347(7)	2742(2)	31(1)
O(4)	131(2)	-672(5)	1102(2)	29(1)	C(7)	776(8)	-2787(19)	3409(6)	33(3)
N(1)	-1032(2)	4336(6)	428(2)	26(1)	C(8)	618(8)	-4173(17)	4156(6)	40(2)
C(1)	-1670(3)	5061(7)	1010(2)	33(1)	C(9)	244(6)	-6372(12)	3850(4)	22(2)
C(2)	-2729(8)	5232(20)	452(7)	46(3)	C(7*)	989(8)	-2863(17)	3582(6)	26(3)
C(3)	-3288(13)	3947(28)	984(10)	92(5)	C(8*)	1014(7)	-4558(16)	4259(5)	35(2)
C(4)	-2739(7)	2251(18)	1377(6)	47(3)	C(9*)	900(11)	-6574(22)	3939(7)	76(4)
C(2*)	-2614(8)	5769(18)	656(6)	36(3)	C(10)	632(4)	-6715(7)	3069(3)	45(1)
C(3*)	-3332(9)	5014(22)	1109(8)	60(3)					

Hydrogen Fractional Coordinates ($\times 10^4$) and Isotropic Displacement Parameters ($Å^2 \times 10^3$) for CMP

	x	y	z	U(eq)		x	y	z	U(eq)
H(1A)	-1465(3)	6515(7)	1276(2)	40	H(8B)	155(8)	-3420(17)	4457(6)	48
H(2A)	-2951(8)	6796(20)	380(7)	55	H(9A)	-461(6)	-6365(12)	3753(4)	26
H(2B)	-2742(8)	4520(20)	-88(7)	55	H(9B)	464(6)	-7566(12)	4246(4)	26
H(3A)	-3503(13)	4957(28)	1392(10)	110	H(7*1)	1611(8)	-2101(17)	3606(6)	32
H(3B)	-3860(13)	3304(28)	649(10)	110	H(7*2)	488(8)	-1730(17)	3615(6)	32
H(4A)	-2694(7)	982(18)	1002(6)	57	H(8*1)	1632(7)	-4470(16)	4624(5)	42
H(4B)	-3017(7)	1712(18)	1854(6)	57	H(8*2)	500(7)	-4240(16)	4586(5)	42
H(2*1)	-2630(8)	7419(18)	629(6)	43	H(9*1)	407(11)	-7352(22)	4198(7)	91
H(2*2)	-2755(8)	5191(18)	91(6)	43	H(9*2)	1504(11)	-7404(22)	4088(7)	91
H(3*1)	-3902(9)	4504(22)	736(8)	72	H(10A)	186(4)	-7601(7)	2679(3)	54
H(3*2)	-3523(9)	6231(22)	1455(8)	72	H(10B)	1254(4)	-7494(7)	3168(3)	54
H(4*1)	-3174(10)	1751(25)	1376(9)	93	H(11)	-1225(30)	2877(78)	200(24)	39(12)
H(4*2)	-3078(10)	3327(25)	2167(9)	93	H(12)	-415(29)	4064(62)	713(22)	23(10)
H(5A)	-1288(4)	2094(8)	1648(3)	57	H(13)	-1058(29)	5341(72)	-10(26)	33(11)
H(5B)	-1755(4)	3893(8)	2190(3)	57	H(21)	2022(33)	-4590(76)	2604(27)	41(13)
H(6A)	156(3)	-4012(7)	2351(2)	37	H(22)	1605(29)	-2710(77)	2068(24)	37(12)
H(7A)	270(8)	-1648(19)	3285(6)	39	H(23)	1467(28)	-5281(68)	1864(24)	27(11)
H(7B)	1401(8)	-2023(19)	3508(6)	39	H(4O)	-319(29)	-450(66)	785(23)	22(11)
H(8A)	1225(8)	-4361(17)	4530(6)	48					

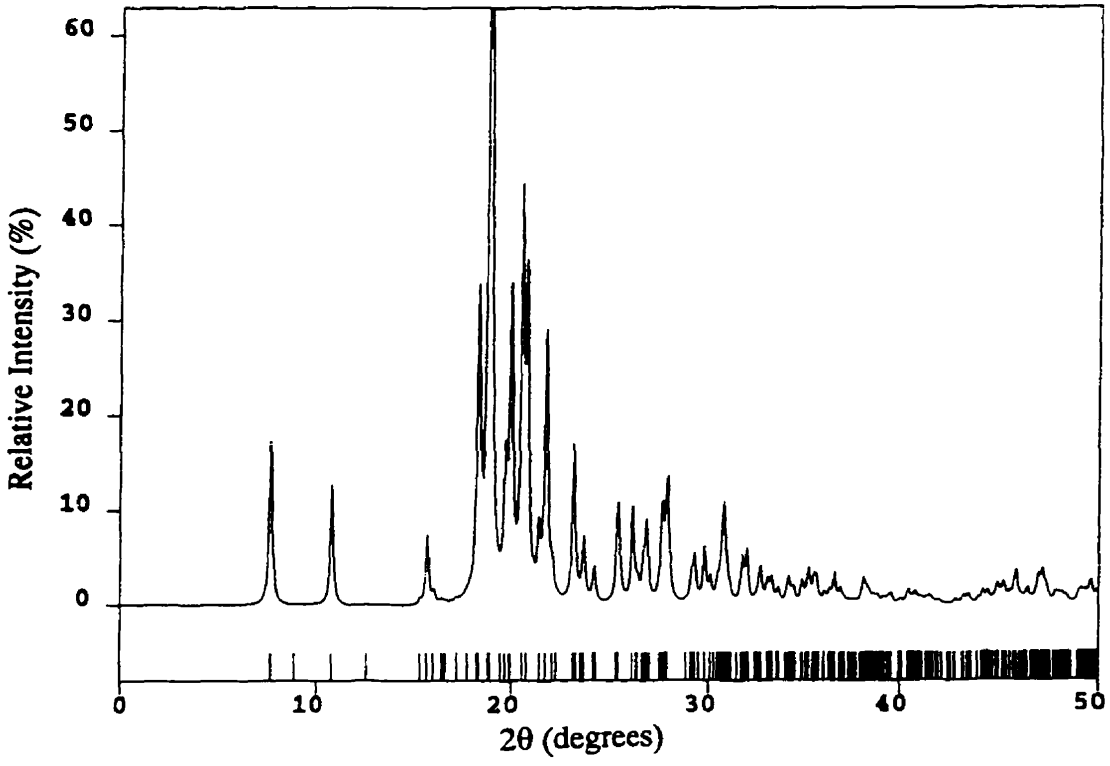

h	k	l	d-spacing	2θ	Relative Intensity	h	k	l	d-spacing	2θ	Relative Intensity
1	0	-1	11.5474	7.656	19.79%	2	1	5	2.5474	35.23	1.30%
0	0	2	8.1974	10.792	14.57%	5	1	0	2.5424	35.301	2.94%
2	0	-2	5.7737	15.346	0.50%	3	2	-1	2.5245	35.56	1.28%
0	1	1	5.6279	15.746	8.33%	3	2	0	2.5232	35.579	1.02%
1	1	0	5.511	16.082	1.28%	2	2	-3	2.5204	35.62	0.52%
1	0	3	4.854	18.276	15.05%	4	1	3	2.5153	35.695	1.25%
0	1	2	4.8374	18.339	23.59%	3	0	5	2.515	35.699	0.85%
1	1	-2	4.7027	18.87	100.00%	0	1	6	2.4862	36.127	0.80%
3	0	-1	4.6879	18.93	31.40%	3	2	-2	2.4679	36.404	1.25%
2	1	-1	4.5047	19.707	13.61%	2	1	-6	2.4504	36.673	3.49%
1	1	2	4.4545	19.932	35.10%	5	1	-3	2.4342	36.926	1.54%
3	0	1	4.3326	20.498	45.60%	5	0	3	2.3586	38.154	2.66%
2	1	1	4.2852	20.728	35.63%	2	2	-4	2.3513	38.277	0.93%
2	1	-2	4.1576	21.371	7.07%	6	0	0	2.3397	38.474	0.69%
0	0	4	4.0987	21.682	32.22%	3	1	-6	2.3304	38.635	0.80%
0	1	3	4.0378	22.013	3.00%	3	1	5	2.319	38.832	0.91%
3	0	-3	3.8491	23.106	19.20%	4	1	4	2.2985	39.192	0.54%
1	1	3	3.7717	23.587	7.56%	4	2	-1	2.2873	39.391	0.61%
3	1	-1	3.6922	24.103	0.95%	4	2	0	2.2787	39.548	1.20%
3	1	0	3.6881	24.13	3.41%	3	0	-7	2.2318	40.414	0.89%
3	1	-2	3.5217	25.289	1.84%	0	2	5	2.2118	40.796	1.34%
3	1	1	3.511	25.367	5.05%	5	1	3	2.1947	41.128	0.54%
4	0	0	3.5096	25.377	7.56%	4	1	-6	2.1724	41.569	0.54%
4	0	-2	3.4158	26.086	11.45%	1	2	5	2.1518	41.985	0.51%
1	1	-4	3.385	26.328	1.98%	1	1	7	2.1115	42.826	0.66%
2	1	3	3.3445	26.653	3.66%	4	1	5	2.0945	43.191	0.70%
2	0	4	3.33	26.771	1.33%	3	2	-5	2.0822	43.46	0.86%
3	0	3	3.3185	26.865	8.81%	5	2	-1	2.0606	43.938	0.52%
3	1	-3	3.2385	27.542	2.31%	5	2	0	2.0487	44.208	1.26%
3	1	2	3.2246	27.662	9.50%	6	1	2	2.0373	44.469	1.34%
2	1	-4	3.2056	27.83	5.74%	0	2	6	2.0189	44.895	1.98%
1	1	4	3.2004	27.876	10.00%	4	0	6	2.0154	44.977	0.59%
4	0	2	3.0653	29.131	2.92%	2	1	7	2.0057	45.206	2.04%

4	1	-1	3.0489	29.292	4.95%	5	1	-6	2.0008	45.323	0.54%
0	2	0	2.996	29.821	6.63%	5	0	5	1.9911	45.556	0.81%
4	1	-2	2.9675	30.114	2.51%	7	0	-3	1.9806	45.812	1.64%
1	2	0	2.93	30.508	2.00%	3	0	7	1.9797	45.834	0.75%
3	1	-4	2.9172	30.645	2.47%	1	3	0	1.9774	45.89	2.52%
3	1	3	2.9031	30.799	3.63%	7	0	1	1.9558	46.426	1.53%
1	2	-1	2.9	30.832	6.26%	6	1	3	1.9342	46.977	1.93%
3	0	-5	2.8958	30.878	2.05%	3	2	-6	1.9328	47.013	0.68%
1	1	-5	2.8933	30.905	1.62%	1	3	-2	1.9315	47.044	0.51%
1	2	1	2.8689	31.174	0.87%	3	2	5	1.9263	47.181	3.23%
0	2	2	2.814	31.799	4.82%	7	1	-1	1.9205	47.333	0.77%
4	1	-3	2.8063	31.889	0.67%	2	3	-1	1.9171	47.421	0.81%
2	1	-5	2.7928	32.046	5.69%	7	1	0	1.9018	47.826	0.54%
0	0	6	2.7325	32.774	2.17%	2	3	1	1.8991	47.898	0.56%
4	1	2	2.729	32.817	2.06%	2	0	8	1.8928	48.067	0.70%
5	0	1	2.7012	33.163	2.35%	3	1	-8	1.888	48.198	0.70%
2	0	-6	2.6852	33.367	2.76%	7	1	-3	1.8805	48.401	0.63%
2	2	-2	2.6593	33.702	1.37%	1	2	-7	1.8579	49.03	0.68%
0	2	3	2.6271	34.128	0.62%	5	1	-7	1.8516	49.207	0.84%
1	2	-3	2.6164	34.272	2.68%	6	2	0	1.844	49.422	0.66%
4	1	-4	2.6007	34.484	1.47%	2	3	-3	1.8359	49.655	2.05%
2	2	2	2.5669	34.953	2.07%	7	1	-4	1.8265	49.929	1.39%
5	1	-1	2.5654	34.975	0.67%						

(x) 1,8-Diammoniumoctane Dihydrogen Phosphate (DODP), $[^{+}H_3N(CH_2)_8NH_3^{+}][H_2N(CH_2)_8NH_2][H_2PO_4^{-}]_2$

Fractional Atomic Coordinates ($\times 10^4$) and Equivalent Isotropic Displacement Parameters ($Å^2 \times 10^3$) for DODP

	x	y	z	U(eq)		x	y	z	U(eq)
P(1)	2618	187	1717		C(4)	1366	-2095	-573	
O(1)	3152	881	2328		C(7)	3197	2245	-191	
O(2)	2303	584	91		C(6)	3763	2516	-111	
O(3)	2706	-1182	1843		C(5)	4049	1340	-299	
O(4)	2242	575	2683		C(9)	5000	0	0	
N(1)	1876	-2713	307		C(8)	4611	1407	-181	
C(1)	261	-297	509		C(10)	4248	730	878	
C(2)	570	-913	-464		C(9)	5412	410	-572	
C(3)	1094	-1505	517						

Hydrogen Fractional Coordinates ($\times 10^4$) and Isotropic Displacement Parameters ($Å^2 \times 10^3$) for DODP

	x	y	z	U(eq)		x	y	z	U(eq)
H(1A)	2079	-3116	-263		H(2B)	261	-1471	-1127	
H(1B)	2168	-2195	930		H(3A)	952	-2083	1122	
H(1C)	1732	-3243	867		H(3B)	1412	-956	1172	
H(1D)	568	261	1178		H(4A)	1040	-2626	-1239	
H(1E)	104	-861	1103		H(4B)	1505	-1510	-1173	
H(2A)	718	-345	-1069						

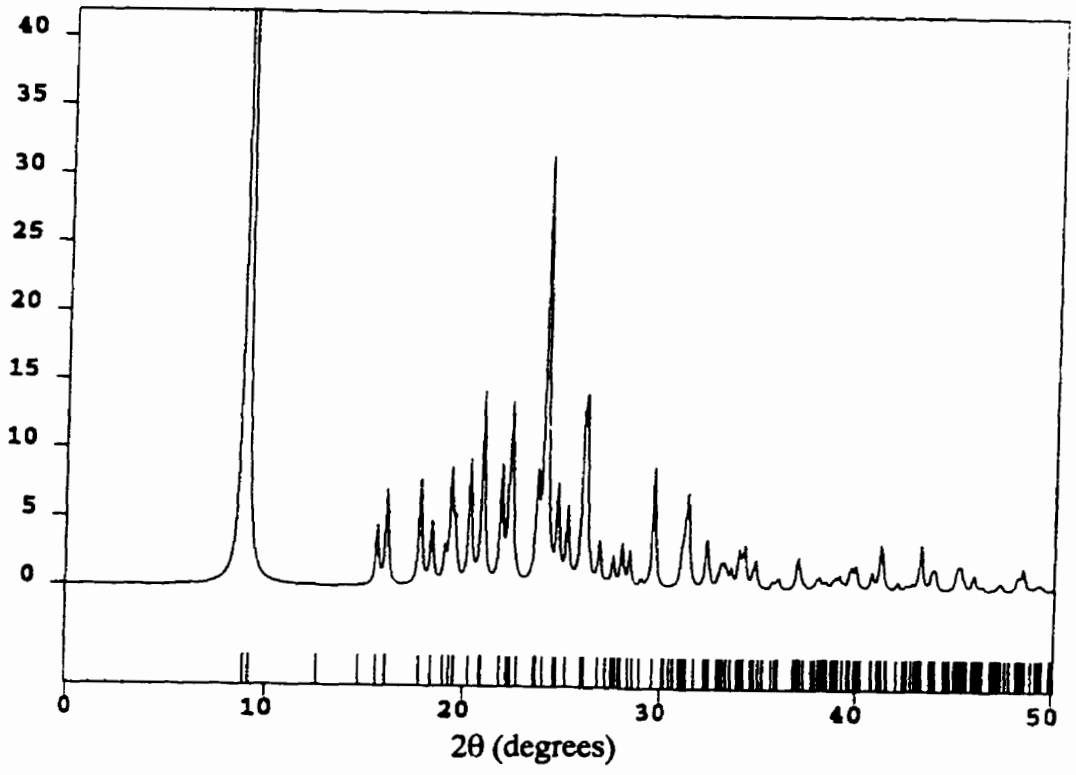

h	k	l	d-spacing	2θ	Relative Intensity	h	k	l	d-spacing	2θ	Relative Intensity
2	0	0	9.9807	8.86	100.00%	8	0	-4	2.0021	45.293	1.42%
4	2	0	3.7032	24.03	31.40%	5	3	0	2.707	33.091	1.32%
1	1	-2	4.2523	20.89	14.12%	9	1	-2	2.2566	39.951	1.31%
2	2	1	3.9752	22.364	12.29%	2	2	-3	2.6962	33.228	1.26%
5	1	-2	3.4162	26.083	10.90%	2	4	0	2.6622	33.665	1.24%
0	2	2	3.4334	25.95	9.62%	3	1	-4	2.2688	39.726	1.22%
2	2	2	3.018	29.599	9.15%	4	4	-1	2.4303	36.987	1.20%
0	0	2	4.3826	20.262	9.02%	1	3	-1	3.4196	26.057	1.16%
3	1	-2	4.067	21.853	8.27%	7	1	-3	2.4256	37.061	1.08%
2	0	-2	4.6039	19.278	7.86%	1	1	-4	2.2138	40.756	1.04%
4	0	0	4.9904	17.773	7.76%	6	0	-4	2.1871	41.278	0.98%
0	2	0	5.5245	16.042	6.98%	4	2	-3	2.6235	34.176	0.95%
2	0	2	3.6031	24.708	6.76%	1	1	4	2.0678	43.778	0.95%
6	2	0	2.85	31.386	6.22%	4	0	-4	2.3019	39.131	0.90%
4	2	-1	3.7526	23.709	5.44%	1	1	3	2.6818	33.411	0.89%
2	2	-2	3.5368	25.179	5.42%	2	0	4	2.0075	45.165	0.86%
2	2	0	4.8335	18.355	4.51%	3	3	-3	2.3578	38.167	0.76%
3	1	0	5.7	15.545	4.34%	2	4	3	1.8877	48.206	0.74%
4	0	-2	4.0041	22.2	3.89%	10	2	0	1.8774	48.488	0.73%
2	2	-1	4.5474	19.52	3.73%	7	3	1	2.0592	43.97	0.72%
6	0	0	3.3269	26.796	3.13%	2	4	1	2.4878	36.103	0.69%
4	0	2	2.8622	31.249	3.06%	0	2	3	2.5828	34.732	0.68%
3	3	-1	3.1922	27.949	2.87%	6	0	2	2.3114	38.966	0.67%
2	4	-1	2.6113	34.341	2.79%	9	3	-1	1.9747	45.956	0.65%
0	0	4	2.1913	41.195	2.65%	1	5	-1	2.1488	42.048	0.62%
6	4	-2	2.0911	43.266	2.61%	6	2	1	2.5117	35.748	0.60%
4	2	1	3.1488	28.343	2.57%	3	1	2	3.0827	28.963	0.54%
0	4	1	2.6345	34.029	2.43%	6	4	1	1.9733	45.991	0.54%
1	1	2	3.7735	23.576	2.33%	3	1	4	1.8771	48.495	0.54%
0	2	1	4.6736	18.988	2.13%	2	4	-2	2.3686	37.987	0.53%
4	2	-2	3.2421	27.511	2.04%	8	2	0	2.274	39.632	0.53%
5	3	-2	2.5716	34.888	1.92%	9	1	-3	2.0948	43.185	0.50%
1	3	-2	2.8768	31.087	1.69%	3	5	-1	2.0888	43.315	0.50%
6	2	-2	2.7692	32.327	1.66%	6	4	-3	1.9195	47.357	0.50%
7	1	-2	2.7629	32.402	1.63%						

(xi) Octylammonium Dihydrogen Phosphate (ODP), $[CH_3(CH_2)_7NH_3^+][H_2PO_4^-]$

Fractional Atomic Coordinates ($\times 10^4$) and Equivalent Isotropic Displacement Parameters ($Å^2 \times 10^3$) for ODP

	x	y	z	U(eq)		x	y	z	U(eq)
P(1)	3409(2)	7079(1)	2396(1)	16(1)	C(1)	9223(8)	10911(1)	2499(5)	33(1)
O(1)	2745(9)	7133(1)	460(5)	22(1)	C(2)	7418(7)	10542(1)	2497(5)	26(1)
O(1*)	775(9)	6967(1)	1319(6)	24(1)	C(3)	9238(7)	10175(1)	2503(4)	21(1)
O(2)	4685(9)	7459(1)	3198(5)	21(1)	C(4)	7420(7)	9807(1)	2490(4)	22(1)
O(2*)	4786(9)	7459(1)	1603(5)	19(1)	C(5)	9256(7)	9439(1)	2490(4)	22(1)
O(3)	812(8)	6946(1)	3593(5)	19(1)	C(6)	7412(7)	9072(1)	2485(4)	23(1)
O(3*)	2779(10)	7167(1)	4427(5)	26(1)	C(7)	9246(6)	8704(1)	2494(4)	21(1)
O(4)	5731(6)	6751(1)	2514(4)	32(1)	C(8)	7314(6)	8347(1)	2461(4)	20(1)
N(1)	9087(6)	7989(1)	2470(4)	27(1)					

Hydrogen Fractional Coordinates ($\times 10^4$) and Isotropic Displacement Parameters ($Å^2 \times 10^3$) for ODP

	x	y	z	U(eq)		x	y	z	U(eq)
H(4O)	7223(89)	6802(12)	2489(54)	29(12)	H(4B)	6169(7)	9807(1)	1427(4)	29(2)
H(1A)	7896(6)	7786(1)	2410(4)	29(2)	H(4C)	6186(7)	9805(1)	3543(4)	29(2)
H(1B)	10155(6)	7977(1)	3494(4)	29(2)	H(5A)	10510(7)	9438(1)	3552(4)	29(2)
H(1C)	10272(6)	7988(1)	1513(4)	29(2)	H(5B)	10484(7)	9439(1)	1434(4)	29(2)
H(1C)	7935(8)	11130(1)	2489(5)	29(2)	H(6A)	6170(7)	9072(1)	1417(4)	29(2)
H(1D)	10433(8)	10917(1)	1436(5)	29(2)	H(6B)	6171(7)	9073(1)	3535(4)	29(2)
H(1E)	10445(8)	10918(1)	3575(5)	29(2)	H(7A)	10462(6)	8699(1)	3573(4)	29(2)
H(2A)	6165(7)	10540(1)	1435(5)	29(2)	H(7B)	10505(6)	8702(1)	1452(4)	29(2)
H(2B)	6184(7)	10541(1)	3551(5)	29(2)	H(8A)	6060(6)	8349(1)	3505(4)	29(2)
H(3A)	10482(7)	10175(1)	3569(4)	29(2)	H(8B)	6092(6)	8353(1)	1385(4)	29(2)
H(3B)	10479(7)	10175(1)	1453(4)	29(2)					

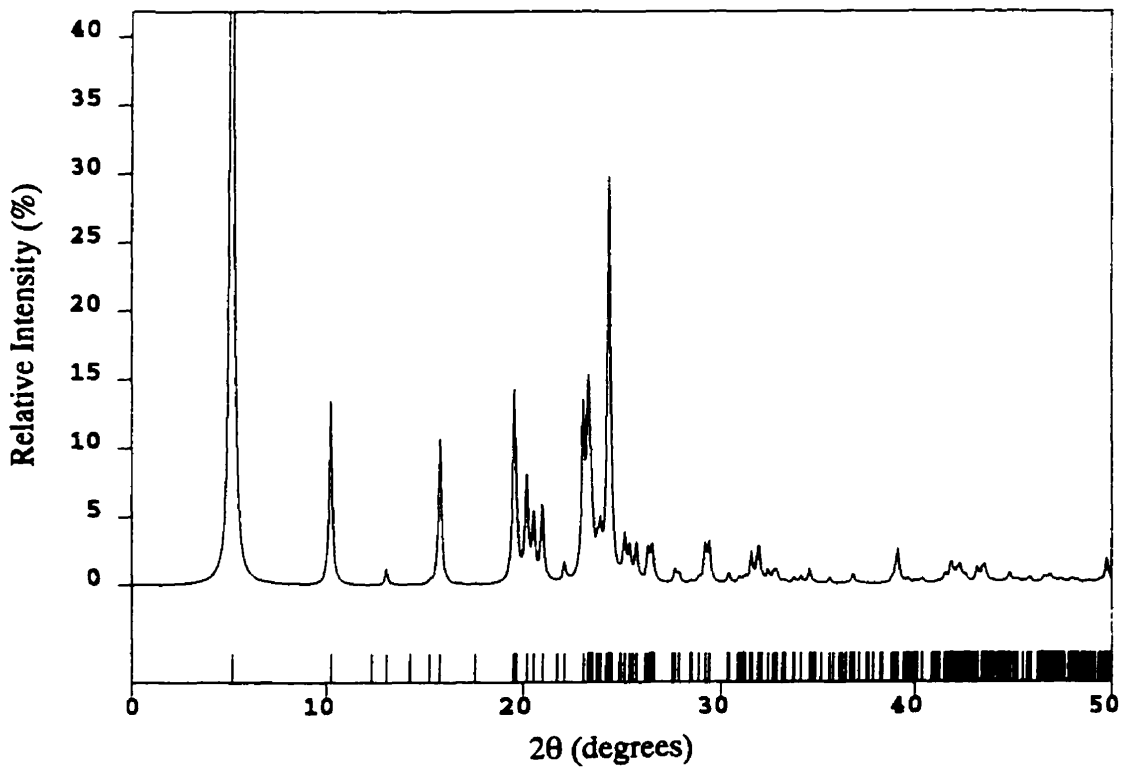

h	k	l	d-spacing	2θ	Relative Intensity	h	k	l	d-spacing	2θ	Relative Intensity
0	2	0	17.326	5.1	100.00%	1	6	-1	3.2251	27.658	1.02%
0	4	0	8.663	10.211	13.51%	1	6	1	3.2022	27.86	0.64%
0	2	1	6.7488	13.118	1.16%	1	7	-1	3.0576	29.207	2.58%
0	4	1	5.5946	15.84	10.75%	1	7	1	3.038	29.399	2.72%
0	6	1	4.5358	19.57	13.21%	1	9	0	2.9401	30.401	0.74%
1	1	0	4.5149	19.662	1.66%	1	2	-2	2.8321	31.59	1.91%
1	2	0	4.4041	20.162	7.43%	1	2	2	2.8013	31.947	1.57%
0	8	0	4.3315	20.503	4.60%	0	8	2	2.7973	31.994	1.46%
1	3	0	4.2364	20.969	5.57%	1	10	0	2.7576	32.467	0.78%
1	4	0	4.0308	22.052	1.34%	1	9	-1	2.7357	32.734	0.68%
1	1	-1	3.8636	23.019	11.91%	1	9	1	2.7217	32.907	0.70%
1	1	1	3.8244	23.258	11.77%	1	5	2	2.6268	34.132	0.51%
1	5	0	3.8057	23.374	3.93%	1	11	0	2.5907	34.622	1.09%
1	2	-1	3.7935	23.45	2.08%	1	12	0	2.4387	36.856	0.72%
1	2	1	3.7563	23.685	1.54%	1	13	0	2.3004	39.158	2.46%
0	8	1	3.7287	23.863	2.76%	1	1	-3	2.1586	41.847	1.14%
1	3	-1	3.6847	24.153	0.75%	1	2	-3	2.1462	42.101	0.64%
0	0	2	3.6638	24.293	29.43%	1	1	3	2.1381	42.268	1.21%
1	3	1	3.6506	24.381	0.85%	1	4	-3	2.0984	43.107	1.09%
1	4	-1	3.547	25.105	2.96%	1	14	-1	2.0879	43.334	0.66%
1	4	1	3.5166	25.326	2.17%	1	4	3	2.0795	43.518	0.79%
0	10	0	3.4652	25.708	2.60%	1	6	-3	2.0255	44.742	0.51%
1	5	-1	3.3907	26.283	2.23%	0	0	4	1.8319	49.773	1.93%
1	5	1	3.3641	26.494	2.38%						

(xii) Decylammonium Dihydrogen Phosphate (DDP), $[CH_3(CH_2)_9NH_3^+][H_2PO_4^-]$

Fractional Atomic Coordinates ($\times 10^4$) and Equivalent Isotropic Displacement Parameters ($Å^2 \times 10^3$) for DDP

	x	y	z	U(eq)		x	y	z	U(eq)
P(1)	2621(2)	2142(1)	783(1)	17(1)	P(2)	-2483(2)	2873(1)	811(1)	16(1)
O(1)	2691(5)	1849(1)	-358(4)	24(1)	O(5)	-3609(4)	2977(1)	2103(3)	21(1)
O(2)	3365(4)	2465(1)	117(3)	22(1)	O(6)	-3230(5)	2535(1)	143(3)	23(1)
O(3)	552(5)	2202(1)	1117(4)	25(1)	O(7)	-478(4)	2816(1)	1119(3)	22(1)
O(4)	3649(4)	2031(1)	2118(3)	22(1)	O(8)	-2710(5)	3154(1)	-390(4)	23(1)
N(1)	2724(6)	2924(1)	2925(5)	20(1)	N(2)	2315(6)	2925(1)	-2023(5)	20(1)
C(1)	2542(7)	3238(1)	3823(5)	21(1)	C(11)	2492(7)	3240(1)	-1152(5)	20(1)
C(2)	2562(7)	3549(1)	2870(5)	22(1)	C(12)	2450(7)	3548(1)	-2119(5)	21(1)
C(3)	2521(7)	3870(1)	3787(5)	21(1)	C(13)	2498(7)	3871(1)	-1215(5)	22(1)
C(4)	2515(7)	4192(1)	2874(5)	21(1)	C(14)	2483(7)	4190(1)	-2131(5)	21(1)
C(5)	2508(7)	4513(1)	3786(5)	22(1)	C(15)	2507(7)	4513(1)	-1219(5)	22(1)
C(6)	2511(7)	4834(1)	2874(5)	20(1)	C(16)	2495(7)	4834(1)	-2130(5)	20(1)
C(7)	2506(7)	5155(1)	3792(5)	22(1)	C(17)	2491(7)	5155(1)	-1216(5)	22(1)
C(8)	2522(7)	5476(1)	2880(5)	20(1)	C(18)	2476(7)	5476(1)	-2120(5)	21(1)
C(9)	2513(7)	5797(1)	3789(5)	25(1)	C(19)	2488(7)	5796(1)	-1208(5)	25(1)
C(10)	2521(7)	6118(1)	2886(6)	32(1)	C(20)	2471(8)	6117(1)	-2120(6)	32(1)

Hydrogen Fractional Coordinates ($\times 10^4$) and Isotropic Displacement Parameters ($Å^2 \times 10^3$) for DDP

	x	y	z	U(eq)		x	y	z	U(eq)
H(1A)	2629(64)	2753(13)	3595(55)	22(5)	H(2E)	1290(73)	2931(12)	-2507(55)	22(5)
H(1B)	3850(71)	2952(12)	2385(53)	22(5)	H(11A)	3651(7)	3235(1)	-594(5)	22(2)
H(1C)	1887(69)	2943(12)	2217(56)	22(5)	H(11B)	1486(7)	3252(1)	-441(5)	22(2)
H(1D)	3556(7)	3250(1)	4541(5)	22(2)	H(12A)	1332(7)	3545(1)	-2729(5)	22(2)
H(1E)	1389(7)	3230(1)	4375(5)	22(2)	H(12B)	3507(7)	3543(1)	-2783(5)	22(2)
H(2A)	1496(7)	3546(1)	2203(5)	22(2)	H(13A)	1434(7)	3874(1)	-558(5)	22(2)
H(2B)	3672(7)	3548(1)	2263(5)	22(2)	H(13B)	3605(7)	3870(1)	-593(5)	22(2)
H(3A)	3594(7)	3872(1)	4447(5)	22(2)	H(14A)	1383(7)	4190(1)	-2762(5)	22(2)
H(3B)	1422(7)	3866(1)	4406(5)	22(2)	H(14B)	3555(7)	4189(1)	-2779(5)	22(2)
H(4A)	3601(7)	4193(1)	2241(5)	22(2)	H(15A)	1433(7)	4514(1)	-572(5)	22(2)
H(4B)	1428(7)	4191(1)	2227(5)	22(2)	H(15B)	3605(7)	4513(1)	-586(5)	22(2)
H(5A)	1418(7)	4513(1)	4415(5)	22(2)	H(16A)	1406(7)	4833(1)	-2773(5)	22(2)

H(5B)	3591(7)	4513(1)	4436(5)	22(2)	H(16B)	3579(7)	4835(1)	-2766(5)	22(2)
H(6A)	1427(7)	4834(1)	2225(5)	22(2)	H(17A)	1409(7)	5153(1)	-578(5)	22(2)
H(6B)	3600(7)	4834(1)	2244(5)	22(2)	H(17B)	3582(7)	5156(1)	-574(5)	22(2)
H(7A)	1413(7)	5156(1)	4417(5)	22(2)	H(18A)	1381(7)	5476(1)	-2756(5)	22(2)
H(7B)	3586(7)	5154(1)	4446(5)	22(2)	H(18B)	3553(7)	5476(1)	-2763(5)	22(2)
H(8A)	1444(7)	5476(1)	2225(5)	22(2)	H(19A)	3584(7)	5796(1)	-572(5)	22(2)
H(8B)	3616(7)	5475(1)	2257(5)	22(2)	H(19B)	1411(7)	5796(1)	-564(5)	22(2)
H(9A)	1422(7)	5797(1)	4416(5)	22(2)	H(20A)	2517(50)	6313(1)	-1469(6)	52(7)
H(9B)	3594(7)	5797(1)	4442(5)	22(2)	H(20B)	1355(24)	6125(5)	-2712(30)	52(7)
H(10A)	2535(50)	6313(1)	3541(6)	52(7)	H(20C)	3528(27)	6119(4)	-2766(29)	52(7)
H(10B)	1428(25)	6126(4)	2266(29)	52(7)	H(1O)	2334(67)	1899(12)	-1149(58)	21(14)
H(10C)	3603(26)	6122(4)	2267(29)	52(7)	H(3O)	244(96)	2453(20)	1091(76)	80(23)
H(2C)	2584(66)	2743(13)	-1540(54)	22(5)	H(6O)	-4387(103)	2511(20)	275(81)	85(28)
H(2D)	3140(67)	2899(12)	-2776(57)	22(5)	H(8O)	-2224(80)	3069(15)	-1232(67)	46(17)

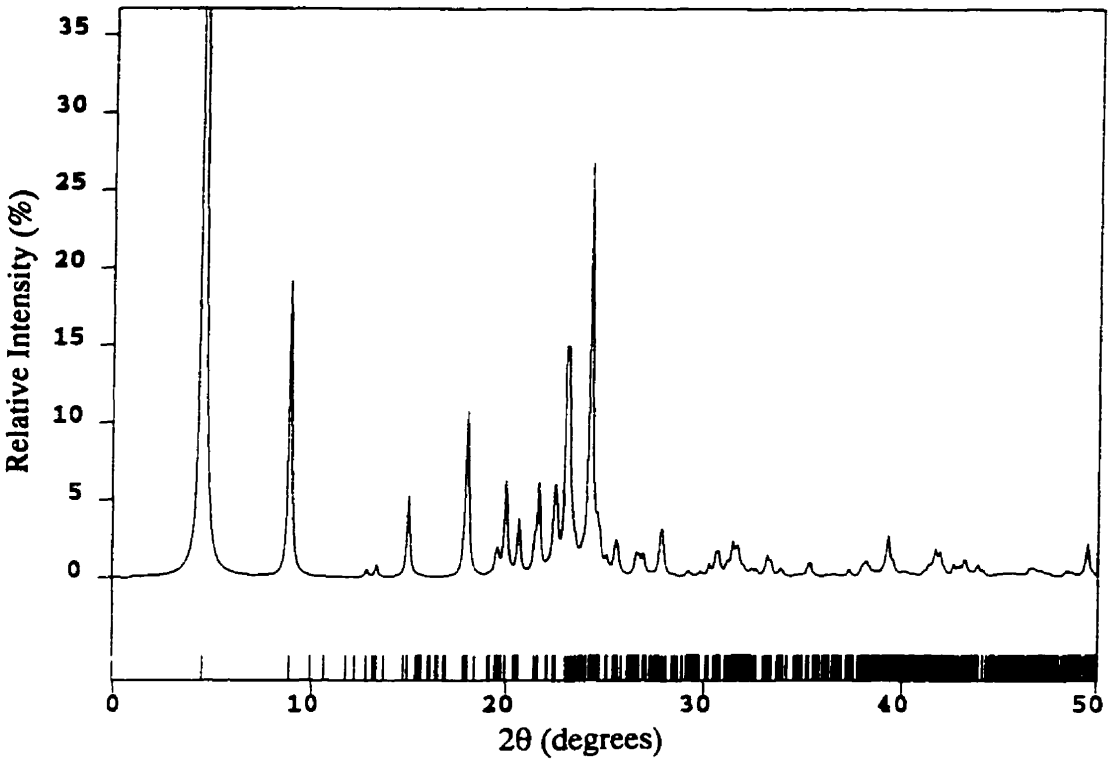

h	k	l	d-spacing	2θ	Relative Intensity	h	k	l	d-spacing	2θ	Relative Intensity
0	2	0	19.8745	4.446	100.00%	1	5	-2	3.4963	25.475	1.06%
0	4	0	9.9373	8.898	19.21%	1	5	2	3.4765	25.623	1.16%
1	2	0	6.9001	12.829	0.51%	1	6	-2	3.3564	26.556	1.14%
0	6	0	6.6248	13.365	0.82%	1	6	2	3.3388	26.698	0.93%
1	4	0	5.9133	14.981	5.35%	0	12	0	3.3124	26.915	1.23%
0	8	0	4.9686	17.851	1.59%	1	7	-2	3.2109	27.783	2.03%
1	6	0	4.9233	18.017	10.48%	1	7	2	3.1955	27.92	2.12%
0	0	2	4.5654	19.443	0.90%	2	8	0	2.9566	30.227	0.77%
0	1	2	4.5355	19.572	1.20%	1	9	-2	2.9204	30.611	1.23%
0	2	2	4.4495	19.954	6.19%	1	9	2	2.9088	30.736	1.29%
0	3	2	4.3163	20.576	3.61%	2	2	-2	2.846	31.432	1.41%
0	4	2	4.1485	21.418	1.81%	0	11	2	2.8334	31.575	0.61%
1	8	0	4.1177	21.581	5.72%	2	2	2	2.8247	31.675	1.30%
0	10	0	3.9749	22.366	2.94%	2	10	0	2.7	33.18	0.93%
0	5	2	3.959	22.457	4.06%	0	12	2	2.6811	33.42	0.65%
1	1	-2	3.8745	22.953	11.69%	0	13	2	2.5405	35.329	0.73%
1	1	2	3.8475	23.116	11.55%	0	14	2	2.411	37.294	0.50%

1	2	-2	3.8204	23.282	1.11%	0	15	2	2.2918	39.311	1.94%
1	2	2	3.7946	23.443	0.93%	3	1	-2	2.1644	41.729	1.23%
1	3	-2	3.7351	23.822	0.59%	3	1	2	2.1504	42.015	1.25%
1	3	2	3.711	23.979	0.64%	3	4	-2	2.1179	42.691	0.66%
2	0	0	3.6789	24.191	26.80%	3	4	2	2.1047	42.972	0.55%
1	4	-2	3.6248	24.558	2.00%	1	16	-2	2.0942	43.197	0.66%
1	4	2	3.6027	24.711	1.70%	1	16	2	2.0899	43.29	0.54%
0	7	2	3.558	25.026	0.87%	4	0	0	1.8394	49.554	1.77%
1	10	0	3.4972	25.469	0.59%						

IMAGE EVALUATION TEST TARGET (QA-3)

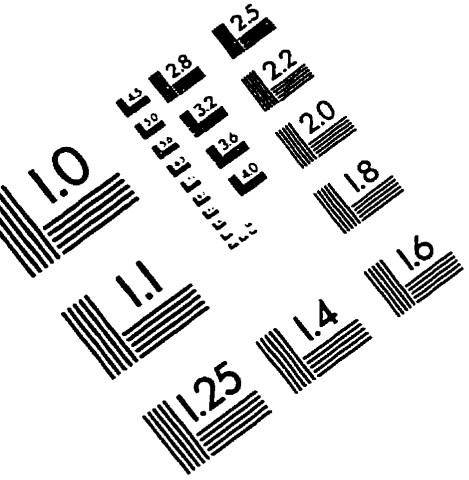

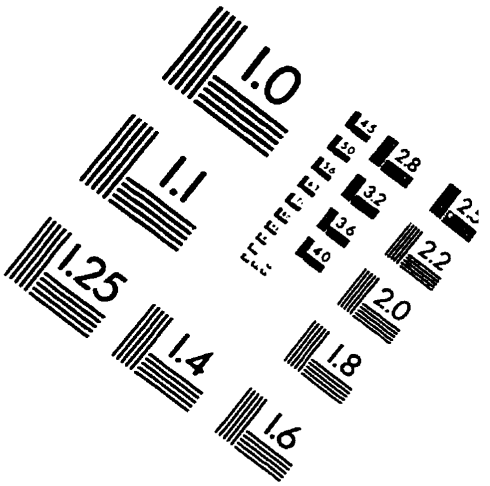

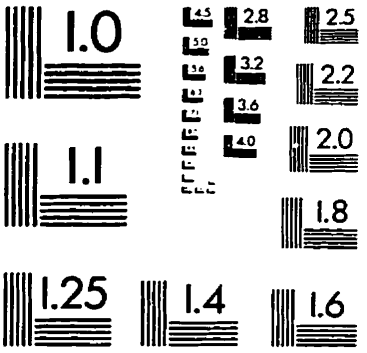

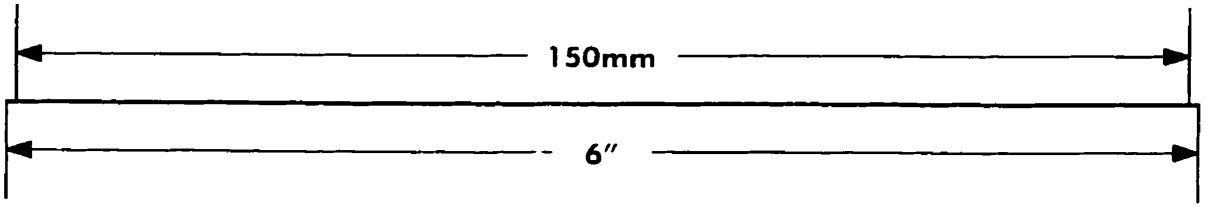

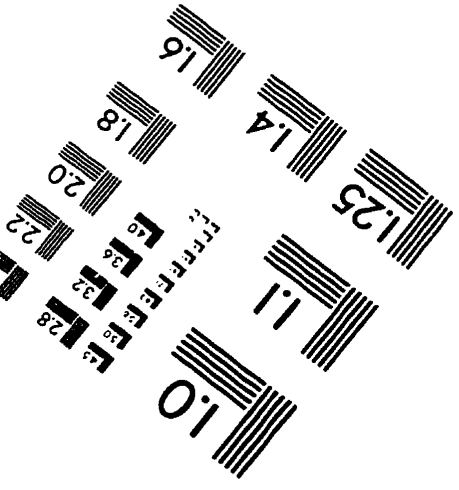

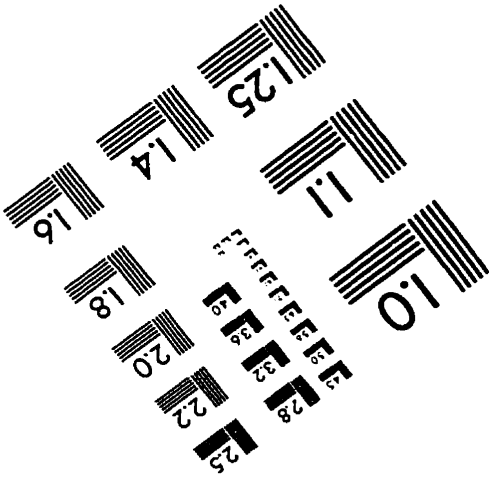

APPLIED IMAGE, Inc
1653 East Main Street
Rochester, NY 14609 USA
Phone: 716/482-0300
Fax: 716/288-5989